



**Treatment of Leachates from Urban Sanitary Landfills through
Integration of Biological and Photo-Chemical Oxidation Processes
combining Natural and Artificial Radiation**

*Thesis submitted in partial fulfilment of the requirements for the degree of
Doctor of Philosophy in Environmental Engineering, at the Faculty of
Engineering, University of Porto*

Tânia Filomena Castro Valente Silva

Supervisor: Doutor Vítor Jorge Pais Vilar

Co-Supervisor: Doutor Rui Alfredo da Rocha Boaventura

LSRE-Laboratory of Separation and Reaction Engineering - Associate Laboratory LSRE-LCM
Department of Chemical Engineering
Faculty of Engineering
University of Porto
December, 2015

Acknowledgments

After four years of this doctoral program, it would not be entirely fair do not express my sincere thanks to all of those who, directly or indirectly, have contributed to the concretization of this work.

First of all, I would like to deeply acknowledge to my supervisors, Dr. Vítor Vilar and Dr. Rui Boaventura, the opportunity given me to perform this thesis under their guidance, as well as their assiduous and enriching presence in the discussion and resolution of the difficulties encountered, especially on troubled moments that have emerged during the work, and their constructive criticism that have become precious, acknowledging that without their help and valuable knowledge it would not have been possible to meet all the objectives.

A mention must be made to the following institutions that supported this work: the Foundation for Science and Technology (FCT) for the doctoral grant (SFRH/BD/73510/2010); the Associated Laboratory of Separation and Reaction Engineering (LSRE) and Catalysis Materials (LCM), Faculty of Engineering of the University of Porto (FEUP). The project PEst-C/eqB/LA0020/2013, financed by FCT and FEDER through COMPETE, and by QREN, ON2 (North Portugal Regional Operational Programme) and FEDER through project NORTE-07-0124-FEDER- 0000008.

I am very grateful to EFACEC Engineering and Systems, S.A, mainly to Eng. Amélia Fonseca and Eng. Isabel Saraiva, for the financial and technical support, providing me the infrastructures and required conditions, without which this research would not have been possible.

I gratefully acknowledge to all workers of the sanitary landfill where this research was conducted, who have always received me willingly and let me use their facilities to develop my work. Especially, I would like to acknowledge to Dr. Andreia Costa and Sr. Nuno Barbosa, who became good friends, for sharing their workspace and their knowledge with me, for always help me when I needed and for making my days more pleasant.

I also am very thankful for the collaborative work developed with: Dr. Elisabete Silva and Dr. Ana Cunha-Queda, from the School of Technology of the Polytechnic Institute of Viseu (ESTGV) and Faculty of Agricultural Sciences (ISA) of the Technical University of Lisbon (UTL); Dr. Augusta Sousa, Dr. Carlos Gonçalves and Dr. Fátima Alpendurada from the Water Institute of the Northern Region (IAREN); and Dr. Joana Bondoso, Dr. Rita Lopes and Dr. Olga Nunes from Laboratory from Process Engineering, Environment, Biotechnology and Energy (LEPABE).

A special thanks for those who somehow helped me, contributing for the accomplishment of my work: Petrick Soares, Rui Gomes, Diego Manenti, Bruno Souza, Carmen Rodrigues, Eloísa Vieira and Juan Soller.

I would like to thank to all my colleagues at LSRE for the partnership and good work environment, over the last few years. Thanks to those who shared with me many refreshing morning coffees, peculiar lunches and lab routines: André Fonseca, André Monteiro, Petrick Soares, João Pereira, Ariana Pintor, Livia Xerez, Filipe Lopes, Joana Pereira, Francisca Moreira, Tatiana Pozdniakova, Catarina Ferreira, Fabiola Hackbarth and Caio Rodrigues-Silva.

A particular thanks to my friends Diana Machado, Raquel Rocha and Sofia Lima for the great moments of conviviality, for supporting me along the trodden way and mostly for their genuine friendship over the past few years.

To my family, especially my parents and my brother, I express my frank acknowledgment, for all the help and strength that always instilled in me throughout my personal and academic life.

Finally, to my husband, Bruno, I would like to express my sincere gratitude for his love, friendship and support in all times, for have given me strength in the most difficult moments and for the encouragement along this journey.

To all my genuine thanks!

With love to my parents, brother and husband

Abstract

The disposal of municipal solid wastes in sanitary landfills unavoidably leads to the production of leachate, which results from the rainwater percolation through the waste mass, biochemical reactions in waste's cells and water contained in the wastes. The leachate presents a composition extremely complex and variable. Furthermore, this kind of effluent, especially the one from landfills designated "old", presents low biodegradability, mainly due to humic substances (HS), which difficult its treatment by conventional biological processes. Advanced oxidation processes (AOPs) have been recognized as highly efficient in biodegradability enhancement of different recalcitrant wastewaters. The present thesis had as main purpose the development and optimization of a multistage methodology for the treatment of mature landfill leachates, targeting mostly the discharge into water bodies, at appellative costs.

Firstly, an integrated leachate treatment strategy was proposed, combining (i) a solar photo-Fenton (PF) reaction (80 mg Fe^{2+} , pH 2.8), to enhance the biodegradability of the leachate from an aerated lagoon, with (ii) an activated sludge biological oxidation (ASBO), under aerobic and anoxic conditions, to eliminate the nitrogen compounds and the remaining biodegradable organic matter. Then, a multistage treatment system was designed for the treatment of a raw landfill leachate integrating (i) an ASBO, to remove the biodegradable organic matter and most of the nitrogen, with (ii) a solar PF process, to enhance the biodegradability of the bio-treated leachate, considering or not the removal of acid sludge after acidification, and (iii) an ASBO, as final polishing step. Both treatment sequences were performed in a pre-industrial scale plant composed by (i) a photocatalytic system with 39.52 m² of compound parabolic collectors (CPCs) and 2.5 m³ recirculation tank and (ii) a 3.5 m³ capacity biological reactor. The experimental unit was installed at the sanitary landfill in order to assess the treatment efficiency, under real circumstances of leachate variability and weather conditions.

A physico-chemical characterization of the leachate after aerobic lagooning, along 1-year, reinforced its high recalcitrant nature, mainly associated with the presence of humic substances (HS), which contribute by about 59% to the dissolved organic carbon (DOC). The raw leachate, collected before the aerobic lagooning, was also characterized by a high concentration of HS (1.2 g $\text{C}_{\text{HS}}/\text{L}$), representing 39% of the DOC content, and a high nitrogen content, mainly in the form of ammonium nitrogen ($> 3.8 \text{ g NH}_4^+\text{-N/L}$). Performing a biological oxidation before the solar PF reaction allowed 95% removal of the total nitrogen and 39% mineralization, remaining only the recalcitrant organic fraction (mostly HS, representing 57% of DOC). Under aerobic conditions, the highest nitrification rate obtained was 8.2 mg $\text{NH}_4^+\text{-N}/(\text{h.g VSS})$, and under anoxic conditions, the maximum denitrification rate was 5.8 mg $(\text{NO}_2^-\text{-N}+\text{NO}_3^-\text{-N})/(\text{h.g VSS})$, corresponding to a C/N consumption ratio of 2.4 mg $\text{CH}_3\text{OH}/\text{mg} (\text{NO}_2^-\text{-N}+\text{NO}_3^-\text{-N})$.

The phototreatment process led to the depletion of HS $>80\%$, of low-molecular-weight carboxylate anions $>70\%$ and other organic micropollutants, thus resulting in a total biodegradability increase of $>70\%$.

However, it was observed that the photo-reaction efficiency was strongly affected by the (i) weather conditions, mainly due to low irradiances and temperatures in the winter season, associated to the effects of the Fenton thermal reaction and molar fraction of ferric species, (ii) presence of humic acids, related to the dark-brown colour intrinsic to leachates, (iii) high amount of total suspended solids (TSS), resulting from the precipitation of some organic compounds with ferric ions, after acidification and during reaction, and (iv) high amounts of sulphate ions provided by the sulphuric acid addition to perform the initial acidification for the PF reaction. The non-elimination of the produced acid sludge decreases the PF reaction efficiency (~30%), due to the low light transmission caused by the high amount of TSS that compete with H₂O₂ and iron species as photons absorbers. Besides, higher amounts of H₂O₂ and energy were required for the degradation of additional particulate organic matter. The low temperatures observed during the winter likewise affected the biological process after the chemical oxidation step.

The combined use of PF and ASBO processes allowed to obtain a final treated leachate in compliance with legal discharge limits regarding water bodies, imposed by Portuguese Legislation, with the exception of sulphate ions. However, even at optimal conditions, a scale-up of the PF system (considering the consumption of 180 mM of H₂O₂ and 30 kJ_{UV}/L of accumulated UV energy), for the treatment of 100 m³ per day of a sanitary landfill leachate previously treated in a biological system, revealed the need of 6056 m² of CPCs or 39 UV lamps (with 4kW and 20,000-h of lifetime each) to achieve a COD of 150 mg O₂/L by a subsequent ASBO. Combining natural and artificial radiation, it would be need 3862 m² of CPCs and 30 UV lamps. Total PF costs were calculated based on the project's contingencies, engineering and setup, spare parts, personnel, maintenance, electricity and chemicals supplies. Thus, the total unitary costs at the optimal conditions were (i) 11.0 €/m³ using only CPCs, (ii) 11.7 €/m³ resorting just to UV lamps, and (iii) 10.9 €/m³ combining CPCs and UV lamps. The cost of the H₂O₂ reactant represents more than 30% of the total yearly cost.

Considering all drawbacks and the high treatment costs associated to the PF reaction, the implementation of a preliminary biological nitrification followed by a physico-chemical process seemed to be the best option to reduce the amount of sulphates and photons absorbers species, respectively, during photo-oxidation. So, it was decided to adapt the pre-industrial plant to work according to this new methodology. However, in the meantime, complementary tests, at lab-scale, were performed, in order to assess the effect of (i) the main PF reaction variables on the treatment of a leachate collected at the end of a leachate treatment plant (LTP), which includes aerated lagooning followed by aerated activated sludge and a final coagulation-flocculation step, and (ii) the main nitrification and denitrification variables on the nitrogen's biological removal via nitrite, from mature leachates.

The best PF reaction rate was obtained for: pH = 2.8 (acidification agent: H₂SO₄); T = 30 °C; [Fe²⁺] = 60 mg/L and UV irradiance = 44 W_{UV}/m², achieving 72% mineralization after 25 kJ_{UV}/L of accumulated UV energy and 149 mM of H₂O₂ consumed. The denitrification process, which was mediated

by bacteria from the genus *Hyphomicrobium*, showed to be sensitive to variations in the pH, temperature and phosphate concentration. While, the nitrification reaction, which was mediated by bacteria from the family *Nitrosomonadaceae*, did not suffer significant change when DO content was changed, but showed itself susceptible to pH and temperature variations.

Finally, it was adopted an integrated leachate treatment strategy, involving (i) ASBO, under aerobic conditions, to remove leachate's alkalinity and the biodegradable organic carbon fraction (ii) a coagulation/sedimentation step (240 mg Fe³⁺/L, at pH 4.2, 14-hours settling), to promote humic acids precipitation and reduce the amount of TSS, and (iii) photo-oxidation through PF reaction (60 mg Fe²⁺, at pH 2.8), combining solar and artificial radiation (given the reduced solar energy in winter time), to promote the recalcitrant molecules degradation and consequent biodegradability enhancement, until the point (DOC \approx 250 mg/L) wherein a downstream biological treatment would allow to meet the discharge limit into water bodies (COD < 150 mg O₂/L).

The results demonstrate that the ASBO applied to a leachate after aerobic lagooning, with high organic and nitrogen content and low biodegradability, was capable to oxidise between 62 and 99% of the ammonium nitrogen, consuming only its own alkalinity, which means alkalinity reductions between 70 and 100%. The coagulation/sedimentation stage led to the humic acids precipitation, promoting a marked change in leachate colour, from dark-brown to yellowish-brown (related to fulvic acids), accompanied by reductions up to 66% on DOC and 92% on TSS, obtaining an amount of acid sludge of about 300 mL/L. These pre-treatments led to an effluent in agreement with the sulphate discharge limit (2 g/L) into water bodies.

From the PF trials, it was concluded that the best option would be combining natural sunlight with artificial radiation (\sim 1.3 kW/m³), thus optimizing the indirect costs. According to Zahn-Wellens test, a leachate after coagulation (419 mg DOC/L) would have to be photo-oxidized until a DOC lesser than 300 mg/L, consuming about 100 mM of H₂O₂ and 7.4 kJ/L of accumulated UV energy, in order to achieve an effluent than can be biologically treated in compliance with the COD discharge limit into water bodies. The biological process subsequent to the photocatalytic system would promote a 59% mineralization, being the final COD of approximately 115 mg O₂/L.

The scale-up of a PF facility with a capacity to treat 100 m³ of leachate/day showed the need to implement 1500 m² of CPCs or 38 UV-Vis lamps (4kW, 20,000-h of lifetime, working 6 daily hours), targeting a COD < 150 mg O₂/L. Combining solar and artificial radiation, it would be need 957 m² of CPCs and 30 lamps (considering the month of lesser and higher irradiance, respectively). The cost of the PF step decreased by about 50% when compared to the initial approach: 5.7 €/m³, resorting just to CPCs; 5.8 €/m³, using only UV-Vis Lamps; and 5.7 €/m³, combining CPCs and lamps. The cost with H₂O₂ corresponds to about 44% of the total yearly cost.

Resumo

A deposição de resíduos sólidos urbanos em aterros sanitários conduz forçosamente à produção de lixiviado, o qual resulta da percolação da água da chuva através da massa de resíduos, de reações bioquímicas nas células de resíduos e da própria água contida nos resíduos. O lixiviado apresenta uma composição extremamente complexa e variável. Além disso, este tipo de efluente, especialmente os provenientes de aterros designados “velhos”, apresenta baixa biodegradabilidade, principalmente devido à presença de substâncias húmicas (SH), o que dificulta o tratamento por processos biológicos convencionais. Os processos de oxidação avançados (POAs) têm sido reconhecidos como altamente eficientes no aumento da biodegradabilidade de diferentes efluentes recalcitrantes. A presente tese teve como objetivo principal o desenvolvimento e otimização de uma metodologia, composta por vários estágios, para o tratamento de lixiviados dos aterros maduros, visando principalmente a descarga em meio hídrico, a custos apelativos.

Em primeiro lugar, uma estratégia de tratamento de lixiviados integrada foi proposta, combinando (i) reação de foto-Fenton (FF) solar (80 mg de Fe^{2+} , pH 2,8), para aumentar a biodegradabilidade do lixiviado proveniente de uma lagoa arejada, e (ii) oxidação biológica com lamas ativadas (OBLA), sob condições aeróbias e anóxicas, para eliminar os compostos azotados e a matéria orgânica biodegradável remanescente. Em seguida, um sistema de tratamento de vários estágios foi concebido para o tratamento de lixiviado bruto, integrando: (i) uma OBLA, para remover a matéria orgânica biodegradável e a maior parte do azoto, com (ii) um processo de FF solar, para aumentar a biodegradabilidade do lixiviado bio-tratado, considerando ou não a remoção de lamas de ácidas após acidificação, e (iii) uma OBLA, como etapa final de polimento. Ambas as sequências de tratamento foram realizados numa unidade à escala pré-industrial constituída por (i) um sistema fotocatalítico composto por 39,52 m² de coletores parabólicos compostos (CPCs) e tanque de recirculação com 2,5 m³ e (ii) um reator biológico com 3,5 m³ de capacidade. A unidade experimental foi instalada no aterro sanitário, a fim de avaliar a eficiência do tratamento, em condições reais de variabilidade do lixiviado e das condições meteorológicas.

A caracterização físico-química do lixiviado após lagunagem aeróbia, ao longo de 1 ano, reforçou a sua natureza recalcitrante, principalmente associada à presença de SH, que contribuem em cerca de 59% para o carbono orgânico dissolvido (COD). O lixiviado bruto, recolhido antes do processo de lagunagem aeróbia, também foi caracterizado por uma elevada concentração de SH (1,2 g $\text{C}_{\text{SH}}/\text{L}$), que representa 39% do teor de COD, e um elevado teor de azoto, principalmente sob a forma de azoto de amoniacal ($> 3,8 \text{ g N-NH}_4^+/\text{L}$). A realização de uma oxidação biológica antes da reação de FF permitiu obter uma remoção de 95% do azoto total e 39% de mineralização, permanecendo apenas a fração orgânica recalcitrante (principalmente SH, representando 57% do COD). Em condições aeróbias, a maior taxa de nitrificação obtida foi de 8,2 mg $\text{N-NH}_4^+ / (\text{h.g SSV})$, e sob condições anóxicas, a taxa máxima de desnitrificação foi de 5,8 mg $(\text{N-NO}_2^- + \text{N-NO}_3^-) / (\text{h.g SSV})$, correspondendo a uma razão de consumo C/N de 2,4 mg $\text{CH}_3\text{OH} / \text{mg} (\text{N-NO}_2^- + \text{N-NO}_3^-)$.

O processo de fototratamento conduziu à depleção de SH (>80%), de carboxilatos de baixo peso molecular (>70%) e outros micro-poluentes, resultando assim num aumento total de biodegradabilidade maior do que 70%. Contudo, a eficácia da foto-reação foi claramente afetada (i) pelas condições meteorológicas, principalmente devido aos baixos níveis de irradiância e temperaturas no inverno, associados aos efeitos da reação térmica de Fenton e da fração molar das espécies férricas, (ii) pela presença de ácidos húmicos, relacionada com a cor castanho-escuro intrínseca dos lixiviados, (iii) pela quantidade elevada de sólidos suspensos totais (SST), resultantes da precipitação de alguns compostos orgânicos com iões férricos, após acidificação e durante a reação, e (iv) pelas quantidades elevadas de iões de sulfato providos pela adição de ácido sulfúrico para realizar a acidificação inicial da reação de FF. O facto de não eliminar as lamas ácidas produzidas contribui para a diminuição da eficiência da reação de FF (~30%), devido à baixa transmissibilidade da luz provocada pela elevada quantidade de SST, que competem com o H₂O₂ e as espécies de ferro como absorvedores de fotões. Além disso, foram necessárias quantidades mais elevadas de H₂O₂ e de energia para a degradação da matéria orgânica particulada adicional. As baixas temperaturas observadas durante o inverno afetaram de igual modo o processo biológico após a etapa de oxidação química.

O uso combinado dos processos de FF e de OBLA permitiu obter um lixiviado tratado em conformidade com os limites de descarga legais em meio hídrico, impostos pela legislação portuguesa, com a exceção do iões sulfato. Todavia, mesmo em condições ideais, o *scale-up* do sistema FF (considerando-se o consumo de 180 mM de H₂O₂ e 30 kJ_{UV}/L de energia UV acumulado), para o tratamento de 100 m³ por dia de um lixiviado de aterro sanitário tratado previamente num sistema biológico, revelou a necessidade de 6056 m² de CPCs ou 39 lâmpadas UV (com 4 kW e 20.000 h de tempo de vida, cada uma) para atingir uma CQO de 150 mg O₂/L numa OBLA subsequente. Combinando radiação natural e artificial, seriam necessários 3862 m² de CPCs e 30 lâmpadas UV. Os custos totais da etapa de FF foram calculados considerando contingências de projeto, engenharia e montagem, peças de reposição, pessoal, manutenção, energia elétrica e produtos químicos. Assim, o custo total unitário, em condições ótimas, foram: (i) 11,0 €/m³, utilizando apenas CPCs, (ii) 11,7 €/m³, recorrendo apenas a lâmpadas UV, e (iii) 10,9 €/m³, combinando CPCs e lâmpadas UV. O custo do H₂O₂ representa mais de 30% do custo total anual.

Considerando todas as desvantagens e os elevados custos de tratamento associados à reação de FF, a aplicação de uma nitrificação preliminar, seguido por um processo físico-químico pareceu ser a melhor opção para reduzir a quantidade de sulfatos e de espécies absorvedores de fotões, respetivamente, durante a foto-oxidação. Assim, decidiu-se adaptar a unidade pré-industrial para trabalhar de acordo com esta nova metodologia. No entanto, nesse meio tempo, testes complementares, à escala laboratorial, foram realizados, de forma a avaliar o efeito (i) das principais variáveis da reação de FF no tratamento de lixiviados recolhidos no final de uma estação de tratamento de lixiviados (ETL), que inclui lagunagem aeróbia, seguido por lamas ativadas, em regime aeróbico, e uma etapa final de coagulação-floculação, e (ii) as principais variáveis de nitrificação e desnitrificação, na remoção biológica do azoto de lixiviados maduros, via nitrito.

A melhor velocidade da reação de FF foi obtida nas seguintes condições: pH = 2,8 (agente de acidificação: H₂SO₄); T = 30 °C; [Fe²⁺] = 60 mg/L e irradiância UV = 44 W_{UV}/m², alcançando uma mineralização de 72%,

consumindo 25 kJ_{UV}/L de energia UV acumulada e 149 mM de H₂O₂. O processo de desnitrificação, que foi mediado por bactérias do género *Hyphomicrobium*, mostrou ser sensível às variações de pH, temperatura e concentração de fosfato. Enquanto, a reação de nitrificação, que foi mediada por bactérias da família *Nitrosomonadaceae*, não sofreu alteração significativa face a variações na concentração de oxigénio dissolvido, mas mostrou-se suscetível a variações de pH e temperatura.

Finalmente, foi adotada uma estratégia integrada de tratamento de lixiviados, envolvendo (i) uma OBLA, em regime aeróbio, para remover a alcalinidade do lixiviado e a fração de carbono orgânico biodegradável (ii) uma etapa de coagulação/sedimentação (240 mg Fe³⁺/L, pH 4,2, 14 horas de decantação), para promover a precipitação dos ácidos húmicos e reduzir a quantidade de SST, e (iii) uma foto-oxidação por meio da reação de FF (60 mg de Fe²⁺, pH 2,8), combinando radiação solar e artificial (dado a energia solar reduzida no inverno), para promover a degradação de moléculas recalcitrantes e consequente aumento da biodegradabilidade, até ao ponto (COD ≈ 250 mg/L), em que um tratamento biológico a jusante permitiria atingir o limite de descarga em corpos de água (CQO < 150 mg de O₂/L).

Os resultados demonstraram que a OBLA aplicada a um lixiviado após lagunagem aeróbica, com elevado teor orgânico e de azoto e baixa biodegradabilidade, foi capaz de oxidar entre 62 e 99% do azoto amoniacal, consumindo somente a sua alcalinidade, verificando-se reduções de alcalinidade entre 70 e 100%. A fase de coagulação/sedimentação levou à precipitação ácidos húmicos, promovendo uma mudança acentuada na cor do lixiviado, de negro/acastanhado para amarelo/acastanhado (característica dos ácidos fúlvicos), acompanhada de reduções até 66% do COD e 92% do SST, obtendo uma quantidade de lamas ácidas de cerca de 300 mL/L. A realização destes pré-tratamentos conduziu a um efluente de acordo com o limite de descarga para o sulfato (2 g/L) em meio hídrico.

A partir dos ensaios de FF concluiu-se que a melhor opção seria combinar luz solar natural com radiação artificial (~ 1,3 kW/m³), otimizando os custos indiretos. De acordo com o teste de Zahn-Wellens, um lixiviado após coagulação (419 mg de COD/L) teria de ser foto-oxidado até apresentar um COD menor que 300 mg/L, consumindo cerca de 100 mM de H₂O₂ e 7,4 kJ/L de energia UV acumulada, de modo a se obter um efluente que pode ser biologicamente tratada de acordo com o limite de descarga do CQO em corpos de água. O processo biológico subsequente ao sistema fotocatalítico iria promover uma mineralização de 59%, sendo o CQO final de aproximadamente 115 mg O₂/L.

O *scale-up* de uma instalação de FF, com uma capacidade para tratar 100 m³ de lixiviado por dia mostrou a necessidade de implementar 1500 m² de CPCs ou 38 lâmpadas UV-Vis (4 kW, 20.000 h de vida, 6 horas diárias de trabalho), visando uma CQO < 150 mg de O₂/L. Combinando radiação solar e artificial, seriam necessários 957 m² de CPCs e 30 lâmpadas (considerando-se o mês de menor e maior irradiância, respetivamente). O custo da etapa de FF diminuiu cerca de 50% comparativamente à abordagem inicial: 5,7 €/m³, recorrendo apenas a CPCs; 5,8 €/m³, usando apenas lâmpadas UV-Vis; e 5,7 €/m³, combinando CPCs e lâmpadas. O custo com H₂O₂ corresponde a cerca de 44% do custo total anual.

Table of Contents

Page

1 Introduction	1
1.1 Production and disposal of solid waste	3
1.2 Production, composition and characterization of landfill leachates	8
1.3 Leachate treatment systems	14
1.3.1 Leachate channelling	19
1.3.2 Biological degradation	19
1.3.3 Physical and chemical processes	21
1.3.4 Membrane filtration	24
1.3.5 Leachate treatment systems in Portugal	26
1.4 Advanced oxidation processes	28
1.5 Aim of the work and thesis outline	36
1.6 References	40
2 Materials and methods	49
2.1 Chemicals	51
2.2 Experimental setups	54
2.2.1 Solar pre-industrial scale plant	54
2.2.2 Lab-scale photoreactor	59
2.2.3 Lab-scale biological reactor	61
2.2.4 Solar/UV pre-industrial scale plant	63
2.3 Experimental procedure	69
2.3.1 Solar pre-industrial scale experiments	69
2.3.2 Lab-scale photo-Fenton experiments	72
2.3.3 Lab-scale biological experiments	73
2.3.4 Solar/UV pre-industrial scale experiments	74
2.4 Analytical methods	76
2.5 Biodegradability assays	79
2.6 Target and non-target screening of persistent organic micropollutants	80
2.7 16S rRNA gene barcode 454-pyrosequencing	81
2.7.1 DNA extraction and 454-pyrosequencing analysis	81
2.7.2 Post run analysis	81
2.8 References	83
3 Integration of solar photo-Fenton and biological oxidation processes for leachate treatment at pre-industrial scale	85
3.1 Introduction	87
3.2 Experimental methodology	90
3.3 Results and discussion	91
3.3.1 Leachate characterization	91
3.3.2 Solar photo-Fenton process	94

3.3.3	Evaluation of combined photo-Fenton and biological treatment	105
3.4	Conclusions	111
3.5	References	112
4	Integration of solar photo-Fenton and biological oxidation processes for leachate treatment at pre-industrial scale - Biodegradability enhancement assessment	117
4.1	Introduction	119
4.2	Experimental methodology.....	120
4.3	Results and discussion.....	121
4.3.1	Leachate characterization.....	121
4.3.2	Biodegradability enhancement during solar photo-Fenton reaction	123
4.3.3	Integrated systems: solar photo-Fenton pre-oxidation/biological nitrification and denitrification	131
4.4	Conclusions	135
4.5	References	136
5	Integration of biological nitrification-denitrification, solar photo-Fenton and biological oxidation processes for raw leachate treatment, at pre-industrial scale.....	139
5.1	Introduction	141
5.2	Experimental methodology.....	142
5.3	Results and discussion.....	143
5.3.1	Leachate characterization.....	143
5.3.2	1 st Biological oxidation	143
5.3.3	Solar photo-Fenton Oxidation.....	149
5.3.4	2 nd Biological oxidation	154
5.3.5	Organic trace contaminants identification and evolution profile	155
5.4	Conclusions	164
5.5	References	165
6	Scale-up and economic analysis of the photo-Fenton system for landfill leachate treatment.....	169
6.1	Introduction	171
6.2	Experimental methodology.....	175
6.3	Results and discussion.....	176
6.3.1	Bio-treated leachate characterization	176
6.3.2	Performance of the biological and photo-Fenton oxidation processes.....	176
6.3.3	Evaluation of the yearly solar irradiation and CPCs area requirements.....	177
6.3.4	Solar UV photons versus electric UV photons.....	181
6.3.5	Assessment of CPCs area and UV lamps requirements according to monthly variations of solar radiation.....	186
6.3.6	Reagents costs	187
6.3.7	Total cost: comparison of the leachate phototreatment using CPCs and/or UV lamps.....	190
6.4	Conclusions	198
6.5	References	199

7 Evaluation of solar photo-Fenton reaction parameters on the treatment of landfill leachate after biological and physico-chemical oxidation, at lab-scale	203
7.1 Introduction	205
7.2 Experimental methodology	206
7.3 Results and discussion.....	207
7.3.1 Leachate characterization.....	207
7.3.2 Solar photo-Fenton reaction: Influence of iron concentration	208
7.3.3 Solar photo-Fenton reaction: Influence of solution pH.....	209
7.3.4 Solar photo-Fenton reaction: Influence of temperature	216
7.3.5 Solar photo-Fenton reaction: Influence of acid type.....	220
7.3.6 Solar photo-Fenton reaction: Influence of irradiance	224
7.4 Conclusions	227
7.5 References	228
8 Nitrification and denitrification kinetic parameters of a mature sanitary landfill leachate	231
8.1 Introduction	233
8.2 Experimental methodology	235
8.3 Results and discussion.....	237
8.3.1 Nitrification.....	237
8.3.2 Denitrification.....	243
8.3.3 Characterization of the bacterial communities.....	246
8.4 Conclusions	252
8.5 References	253
9 Depuration of mature sanitary landfill leachate using biological nitrification followed by coagulation and photo-Fenton reaction, combining solar and artificial radiation, at pre-industrial scale	257
9.1 Introduction	259
9.2 Experimental methodology	261
9.3 Results and discussion.....	263
9.3.1 Evaluation of the biological oxidation efficiency	263
9.3.2 Evaluation of the coagulation/sedimentation efficiency	270
9.3.3 Evaluation of the photo-Fenton reaction efficiency	279
9.3.4 Biodegradability assessment	290
9.3.5 Economic analysis	296
9.3.6 European patent and semi-industrial scale plant.....	305
9.4 Conclusions	307
9.5 References	310
10 Final Remarks	313
10.1 Conclusions	315
10.1.1 Integration of solar photo-Fenton reaction with biological oxidation.....	315
10.1.2 Integration of biological oxidation with coagulation and solar/UV photo-Fenton process	318
10.2 Suggestions for future work	322

List of Figures

Page

Figure 1.1. Evolution of the global solid waste production (adapted from Hoornweg et al. [1]).....	3
Figure 1.2. Evolution of the municipal solid waste (MSW) production in the European Union (*- Netherlands, Romania, Belgium, Greece, Portugal, Austria, Hungary, Bulgaria and Sweden; **- Denmark, Czech Republic, Ireland, Finland, Croatia (data from 2004), Slovakia, Lithuania, Slovenia, Latvia, Estonia, Cyprus, Luxemburg and Malta) (source: Eurostat [3]).	4
Figure 1.3. Development of the municipal solid waste (MSW) treatment in the European Union (source: Eurostat [3]).....	5
Figure 1.4. Evolution of the Municipal solid waste (MSW) produced according to type of treatment method in Portugal (source: Eurostat [3]).	6
Figure 1.5. Portuguese systems of urban waste management [9].....	7
Figure 1.6. Water cycle in a sanitary landfill (adapted from Renou et al. [14]).....	9
Figure 1.7. COD balance of the biodegradable organic matter during the anaerobic solid waste degradation (adapted from Renou et al. [14]).	10
Figure 1.8. Average annual values of global radiation (kWh/m ²) [102].	30
Figure 2.1. Solar pre-industrial unit combining photocatalytic and biological oxidation systems.....	54
Figure 2.2. Flow diagram of the solar pre-industrial unit.....	55
Figure 2.3. Lab-scale photoreactor plant (a): solar radiation simulator (b), CPC (c) and flow diagram (d).	59
Figure 2.7. Lab-scale biological reactor and respective schematic representation.....	61
Figure 2.4. Solar/UV pre-industrial unit combining biological and chemical oxidation systems.	63
Figure 2.5. Flow diagram of the solar/UV pre-industrial unit.....	64
Figure 2.6. UV-Vis lamp spectrum.	67
Figure 3.1. Evolution of the leachate's characteristics after lagooning, during 2010-2011, in terms of DOC, COD and BOD ₅ (a) and nitrogen (b).	93
Figure 3.2. Speciation diagram of iron (III) species (80 mg Fe/L) as a function of pH, at 25°C and at an ionic strength of 0.5 M, in the presence of: (a) 2 g/L sulphate and 4 g/L chloride (b) 12 g/L sulphate and 3 g/L chloride; (c) 12 g/L sulphate, 3 g/L chloride and 50 mg/L oxalic acid and (d) 12 g/L sulphate, 3 g/L chloride and 200 mg/L oxalic acid (all the equilibrium constants [41-45] were corrected for an ionic strength of 0.5 M with Davies and Debye-Hückel equations).....	98
Figure 3.3. DOC (□,■), H ₂ O ₂ consumption (○,●) and TDI concentration (△,▲) evolution as a function of the accumulated UV energy per liter of leachate during the photo-Fenton process (pH = 2.8; [Fe ²⁺] = 80 mg/L). Solid symbols: Experiment 5; Open symbols: Experiment 6.	99

- Figure 3.4.** Effect of the suspended solids recirculation on the photo-Fenton reaction. (□,■) - DOC, (○,●) - H₂O₂ consumed; (△,▲) - TDI; (◁,◄) – temperature. Solid symbols: Experiment 22 (without stirring); Open symbols: Experiment 23 (with stirring). 100
- Figure 3.5.** Effect of leachate temperature on the photo-Fenton reaction. (□,■) - DOC, (○,●) - H₂O₂ consumed; (△,▲) - TDI; (◇,◆) – temperature. Solid symbols: Experiment 5 (T_m = 37°C); Open symbols: Experiment 21 (T_m = 21°C). 103
- Figure 3.6.** Evaluation of the possible iron sludge recycling in the photo-Fenton process. 104
- Figure 3.7.** Biodegradability of photo-treated leachate: (a) DOC and COD; (b) nitrogen. 106
- Figure 3.8.** Leachate mineralization by the combined system: photo-Fenton (DOC, H₂O₂ consumed and Q_{UV} in function of the illumination time); biological nitrification/denitrification (DOC and nitrogen species as function of time). (a) Experiment 20; (b) Experiment 21. ■ - DOC; △ - H₂O₂ consumed; ★ - Q_{UV}; ● - Total Nitrogen; ○ - Ammonium (NH₄⁺-N); ◇ - Nitrate (NO₃⁻-N); ▽ - Nitrite (NO₂⁻-N); ▣ - Dissolved Oxygen. ... 109
- Figure 3.9.** DOC concentration and DOC removal percentage obtained for the photo-Fenton and biological processes, experiments 18 to 25. △ - Initial DOC (leachate after lagooning); □ - DOC after the Photo-Fenton reaction; ◇ - DOC after the biological oxidation process. 110
- Figure 4.1.** DOC (■), COD (□), AOS (▲), and COS (△) evolution as a function of the hydrogen peroxide consumption during the photo-Fenton process: (a) with (Exp. A) and (b) without (Exp. B) sludge removal... 123
- Figure 4.2.** Zahn-Wellens test for samples taken during the photo-Fenton process, (a) with (Exp. A) and (b) without (Exp. B) sludge removal: reference (■); initial (◄); after acidification and iron sulphate addition (◁); 50 (☆), 100 (★), 150 (○), 200 (●,●), 250 (△,△), 300 (▲) and 350 (□) mM of H₂O₂ consumed. 124
- Figure 4.3.** Evaluation of DOC and COD during the Zahn-Wellens test at day 0 and day 28: (a) with (Exp. A) (b) and without (Exp. B) sludge removal after acidification. 125
- Figure 4.4.** Evaluation of DOC at acidic (▨) or neutralized (▩) conditions and low-molecular-weight carboxylate anions (LMCA)/DOC ratio (●) as a function of hydrogen peroxide consumption during photo-Fenton process: (a) with (Exp. A) and (b) without (Exp. B) sludge removal after acidification. 126
- Figure 4.5.** DOC (■), absorbance at 254 nm (▲), polyphenols (△) and dissolved iron concentration (□) evolution as a function of hydrogen peroxide consumption during the photo-Fenton process (pH = 2.8; [Fe²⁺] = 80 mg/L): with (Exp. A) (a) and without (Exp. B) (b) sludge removal after acidification. 130
- Figure 4.6.** Evaluation of the photo-Fenton reaction. (■,□) - DOC; (●,○) - H₂O₂ consumed; (▲,△) Dissolved Iron; (★,☆) – Temperature; (◆,◇) – Average irradiation. Solid symbols: Exp. C (without sludge removal); Open symbols: Exp. D (without sludge removal). 132
- Figure 4.7.** Leachate mineralization by the combined system: photo-Fenton (DOC and H₂O₂ consumed in function of the illumination time); biological nitrification/denitrification (DOC and nitrogen species as function of time). (a) Exp. B (without sludge removal); (b) Exp. C (without sludge removal). ■ - DOC; △ - H₂O₂ consumption; ● - Total Nitrogen; ○ - Ammonium (NH₄⁺-N); ◇ - Nitrate (NO₃⁻-N); ▽ - Nitrite (NO₂⁻-N). 134
- Figure 5.1.** Biological nitrification/denitrification of the raw leachate. ■ - DOC; ● - Total Dissolved Nitrogen; ○ - Ammonium (NH₄⁺-N); ◇ - Nitrate (NO₃⁻-N); △ - Nitrite (NO₂⁻-N); ★ - Temperature (T); ☆ - pH; ◁ - Dissolved Oxygen (DO). 145

- Figure 5.2.** DOC (□,■), H₂O₂ consumption (○,●), total dissolved iron (TDI) concentration (△,▲), temperature (T - ☆,★) and average radiation intensity (I - ◆,◇) evolution as a function of the accumulated UV energy per liter of leachate during the photo-Fenton process (pH = 2.8; [Fe²⁺] = 80 mg/L), with (open symbols) and without (solid symbols) sludge removal. 150
- Figure 5.3.** Biological/photo-Fenton/Biological treatment sequence of the raw leachate. ■ - DOC; ● - Total Dissolved Nitrogen; ○ - Ammonium (NH₄⁺-N); ◇ - Nitrate (NO₃⁻-N); △ - Nitrite (NO₂⁻-N)..... 151
- Figure 5.4.** Zahn-Wellens test for samples collected before and after the 1st biological treatment and after acidification (cross symbols), and for some samples taken during the photo-Fenton process without (solid symbols) and with (open symbols) sludge removal after acidification: ▲ - Raw Leachate; ▣ - LBT1; ◆ - LAA; ● - S₁; ▲ - S₂; ■ - S₃; ○ - S₁' ; △ - S₂' ; ◇ - S₃' ; □ - S₄' ; ● - Reference..... 152
- Figure 5.5.** Evaluation of DOC and COD during the Zahn-Wellens test at day 0 and day 28; percentage of biodegradation (*D_t*) during Zahn-Wellens test at day 8 and day 28; low-molecular-weight carboxylate anions (LMCA) and LMCA/DOC ratio, during combined system 1st biological treatment (BT1)/photo-Fenton reaction (PFR), without (a) and with (b) sludge removal after acidification (Acid.). 153
- Figure 5.6.** Non-target screening analysis of leachate samples, collected at different treatment points, by the four methods described in Chapter 2 (section 2.6): (a) VOCs; (b) PAHs, PCBs and phthalates; (c) pesticides; (d) phenols. Identification of contaminants removed and formed during different treatment stages (correspondence between the compound and the respective peak number is displayed in the Table 5.4) (RL – Raw Leachate; LBT1 – Leachate after 1st biological treatment; LPFN - Leachate after Photo-Fenton reaction and neutralization; LBT2 – Leachate after 2nd biological treatment (final effluent)). 158
- Figure 6.1.** Average global UV irradiance (◇ - *I_m*), insolation (■ - *t_m*) and ‘cloud factor’ (◆ - *f_c*) for global UV irradiance during the years 2010 and 2011 nearby Porto, Portugal..... 179
- Figure 6.2.** Illustrative scheme of the CPCs’ configuration to a local with 41° of latitude. 180
- Figure 6.3.** Costs of UV photons collected using CPCs and UV photons generated with electric lamps (electricity costs of (a) 0.15 €/kWh and (b) 0.10 €/kWh) (Based on Gálvez and Rodríguez [18] and information obtained in a market study)..... 185
- Figure 6.4.** Assessment of CPCs area (bars) and number of lamps (lines) required for each month of the year, considering different operating conditions. 187
- Figure 6.5.** Yearly total cost of reagents for the optimal conditions, with and without methanol contribution, considering target COD values of 150 and 1000 mg O₂/L..... 189
- Figure 6.6.** Total cost for the sanitary landfill leachate’s treatment using different set-ups..... 196
- Figure 7.1.** Evaluation of the DOC (closed symbols), H₂O₂ consumed (crossed symbols) and TDI concentration (open symbols) during the photo-Fenton reaction for different iron concentrations. Operational conditions: pH = 2.8 (H₂SO₄), T = 20°C, I = 40 W_{UV}/m²; (■, □, ▣) – [Fe] = 20 mg/L; (▲, △, ▴) – [Fe] = 40 mg/L; (●, ○, ⊕) – [Fe] = 60 mg/L; (◆, ◇, ⊕) – [Fe] = 80 mg/L; (★, ☆, ✨) – [Fe] = 100 mg/L. 208
- Figure 7.2.** Evaluation of the DOC (closed symbols), H₂O₂ consumed (open symbols), pH (H₂SO₄) (semi-filled symbols) and TDI concentration (crossed symbols) during photo-Fenton reaction for different pH values. Operational conditions: [Fe] = 60 mg/L, T = 20°C, I = 40 W_{UV}/m²; (■, □, ▣, ⊕) – pH = 2.0; (●, ○, ⊕) – pH = 2.4; (▲, △, ▴, ⊕) – pH = 2.8; (★, ☆, ✨, ⊕) – pH = 3.2; (◆, ◇, ⊕, ⊕) – pH = 3.6. 211

- Figure 7.3.** Theoretical Fe^{3+} speciation diagrams as a function of solution pH in the conditions of the experiments performed at different pH values: (a) 2.0; (b) 2.4; (c) 2.8; (d) 3.2; and (e) 3.6. Comparison of the theoretical molar fraction of FeOH^{2+} as a function of pH in the conditions of the experiments performed at different pH values (f): 2.0 (■); 2.4 (●); 2.8 (▲); 3.2 (★); and 3.6 (◆).213
- Figure 7.4.** Representation of the pseudo-first-order kinetic constant for DOC degradation as a function of the theoretical FeOH^{2+} concentration, for the tests performed at different values of pH (a) and temperature (b).216
- Figure 7.5.** Evaluation of the DOC (closed symbols), H_2O_2 consumed (open symbols), temperature (semi-filled symbols) and TDI concentration (crossed symbols) during the photo-Fenton reaction for different temperature values. Operational conditions: pH = 2.8 (H_2SO_4); $[\text{Fe}] = 60 \text{ mg/L}$, $I = 40 \text{ W}_{\text{UV}}/\text{m}^2$; (■, □, ▣, ⊞) – T = 10°C; (●, ○, ⊙, ⊕) – T = 20°C; (▲, △, ⊲, ⊳) – T = 30°C; (★, ☆, ☆, ☆) – T = 40°C; (◆, ◇, ◆, ⊕) – T = 50°C.217
- Figure 7.6.** Theoretical Fe^{3+} speciation diagrams as a function of solution pH in the conditions of the experiments performed at different temperature values: (a) 10°C; (b) 20°C; (c) 30°C; (d) 40°C; and (e) 50°C. Comparison of the theoretical molar fraction of FeOH^{2+} as a function of pH in the conditions of the experiments performed at different temperature values (f): 10°C (■); 20°C (●); 30°C (▲); 40°C (★); and 50°C (◆).219
- Figure 7.7.** Evaluation of the DOC (closed symbols), H_2O_2 consumed (open symbols) and TDI concentration (crossed symbols) during the photo-Fenton reaction for different acid types. Operational conditions: pH = 2.8; T = 30°C; $[\text{Fe}] = 60 \text{ mg/L}$, $I = 40 \text{ W}_{\text{UV}}/\text{m}^2$; (■, □, ⊞) – H_2SO_4 ; (●, ○, ⊕) – HCl; (◆, ◇, ⊕) – $\text{H}_2\text{SO}_4 + \text{HCl}$222
- Figure 7.8.** Theoretical Fe^{3+} speciation diagrams as a function of solution pH in the conditions of the experiments performed with different acid types: (a) H_2SO_4 ; (b) HCl; (c) $\text{H}_2\text{SO}_4 + \text{HCl}$. Comparison of the theoretical molar fraction of FeOH^{2+} as a function of pH in the conditions of the experiments performed with different acid types (d): H_2SO_4 (■); HCl (●) and $\text{H}_2\text{SO}_4 + \text{HCl}$ (◆).223
- Figure 7.9.** Evaluation of the DOC (closed symbols), H_2O_2 consumed (open symbols) and TDI concentration (crossed symbols) during the photo-Fenton reaction for different values of solar irradiance. Operational conditions: pH = 2.8 (H_2SO_4); T = 30°C; $[\text{Fe}] = 60 \text{ mg/L}$; (■, □, ⊞) – I = 22 $\text{W}_{\text{UV}}/\text{m}^2$; (●, ○, ⊕) – I = 44 $\text{W}_{\text{UV}}/\text{m}^2$; (◆, ◇, ⊕) – I = 68 $\text{W}_{\text{UV}}/\text{m}^2$225
- Figure 8.1.** Evolution of total dissolved nitrogen (■), total ammonia nitrogen (■ - $\text{NH}_4^+\text{-N} + \text{NH}_3\text{-N}$), free ammonia (□ - $\text{NH}_3\text{-N}$), total nitrite-nitrogen (▲ - $\text{NO}_2^-\text{-N}$), alkalinity (○), pH (---) and dissolved oxygen (—) during a nitrification test (pH not controlled, OD = 0.5-1.0, T = 25 °C, VSS = 2.76 g/L).239
- Figure 8.2.** Representation of the (.1) TAN removed/VSS ratio, and the (.2) $\text{NO}_2^-\text{-N}$ produced/VSS ratio, as a function of time, and the (.3) alkalinity removed, as a function of TNN removed, along all nitrification tests, for different (a) temperature values (15 °C, ■; 20 °C, ▲; 25 °C, ● and 30 °C, ◆), (b) DO intervals (0.5-1.0 mg/L, □; 1.0-2.0 mg/L, △ and 2.0-4.0 mg/L, ○) and (c) pH intervals (6.5-7.5, ⊕; 7.5-8.5, ▲ and not controlled, ⊞).241
- Figure 8.3.** Evolution of the pH profile along the test carried out in the pH interval of 6.5-7.5, between the 8 and 12 hours.242
- Figure 8.4.** Representation of the (.1) $\text{NO}_2^-\text{-N}$ reduced/VSS ratio, as a function of time, and the (.2) methanol consumed and (.3) alkalinity removed, as a function of $\text{NO}_2^-\text{-N}$ reduced, along all denitrification tests,

- regarding (a) different pH intervals (6.5-7.0, □; 7.0-7.5, ○; 7.5-8.0, △; 8.0-8.5, ◇ and 8.5-9.5, ☆), (b) different temperatures (20 °C, ▣; 25 °C, ⊕ and 30 °C, ▲) and (c) the addition (■) or not (●) of phosphate ions..... 245
- Figure 8.5.** PCoA biplot depicting the dissimilarities between the bacterial communities from each biological sludge sample, based on the unweighted UniFrac distances. 247
- Figure 8.6.** Relative abundance of the members affiliated to the different phyla present in each biological sludge sample. Phyla with abundance ranging from 0.1-1% include *Acidobacteria*, *Chloroflexi*, *Gemmatimonadetes*, GNO2, SAR406, *Spirochaetes*, *Synergistetes*, *Thermotogae*, TM7, *Verrucomicrobia* and WPS-2. Phyla with abundance < 0.1% include OD1, OP9, OP11, SR1, WS6, WYO..... 248
- Figure 9.1.** Variation of the alkalinity (▣) and ammonium nitrogen content (■) at the end of the biological treatment..... 266
- Figure 9.2.** Amount of ammonium nitrogen eliminated (▣), time required for the nitrification reaction (■), maximum contents of free ammonia (—) and free nitrous acid (***), and average values of temperature (□), dissolved oxygen (△) and pH (◇), for each biological test..... 267
- Figure 9.3.** Evolution of total suspended solids (TSS), volatile suspended solids (VSS), 30-min settled sludge volume (SSV_{30-min}) and sludge volumetric index (SVI), in the biological reactor, along the experimental period..... 268
- Figure 9.4.** Evolution of the supernatant colour for coagulant doses from 0 to 600 mg Fe³⁺/L. 272
- Figure 9.5.** Dissolved organic carbon (DOC), 30-min settled sludge volume (SS) and total suspended solids (TSS) in the supernatant, as a function of coagulant concentration (pH 4.2)..... 272
- Figure 9.6.** Extraction of humic substances from landfill leachate. (a) XAD-8 resin column after passing the leachate previously nitrified and acidified. (b) Eluate samples collected at different times. 273
- Figure 9.7.** Comparison between the test performed in the pre-industrial scale plant using 240 mg Fe³⁺/L (b), with the tests performed in the jar-test using 240 (a) and 360 (c) mg Fe³⁺/L. 273
- Figure 9.8.** Variation of the initial values of alkalinity (▣) and NH₄⁺-N (▣), final pH (▣) and sulphate increment (▣), during the coagulation step..... 277
- Figure 9.9.** Evolution of DOC (▣) and COD (▣) removal along the experimental period, and values of DOC (—) and COD (—) at the end of the coagulation step..... 277
- Figure 9.10.** Evaluation of DOC (closed symbols), H₂O₂ consumed (open symbols) and TDI concentration (cross symbols), during photo-Fenton reaction (pH = 2.8, [Fe] = 60 mg/L), for the experiments performed with solar radiation, with (1 - ■, □, ▣; 2 - ●, ○, ⊕) and without (5' - ▲, △, ▴) pre-treatment (aerobic biological oxidation and coagulation). 281
- Figure 9.11.** Progression of H₂O₂ (▣) and NaOH (—) consumption, and initial values of NO₂⁻-N (▣) and pH (—), at the beginning of photo-Fenton reactions, using solar (S) and/or artificial (A) radiation (R), along the experiments. 282
- Figure 9.12.** Distribution diagram of the molar fractions of nitrous acid (—) and nitrite ion (—), as a function of pH (T = 25 °C). 283
- Figure 9.13.** Evaluation of DOC (closed symbols), H₂O₂ consumed (open symbols) and TDI concentration (cross symbols), during the photo-Fenton treatment (pH = 2.8, [Fe] = 60 mg/L) of the bio-coagulated treated leachate using solar radiation, 4 UV-Vis lamps and 4 UV-Vis lamps (without coagulation; pH = 3.0)..... 284

Figure 9.14. Evaluation of DOC (closed symbols), H ₂ O ₂ consumed (open symbols), TDI concentration (cross symbols) and pH (semi-filled symbols) during the photo-Fenton treatment (pH = 2.8, [Fe] = 60 mg/L) of the bio-coagulated treated leachate using 4 UV-Vis lamps and combining solar radiation with 4 UV-Vis lamps after coagulation with 240 mg Fe ³⁺ /L and 120 mg Fe ³⁺ /L.	286
Figure 9.15. Evaluation of DOC (closed symbols), H ₂ O ₂ consumed (open symbols) and TDI concentration (cross symbols), during the photo-Fenton treatment (pH = 2.8, [Fe] = 60 mg/L) of the bio-coagulated treated leachate, using 4 lamps of 1000 W (9 – ▲, △, ▴), 2 lamps of 1200 W (12 – ■, □, ⊞) and 2 lamps of 850 W (13 – ●, ○, ⊕).....	288
Figure 9.16. Evolution of DOC removal in the biological, coagulation/sedimentation and photo-oxidation processes, as well as the initial and final DOC of each stage.	289
Figure 9.17. Evolution of DOC and nitrogen content (NH ₄ ⁺ -N - ■, NO ₂ ⁻ -N - ■ and NO ₃ ⁻ -N - ■) along all stages of the multi-treatment process, as a function of time, for the experiment in the best conditions.	290
Figure 9.18. Evaluation of DOC (■), H ₂ O ₂ consumed (●), TDI concentration (◆), TSS content (▲), Q _{UV} (★), pH (⊞) and temperature (⊕), as a function of accumulated UV energy and H ₂ O ₂ consumed during the photo-oxidation of the bio-coag-treated leachate.	291
Figure 9.19. Progress of the DOC (●), COD (○), AOS (■), COS (□) and Abs254 (▲), as a function of the H ₂ O ₂ consumed, along experiment 15.	293
Figure 9.20. Evolution of low-molecular-weight carboxylate anions (LMCA) concentration and LMCA/DOC ratio, along experiment 15.	293
Figure 9.21. Zahn-Wellens test results for samples collected along experiment 15: Reference (■); BR15.0 (⊕); CT15F (⊕); 29 (▲), 59 (⊞), 76 (◀), 83 (▶), 106 (●) and 127 (◉) mM of H ₂ O ₂ consumed.	294
Figure 9.22. Evaluation of DOC and COD at day 0 and 28 of the Zahn-Wellens test and percentage of biodegradability at day 28.	295
Figure 9.23. Annual cost of the reagents employed in each treatment step.	298
Figure 9.24. Estimative of the CPCs unitary cost as a function of their area, through a power regression used for the calculation of the total expense with CPCs, targeting a COD of 1000 (a) and 150 (b) mg O ₂ /L.	301
Figure 9.25. Representation of the total unitary cost of the treatment using artificial light, as a function of the lamps operating time in order to obtain a COD lesser than 150 and 1000 mg O ₂ /L.	302
Figure 9.26. Comparison between the total cost of the leachate phototreatment obtained in this chapter and in Chapter 6 (*), considering different process setups, aiming a COD of 150 and 1000 mg O ₂ /L.	305
Figure 9.27. Semi-industrial plant for the treatment of 20 m ³ /day of leachate, developed under the project Advanced LFT.	306

List of Tables

Page

Table 1.1. Leachate classification according to the landfill age (adapted from: Renou et al. [14], Foo and Hameed [22] and Li et al. [23]).	12
Table 1.2. Emission limit values (ELV) for the discharge of wastewaters (Decree-Law no. 236/98).	13
Table 1.3. Overview of the main leachate treatment processes (adapted from Abbas et al. [25], O’Leary and Tchobanoglous [19] and Renou et al. [14]).	15
Table 1.4. Performance of different biological processes on the landfill leachate treatment.	20
Table 1.5. Performance of different physical and chemical processes on landfill leachate treatment.	22
Table 1.6. Performance of the different membrane filtration processes on the landfill leachate treatment.	25
Table 1.7. Leachate treatment plants (LTP) installed at the Portuguese sanitary landfills and final destination of the treated leachate [63].	27
Table 1.8. Oxidation potential of different species.	29
Table 1.9. Typical AOPs [14, 26].	29
Table 1.10. Performance of the different AOPs on the landfill leachate treatment.	31
Table 1.11. Main photo-Fenton reaction parameters and their respective effect (updated from Pereira [119]).	34
Table 2.1. Chemicals description.	51
Table 2.2. Description of the solar pre-industrial unit constituents.	56
Table 2.3. Description of solar/UV pre-industrial unit constituents.	65
Table 2.4. Physico-chemical parameters and their analytical methods	76
Table 3.1. Characterization of the sanitary landfill leachate after aerobic lagooning throughout 1-year.	92
Table 3.2. Characterization of the landfill leachate before photo-Fenton process.	95
Table 3.3. Characterization of the landfill leachate before photo-Fenton process.	96
Table 3.4. Characteristics of the photo-treated leachate after neutralization.	105
Table 3.5. Characteristics of the photo-bio-treated leachate.	107
Table 3.6. Operating conditions in the biological reactor.	108
Table 4.1. Characterization of the sanitary landfill leachate after aerobic lagooning throughout 1-year.	122
Table 4.2. Process variables as performance indicators.	128
Table 5.1. Physico-chemical characterization of the landfill leachate at different treatment phases.	144

Table 5.2. Process variables as performance indicators.....	147
Table 5.3. Contaminants' concentrations ($\mu\text{g/L}$) along the leachate treatment process.....	156
Table 5.4. Contaminants identified in the different leachate samples collected along the treatment process, after target and non-screening analyses by the four methods described in Chapter 2 (section 2.6): structural characterization, fitting probability and removal efficiency during the different treatment stages (RL-Raw Leachate; LBT1-Leachate after 1 st biological treatment; LPFN-Leachate after Photo-Fenton reaction and neutralization; LBT2-Leachate after 2 nd biological treatment (final effluent)).	159
Table 6.1. Total expenditure with different treatment strategies using AOPs.	172
Table 6.2. Characteristics of the bio-treated leachate used in the photo-Fenton reactions.	175
Table 6.3. Operation data for the treatment of $100 \text{ m}^3/\text{day}$ of sanitary landfill leachate.	178
Table 6.4. Estimative of the unitary cost of the CPCs according to their area.	181
Table 6.5. Estimative of costs to capture of 1.1×10^{30} , 1.8×10^{30} , 2.4×10^{30} and 3.9×10^{30} solar UV photons at different conditions of solar irradiation (FCR = 12%, 20 years).	182
Table 6.6. Estimative of costs associated to the generation of electric UV photons (lamps with 4 kW, 20,000 hours of total operation and 8760 hours of yearly operation (t_{LO})), comparing electricity cost of 0.10 and 0.15 €/kWh (FCR=12%, 20 years).	183
Table 6.7. Cost associated to reagents consumption, considering different operability conditions.....	188
Table 6.8. Yearly cost associated to sanitary landfill leachate treatment using CPC technology considering different operating conditions.	191
Table 6.9. Yearly cost associated to sanitary landfill leachate treatment with resource to UV lamps (4 kW, 20000 hours of total operation and 8760 hours of yearly operation) considering different operating conditions.....	192
Table 6.10. Yearly cost associated to sanitary landfill leachate treatment combining CPCs technology with UV lamps (4 kW, 20,000 hours of total operation and 8,760 hours of yearly operation) considering different operating conditions.	193
Table 7.1. Characterization of sanitary landfill leachate samples, at the outlet of the LTP (after coagulation/flocculation), used for the experiments with sulphuric and hydrochloric acids.....	206
Table 7.2. Operational conditions used in the photo-Fenton experiments.....	207
Table 7.3. Variables and kinetic parameters of the photo-Fenton process for all experiments.	210
Table 7.4. Concentration of iron, chloride and sulphate added in the photo-Fenton reaction, and theoretical molar fraction of Fe^{3+} species, associated to pH value in different experiments.....	214
Table 8.1. Operating conditions adopted in the nitrification and denitrification tests.	236
Table 8.2. Physico-chemical characterization of the leachate used in the nitrification and denitrification tests.	237
Table 8.3. Operating conditions and kinetic parameters of the nitrification process for all experiments.....	238
Table 8.4. Operating conditions and kinetic parameters of the denitrification process for all experiments.	244

Table 8.5. Diversity indices of the bacterial communities of the nitrification (N) and denitrification (D) reactors, at the initial (I), middle (M) and final (F) treatment stages.	247
Table 8.6. Relative abundance (> 1%) of the families belonging to the bacterial phyla with an abundance higher than 1% in nitrification or/and denitrification reactors.	250
Table 9.1. Description of the tests performed.....	262
Table 9.2. Physico-chemical characterization of the landfill leachate before and after biological treatment. .	264
Table 9.3. Physico-chemical characterization of the landfill leachate before and after coagulation/sedimentation process.....	275
Table 9.4. Main characteristics of the leachate after the photo-oxidation process.	280
Table 9.5. Operation data for the treatment of 100 m ³ per day of sanitary landfill leachate.	297
Table 9.6. Cost associated to reagents consumption on each treatment step.	298
Table 9.7. Yearly cost associated to the leachate phototreatment using CPCs technology and/or UV-Vis lamps (4 kW, 20,000 hours of useful lifetime), considering the operability conditions of the test 15, in order to obtain a COD below 150 and 1000 mg O ₂ /L.	300
Table 9.8. CPCs area and number of UV lamps required for all months of the year, targeting a final COD value of 150 or 1000 mg O ₂ /L.	303

Notation

Latin letters

A_{CPC}	Total collectors area needed for the treatment of 100 m ³ of bio-treated leachate per day (m ²)
A_{land}	Land area required for the CPCs implementation (m ²)
A_r	Illuminated collector surface area (m ²)
BOD_5	Biochemical oxygen demand (mg O ₂ /L)
c	speed of light (3.0×10 ⁸ m/s)
C_A	DOC of the sample measured 3-h after starting the Zahn-Wellens test (mg/L)
C_B	DOC of the blank measured at the sampling time t during the Zahn-Wellens test (mg/L)
C_{BA}	DOC of the blank measured 3-h after starting the Zahn-Wellens test (mg/L)
C_L	Cost of 1-lamp (€)
C_{LR}	Annual cost associated to the labor needed to the UV lamp replacement (€)
$C_{LR,IL}$	Costs with the labor to replace 1-lamp (€)
COD	Chemical oxygen demand (mg O ₂ /L)
CPC	Compound parabolic collector
C_R	Annual cost associated to the UV lamp replacement (€)
C_t	DOC of the sample measured at the sampling time t during the Zahn-Wellens test (mg/L)
DIC	Dissolved inorganic carbon (mg/L)
DO	Dissolved Oxygen (mg/L)
DOC	Dissolved organic carbon (mg/L)
DOC_f	Final dissolved organic carbon concentration (mg C/L)
DOC_i	Initial dissolved organic carbon concentration (mg C/L)
D_t	Percentage of biodegradation (%)
E_{CPC}	Energy captured by the CPCs (kJ)
E_L	Lamp electricity consumption (kJ)
E_m	Monthly accumulated UV energy (kJ/m ²)
E_{ph}	Energy of 1-photon (J)
E_y	Yearly accumulated UV energy (kJ/m ²)
FCR	Fixed charge rate (12%, considering 20-year plant depreciation)
Fe_m	Average dissolved iron concentration during photo-Fenton experiment (mg/L)
h	Planck constant (6.63×10 ⁻³⁴ J×s)
HS	Humic substances (mg C _{HS} /L)
I_m	Yearly average global UV radiation power (W/m ²)

I_{UV}	Average UV irradiance power during photo-Fenton experiment (W/m ²)
$LMCA$	Low molecular-weight carboxylate anions (mg/L)
LTC	Lamp total cost (€)
N_D	Total dissolved nitrogen (mg/L)
N_L	Number of UV lamps
N_{ps}	Number of photons emitted up to wavelength of 387 nm per unit of time and potency according to the standard ASTM solar spectrum (5.8×10^{21} photons/W/h)
N_T	Total nitrogen (mg/L)
N_{uv}	Number of photons emitted up to wavelength of 387 nm
OC	Operating cost (€)
ORP	Oxidation-reduction potential (mV)
$PETC$	Principal equipment total cost (€)
pH_m	Average pH value during photo-Fenton experiment
P_L	Lamp power (W)
P_T	Total phosphorus (mg/L)
Q_d	Daily flow (m ³ /day)
Q_{UV}	Accumulated UV energy received on any surface in the same position with regard to the sun (kJ/L)
$Q_{UV,L}$	Accumulated UV energy emitted by the UV-Vis lamps and received by the leachate existing inside the photoreactor (kJ/L)
$Q_{UV,T}$	Total accumulated UV energy ($Q_{UV} + Q_{UV,L}$), when solar and artificial radiation are simultaneously used (kJ/L).
SSV_{30-min}	30-min settled sludge volume (mL/L)
t	Sampling time (h)
T	Temperature (°C)
TCR	Total capital required (€)
TDC	Total direct cost (€)
TDI	Total dissolved iron (mg/L)
T_{fm}	Mass treatment factor (g/h/ m ²)
T_{fv}	Volumetric treatment factor (L/h/ m ²)
t_{ins}	Total yearly hours of insolation (h)
t_{LL}	Lamp life time (h)
t_{LO}	Yearly lamp operation time (h)
T_m	Average temperature during photo-Fenton experiment (°C)
t_n	Time corresponding to n-water sample (s)

TOC	Total organic carbon (mg/L)
t_{PF}	Phototreatment time (h)
TSS	Total suspended solids (mg/L)
TYC	Total yearly cost (€)
UC	Unitary cost (€/m ³)
$\overline{UV}_{G,n}$	Average solar ultraviolet radiation measured during Δt (W/m ²)
V_m	Monthly volume of leachate generated from the sanitary landfill (m ³)
VSS	Volatile suspended solids (mg/L)
V_t	Total reactor volume (L)
V_y	Yearly volume of leachate generated from the sanitary landfill (m ³)
Δm	Amount of organic substances removed during phototreatment (g)
Δt	Time interval between the collection of two samples, during photo-Fenton reaction ($t_n - t_{n-1}$) (s)

Greek letters

η	Lamp efficiency
λ	Wavelength (nm)
ρ	Density (kg/L)
φ	Photonic flux (photons/s)

1 Introduction

This first chapter presents an overview of the problematics associated with the production and remediation of mature leachates from urban sanitary landfills, as well as current and potential decontamination methods. Biological nitrification-denitrification, coagulation and photo-Fenton oxidation processes used for leachate treatment are herein described and complemented with a briefly survey of the current literature. The objectives and the thesis outline are also provided, at the end of the chapter.

1.1 Production and disposal of solid waste

Since that humankind settled in communities, and mostly over the last decades, the increasing production of municipal solid wastes is an unavoidable consequence of the technological and scientific development together with the high consumption standards by society. The waste production has been proportional to urban population growth, cities' development and increasing of the consumption levels. Currently, solid waste management is one of the most important environmental challenges and represents one of the greatest costs to the municipality budgets. At the beginning of twenty century, about 87% of the world's population lived in rural communities, being the urban citizens solely 220 million. They generated about 300 thousand tonnes of solid waste per day, as could be seen in Figure 1.1. At the end of the century, the urban population increased to 2.9 billion (49% of global population), who produced more than 3 million tonnes of rubbish per day. It is expected that by 2025, the amount of generated solid waste will be the double, and by 2100, the waste production will exceed 11 million tonnes per day (considering a global population of 9.5 billion and 80% urbanization). At present, the member countries of the Organisation for Economic Co-operation and Development (OECD) are the main producers of solid waste, with a slight tendency to grow up to 2050 and to decrease after that, achieving 2 million tonnes per day, in 2100. On the other hand, the countries from Sub-Saharan Africa and South Asia show the propensity to continuous increasing of the waste volume until 2100, reaching up to approximately 3.2 and 2 million tonnes per day, respectively [1].

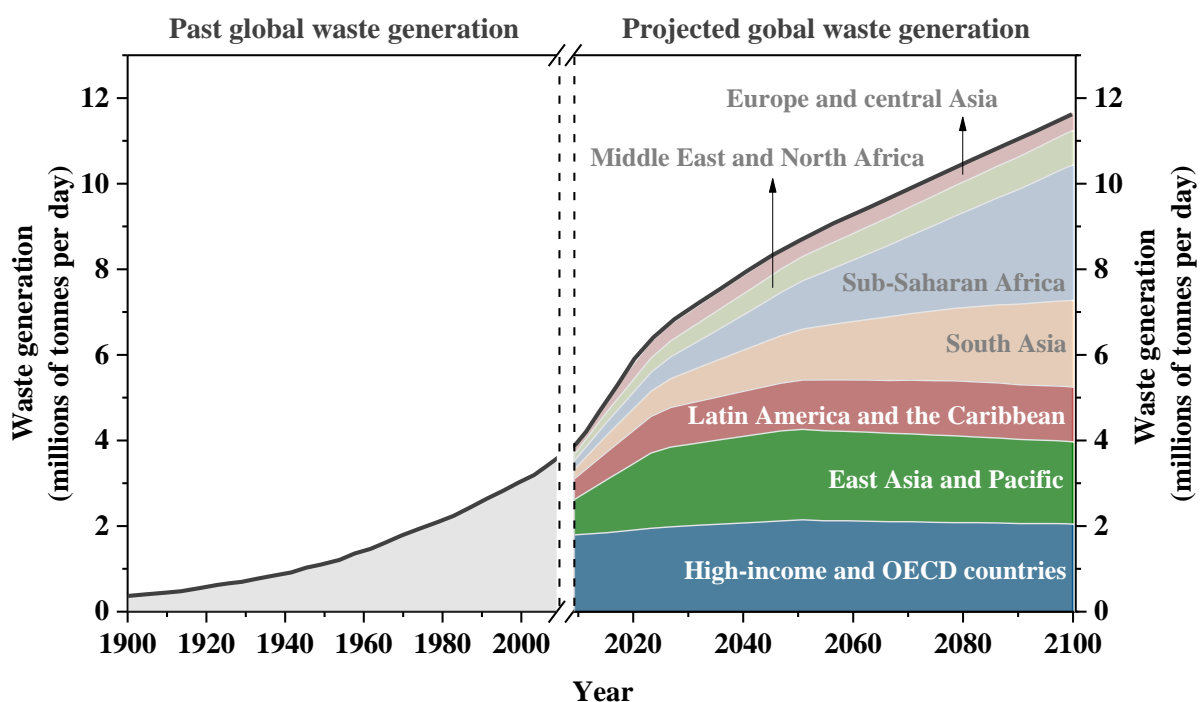


Figure 1.1. Evolution of the global solid waste production (adapted from Hoornweg et al. [1]).

During the past few years, in the European Union (EU), 1.1 thousand million tonnes of solid waste are produced every year [2], from which approximately 250 million tonnes are related to municipal solid wastes (MSW), corresponding to an annual average of 509 kilograms per capita (see Figure 1.2). According to Eurostat data [3], the member countries of EU that generate more MSW per capita and year are Cyprus, Luxembourg, Ireland and Denmark (> 650 kilograms), while Romania, Latvia, Poland, Czech Republic and Slovakia generate less than 350 kilograms. The problematics of waste elimination is international in scope, with many countries suffering from similar problems. For decades, the response of the majority of Governments and waste sector operators passed by burning or burying the waste [4]. Numerous efforts have been developed, at the community level, to apply the waste hierarchy aiming at the waste prevention and management imposed by the Waste Framework Directive 2008/98/EC, of the European Parliament and of the Council [5]. Thus, the EU Member States have been encouraged to, firstly, reduce and reuse the waste, then promote recycling and recovery, under appropriate conditions, and, only as a last resource, to resort to safe enclosure. Despite being the last option in the management hierarchy, a significant amount of municipal waste continues to have as the final destination the landfilling (see Figure 1.3).

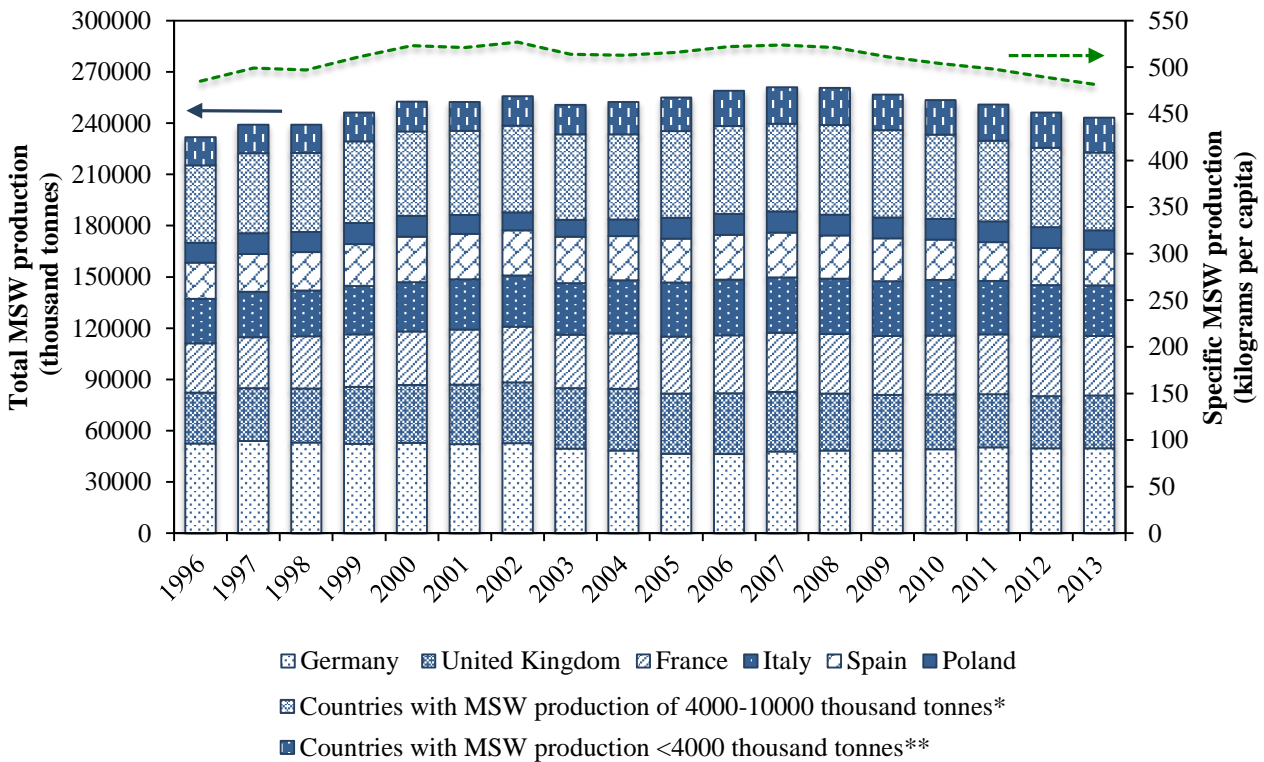


Figure 1.2. Evolution of the municipal solid waste (MSW) production in the European Union (*- Netherlands, Romania, Belgium, Greece, Portugal, Austria, Hungary, Bulgaria and Sweden; **- Denmark, Czech Republic, Ireland, Finland, Croatia (data from 2004), Slovakia, Lithuania, Slovenia, Latvia, Estonia, Cyprus, Luxemburg and Malta) (source: Eurostat [3]).

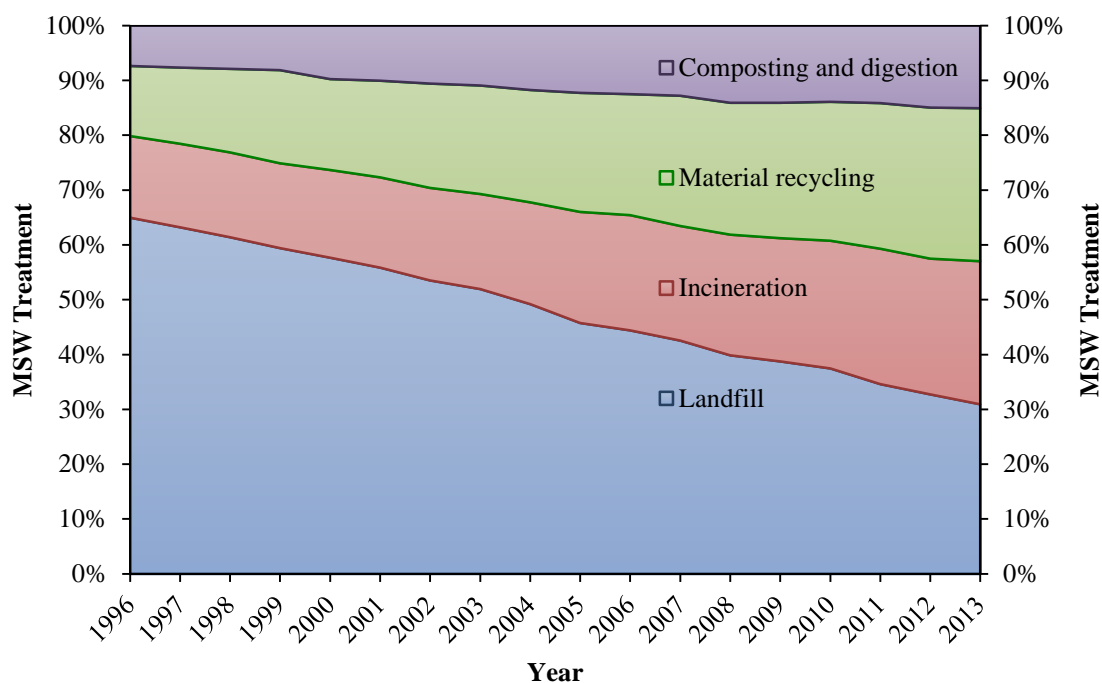


Figure 1.3. Development of the municipal solid waste (MSW) treatment in the European Union (source: Eurostat [3]).

Considering the last 18 years, Portugal achieved its peak of waste production between 2008 and 2010, being generated, on average, 5,475 thousand tonnes of MSW per year, the equivalent to 518 kilograms per habitant (see Figure 1.4). After that, the waste generation profile shows a decreasing tendency, being registered in 2013 a total yearly production of 4598 thousand tonnes of MSW, corresponding to 440 kilograms per capita (~1.2 kilograms per day), which was 8.5% lesser than the value corresponding to all EU member countries (see Figure 1.2). This performance shows that the Portuguese population has been made aware of the problematics associated with the high production of wastes and their disposal.

Until the end of the 90s, the municipal waste management, in Portugal, consisted in the deposition of the waste into open-air dumps (76%) and “controlled” dumps (14%), thus causing the pollution of the air, soil, surface water and groundwater, resulting in risks to the population health [6]. In 1997, the Strategic Plan for Municipal Solid Waste (PERSU, in Portuguese: Plano Estratégico para os Resíduos Sólidos Urbanos) was approved, being reissued later in 1999, which had as main objective to structure the strategies for the municipal waste management regarding the period 1997-2006 [7]. This document was based on strategic principles of the European Union for the sector with the application of a hierarchy of principles by placing firstly prevention, followed by recycling and, as solution of end line, the safe enclosure [8].

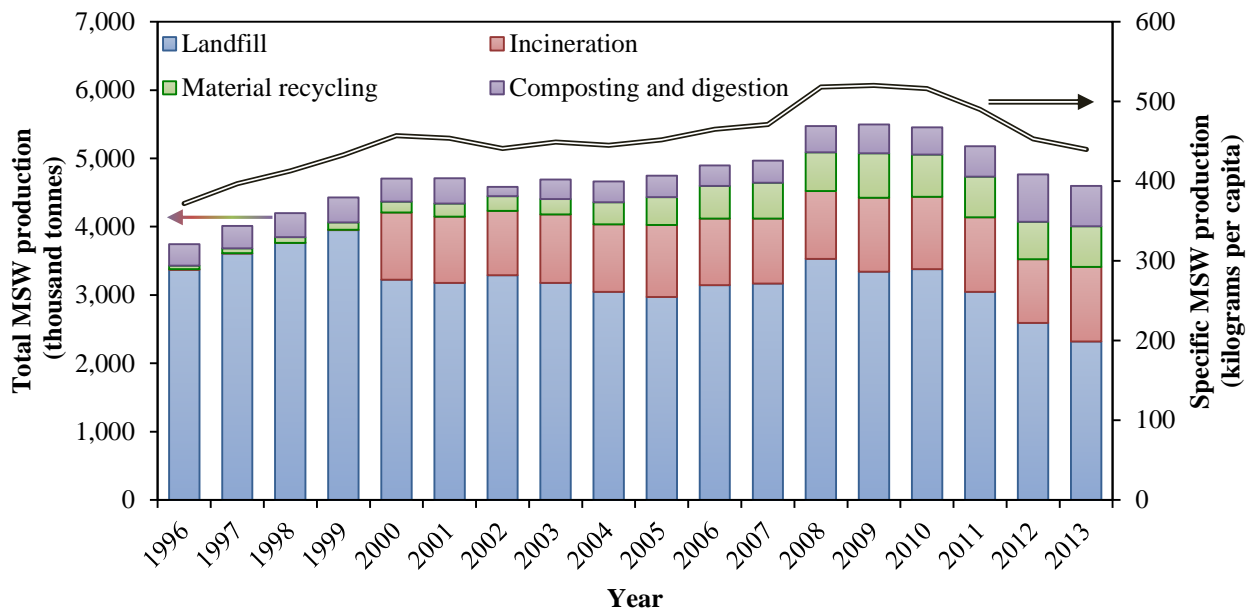


Figure 1.4. Evolution of the Municipal solid waste (MSW) produced according to type of treatment method in Portugal (source: Eurostat [3]).

After the PERSU application, key steps were given on the implementation of a waste policy. The urban waste management has undergone an evolution of political and legislative character. Firstly, the closure of all dumps was established, then management companies were reorganized by creating multi-municipal and inter-municipal systems, disposal and valorisation infrastructures were built up and, finally, selective collection's systems were created [7]. The closure of dumps led to their replacement by landfills, which began operating nationwide [6]. Sanitary landfill consists in a facility for waste disposal onto or into land (underground), including (i) the internal waste disposal sites (landfill where a producer of waste carries out its own waste disposal at the production site) and (ii) a permanent site (for a period longer than one year), used for temporary storage (Decree-Law no. 183/2009). Landfilling remains as the predominant municipal waste treatment option both at European level as in Portugal (see Figure 1.3 and Figure 1.4). In 2013, 13% of MSW were selectively collected while the 87% remaining were inferentially collected, having as a main destination the disposal in landfill (50%), followed by energy recovery (24%) and the organic valorisation (13%) (Figure 1.4).

The current waste management policy that is embodied in Decree-Law no. 178/2006, of 5th September, establishes the general system of waste management. This diploma clarifies the need to draw up a new specific plan for municipal waste management, reviewing the strategy manifested on PERSU. PERSU II, which was approved by Ordinance no. 187/2007, of 12th February, is a municipal waste management strategic instrument for the period 2007-2016.

The municipal waste management activity is a concept that comprises the activities of deposition, collection, transport, storage, sorting, recovery and disposal of waste from households, as well as other waste which, because of its nature or composition, presents similar features to waste from households [9]. In Portugal, the System of Urban Waste Management (SGRU, in Portuguese: Sistema de Gestão de Resíduos Urbanos) presents a structure composed of human resources, logistics, equipment and infrastructures, whose purpose is to implement the activities associated with the management of the municipal wastes. As can be seen in Figure 1.5, at the beginning of 2011 there were 23 SGRU geographically spread all over continental territory, of which 12 are Multimunicipal and 11 Intermunicipal. The Multimunicipal systems (by assignment or grant) are identified with capital letters and the systems represented in lowercase are Intermunicipal systems (isolated municipalities or in combination) [9].

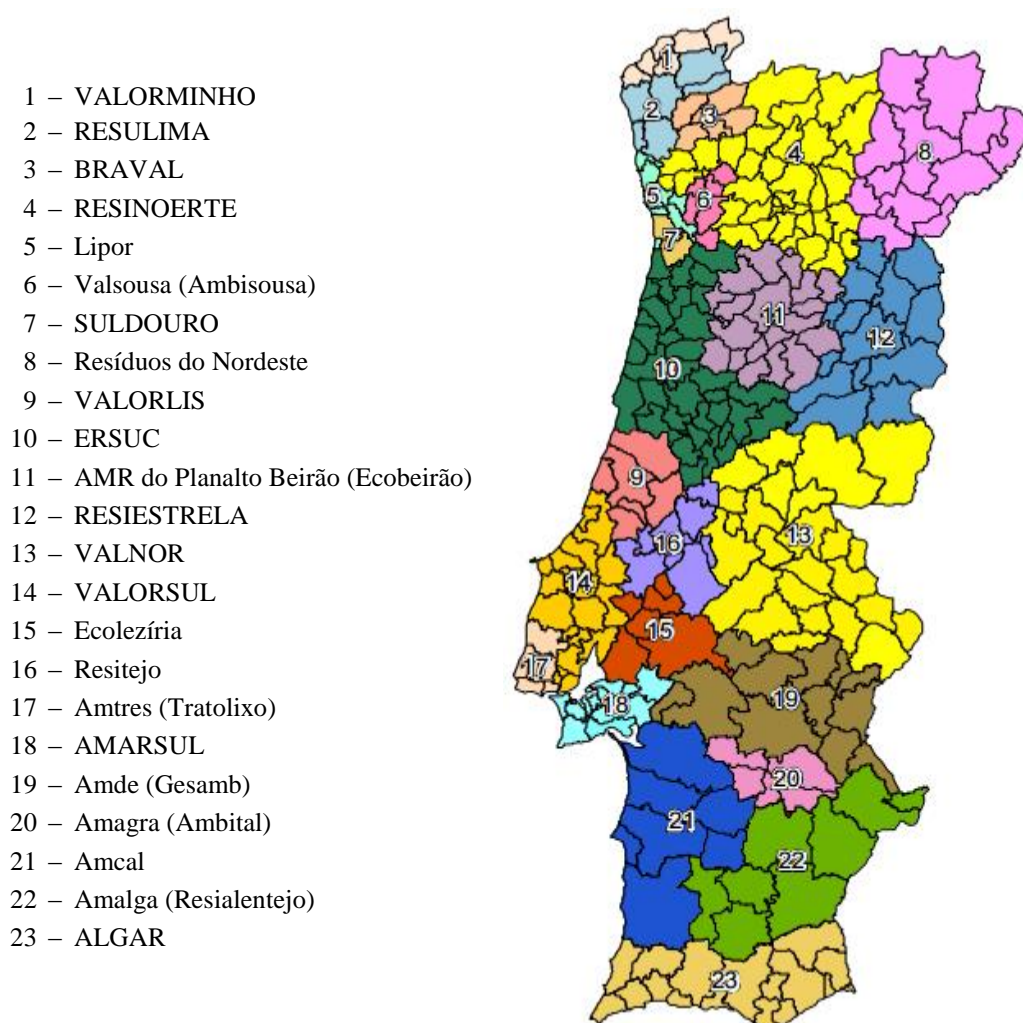


Figure 1.5. Portuguese systems of urban waste management [9].

The current SGRUs combine integrated solutions of recovery, treatment and technical confinement, thus minimizing the deposition of waste in landfills. However, the MSW disposal in landfill is, presently, a fundamental practice in an integrated system of waste management, either as end of line solution to refuse produced in other treatment processes (e.g. composting, incineration, anaerobic digestion of the organic fraction of the municipal waste), either as single treatment option [6, 10].

Sanitary landfills are infrastructures designed to protect the public health and the environment from the negative impacts associated with waste disposal. The landfill is one of the most used municipal waste management methods due to the maturity of the technology and the economic benefits [11]. Nevertheless, despite the technological development, this type of waste disposal is associated with various environmental impacts, most notably the impacts related to the production of leachate due to possible pollution of soil, groundwater and surface water. The leachates result from the water contained in the waste, the physicochemical and biological decomposition of waste and, especially, the percolation of rainwater through the mass of waste, accompanied by extraction of dissolved materials and/or in suspension [12, 13]. A landfill can be considered a biochemical reactor in which the inputs are waste, rainwater and energy, and the outputs are biogas and leachate, resulting from the degradation of the waste mass and from the precipitation [12].

The Decree-Law no. 183/2009 establishes the specific technical characteristics for each landfill class: i) landfill for inert waste; ii) landfill for non-hazardous waste; and iii) landfill for hazardous waste. Landfills, according to the respective class, namely the MSW landfills, which are integrated in the class of "landfill for non-hazardous waste", must fulfil the technical requirements of Annex I of the Decree-Law no. 183/2009. One of the requirements, related to the control of emissions and protection of the soil and the water, demands that the collected leachates must have a treatment and a final destination adequate, in accordance with the applicable legislation, being one of the biggest challenges to face in the management of these infrastructures, assuming itself as one of the most important pollution control processes.

1.2 Production, composition and characterization of landfill leachates

The leachate production results from the percolation of rainwater through the waste mass, biochemical processes in the waste cells, the water retained by the waste and water released as a result of the same decomposition reactions [6, 14].

The amount of leachate (L) produced over a given period of time can be estimated by conducting a water balance (Eq. (1.1)), taken into account the water streams entering and leaving the landfilling system (Figure 1.6), namely: accumulated precipitation (P) (in mm), surface water influx (R_{int}) (in mm), groundwater influx (I) (in mm), average evapotranspiration (EV) (mm), and surface run-off (R_{ext}) (in mm) [6, 14].

$$L = P + R_{int} + I - EV - R_{ext} \quad (1.1)$$

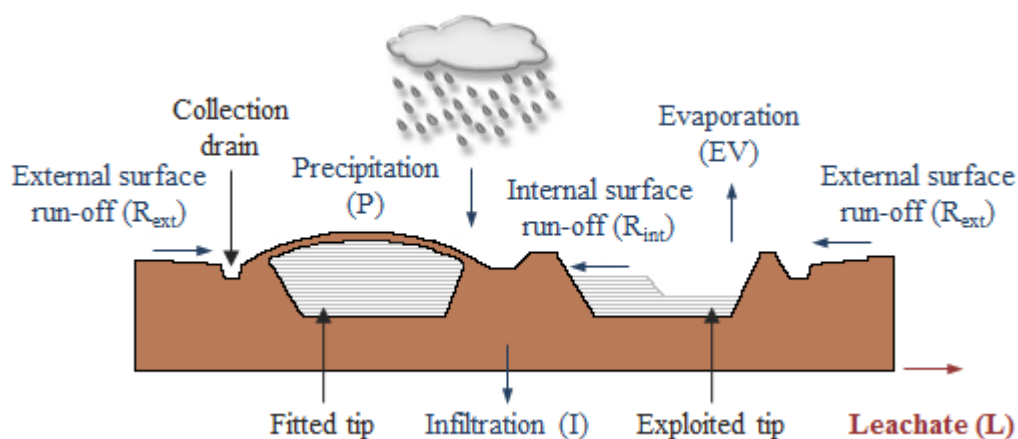


Figure 1.6. Water cycle in a sanitary landfill (adapted from Renou et al. [14]).

One of the factors having a huge influence on leachate production is the weather because it affects the precipitation and evaporation. The production of leachate also depends on the waste nature, especially its water content and compaction degree. The leachate production is generally higher when the waste is less compacted, since compaction decreases the infiltration rates [14, 15]. The maximum leachate production usually occurs at the end of winter and throughout the spring. An expeditious way to estimate the theoretical value of the amount of leachate is to assume that, in the absence or insufficiency of information, the value is about 30% of the average annual rainfall [6].

Leachate quality is also affected by the decomposition degree of the organic waste disposed in the landfill. After disposal, the biodegradable waste is initially decomposed by biological aerobic processes, of relatively short duration, and then by longer anaerobic processes [8, 16]. Depending on the decomposition stage, i.e. if the organic waste underwent partial or total biological anaerobic degradation, the leachates can present a variety of intermediate products along with other soluble recalcitrant materials [15].

The aerobic phase corresponds to the first stage of organic matter degradation. This is a period of 2/3 months, in which the oxygen initially present in the pores of the waste mass is diffused through the upper layers, enabling the aerobic microorganisms' activity. After that, the oxygen is depleted due to the aerobic metabolism and reconditioning operations. In this phase, the atmospheric oxygen is the final electron acceptor of the exothermic oxidation-reduction reactions. So, during this period, elevated temperatures are achieved in the waste mass. This results also in the production of water and carbon dioxide [8, 17].

The identification and demarcation of the anaerobic phases of the solid waste degradation often differs between the existing publications. In this thesis, the anaerobic process is divided into four main phases (see Figure 1.7): i) hydrolysis; ii) acidogenesis; iii) acetogenesis and iv) methanogenesis [8, 14].

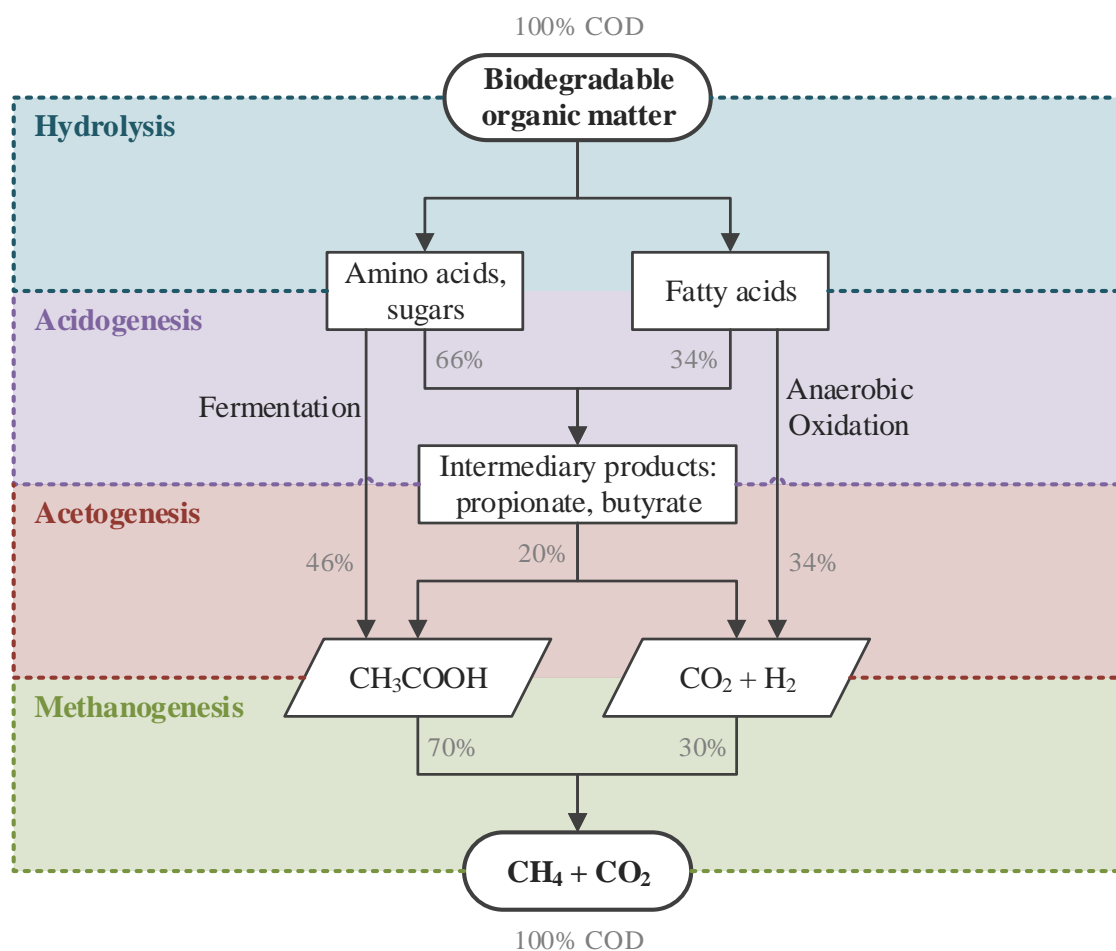


Figure 1.7. COD balance of the biodegradable organic matter during the anaerobic solid waste degradation (adapted from Renou et al. [14]).

The hydrolysis step consists in the conversion of organic polymers (proteins, carbohydrates and lipids) into soluble products through the action of extracellular enzymes. These enzymes are secreted by fermentative bacteria. The resulting products are organic monomers, including amino acids, sugars and long-chain organic acids. The factors that affect the degree and the rate of the hydrolysis are: temperature; residence time; composition of the substrate; particle size; pH of the medium; concentration of ammonium; and concentration of hydrolysis products [8, 18, 19].

During the acidogenesis or fermentation stage, the products resulting from hydrolysis are transported to the interior of fermentative bacteria cells, occurring their transformation to intermediate products (volatile fatty acids (VFA), alcohols, etc.), carbon dioxide and hydrogen. The VFA formed constitute the most important intermediates in the anaerobic digestion process, encompassing various lower-molecular-weight carboxylic acids, e.g. acetic and propionic acids (CH_3COOH , $\text{C}_2\text{H}_5\text{COOH}$), formed in greater quantities [8, 18, 19].

In the acetogenesis step occurs the transformation of the products resulting from acidogenesis in acetic acid (CH_3COOH), carbon dioxide (CO_2) and hydrogen (H_2) by acetogenic bacteria. The pH of the leachate goes down to 5 or lower values due to the presence of organic acids and high concentrations of CO_2 in the landfill. The biochemical oxygen demand (BOD_5), chemical oxygen demand (COD) and conductivity of the leachate significantly increase during this phase due to the presence of organic acids in the leachate. Due to the low pH of the leachate, inorganic compounds, mainly heavy metals, are solubilized. Many essential nutrients are also removed from the leached at this stage [8, 19].

The methanogenesis is the final stage and is the one that controls the anaerobic digestion process, being directly responsible by the production of methane (CH_4). The conversion of the H_2 and CH_3COOH into CH_4 and CO_2 is performed by methanogenic bacteria, increasing the leachate's pH to values close to the neutrality (about 6.8 to 8). While pH value increases, the values of BOD_5 , COD and conductivity decrease. At higher pH values, few are the inorganic constituents that remain in solution, as result the concentration of heavy metals in the leachate is reduced [8, 19, 20].

After the biodegradable organic material has been converted into CH_4 and CO_2 , during the previous phase, the maturation phase occurs. The mixture continues to migrate through the waste mass and the biodegradable material previously unavailable is converted. The gas generation rate considerably decreases, since the majority of nutrients were already removed during the previous stages and the remaining substrates in the landfill are slowly biodegradable. During the maturation phase, the leachate contains a high content of humic and fulvic acids (HA and FA), which are hardly degraded by biological processes [19].

The leachate composition varies according to the age of the landfill, climatic conditions, soil properties and type of waste, and it can be characterized in terms of dissolved organic matter (including recalcitrant compounds), inorganic macrocomponents, heavy metals and xenobiotic organic compounds [11, 14, 21]. Despite the composition of the leachate significantly changes along time, three types of leachate were defined according to the age of the landfill: young, intermediate and old. The relationship between the landfill's age and the leachate's characteristics is shown in Table 1.1.

Table 1.1. Leachate classification according to the landfill age (adapted from: Renou et al. [14], Foo and Hameed [22] and Li et al. [23]).

Leachate	Young	Intermediate	Old
Age (years)	<5	5-10	>10
pH	<6.5	6.5-7.5	>7.5
COD (mg/L)	>10 000	4 000 – 10 000	<4 000
BOD ₅ /COD	0.5 – 1.0	0.1 – 0.5	<0.1
Biodegradability	Important	Medium	Low
Organic Compounds	80% of VFA ^a	5-30% of VFA ^a + HA ^b and FA ^c	HA ^b and FA ^b
Ammonia Nitrogen (mg N/L)	< 400	-	> 400
Heavy metals (mg/L)	Low-Medium	Low	Low

^aVolatile fatty acids; ^bHumic acids; ^cFulvic acids.

The leachates from new landfills (<5 years) are characteristic of the acid phase of waste decomposition. They present a high BOD₅/COD ratio, being indicative of their high biodegradability, high concentrations of COD (30,000-60,000 mg/L) and BOD₅ (4000-13,000 mg/L), moderate levels of ammonia nitrogen and alkalinity and a low pH value. The highest fraction of the organic matter is related to low molecular weight compounds such as volatile fatty acids (VFA) resulting from the anaerobic fermentation [11, 14, 21, 23].

When the age of the landfill increases, there is a decrease in the concentration of organic compounds as result from the anaerobic decomposition. So, more stabilized leachates are produced, which are characterized by reduced COD values, high pH (7.5 to 8.5) and low BOD₅/COD ratio, due to the releasing of recalcitrant organic molecules from the waste [14, 20, 23]. Most organic compounds present in the stabilized leachate have a high molecular weight, such as humic substances [11, 21, 24]. At this phase, so called methanogenic, the concentration of some inorganic macrocomponents in the leachate (such as calcium, magnesium, iron and manganese) is low due to high pH (which decreases the solubility enhancing the reactions of precipitation and sorption) and to low content of dissolved organic matter (which could originate complexes with the cations) [20].

Due to the characteristics of the sanitary landfill leachates, it turns out that their production is a problem in the environmental context, and it is vital their proper management, given the associated risks of contamination of water bodies (surface and underground) and soil underlying the landfill. The discharge of leachate into water bodies or soil is covered by Decree-Law no. 236/98, of 1st August 1998 (Table 1.2), which establishes the Emission Limit Values for wastewaters discharge in surface, coastline and territorial waters, groundwater and soil, promoting the quality of the aquatic environment and the protection of the public health and soils.

Table 1.2. Emission limit values (ELV) for the discharge of wastewaters (Decree-Law no. 236/98).

Parameter	Unities	ELV ^a
pH	Sörensens scale	6.0-9.0
Temperature	°C	Increase of 3°C ^b
BOD ₅ (at 20°C)	mg O ₂ /L	40
COD	mg O ₂ /L	150
TSS	mg/L	60
Aluminium	mg Al/L	10
Total iron	mg Fe/L	2.0
Odour	-	Not detectable at a dilution of 1:20
Colour	-	Not visible at a dilution of 1:20
Free residual chlorine	mg Cl ₂ /L	0.5
Total residual chlorine	mg Cl ₂ /L	1.0
Phenols	mg C ₆ H ₅ OH /L	0.5
Oil and grease	mg/L	15
Sulphides	mg S/L	1.0
Sulphites	mg SO ₃ /L	1.0
Sulphates	mg SO ₄ /L	2000
Total phosphorus	mg P/L	10 3 (in waters that feed lagoons or reservoirs) 0.5 (in lagoons or reservoirs)
Ammonium nitrogen	mg NH ₄ /L	10
Total nitrogen	mg N/L	15
Nitrates	mg NO ₃ /L	50
Aldehydes	mg/L	1.0
Total arsenic	mg As/L	1.0
Total lead	mg Pb/L	1.0
Total cadmium	mg Cd/L	0.2
Total chromium	mg Cr/L	2.0
Hexavalent chromium	mg Cr (VI)/L	0.1
Total copper	mg Cu/L	1.0
Total nickel	mg Ni/L	2.0
Total mercury	mg Hg/L	0.05
Total cyanide	mg CN/L	0.5
Mineral oils	mg/L	15
Detergents (sodium lauryl sulphate)	mg/L	2.0 ^c

^aThe ELV is understood as the monthly average, which is defined as the arithmetic mean of the average daily referring to the days of 1-month operation, which should not be exceeded. The daily value, based on a representative sample of the wastewater discharged during a period of 24-hours cannot exceed twice the monthly average value (the 24-hours composed sample must take into account the discharge regime of the wastewater produced); ^bTemperature of the receiving water body after the wastewater discharge, measured at 30 m downstream from the discharging point; ^cValue relative to the industrial plant's discharge for the HCH production and/or lindane extraction.

1.3 Leachate treatment systems

Due to the large variability of leachates, both in quantity and quality, influenced by factors such as the waste mass composition deposited, rainwater and type of management and operation of the landfill, the definition of a treatment line able to be effective in all situations is not easy. The leachate treatment systems are often similar to traditional treatment methods used for urban wastewater, including biological (aerobic and anaerobic) and physical-chemical processes, although the processing is much more challenging. Several authors have presented reviews on different approaches used for the landfill leachate treatment [14, 15, 19, 25, 26]. From these works it is possible to divide the leachate treatment systems into four different groups (see Table 1.3):

- i) leachate channelling (combined treatment with domestic sewage and recycling back through the landfill);
- ii) biological degradation (aerobic and anaerobic processes);
- iii) chemical and physical methods (flotation, coagulation/flocculation, chemical precipitation, adsorption, ammonium stripping, chemical oxidation and ion exchange);
- iv) membrane filtration (microfiltration, ultrafiltration, nanofiltration and reverse osmosis).

Regardless the technology chosen to treat the leachate, it is usual to have a stabilization lagoon upstream, in order to promote the regularization and homogenization of the flowrate resulting from situations of irregular or intense rainfall [10, 27]. Pure oxygen or air must be injected in these lagoons to avoid uncomfortable odors, due to the anaerobic biochemical processes, and to foment the nitrification reactions. A good management of the stabilization lagoons is of extreme importance, in order to prevent the contamination of the waterways and soil.

Table 1.3. Overview of the main leachate treatment processes (adapted from Abbas et al. [25], O’Leary and Tchobanoglous [19] and Renou et al. [14]).

	Treatment Process	Effectiveness			Main application	Benefits	Drawbacks
		YL ^a	IL ^b	OL ^c			
Leachate Channelling	Combined treatment with domestic sewage	Good	Fair	Poor	General treatment	Easy maintenance and low operating costs. No need for nutrients addition, since the leachate contains nitrogen and the sewage contains phosphorous.	Reduction of the treatment efficiency and increase of the effluent load, due to the presence of recalcitrant compounds and heavy metals in the leachate.
	Recycling	Good	Fair	Poor	Improvement of leachate quality and stabilization	One of the least expensive. Improvement of leachate quality. Less time required for stabilization.	High recirculation rates can affect the waste anaerobic degradation, e.g. methanogenesis inhibition. Very high volumes of recirculated leachate can lead to saturation, ponding and acidic conditions.
Biological Biodegradation	Aerated lagoons^e	Good	Fair	Poor	Biodegradable organic matter removal and ammonium nitrification	Low operation and maintenance costs. Anoxic zones inside the lagoon promote nitrogen removal via nitrite/nitrate denitrification.	Need for large areas. Not completely satisfactory for strict requirements. Strong temperature-dependence.
	Activated Sludge^{d,e}	Good	Fair	Poor	Biodegradable organic matter removal and ammonium nitrification	Effective for the removal of biodegradable organic carbon, nutrients and ammonium.	Excess of sludge production. Inadequate sludge settleability. Need for longer aeration times. High energy requirements. Need for secondary settlement. Possible need for antifoam. Microbial inhibition due to high ammonium-nitrogen load. Strong temperature-dependence.
	Sequencing Batch Reactor^{d,e} (SBR)	Good	Fair	Poor	Biodegradable organic matter removal and ammonium nitrification	Alternating the operating regime between aerobic and anoxic, total nitrogen can also be removed by nitrification and denitrification reactions. Great flexibility considering the high degree of leachate variability.	Similar to activated sludge but without secondary settlement. Applicable to relatively low flow rates.

Table 1.3. Overview of the main leachate treatment processes (adapted from Abbas et al. [25], O’Leary and Tchobanoglous [19] and Renou et al. [14]).

	Treatment Process	Effectiveness			Main application	Benefits	Drawbacks
		YL ^a	IL ^b	OL ^c			
Biological Biodegradation	Moving bed biofilm and trickling filters^{d,f}	Good	Fair	Poor	Biodegradable organic matter removal and ammonium nitrification	Neither losses of active biomass nor long sedimentation periods. Nitrification is less affected by low temperatures and by inhibition due to high ammonium content than in the suspended-growth biomass processes.	Need for operation at high dissolved oxygen content to maintain high nitrification rates [28]. High capital costs [26]. Trickling filter is not volume-effective and nuisance odour may prevail [29, 30].
	Anaerobic systems^g	Good	Fair	Poor	Biodegradable organic matter removal and nitrite/nitrate denitrification	Conservation of energy and production of very few sludge. Possibility for using the biogas produced for external purposes. Low doses of phosphorus required for bacterial growth [26].	Low reaction rates. Heavy metals can hamper digestion [26]. Ammonia toxicity and high residual ammonia concentration [26]. Susceptible to changes in pH and temperature [26].
	Nitrification/denitrification	Good	Fair	Poor	Nitrogen removal	Nitrification/denitrification process can be accompanied by carbon removal and can occur in the biological systems reported above, alternating between the presence and absence of oxygen, respectively.	
Chemical and Physical Methods	Flotation	-	-	-	Suspended matter removal	Low capital investment and operating costs [31]. High efficiency of separation [31]. Also effective on BOD ₅ , COD and turbidity removal [32]. Robust against influent variations [32]. Need for lesser implementation areas than normal clarifiers [32]. Easy installation and set-up [32].	Reduced applicability when used as a single process. For better results the flotation processes must be used together with coagulation, in order to facilitate the destabilization of colloidal particles [31].
	Coagulation/flocculation	Poor	Fair	Fair	Suspended matter and heavy metals removal	The simplest physical-chemical technique for leachate treatment [33]. Effective pre-treatment process when used prior to biological treatment or reverse osmosis [33]. Efficient polishing treatment for the removal/reduction of recalcitrant organic matter [33].	High sludge production and need for adequate disposal. Possible increase of the concentrations of iron or aluminium in the liquid phase. Not suitable for full treatment [33]. Inefficiency on nitrogen removal [33]. Low removal efficiency on high strength leachate [33]

Table 1.3. Overview of the main leachate treatment processes (adapted from Abbas et al. [25], O’Leary and Tchobanoglous [19] and Renou et al. [14]).

Treatment Process	Effectiveness			Main application	Benefits	Drawbacks	
	YL ^a	IL ^b	OL ^c				
Chemical and Physical Methods	Chemical precipitation	Poor	Fair	Poor	Ammonium and metals removal	Extensively employed as leachate pre-treatment due to its simplicity, capability and low-cost equipment [33]. Also efficient on refractory compounds.	Sludge production requires the disposed as hazardous waste. Relatively expensive chemicals [33].
	Adsorption	Poor	Fair	Good	Organic matter removal	Proven technology. Better COD reduction than the chemical methods. More effective leachate treatment when used together with biological oxidation or as a stage of an integrated chemical-physical-biological process.	Variable costs depending on leachate. Need for frequent regeneration of columns or an equivalently high consumption of powdered activated carbon.
	Ammonium stripping	Poor	Fair	Fair	Ammonium removal	High removal efficiency. Lower operating costs than for reverse osmosis and nanofiltration [33].	May require other equipment for air pollution control, since ammonia gas is released to the atmosphere. High pH value is required. Scaling of alkalinity, when lime is used for rise pH in the stripping tower. pH adjustment prior to discharge.
	Chemical oxidation	Poor	Fair	Fair	Organic matter removal	Greatly suitable for non-biodegradable compounds removal. Capable to reach complete mineralization. Biodegradability enhancement of recalcitrant organic pollutants.	Works better on diluted waste streams. The use of chlorine can lead to the formation of chlorinated compounds. High demand of electrical energy resulting in rather high treatment costs. For complete mineralization, high oxidant doses would be required. Some intermediate products can increase the leachate toxicity.
	Ion exchange	Good	Good	Good	Dissolved inorganic compounds removal	Effective removal of traces of metal impurities, meeting stricter discharge standards.	Useful only as a relaying treatment after biological processes. High treatment cost. Previous suspended solids removal is required.

Table 1.3. Overview of the main leachate treatment processes (adapted from Abbas et al. [25], O’Leary and Tchobanoglous [19] and Renou et al. [14]).

	Treatment Process	Effectiveness			Main application	Benefits	Drawbacks
		YL ^a	IL ^b	OL ^c			
Membrane Filtration	Microfiltration	Poor	-	-	Suspended matter removal	Efficient as pre-treatment for the other membrane processes or along with chemical treatments.	Useful only as a relaying treatment.
	Ultrafiltration	Poor	-	-	Removal of bacteria and high molecular weight organic compounds	Proficient on suspended matter removal either by direct filtration or together with biological treatment, by replacing the sedimentation unit. Effective as a pre-treatment for reverse osmosis process.	Costly and membranes are subject to fouling. Strongly dependent of the kind of material constituting the membrane.
	Nanofiltration	Good	Good	Good	Removal of organic, inorganic and microbial contaminants	Versatile technology capable to meet multiple water quality objectives. Combined with physical methods allows to obtain a satisfactory organic matter removal	Costly and need for lower pressure than reverse osmosis. Membrane fouling.
	Reverse osmosis	Good	Good	Good	Removal of organic and inorganic matter, suspended and dissolved	More efficient than conventional methods and the other membrane filtration processes.	Expensive process. Membrane fouling. Extensive pre-treatment is required. Problem with the concentrates disposal.

^aYoung leachate; ^bIntermediate leachate; ^cOld leachate; ^dUnder aerobic conditions; ^eSuspended-growth biomass process; ^fAttached-growth biomass process; ^g Comprises all suspended-growth and attached-growth biomass processes, which are quite similar to those ones used under aerobic conditions.

1.3.1 Leachate channelling

The co-treatment of landfill leachate with domestic sewage is a very attractive approach, both at technical and economic level, throughout the conception and exploration of the sanitary landfill, since there is no need for the full treatment facility construction, reducing the associated expenses. Besides the good cooperation between the different involved entities, for the implementation of this process it is necessary to take into account if: i) exists a wastewater treatment plant (WWTP) in the vicinity of the landfill, or a sewerage system that forwards the leachate to the WWTP; ii) the WWTP has capability to qualitatively and quantitatively assimilate the leachate flow-rates; iii) the treatment methodology applied in the WWTP is compatible with the leachate's characteristics. However, this alternative has been questioned due to the presence of recalcitrant organic matter and heavy metals, since the treatment efficiency may be reduced and the effluent concentration can be increased [14, 15]. In fact, a study performed by Ferraz et al. [34] disclosed that the co-treatment of domestic wastewater with 5% (v/v) leachate (pre-treated by air stripping) led to the reduction of hardly biodegradable organic matter as a result of dilution and not of biodegradation.

Recycling leachate back through the landfill was largely used in the past due to its low cost and fast leachate's stabilization [14], being possible to produce an effluent with low organic load in a relatively short period of time. Nevertheless, the recirculation does not constitutes a complete solution for leachate treatment, but instead could be used as a complement, since (i) the precipitation can exceed the evaporation (increasing the volume to recirculate and thus exceeding the absorption capacity by the system) and (ii) the recalcitrant organic compounds as well as some inorganic ones cannot be removed [8, 14]. So, this technique should only be used with the purpose of promoting the waste biodegradation process in the landfill.

1.3.2 Biological degradation

Due to its simplicity, reliability, high cost-effectiveness and to the high nitrogen content (mostly as ammonium) inherent in this type of effluent, the biological process is almost always applied in leachate treatment plants (LTPs) [14, 35]. Up to date, the nitrification reaction followed by a denitrification step, mediated by microorganisms with aerobic and anoxic metabolisms, respectively, is the biological process most used for nitrogen removal from wastewaters [36]. However, regarding the organic contaminants, biological treatment only has a good performance in young leachates, where the organic matter content is mainly biodegradable (Table 1.4).

Table 1.4. Performance of different biological processes on the landfill leachate treatment.

Process	Initial characterization	Removal (%)	Observations	Reference
Activated Sludge (Aerobic)	COD=270-1000 mg/L NH ₄ ⁺ -N=53-270 mg/L	25-55 COD >88 BOD 61, 95,100 NH ₄ ⁺	Anaerobically pretreated leachate V=3.75 L; HRT=3-4 d T=5°C, 7°C and 10°C	Hoilijoki et al. [37]
UASB + Activated sludge (AS)	COD=24,000 mg/L BOD ₅ /COD=0.45 TKN = 1766 mg/L NH ₄ ⁺ -N=1682 mg/L	UASB: 87 COD >80 NO ₃ ⁻ -N AS: >99 NH ₄ ⁺ -N 74 COD (97 T)	UASB: V=20 L; T=36°C; HRT=2 d AS: V=40 L; T=23 °C; HRT=4 d RS=100%;R=300%	Im et al. [38]
UASB + Activated sludge (AS)	COD=2900 mg/L BOD ₅ /COD=0.66 TN = 200 mg/L NH ₄ ⁺ -N=170 mg/L	58 COD (UASB) 75 COD (AS) 90 COD (Total) 45 TN (AS) 80 NH ₄ ⁺ -N (AS)	T=24 °C UASB: V=0.38 L AS: V=0.5 L; DO > 2 mg/L; RS ratio of 5:1	Kettunen et al. [39]
Aerated SBR	COD=757 mg O ₂ /L NH ₄ ⁺ -N=362 mg/L BOD ₅ /COD=0.14	48.0 COD ≈100 NH ₄ ⁺ -N	Raw leachate V=6L; T=20-25 °C; HRT=2 d	Kulikowska and Klimiuk [40]
Anoxic SBR	COD=394 mg O ₂ /L NO ₃ ⁻ -N=320 mg/L BOD ₅ /COD=0.02	99.7 NO ₃ ⁻ -N	Aerobically treated leachate T=20-25 °C; HRT=1 d 3.6 mg COD*/mg NO _x -N (*COD from methanol)	
SBR	COD=528-3060 mg/L NH ₄ ⁺ -N=167-1519 mg/L BOD ₅ =30-1000 mg/L pH=7.55-8.70	40-50 COD >99% NH ₄ ⁺ -N	V=24 L; T=20 °C; SRT=25 d Full cycle=24 h (4×5.75 h) Anoxic phase=1-2 h Oxic phase=3.75-4.75 h	Spagni et al. [41]
SBR	COD=1769-2623 mg/L NH ₄ ⁺ -N=933-1406 mg/L BOD ₅ /COD≈0.2	20-30 COD >98 NH ₄ ⁺ -N >95 TN	V=24 L; T=20 °C; SRT=20-25 d Full cycle=24 h (4×5.75 h) Anoxic/oxic phase=2/3.75 h	Spagni and Marsili-Libelli [42]
UASB + SBR	COD=1237-13500 mg/L NH ₄ ⁺ -N=738-2400 mg/L BOD ₅ =550-6500 mg/L pH=7.1-8.5	77-99 COD 89-99.9 NH ₄ ⁺ -N 95-99 TN	UASB: V=3 L; T=30 °C HRT=14-48 h; R=50-300% SBR: V=9 L; T=9-32 °C Full cycle=variable Anoxic/oxic phase=30 min	Sun et al. [43]
Anoxic digestion (batch)	COD=7720 mg O ₂ /L TOC=2420 mg/L NH ₄ ⁺ -N=1694 mg/L BOD ₅ /COD=0.28	46 COD 65 TOC 45 NH ₄ ⁺ -N 91 BOD ₅	Raw leachate V=150 L T=35 °C HRT= 90 d	Trabelsi et al. [44]
Aerated submerged biological reactor		84 COD 45 NH ₄ ⁺ -N 91 BOD ₅	Leachate after anoxic digestion V=3×30 L (in series); T=20-25°C; HRT=7 d Bio-film supported in synthetic PVC fiber (57 m ² /m ³)	
Moving bed biofilm	COD=800-1300 mg/L NH ₄ ⁺ -N=460-600 mg/L BOD ₇ =30-140 mg/L	20-30 COD 79-99.6 NH ₄ ⁺ -N	Aerated conditions; pH=7.5 V=0.22-0.60 L T=5-20 °C; HRT=2-5 d	Welander et al. [45]

Legend: HTR – Hydraulic retention time; SRT – Solid retention time; UASB – Upflow anaerobic sludge blanket; R – recirculation of the SBR-nitrified supernatant; DO – dissolved oxygen; RS – return sludge recirculation; T – Total.

Table 1.4 summarizes different types of biological processes applied to sanitary landfill leachates treatment, including removal percentages of nitrogen and organic compounds. Among them, there is a work presented by Im et al. [38], where a biological system composed by an upflow anaerobic biofilm reactor (20 L, 36 °C), an aerobic activated sludge reactor (40 L, 23 °C) and a clarifier (5 L), is proposed as a feasible process to treat organic and nitrogen compounds in an immature leachate (COD=24 g/L, BOD₅/COD=0.45, NH₄⁺-N=1682 mg/L). Applying a return sludge flow ratio of 100% (from the clarifier to the aerobic reactor), a recirculation flow ratio of 300% (from the aerobic to the anaerobic reactor) and hydraulic retention times of 2 and 4 days in the anaerobic and aerobic reactors, respectively, they were able to denitrify more than 80% of the nitrate, without external carbon source addition, and nitrify more than 99% of the ammonium nitrogen, in the anaerobic and aerobic reactors, respectively. Relatively to the organic matter balance, in the anaerobic reactor, 87% of COD was removed to the denitrification and methanogenesis reactions, and in the aerobic reactor, 74% of COD was mineralized, totalizing a 97% COD depletion. Spagni and Marsili-Libelli [42] reported a study on the treatment of a leachate generated in old landfills (COD=1769-2623 mg/L, BOD₅/COD≈0.2, NH₄⁺-N=933-1406 mg/L) by a sequencing batch reactor, in order to remove the nitrogen load. Nitrification and nitrogen removal (with external carbon source addition) were frequently greater than 98% and 95%, respectively, whereas COD reduction was around 20-30%.

1.3.3 Physical and chemical processes

When the leachate's BOD₅/COD ratio becomes too low, prevailing the refractory organic matter, and the biological technologies can no longer remove the organic content, physical and chemical processes can be a suitable treatment approach [15, 46]. This treatment is usually used to reduce suspended solids, colloidal particles, colour, floating material and toxic compounds. In contrast to biological processes, physical and chemical technologies cannot be applied as an individual treatment, instead they can effectively be used as a pre-treatment or a polishing step, in combination with other treatment processes, as well as to treat a specific contaminant, such as ammonia [14, 16]. Particularly, the most prominent treatments are flotation [31, 32], coagulation/flocculation [47-49], chemical precipitation [50, 51], adsorption by activated carbon [22, 52], ammonia stripping [46, 50] and chemical oxidation [53-56]. Table 1.5 lists some research studies performed in the scope of landfill leachate treatment via physical and chemical technologies.

Table 1.5. Performance of different physical and chemical processes on landfill leachate treatment.

Process	Initial characterization	Removal (%)	Observations	Reference
Flotation	COD=2667 mg/L Colour=4059 PtCo Turbidity=248 FAU NH ₃ -N=1760 mg/L pH=8.0	36 COD	Only DAF	Palaniandy et al. [32]
		33 Colour 32 Turbidity	Q=6 L/min; P=400 kPa; IT=2 min; RT=10 min	
Flotation + Coagulation	COD=2610 mg/L Colour=4000 PtCo Turbidity=259 FAU NH ₃ -N=1975 mg/L pH=8.1	79 COD	DAF + Coagulation	Adlan et al. [31]
		70 Colour 42 Turbidity	(2.3 g/L alum; pH=7) Q=4L/min; P=600 kPa; IT=4 min; RT=20 min	
Coagulation/ Flocculation	COD=4100 mg/L BOD ₅ /COD=0.05 Turbidity=1800 NTU NH ₄ ⁺ -N=1040 mg/L pH=8.2	55 COD	Ferric chloride: 0.035 mol Fe ³⁺ /L	Amokrane et al. [47]
		94 Turbidity	pH=5.1	
Coagulation/ Flocculation	COD=5350 mg/L BOD ₅ /COD=0.20 pH=7.9	42 COD	Alum: 0.035 mol Al ³⁺ /L	Tatsi et al. [48]
		87 Turbidity	pH=5.6	
Coagulation/ Flocculation	COD=70,900 mg/L BOD ₅ /COD=0.38 pH=6.2	45 COD	Lime: 7g/L Ca(OH) ₂ ; pH=12	Tatsi et al. [48]
		75 COD 66 COD	Ferric chloride: 1.5 g Fe ³⁺ /L Alum: 0.7 g Al ³⁺ /L; pH = 10	
Coagulation/ Flocculation	COD=5050 mg/L BOD ₅ /COD=0.17 pH=8	30 COD	Lime: 7g/L Ca(OH) ₂ ; pH=12	Ntampou et al. [49]
		25 COD 38 COD	Ferric chloride: 0.5 g Fe ³⁺ /L Alum: 1.5 g Al ³⁺ /L	
Chemical precipitation	COD=4024 mg/L NH ₄ ⁺ -N=2240 mg/L pH=7.7	72 COD	FeCl ₃ : 7 mM Fe; pH=5.2	Ozturk et al. [50]
		38 Colour		
Ammonia Stripping	COD=5730 mg/L NH ₄ ⁺ -N=1025 mg/L pH=7.9	62 COD	PACl-18: 11 mM Al; pH=5.7	Huang et al. [51]
		38 Colour		
Chemical precipitation	COD=4295 mg/L BOD ₅ /COD=0.49 NH ₄ ⁺ -N=1750 mg/L	50 COD	Struvite (MAP) precipitation	Pirbazari et al. [52]
		85 NH ₄ ⁺ -N	Mg:NH ₄ :PO ₄ =1:1:1; pH=9.2 (MgCl ₂ .6H ₂ O+NaH ₂ PO ₄ .2H ₂ O)	
Adsorption by activated carbon	COD=879-940 mg/L BOD ₅ /COD=0.004 pH=7.5	25 COD	pH=12; 17 h of aeration time	Martinen et al. [46]
		85 NH ₄ ⁺ -N		
Ammonia Stripping	COD=190-920 mg/L NH ₄ ⁺ -N=74-220 mg/L pH=7.9	9 COD	Struvite precipitation	Huang et al. [51]
		82 NH ₄ ⁺ -N	Mg:N:P=3:1:1; pH=5.3-8.4 (MgO+H ₃ PO ₄)	
Adsorption by activated carbon	COD=879-940 mg/L BOD ₅ /COD=0.004 pH=7.5	~91 COD	Pre-treated leachate (0.8 L/h)	Pirbazari et al. [52]
		dark colour- -colourless	Granular carbon (1031 m ² /g) Stainless steel column (1.25m×60mm; 16 kg of carbon)	
Ammonia Stripping	COD=190-920 mg/L NH ₄ ⁺ -N=74-220 mg/L pH=7.9	4-21 COD	pH=11; 24 h of aeration time	Martinen et al. [46]
		89, 64 NH ₄ ⁺ -N	T=20,6 °C	

Legend: DAF – Dissolved air flotation; IT – Injection time; RT – Retention time; Alum - aluminium sulphate, Al₂(SO₄)₃.18H₂O; PACl-18 - poly-aluminium chloride; MAP - Magnesium ammonium phosphate, MgNH₄PO₄.6H₂O.

Flotation has been widely used for the removal of colloids, ions, macromolecules, microorganisms and fibres from wastewaters, but there are few studies reporting this application on the leachate remediation [14]. Combining flotation with coagulation, it is possible to achieve COD removals higher than 75% [31, 32]. This technique is a good option when the available land area does not allow the construction of settling tanks [57].

Coagulation/flocculation has been effectively employed for leachate treatment from mature landfills, as could be seen in Table 1.5. The affinity for old leachates is due to the fact that these are mainly constituted by humic and fulvic acids. Actually, Yoon et al. [58], using an ultrafiltration system for the organic compounds fractionation, showed that along the coagulation process of a leachate from an aerated lagoon, the organics with MW > 500 Da were removed more easily (59 – 73%) than the organics with a MW < 500 Da (18%). Coagulation is extensively used as pre-treatment of biological processes and reverse osmosis (avoiding the membrane fouling) or as polishing step to remove bio-refractory compounds [14].

Usually, chemical precipitation and ammonia stripping are used when the leachate presents a high ammonium content, due to its efficiency, process simplicity and cheap equipment [16]. However, a high chemicals dosage and additional air pollution control are required for chemical precipitation and ammonia stripping, respectively. These technologies allow obtaining ammonium abatements greater than 80% (Table 1.5). Even though, adsorption leads to better results than chemical methods. However, the regular need to regenerate or replace the adsorbent means high associated costs, which often makes this option unfeasible [15, 57].

Chemical oxidation has been subject of many studies about wastewater treatment containing non-biodegradable organic matter, including landfill leachates. The main focus of interest from various authors [53-56] is Advanced Oxidation Processes (AOPs), which have been positively applied in the treatment of stabilized leachates. AOPs are able to oxidize organic substances with the perspective of full mineralization or biodegradability's enhancement until obtaining a range of values that allows the coupling with a subsequent biological treatment. AOPs will be subject to further description in the next sub-chapter.

The combination of biological processes with physical-chemical technologies minimizes the drawbacks of each individual treatment, optimizing the effectiveness of the overall process. Furthermore, the UK Environment Agency presented in 2007 a guidance for the treatment of landfill leachates [57], which indicated that the Best Available Technology for leachates treatment relied on the adoption of a multistage treatment process, possibly involving the use of primary, secondary, and tertiary processes, adjusted to the type of leachate, including the different technologies aforementioned.

1.3.4 Membrane filtration

Membrane separation processes involve the use of synthetic membranes, porous or semipermeable, to separate small solid particles, molecules or even dissolved ionic compounds from water. The separation process is based on a hydraulic pressure gradient, where a certain pressure is applied to the more concentrated solution, compelling the water to flow from the higher concentration to the lower concentration through the membrane. The liquid that passes through the semipermeable membrane is designed as permeate and the liquid containing the retained compounds is designed as concentrate. The main membrane processes used on leachate treatment are (i) microfiltration (MF), (ii) ultrafiltration (UF), (iii) nanofiltration (NF) and (iv) reverse osmosis (RO). Basically, the difference between each method is the membrane pore size and the driving force intensity [14, 26, 59]. Table 1.6 presents some applications of membrane filtration processes for leachate treatment.

Concerning membrane separation technologies, NF and RO seem to be the best choices (see Table 1.6). MF and UF do not allow an effective removal of the organic matter (<50%), so they could be used prior to NF and RO processes, in order to prevent membrane fouling, which is one of the main disadvantages of the membrane filtration (see Table 1.3). Membrane fouling can also be avoided by using a coagulation process as pre-treatment. Commonly, RO is preceded by biodegradation, lime precipitation or hybrid systems combining biological and chemical oxidation treatment [26, 52, 60].

During the late 90s, in Germany, the Netherlands, Belgium, France, Portugal and Spain, a lot of reverse osmosis (RO) leachate treatment systems were designed with an aerated lagoon upstream from a 2-stages RO plant. This configuration presented as advantage the aerated lagoon, which significantly reduced the nitrogen and organic matter load. Although the production of a high quality effluent (permeate) was a significant advantage of the RO process, the non-biodegradable components of the leachate, such as chloride, residual COD and heavy metals, were present in the concentrate, which could be 10%-25% of the leachate's volume [57].

Additionally, all chemicals required for the effective operation of an RO plant, such as citric acid, membrane cleaner and anti-scaling detergents (up to 0.3% per cubic meter of treated leachate) were also present in the concentrate. The final destination of the concentrate is a key factor to be addressed, and normally the concentrate is returned to the landfill or disposed of off-site. The return of concentrate to the landfill leads to an increase of COD and $\text{NH}_4^+\text{-N}$ concentration in the leachate, as well as an increase in electrical conductivity [57].

Table 1.6. Performance of the different membrane filtration processes on the landfill leachate treatment.

Process	Initial characterization	Removal (%)	Observations	Reference
MF	COD=2300 mg/L BOD ₅ /COD=0.30 pH=7.25	25-35 COD	Polypropylene tubular membrane $v=4.1-4.3$ m/s; cut-off:0.2 μ m; T=20°C; surface area (a) =0.11 m ²	
UF (after MF)	COD=1700 mg/L BOD ₅ /COD=0.29	5-10 COD	Polysulphone tubular membrane $v=4.1-4.3$ m/s; cut-off:50-80 kDa; T=20°C; a=0.15 m ²	Piatkiewicz et al. [61]
RO (after UF)	COD=1820 mg/L BOD ₅ /COD=0.30	-	Spiral wound $v=4.1-4.3$ m/s; T=20°C	
NF	COD=550 mg/L NH ₄ ⁺ -N=220 mg/L COD=600 mg/L NH ₄ ⁺ -N=74 mg/L COD=200 mg/L NH ₄ ⁺ -N<1 mg/L	56 COD 27 NH ₄ ⁺ -N 66 COD 50 NH ₄ ⁺ -N 83 COD - NH ₄ ⁺ -N	Polymer membrane Desal 5 DL $v=3$ m/s; cut-off:200-300 Da; P=6-8 bar; T=25°C; a=45 cm ²	Marttinen et al. [46]
UF	COD=1660 mg/L	49 COD	Polysulfone $v=2.5$ m/s; cut-off:300 kDa; P=0.3 MPa; T=25°C; a=0.025 m ²	Bohdziewicz et al. [60]
RO (after UF)	COD=846 mg/L	93 COD	Cellulose acetate (SS) $v=1.5$ m/s; P=2.76 MPa; T=25°C; a=0.0155 m ²	
NF	COD=500 mg/L BOD ₅ /COD=0.01	74/80 COD	Polyacrilonitrile/Polypropylene $v=3$ m/s; cut-off:450 Da; P=2 MPa; T=25°C; a=490 cm ²	Trebouet et al. [62]
RO	COD=1749 mg/L	96-98	Spiral wound $v=1.5$ m/s; P=20-53 bar; T=28°C	Bohdziewicz et al. [60]

In general, there is no technology that, acting alone, is able to treat effluents with such recalcitrant organic fraction and as high organic and inorganic load as in the leachate. The best solution is based on combined systems being able to achieve a cost/effective treatment technology. The treatment strategy is going to be dependent on the leachate quality and on the water discharge standards imposed by the local authorities.

1.3.5 Leachate treatment systems in Portugal

In Portugal, the main treatment systems used in the leachate treatment plants (LTP) are: i) activated sludge biological oxidation (ASBO) followed by physico-chemical treatment (in 25% of cases); and ii) ASBO or aerated lagoons, followed by reverse osmosis membranes (32% of cases). The most basic treatments consist in aerated or stabilization lagoons and represent 15% of the LTP. There are two cases (6%) wherein the polishing treatment, downstream from the biological treatment, consists in macrophytes beds. Table 1.7 presents the leachate treatment systems used in Portuguese LTP and the respective leachate final destination.

According to municipal waste management entities, in 19% of the 42 existing landfills the produced leachate is directly discharged into sewerage systems for full treatment in wastewater treatment plants. In other cases, the leachate is sent to the landfill's LTP, (i) either for pre-treatment, followed by final treatment at the municipal WWTP, situation that occurs in 47% of cases, (ii) or for complete treatment, followed by discharge into water bodies. According to data supplied by the same entities, in 2006, about one thousand millions of cubic meters of leachate were sent to LTP. An analysis aiming at evaluating the LTP's operation allowed to conclude that, in about 80% of existing landfills, the leachate treatment efficiencies obtained were lower than the initially predicted [63].

Results obtained from a study carried out by the IRAR demonstrated, in fact, an elevated inconstancy, both on the quality and on the quantity of the leachates fed to the evaluated LTP. It was also found that the removal efficiencies of BOD₅ and COD were lesser than expected, which does not allow the fulfilment of the emission limit values imposed by the legislation. This is due to the poor effluent biodegradability, whereby the resort to biochemical processes is not enough. In this study, reverse osmosis was the treatment technology that displayed the best results, especially when it was proceeded by biological processes [63]. In terms of cost-effectiveness, the best option is the use of biological technologies. However this kind of treatment is only fully suitable to young leachates, as these are quite biodegradable. For old leachates, it proved to be inefficient due to the presence of recalcitrant compounds, thus being required the use of an additional process at downstream [64].

Currently, in Portugal, the existing landfills are mostly recent and generate significant amounts of leachate. Given the current problematics of the leachate management, which is largely related to the lack of efficiency of the operating systems, and a society when environmental issues are increasingly pressing, the optimization of these treatment systems is essential to prevent the pollution of water bodies and soils.

Table 1.7. Leachate treatment plants (LTP) installed at the Portuguese sanitary landfills and final destination of the treated leachate [63].

Treatment system	LTP		Final destination
Aeration lagoon + Reverse osmosis	ALGAR	BARLAVENTO	Water bodies
		SOTAVENTO	
	REBAT		
	RESIDOURO		
RESIOESTE			
Anaerobic lagoon + Reverse osmosis	GESAMB		Water bodies
Activated sludge + Reverse osmosis	ECOBEIRÃO		Water bodies
	LIPOR		
	RAIA - PINHAL		
Physico-chemical treatment + Evaporation + Condensation + Activated sludge	RESÍDUOS DO NORDESTE		Water bodies
Stabilization lagoon + Aeration lagoon + Macrophytes beds	AMCAL		Water bodies
Aeration lagoon	AMBILITAL		Null discharge/ inoperable
	AMBISOUSA	PENAFIEL	
	VALNOR	ABRANTES	WWTP/inoperable
Stabilization lagoon	AMARSUL	PALMELA	WWTP
Aeration lagoon + Physico-chemical treatment	VALE DO DOURO NORTE		Water bodies/ inoperable
Aeration lagoon + Macrophytes beds	VALORLIS		WWTP
Activated sludge	AMTRES		WWTP
Activated sludge + Physico-chemical treatment	VALNOR	AVIS	WWTP
	AMBISOUSA	LUSTOSA	
	ERSUC	COIMBRA	
		AVEIRO	
	RESAT		
	SULDOURO		
	VALORMINHO		
	VALORSUL		
Physico-chemical treatment + Activated sludge	RESIURB		Water bodies/ inoperable
	RESULIMA		WWTP
Physico-chemical treatment + Filtration* + Activated sludge	BRAVAL		WWTP
Filtration* + Activated sludge + Physico-chemical treatment	RESIALENTEJO		WWTP
Aeration lagoon + Filtration* + Physico-chemical treatment	RESITEJO		Water bodies/ inoperable
Direct discharge into WWTP (without any treatment)	AMAVE	SANTO TIRSO	WWTP
	AMARSUL	GONÇA	
		SEIXAL	
ERSUC	FIGUEIRA DA FOZ		

*Sand filter with forced ventilation

1.4 Advanced oxidation processes

The elimination of persistent organic compounds (low biodegradability) is one of the most significant problems in the treatment of industrial wastewater and effluents from farms and household (containing pesticides, herbicides, fertilizers, detergents, etc.). The search for effective ways to remove these compounds is of general interest in order to comply with the discharge regulations and fundamentally enable the reuse of water.

The conventional wastewater treatments, based on various mechanical, biological, physical and chemical processes, presents limitations in their applicability, efficiency and costs. For instance, processes such as adsorption on activated carbon or air stripping, only allow the separation of contaminants, leading to their concentration in a solid matrix or their transference into the gas phase, respectively. Therefore, they are not an environmentally sustainable long-term solution. The incineration is capable of converting toxic compounds into carbon dioxide, water and inorganic acids, but a defective operation can cause the emission of not destroyed constituents and organic products of incomplete combustion, turning this waste disposal method a source of controversy.

Among the chemical oxidation technologies, the advanced oxidation processes (AOPs) have been recognized as highly efficient on treatment and biodegradability enhancement of different recalcitrant effluents, including textile [65-67], cork [68, 69], winery [70-73], pharmaceutical [74-76], paper mill [77] and wastewater from WWTP [78], olive mill wastewaters [79], pesticide-containing wastewaters [80, 81], leachates from sanitary landfills [11, 54, 82-89] and many others as report by Oller et al. [90]. AOPs have also shown effective results on the disinfection of drinking water contaminated with humic acids and microorganisms, such as *E. coli* [91], *E. faecalis* [92] and cyanobacteria [93].

The efficiency of these systems is based on the production of strong oxidizing species, e.g. hydroxyl radical (HO[•]), which can oxidize most of the organic molecules until complete mineralization. The hydroxyl radical has an oxidizing potential (+ 2.8 V) higher than other traditional oxidants (ozone, hydrogen peroxide, chlorine dioxide and chlorine), as can be seen in Table 1.8. Hydroxyl radicals are non-selective, so they are able to react with virtually all classes of organic and inorganic compounds, leading, as mentioned above, to their total mineralization or the formation of more biodegradable intermediates. This methodology can be applicable to a wide variety of natural matrices and the decontamination occurs by degradation of pollutants and not by a simple phase transfer [94].

Table 1.8. Oxidation potential of different species.

Oxidant agent	E° (V)
Fluorine	3.03 ^{a, c} , 3.06 ^b
Hydroxyl radical	2.80 ^{a, b, c}
Sulfate radical	2.60
Singlet Oxygen	2.42 ^{a, b, c}
Ozone	2.07 ^a , 2.08 ^b
Hydrogen peroxide	1.77 ^a , 1.78 ^b
Perhydroxyl radical	1.70 ^c
Permanganate	1.67 ^a
Chlorine dioxide	1.50 ^a , 1.27 ^b , 1.57 ^c
Hypochlorite	1.49 ^b
Chlorine	1.36 ^{a, b, c}
Molecular oxygen	1.23 ^b
Bromine	1.09 ^{a, c}
Iodine	0.54 ^a , 0.59 ^c

^aAl-Momani [95]; ^bTchobanoglous et al. [96]; ^cGernjak et al. [97].

Hydroxyl radical can be generated by different AOPs, which can be divided into photochemical processes, if in the presence of radiation, and non-photochemical processes, if no radiation is required [26], as described in Table 1.9. The mechanisms and characteristics of these processes have been described in detail in other studies regarding general and particular aspects of each method or combination thereof [53, 98-101].

Table 1.9. Typical AOPs [14, 26].

Non-photochemical	Photochemical
Ozonation (O ₃) at high pH (>8.5)	O ₃ /UV
O ₃ /H ₂ O ₂	H ₂ O ₂ /UV
Ozone/catalyst	O ₃ /H ₂ O ₂ /UV
Fenton (H ₂ O ₂ /Fe ²⁺)	Photo-Fenton
Electro-Fenton	Electro-Photo-Fenton
	TiO ₂ /UV
	TiO ₂ /H ₂ O ₂ /UV
	Photolysis

One of the biggest problems of the AOPs is the high cost associated with the reagents (e.g. H_2O_2) and energy consumption (UV radiation production). The reagents consumption can be reduced by using catalysts. With regard to energy consumption, this aspect can be overcome using solar radiation, with the advantages inherent in the use of a renewable energy source, clean and free of charge. Portugal is one of the European countries with greater availability of solar radiation (see Figure 1.8), both in terms of hours of sunshine, and in terms of annual global solar radiation. In Portugal, the annual average number of hours of sunshine varies between 2200 and 3000, while, for example, in Germany, ranges from 1200 to 1700 hours. At a time where sustainable development and, in particular, the use of renewable resources, focuses the attention of so many people, it is important to explore better this wealth.

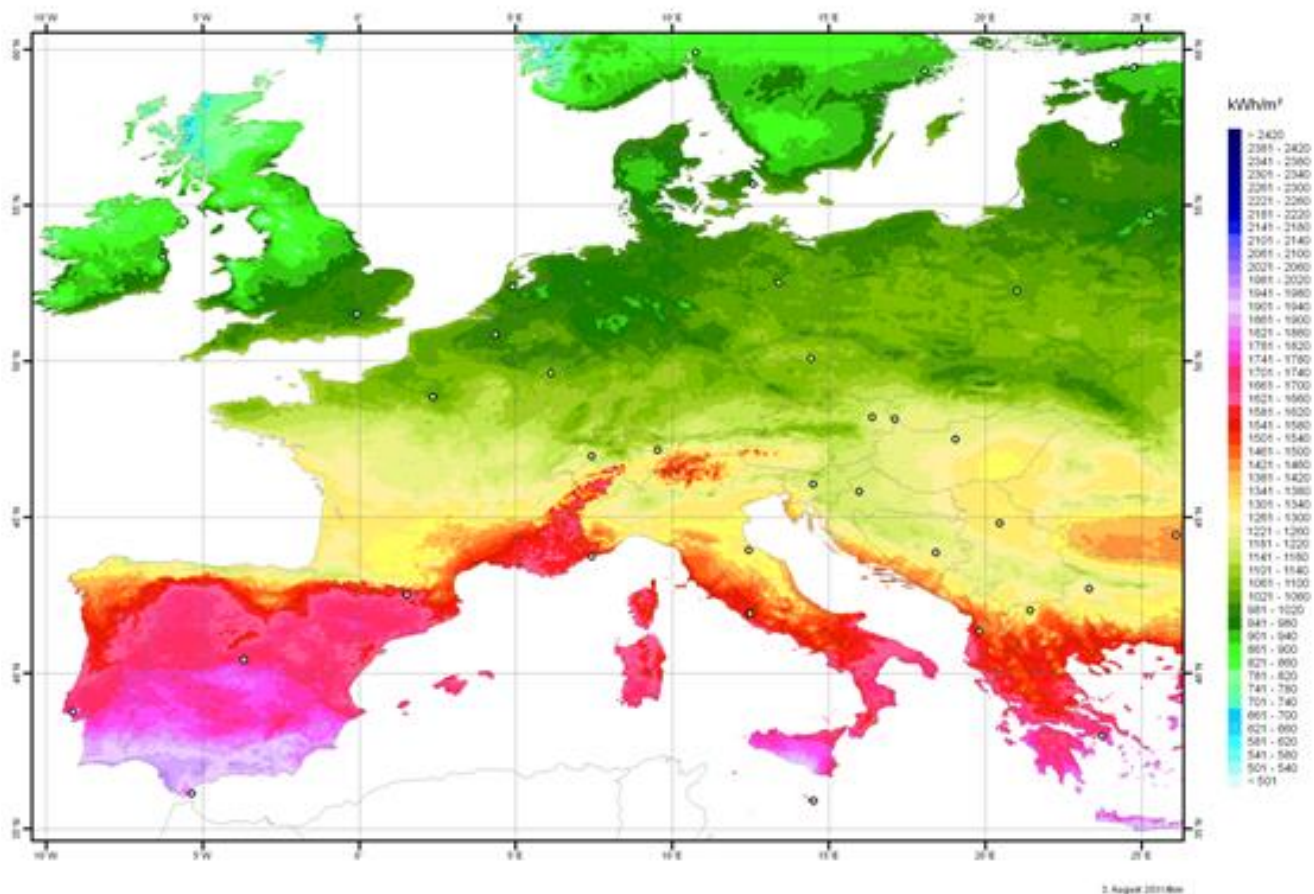


Table 1.10. Performance of the different AOPs on the landfill leachate treatment.

Process	Initial characterization	Removal (%)	Observations	Reference
O ₃	COD=1010 mg/L Colour=2300 units	57-81 COD 78-89 Colour	Air flow rate = 4 L/min O ₃ =1.5-2 g/h; t=240 min	Ntampou et al. [49]
O ₃	COD=5230 mg/L BOD ₅ /COD=0.1	27 COD BOD ₅ /COD=0.1	Air flow rate = 200 mL/min O ₃ =80 g/m ³ ; t=60 min	Tizaoui et al. [56]
O ₃ /H ₂ O ₂	pH=8.7	48 COD BOD ₅ /COD=0.7	H ₂ O ₂ =2 g/L	
O ₃ /UV	TOC = 430 mg/L	51-40 TOC	Air flow rate = 540-200 L/h O ₃ =100 g/m ³ ; t=250 min; P=300 W	
O ₃ /H ₂ O ₂ /UV		57 TOC	Air flow rate = 540 L/h O ₃ =100 g/m ³ ; t=250 min P=200-400W; H ₂ O ₂ =1 mL/min	Wenzel et al. [103]
H ₂ O ₂ /UV		42 TOC	Air flow rate = 540 L/h t=250 min; H ₂ O ₂ =1 mL/min	
H ₂ O ₂ /UV		23 DOC	Solar Radiation Q= 500 kJ/L; H ₂ O ₂ =1350 mM	
Fe ²⁺ /H ₂ O ₂ /UV	COD=3270-4575 mg/L DOC=954-1220 mg/L	86 DOC	pH=2.6-2.9; Q= 110 kJ/L; Fe ²⁺ =60 mg/L; H ₂ O ₂ =306 mM	Rocha et al. [55]
TiO ₂ /UV	BOD ₅ /COD=0.04-0.07	26 DOC	TiO ₂ =200 mg/L; Q=1019 kJ/L pH=5	
TiO ₂ /H ₂ O ₂ /UV		79 DOC	TiO ₂ =200 mg/L; Q= 111 kJ/L pH=4; H ₂ O ₂ =267 mM	
TiO ₂ /UV	COD=1260-1673 mg/L TOC=269-428 mg/L BOD ₅ =27-111 mg/L	80 COD 90 TOC	TiO ₂ =3000 mg/L; pH=4; I=21 W/cm ² ; t=12 h	Cho et al. [104]
Fe/H ₂ O ₂	COD=2072 mg/L TOC=769 mg/L	70 COD ~68 DOC	pH=2.5; T=25 °C; Fe ²⁺ =50 mM; H ₂ O ₂ =75 mM; t=60 min	Hermosilla et al. [11]
Fe/H ₂ O ₂ /UV	BOD ₅ /COD=0.17		pH=2.5; T=25 °C; V=4 L; t≈240 min; P=400 W; Fe ²⁺ =1.6 mM; H ₂ O ₂ =75 mM	
Fe ²⁺ /H ₂ O ₂	COD=3420 mg/L DOC=1045 mg/L	24 DOC	pH=2.8; T=17-35 °C; t=11 days; Fe ²⁺ =20 mg/L; H ₂ O ₂ =54 mM	Vilar et al. [105]
Fe ²⁺ /H ₂ O ₂ /UV	BOD ₅ /COD=0.07	86 DOC	Solar Radiation: Q= 206 kJ/L pH=2.8; T=15-43 °C; Fe ²⁺ =20 mg/L; H ₂ O ₂ =366 mM	
UV/H ₂ O ₂		-52 COD	I=1.4 W/cm ² ; H ₂ O ₂ =2000 mg/L; pH=3; t=20 min	
EC	COD=2350 mg/L	~20 COD	Current=2.0 A; pH=3; t=20 min	Altin [106]
EF	BOD ₅ /COD=0.39	~70 COD	H ₂ O ₂ =2000 mg/L; pH=3; Current=2.0 A; t=20 min	
PEF		~80 COD	I=1.4 W/cm ² ; H ₂ O ₂ =2000 mg/L; pH=3; Current=2.0 A; t=20 min	

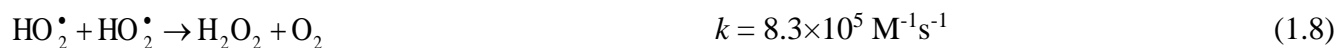
EC – electro-coagulation; EF – electro-Fenton; PEF – photo-electro-Fenton.

Considering all the AOPs, the photo-Fenton reaction seems to be the more adequate to the treatment of landfill leachate (Table 1.10). Specially, the solar-driven photo-Fenton process has been reported as the best option in terms of integrated environmental and economic point of view, taken into account its life-cycle greenhouse gas emission and life-cycle cost [107]. Results reported by Vilar et al. [105] and Rocha et al. [55] also showed that the solar photo-Fenton process can be selected as the best option for the pre-oxidation of mature leachates, after preliminary biological lagooning, promoting biodegradability's enhancement [88, 108, 109], which makes possible the combination with a further biological oxidation system.

In 1894, H.J.H. Fenton discovered that using a primary oxidant, such as hydrogen peroxide (H_2O_2), together with iron salts, as catalyst, many organic molecules could be oxidised. However, the application of Fenton's reagent as oxidation process for destruction of toxic organic compounds only began in 1960 [110, 111]. Two mechanisms were proposed to describe Fenton's reaction, the first one formulates a radical chain reaction (Haber-Weiss mechanism) and the second one an ionic mechanism (Kremer-Stein mechanism) [97]. In the mechanism generally accepted for Fenton reaction (Haber-Weiss mechanism), in acidic aqueous solutions, the Fe^{2+} is oxidised to Fe^{3+} by H_2O_2 , leading to the formation of HO^\bullet radicals (Eq. (1.2)) [112, 113].

Commonly, it is accepted, that in the absence of light, the origin of HO^\bullet radical is represented by the free radicals mechanism proposed by the Eqs. (1.2), (1.3), (1.4) and (1.6) [114]. The Fenton reaction is described by Eqs. (1.2) to (1.9), which represent the reactions of the Fe^{2+} , Fe^{3+} and H_2O_2 , in the absence of other ions and organic substances. In this conditions, the HO^\bullet radical formed can oxidize Fe^{2+} , according to Eq. (1.5) [97, 113]. The Eqs. (1.2), (1.3) and (1.6) establish a chain reaction, leading to continuous generation of HO^\bullet radicals and, as such, the continuous degradation of the organic contaminants [110].





The Fenton process consists of four steps, namely, oxidation reaction, neutralization, coagulation/flocculation and precipitation, being the organic substances removed during oxidation and coagulation processes [23, 54, 115].

The photo-Fenton reaction is just the Fenton reaction in the presence of UV-Vis radiation (wavelength < 580 nm). The radiation has a positive effect on the reaction rate by promoting the photo-reduction of ferric ions to ferrous ions, producing additional hydroxyl radicals. The regenerated Fe^{2+} ions react with H_2O_2 , generating more hydroxyl radicals. Thus, only low amounts of iron are needed for the treatment of wastewater by the photo-Fenton process [87, 94, 112, 116, 117].

The main species which absorb radiation are the ferric hydroxide complexes, $\text{Fe}(\text{OH})^{2+}$ and $\text{Fe}(\text{RCO}_2)^{2+}$, allowing the regeneration of Fe^{3+} into Fe^{2+} , followed by photo-induced ligand-to-metal charge-transfer (LMCT) [110, 117]. The intermediate complexes are dissociated according to Eq. (1.10), being the ligand capable of forming a complex with Fe^{3+} (OH^- , H_2O , HO_2^- , Cl^- , R-COO^- , R-OH , R-NH_2) [94].

Depending on the organic ligand, the Fe^{3+} complexes exhibit different behaviour as regards radiation absorption and the reaction (1.10) occurs with different quantum yields (photonic efficiency measure, defined as the number of moles of product formed or reagent consumed per number of moles of photons absorbed) and at different wavelengths (λ) [94, 116].



According to the organic ligand, the product can also be a radical OH^\bullet (Eq. (1.11)) or other radical derived from the ligand [94, 116].



The direct oxidation on an organic ligand is also possible, like shown in Eq. (1.12) for carboxylic acids [94], resulting in the abatement of total organic carbon concentration due to the decarboxylation of organic-acid intermediates [110, 117].



The organic radical (R^\bullet) reacts instantly with O_2 to produce a peroxy radical that subsequently initiates an oxidation reaction (Eq. (1.13)) [11, 118].



The main parameters affecting the efficiency of the photo-Fenton reaction are pH, initial concentrations of Fe^{2+} and H_2O_2 , temperature and irradiance. Table 1.11 only shows a brief description of the influence of these parameters on the photo-Fenton reaction. Further evaluation on this subject will be held in Chapter 7.

Table 1.11. Main photo-Fenton reaction parameters and their respective effect (updated from Pereira [119]).

Parameter	Influence or effect on reaction rates
pH	Controls the distribution of dissolved ferrous and ferric iron hydroxide species, which have different molar absorption coefficients. Optimal pH ~ 2.8 avoids precipitation and maximizes quantum yields.
Iron concentration	Increasing iron concentration increases reaction rates. Relation is not proportional and levels off due to attenuation of incident radiation. Optimization needs to consider reactor geometry and inner filter effects.
H_2O_2	Optimum H_2O_2 concentration must be found. Lower concentrations lead to a rate reduction of Fenton reaction, while higher ones lead to an unfavourable competition for HO^\bullet radicals.
Temperature	Increasing temperature customarily increases reaction rates, up to the point where hydrogen peroxide is inefficiently consumed and ferric ions precipitates.
Irradiance	Useful radiation absorption over the UV/Vis spectrum, especially in the presence of carboxylate anions. Excess radiation favours parallel occurrence of thermal reactions. Optimization of optical pathlength greatly reduces the amount of necessary photons.
Substrate concentration and characteristics	Higher concentrations require longer treatment times and are prone to cause inner filter effects. Released inorganic ions can interfere with the degradation process (e.g.: precipitation of iron by phosphate).

The applicability of this technology in the treatment of leachate does not presuppose the complete mineralization of the contaminants using hydroxyl radicals, but instead, it assumes the oxidation of recalcitrant compounds by photochemical processes, until achieving a biodegradability level compatible with a conventional biological oxidation system.

Bae et al. [120] published a work dealing with the treatment of mature landfill leachates by an integrated treatment system composed by (i) an anaerobic filter (AF) (35 °C); followed by a 2-stage activated sludge (AS) (25°C) reactor with recirculation to AF, (ii) a Fenton process (pH 3.5) and (iii) a post-AS reactor (25 °C). The overall system was able to completely remove 1400-1800 mg/L of ammonium nitrogen, leaving 200 mg/L of nitrate nitrogen. Also, 4000-7000 mg/L of COD in the raw leachate was reduced to 150-200 mg/L.

Vilar et al. [88] proposed the combination of a solar photo-Fenton (60 mg Fe²⁺/L) process with a biological nitrification-denitrification system for the decontamination of a stabilized landfill leachate, collected after aerobic lagooning, using photocatalytic (4.16 m² of Compound parabolic Collectors – CPCs) and biological (immobilized biomass reactor) systems. They achieved a COD lesser than 250 mg/L and a complete removal of nitrogen compounds from the photo-pre-treated leachate via biological nitrification-denitrification, after previous neutralization/sedimentation of iron sludge.

Cassano et al. [82] compared several combined/integrated biological AOPs setups for the treatment of a medium-age landfill leachate. Setups included a sequencing batch biofilter granular reactor (SBBGR), with or without ozone (O₃) enhancement, followed or not by solar photo-Fenton (SphF) polishing step. All treatment strategies demonstrated to be technically suitable to achieve the target COD values of 160 and 500 mg/L (disposal into water bodies and sewers, respectively) and the toxicity goals. However, for the target COD of 160 mg/L, the combination of SBBGR with SphF was economically more convenient.

De Torres-Sociás et al. [121] suggested a combined treatment line for a particular landfill leachate, containing a high organic load (40 g/L as COD and 15 g/L as DOC), consisting of a preliminary physico-chemical stage followed by a solar photo-Fenton process and a final conventional bio-treatment. The results revealed that this multistage treatment was effective on the reduction of the recalcitrant organic content after the conditioning step (17% DOC removal), requiring then a solar photo-treatment (1 mmol Fe²⁺/L) time of 11 hours to generate, after 27% mineralization, a non-toxic and biodegradable effluent.

The combination of photochemical and biological processes reduces the treatment time and the total cost, since the required solar collectors area can be significantly reduced. The most suitable conditions for the biological treatment are obtained when the phototreatment time is only enough to get a high efficiency in the biological treatment. Longer times of phototreatment only will oxidise biologically degradable substances, without any benefit.

1.5 Aim of the work and thesis outline

In the last decades the production of waste increased significantly due to excessive population growth and to the changing of their consumption habits. Landfilling is the most used final waste disposal method around the world. However, one of the environmental problems associated with the disposal of municipal waste in landfills is the generation of leachate, which is a wastewater characterized by high concentrations of organic and inorganic contaminants, including humic substances, ammonium nitrogen, heavy metals, xenobiotic compounds that need to be removed due to their toxicity and consequent impacts on the environment. Besides that, the leachates also present high variability in their quantity and quality, along the year, which makes the definition of an efficient treatment line for all situations very difficult.

Due to their cost-effectiveness, biological treatments are usually used to remove biodegradable organic compounds. These are effective in the treatment of leachate from young landfills but are ineffective in the treatment of stabilized leachate due to the presence of recalcitrant compounds, mainly humic substances. Its recalcitrant nature leads to the need for alternative technologies implementation to efficiently remove the organic load present in these effluents. AOPs are able to degrade a wide range of compounds from stabilized landfill leachates. Despite their high effectiveness, they become quite expensive if applied alone. Having in mind that the leachate presents high contents of nitrogen and recalcitrant organic matter and aiming at a significant reduction on the leachate treatment cost, the best strategy, for leachate remediation, seems to be the integration of biological and chemical oxidation processes.

The main objective of this thesis was to develop and optimize a multistage methodology for the treatment of mature landfill leachates, targeting mostly the discharge into water bodies, at comfortable costs. Regardless the multistage treatment system used, the treatment strategy always involved an activated sludge biological oxidation (ASBO) and a photo-Fenton (PF) reaction. Later, it was also incorporated a coagulation/sedimentation stage. All processes were tested at lab and pre-industrial scale units equipped with (i) a biological reactor prepared to work under aerobic and anoxic conditions, and (ii) a photoreactor equipped with compound parabolic collectors (CPCs) and/or UV-Vis lamps. In order to accomplish the main purpose, several partial objectives were addressed:

- i) Leachate characterization along all stages;
- ii) Assessment of the efficiency of each treatment stage, namely:
 - a. Biological reactor, under aerobic and anoxic conditions, and its dependence on the main nitrification and denitrification variables for nitrogen removal;

- b. Photo-Fenton reactor, considering the effect of the main reaction variables and the use of natural sunlight and/or artificial radiation;
 - c. Coagulation/sedimentation process, for different ferric ion concentration and pH values;
- iii) Evaluation of the efficiency of the combined treatments, concerning the leachate characteristics' variability, availability of solar radiation throughout the year, biodegradability enhancement during the photo-oxidation processes, iron reutilization in consecutive oxidation processes and different values of pH and settling times during coagulation;
- iv) Economic analysis of the phototreatment step, based on different tests conducted under different treatment strategies.

The present thesis is structured in 10 chapters:

Chapter 1 corresponds to the present introductory section, wherein the main questions associated with the production and remediation of mature leachates from urban sanitary landfills are identified, as well as current and potential decontamination methods, complemented with a briefly survey of current literature.

Chapter 2 presents a description of all chemical reagents and experimental setups used, as well as the experimental procedures and analytical methods employed.

In the Chapter 3, a strategy for the treatment of leachates from sanitary landfills after lagooning pretreatment, combining solar PF oxidation process with an ASBO, at a near industrial plant, is proposed. An extensive physico-chemical characterization of the leachate after lagooning was performed over 1-year. The efficiency of the combined treatment is evaluated taking into account the leachate characteristics' variability, availability of solar radiation throughout the year, and different process variables, such as the amount of hydrogen peroxide necessary to reach the required COD target value, biodegradability enhancement during the photo-oxidation process, iron reutilization in consecutive oxidation processes, removal of the acidic sludge resulting from the acidification process and leachate temperature/average solar power. The elimination of the remaining organic carbon fraction and nitrogen compounds after the pre-oxidation step is also assessed in an ASBO, under aerobic and anoxic conditions, considering the composition variability of the photo-treated leachate. Nitrification and denitrification reaction rates were also evaluated.

In the Chapter 4, the efficiency and performance of the (i) PF reaction, concerning sludge removal after acidification and the optimum phototreatment time to reach a biodegradable wastewater that can be further oxidized in a biological reactor and, (ii) ASBO process, calculating the nitrification and

denitrification reaction rates, alkalinity balance and methanol necessary as external carbon source, is evaluated using the plant presented in Chapter 3. Leachate biodegradability enhancement by means of a solar-driven PF process was quantified by direct biodegradability tests, as Zahn-Wellens method, and indirect measurements as the average oxidation state (AOS), low-molecular-weight carboxylic acids content (fast biodegradable character) and humic substances (recalcitrant character) concentration.

In Chapter 5 a multistage treatment system, at pre-industrial scale, is proposed for the treatment of a mature raw landfill leachate, including: (i) an ASBO, under aerobic and anoxic conditions; (ii) a solar PF process to enhance the bio-treated leachate biodegradability, with and without sludge removal after acidification; and (iii) a final polishing step, with further ASBO. The efficiency of the overall treatment process, as well as the efficiency of each treatment stage was assessed.

Chapter 6 presents the scale-up and cost analysis of a PF process, using solar and/or artificial radiation, for the treatment of 100 m³ per day of a sanitary landfill leachate previously oxidized in a biological system, taking into account the CPCs (compound parabolic collectors) area and land requirements for their installation and/or the number of UV lamps (with 4 kW and 20,000-h of lifetime each), considering (i) the average global UV irradiance and insolation, in the specific location of the sanitary landfill, and (ii) the amount of UV energy and H₂O₂ necessary for the PF reaction, in order to achieve target COD values of 1000 and 150 mg O₂/L, regarding the Portuguese regulations for discharges into sewerage systems and water bodies, respectively.

In the Chapter 7, it is reported the effect of the main PF reaction variables on the treatment of a sanitary landfill leachate collected at the outlet of a leachate treatment plant, which includes aerated lagooning followed by aerated activated sludge and a final coagulation-flocculation step. The PF experiments were performed in a lab-scale CPC photoreactor using artificial solar radiation and the photocatalytic reaction rate was determined while varying the total dissolved iron concentration, solution pH, operating temperature, type of acid used for acidification and UV irradiance. The role of ferric hydroxides, ferric sulphate and ferric chloride species, by taking advantage of ferric speciation diagrams, in the efficiency of the PF reaction when applied to leachate oxidation, is also assessed.

Chapter 8 discloses the effect of the main nitrification and denitrification variables on the nitrogen's biological removal via nitrite, from mature leachates, collected after aerobic lagooning, using a 1-L lab-scale batch reactor, equipped with a pH, temperature and dissolved oxygen (DO) control system, in order to determine the reaction kinetic constants at unchanging conditions. The nitrification reaction rate was evaluated while varying the operating temperature, DO concentration interval and solution pH. The denitrification kinetic constants and the methanol consumption were calculated for different values of

pH, temperature and amount of added phosphate, using the previously nitrified effluent. The characterization of the biological communities was also performed, by a 454-pyrosequencing analysis of the 16S rRNA gene.

In the Chapter 9 a new methodology for the treatment of landfill leachates, after aerobic lagooning, is studied, at a scale close to industrial, involving an aerobic biological pre-oxidation by activated sludge, a coagulation/sedimentation step and a photo-oxidation process (PF reaction), combining solar and artificial radiation. The efficiency of the overall treatment process, as well as the efficiency of each treatment stage was assessed. The scale-up and economic assessment of a PF process is also presented, assuming the treatment of 100 m³/day of a leachate previously oxidized in a biological and coagulation system, in order to achieve COD values below 1000 and 150 mg O₂/L, according to the Portuguese regulations for discharges into sewerage systems and water bodies, respectively.

Finally, Chapter 10 is dedicated to the final remarks, where the most relevant results and conclusions are reported and some suggestions for future work are proposed.

1.6 References

- [1] D. Hoornweg, P. Bhada-Tata, C. Kennedy, Environment: Waste production must peak this century, *Nature*, 502 (2013) 615-617.
- [2] IRAR, Gestão e tratamento de lixiviados produzidos em aterros sanitários de resíduos urbanos”, Instituto Regulador de Águas e Resíduos, Relatório IRAR nº3, 2008, pp. 3-43.
- [3] EUROSTAT (2015), Available at http://appsso.eurostat.ec.europa.eu/nui/show.do?dataset=env_wasmun&lang=en on 1st July 2015.
- [4] A.D. Read, P. Phillips, G. Robinson, Landfill as a future waste management option in England: the view of landfill operators, *Resources, conservation and recycling*, 20 (1997) 183-205.
- [5] EC (2008), Directive 2008/98/EC of the European Parliament and of the Council of 19 November 2008 on waste and repealing certain directives (Waste framework directive), *Official Journal of the European Union*, Available at <http://eur-lex.europa.eu/legal-content/EN/TXT/PDF/?uri=CELEX:32008L0098&from=EN> on 18th July 2015.
- [6] G. Martinho, F. Santana, J. Santos, A. Brandão, I. Santos, Gestão e tratamento de lixiviados produzidos em aterros sanitários de resíduos urbanos (Management and treatment of leachate from municipal solid waste sanitary landfills), in, DCEA/FCT/UNL. Relatório IRAR, 2008.
- [7] ERSAR, Relatório Anual do Sector de Águas e Resíduos em Portugal, in, Entidade Reguladora dos Serviços de Águas e Resíduos, 2010.
- [8] M.A.T. Russo, Avaliação dos processos de transformação de resíduos sólidos urbanos em aterro sanitário, in: *Civil Engineering*, Universidade do Minho, Braga, Portugal, 2006.
- [9] APA, Resíduos Urbanos em 2010, in, Agência Portuguesa do Ambiente, 2011.
- [10] J.Q. Levy, A.J. Cabeças, Resíduos sólidos urbanos – princípios e processos, AEPISA, Lisboa, 2006.
- [11] D. Hermosilla, M. Cortijo, C.P. Huang, Optimizing the treatment of landfill leachate by conventional Fenton and photo-Fenton processes, *Science of the Total Environment*, 407 (2009) 3473-3481.
- [12] G. Tchobanoglous, H. Theisen, S. Vigil, *Integrated solid waste management: engineering principles and management issues*, McGraw-Hill, New York, 1993.
- [13] S.R. Qasin, W. Chiang, *Sanitary landfill leachate – generation control and treatment*, Technomic Publishing Company, Inc. Lancaster, USA, 1994.
- [14] S. Renou, J. Givaudan, S. Poulain, F. Dirassouyan, P. Moulin, Landfill leachate treatment: Review and opportunity, *Journal of Hazardous materials*, 150 (2008) 468-493.
- [15] J. Lema, R. Mendez, R. Blazquez, Characteristics of landfill leachates and alternatives for their treatment: a review, *Water, Air, and Soil Pollution*, 40 (1988) 223-250.
- [16] T.A. Kurniawan, W.-h. Lo, G.Y. Chan, Physico-chemical treatments for removal of recalcitrant contaminants from landfill leachate, *Journal of Hazardous materials*, 129 (2006) 80-100.
- [17] P. Kjeldsen, M.A. Barlaz, A.P. Rooker, A. Baun, A. Ledin, T.H. Christensen, Present and Long-Term Composition of MSW Landfill Leachate: A Review, *Critical Reviews in Environmental Science and Technology*, 32 (2002) 297-336.

- [18] M.T.L. Santos, Contribuição para o estudo da digestão anaeróbia de resíduos orgânicos, Dissertação de Doutoramento, Faculdade de Ciências e Tecnologia, Universidade Nova de Lisboa, 2010.
- [19] P.R. O’Leary, G. Tchobanoglous, Landfilling, in: G. Tchobanoglous, F. Kreith (Eds.) Handbook of Solid Waste Management, McGraw-Hill, 2002.
- [20] T.H. Christensen, P. Kjeldsen, P.L. Bjerg, D.L. Jensen, J.B. Christensen, A. Baun, H.-J. Albrechtsen, G. Heron, Biogeochemistry of landfill leachate plumes, Applied Geochemistry, 16 (2001) 659-718.
- [21] O. Primo, M.J. Rivero, I. Ortiz, Photo-Fenton process as an efficient alternative to the treatment of landfill leachates, Journal of Hazardous materials, 153 (2008) 834-842.
- [22] K.Y. Foo, B.H. Hameed, An overview of landfill leachate treatment via activated carbon adsorption process, Journal of Hazardous materials, 171 (2009) 54-60.
- [23] W. Li, Q. Zhou, T. Hua, Removal of organic matter from landfill leachate by advanced oxidation processes: a review, International Journal of Chemical Engineering, 2010 (2010) 1-10.
- [24] J.L. De Morais, P.P. Zamora, Use of advanced oxidation processes to improve the biodegradability of mature landfill leachates, Journal of Hazardous materials, 123 (2005) 181-186.
- [25] A.A. Abbas, G. Jingsong, L.Z. Ping, P.Y. Ya, W.S. Al-Rekabi, Review on Landfill Leachate Treatments, Journal of Applied Sciences Research, 5 (2009) 534-545.
- [26] J. Wiszniowski, D. Robert, J. Surmacz-Gorska, K. Miksch, J. Weber, Landfill leachate treatment methods: A review, Environmental Chemistry Letters, 4 (2006) 51-61.
- [27] S.R. Qasim, W. Chiang, Sanitary landfill leachate: generation, control and treatment, CRC Press, 1994.
- [28] M.X. Loukidou, A.I. Zouboulis, Comparison of two biological treatment processes using attached-growth biomass for sanitary landfill leachate treatment, Environmental Pollution, 111 (2001) 273-281.
- [29] B. Rusten, B. Eikebrokk, Y. Ulgenes, E. Lygren, Design and operations of the Kaldnes moving bed biofilm reactors, Aquacultural engineering, 34 (2006) 322-331.
- [30] E. Engineering (2015), Trickling Filter – Classification and Mechanism, Engineering Articles, Available at <http://www.engineeringarticles.org/civil/environmental/trickling-filter-classification-and-mechanism/> on 15th August 2015.
- [31] M.N. Adlan, P. Palaniandy, H.A. Aziz, Optimization of coagulation and dissolved air flotation (DAF) treatment of semi-aerobic landfill leachate using response surface methodology (RSM), Desalination, 277 (2011) 74-82.
- [32] P. Palaniandy, M.N. Adlan, H.A. Aziz, M.F. Murshed, Application of dissolved air flotation (DAF) in semi-aerobic leachate treatment, Chemical Engineering Journal, 157 (2010) 316-322.
- [33] S.Q. Aziz, H.A. Aziz, M.J.K. Bashir, A. Mojiri, Municipal Landfill Leachate Treatment Techniques: An Overview, in: H.A. Aziz, A. Mojiri (Eds.) Wastewater Engineering: Advanced Wastewater Treatment Systems, 2014.
- [34] F.M. Ferraz, J. Povinelli, E. Pozzi, E.M. Vieira, J.C. Trofino, Co-treatment of landfill leachate and domestic wastewater using a submerged aerobic biofilter, Journal of Environmental Management, 141 (2014) 9-15.

- [35] U.E. Agency, Guidance for the Treatment of Landfill Leachate, Integrated Pollution Prevention and Control (IPPC), in, Sector Guidance Note IPPC S5.03, 2007.
- [36] G. Ruiz, D. Jeison, O. Rubilar, G. Ciudad, R. Chamy, Nitrification–denitrification via nitrite accumulation for nitrogen removal from wastewaters, *Bioresource Technology*, 97 (2006) 330-335.
- [37] T.H. Hoilijoki, R.H. Kettunen, J.A. Rintala, Nitrification of anaerobically pretreated municipal landfill leachate at low temperature, *Water Research*, 34 (2000) 1435-1446.
- [38] J.-h. Im, H.-j. Woo, M.-w. Choi, K.-b. Han, C.-w. Kim, Simultaneous organic and nitrogen removal from municipal landfill leachate using an anaerobic-aerobic system, *Water Research*, 35 (2001) 2403-2410.
- [39] R.H. Kettunen, T.H. Hoilijoki, J.A. Rintala, Anaerobic and sequential anaerobic-aerobic treatments of municipal landfill leachate at low temperatures, *Bioresource Technology*, 58 (1996) 31-40.
- [40] D. Kulikowska, E. Klimiuk, Removal of organics and nitrogen from municipal landfill leachate in two-stage SBR reactors, *Polish Journal of Environmental Studies*, 13 (2004) 389-396.
- [41] A. Spagni, M.C. Lavagnolo, C. Scarpa, P. Vendrame, A. Rizzo, L. Luccarini, Nitrogen removal optimization in a sequencing batch reactor treating sanitary landfill leachate, *Journal of Environmental Science and Health Part A*, 42 (2007) 757-765.
- [42] A. Spagni, S. Marsili-Libelli, Nitrogen removal via nitrite in a sequencing batch reactor treating sanitary landfill leachate, *Bioresource Technology*, 100 (2009) 609-614.
- [43] H. Sun, Y. Peng, X. Shi, Advanced treatment of landfill leachate using anaerobic–aerobic process: Organic removal by simultaneous denitrification and methanogenesis and nitrogen removal via nitrite, *Bioresource Technology*, 177 (2015) 337-345.
- [44] I. Trabelsi, I. Sellami, T. Dhifallah, K. Medhioub, L. Bousselmi, A. Ghrabi, Coupling of anoxic and aerobic biological treatment of landfill leachate, *Desalination*, 246 (2009) 506-513.
- [45] U. Welander, T. Henrysson, T. Welander, Nitrification of landfill leachate using suspended-carrier biofilm technology, *Water Research*, 31 (1997) 2351-2355.
- [46] S.K. Marttinen, R.H. Kettunen, K.M. Sormunen, R.M. Soimasuo, J.A. Rintala, Screening of physical–chemical methods for removal of organic material, nitrogen and toxicity from low strength landfill leachates, *Chemosphere*, 46 (2002) 851-858.
- [47] A. Amokrane, C. Comel, J. Veron, Landfill leachates pretreatment by coagulation-flocculation, *Water Research*, 31 (1997) 2775-2782.
- [48] A.A. Tatsi, A.I. Zouboulis, K.A. Matis, P. Samaras, Coagulation–flocculation pretreatment of sanitary landfill leachates, *Chemosphere*, 53 (2003) 737-744.
- [49] X. Ntampou, A.I. Zouboulis, P. Samaras, Appropriate combination of physico-chemical methods (coagulation/flocculation and ozonation) for the efficient treatment of landfill leachates, *Chemosphere*, 62 (2006) 722-730.
- [50] I. Ozturk, M. Altinbas, I. Koyuncu, O. Arikan, C. Gomec-Yangin, Advanced physico-chemical treatment experiences on young municipal landfill leachates, *Waste Management*, 23 (2003) 441-446.

- [51] H. Huang, D. Xiao, Q. Zhang, L. Ding, Removal of ammonia from landfill leachate by struvite precipitation with the use of low-cost phosphate and magnesium sources, *Journal of Environmental Management*, 145 (2014) 191-198.
- [52] M. Pirbazari, V. Ravindran, B.N. Badriyha, S.-H. Kim, Hybrid membrane filtration process for leachate treatment, *Water Research*, 30 (1996) 2691-2706.
- [53] T.A. Kurniawan, W.-h. Lo, G.Y.S. Chan, Radicals-catalyzed oxidation reactions for degradation of recalcitrant compounds from landfill leachate, *Chemical Engineering Journal*, 125 (2006) 35-57.
- [54] M. Umar, H.A. Aziz, M.S. Yusoff, Trends in the use of Fenton, electro-Fenton and photo-Fenton for the treatment of landfill leachate, *Waste Management*, 30 (2010) 2113-2121.
- [55] E.M.R. Rocha, V.J.P. Vilar, A. Fonseca, I. Saraiva, R.A.R. Boaventura, Landfill leachate treatment by solar-driven AOPs, *Solar Energy*, 85 (2011) 46-56.
- [56] C. Tizaoui, L. Bouselmi, L. Mansouri, A. Ghrabi, Landfill leachate treatment with ozone and ozone/hydrogen peroxide systems, *Journal of Hazardous materials*, 140 (2007) 316-324.
- [57] U.E. Agency, Guidance for the Treatment of Landfill Leachate, Sector Guidance Note IPPC S5.03, in: I.P.P.a.C. (IPPC) (Ed.), 2007.
- [58] J. Yoon, S. Cho, Y. Cho, S. Kim, The characteristics of coagulation of fenton reaction in the removal of landfill leachate organics, *Water Science and Technology*, 38 (1998) 209-214.
- [59] Metcalf, Eddy, *Wastewater Engineering Treatment and Reuse*, 4th ed., Metcalf & Eddy, 2005.
- [60] J. Bohdziewicz, M. Bodzek, J. Górska, Application of pressure-driven membrane techniques to biological treatment of landfill leachate, *Process Biochemistry*, 36 (2001) 641-646.
- [61] W. Piatkiewicz, E. Biemacka, T. Suchecka, A polish study: treating landfill leachate with membranes, *Filtration & separation*, 38 (2001) 22-23.
- [62] D. Trebouet, J.P. Schlumpf, P. Jaouen, F. Quemeneur, Stabilized landfill leachate treatment by combined physicochemical-nanofiltration processes, *Water Research*, 35 (2001) 2935-2942.
- [63] IRAR, Gestão e tratamento de lixiviados produzidos em aterros sanitários de resíduos urbanos, Relatório IRAR nº 03/2008, Lisboa, 2008.
- [64] E.S.K. Chian, F.B. DeWalle, Sanitary landfill leachate and their treatment, *Journal of the Environmental Engineering Division* 2(1976) 411-431.
- [65] P. Hörsch, A. Speck, F.H. Frimmel, Combined advanced oxidation and biodegradation of industrial effluents from the production of stilbene-based fluorescent whitening agents, *Water Research*, 37 (2003) 2748-2756.
- [66] V.J.P. Vilar, L.X. Pinho, A.M.A. Pintor, R.A.R. Boaventura, Treatment of textile wastewaters by solar-driven advanced oxidation processes, *Solar Energy*, 85 (2011) 1927-1934.
- [67] P.A. Soares, T.F.C.V. Silva, D.R. Manenti, S.M.A.G.U. Souza, R.A.R. Boaventura, V.J.P. Vilar, Insights into real cotton-textile dyeing wastewater treatment using solar advanced oxidation processes, *Environmental Science and Pollution Research*, 21 (2014) 932-945.
- [68] V.J.P. Vilar, M.I. Maldonado, I. Oller, S. Malato, R.A.R. Boaventura, Solar treatment of cork boiling and bleaching wastewaters in a pilot plant, *Water Research*, 43 (2009) 4050-4062.

- [69] A.M.A. Pintor, V.J.P. Vilar, R.A.R. Boaventura, Decontamination of cork wastewaters by solar-photo-Fenton process using cork bleaching wastewater as H₂O₂ source, *Solar Energy*, 85 (2011) 579-587.
- [70] F.J. Benitez, J.B.d. Heredia, F.J. Real, J.L. Acero, Purification kinetics of winery wastes by ozonation, anaerobic digestion and ozonation plus anaerobic digestion, *Journal of Environmental Science and Health*, A34 (1999) 2023-2041.
- [71] J.B. de Heredia, J. Torregrosa, J. Dominguez, E. Partido, Degradation of wine distillery wastewaters by the combination of aerobic biological treatment with chemical oxidation by Fenton's reagent, *Sustainable Viticulture and Winery Wastes Management*, 51 (2005) 167-174.
- [72] R. Mosteo, J. Sarasa, M.P. Ormad, J. Ovelleiro, Sequential solar photo-Fenton-biological system for the treatment of winery wastewaters, *Journal of Agricultural and Food Chemistry*, 56 (2008) 7333-7338.
- [73] B.S. Souza, F.C. Moreira, M.W. Dezotti, V.J. Vilar, R.A. Boaventura, Application of biological oxidation and solar driven advanced oxidation processes to remediation of winery wastewater, *Catalysis Today*, 209 (2013) 201-208.
- [74] C. Sirtori, A. Zapata, I. Oller, W. Gernjak, A. Agüera, S. Malato, Decontamination industrial pharmaceutical wastewater by combining solar photo-Fenton and biological treatment, *Water Research*, 43 (2009) 661-668.
- [75] J.H. Pereira, M.T. Borges, O. González, S. Esplugas, V.J.P. Vilar, R.A.R. Boaventura, Photocatalytic degradation of oxytetracycline using TiO₂ under natural and simulated solar radiation, *Chemosphere*, submitted (2011).
- [76] J.H.O.S. Pereira, A.C. Reis, V. Homem, J.A. Silva, A. Alves, M.T. Borges, R.A.R. Boaventura, V.J.P. Vilar, O.C. Nunes, Solar photocatalytic oxidation of recalcitrant natural metabolic by-products of amoxicillin biodegradation, *Water Research*, 65 (2014) 307-320.
- [77] A.M. Amat, A. Arques, F. Lopez, M.A. Miranda, Solar photo-catalysis to remove paper mill wastewater pollutants, *Solar Energy*, 79 (2005) 393-401.
- [78] V.J.P. Vilar, A.I.E. Gomes, R.A.R. Boaventura, Solar Detoxification of a Recalcitrant Colour Real Effluent from a Wastewater Treatment Plant, *Photochemical & Photobiological Sciences*, 8 (2009) 691-698.
- [79] J. Beltrán-Heredia, J. Torregrosa, J. García, J. Domínguez, J. Tierno, Degradation of olive mill wastewater by the combination of Fenton's reagent and ozonation processes with an aerobic biological treatment, *Water Science & Technology*, 44 (2001) 103-108.
- [80] A. Zapata, S. Malato, J.A. Sánchez-Pérez, I. Oller, M.I. Maldonado, Scale-up strategy for a combined solar photo-Fenton/biological system for remediation of pesticide-contaminated water, *Catalysis Today*, 151 (2010) 100-106.
- [81] V.J.P. Vilar, F.C. Moreira, A.C.C. Ferreira, M.A. Sousa, C. Gonçalves, M.F. Alpendurada, R.A.R. Boaventura, Biodegradability enhancement of a pesticide-containing bio-treated wastewater using a solar photo-Fenton treatment step followed by a biological oxidation process, *Water Research*, 46 (2012) 4599-4613.

- [82] D. Cassano, A. Zapata, G. Brunetti, G. Del Moro, C. Di Iaconi, I. Oller, S. Malato, G. Mascolo, Comparison of several combined/integrated biological-AOPs setups for the treatment of municipal landfill leachate: Minimization of operating costs and effluent toxicity, *Chemical Engineering Journal*, 172 (2011) 250-257.
- [83] S. Cortez, P. Teixeira, R. Oliveira, M. Mota, Evaluation of Fenton and ozone-based advanced oxidation processes as mature landfill leachate pre-treatments, *Journal of Environmental Management*, 92 (2011) 749-755.
- [84] P.-J. He, Z. Zheng, H. Zhang, L.-M. Shao, Q.-Y. Tang, PAEs and BPA removal in landfill leachate with Fenton process and its relationship with leachate DOM composition, *Science of the Total Environment*, 407 (2009) 4928-4933.
- [85] J.J. Wu, C.-C. Wu, H.-W. Ma, C.-C. Chang, Treatment of landfill leachate by ozone-based advanced oxidation processes, *Chemosphere*, 54 (2004) 997-1003.
- [86] J. Blanco-Galvez, P. Fernández-Ibáñez, S. Malato-Rodríguez, Solar Photocatalytic Detoxification and Disinfection of Water: Recent Overview, *Journal of Solar Energy Engineering*, 129 (2007) 4-15.
- [87] S. Malato, J. Blanco, D.C. Alarcon, M.I. Maldonado, P. Fernandez-Ibanez, W. Gernjak, Photocatalytic decontamination and disinfection of water with solar collectors, *Catalysis Today*, 122 (2007) 137-149.
- [88] V.J.P. Vilar, E.M.R. Rocha, F.S. Mota, A. Fonseca, I. Saraiva, R.A.R. Boaventura, Treatment of a sanitary landfill leachate using combined solar photo-Fenton and biological immobilized biomass reactor at a pilot scale, *Water Research*, 45 (2011) 2647-2658.
- [89] M. Vedrenne, R. Vasquez-Medrano, D. Prato-Garcia, B.A. Frontana-Uribe, J.G. Ibanez, Characterization and detoxification of a mature landfill leachate using a combined coagulation–flocculation/photo Fenton treatment, *Journal of Hazardous materials*, 205–206 (2012) 208-215.
- [90] I. Oller, S. Malato, J. Sánchez-Pérez, Combination of advanced oxidation processes and biological treatments for wastewater decontamination—a review, *Science of the Total Environment*, 409 (2011) 4141-4166.
- [91] A.I. Gomes, J.C. Santos, V.J.P. Vilar, R.A.R. Boaventura, Inactivation of Bacteria *E. coli* and photodegradation of humic acids using natural sunlight, *Applied Catalysis B: Environmental*, 88 (2009) 283-291.
- [92] A.I. Gomes, V.J.P. Vilar, R.A.R. Boaventura, Inactivation Kinetics of *E. coli* and *E. faecalis* in Distilled and Natural Waters by Solar Photocatalysis, in: 5th European Meeting on Solar Chemistry and Photocatalysis: Environmental Applications (SPEA 5), Sicilia - 4-8 October, 2008.
- [93] L. Pinho, X., J. Azevedo, V. Vasconcelos, M., V. Vilar, J. P., R.A.R. Boaventura, Decomposition of *Microcystis aeruginosa* and Microcystin-LR by TiO₂ Oxidation Using Artificial UV Light or Natural Sunlight, *Journal of Advanced Oxidation Technologies*, 15 (2012) 98-106.
- [94] S. Malato, P. Fernández-Ibáñez, M.I. Maldonado, J. Blanco, W. Gernjak, Decontamination and disinfection of water by solar photocatalysis: Recent overview and trends, *Catalysis Today*, 147 (2009) 1-59.
- [95] F. Al-Momani, Combination of photo-oxidation processes with biological treatment, *Universitat de Barcelona*, 2003.

- [96] G. Tchobanoglous, F.L. Burton, H.D. Stensel, Wastewater engineering: treatment and reuse. Metcalf & Eddy, Inc., McGraw-Hill, New York, (2003).
- [97] W. Gernjak, M.I. Maldonado, M. Fuerhacker, S. Malato, Solar photo-Fenton treatment of EU priority substances: Process parameters and control strategies, Editorial CIEMAT, 2006.
- [98] J.M. Poyatos, M. Muñoio, M. Almecija, J. Torres, E. Hontoria, F. Osorio, Advanced oxidation processes for wastewater treatment: state of the art, *Water, Air, and Soil Pollution*, 205 (2010) 187-204.
- [99] S. Malato, J. Blanco, A. Vidal, D. Alarcón, M.I. Maldonado, J. Cáceres, W. Gernjak, Applied studies in solar photocatalytic detoxification: an overview, *Solar Energy*, 75 (2003) 329-336.
- [100] J.J. Pignatello, E. Oliveros, A. MacKay, Advanced oxidation processes for organic contaminant destruction based on the fenton reaction and related chemistry, *Critical Reviews in Environmental Science and Technology*, 36 (2006) 1-84.
- [101] R. Andreozzi, V. Caprio, A. Insola, R. Marotta, Advanced oxidation processes (AOP) for water purification and recovery, *Catalysis Today*, 53 (1999) 51-59.
- [102] Meteonorm (2011), Available at <http://meteonorm.com/download/maps/> on 1st April 2012.
- [103] A. Wenzel, A. Gahr, R. Niessner, TOC-removal and degradation of pollutants in leachate using a thin-film photoreactor, *Water Research*, 33 (1999) 937-946.
- [104] S.P. Cho, S.C. Hong, S.-I. Hong, Photocatalytic degradation of the landfill leachate containing refractory matters and nitrogen compounds, *Applied Catalysis B: Environmental*, 39 (2002) 125-133.
- [105] V.J.P. Vilar, J.M.S. Moreira, A. Fonseca, I. Saraiva, R.A.R. Boaventura, Application of Fenton and Solar Photo-Fenton Processes to the Treatment of a Sanitary Landfill Leachate in a Pilot Plant with CPCs, *Journal of Advanced Oxidation Technologies*, 15 (2012) 107-116.
- [106] A. Altin, An alternative type of photoelectro-Fenton process for the treatment of landfill leachate, *Separation and Purification Technology*, 61 (2008) 391-397.
- [107] I. Muñoz, S. Malato, A. Rodríguez, X. Doménech, Integration of Environmental and Economic Performance of Processes. Case Study on Advanced Oxidation Processes for Wastewater Treatment, *Journal of Advanced Oxidation Technologies*, 11 (2008) 270-275.
- [108] V.J.P. Vilar, S.M.S. Capelo, T.F.C.V. Silva, R.A.R. Boaventura, Solar photo-Fenton as a pre-oxidation step for biological treatment of landfill leachate in a pilot plant with CPCs, *Catalysis Today*, 161 (2011) 228-234.
- [109] J.L. de Morais, P.P. Zamora, Use of advanced oxidation processes to improve the biodegradability of mature landfill leachates, *Journal of Hazardous materials*, 123 (2005) 181-186.
- [110] G. Sagawe, A. Lehnard, M. Lübber, D. Bahnemann, The insulated solar Fenton hybrid process: fundamental investigations, *Helvetica Chimica Acta*, 84 (2001) 3742-3759.
- [111] H. Zhang, H.J. Choi, C.-P. Huang, Optimization of Fenton process for the treatment of landfill leachate, *Journal of Hazardous materials*, 125 (2005) 166-174.

-
- [112] F. Torrades, J. García-Montaño, J. Antonio García-Hortal, X. Domènech, J. Peral, Decolorization and mineralization of commercial reactive dyes under solar light assisted photo-Fenton conditions, *Solar Energy*, 77 (2004) 573-581.
- [113] R.F.P. Nogueira, A.G.Trovó, M.R.A. Silva, R.D. Villa, C. Oliveira, Fundamentos e aplicações ambientais dos processos Fenton e foto-Fenton, *Quimica Nova*, 30 (2007) 400-408.
- [114] J.J. Pignatello, D. Liu, P. Huston, Evidence for an additional oxidant in the photoassisted Fenton reaction, *Environmental Science & Technology*, 33 (1999) 1832-1839.
- [115] Y. Deng, Physical and oxidative removal of organics during Fenton treatment of mature municipal landfill leachate, *Journal of Hazardous materials*, 146 (2007) 334-340.
- [116] W. Gernjak, M. Fuerhacker, P. Fernandez-Ibanez, J. Blanco, S. Malato, Solar photo-Fenton treatment- Process parameters and process control, *Applied Catalysis B: Environmental*, 64 (2006) 121-130.
- [117] M. Rodríguez, S. Malato, C. Pulgarin, S. Contreras, D. Curcó, J. Giménez, S. Esplugas, Optimizing the solar photo-Fenton process in the treatment of contaminated water. Determination of intrinsic kinetic constants for scale-up, *Solar Energy*, 79 (2005) 360-368.
- [118] S.M. Kim, A. Vogelpohl, Degradation of Organic Pollutants by the Photo-Fenton-Process, *Chemical engineering & technology*, 21 (1998) 187-191.
- [119] J.H.O.S. Pereira, Solar Photocatalytic Degradation of Antibiotics: Chemical, Ecotoxicological and Biodegradability Assessment, in: Department of Chemical Engineering, University of Porto, Faculty of Engineering, 2014.
- [120] B. Bae, E. Jung, Y. Kim, H. Shin, Treatment of landfill leachate using activated sludge process and electron-beam radiation, *Water Research*, 33 (1999) 2669-2673.
- [121] E. De Torres-Socías, L. Prieto-Rodríguez, A. Zapata, I. Fernández-Calderero, I. Oller, S. Malato, Detailed treatment line for a specific landfill leachate remediation. Brief economic assessment, *Chemical Engineering Journal*, 261 (2015) 60-66.

2 Materials and methods

This chapter presents a detailed description of all chemical reagents and experimental setups used throughout this thesis, as well as of the experimental procedures implemented to meet the proposed objectives. A brief description of the employed analytical methods is also given.

The experimental work was mostly developed in a Municipal Solid Waste Sanitary Landfill located in northern Portugal, and also in the Laboratory of Separation and Reaction Engineering (LSRE), at the Department of Chemical Engineering (DEQ), Faculty of Engineering University of Porto (FEUP).

2.1 Chemicals

Photo-Fenton experiments were performed using hydrogen peroxide, iron (II) sulphate heptahydrate ($\text{FeSO}_4 \cdot 7\text{H}_2\text{O}$), as iron source, and sulphuric acid, hydrochloric acid and sodium hydroxide for pH adjustments.

Coagulation tests were accomplished by employing ferric chloride and sulphuric acid.

In the activated sludge biological reactor, sodium hydroxide and sulphuric acid were also used for pH control, and methanol was added as an external carbon source in the denitrification stage.

Ultrapure and pure water were produced by a Millipore system (Direct-Q model) and a reverse osmosis system (Panice[®]), respectively.

Table 2.1 shows a brief description of all reagents employed in the different reactions and analytical methods. All the chemicals used in the analytical methods were analytical grade.

Table 2.1. Chemicals description.

Reagent	MF ^a	% w/w	ρ^b (kg/L)	MW ^c (g/mol)	Supplier	Purpose
Ferrous sulphate heptahydrate	$\text{FeSO}_4 \cdot 7\text{H}_2\text{O}$	-	-	278.05	Quimitécnica	Photo-Fenton tests at pre-industrial scale (PIS)
Hydrochloric acid	HCl	33	1.16	36.46		
Hydrogen peroxide	H_2O_2	25; 50 ^d	1.10	34.02		
Sodium hydroxide	NaOH	30	1.33	40.00		
Sulphuric acid	H_2SO_4	98	1.84	98.08		
Sodium hydroxide	NaOH	30	1.33	40.00	Quimitécnica	Biological treatment at PIS
Methanol	CH_3OH	-	0.79	32.04		
Sulphuric acid	H_2SO_4	98	1.84	98.08		
Ferric chloride	FeCl_3	40	1.44	162.20	Quimitécnica	Coagulation process at PIS
Sulphuric acid	H_2SO_4	98	1.84	98.08		
Ferrous sulphate heptahydrate	$\text{FeSO}_4 \cdot 7\text{H}_2\text{O}$	-	-	278.05	Panreac	Photo-Fenton tests at lab-scale
Hydrochloric acid	HCl	37	1.16	36.46	Merck	
Hydrogen peroxide	H_2O_2	50 ^d	1.10	34.02	Quimitécnica	
Sodium hydroxide	NaOH	-	-	40.00	Merck	
Sulphuric acid	H_2SO_4	96	1.84	98.08	Pronalab	
Ammonium monovanadate	NH_4VO_3	-	-	116.97	Merck	Hydrogen peroxide analysis
Sulphuric acid	H_2SO_4	96	1.84	98.08	Pronalab	
1,10-phenanthroline 1-hydrate	$\text{C}_{12}\text{H}_8\text{N}_2 \cdot \text{H}_2\text{O}$	-	-	198.23	Panreac	Iron analysis
Acetic acid	CH_3COOH	100	1.05	60.05	Fisher	
Ammonium acetate	$\text{NH}_4\text{C}_2\text{H}_3\text{O}_2$	-	-	77.08	Fisher	
L-ascorbic acid	$\text{C}_6\text{H}_8\text{O}_6$	-	-	176.12	Acrós	

Table 2.1. Chemicals description.

Reagent	MF ^a	% w/w	ρ^b (kg/L)	MW ^c (g/mol)	Supplier	Purpose
Caffeic Acid (SS ^e)	C ₉ H ₈ O ₄	-	-	180.16	Merck	Polyphenols analysis
Folin-Ciocalteu's Reagent DC	-	-	1.23	-	Panreac	
Sodium carbonate	Na ₂ CO ₃	-	-	105.99	Merck	
Potassium hydrogen phthalate (TDC SS ^e)	C ₈ H ₅ KO ₄	-	-	204.22	ISAZA	Standard solutions (SS) for TC-TOC-TN analyser calibration
Hydrogen carbonate (TIC SS ^e)	HCO ₃ ⁻	-	-	61.02		
Sodium carbonate (TIC SS ^e)	Na ₂ CO ₃	-	-	105.99		
Potassium nitrate (TDN SS ^e)	KNO ₃	-	-	101.10		
Chloride, nitrate and sulphate SS ^e	NaCl	1000 ^f	1.00	58.44	Merck	SS for anions calibration in ionic chromatography and respective eluent
	NaNO ₃			84.99		
	Na ₂ SO ₄			142.04		
Fluoride, phosphate and bromide SS ^e	NaF	1000 ^g	1.00	41.99		
	KH ₂ PO ₄			136.09		
	NaBr			102.89		
Nitrite SS ^e	NaNO ₂	999 ^h	1.00	68.98		
Sodium hydroxide	NaOH	1.000 ⁱ	1.04	40.00		
Acetate SS ^e	C ₂ H ₄ O ₂		1.00	60.05	Fluka	SS for low molecular weight carboxylate anions calibration in ionic chromatography and respective eluent
Citrate SS ^e	C ₆ H ₈ O ₇		1.00	192.12		
Formate SS ^e	CH ₂ O ₂		1.00	46.13		
Malonate SS ^e	C ₃ H ₄ O ₄	1000 ^k	1.00	104.06		
Oxalate SS ^e	C ₂ H ₂ O ₄		1.00	90.03		
Phthalate SS ^e	C ₈ H ₆ O ₄		1.00	166.13		
Propionate SS ^e	C ₃ H ₆ O ₂		1.00	74.08		
L(-)-malic acid (maleate SS ^e)	C ₄ H ₆ O ₅	-	-	134.09	Acrós	
Pyruvic acid (pyruvate SS ^e)	C ₃ H ₄ O ₃	98	1.27	88.06	Aldrich	
Valeric acid (valerate SS ^e)	C ₅ H ₁₀ O ₂	≥99	0.94	102.13		
Potassium hydroxide (eluent generator cartridge)	KOH	22.4	1.21	56.11	Dionex	
Ammonium SS ^e	NH ₄ Cl		1.00	53.49	Merck	SS for cations calibration in ionic chromatography and respective eluent
Calcium SS ^e	CaCl ₂		1.00	110.98		
Magnesium SS ^e	MgCl ₂ .6H ₂ O	1000 ^j	1.00	203.31		
Potassium SS ^e	KCl		1.00	74.55		
Sodium SS ^e	NaCl		1.00	58.44		
Lithium SS ^e	LiCl	-	-	42.39		
Methanesulfonic acid	CH ₃ SO ₃ H	≥99	1.48	96.11		
Potassium dichromate	K ₂ Cr ₂ O ₇	-	-	294.19	Merck	Chemical oxygen demand analysis
Potassium hydrogen phthalate (COD SS ^e)	C ₈ H ₅ KO ₄	-	-	204.22	Merck	
Silver sulphate	Ag ₂ SO ₄	-	-	311.80	Merck	
Sulphuric acid	H ₂ SO ₄	96	1.84	98.08	Pronalab	

Table 2.1. Chemicals description.

Reagent	MF ^a	% w/w	ρ^b (kg/L)	MW ^c (g/mol)	Supplier	Purpose
Ammonium chloride	NH ₄ Cl	-	-	53.49	VWR	
Calcium chloride dihydrate	CaCl ₂ .2H ₂ O	-	-	147.02	VWR	
Dipotassium hydrogen phosphate	K ₂ HPO ₄	-	-	174.20	Merck	
Disodium hydrogen phosphate dihydrate	Na ₂ HPO ₄ .2H ₂ O	-	-	178.00	Merck	Mineral medium for Zahn-Wellens and BOD ₅ tests
Iron (III) chloride hexahydrate	FeCl ₃ .6H ₂ O	-	-	270.30	Chem-lab	
Magnesium sulphate heptahydrate	MgSO ₄ .7H ₂ O	-	-	246.47	Panreac	
Potassium dihydrogen phosphate	KH ₂ PO ₄	-	-	136.09	VWR	
Alpha-D-glucose	C ₆ H ₁₂ O ₆	-	-	180.16	Fisher	Zahn-Wellens
N-Allylthiourea	C ₄ H ₈ N ₂ S	-	-	116.19	Merk	BOD ₅
Sodium hydroxide pellets	NaOH	-	-	40.00	Merck	
Ammonium molybdate	(NH ₄) ₆ Mo ₇ O ₂₄ .4H ₂ O	-	-	1235.8 6	Merck	
Ammonium monovanadate	NH ₄ VO ₃	-	-	116.97	Merck	
Ammonium persulphate	(NH ₄) ₂ S ₂ O ₈	-	-	228.20	Sigma	Total phosphorus analysis
Hydrochloric acid	HCl	37	1.16	36.46	Fisher	
Phenolphthalein indicator	C ₂₀ H ₁₄ O ₄	0.5 ^l	0.92	318.32	Sigma	
Potassium dihydrogen orthophosphate (P _T SS ^e)	KH ₂ PO ₄	-	-	136.09	VWR	
Sodium hydroxide	NaOH	-	-	40.00	Merck	
Sulphuric acid	H ₂ SO ₄	96	1.84	98.08	Pronalab	
Acetonitrile	CH ₃ CN	-	0.79	41.05	Merck	
Hydrochloric acid	HCl	37	1.16	36.46	Fisher	
Diethyl ether	(CH ₃ CH ₂) ₂ O	-	0.71	74.12	Sigma-Aldrich	Humic substances analysis
Supelite DAX-8	-	-	-	-	Supelco	
Methanol	CH ₃ OH	-	0.79	32.04	Basic	
Sodium hydroxide	NaOH	-	-	40.00	Merck	

^aMolecular formula; ^bDensity; ^cMolecular weight; ^dConcentration in weight/volume percentage; ^eStandard solution; ^fConcentration of Cl⁻, NO₃⁻ and SO₄²⁻, expressed in mg/L; ^gConcentration of F⁻, PO₄³⁻ and Br⁻, expressed in mg/L; ^hNO₂⁻ concentration, expressed in mg/L; ⁱConcentration expressed in mol/L; ^jConcentration of NH₄⁺, Ca²⁺, Mg²⁺, K⁺ and Na⁺, expressed in mg/L; ^kConcentration of acetate, citrate, formate, malonate, oxalate, phthalate and propionate, expressed in mg/L; ^lPercentage in ethanol:water (1:1).

2.2 Experimental setups

The various sets of experiments carried out during this thesis were performed in different experimental facilities, which are described below.

2.2.1 Solar pre-industrial scale plant

The first set of combined experiments described in the Chapters 3, 4, 5 and 6 was carried out in a mobile unit at pre-industrial scale, installed at a sanitary landfill (Figure 2.1), constructed for the treatment *in-situ* of 1-2 m³ of leachate (operation in batch mode). This facility is composed by a solar photocatalytic pre-oxidation system and a biological oxidation system. The schematic diagram of the entire plant is shown in Figure 2.2.



Figure 2.1. Solar pre-industrial unit combining photocatalytic and biological oxidation systems.

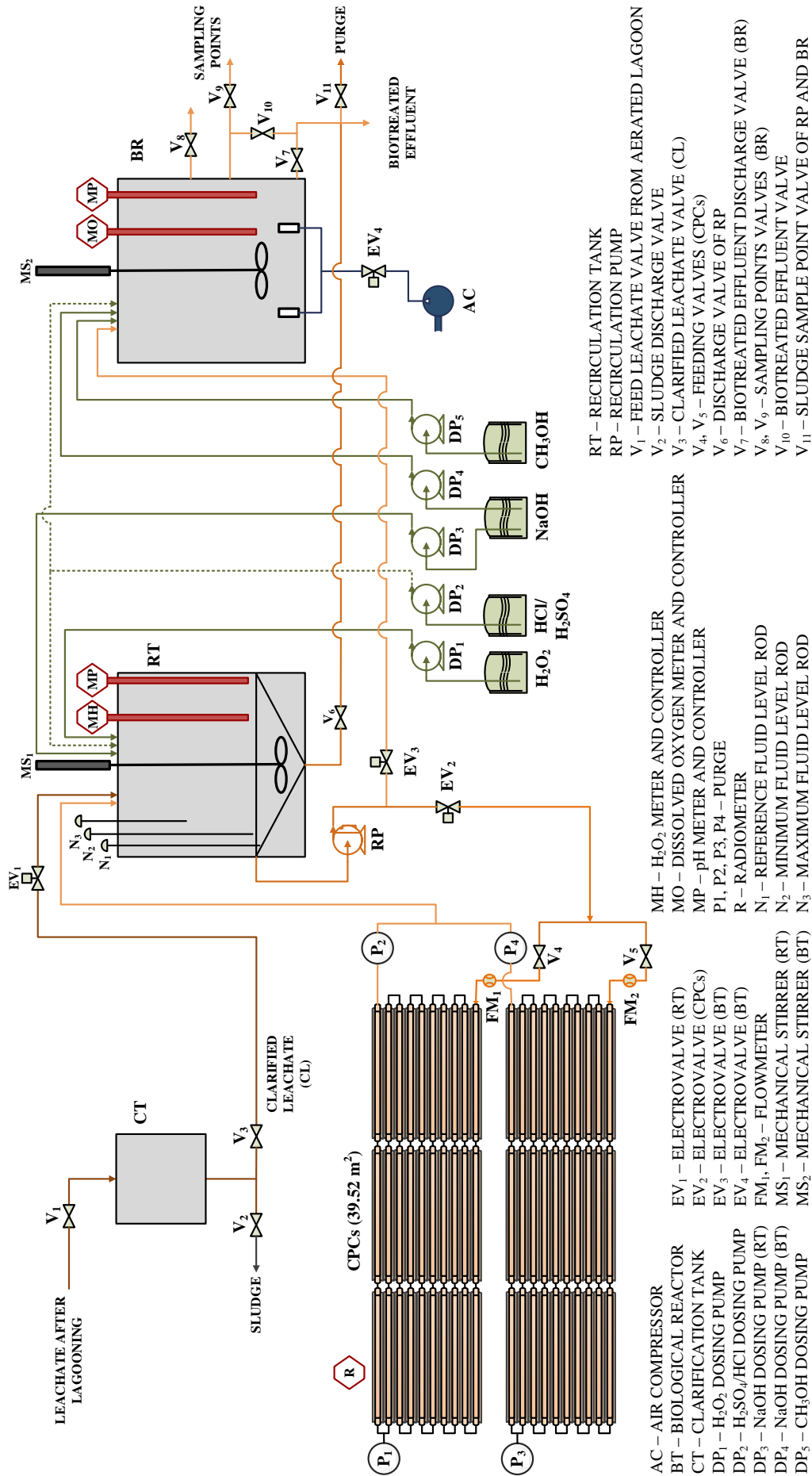


Figure 2.2. Flow diagram of the solar pre-industrial unit.

Table 2.2 shows the characteristics of the components present in the experimental facility previously described.

Table 2.2. Description of the solar pre-industrial unit constituents.

Element	Acronym	Brand	Model	Characteristics
Air compressor	AC	Maquinaria Disber S.L.	CD-2/24L	P = 8 bar V = 24 L Q = 198 L/min
Biological reactor	BR	Colberge	DPC3500	PE-HD cylindrical flat-bottom tank D = 1.6 m H = 2.0 m V = 3.5 m ³
Dosing pumps	DP ₁ DP ₂ DP ₃ DP ₅	Colberge	MP643-552	Q _{max} = 13 L/h
	DP ₄	Milton Roy	CEGA5M1T3	Q _{max} = 5 L/h
Electrovalves	EV ₁ EV ₂ EV ₃ EV ₄	Ebro Armaturen	EB4DM	P _{max} = 8 bar
H ₂ O ₂ meter and controller	MH	Grundfos Alldos	Conex DIA-1	WP7 sensor
Mechanical Stirrers	MS ₁ MS ₂	Colberge	VLS 5550	76 rpm
Oxygen dissolved meter and controller	MO	Colberge	Aqs- *S*	Oxygen electrode Pg 13.5 (ord. no. 21100)
pH meter and controller	MP	Colberge	Aqs- *S*	Sensorex sensor, model S653/S653W
Radiometer	R	Kipp & Zonen	CUV4	$\lambda = 299 - 384\text{nm}$ I = 0 to 100 W/m ² Sensitivity = 1 mV.m ² /W Response time < 1s
Recirculation pump	RP	Pan World	NH-250PS	Q _{máx} = 65 L/min
Recirculation tank	RT	Colberge	TFC2500Z	PE-HD cylindrical conic tank $\phi = 1.6\text{ m}$ H = 2.0 m V = 2.5 m ³

2.2.1.1 Solar CPC reactor

The photo-Fenton experiments were performed in a pre-industrial CPC-based plant under natural sunlight, constituted by 2 separate parallel rows of 10 and 9 CPC modules (10 tubes/module, 2.08 m²/module) connected by polypropylene junctions, with a total collector surface of 39.52 m², mounted on a fixed platform tilted 41° (local latitude), oriented South. The CPC tubes are made of borosilicate glass (Schott-Duran type 3.3, Germany, cut-off at 280 nm, internal diameter 46.4 mm, length 1500 mm and thickness 1.8 mm) connected by polypropylene junctions. Each of the CPC rows is connected to a cylindrical conic recirculation tank.

The leachate, previously decanted in a clarification tank (CT), was pumped from the recirculation tank (RT) to the CPCs using a centrifugal pump (RP) at a maximum flow rate of 65 L/min, regulated by two flowmeters (FM₁ and FM₂). The plant can be operated in two ways: (i) using the two CPC modules (illuminated volume of 482 L) or (ii) using just one module of 10 (illuminated volume of 254 L) or 9 CPCs (illuminated volume of 228 L). The RT is equipped with a mechanical stirrer (MS₁), a pH sensor and controller (MP), a H₂O₂ sensor and controller (MH) and three dosing pumps for H₂O₂ (DP₁), H₂SO₄/HCl (DP₂), and NaOH (DP₃) addition.

The photoreactor is an autonomous system, controlled by an abstract computer (Magelis, Schneider Electric), constituted by three electrovalves (EV₁, EV₂ and EV₃), three level rods (N₁, N₂ and N₃) and three valves (V₄, V₅ and V₆).

The intensity of solar UV radiation was measured by a global UV radiometer (R) mounted on the CPC modules at the same angle, which provided data in terms of incident W_{UV}/m^2 . Equation (2.1) allows to calculate the amount of accumulated UV energy ($Q_{UV,n}$, kJ/L) received on any surface in the same position with regard to the Sun, per unit of water volume inside the reactor, in the time interval Δt [1]:

$$Q_{UV,n} = Q_{UV,n-1} + \Delta t_n \overline{UV}_{G,n} \frac{A_r}{1000 \times V_t}; \quad \Delta t_n = t_n - t_{n-1} \quad (2.1)$$

Where:

t_n - time corresponding to the n -water sample (s)

V_t - total reactor volume (L)

A_r - illuminated collector surface area (m²)

$\overline{UV}_{G,n}$ - average ultraviolet radiation (W/m²) measured during the period Δt_n (s).

2.2.1.2 *Biological oxidation system*

The biological oxidation system is composed by a cylindrical flat-bottom tank (BR), equipped with a mechanical stirrer (MS₂), a pH control unit (MP) for pH adjustment using either H₂SO₄ or NaOH dosing metering pumps (DP₂ and DP₄, respectively), a dissolved oxygen sensor and controller (MO), and a methanol dosing pump (DP₅). A blower (AC) was used to supply air in order to maintain the selected range of dissolved oxygen concentration in the tank using a ceramic diffuser at the bottom of the BR.

The biological reactor is an autonomous system, controlled by an abstract computer (Magelis, Schneider Electric), constituted by one electrovalve (EV₄) and four discharge valves (V₇, V₈, V₉ and V₁₀).

2.2.2 Lab-scale photoreactor

The effect of the main photo-Fenton (PF) reaction variables on the treatment of the sanitary landfill leachate collected at the outlet of a leachate treatment plant (LTP), presented in the Chapter 7, was assessed in a lab-scale CPC photoreactor equipped with a sunlight simulator. Figure 2.3 presents different views and a schematic representation of the lab-scale photoreactor.

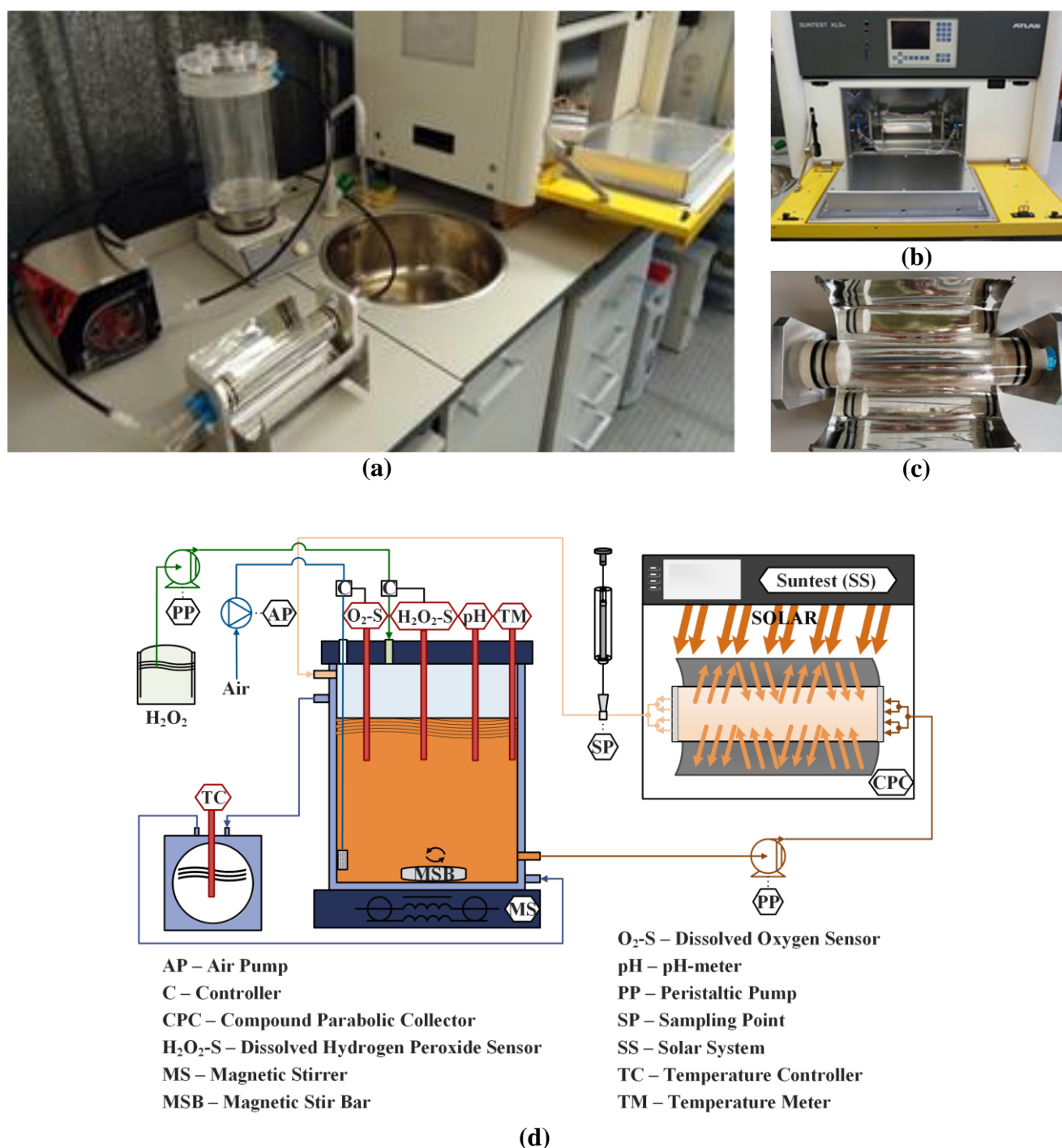
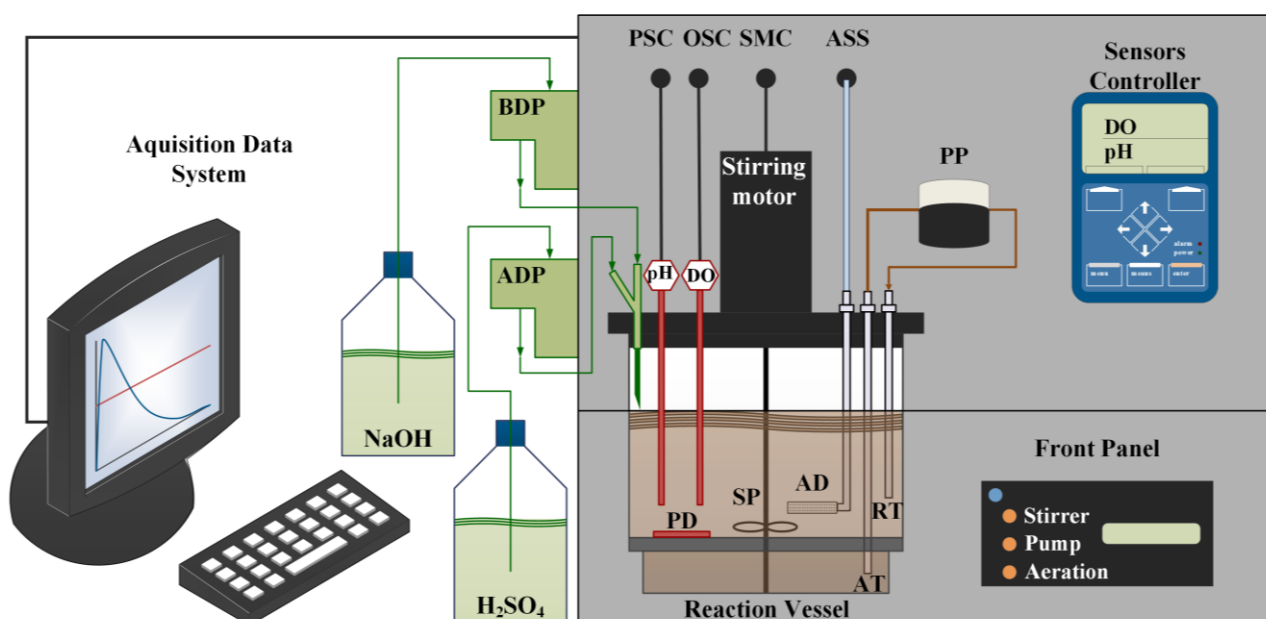


Figure 2.3. Lab-scale photoreactor plant (a): solar radiation simulator (b), CPC (c) and flow diagram (d).

The photocatalytic system includes: i) a solar radiation simulator (ATLAS, model SUNTEST XLS+) with 1100 cm² of exposition area, a 1700 Watt air-cooled xenon arc lamp, a daylight filter and quartz filter with IR coating; ii) a compound parabolic collector (CPC) with 0.023 m² of illuminated area constituted by anodized aluminium reflectors and a borosilicate tube (Schott-Duran type 3.3, Germany, cut-off at 280 nm, internal diameter 46.4 mm, length 160 mm and thickness 1.8 mm); iii) a glass vessel (1 L capacity) with a cooling jacket coupled to a refrigerated thermostatic bath (Lab. Companion, model RW-0525G) to ensure a constant temperature during the experiment; iv) a magnetic stirrer (Velp Scientifica, model ARE) for complete homogenization of the solution inside the glass vessel; v) a peristaltic pump (Ismatec, model Ecoline VC-380 II, with a flow rate of 0.63L/min) to promote water recirculation between the CPC and the glass vessel; vi) pH and temperature meter (VWR symphony - SB90M5). All systems are connected by Teflon tubing. The intensity of the UV radiation was measured by a broadband UV radiometer (Kipp & Zonen B.V., model CUV5) placed inside the sunlight simulator at the same level as the photoreactor centre. The radiometer was plugged into a handheld display unit (Kipp & Zonen B.V., model Meteon) to record the incident irradiance (W/m²).

2.2.3 Lab-scale biological reactor

The effect of the main nitrification and denitrification reaction variables on nitrogen species removal from leachate samples, presented in the Chapter 8, was evaluated in a Respirometer (BM-Advanced, Surcis) equipped with a pH, temperature and dissolved oxygen control system, simulating a lab-scale batch bioreactor. Figure 2.4 shows the view and schematic representation of the respirometer.



Legend:

AD – Air Diffuser
ADP – Acid Dosing Pump
ASS – Air Supply Source
AT – Aspiration Tube

BDP – Base Dosing Pump
OD – Dissolved Oxygen Sensor
OSC – Oxygen Sensor Connector
PD – Peltier Device
pH – pH sensor

PP – Peristaltic Pump
PSC – pH Sensor Connector
RT – Return Tube
SMC – Stirring Motor Connector
SP – Stirring Paddle

Figure 2.4. Lab-scale biological reactor and respective schematic representation.

The respirometric system is composed by: (i) a glass reaction vessel with an approximate useful volume of 1.2 L; (ii) a stirring system composed by a stirrer motor, stirring paddles, partition plate, one-sense membrane device, air diffuser and aspiration and returning tubing, (iii) a peristaltic pump for the mixed liquor recirculation from the aspiration tube to the return tube (tygon tubing with internal diameter of 4.8 mm); (iv) a set of pH and DO sensors located inside the reaction vessel and an internal Peltier device for heating and cooling, keeping the solution temperature in the desired values; (v) sensor controller, where the measurements of pH, OD and temperature can be seen and the calibration of pH and DO sensors are made; (vi) a set of connectors, where the dissolved oxygen and pH sensors and the stirring motor are linked, and from which the air is supplied to the reaction vessel through the air diffuser; (vii) pumping and injection system for pH control, which includes acid and base dosing pumps; (viii) a front panel, which indicates if the equipment and the agitation, pumping and aeration systems are switched on; and (ix) an acquisition data system by means of a specific BM software.

2.2.4 Solar/UV pre-industrial scale plant

Based on the outcomes obtained in the lab-scale photoreactor and in the solar pre-industrial scale plant, it was necessary to modify the last one, in order to be possible to (i) perform a coagulation/sedimentation step before the photo-Fenton reaction and (ii) operate with solar and/or artificial irradiation, which results will be presented in Chapter 9. Therefore, the amended facility is composed by three systems: biological oxidation; coagulation/sedimentation and photo-oxidation. The views and the schematic representation of the plant are shown in Figure 2.5 and Figure 2.6, respectively.



Figure 2.5. Solar/UV pre-industrial unit combining biological and chemical oxidation systems.

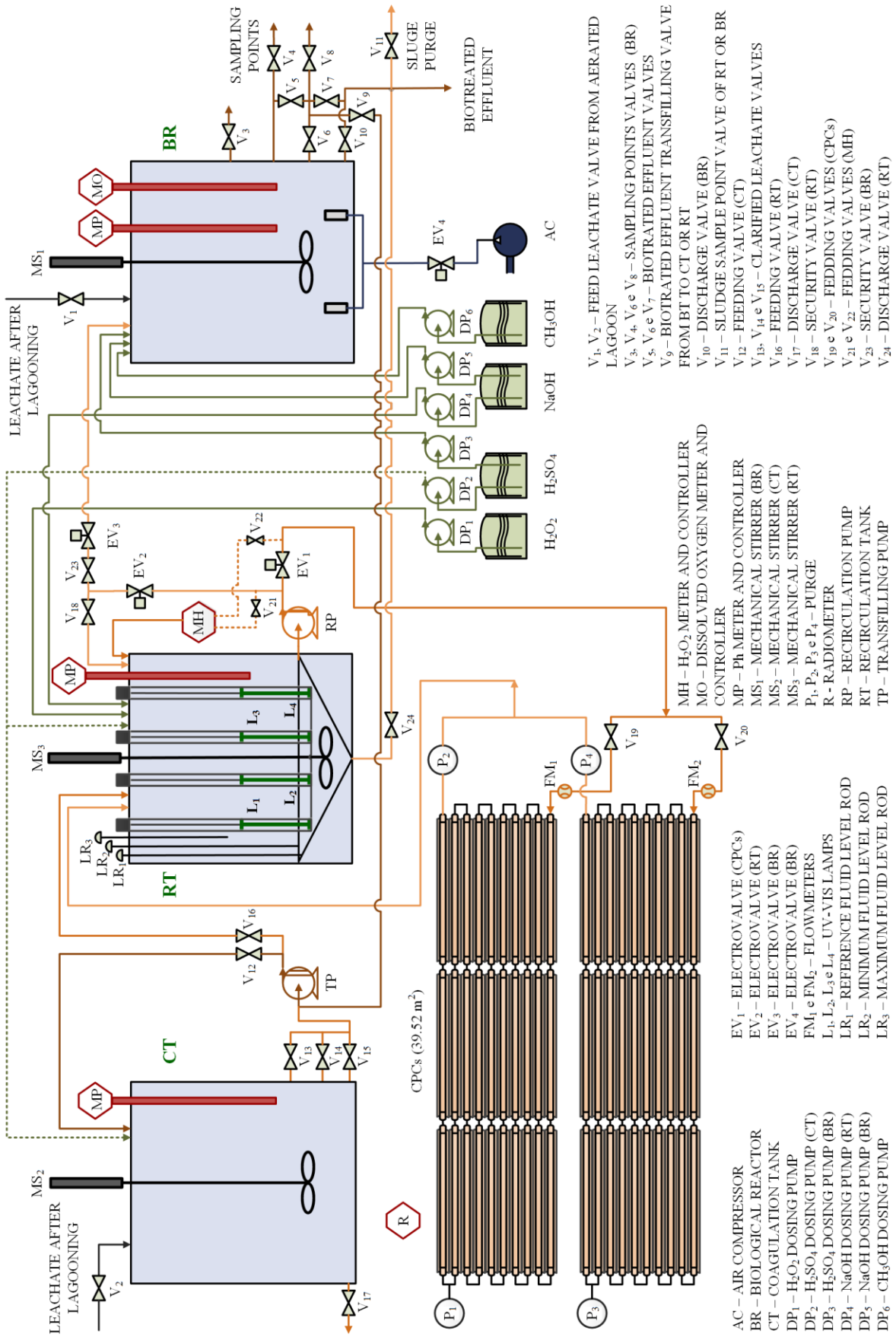


Figure 2.6. Flow diagram of the solar/UV pre-industrial unit.

Table 2.3 shows the characteristics of the components present in the experimental facility previously described.

Table 2.3. Description of solar/UV pre-industrial unit constituents.

Element	Acronym	Brand	Model	Characteristics
Air compressor	AC	Maquinaria Disber S.L.	CD-2/24L	P = 8 bar V = 24 L Q = 198 L/min
Biological reactor	BR	Colberge	DPC3500	PE-HD cylindrical flat-bottom tank D = 1.6 m H = 2.0 m V = 3.5 m ³
Coagulation tank	CT	Colbergue	DPC3000	PE-HD cylindrical flat-bottom tank D = 1.47 m H = 2.0 m V = 3.0 m ³
Dosing pumps	DP ₁	Colberge	MP643-552	Q _{max} = 13 L/h
	DP ₂			
	DP ₃			
	DP ₄			
	DP ₅	Milton Roy	CEGA5M1T3	Q _{max} = 5 L/h
	DP ₆	Colberge	MP643-552	Q _{max} = 14.9 L/h
Electrovalves	EV ₁	Ebro Armaturen	EB4DM	P _{max} = 8 bar
	EV ₂			
	EV ₃			
	EV ₄			
H ₂ O ₂ meter and controller	MH	Grundfos Alldos	Conex DIA-1	WP7 sensor
UV lamps	L ₁	Uv-technik	UV-Lamp UVH 4019/28 F-1	Doping: Iron Rated power = 0.85/1.0/1.2 kW L = 405 mm
	L ₂			UV-C, UV-B, UV-A and Vis light Sealing temperature = 350 °C
	L ₃			Useful lifetime: 750 – 1250 h Quartz sleeves: D _{ext.} = 45 mm;
	L ₄			Thickness = 2 mm; ΔT = 700 – 900 °C
Mechanical stirrers	MS ₁	Colberge	VLS 5550	76 rpm
	MS ₂			104 rpm
	MS ₃			76 rpm
Dissolved oxygen meter and controller	MO	Colberge	Aqs- *S*	Oxygen electrode Pg 13.5 (ord. no. 21100)
pH meter and controller	MP	Colberge	Aqs- *S*	Sensorex sensor, model S653/S653W

Table 2.3. Description of solar/UV pre-industrial unit constituents.

Element	Acronym	Brand	Model	Characteristics
Radiometer	R	Kipp & Zonen	CUV4	$\lambda = 299 - 384\text{nm}$ $I = 0 \text{ to } 100 \text{ W/m}^2$ Sensitivity = $1 \text{ mV.m}^2/\text{W}$ Response time < 1s
Recirculation pump	RP	Pan World	NH-250PS	$Q_{\text{max}} = 65 \text{ L/min}$
Recirculation tank	RT	Colberge	TFC2500Z	PE-HD cylindrical conic tank $\phi = 1.6 \text{ m}$ $H = 2.0 \text{ m}$ $V = 2.5 \text{ m}^3$
Transfilling pump	TP	Pan World	NH-50PX-X	$Q_{\text{max}} = 24 \text{ L/min}$

2.2.4.1 Biological oxidation system

The biological oxidation system is composed by a cylindrical flat-bottom tank (BR), equipped with a mechanical stirrer (MS₁), a pH control unit (MP) for pH adjustment using either H₂SO₄ or NaOH dosing metering pumps (DP₃ and DP₅, respectively), a dissolved oxygen sensor and controller (MO), and a methanol dosing pump (DP₆). A blower (AC) was used to supply air in order to maintain the selected range of dissolved oxygen concentration inside the tank, using a ceramic diffuser at bottom of the BR.

The biological reactor is an autonomous system controlled by an abstract computer (Magelis, Schneider Electric), constituted by one electrovalve (EV₄) and nine discharge valves (V₃ - V₁₁).

2.2.4.2 Coagulation/sedimentation system

The coagulation/sedimentation system is constituted by a cylindrical flat-bottom tank (CT), a mechanical stirrer (MS₂), a pH control unit (MP) for pH adjustment using a H₂SO₄ dosing pump (DP₂). The clarified leachate is transferred to the photoreactor by means of a transfilling pump (TP), opening the valve (V₁₆) downstream of the pump and one of the three valves (V₁₃, V₁₄ and V₁₅) arranged at different heights of the CT, taking into account the acid sludge volume.

2.2.4.3 Solar/UV photo-oxidation system

The photo-Fenton experiments were performed in a photoreactor, under natural and/or artificial irradiation, constituted by 2 separate parallel rows of 10 and 9 CPC modules (10 tubes/module, 2.08 m²/module) connected by polypropylene junctions, with a total collector surface of 39.52 m², mounted on a fixed platform tilted 41° (local latitude), oriented South. The CPC tubes are made of borosilicate glass (Schott-Duran type 3.3, Germany, cut-off at 280 nm, internal diameter 46.4 mm, length 1500 mm and thickness 1.8 mm) connected by polypropylene junctions. Given the difficulty of filling the CPCs, due to the air present inside the borosilicate tubes, there are four purges (P₁, P₂, P₃ and P₄), before and after of each CPCs row. The plant can be operated in two ways: (i) using the two CPC modules (illuminated volume of 482 L) or (ii) using just one module of 10 (illuminated volume of 254 L) or 9 CPCs (illuminated volume of 228 L). Each of the CPC rows is connected to the cylindrical conic recirculation tank (RT). Besides CPCs, the photo-oxidation system also contains four independent UV-Vis lamps (L₁, L₂, L₃ and L₄) placed equidistantly 0.5 m from the center of the reactor, whose spectrum can be seen in Figure 2.7. All lamps are coated with quartz sleeves and can operate at different rated powers (850, 1000 and 1200 W), depending on the electrical connections. This system can be operated using singly CPCs or lamps, or simultaneously CPCs and lamps.

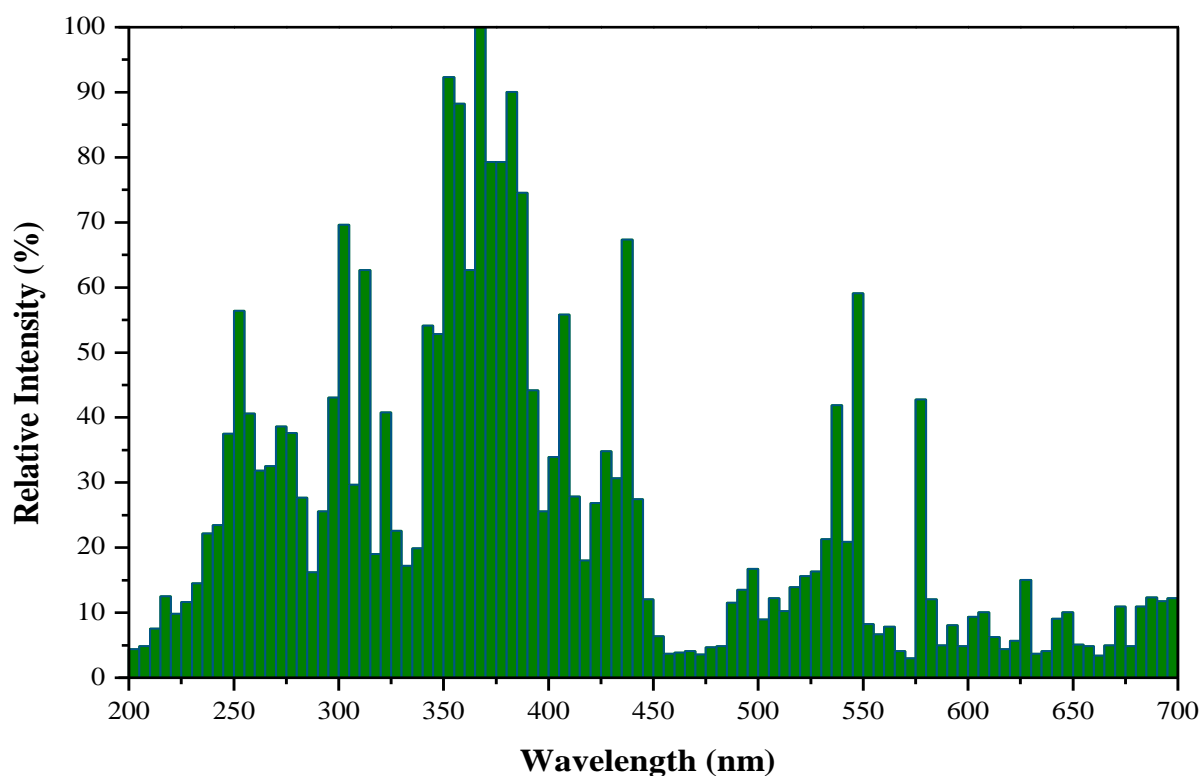


Figure 2.7. UV-Vis lamp spectrum.

The clarified leachate fed to the RT can be: (i) pumped through CPCs by means of a centrifugal pump (RP), at a maximum flow rate of 65 L/min, regulated by two globe valves (V_{19} and V_{20}) connected to two flowmeters (FM_1 and FM_2), in case where the CPCs are used, individually or simultaneously with the lamps; or (ii) only recirculated to the RT, using the same pump, in the case where the lamps are exclusively used. This recirculation process is performed in order to enhance the turbulence inside the RT, maximizing the absorption of light by the iron species and for the correct on-line H_2O_2 concentration measurement and control.

The RT is equipped with a mechanical stirrer with double helix (MS_3), in order to increase the turbulence inside the reactor, a pH sensor and controller (MP), a H_2O_2 sensor and controller (MH) and three dosing pumps for H_2O_2 (DP_1), H_2SO_4 (DP_2) and NaOH (DP_4) addition. The photoreactor is an autonomous system, controlled by an abstract computer (Magelis, Schneider Electric), constituted by three electrovalves (EV_1 , EV_2 and EV_3), three level rods (LR_1 , LR_2 and LR_3) and three valves (V_{16} , V_{18} and V_{24}).

The intensity of solar UV radiation was measured by a global UV radiometer (R) mounted on the CPC modules at the same angle, which provided data in terms of incident W_{UV}/m^2 . Equation (2.1), presented in the sub-section 2.2.1.1, allows to obtain the amount of accumulated UV energy ($Q_{UV,n}$, kJ/L), when the CPCs are used. The amount of accumulated UV energy ($Q_{UV,L,n}$, kJ/L) emitted by the UV-Vis lamps and received by the leachate existing inside the photoreactor, is given by Equation (2.2). When solar and artificial radiation are simultaneously used, the amount of accumulated UV energy ($Q_{UV,T,n}$, kJ/L) is calculated as the sum of Equations (2.1) and (2.2), according to Equation (2.3).

$$Q_{UV,L,n} = Q_{UV,L,n-1} + \frac{N_L \times \eta \times P_L \times \Delta t_n}{V_t}; \quad \Delta t_n = t_n - t_{n-1} \quad (2.2)$$

$$Q_{UV,T,n} = Q_{UV,T,n-1} + \frac{\Delta t_n}{V_t} \left(N_L \times \eta \times P_L + \frac{\overline{UV}_{G,n} \times A_r}{1000} \right); \quad \Delta t_n = t_n - t_{n-1} \quad (2.3)$$

Where:

t_n - time corresponding to the n -water sample (s)

V_t - total reactor volume (L)

N_L - number of UV-Vis lamps

η – useful ultraviolet radiation fraction

P_L – rated power (kW) of the UV-Vis lamp used during the period Δt_n (s).

2.3 Experimental procedure

The specific procedures used to carry out the various sets of experiments in the different facilities are described below.

2.3.1 Solar pre-industrial scale experiments

The first set of experiments carried out at the solar pre-industrial scale unit, which results are presented in the Chapters 3, 4 and 5, was based on an integrated leachate treatment strategy composed by a solar photo-Fenton reaction and an activated sludge process, under aerobic and anoxic conditions. In the Chapters 3 and 4 this was the sequence of treatment adopted (see subsection 2.3.1.1), while in the Chapter 5, a biological process was also added before the photo-oxidation step (see subsection 2.3.1.2). In the next subsections, the experimental procedure of each step is described.

2.3.1.1 *Photo-treatment/Biological treatment*

a) Photo-treatment

The clarification tank was filled by gravity with 2 m³ of leachate from the aerobic lagoon by opening valve 1 (valves 2 and 3 closed). After a 3-h sedimentation period, the clarified leachate flowed by gravity to the recirculation tank (RT) (valve 3 and electrovalve 1 open) and the sludge, if necessary, was removed by opening valve 2. The volume of leachate (1.3–1.4 m³) was controlled by three level rods (minimum, maximum and reference). A first control sample was taken for leachate characterization after 15 min of mechanical stirring.

The pH value was adjusted to 3.0 through the addition of sulphuric and/or hydrochloric acids under mechanical stirring and another sample was taken after pH stabilization. Then, iron sulphate salt (80 mg Fe²⁺/L) and H₂O₂ (500 mg/L) were manually and automatically added, respectively, leading to a final pH of 2.8. The dissolved iron content initially present in the leachate was not taken into account. Afterwards, electrovalve 2 was open, the leachate was pumped into the CPCs and the photo-Fenton reaction started.

Hydrogen peroxide concentration was controlled online between 100 and 500 mg/L, through the addition of commercial H₂O₂ solution (50% (w/v)). Samples were collected at pre-defined times to evaluate the degradation process. pH was not controlled during the photo-Fenton reaction. Reaction was stopped automatically when the consumption of H₂O₂ or amount of UV radiation (integrated by the UV radiometer) reached the set point. At that moment, the pump was turned off and the photo-treated leachate returned to the recirculation tank by gravity.

For biodegradability tests, presented in the Chapter 4, two photo-Fenton experiments were performed maintaining all parameters, with exception of H₂O₂ dose. In one of those experiments, after the acidification procedure, sludge was completely removed, and only supernatant leachate was used. In these experiments, a small amount of H₂O₂ was added to the photoreactor, and after H₂O₂ total consumption, a sample was taken for bioassays and a new dose of H₂O₂ was added. This procedure of “addition-total consumption-sample collection-addition” is important since it prevents any reaction in dark conditions after sample collection during storage, and possible interferences in bioassays. Considering this procedure, experimental data must be expressed in terms of H₂O₂ consumption and not accumulated UV energy per litre of leachate.

Finally, the photo-treated leachate was neutralized with NaOH to a pH ca. 7, under mechanical stirring, leading to iron precipitation and followed by a 3-h sedimentation period for iron sludge settling.

b) Biological treatment

The biological reactor was initially colonized by activated sludge, collected in a conventional municipal WWTP, and small amounts of raw leachate were further added during 1-month in order to allow the biomass to adapt to such complex wastewater.

Afterwards, the clarified photo-treated-neutralized leachate (1 m³) was pumped into the biological reactor. The biological reactor was operated under aerobic and anoxic conditions, to promote not only nitrogen removal by nitrification and denitrification reactions, but also to remove the biodegradable organic carbon fraction. Furthermore, taking into account the low carbon/nitrogen ratio of the photo-treated leachate, methanol was used as an external carbon source to achieve complete denitrification. pH was controlled between 6.5 and 8.5 during nitrification and denitrification reactions. Along the nitrification process, oxygen concentration was maintained between 0.5 and 2 mg O₂/L. For the denitrification reaction, the air blower was turned off (the mechanical stirrer remained on, to avoid sludge settling) and the dissolved oxygen concentration was kept below the detection limit (<0.05 mg O₂/L). After complete nitrogen removal, and further clarification (2–4 hours) of the wastewater, the photo-bio-treated leachate was discharged.

2.3.1.2 Biological treatment/photo-treatment/biological treatment

a) 1st Biological treatment

The biological reactor was initially colonized using activated sludge from a conventional municipal wastewater treatment plant (WWTP), and small amounts of raw leachate were added during one month,

in order to adapt the biomass to the high-strength wastewater. After this preliminary adaption period, the clarified raw leachate (2.5 m³) was pumped into the biological reactor containing the biomass. The biological reactor was operated under aerobic and anoxic conditions, to promote nitrogen removal by nitrification and denitrification reactions, respectively, and the complete oxidation of the biodegradable organic carbon fraction. Furthermore, and taking into account the low carbon/nitrogen ratio of the raw leachate, methanol was used as an external carbon source to promote complete denitrification. pH was controlled in the range between 7.5 and 9.0 along nitrification and denitrification reactions. During nitrification, oxygen concentration was maintained above 0.5 mg O₂/L. Over denitrification reactions, the air blower was turned off (mechanical stirrer remained turned on, in order to avoid sludge settling) and dissolved oxygen concentration was always below the detection limit (<0.05 mg O₂/L).

b) Solar photo-treatment

After the 1st biological treatment and further wastewater clarification, the bio-treated leachate was pumped into the recirculation tank of the photocatalytic system to proceed with the photo-Fenton oxidation. A first control sample was taken after 15 min of mechanical stirring for bio-treated leachate characterization.

The pH value was adjusted to 3.0 through the addition of sulphuric acid, under mechanical stirring, and another sample was taken after pH stabilization. In order to evaluate the influence of sludge removal on the photo-Fenton reaction, the acidified bio-treated leachate was divided in two parts: half the volume was transferred to another tank, followed by sludge settling, and the supernatant was transferred back again to the recirculation tank, to perform the photo-oxidation reaction. In the experiments with and without sludge removal after acidification, 0.9 and 0.8 m³ of acidified bio-treated leachate was used, respectively.

Then, iron sulphate salt (80 mg Fe²⁺/L) and a first dose of H₂O₂ (500 mg/L) was added manually and automatically to the wastewater, respectively, achieving a final pH value of 2.8. The presence of dissolved iron in the leachate (7.9 mg/L) was not taken into account. Then, the acidified-bio-treated leachate was pumped through the CPCs (10 CPCs modules; 20.8 m²) and the photo-Fenton reaction started.

Hydrogen peroxide was controlled online between 100 and 500 mg/L, through the addition of commercial H₂O₂ (50% (w/v)) solution. Samples were taken at pre-defined times to evaluate the degradation process. Reactions stopped automatically when the consumption of H₂O₂ or the amount of

UV radiation (integrated by the UV radiometer) reached the set point. At this moment, the pump was turned off and the bio-photo-treated leachate returned to the recirculation tank by gravity.

Finally, the bio-photo-treated leachate was neutralized with NaOH to a pH around 7, under mechanical stirring, leading to iron precipitation, followed by an iron sludge settling period of 3 hours.

c) 2nd Biological treatment

The clarified neutralized photo-bio-treated leachate (0.6 m³) was pumped into the biological reactor containing the settled biomass. The biological reactor was operated under the same conditions than the first one. After oxidation of the biodegradable organic carbon content, and further clarification of the wastewater, the bio-photo-bio-treated leachate was discharged.

2.3.2 Lab-scale photo-Fenton experiments

In order to assess the effect of the main photo-Fenton reaction parameters on leachate treatment, which results are presented in Chapter 7, the recirculation glass vessel of the lab-scale prototype (Figure 2.3) was filled with 1 L of pre-treated (biological oxidation and physico-chemical process) leachate, homogenized (magnetic stirrer) and recirculated to the CPC unit during ca. 30 minutes in the darkness. Then, a first sample was taken. Meanwhile, the temperature set-point of the refrigerated thermostatic bath was adjusted to keep the leachate in the intended temperature (10, 20, 30, 40 or 50°C). The SUNTEST was switched on (keeping the photoreactor covered with an aluminium sheet) and the irradiance was set at 250, 500 and 750 W/m², which is equivalent to 22, 44 and 68 W_{UV}/m², measured in the wavelength range 280 - 400 nm. Then, the leachate was acidified with H₂SO₄, HCl or H₂SO₄+HCl until the desired pH (2.0, 2.4, 2.8, 3.2 and 3.6) and ferrous sulphate was added to achieve the concentrations of 20, 40, 60, 80 and 100 mg/L, taking into account the initial dissolved iron content. After about 10 min, a second sample was analysed for total dissolved iron (TDI) concentration control. Finally, the CPC was uncovered and the first dose of H₂O₂ was added to start the photo-Fenton reaction. Additional samples were taken at pre-defined times in order to follow the degradation process. The concentration of H₂O₂ was maintained in excess, between 100 and 500 mg/L during the entire reaction, by adding the amounts required to compensate the consumed ones, as indicated by the analyses performed throughout the experiments.

The iron (III) speciation diagrams, presented in the Chapter 7, were obtained from the chemical equilibrium modelling system MINEQL+ [2], taking into account (i) the formation of Fe(OH)₃ (s) and (ii) the equilibrium constants of the iron-water, iron-sulphate and iron-chloride complexes, as well as (iii) the respective reaction enthalpies.

2.3.3 Lab-scale biological experiments

As previously mentioned, the effect of the main biological treatment variables on the leachate's nitrification and denitrification, presented in the Chapter 8, was assessed in a respirometer (Figure 2.4), working as a lab-scale bioreactor.

2.3.3.1 Nitrification kinetics

Initially, the reactor vessel was filled with about 880 mL of sanitary landfill leachate, collected from an LTP aerobic lagoon, previously acidified with sulphuric acid up to the required initial pH (8.5 or 7.5), when it was necessary to vary the pH range. Then, the reaction vessel was placed in the respirometer container and the stirring motor was switched on. After that, the operating temperature (15, 20, 25 and 30°C) and the pH (6.5-7.5, 7.5-8.5 and not controlled) and dissolved oxygen (0.5-1.0, 1.0-2.0 and 2.0-4.0 mg/L) intervals were selected as required, being continuously controlled by the respirometer software. These parameters were constantly measured and recorded online every 60 seconds. Then, the stirring, the aeration and the peristaltic pump were turned on, in order to initiate the system stabilization. Once the temperature was stabilized, centrifuged biomass (20-35 mL) previously adapted both to the aerobic operating regime and to the landfill leachate, was added to the reaction vessel and the first control sample was taken after ca. 1 min. Other samples were collected roughly every hour, during about 14-16 hours, in order to evaluate the nitrification reaction by analysing the dissolved inorganic carbon, ammonium nitrogen, volatile suspended solids and nitrite and nitrate ions content.

2.3.3.2 Denitrification kinetics

Firstly, the reactor vessel was filled with sanitary landfill leachate (900-975 mL), previously nitrified and, when necessary, acidified with sulphuric acid up to the required initial pH (6.5, 7.0, 7.5, 8.0 and 9.0). Then, the reaction vessel was placed in the respirometer container and the stirring motor was switched on. After that, the operating temperature (20, 25 and 30°C) and the pH interval (6.5-7.0, 7.0-7.5, 7.5-8.0, 8.0-8.5 and 8.5-9.0) were selected and controlled throughout the experiment by the respirometer software. These parameters were constantly measured and recorded online every 60 seconds. Then, the stirring and the peristaltic pump were turned on, keeping the aeration off, in order to initiate the system stabilization. Once the temperature was stabilized, centrifuged biomass (25, 50 and 100 mL), previously adapted both to the anoxic operating regime as to the nitrified landfill leachate, was added to the reactor and the first control sample was taken after ca. 1 min. Immediately after the collection of the first sample, methanol was added to start the reaction. Other samples were collected roughly every 2-3 hours (being the collection suspended overnight), during about 12-30 hours, in order to evaluate the denitrification

reaction by analysing the dissolved inorganic and organic carbon, volatile suspended solids and nitrite and nitrate ions concentration.

Regarding the denitrification evaluation, it was also performed one experiment with phosphate ions addition (ca. 30 mg PO₄³⁻-P/L). In this test, the biomass was prepared according to Zahn-Wellens test methodology (as described in the sub-chapter 2.4) and 1.2 mL of the phosphate buffer, also used in the Zahn-Wellens test, was added.

2.3.4 Solar/UV pre-industrial scale experiments

The set of experiments carried out at the solar/UV pre-industrial scale facility, which results are presented in the Chapter 9, was based on an integrated leachate treatment strategy composed by aerobic biological oxidation, coagulation/sedimentation process and photo-Fenton reaction driven by solar and/or artificial radiation. In the following subsections, the experimental procedure of each stage is described.

2.3.4.1 Biological treatment

The biological reactor (BR) was initially fed with the mixed liquor from the biological reactor of the LTP, located at the sanitary landfill in question, since the activated sludge was already properly adapted to the recalcitrant compounds inherent to this kind of wastewater. The succeeding batches (2.0-2.5 m³) were performed with clarified leachate from the secondary settling tank existing at the LTP. The BR from the experimental unit was prepared to operate in aerobic and anoxic conditions. However, during this experimental cycle, the BR was kept to work in aerobic regime in order to remove the alkalinity (via nitrification reaction) and the remaining biodegradable organic matter. After leachate feeding, the mechanical stirring was switched on and a sample was taken for initial leachate characterization.

During the nitrification reaction, the pH was not controlled (decreasing along the reaction) and the BR was continuously aerated, trying to keep the DO content between 0.5 and 1.0 mg O₂/L. However, due to operational limitations, the air supply was not enough for microbial consumption needs, not allowing to maintain the average DO content higher than 0.5 mg O₂/L. The reaction was stopped when the values of alkalinity and/or ammonium nitrogen were close to zero. After that, the biological sludge was settled for 2-4 hours.

2.3.4.2 Coagulation/sedimentation process

After the first biological treatment and further clarification, the bio-treated leachate was pumped to the coagulation tank (CT), and the first sample was taken after ca. 15 minutes of mechanical stirring, for bio-treated leachate characterization. The ferric chloride was manually added (120 or 240 mg Fe³⁺/L), and the pH was automatically adjusted to the required value (2.8, 3.0, 4.2 or 4.5), through sulphuric acid addition. After the addition and mixture of the reactants (about 1 hour), agitation was turned off and acidic sludge was settled down during the pre-defined time (3 or 14 hours), being posteriorly discharged.

2.3.4.3 Solar/UV phototreatment

After the sedimentation period, the clarified effluent was transferred to the recirculation tank (1.0 – 1.8 m³), opening one of the valves 13, 14 or 15 (depending on the height of the acid sludge) and the valve 16, and a sample was taken after ca. 15 minutes of mechanical stirring, for bio-coagulated leachate characterization. Then, iron sulphate salt was manually added in order to obtain a Fe²⁺ concentration of 60 mg/L, and the first dose of H₂O₂ was automatically added, in a concentration not exceeding 500 mg/L to minimize the use of the reagent in parallel reactions. Afterwards, (i) the electrovalve 1 (electrovalve 2 closed) was open and the leachate was pumped into the CPCs (10 CPCs modules; 20.8 m²), when it was intended to use only CPCs or the combination of solar and artificial radiation, or (ii) the electrovalve 2 and valve 18 were open (electrovalve 1 and 3 and valve 23 closed), the UV-Vis lamps were switched on and the leachate was recirculated within the recirculation tank, when it was intended only to use artificial radiation.

In the preliminary phase of the photo-Fenton oxidation, the H₂O₂ was quickly consumed, associated with the indirect oxidation of nitrite ions to nitrate ions, and the solution pH rapidly dropped to values lesser than 2.8, whereby it was necessary to add sodium hydroxide to correct the pH value. From this moment on, it was possible to control the H₂O₂ concentration between 100 and 500 mg/L, through the addition of a commercial H₂O₂ solution (50% (w/v)). Samples were collected at pre-defined times to evaluate the degradation process.

Reaction was stopped automatically when the consumption of H₂O₂ or amount of UV radiation (integrated by the UV radiometer) reached the set point (the equivalent to a DOC content of 250 mg/L). At that moment, the pump was turned off and the photo-treated leachate returned to the recirculation tank by gravity. Finally, the photo-treated leachate was neutralized with NaOH to a pH ca. 7, under mechanical stirring, leading to iron precipitation and followed by a 3-h sedimentation period for iron sludge settling.

2.4 Analytical methods

Table 2.4 presents the diverse physico-chemical parameters analysed during the present experimental work, as well as the respective analytical methods employed.

Table 2.4. Physico-chemical parameters and their analytical methods

Parameter	Methodology
Anions ^a	Chloride (Cl ⁻), nitrite (NO ₂ ⁻), sulphate (SO ₄ ²⁻), nitrate (NO ₃ ⁻) and phosphate (PO ₄ ³⁻) were quantified by ion chromatography using a Dionex ICS-2100 apparatus, equipped with a IonPac [®] AS11-HC (4 × 250 mm) column at 30 °C and an anion self-regenerating suppressor (ASRS [®] 300, 4 mm), under isocratic elution of 30 mM NaOH at a flow rate of 1.5 mL/min, during 12 minutes.
Aromatic compounds ^a	The presence and content of aromatic compounds was qualitatively evaluated by UV spectrometry at 254 nm (Abs ₂₅₄).
BOD ₅	Biochemical oxygen demand at 5 days (BOD ₅) was determined according to the Standard Methods, 5210-B test, using an OxiTop [®] (manometric respirometry) [3].
Cations ^a	Sodium (Na ⁺), ammonium (NH ₄ ⁺), potassium (K ⁺), magnesium (Mg ²⁺) and calcium (Ca ²⁺) were determined by ion chromatography using a Dionex DX-120 device equipped with a IonPac [®] CS12A (4 × 250 mm) column at ambient temperature and a cation self-regenerating (CSRS [®] Ultra II, 4 mm) suppressor, under isocratic elution of 20 mM methanesulfonic acid at a flow rate of 1.0 mL/min, during 12 minutes.
COD	Chemical oxygen demand (COD) was measured according to the Standard Methods, 5220-D test, using a WTW thermoreactor (model CR4200) and a WTW photometer (model Photolab S12). COD was also quantified by Merck [®] Spectroquant kits (ref: 1.14541.0001).
Colour and Turbidity	Colour (expressed in terms of Pt-Co units; samples were diluted 20 times) and turbidity were measured in a spectrophotometer (Hach, model DR 2010).
DO	Dissolved oxygen (DO) was measured by (i) a dissolved oxygen meter and controller from Colberge (model Aqs- *S*), with an oxygen electrode Pg 13.5 (ord. no. 21100), and (ii) multiparameter meter HI9828, from Hanna Instruments (sensor HI769828, Hanna Instruments).
DOC ^a	Dissolved organic carbon (DOC) was determined by NDIR spectrometry in a TC-TOC-TN analyser equipped with ASI-V autosampler (Shimadzu, model TOC-V _{CSN}) after calibration with standard solutions of potassium hydrogen phthalate (total carbon) and a mixture of sodium hydrogen carbonate/sodium carbonate (inorganic carbon). DOC was given by the difference between TDC (Total Dissolved Carbon) and DIC (Dissolved Inorganic Carbon) (DOC=TDC-DIC).

Table 2.4. Physico-chemical parameters and their analytical methods

Parameter	Methodology
TDI ^{a,b} (Fe ²⁺ + Fe ³⁺)	Colorimetric determination of total dissolved iron (TDI) content was done with 1,10-phenantroline according to ISO 6332 [4], using a spectrophotometer (Merck, model Spectroquant® Pharo 100 or Hach, model DR 2010) at 510 nm.
H ₂ O ₂ ^{a,b}	<p>The hydrogen peroxide (H₂O₂) concentration during experiments was determined by the vanadate method [5], based on the reaction of H₂O₂ with ammonium metavanadate in acidic medium, which results in the formation of a red-orange colour peroxovanadium cation, with maximum absorbance at 450 nm, using a spectrophotometer (Merck, model Spectroquant® Pharo 100 or Hach, model DR 2010).</p> <p>H₂O₂ was measured using a H₂O₂ meter and controller from Grundfos Alldos (model Conex DIA-1), with a WP7 sensor.</p>
HS	Leachate extraction for humic substances (HS) was performed by the acid-base treatment method [3]. Briefly, leachate samples were filtered through 0.45 µm cellulose membrane filters and acidified to pH 2.0. Acidified leachates were percolated through a DAX-8 resin column. The preparative cleaning of the resin is described by Thurman and Malcom [6]. After percolating the whole sample through the adsorption column, HS were eluted from the DAX-8 resin using 0.1 M NaOH, in reverse flow. HS concentration in the eluted solution was measured in terms of mg C _{HS} /L using a TC-TOC-TN analyzer (Shimadzu, model TOC-V _{CSN}).
LMCA ^a	Low molecular-weight carboxylate anions, namely, acetate, propionate, formate, pyruvate, valerate, malonate, maleate, oxalate, phthalate and citrate were quantified by ion chromatography using a Dionex ICS-2100 apparatus, equipped with a IonPac® AS11-HC (4 × 250 mm) column at 30 °C and an anion self-regenerating suppressor (ASRS® 300, 4 mm), under gradient elution which comprised a pre-run of 8 min with 1 mM KOH, 20 min with 30 mM KOH and 10 min with 60 mM KOH, at a flow rate of 1.5 mL/min, using an eluent generator cartridge (Dionex, RFIC™).
N _D ^a	Total dissolved nitrogen (N _D) was measured in a TC-TOC-TN analyser coupled with a TNM-1 unit (Shimadzu, model TOC-V _{CSN}), by thermal decomposition and NO detection by chemiluminescence method, calibrated with standard solutions of potassium nitrate.
N _T	Total nitrogen was determined by Merck® Spectroquant kits (ref: 1.14763.0001), using a WTW thermoreactor (model CR4200) and a WTW photometer (model Photolab S12).
ORP	Oxidation-reduction potential (ORP) was measured by (i) an ORPSension1 meter, from Hach, and (ii) a multiparameter meter HI9828, from Hanna Instruments (sensor HI769828, Hanna Instruments).

Table 2.4. Physico-chemical parameters and their analytical methods

Parameter	Methodology
pH	pH was measured by (i) a pH meter and controller from Colberge (model Aqs- *S*), with a Sensorex sensor (model S653/S653W), (ii) a multiparameter meter HI9828, from Hanna Instruments (sensor HI769828, Hanna Instruments), and (iii) a pH meter VWR symphony - SB90M5.
Polyphenols ^{a,b}	Total polyphenols were quantified by spectrometry (Merck, model Spectroquant® Pharo 100 or Hach, model DR 2010) at 765 nm, using the reagent Folin-Ciocalteau [7], and expressed as mg/L of caffeic acid.
P _T	Total phosphorus (P _T) was measured, in samples pre-treated by persulphate digestion method, according to the Standard Methods, 4500-P C test, using a WTW thermoreactor (model CR4200) and a WTW photometer (model Photolab S12).
SSV _{30-min}	30-min settled sludge volume (SSV _{30-min}) was measured according to Standard Methods [3], 2710-C test.
T	Temperature (T) was measured by (i) an ORPSension1 meter, from Hach, (ii) a multiparameter meter HI9828, from Hanna Instruments (sensor HI769828, Hanna Instruments), and (iii) a pH meter VWR symphony - SB90M5.
TSS	Total suspended solids (TSS) was measured by gravimetry, drying the solid residue at 105 °C, according to Standard Methods [3], 2540-D test.
VSS	Volatile suspended solids (VSS) was determined by gravimetry, after suspended solids oxidation at 550 °C, according to Standard Methods [3], 2540-E test.

^aAll samples were filtrated through 0.45 µm Nylon membrane filters before analysis; ^bDue to the leachate's absorption at the selected wavelengths, a blank/control sample (diluted as for the colorimetric analyses) was always prepared, and the absorbance measured at the same wavelength for correction.

2.5 Biodegradability assays

Before biological tests and other analyses involving chemical oxidation, the excess of H_2O_2 in the samples was removed by adding a small volume of 0.1 g/L solution of catalase (2500 U per mg bovine liver), after pH adjustment to pH 6.5-7.5. Although catalase contribution to DOC and COD is negligible, a blank solution with the same amount of catalase added to the leachate samples was prepared in pure water, for DOC and COD corrections on leachate samples.

A 28 days Zahn-Wellens biodegradability test was performed according to the EC protocol, Directive 88/303/EEC [8]. 250 mL of the pre-treated samples, collected at different photo-Fenton times, without hydrogen peroxide and at neutral pH, were added to an open borosilicate glass beaker, magnetically stirred and kept in the dark at 25°C. Activated sludge from a WWTP located in Porto, previously centrifuged, was added to the samples, as well as some mineral nutrients (KH_2PO_4 , K_2HPO_4 , Na_2HPO_4 , NH_4Cl , $CaCl_2$, $MgSO_4$ and $FeCl_3$). Control and blank experiments were prepared using glucose (highly biodegradable) as carbon source, and distilled water, respectively, further added with mineral nutrients and activated sludge. The percentage of biodegradation (D_t) was calculated by the following equation:

$$D_t = \left[1 - \frac{C_t - C_B}{C_A - C_{BA}} \right] \times 100 \quad (2.4)$$

where C_A and C_{BA} are the DOC (mg/L) in the sample and in the blank, measured 3-h after starting the experiment, C_t and C_B are the DOC (mg/L) in the sample and in the blank, measured at the sampling time t . Photo-Fenton pre-treated samples are considered biodegradable when D_t is higher than 70% [9].

2.6 Target and non-target screening of persistent organic micropollutants

Leachate samples screening analyses for volatile organic compounds (VOCs), pesticides, phenols, phthalates, polycyclic aromatic hydrocarbons (PAHs) and polychlorinated biphenyls (PCBs) were performed by solid-phase microextraction, followed by gas chromatography coupled to mass spectrometry (SPME-GC-MS).

Leachate samples collected at different treatment stages (Chapter 5) were first extracted using a polydimethylsiloxane/divinylbenzene (PDMS-DVB) fibre (60 mm), supplied by Supelco (Bellefonte, PA, USA) for the analysis of semivolatile pollutants, while for the analysis of VOCs a Carboxen/PDMS 75 mm fibre was used. Samples collected at an earlier treatment stage, i.e., prior to the phototreatment step, were first diluted (1:10) in some cases, owing to their dark-brown colour and intense turbidity. For subsequent analyses, 10 mL samples were used for COVs extraction (headspace), 18 mL for pesticides, phthalates, PAHs and PCBs (fibre immersion), and 18 mL acidified with sulfuric acid to pH 2 for phenols extraction (fibre immersion). In immersion mode, extractions were conducted over 60 min, at 60 °C and under constant stirring at 250 rpm. Two different GC-MS systems were employed for the overall characterization: (i) for pesticides, phenols, phthalates, PAHs and PCBs, a Varian CP 3800 (Walnut Creek, CA, USA) gas chromatograph was used, equipped with a fused-silica capillary column coated with 5% diphenylmethylsiloxane (DPMS), VF-5 MS (30m × 0.25 mm I.D., 0.25 µm film thickness), coupled to a 4000 ion trap mass spectrometer, from Varian Instruments (Walnut Creek, CA, USA); (ii) for VOCs, analyses were carried out in a Varian 3400 CX (Walnut Creek, CA, USA) gas chromatograph, equipped with a BR-624 capillary column (30m × 0.25 mm I.D., 1.4 µm film thickness), coupled to a Saturn 2000 ion trap mass spectrometer, from Varian Instruments (Sunnyvale, CA, USA). Mass spectrometers were operated in full-scan mode, in the range between 35 and 420 m/z.

Further details on the analytical methods herein employed for target quantitative analysis of the different organic micropollutants can be found in Gonçalves and Alpendurada [10], Beceiro-González et al. [11] and Guimarães et al. [12]. For non-target screening analyses, spectra of unidentified chromatographic peaks, not present in the respective blank/negative control chromatogram, were compared against reference spectra included in the US National Institute of Standards and Technology (NIST) database, after background subtraction.

2.7 16S rRNA gene barcode 454-pyrosequencing

2.7.1 DNA extraction and 454-pyrosequencing analysis

To characterize the bacterial communities present in the activated sludge under nitrification (N) and denitrification (D) treatments (Chapter 8), a barcode pyrosequencing approach was used. Genomic DNA was extracted from activated sludge samples at three different time points of each treatment (initial (I), middle (M) and final (F)). For each sample, two DNA extractions were performed using the Power Soil™ DNA Isolation Kit (MO BIO) as described elsewhere [13], and collecting the two extracts in a single tube. DNA was further purified (Bacteria genomicPrep Mini Spin Kit, Amersham Biosciences, NJ). The DNA concentration in the final extracts [Qubit® Fluorometer (Invitrogen) with QuantiTMM dsDNA HS assay kit] was c. 60 µg/mL. DNA extracts were used as template for the amplification by PCR of the hypervariable V3–V4 region of the 16S rRNA gene using the primers V3F (5'-ACTCCTACGGGAGGCAG-3') and V4R (5'-TACNVRRGTHCTAATYC-3') [14]. The PCR amplifications were performed in duplicate for each DNA extract as described elsewhere [15]. Briefly, the PCR mixtures (25 µL) contained 0.2 mM dNTPs (Bioron, Ludwigshafen am Rhein, Germany), 0.2 µM of each primer, 5% DMSO (Roche Diagnostics GmbH, Mannheim, Germany), 1 × Advantage 2 Polymerase Mix (Clontech, Mountain View, CA), 1 × Advantage 2 PCR Buffer and 1–3 µL of target DNA (corresponding to 20 ng), and cycling conditions consisted of a first denaturation step at 94 °C for 4 min, followed by 20 cycles at 94 °C (30 s), 44 °C (45 s) and 68 °C (60 s) and a final 2 min extension at 68 °C. The amplicons were quantified by fluorimetry with PicoGreen dsDNA quantitation kit (Invitrogen, Life Technologies, Carlsbad, CA,) and pooled at equimolar concentrations. Pyrosequencing libraries were obtained using the 454 Genome Sequencer FLX platform according to standard 454 protocols (Roche 454 Life Sciences, Branford, CT) at Biocant (Cantanhede, Portugal). The raw reads have been deposited into the NCBI short-reads archive database (accession numbers: SAMN03647091 – DI; SAMN03647092 – DM; SAMN03647093 – DF; SAMN03647094 – NI; SAMN03647095 – NM and SAMN03647096 – NF).

2.7.2 Post run analysis

QIIME pipeline was used to process and analyse the 16S rRNA gene data generated from pyrosequencing [16]. Briefly, sequences shorter than 300 bp and with quality scores lower than 25 were eliminated. Moreover, single sequences (singlet) were removed from each sample data. Sequences (> 300 bp) were assigned to samples by the 8-bp barcodes, grouped into operational taxonomic units (OTUs) using UCLUST [17] with a phylotype threshold of $\geq 97\%$ sequence similarity and were

taxonomically assigned using QIIME defaults. The sequences comprising each OTU were aligned using PYNAST [18] and were classified using Ribosomal Database Project (RDP) classifier [19]. At the 97% identity level, the final OTU table consisted of 20 209 sequences. A phylogenetic tree containing the aligned sequences was produced using FASTTREE [20].

The number of sequences for all the six analysed samples was rarefied (2400 sequences per sample [16]), using the QIIME pipeline, and alpha and beta diversity metrics were determined. Alpha diversity was assessed calculating the richness estimator (Chao 1 [21]) and the diversity indices (Simpson [22], Shannon [23] and PD [24]). Beta diversity patterns of rarefied samples were assessed using the UniFrac metric [25].

2.8 References

- [1] S. Malato, J. Blanco, A. Vidal, C. Richter, Photocatalysis with solar energy at a pilot-plant scale: an overview, *Applied Catalysis B: Environmental*, 37 (2002) 1-15.
- [2] W.D. Schecher, D.C. McAvoy, MINEQL+. A Chemical Equilibrium Modeling System, Version 4.6 for Windows, Environmental Research Software, Hallowell, ME, 2007.
- [3] L.S. Clesceri, A.E. Greenberg, A.D. Eaton, Standard Methods for Examination of Water & Wastewater, 21st ed. ed., American Public Health Association (APHA), American Water Works Association (AWWA) & Water Environment Federation (WEF), 2005.
- [4] ISO 6332:1988, Water quality - Determination of iron - Spectrometric method using 1,10-phenanthroline, in, 1988.
- [5] R.F.P. Nogueira, M.C. Oliveira, W.C. Paterlini, Simple and fast spectrophotometric determination of H₂O₂ in photo-Fenton reactions using metavanadate, *Talanta*, 66 (2005) 86-91.
- [6] E.M. Thurman, R.L. Malcom, Preparative Isolation of Aquatic Humic Substances, *Environ. Sci. Technol.*, 15 (1981) 463-466.
- [7] O. Folin, V. Ciocalteu, On tyrosine and tryptophane determinations in proteíns, *Journal of Biological Chemistry*, 73 (1927) 627-650.
- [8] EPA, U.S. Environmental Protection Agency, Prevention Pesticides and Toxic Substances (7101). Fates; Transport and Transformation Test Guidelines OPPTS 835.3200 Zahn-wellens/EMPA Test, in, EPA 712-C-96-084, Washington, DC, 1996.
- [9] EMPA, OCDE guideline for testing of chemicals, Adopted by the Council on 17th July 1992, Zahn-wellens/EMPA test, in, Swiss Federal Laboratories for Materials testing and Research, 1992.
- [10] C. Gonçalves, M.F. Alpendurada, Solid-phase micro-extraction-gas chromatography-(tandem) mass spectrometry as a tool for pesticide residue analysis in water samples at high sensitivity and selectivity with confirmation capabilities, *Journal of Chromatography A*, 1026 (2004) 239-250.
- [11] E. Beceiro-González, E. Concha-Graña, A. Guimaraes, C. Gonçalves, S. Muniategui-Lorenzo, M.F. Alpendurada, Optimisation and validation of a solid-phase microextraction method for simultaneous determination of different types of pesticides in water by gas chromatography–mass spectrometry, *Journal of Chromatography A*, 1141 (2007) 165-173.
- [12] A.D. Guimarães, J.J. Carvalho, C. Gonçalves, M.D.F. Alpendurada, Simultaneous analysis of 23 priority volatile compounds in water by solid-phase microextraction-gas chromatography-mass spectrometry and estimation of the method's uncertainty, *International Journal of Environmental Analytical Chemistry*, 88 (2008) 151-164.
- [13] A.R. Lopes, C. Faria, Á. Prieto-Fernández, C. Trasar-Cepeda, C.M. Manaia, O.C. Nunes, Comparative study of the microbial diversity of bulk paddy soil of two rice fields subjected to organic and conventional farming, *Soil Biology and Biochemistry*, 43 (2011) 115-125.
- [14] Y. Wang, P.-Y. Qian, Conservative fragments in bacterial 16S rRNA genes and primer design for 16S ribosomal DNA amplicons in metagenomic studies, *PloS one*, 4 (2009) e7401.

- [15] A.R. Lopes, C.M. Manaia, O.C. Nunes, Bacterial community variations in an alfalfa-rice rotation system revealed by 16S rRNA gene 454-pyrosequencing, *FEMS microbiology ecology*, 87 (2014) 650-663.
- [16] J.G. Caporaso, J. Kuczynski, J. Stombaugh, K. Bittinger, F.D. Bushman, E.K. Costello, N. Fierer, A.G. Pena, J.K. Goodrich, J.I. Gordon, QIIME allows analysis of high-throughput community sequencing data, *Nature methods*, 7 (2010) 335-336.
- [17] R.C. Edgar, Search and clustering orders of magnitude faster than BLAST, *Bioinformatics*, 26 (2010) 2460-2461.
- [18] T.Z. DeSantis, P. Hugenholtz, N. Larsen, M. Rojas, E.L. Brodie, K. Keller, T. Huber, D. Dalevi, P. Hu, G.L. Andersen, Greengenes, a chimera-checked 16S rRNA gene database and workbench compatible with ARB, *Applied and environmental microbiology*, 72 (2006) 5069-5072.
- [19] Q. Wang, G.M. Garrity, J.M. Tiedje, J.R. Cole, Naive Bayesian classifier for rapid assignment of rRNA sequences into the new bacterial taxonomy, *Applied and environmental microbiology*, 73 (2007) 5261-5267.
- [20] M.N. Price, P.S. Dehal, A.P. Arkin, FastTree: computing large minimum evolution trees with profiles instead of a distance matrix, *Molecular biology and evolution*, 26 (2009) 1641-1650.
- [21] A. Chao, Nonparametric estimation of the number of classes in a population, *Scandinavian Journal of statistics*, (1984) 265-270.
- [22] E.H. Simpson, Measurement of diversity, *Nature*, (1949).
- [23] C.E. Shannon, W. Weaver, *The mathematical theory of communication*, University of Illinois Press, Urbana, IL, 1963.
- [24] D.P. Faith, Conservation evaluation and phylogenetic diversity, *Biological conservation*, 61 (1992) 1-10.
- [25] C. Lozupone, R. Knight, UniFrac: a new phylogenetic method for comparing microbial communities, *Applied and environmental microbiology*, 71 (2005) 8228-8235.

3 Integration of solar photo-Fenton and biological oxidation processes for leachate treatment at pre-industrial scale

A strategy for the treatment of leachates from sanitary landfills after lagooning pretreatment is proposed in this chapter. The most recalcitrant organic compounds were eliminated by a solar photo-Fenton oxidation process, leading to a biodegradability enhancement of the leachate and promoting its subsequent oxidation in an activated sludge biological reactor. The integrated leachate treatment process was conducted in a pre-industrial plant, incorporating a photocatalytic system with 39.52 m² of compound parabolic collectors (CPCs) and a 3.5 m³ capacity activated sludge biological reactor, operated under aerated and anoxic conditions. An extensive physico-chemical characterization of the leachate after lagooning was performed during one year, from June 2010 to May 2011, showing its high recalcitrant character mainly associated with the presence of humic substances.

The efficiency of the combined treatment was evaluated concerning the leachate characteristics' variability after lagooning, availability of solar radiation throughout the year, and different operational process variables, such as the amount of hydrogen peroxide necessary to reach the required COD target value, biodegradability enhancement during the photo-oxidation process, iron reutilization in consecutive oxidation processes, removal of the acidic sludge resulting from the acidification process and leachate temperature/average solar power. The elimination of the remaining organic carbon fraction and nitrogen compounds after the pre-oxidation step was also assessed in an activated sludge biological reactor, under aerobic and anoxic conditions, considering the composition variability of the photo-treated leachate. Nitrification and denitrification reaction rates were also evaluated.

This chapter is based on the research article “Silva, T.F.C.V., Silva, M.E.F., Cunha-Queda, A.C., Fonseca, A., Saraiva, I., Boaventura, R.A.R, Vilar, V.J.P, *Sanitary landfill leachate treatment using combined solar photo Fenton and biological oxidation processes at pre-industrial scale*, Chemical Engineering Journal, 228 (2013) 850-866, DOI: 10.1016/j.cej.2013.05.060”.

3.1 Introduction

Sanitary landfill leachates treatment constitutes nowadays one of the major challenges for the scientific community, mainly due to the variability of leachates composition and quantity [1, 2], reinforced by the presence of a complex mixture of recalcitrant organic contaminants. These may include humic and fulvic acids [3], phthalic esters [4, 5] pesticides [6], and many other emerging organic pollutants, in concentration as low as nanograms (ng) or micrograms (μg) per liter (perfluorinated compounds-PFCs, pharmaceuticals and personal care products, polyaromatic hydrocarbons-PAHs) [7], inorganic compounds (chloride, sulphate, bicarbonate and carbonate, sulphide species, alkali and alkaline earth metals, iron and manganese) [8], nitrogen compounds in high concentration [9-11] and heavy metals [8, 12].

Renou et al. [11] and Abbas et al. [13] presented reviews on different approaches used for landfill leachates treatment, divided in five different groups: i) leachate channeling (combined treatment with domestic sewage; recycling back through the landfill); ii) biodegradation (aerobic and anaerobic biological processes); iii) chemical and physical methods (flotation, coagulation/flocculation, chemical precipitation, adsorption, ammonium stripping, chemical oxidation and ion exchange); iv) membrane filtration (microfiltration, ultrafiltration, nanofiltration and reverse osmosis); v) combination of the different processes reported above. The UK Environment Agency presented in 2007 a guidance for the treatment of landfill leachates [14], which indicated that the Best Available Technologies for leachates treatment relied on the adoption of a multistage treatment process, possibly involving the use of primary, secondary, and tertiary processes, adjusted to the type of leachate, including the different technologies aforementioned.

During the late 90s, in Germany, the Netherlands, Belgium, France, Portugal and Spain, a lot of reverse osmosis (RO) leachate treatment systems were designed with an aerated lagoon in front of a 2-stages RO plant [14]. This configuration presented as advantage the aerated lagoon, which significantly reduced $\text{NH}_4^+\text{-N}$ load, BOD_5 and COD due to its biologic activity. Although the production of a high quality effluent (permeate) was a significant advantage of the RO process, considering the removal of non-biodegradable components of the leachate, such as chloride, residual COD and heavy metals, all these contaminants were present in the concentrate, which could be 10%-25% of the leachate's volume [14]. In addition, all chemicals required for the effective operation of an RO plant, such as citric acid, membrane cleaner and anti-scaling detergents (up to 0.3% per cubic meter of treated leachate) were also present in the concentrate [14]. Disposal of concentrate is a key factor to be addressed, and normally the concentrate is returned to the landfill or disposed of off-site. The return of concentrate to the landfill coincides with an increase of COD and $\text{NH}_4^+\text{-N}$ concentration in the leachate, as well as an increase in electrical conductivity [14].

Advanced oxidation processes (AOPs) constitute nowadays a promising technique for the removal of recalcitrant pollutants from landfill leachates, turning them into simpler and easily biodegradable compounds through the generation of powerful reactive chemical species, such as hydroxyl radicals ($\cdot\text{OH}$) [15-20]. Hence, a subsequent biological oxidation step could allow getting in compliance with the discharge limits. Considering the high costs associated with energy and chemicals consumption, research has focused on the development of systems using renewable solar energy as UV photon source to promote the oxidation process [21-24].

Although AOPs constitute a promising technology for the treatment of recalcitrant wastewaters, few demonstration or industrial applications are available: (i) in 1993 a solar TiO_2 photocatalytic plant, with 158 m^2 of parabolic-trough concentrators collectors (PTCs) was installed at Lawrence Livermore National Laboratory for the treatment of groundwater contaminated with trichloroethylene (TCE) [25]; (ii) in 1998, 12 double-skin sheet photoreactors (DSSRs) with a total irradiated area of 27.6 m^2 and total volume of 1 m^3 were installed at Volkswagen AG factory (Wolfsburg, Germany) for the treatment of biologically pre-treated wastewaters [26-28]; (iii) in 2004 two Thin Film Fixed Bed Reactors (TFFBR), with a width of 2.5 m and a length of 10 m, corresponding to a total illuminated area of 50 m^2 , oriented to the South and tilted 20° , were installed at a Tunisian textile industry (Menzel Temime) for the treatment of a biologically pre-treated textile wastewater and further combined with two bioreactors (SBR-Sequential Batch Reactors) with 15 m^3 capacity each one, used for the pre-treatment of the textile effluent [29]; (iv) in 2004 a 150 m^2 plant of compound parabolic collectors (CPCs) and total operation volume of 2.5 m^3 was installed at Albaida (Almeria, Spain) for the treatment of wastewaters contaminated with pesticides, and in 2010 the combination with a biological system based on two 1.23 m^3 immobilized biomass reactors was optimized [30]; (v) in 2007 a 100 m^2 unit of CPCs for the pre-oxidation of a saline industrial wastewater containing 600 mg/L of a recalcitrant pharmaceutical compound, α -methylphenylglycine, was installed at a pharmaceutical company, DSM DIRETIL, which was able to remove 50% of the initial dissolved organic carbon (DOC), being the remaining 45% removed in an aerobic biological treatment system [31].

Considering the application of AOPs to leachates treatment, few full-scale treatment plants have been reported in the literature, mainly using ozonation combined with biological processes. Between 1991 and 2002, 35 different plants combining biological processes and ozonation [32] were operated for the treatment of leachates, at a flow rate varying from $10,000$ to $150,000 \text{ m}^3/\text{year}$, and COD levels between 2000 - 4000 mg/L . The Singhofen landfill leachate treatment plant (Germany) treated $29,200 \text{ m}^3/\text{year}$, combining a biological treatment step, consisting on a denitrification reactor followed by 3 nitrification reactors, a sedimentation tank and a sand filter, with an ozonation/UV stage and a final biological

treatment step [32], producing a final effluent with 200 mg COD/L and 50 mg $\text{NH}_4^+\text{-N/L}$. The facility in Asbach (Germany) used the BIOQUINT® system since 1998 and treated up to 26,000 m³/year, using a raw leachate basin (1000 m³) followed by a biological treatment stage, with a nitrification fixed-bed biofilter (45 m³), and two denitrification fixed-bed biofilters (2×10 m³) and an ozonation system (4 kg O₃/hour), achieving a final effluent with 200 mg COD/L, < 50 mg $\text{NH}_4^+\text{-N/L}$, < 2 NO₂⁻-N/L and < 70 mg N_{total}/L. The landfill leachate treatment plant in Friedrichshafen (Germany) was based on an improved version of the BIOQUINT® system, where the biological treatment stage consisted on nitrification and denitrification activated sludge reactors with 100 and 25 m³ capacity, respectively, followed by an ozonation (1.5 kg O₃/h)/biological recycle step, leading to 82% and 98% removal of COD and nitrogen, respectively [33]. Leachates from a sanitary landfill in Bord-Matin, near Saint-Etienne (France), containing 1750 mg COD/L and 850 mg $\text{NH}_4^+\text{-N/L}$, have been treated since 1972 by a combination of biological nitrification and denitrification processes, followed by chemical precipitation with lime in a lamellar settling tank and a final ozonation step [33].

The present work aims at developing a new strategy for the treatment of landfill leachates, after lagooning, using a solar photo-Fenton oxidation process to degrade the most recalcitrant organic compounds, leading to a biodegradability enhancement of the leachate, which may then be further oxidized in an activated sludge biological reactor. The elimination of the remaining nitrogen compounds fraction was also evaluated in the activated sludge biological reactor, under aerated and anoxic conditions, first promoting the aerobic nitrification of ammonia to nitrite/nitrate and then the anoxic denitrification of nitrate/nitrite to nitrogen gas, using methanol as external carbon source. The efficiency of the treatment strategy was evaluated in a pre-industrial plant, combining a photocatalytic reactor with 39.52 m² of compound parabolic collectors (CPCs) with an activated sludge reactor with 3.5 m³ capacity, during 1-year. The efficiency of the treatment strategy was evaluated to understand the influence of the leachate composition, weather conditions and operational variables of the process (hydrogen peroxide dose necessary to reach the required COD target value, biodegradability enhancement during the photo-oxidation process, re-utilization of iron sludge in the photo-Fenton reaction, elimination of sludge resulting from the acidification process and influence of temperature/average solar power during the reaction). Finally, the first results using a plant close to industrial scale and real leachate samples, under real operational conditions, are herein presented, supporting this system efficiency, sustainable practical application and commercialization.

3.2 Experimental methodology

During the trial period concerning this chapter, 29 leachate samples were collected at a municipal solid waste (MSW) sanitary landfill nearby Porto. Table 3.1 presents the main physico-chemical characteristics of the leachate over 1-year. Each parameter was analysed in duplicate, for each sample. From January to May, only one sample was analysed per month.

All the chemicals used in this work, the detailed description of the experimental unit and respective procedures, as well as the employed analytical methods can be consulted in Chapter 2.

The photo-Fenton reaction efficiency was evaluated in the pre-industrial scale plant during 1-year, in order to better understand the influence of the leachate composition, specific solar radiation conditions and different operational variables of the photo-Fenton process, such as: (i) hydrogen peroxide dose/leachate composition variability (experiments 4–7, 12 and 18); (ii) reutilization of iron sludge (experiments 8–11 and 13–17); (iii) sludge removal resulting from the acidification process (experiments 22–24); (iv) average solar UV irradiation/temperature (experiments 5 and 21); (v) type of acid used for acidification/variability of the leachate's alkalinity (experiments 5, 6, 8, 24 and 25) and (vi) biodegradability enhancement (experiments 19–25).

The biological treatment efficiency was evaluated in the pre-industrial scale plant using a 3.5 m³ reactor, in order to assess the influence of the photo-treated leachate composition, in terms of organic carbon concentration and type (according to the photo-oxidation time) and inorganic species concentration and type, such as nitrogen, sulphate and chloride (experiments 18–25). Nitrification and denitrification reaction rates were also evaluated in experiments 20–25.

3.3 Results and discussion

3.3.1 Leachate characterization

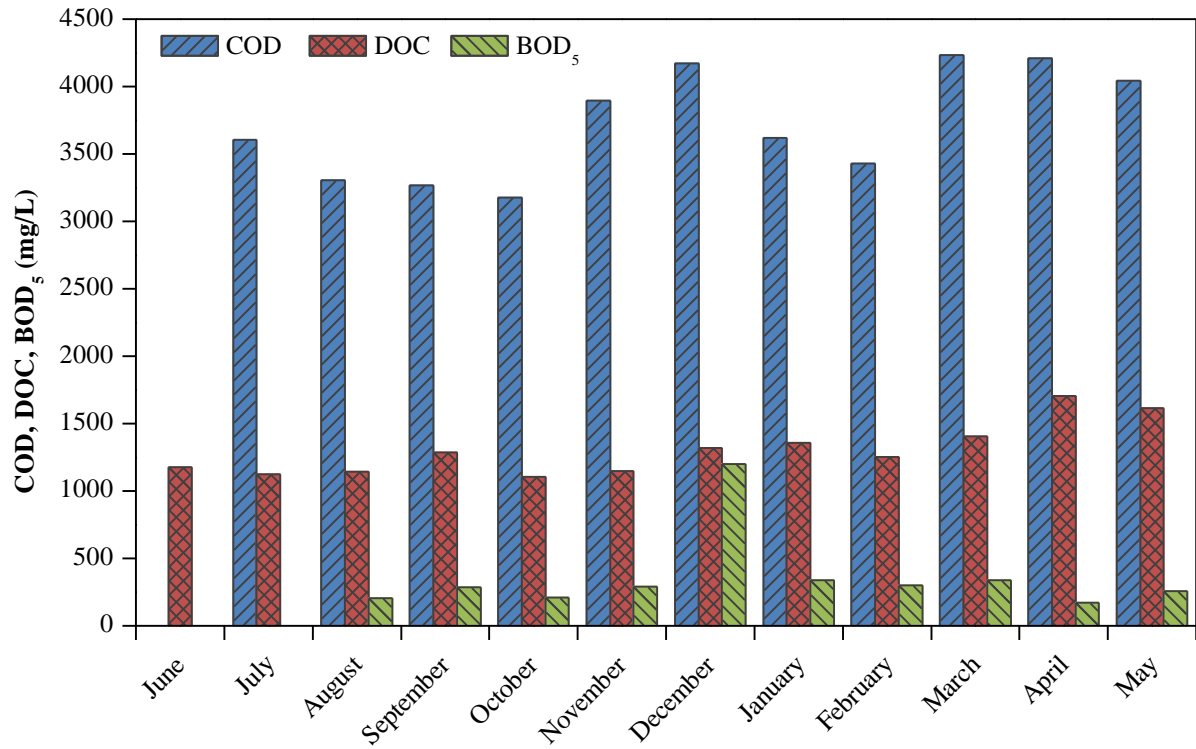
Table 3.1 presents an extensive characterization of leachate samples, after aerobic lagooning, collected at a sanitary landfill located in North Portugal, since June 2010 to May 2011. After the lagooning process, the leachate composition presented a high variability during the year, attributed to: (i) the raw leachate (fed to the lagoon) variability; (ii) the lagoon treatment efficiency, associated with the low liquid oxygen doses used to reduce costs; (iii) the leachate's temperature, which influenced greatly the nitrification and denitrification reactions, leading to a high variability in terms of nitrogen species content and alkalinity.

The leachate presented an intense dark-brown colour associated with its high concentration in humic substances (>1000 mg C_{HS}/L), which corresponded to an average of 59% of the dissolved organic carbon ($DOC = 993\text{--}1707$ mg C/L ; $COD = 2320\text{--}5416$ mg O_2/L), a high nitrogen load ($208\text{--}2989$ mg N/L) and a low BOD_5/COD ratio ($0.04\text{--}0.01$), reflecting a low biodegradability (Figure 3.1a). An exception was spotted in December, with a moderate biodegradability rate ($BOD_5/COD = 0.20\text{--}0.37$), indicating that the lagoon was not working well during that month. Between June and November 2010, the aerated lagoon was working properly and almost all nitrogen compounds and biodegradable organic carbon were completely eliminated (Figure 3.1b). The lower pH values and higher nitrate contents during the summer period (July, August and September) could be explained by the higher doses of injected liquid oxygen, in order to reduce the intense odour associated with high temperatures, consequently leading to an increase in the nitrification reaction rate (and lower values of inorganic carbon associated with alkalinity consumption during nitrification), and simultaneously slower denitrification kinetics (Figure 3.1b). From December 2010 until March 2011, the aerated lagoon presented a lesser nitrogen and organic matter removal efficiency, which was related to the low temperatures observed during that period ($11.7\text{--}16.6^\circ C$), leading to the inhibition of nitrification, and consequent accumulation of ammonium nitrogen, as already reported by Ilies and Mavinic [34]. Between April and May 2011, nitrification was affected by the low dissolved oxygen concentration observed, which favoured the partial oxidation of a small fraction of ammonia to nitrites, instead of nitrates (as reported by Ruiz et al. [35]) leading simultaneously to the decrease on the organic carbon removal efficiency.

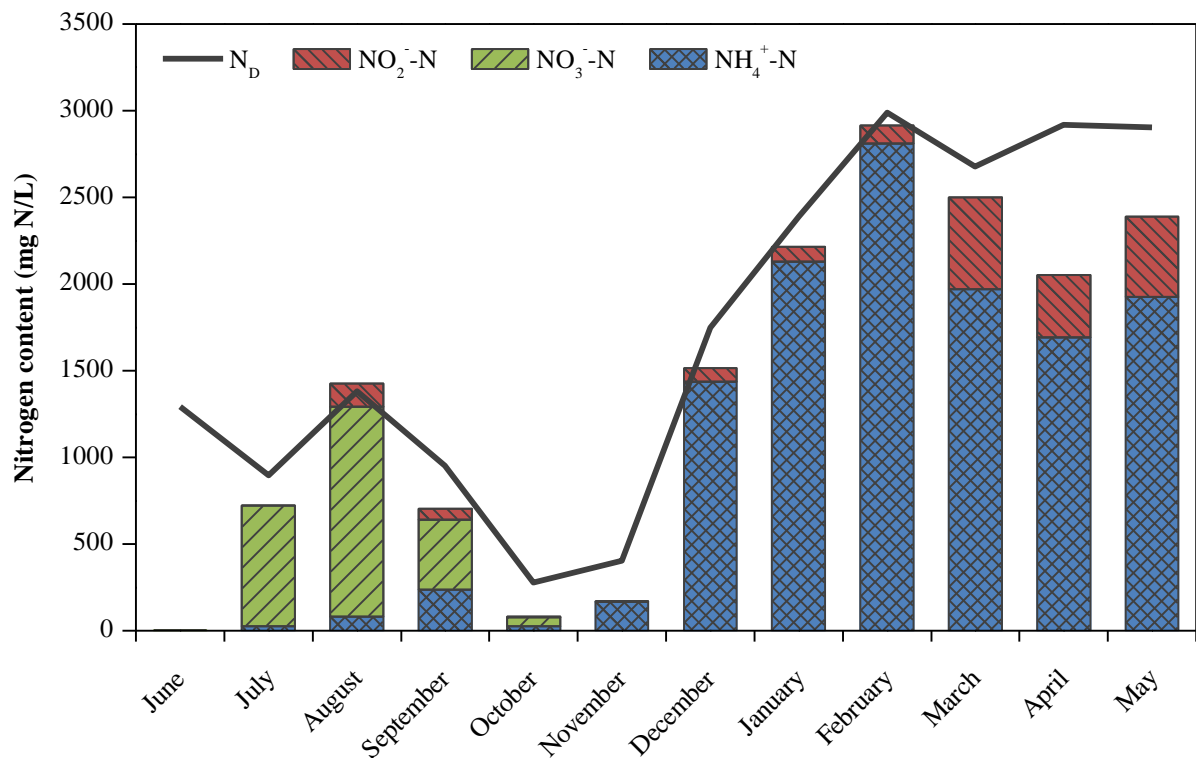
Table 3.1. Characterization of the sanitary landfill leachate after aerobic lagooning throughout 1-year.

Month	June	July	August	September	October	November	December	January	February	March	April	May	Annual
pH	7.8 (7.8-7.9)	7.2 (6.7-7.8)	6.9 (6.5-7.5)	7.5 (7.2-7.7)	7.6 (7.6-7.6)	7.7 (7.6-7.8)	7.6 (7.4-7.8)	7.8	7.9	7.4	8.1	7.7	7.5 (6.5-8.1)
T (°C)	24.8 (23.6-25.9)	25.8 (23.1-28.3)	27.0 (25.3-28.2)	23.6 (22.8-24.8)	20.5 (20.1-20.9)	15.8 (13.9-19.4)	13.5 (13.0-14.0)	16.6	11.7	12.9	26.0	23.8	21.8 (11.7-28.3)
TSS (mg/L)	-	269 (145-435)	302 (121-424)	258 (125-375)	459 (394-523)	766 (405-1085)	453 (375-530)	187	136	52	112	90	329 (52-1085)
TIC (mg C/L)	1548 (1389-1548)	579 (284-1157)	416 (200-885)	1117 (900-1319)	1049 (1026-1071)	1287 (1186-1486)	2262 (2164-2359)	2796	2497	2307	2303	2202	1280 (200-2796)
DOC (mg C/L)	1178 (1118-1238)	1123 (1086-1138)	1145 (993-1266)	1187 (1169-1402)	1104 (995-1213)	1149 (1000-1382)	1320 (1313-1326)	1356	1253	1406	1707	1654	1238 (993-1707)
COD (mg O ₂ /L)	-	3606 (3525-3775)	3307 (2945-3668)	3266 (2320-5416)	3177 (3170-3184)	3895 (3196-4588)	4173 (4147-4199)	3618	3428	4235	4211	4045	3621 (2320-5416)
BOD ₅ (mg O ₂ /L)	-	-	205	285 (150-420)	208 (195-220)	288 (180-450)	1200 (850-1550)	340	300	340	170	255	373 (150-1150)
BOD ₅ /COD	-	-	0.06	0.09 (0.06-0.14)	0.07 (0.06-0.07)	0.07 (0.05-0.10)	0.29 (0.20-0.37)	0.09	0.09	0.08	0.04	0.06	0.10 (0.04-0.37)
Polyphenols (mg caffeic acid/L)	172 (165-179)	144 (134-164)	149 (132-161)	148 (140-156)	155 (151-158)	169 (136-213)	229 (226-232)	157	165	172	190	193	162 (132-232)
TDI (mg (Fe ²⁺ +Fe ³⁺)/L)	16.7 (15.6-17.7)	8.5 (5.9-14.2)	9.1 (1.8-19.9)	16.6 (7.6-29.4)	10.2 (9.0-11.5)	15.7 (9.6-21.7)	19.4 (18.9-19.9)	12.8	10.6	12.0	12.2	11.1	12.9 (1.8-29.4)
Sulphate (mg SO ₄ ²⁻ /L)	195 (167-224)	292 (246-338)	368 (228-597)	327 (275-395)	249 (248-249)	226 (202-239)	138 (132-144)	100	119	128	90	90	248 (90-597)
Chloride (mg Cl ⁻ /L)	3393 (3347-3439)	3365 (3078-3601)	3666 (3513-3767)	4023 (3565-4691)	3374 (3263-3484)	3385 (3173-3601)	3102 (3065-3139)	2834	2867	2888	3148	3082	3440 (2834-4691)
Total Nitrogen (mg N/L)	1291 (841-1742)	896 (323-1224)	1383 (1240-1544)	951 (712-1165)	277 (234-320)	405 (208-724)	1747 (1456-2038)	2390	2989	2678	2917	2905	1303 (208-2989)
Ammonium (mg NH ₄ ⁺ -N/L)	-	24 (1-90)	81 (19-216)	237 (65-344)	27 (8-46)	166 (36-383)	1436 (1173-1699)	2131	2812	1970	1691	1926	591 (1-2812)
Nitrate (mg NO ₃ ⁻ -N/L)	3 (0-6)	698 (9-1126)	1211 (988-1297)	405 (217-691)	52 (21-83)	3 (1-8)	<1 <1	<1	<1	<1	<1	<1	374 (1-1297)
Nitrite (mg NO ₂ ⁻ -N/L)	-	2 (1-5)	133 (1-263)	60 (1-273)	4 (1-9)	<1 <1	79 (74-84)	85	101	529	361	462	91 (1-529)
Total Phosphorous (mg P/L)	-	16.6 (2.6-40.0)	10.9 (7.0-13.4)	26.3 (15.9-44.2)	11.7	18.7 (8.7-30.6)	14.3 (14.0-14.5)	17.5	19.9	26.2	30.6	23.8	19.1 (2.6-44.2)

Values in bold and in parenthesis refer to medium and minimum-maximum values, respectively, obtained during experimental period.



(a)



(b)

Figure 3.1. Evolution of the leachate's characteristics after lagooning, during 2010-2011, in terms of DOC, COD and BOD₅ (a) and nitrogen (b).

3.3.2 Solar photo-Fenton process

3.3.2.1 Kinetics

Between July 2010 and January 2011, 25 experiments were performed, combining solar photo-Fenton with a biological oxidation system for the treatment of leachates after lagooning (Table 3.2). The photo-Fenton reaction was conducted at pH 2.8 and with 80 mg Fe²⁺/L. This pH value was selected for the photo-Fenton reaction to avoid iron precipitation [36]. Previous results [37] showed that the optimum iron concentration for similar leachate and using CPC photoreactors with an internal diameter of 46.4 mm in the presence of high concentrations on sulphates and chlorides, is 80 mg/L (not considering the presence of dissolved iron in the leachate). Thus, the average dissolved iron concentration during the photo-Fenton reaction ranged between 30 and 50 mg (Fe²⁺ + Fe³⁺)/L. An initial 500 mg/L H₂O₂ dose was added and maintained during the reaction between 100 and 500 mg/L, by the addition of small amounts of H₂O₂ as consumed. Bacardit et al. [38] showed that supplying H₂O₂ in multiple small amounts, and maintaining its concentration between 50 and 550 mg H₂O₂/L, improves oxidation reaction rates and minimizes the consumption of H₂O₂ per amount of oxidized COD. Prieto-Rodríguez et al. [39] also reported the same optimal H₂O₂ concentration range to avoid hydrogen peroxide to be rate-limiting if applied in too low concentrations, or in high concentrations, it can compete with contaminants for the generated hydroxyl radicals or to self-decompose into oxygen and water.

Different operational variables of the process were evaluated, such as: the possible reutilization of iron sludge for the photo-Fenton reaction, the elimination of the sludge resulting from the acidification process and the influence of temperature/average solar power during the reaction. In order to prevent sulphate concentrations higher than 2 g/L, which is the discharge limit imposed by the Portuguese legislation, and considering the absence of discharge limit for the chloride concentration, the acidification of the leachate was performed with a mixture of HCl and H₂SO₄, with the exception of experiments 8–11, 24 and 25, for which only H₂SO₄ was used. However, H₂SO₄ is commercially available in a higher concentration (> 96% < > [H⁺] ≈ 37 M) than HCl (37% < > [H⁺] ≈ 12 M), though at similar price, being necessary a substantially higher amount of HCl to acidify the leachate (increasing Cl⁻ concentration relatively to SO₄²⁻). Table 3.3 shows that different doses of HCl and H₂SO₄ or only H₂SO₄ were necessary to achieve a final pH of 3.0, depending on the leachate's alkalinity after lagooning over the year. This was attributed to oxygen deficient conditions and low temperatures in the lagoon, which affected greatly the nitrification reaction.

Table 3.2. Characterization of the landfill leachate before photo-Fenton process.

Exp. ^a	Data	pH	T (°C)	TSS (mg/L)	DIC (mg/L)	CaCO _{3,IC} ^d (mg/L)	DOC (mg/L)	COD (mg/L)	BOD ₅ (mg/L)	Polyphenols (mg caffeic acid/L)	TDI (mg/L)	SO ₄ ²⁻ (mg/L)	Cl ⁻ (mg/L)	N _D (mg/L)	NH ₄ ⁺ -N (mg/L)	NO ₃ ⁻ -N (mg/L)	NO ₂ ⁻ -N (mg/L)	P _T (mg/L)
4	01-07	7.8	25.6	1435	1157	4821	1086	3600	-	164	14.2	246	3388	323	90	9	1	2.6
5	13-07	7.0	26.4	407	575	2396	1129	3775	-	140	7.9	292	3601	859	1	757	<1	40.0
6	21-07	7.2	23.1	145	461	1921	1128	3525	-	142	7.2	289	3078	988	8	747	5	-
7	26-07	7.2	28.3	145	419	1746	1237	3525	-	138	7.1	296	3189	1086	10	852	<1	-
8	30-07	6.7	25.8	214	284	1183	1136	-	-	134	5.9	338	3568	1224	12	1126	<1	7.3
9 ^b	04-08	6.5	27.5	121	200	833	1135	2945	-	132	6.6	340	3665	1377	19	1297	<1	7.0
10 ^b	09-08	6.8	27.1	365	280	1165	989	-	-	108	11.7	762	3526	1556	45	1248	188	11.0
11 ^b	11-08	6.7	28.2	598	299	1246	888	-	-	115	20.3	1059	3705	1430	44	1248	188	11.3
12	27-08	7.5	25.3	424	885	3687	1266	3668	205	152	8.2	306	3718	1240	216	988	6	11.2
13 ^b	02-09	7.7	23.8	125	967	4029	1176	2680	150	156	8.0	314	4035	1165	255	691	10	15.9
14 ^b	06-09	7.7	23.5	206	1146	4776	1042	2860	160	140	23.8	907	4731	1104	322	550	<1	16.6
15 ^b	10-09	7.7	23.2	619	1253	5222	1127	2095	250	143	27.3	840	4532	1017	277	430	<1	20.9
16 ^b	16-09	7.4	24.8	1300	1319	5497	1198	1986	200	153	35.5	801	4711	881	266	281	11	19.9
17 ^b	24-09	7.2	22.8	1675	900	3750	1200	4280	300	148	25.7	811	5452	784	120	256	195	33.6
18	15-10	7.6	20.9	394	1071	4462	1213	3170	220	151	11.5	249	3263	320	46	21	9	-
19	25-10	7.6	20.1	523	1026	4275	995	3184	195	158	9.0	248	3484	234	8	83	<1	11.7
20	02-11	7.6	19.4	1085	1190	4958	1064	3900	180	136	9.6	239	3601	208	36	8	<1	30.8
21	09-11	7.7	13.9	405	1186	4942	1000	3196	235	159	15.9	236	3380	283	79	<1	<1	8.7
22	23-11	7.8	14.4	808	1486	6191	1382	4588	450	213	21.7	202	3173	724	383	1	<1	16.7
23	14-12	7.4	13.1	375	2164	9016	1313	4947	1550	226	19.9	144	3139	1456	1173	<1	74	14.5
24 ^c	30-12	7.8	14.0	530	2359	9829	1326	4199	850	232	18.9	132	3065	2038	1699	<1	84	14.0
25 ^c	18-01 ^c	7.8	16.6	187	2796	11650	1356	3618	340	157	12.8	100	2834	2390	2131	<1	85	17.5

^aExperiment number; ^bISRS-Iron Sludge Recycle Study; ^c2011; ^dAlkalinity values considering that at pH less than 8.0 the inorganic carbon is almost in the form of bicarbonates [40].

Table 3.3. Characterization of the landfill leachate before photo-Fenton process.

Exp. ^a	pH _m ^d	T _m ^d (°C)	Fe _m ^d (mg/L)	t _{PF} (h)	I _{UV} (W/m ²)	Q _{UV} (kJ/L)	[H ₂ O ₂] (mM)	[H ₂ SO ₄] (mM)	[HCl] (mM)	%CaCO ₃ ^e	DOC _i (mg/L)	DOC _{AA} ^f (mg/L)	DOC _{BN} ^g (mg/L)	DOC _f (mg/L)	Min ^h (%)	H ₂ O ₂ /DOC _{ox} ⁱ ($\frac{\text{mg H}_2\text{O}_2}{\text{mg DOC}_{\text{ox}}}$)
4	2.6	32.8	39.6	12.9	27.1	---	83	18	128	58	1086	639	609	622	43	---
5	2.6	37.0	51.6	13.8	23.3	35.0	210	18	38	64	1129	478	177	234	79	29.3
6	2.7	34.4	56.8	6.4	25.5	17.8	99	18	26	61	1128	518	506	510	55	---
7	2.6	38.7	47.5	5.3	34.9	20.2	103	18	26	55	1237	509	525	547	56	---
8 ^b	2.6	40.2	52.3	5.9	24.8	15.9	114	18	0	64	1136	636	571	449	61	20.7
9 ^{b,c}	2.7	37.7	51.0	6.4	34.2	23.8	102	15	0	57	1135	641	587	493	57	23.4
10 ^{b,c}	2.8	37.8	29.0	6.3	25.6	22.7	88	14	0	62	989	773	699	625	37	20.2
11 ^{b,c}	2.7	37.6	45.2	5.2	28.6	21.0	91	16	0	62	888	775	729	729	18	67.3
12	2.6	39.3	53.6	4.0	35.4	14.4	70	31	35	77	1266	691	626	656	48	68.0
13 ^c	2.6	29.5	48.2	5.8	30.6	17.9	70	20	69	74	1176	621	733	724	38	---
14 ^c	2.6	27.1	45.6	12.6	18.3	32.3	72	14	69	70	1042	640	675	649	38	---
15 ^c	2.7	32.8	41.4	4.7	38.3	25.4	74	13	80	71	1127	598	625	689	39	---
16 ^c	2.6	32.0	42.7	6.3	28.0	25.2	72	13	83	73	1198	666	668	777	35	---
17 ^c	2.5	29.6	42.0	7.0	29.3	29.2	72	13	62	62	1200	828	828	867	28	---
18	2.7	31.1	60.2	11.7	25.2	30.0	100	18	75	80	1213	710	674	584	52	27.0
19	2.7	30.1	65.6	14.3	23.1	33.4	140	18	71	79	995	563	538	561	44	---
20	2.7	30.8	48.9	12.8	21.3	27.7	140	18	83	83	1064	542	471	490	54	---
21	2.8	20.8	60.3	35.5	13.9	50.0	190	18	93	76	1000	501	312	324	68	36.5
22	2.9	17.6	42.0	47.7	11.0	53.4	120	18	120	79	1382	797	605	474	66	12.6
23	2.6	17.7	32.7	55.7	12.2	69.2	120	18	150	96	1313	858	700	750	43	---
24 ^b	2.6	16.1	91.0	46.0	6.6	30.8	100	114	0	86	1326	812	576	557	58	13.3
25 ^b	2.6	23.5	56.1	18.3	20.2	37.6	100	149	0	78	1356	696	562	547	60	23.5

^aExperiment number; ^bAcidification with only H₂SO₄; ^cISRS-Iron Sludge Recycle Study; ^dpH_m, T_m and Fe_m corresponds to average pH values, average temperature and average dissolved iron observed during the photo-Fenton experiment; ^ePercentage of consumed acid needed to neutralize the alkalinity ($\text{CaCO}_{3,IC}/[100.08([\text{H}_2\text{SO}_4]+[\text{HCl}]/2)]$, %); ^fDOC After Acidification; ^gDOC Before Neutralization; ^hPhoto-Fenton mineralization ($1-\text{DOC}_f/\text{DOC}_i$, %); ⁱRatio between H₂O₂ consumed and oxidized DOC ($\text{H}_2\text{O}_2/(\text{DOC}_{AA}-\text{DOC}_f) \times 34.02$).

Lower alkalinity values significantly reduce acid consumption during the acidification process (Table 3.2 and Table 3.3). The percentage of consumed acid necessary to neutralize the alkalinity ranged between 55% and 96% of the total acid consumption. Different studies reported that the optimum pH for the photo-Fenton reaction is 2.8 not only because it avoids iron precipitation, but also because the predominant iron species in solution ($T = 25\text{ }^{\circ}\text{C}$; ionic strength (IS) = 0.5 M) are FeOH^{2+} (48.0%), Fe^{3+} (46.9%) and $\text{Fe}(\text{OH})_2^+$ (5.0%) [41-45], being FeOH^{2+} the most photoactive ferric-water complex [36, 46]. However, considering sulphate and chloride contents after acidification and iron addition, the iron (III) speciation diagram (Figure 3.2a) shows that at pH 2.8, the predominant iron species in solution are FeSO_4^+ (69.6%), $\text{Fe}(\text{SO}_4)_2^-$ (23.7%), FeOH^{2+} (2.6%), Fe^{3+} (2.6%) and FeCl^+ (7%) ($[\text{SO}_4^{2-}] = 2\text{ g/L}$; $[\text{Cl}^-] = 4\text{ g/L}$; IS = 0.5 M; $T = 25\text{ }^{\circ}\text{C}$) [41-45], leading to the formation of $\text{SO}_4^{\bullet-}$, OH^{\bullet} and Cl^{\bullet} radicals, respectively, according to Eqs. (2.1)–(3.3) [47]:



According to the speciation diagram, FeOH^{2+} species present the maximum molar fraction (19.5%) at pH 4.1. Since the oxidant power of hydroxyl radicals is higher than sulphate and chloride radicals, an increment of the oxidation rate could be achieved by increasing the pH up to 4.1. Nevertheless, according to ferric ions solubility diagram (data not showed) for pH 4.1 only 0.2 mg Fe^{3+}/L are still soluble. The removal of the leachate's alkalinity prior to the photo-Fenton reaction would be a major aspect in order to reduce the amount of acid necessary and, consequently, the amount of sulphate and chloride ions, which decrease the reaction rates.

Figure 3.3 shows the solar photo-Fenton results for experiments 5 and 6, using different doses of H_2O_2 . After acidification in the photo-Fenton process, it could be observed a DOC abatement of 54–58%. In previous papers, this DOC abatement was either attributed to the formation of foam, which could retain large amounts of DOC, or to the mineralization of the most oxidized organic compounds [22, 23]. However, these two factors could only be responsible for a small fraction of the DOC abatement, since the majority was due to the precipitation of humic acids. For the sanitary landfill leachate with an initial DOC of 1707 mg C/L after lagooning, 59% of the organic carbon content was attributed to humic substances (1008 mg $\text{C}_{\text{HS}}/\text{L}$; HS – humic acids + fulvic acids). After acidification, the DOC abatement was approximately 27% (DOC = 1239 mg C/L), which corresponded to a reduction of the humic substances of approximately 33% (671 mg $\text{C}_{\text{HS}}/\text{L}$; HS/DOC = 54%). This indicated that the precipitation of humic acids (33% of the humic substances), corresponded to approximately 72% of the DOC

abatement. Previous results showed that when the acidified leachate was neutralized again to the same initial pH, the DOC content returned to the initial value [37]. Wu et al. [48], Zhang et al. [49] and Christensen et al. [50] presented humic acids, fulvic acids and Hyl (hydrophilic) DOC fractionation values of approximately 40/41/15 (%), 43/34/57 (%) and 17/25/29 (%), respectively.

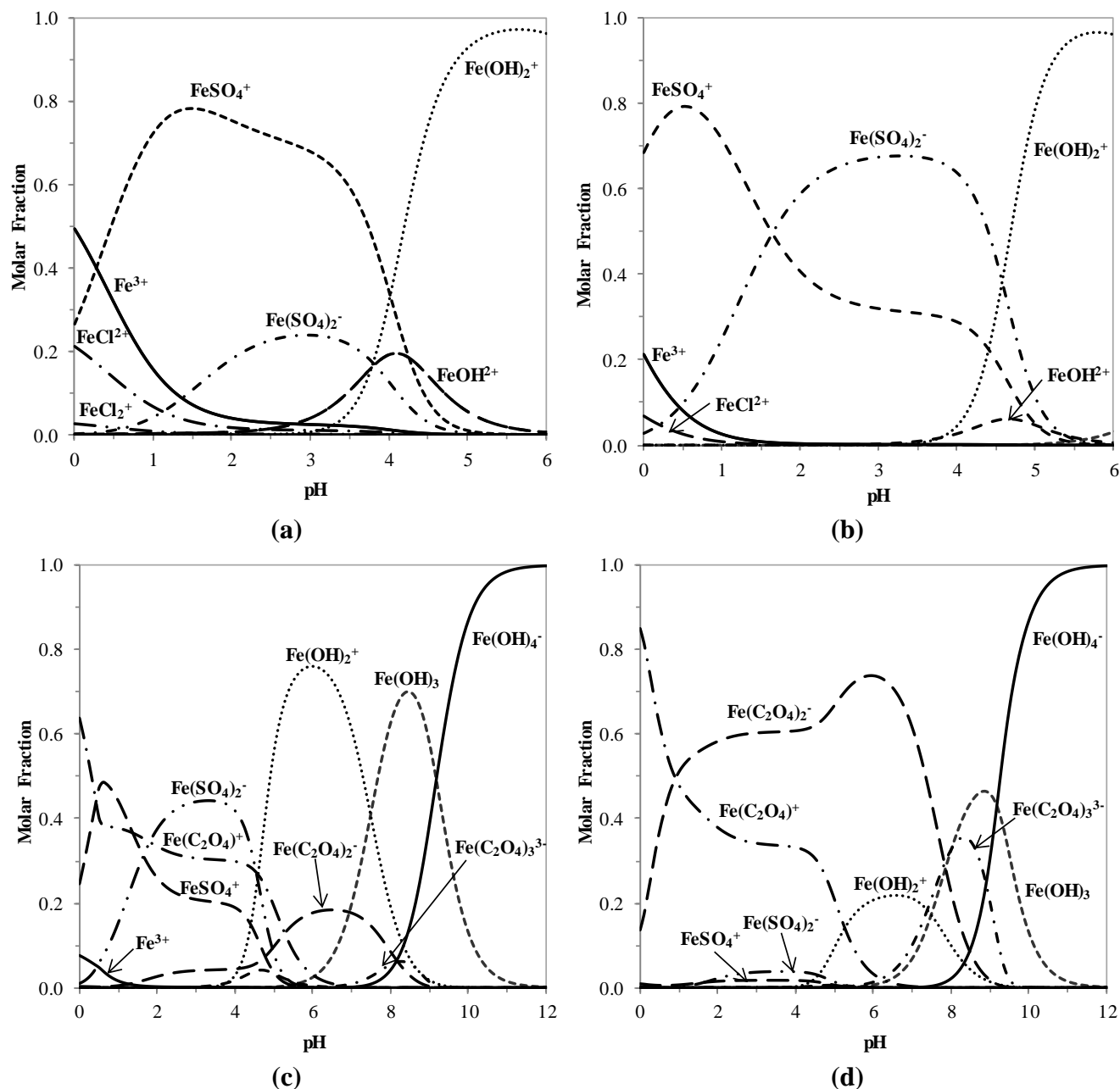


Figure 3.2. Speciation diagram of iron (III) species (80 mg Fe/L) as a function of pH, at 25°C and at an ionic strength of 0.5 M, in the presence of: (a) 2 g/L sulphate and 4 g/L chloride (b) 12 g/L sulphate and 3 g/L chloride; (c) 12 g/L sulphate, 3 g/L chloride and 50 mg/L oxalic acid and (d) 12 g/L sulphate, 3 g/L chloride and 200 mg/L oxalic acid (all the equilibrium constants [41-45] were corrected for an ionic strength of 0.5 M with Davies and Debye-Hückel equations).

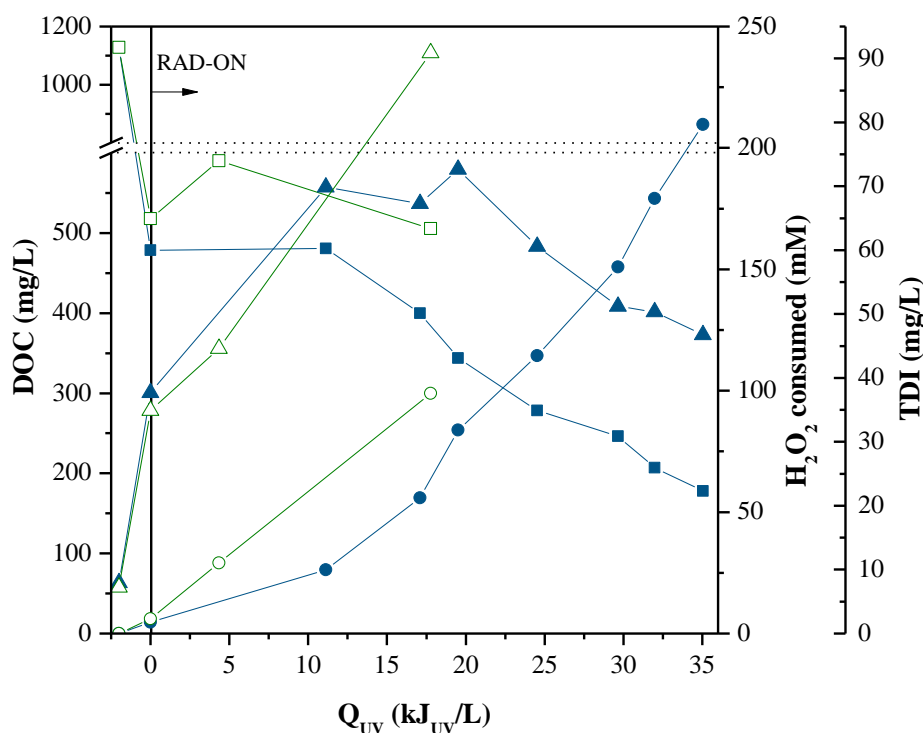


Figure 3.3. DOC (□, ■), H₂O₂ consumption (○, ●) and TDI concentration (△, ▲) evolution as a function of the accumulated UV energy per liter of leachate during the photo-Fenton process (pH = 2.8; [Fe²⁺] = 80 mg/L). Solid symbols: Experiment 5; Open symbols: Experiment 6.

The acid sludge resulting from the acidification reaction had a concentration of 130 mg C_{HS} per gram of sludge, corresponding to the production of 2.7 kg of sludge-HS per cubic meter of leachate. However, the total amount of sludge produced after acidification was greatly dependent on the initial concentration of TSS. In a previous work [37] it was also concluded that the dissolved organic matter reduction related to the preliminary acidification stage was not depend on the type of acid used or the temperature, and lead to a threefold increase of TSS, indicating the significant contribution of the initial leachate TSS for TSS after acidification.

The photo-Fenton reaction kinetic profile showed an initial induction time of 10–15 kJ_{UV}/L (Figure 3.3), after the acidification step, consuming 80–100 mM of H₂O₂ (experiments 4–7), due to: (i) the partial oxidation of more complex organic compounds into simpler ones; (ii) the dissolution of DOC retained in the foam (the foam disappeared during this initial stage of the photo-Fenton reaction); (iii) the suspended solids and intense dark-brown colour of the leachate (competitors with H₂O₂ and iron species as photon absorbents); and also to (iv) the consumption of hydroxyl and other radicals for the partial degradation of humic acids and other organic compounds initially precipitated (constituting the particulate organic matter). After this induction period, the DOC profile followed a pseudo-first-order reaction kinetic.

3.3.2.2 Influence of sludge removal after acidification

In order to assess the influence of the sludge produced after acidification in the photo-Fenton reaction, two experiments were carried out, with (experiment 23) and without (experiment 22) mechanical stirring inside the recirculation tank (in the second case to avoid the recirculation of the settled sludge into the CPCs, since the recirculation pump was located above the conic part of the tank). Figure 3.4 shows that for the same total H_2O_2 consumption (120 mM), at the same average temperature and solar UV power, the mineralization efficiency was higher for the experiment without mechanical stirring. In the experiment with mechanical stirring, it could be observed a high increase of DOC in the initial part of the reaction, related to the dissolution of the organic matter present in the particulate phase. This dissolution was due to the attack of reactive oxygen species to organic compounds present in the particulate phase, leading to more soluble organic compounds.

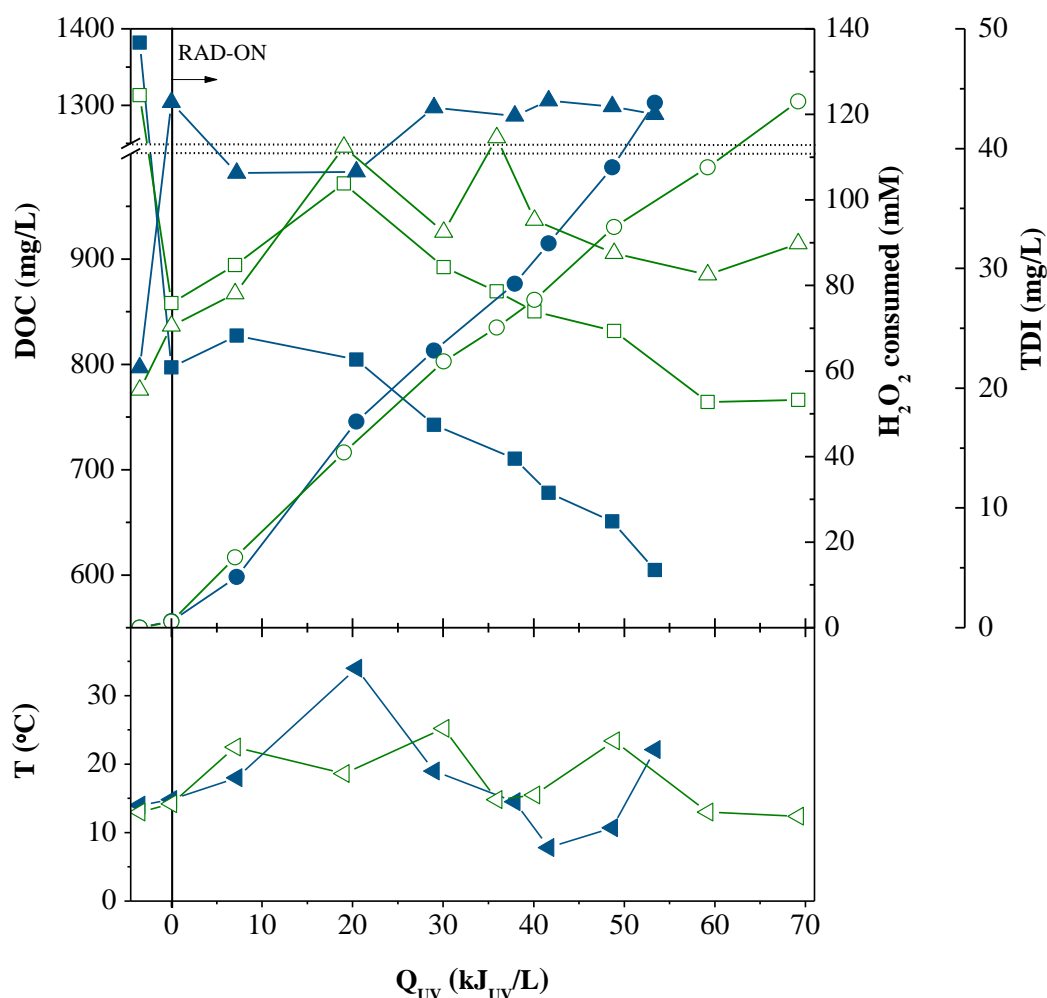


Figure 3.4. Effect of the suspended solids recirculation on the photo-Fenton reaction. (□, ■) - DOC, (○, ●) - H_2O_2 consumed; (△, ▲) - TDI; (◃, ◄) - temperature. Solid symbols: Experiment 22 (without stirring); Open symbols: Experiment 23 (with stirring).

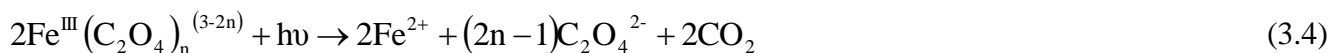
According to these results, it was concluded that the non-elimination of the sludge produced after acidification, decreased the efficiency of the photo-Fenton reaction. The presence of suspended solids also decreases light penetration, competing with H_2O_2 and iron species as photon absorbers, leading to higher reaction times and energy consumption. Moreover, higher energy and H_2O_2 doses were necessary to achieve the same mineralization degree of the organic matter due to the degradation of the particulate organic matter.

To support these conclusions, in experiment 24, after acidification and a sedimentation period of 24-h, the supernatant was pumped from the recirculation tank to another one and back again to the first, after cleaning, and finally, iron and H_2O_2 were added. Taking into account DOC after acidification (beginning of the photo-Fenton reaction), 23.4, 13.3 and 23.5 mg H_2O_2 were consumed per milligram of oxidized DOC, for experiments 9 (without sludge removal), 24 (with sludge removal) and 25 (without sludge removal), respectively. The initial TSS concentration in the leachate after lagooning was 121, 530 and 187 mg/L for the same experiments. Considering that after acidification, TSS concentration increases substantially, it was once again possible to conclude that the presence of particulate organic matter increases H_2O_2 and energy consumption.

In experiments 24 and 25, acidification was performed only with sulphuric acid, and due to the leachate high alkalinity, higher amounts of acid were required (78–86% of added acid was necessary to eliminate the leachate's alkalinity), resulting in high sulphate concentrations. The presence of a high sulphate concentration did not seem to affect the photo-Fenton efficiency (comparing experiments 6 and 7 with 24 and 25), although in this case the iron hydroxide species fraction was insignificant. During the photo-Fenton reaction, a considerable amount of low-molecular-weight carboxylic acids was formed (> 60mg C/L, according to the analysed carboxylic acids) (data not shown), such as oxalic, formic, pyruvic and malonic acids, further supported by pH decrease to values close to 2.4. These carboxylate anions form stable complexes with ferric ions [51].

Taking into consideration the presence of sulphate (12 g $\text{SO}_4^{2-}/\text{L}$), chloride (3 g Cl^-/L) and iron (80 mg Fe/L), the main ferric iron species are (pH = 2.8; IS = 0.5 M; T = 25 °C) [41-45]: $\text{Fe}(\text{SO}_4)_2^- = 66.8\%$ and $\text{FeSO}_4^+ = 32.7\%$ (Figure 3.2b). However, considering an oxalic acid concentration of 50 mg/L (13.3 mg C/L), the main ferric iron complexes are: $\text{Fe}(\text{C}_2\text{O}_4)^{2-} = 3.9\%$; $\text{FeC}_2\text{O}_4^+ = 30.9\%$; $\text{Fe}(\text{SO}_4)_2^- = 43.6\%$ and $\text{FeSO}_4^+ = 21.3\%$ (Figure 3.2c). On the other hand, for an oxalic acid concentration of 200 mg/L, corresponding to 53.3 mg C/L, the main ferric iron complexes are: $\text{Fe}(\text{C}_2\text{O}_4)^{2-} = 60.1\%$; $\text{FeC}_2\text{O}_4^+ = 34.5\%$; $\text{Fe}(\text{SO}_4)_2^- = 3.5\%$ and $\text{FeSO}_4^+ = 1.4\%$ (Figure 3.2d). The presence of low-molecular-weight carboxylate anions and the formation of ferric-carboxylate complexes could explain the high efficiency of the photo-Fenton reaction, even in the presence of high sulphate and chloride concentrations.

This aspect can be attributed to five key aspects: (i) have much higher quantum yields than ferric-water complexes, ferric sulphate and chloride complexes [51, 52]; (ii) can use a higher fraction of the solar radiation spectrum, up to 580 nm; (iii) are more soluble; (iv) are photodecarboxylated under visible radiation; (v) provide a quicker pathway for Fe^{3+} regeneration, thereby accelerating the process [46, 51, 52], according to Eq. (3.4) (taking oxalic acid as example):



3.3.2.3 Influence of temperature/average solar power

Considering that in spring and summer, the insolation and solar radiation power are higher than in autumn and winter, which is correlated with the leachate temperature, it is important to assess the photo-Fenton efficiency in both situations. Experiment 5 was performed in July (summer), with an average solar UV power of approximately 23.3 W/m² and an average temperature of 37.0 °C. On the other hand, experiment 21 was performed in November (autumn), with an average solar UV power of 13.9 W/m² and average temperature of 20.8 °C. Figure 3.5 shows that a higher solar radiation power, associated to higher temperatures, increased the photo-Fenton reaction rate more than three times, mainly due to two different factors: (i) production of more hydroxyl radicals by Fenton thermal reactions involved in ferric ion reduction, particularly through the equations (3.5) - (3.7) [46]; and (ii) increasing of the molar fraction of FeOH^{2+} , which is the most photoactive iron-water complex [53].



Zhang et al. [54] also reported an increase of Fenton reaction rates with temperature, for a leachate with an initial COD of 3000 mg/L. The COD removal efficiency increased from 24.8% to 32.6% as temperature increased from 15 to 36 °C. This effect was also observed for the photo-Fenton degradation of a mixture of commercial pesticides, where the treatment efficiency rose until 42 °C, which could be explained by a faster reduction of Fe^{3+} to Fe^{2+} , making Fe^{2+} available to generate hydroxyl radicals. However, for higher temperatures, the degradation efficiency decreased significantly, due to iron precipitation [55], since its solubility is temperature dependent [56]. Pérez-Moya et al. [57] observed the same behaviour and established a direct relation between of the rise of hydrogen peroxide decomposition rate and temperature, despite this fact was not observed by Zapata et al. [55].

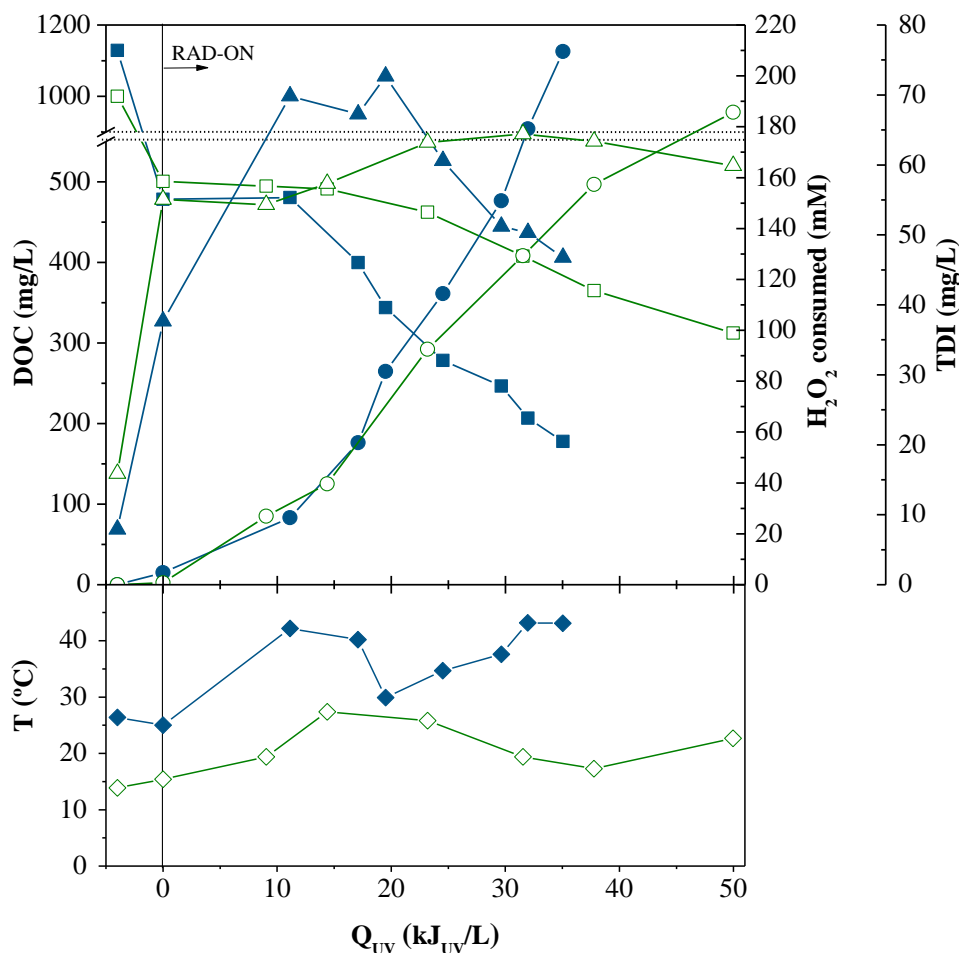


Figure 3.5. Effect of leachate temperature on the photo-Fenton reaction. (□, ■) - DOC, (○, ●) - H₂O₂ consumed; (△, ▲) - TDI; (◇, ◆) – temperature. Solid symbols: Experiment 5 ($T_m = 37^\circ\text{C}$); Open symbols: Experiment 21 ($T_m = 21^\circ\text{C}$).

3.3.2.4 Iron sludge recycling

Two sets of experiments (9–11 and 13–17) were performed to evaluate the possibility of iron sludge recycling for consecutive photo-oxidation cycles, using different leachate samples. After phototreatment, the leachate was neutralized to pH 7, leading to iron precipitation in a small extent, followed by iron sludge settling during 3-h. The supernatant was pumped to the biological reactor and a new leachate sample was fed to the recirculation tank. In experiment 9, 80 ppm of iron was added, while in experiment 10 only the iron sludge resulting from experiment 9 was used, and in experiment 11, 57 mg/L of iron was added; the same iron amount that was lost in the last experiment, resulting in a dissolved iron concentration of 80 mg/L. For experiments 13–17, after each cycle, the amount of iron lost during the previous treatment was always supplied (65, 50, 50 and 42 mg Fe²⁺/L, respectively for experiments 14, 15, 16 and 17), in order to maintain the same dissolved iron concentration.

According to Table 3.3, the mineralization efficiency decreased for successive cycles, associated with the increase of TSS (Figure 3.6), which drastically influenced the photo-Fenton efficiency, as reported above. Another relevant point related to the fact that even for a pH near 7, iron precipitation was minimal (Table 3.4). At the end of the photo-Fenton reaction, ferrous ion was the predominant species, since H_2O_2 was totally consumed. According to the solubility diagrams of ferric and ferrous ions (data not shown) and considering the average concentration of total sulphate (2 g/L), total chloride (4 g/L) and total iron (50 mg/L) species (IS = 0.5 M; T = 25 °C) [41-45], the precipitation of ferrous and ferric ions should start at pH 8.5 and 3.2, respectively. For experiments 20, 21 and 22, a higher precipitation occurred, which could be attributed to the residual H_2O_2 concentration observed, and the main iron species were ferric ions, which obviously precipitated at neutral pH.

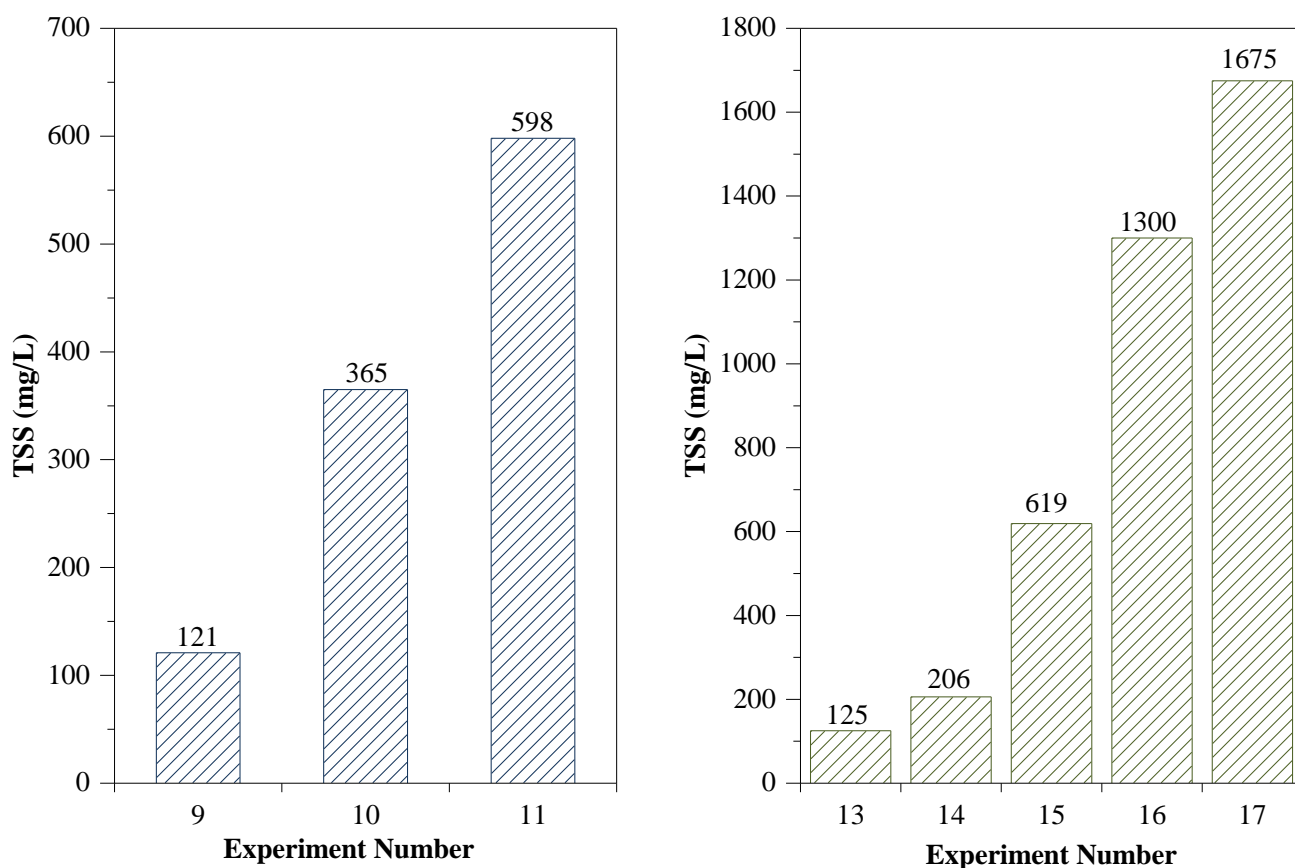


Figure 3.6. Evaluation of the possible iron sludge recycling in the photo-Fenton process.

Table 3.4. Characteristics of the photo-treated leachate after neutralization.

Exp. ^a	Data	pH	T (°C)	DOC _f (mg/L)	COD (mg/L)	TDI (mg/L)	SO ₄ ²⁻ (mg/L)	Cl ⁻ (mg/L)	N _D (mg/L)	NH ₄ ⁺ -N (mg/L)	NO ₃ ⁻ -N (mg/L)	P _T (mg/L)
4	05-07	6.8	33.4	622	1690	43.4	2070	5953	353	100	61	2.0
5	15-07	6.7	32.2	234	613		2418	4081	785	36	704	-
6	22-07	6.7	29.2	510	1052	26.4	1985	3572	968	30	706	2.8
7	27-07	6.9	38.7	547	1010	43.8	2035	3685	1091	31	836	3.1
8	03-08	6.5	24.8	449	902	39.3	2360	3544	1212	31	1074	3.0
9	06-08	6.9	36.0	493	841	36.3	2097	3559	1585	36	1176	8.3
10	10-08	6.7	42.1	625	1026	21.1	2215	3550	1575	51	1164	6.2
11	13-08	6.7	33.5	729	-	45.2	2366	3542	1439	74	1155	6.7
12	30-08	6.7	29.7	656	-	47.3	3307	4987	1293	227	641	6.8
13	03-09	6.8	33.1	724	1480	64.5	2186	6402	1193	266	673	7.9
14	08-09	6.8	33.2	649	1080	48.2	2105	6949	1105	325	526	5.8
15	15-09	6.8	26.4	689	1150	50.6	2117	7090	1014	269	442	8.0
16	21-09	6.8	27.8	777	1440	42.3	2051	7354	964	257	335	7.2
17	28-09	6.8	25.9	867	1640	32.9	2130	7107	827	119	455	9.2
18	20-10	6.5	22.1	584	1610	52.0	2131	6117	278	59	25	-
19	28-10	7.0	22.3	561	1304	19.8	2191	5954	213	26	79	4.6
20	05-11	6.9	25.6	490	1244	8.6	2184	6368	190	43	13	2.5
21	17-11	6.8	14.9	324	905	3.9	2000	5726	245	81	<1	<1.0
22	09-12	6.6	13.4	474	1210	8.7	1613	5171	439	421	<1	<1.0
23	29-12	7.1	13.5	750	2147	18.8	2188	8792	1589	1213	<1	<1.0
24 ^b	14-01	6.9	16.4	557	1506	36.6	12081	2658	2006	1708	<1	3.8
25 ^b	28-01	6.9	13.0	547	1383	30.9	12813	3733	1922	1607	6	7.7

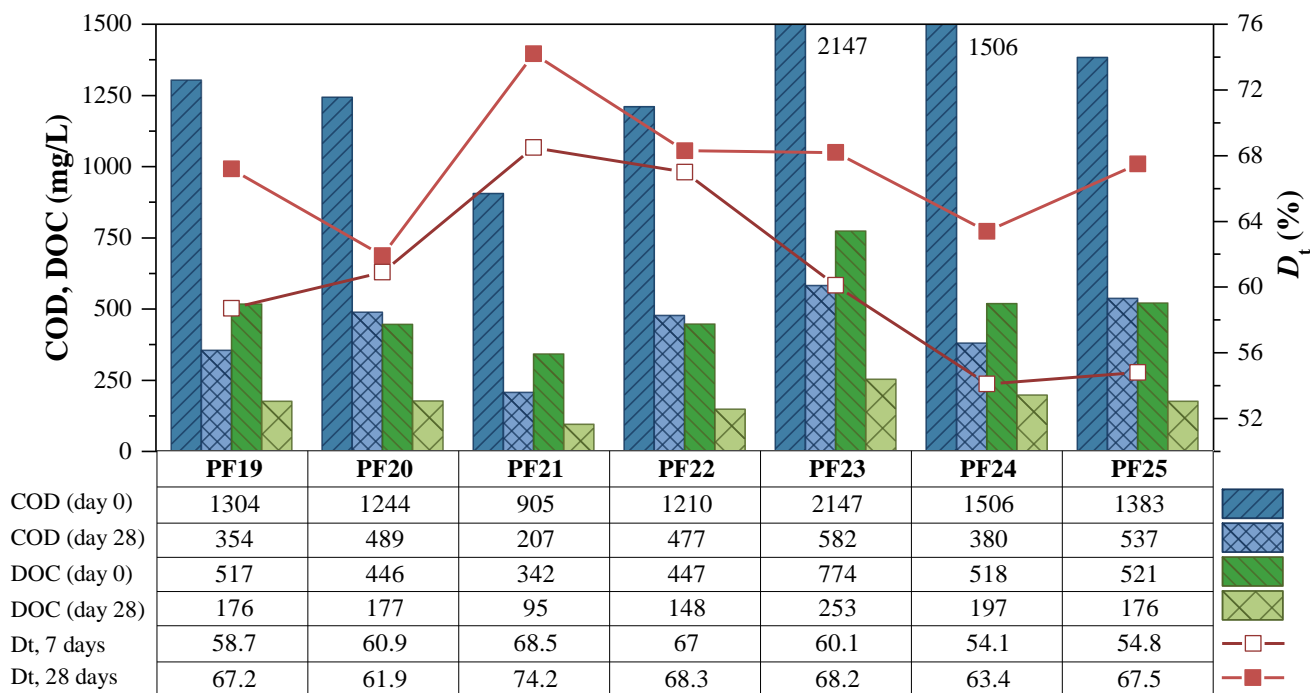
^aExperiment number; ^b2011; *NO₂⁻-N(mg/L)<0.7, with exception for experiment 12 (NO₂⁻-N= 15 mg/L).

3.3.3 Evaluation of combined photo-Fenton and biological treatment

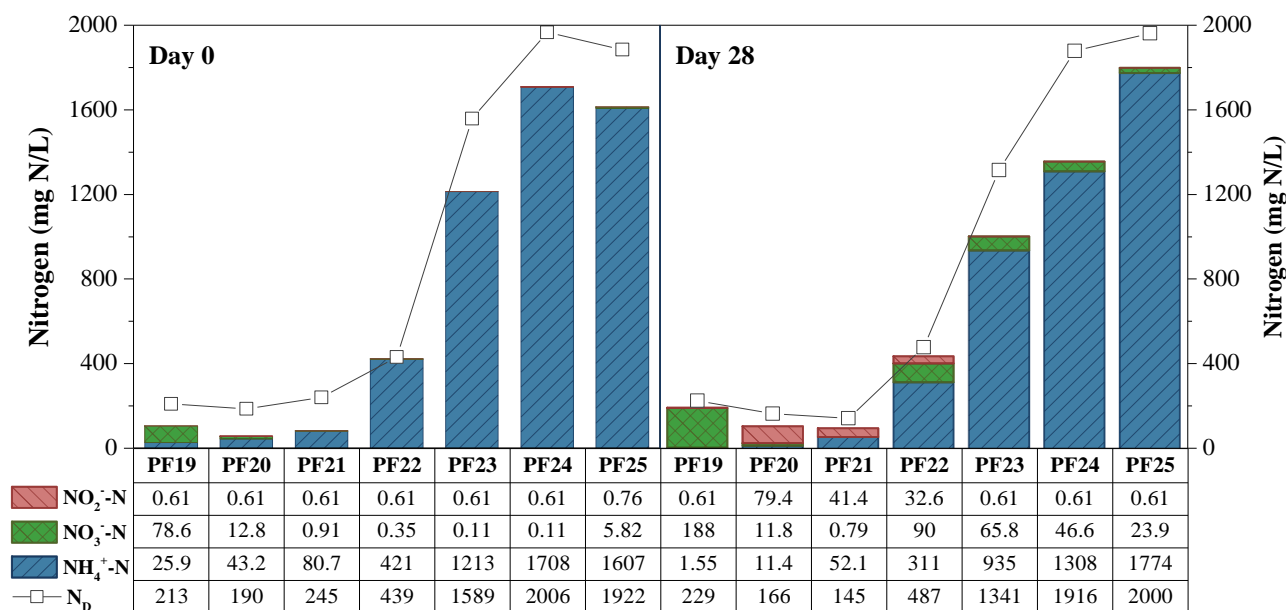
3.3.3.1 Biodegradability of the photo-treated samples

In order to assess the biodegradability of the photo-treated leachate and taken into account the variability of leachate composition, different doses of H₂O₂, solar radiation power and temperatures, a Zahn-Wellens test was performed for the photo-treated neutralized samples of experiments 19–25. Figure 3.7 shows that after 7 days, the biodegradable organic carbon fraction was almost completely removed, when comparing to values obtained after 28 days. On average, almost 70% of the organic carbon present in the photo-treated leachate was biodegradable. Values of COD below 500 mg O₂/L (DOC < 225 mg C/L) were reached in almost all experiments after 28 days of the Zahn–Wellens test, which are in agreement with the discharges limits into sewer (< 1000 mg O₂/L), consuming an amount

of H_2O_2 between 100 and 140 mM. For a more stringent COD value (<150 mg O_2/L), considering the discharge limit into water bodies, the required dose of H_2O_2 was almost 200 mM. Regarding nitrogen species concentration, during the 28 days of the Zahn–Wellens test, the total nitrogen remained approximately constant and nitrification occurred only in a short extent. For the development of nitrifying bacteria it is normally necessary a high residence time and high sludge age. Almost no denitrification occurred because aeration was provided during the entire test.



(a)



(b)

Figure 3.7. Biodegradability of photo-treated leachate: (a) DOC and COD; (b) nitrogen.

3.3.3.2 Evaluation of biological nitrification and denitrification

Table 3.5 shows the characteristics of the photo-bio-treated leachate for experiments 18–25. During these experiments, the biological reactor presented average values of TSS, VSS, VSS/TSS ratio, SSV_{30-min}, SVI and F/M ratio of 2.6 g/L, 1.5 g/L, 58%, 217 mL/L, 85 mL/g and 0.54 g COD/g VSS/day (Table 3.6). Typical values for the BOD F/M ratio reported in the literature vary from 0.04 g substrate/g biomass/day for extended aeration processes to 1.0 g/g/day for high rate processes [58]. Normally, values of SVI below 100 mL/g show a good settling sludge [58].

Table 3.5. Characteristics of the photo-bio-treated leachate.

Parameter	Experiment								ELV ^a
	18	19	20	21	22	23	24	25	
Data	28-out	05-nov	22-nov	09-dez	29-dez	14-01 ^b	28-01 ^b	11-03 ^b	
pH	7.4	7.8	8.1	7.9	6.5	6.5	6.5	7.9	6-9
T (°C)	18.2	19.6	12.9	14.5	12	13.3	10	15.7	-
TSS (mg/L)	216	200	400	181	270	293	155	54	60
DIC (mg/L)	49 (109)	50 (43)	71 (80)	53 (32)	3.7 (6.5)	0	39 (41)	19 (32)	-
DOC (mg/L)	112 (248)	104 (90)	112 (126)	92 (56)	157 (274)	198 (271)	203 (212)	95.3 (160)	-
COD (mg/L)	584 (621)	530 (224)	624 (316)	286 (174)	287 (501)	405 (556)	344 (359)	300 (504)	150
BOD₅ (mg/L)	143	55	60	135	21	12	-	-	40
TDI (mg/L)	1.2 (3.5)	2.0 (4.9)	2.3 (4.5)	1.9 (2.7)	2.9 (5.7)	3.4 (7.6)	6.4 (15.4)	9.9 (20.1)	-
SO₄²⁻ (mg/L)	911 (2142)	1313 (2103)	1622 (2181)	1704 (1940)	1844 (1779)	1794 (1996)	5427 (11991)	6885 (10939)	2000
Cl⁻ (mg/L)	2494 (5909)	3700 (5907)	4110 (5625)	4615 (5638)	5441 (5845)	5983 (7925)	4481 (2484)	2461 (2180)	-
N_D (mg/L)	89 (207)	83 (132)	19 (30)	44 (108)	224 (531)	611 (1365)	1032 (1866)	1152 (1640)	15
NH₄⁺-N (mg/L)	6 (15)	<2 (3)	<2 (4)	<2 (4)	86 (240)	438 (1086)	874 (1674)	623 (881)	7.8
NO₃⁻-N (mg/L)	68 (60)	74 (81)	6 (2)	<1	32 (56)	24 (<1)	8 (<1)	<1	11
NO₂⁻-N (mg/L)	<1	<1	<1	2	25 (<1)	40 (<1)	34 (<1)	169 (6)	-
P_T (mg/L)	11.6 (-)	5.9 (3.0)	4.9 (2.6)	4.1 (<1)	5.3 (<1)	5.5 (<1)	3.6 (2.9)	1.1 (1.6)	10
Color (Pt-Co units)	35	34	103	55	65	76	62	26	-
Turbidity (NTU)	84	59	370	161	191	254	144	43	-

^aELV – Emission Limit Values ; ^b2011; *values in parenthesis refers to the concentration without the contribution of the last biological treatment, considering that the remaining organic matter is recalcitrant.

Table 3.6. Operating conditions in the biological reactor.

Experiment	Data	pH	T (°C)	TSS (mg/L)	VSS (mg/L)	VSS/TSS (%)	SSV _{30-min} ^a (mL/L)	SVI ^b (mL/g)	F/M ratio ^c (g COD/g VSS/day)
18	28-10	7.5	17.6	2600	1430	55	180	69	0.64
19	05-11	7.6	17.1	2937	1600	54	180	61	0.47
20	22-11	7.6	15.5	2720	1540	57	190	70	0.46
21	09-12	7.8	11.2	2640	1440	55	190	72	0.36
22	29-12	7.0	10.5	2400	1495	62	235	98	0.46
23	14-01 ^d	6.5	13.6	2240	1388	62	220	98	0.88
24	28-01 ^d	6.7	10.7	2275	1420	62	210	92	0.61
25	11-03 ^d	6.8	13.4	2695	1510	56	330	122	0.52

^aSS₃₀ – Settled Sludge Volume after 30 minutes; ^bSVI – Sludge Volume Index; ^cF/M – food to microorganism (biomass) ratio.

If denitrification is to be considered after a nitrification process, partial nitrification to nitrite implies 25% less oxygen demand compared to complete nitrification. This shortcut of the nitrate would mean a reduction in the total carbon source required for denitrification, since carbon is needed for conversion of nitrate to nitrite, which can yield up to 40% savings in methanol consumption [23]. Alleman [59] showed that the optimal pH values were between 7.9 and 8.2 for nitrification and between 7.2 and 7.6 for denitrification. Ruiz et al. [35] studied the nitrification of synthetic wastewater with high ammonia concentration (10 g NH₄⁺-N/L) at a temperature of 30 °C, and concluded that for pH values lower than 6.45 and higher than 8.95 complete inhibition of nitrification took place. Setting a DO concentration in the reactor of 0.7 mg/L, it was possible to accumulate more than 65% of the loaded ammonia nitrogen as nitrite, with a 98% ammonia conversion, representing a reduction of 20% in oxygen consumption. For DO concentration below than 0.5 mg/L, ammonia was accumulated, and over a DO of 1.7 mg/L, complete nitrification to nitrate was achieved.

Figure 3.8 summarizes the results obtained for leachate treatment combining chemical (solar photo-Fenton) and biological processes, for experiments 20 and 21. The global DOC removal efficiency of the combined system was approximately 90%, corresponding to 54% (140 mM H₂O₂ consumed) and 68% (190 mM H₂O₂ consumed) for the chemical oxidation and 34% and 27% for the biological oxidation, respectively for experiments 20 and 21. Considering experiments 18–25, the average DOC removal efficiency for the integrated system was 55% and 31%, respectively for the photo and biological oxidation (Figure 3.9). Figure 3.8 also shows the evolution of the nitrogen species during the biological treatment, enabling 90% and 56% of total nitrogen removal, respectively for experiments 20 and 21.

Dissolved oxygen concentration and points of methanol addition, as external carbon source, for the denitrification reaction are also presented in Figure 3.8. In experiment 21, methanol was added with the only purpose of verifying if the biological sludge was active. It was noted that, in some cases, nitrification and denitrification processes occurred simultaneous, which was attributed to some problems in the air compressor, leading to non-aerated zones inside the biological reactor.

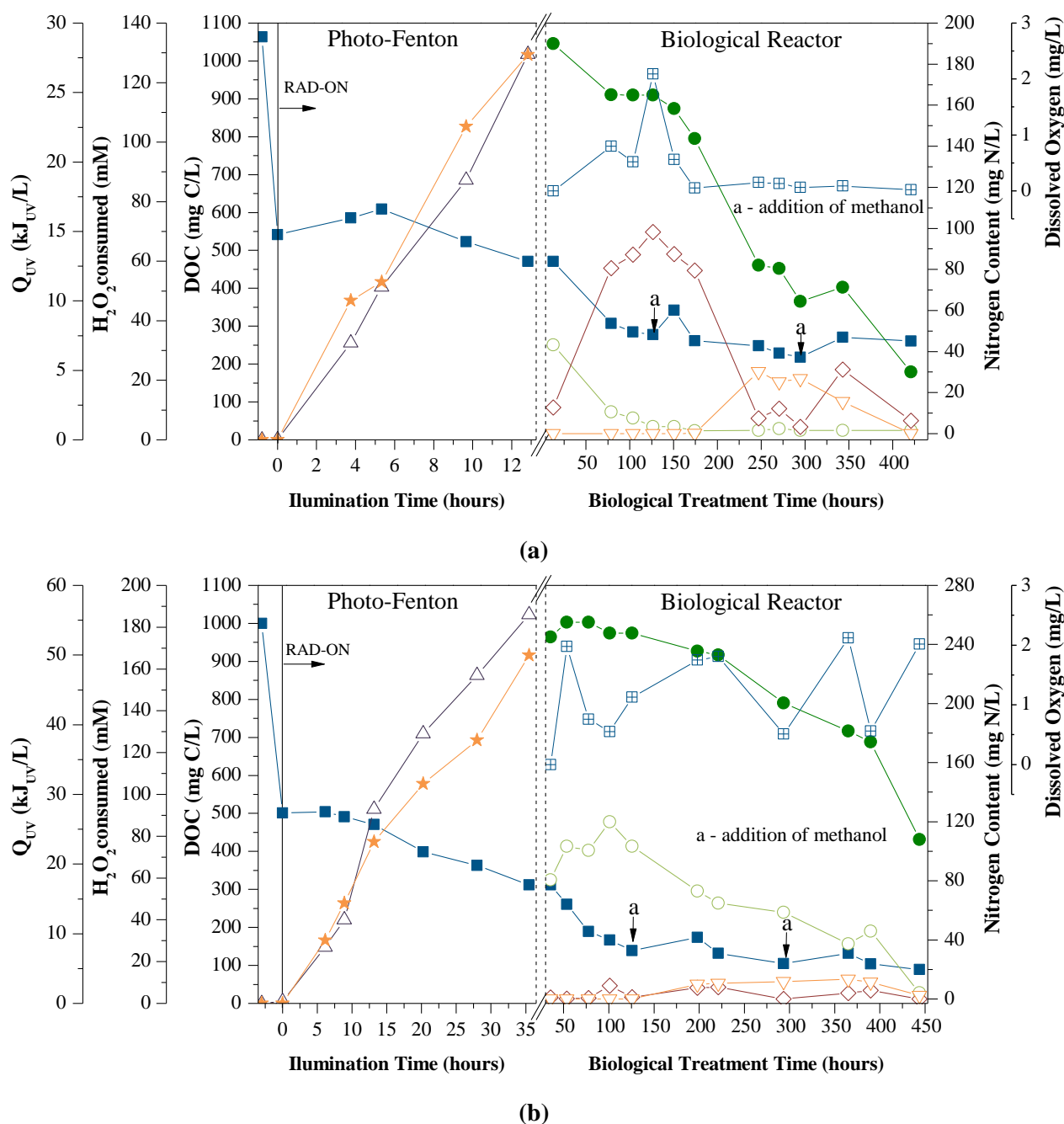


Figure 3.8. Leachate mineralization by the combined system: photo-Fenton (DOC, H₂O₂ consumed and Q_{UV} in function of the illumination time); biological nitrification/denitrification (DOC and nitrogen species as function of time). (a) Experiment 20; (b) Experiment 21. ■ - DOC; △ - H₂O₂ consumed; ★ - Q_{UV} ; ● - Total Nitrogen; ○ - Ammonium (NH₄⁺-N); ◇ - Nitrate (NO₃⁻-N); ▽ - Nitrite (NO₂⁻-N); ☐ - Dissolved Oxygen.

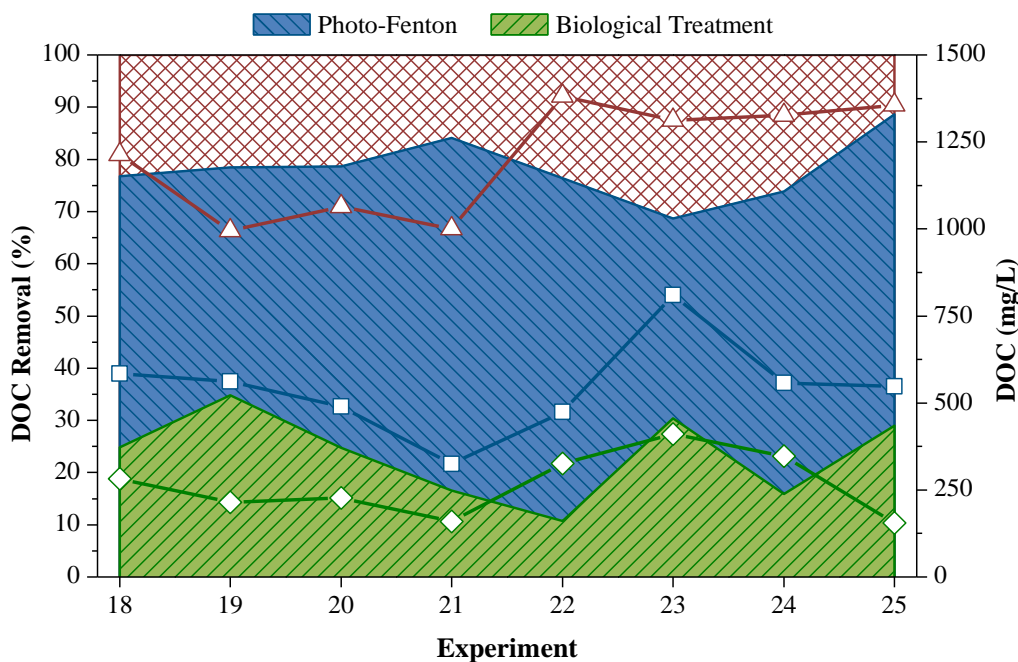


Figure 3.9. DOC concentration and DOC removal percentage obtained for the photo-Fenton and biological processes, experiments 18 to 25. \triangle - Initial DOC (leachate after lagooning); \square - DOC after the Photo-Fenton reaction; \diamond - DOC after the biological oxidation process.

The obtained nitrification rates were 0.06, 0.05, 0.16, 0.14, 0.03 and 0.49 mg $\text{NH}_4^+\text{-N}$ per hour and g VSS (volatile suspended solids), respectively for experiments 20–25. The maximum denitrification rate was 0.27 mg ($\text{NO}_2^-\text{-N} + \text{NO}_3^-\text{-N}$) per hour and g VSS with a C/N ratio of 6.4 mg CH_3OH per mg ($\text{NO}_2^-\text{-N} + \text{NO}_3^-\text{-N}$). The high treatment times needed for the nitrification and denitrification reactions, taking into consideration the low nitrification and denitrification rates, were associated with the low temperatures (6.9–15.5 °C) observed between November 2010 and January 2011. Ilies et al. [34] showed that nitrification and denitrification processes suffered major inhibitions when temperature decreased from 20 to 10 °C. Isaka et al. [60] showed that using nitrifying bacteria entrapped in a gel carrier increased the nitrification rates at low temperatures (0.71 kg $\text{N}/\text{m}^3/\text{day}$ at 10 °C, $\text{DO} > 7$ mg/L, $7.5 < \text{pH} < 8.0$). Cassano et al. [15] further presented several integrated biological processes – AOPs for the treatment of leachates from a medium-age sanitary landfill, characterized by DOC, COD and $\text{NH}_4^+\text{-N}$ in the ranges 0.9–1.2 g C/L, 2.8–3.6 g O_2/L and 1.5–2 g $\text{NH}_4^+\text{-N}/\text{L}$, achieving 61%, 54% and 99% removals, respectively, using a SBBGR (Sequential Batch Biofilter Granular Reactor). High biological oxidation rates were achieved using a high sludge age (i.e., about 800 days), which led to a biomass concentration as high as 46 g TSS/L (VSS/TSS: 0.7–0.8).

In the following chapters, other studies about leachates treatment using combined chemical and biological oxidation processes at pre-industrial scale plant will be presented, regarding the identification and quantification of recalcitrant organic compounds and degradation by-products, improvement of nitrification and denitrification biological rates and minimization of operational costs.

3.4 Conclusions

The leachate after lagooning pre-treatment showed a low biodegradability, mainly due to the presence of a high concentration of humic substances, besides the high nitrogen load, mainly in the form of ammonium. Considering the characteristics of the leachate after lagooning, a complete leachate treatment strategy was proposed, combining: (i) a solar photo-Fenton system, as pre-oxidation process, leading to an enhancement of the leachate's biodegradability, higher than 70%, according to the Zahn-Wellens test; with (ii) an activated sludge biological process, under aerobic and anoxic conditions, allowing to oxidize the remaining biodegradable organic fraction and completely eliminate nitrogen compounds, through ammonium nitrification into nitrates/nitrites and denitrification to nitrogen gas, with the addition of an external carbon source. A pre-industrial plant, incorporating a solar photocatalytic system with 39.52 m² of CPCs and an activated sludge reactor with 3.5 m³ capacity, was constructed and installed in a sanitary landfill in order to evaluate the treatment efficiency, under real circumstances of leachate variability and weather conditions.

The leachate acidification to pH near 3.0 led to 54–58% DOC abatement, mainly associated with humic acids precipitation. The non-elimination of the acid sludge produced after acidification, decreased the photo-Fenton reaction efficiency, which was due to the lower light transmission caused by the higher amount of suspended solids that competed with H₂O₂ and iron species as photons absorbers. Therefore, higher amounts of H₂O₂ and energy were necessary to degrade also the particulate organic matter. The reutilization of iron sludge in consecutive oxidation treatments was not viable due to the increase of suspended solids, leading to lower reaction rates. The leachate photo-oxidation was strongly affected by weather conditions, mainly due to low leachate temperatures in the winter season, causing low reaction rates, associated to the effects of the Fenton thermal reaction and molar fraction of ferric species. In order to achieve COD target values below 500 mg O₂/L and 150 mg O₂/L (in agreement with the discharge limit into water bodies) after the final biological oxidation, it was necessary, for the photo-oxidation, a hydrogen peroxide concentration between 100–140 mM and almost 200 mM, respectively. The great efficiency of the photo-Fenton reaction, even in the presence of high concentrations of sulphate and chloride ions, was attributed to the formation of ferricarboxylate complexes.

Biological nitrification and denitrification reactions were strongly affected by the low temperatures observed during the winter season. The global DOC removal efficiency of the combined system was approximately 86%, corresponding to 55% for chemical oxidation and 31% for biological oxidation.

3.5 References

- [1] D. Kulikowska, E. Klimiuk, The effect of landfill age on municipal leachate composition, *Bioresource Technology*, 99 (2008) 5981-5985.
- [2] A.A. Tatsi, A.I. Zouboulis, A field investigation of the quantity and quality of leachate from a municipal solid waste landfill in a Mediterranean climate (Thessaloniki, Greece), *Advances in Environmental Research*, 6 (2002) 207-219.
- [3] H.-j. Fan, H.-Y. Shu, H.-S. Yang, W.-C. Chen, Characteristics of landfill leachates in central Taiwan, *Science of the Total Environment*, 361 (2006) 25-37.
- [4] S. Jonsson, J. Ejlerthsson, B.H. Svensson, Behaviour of mono- and diesters of o-phthalic acid in leachates released during digestion of municipal solid waste under landfill conditions, *Advances in Environmental Research*, 7 (2003) 429-440.
- [5] S.K. Marttinen, R.H. Kettunen, J.A. Rintala, Occurrence and removal of organic pollutants in sewages and landfill leachates, *The Science of The Total Environment*, 301 (2003) 1-12.
- [6] C.B. Öman, C. Junestedt, Chemical characterization of landfill leachates - 400 parameters and compounds, *Waste Management*, 28 (2008) 1876-1891.
- [7] T. Eggen, M. Moeder, A. Arukwe, Municipal landfill leachates: a significant source for new and emerging pollutants, *Science of the Total Environment*, 408 (2010) 5147-5157.
- [8] T.H. Christensen, P. Kjeldsen, P.L. Bjerg, D.L. Jensen, J.B. Christensen, A. Baun, H.-J. Albrechtsen, G. Heron, Biogeochemistry of landfill leachate plumes, *Applied Geochemistry*, 16 (2001) 659-718.
- [9] N. Calace, A. Liberatori, B.M. Petronio, M. Pietroletti, Characteristics of different molecular weight fractions of organic matter in landfill leachate and their role in soil sorption of heavy metals, *Environmental Pollution*, 113 (2001) 331-339.
- [10] E.S.K. Chian, F.B. DeWalle, Sanitary landfill leachates and their treatment, *Journal of the Environmental Engineering Division*, (1976) 411-431.
- [11] S. Renou, J.G. Givaudan, S. Poulain, F. Dirassouyan, P. Moulin, Landfill leachate treatment: Review and opportunity, *Journal of Hazardous Materials*, 150 (2008) 468-493.
- [12] D.L. Jensen, A. Ledin, T.H. Christensen, Speciation of heavy metals in landfill-leachate polluted groundwater, *Water Research*, 33 (1999) 2642-2650.
- [13] A.A. Abbas, G. Jingsong, L.Z. Ping, P.Y. Ya, W.S. Al-Rekabi, Review on Landfill Leachate Treatments, *American Journal of Applied Sciences*, 6 (2009) 672-684.
- [14] U.E. Agency, Guidance for the Treatment of Landfill Leachate, Sector Guidance Note IPPC S5.03, in: I.P.P.a.C. (IPPC) (Ed.), 2007.
- [15] D. Cassano, A. Zapata, G. Brunetti, G. Del Moro, C. Di Iaconi, I. Oller, S. Malato, G. Mascolo, Comparison of several combined/integrated biological-AOPs setups for the treatment of municipal landfill leachate: Minimization of operating costs and effluent toxicity, *Chemical Engineering Journal*, 172 (2011) 250-257.

- [16] S. Cortez, P. Teixeira, R. Oliveira, M. Mota, Evaluation of Fenton and ozone-based advanced oxidation processes as mature landfill leachate pre-treatments, *Journal of Environmental Management*, 92 (2011) 749-755.
- [17] P.-J. He, Z. Zheng, H. Zhang, L.-M. Shao, Q.-Y. Tang, PAEs and BPA removal in landfill leachate with Fenton process and its relationship with leachate DOM composition, *Science of the Total Environment*, 407 (2009) 4928-4933.
- [18] D. Hermosilla, M. Cortijo, C.P. Huang, Optimizing the treatment of landfill leachate by conventional Fenton and photo-Fenton processes, *Science of the Total Environment*, 407 (2009) 3473-3481.
- [19] M. Umar, H.A. Aziz, M.S. Yusoff, Trends in the use of Fenton, electro-Fenton and photo-Fenton for the treatment of landfill leachate, *Waste Management*, 30 (2010) 2113-2121.
- [20] J.J. Wu, C.-C. Wu, H.-W. Ma, C.-C. Chang, Treatment of landfill leachate by ozone-based advanced oxidation processes, *Chemosphere*, 54 (2004) 997-1003.
- [21] I. Oller, S. Malato, J.A. Sánchez-Pérez, Combination of Advanced Oxidation Processes and biological treatments for wastewater decontamination—A review, *Sci. Total Environ.*, 409 (2011) 4141-4166.
- [22] V.J.P. Vilar, S.M.S. Capelo, T.F.C.V. Silva, R.A.R. Boaventura, Solar photo-Fenton as a pre-oxidation step for biological treatment of landfill leachate in a pilot plant with CPCs, *Catalysis Today*, 161 (2011) 228-234.
- [23] V.J.P. Vilar, E.M.R. Rocha, F.S. Mota, A. Fonseca, I. Saraiva, R.A.R. Boaventura, Treatment of a sanitary landfill leachate using combined solar photo-Fenton and biological immobilized biomass reactor at a pilot scale, *Water Research*, 45 (2011) 2647-2658.
- [24] V.J.P. Vilar, J.M.S. Moreira, A. Fonseca, I. Saraiva, R.A.R. Boaventura, Application of Fenton and Solar Photo-Fenton Processes to the Treatment of a Sanitary Landfill Leachate in a Pilot Plant with CPCs, *Journal of Advanced Oxidation Technologies*, 15 (2012) 107-116.
- [25] M.S. Mehos, C.S. Turchi, Field testing solar photocatalytic detoxification on TCE-contaminated groundwater, *Environmental Progress*, 12 (1993) 194-199.
- [26] R. Dillert, A.E. Cassano, R. Goslich, D. Bahnemann, Large scale studies in solar catalytic wastewater treatment, *Catalysis Today*, 54 (1999) 267-282.
- [27] R. Dillert, S. Vollmer, M. Schober, J. Theurich, D. Bahnemann, H.J. Arntz, K. Pahlmann, J. Wienefeld, T. Schmedding, G. Sager, Photocatalytic Treatment of an Industrial Wastewater in the Double-Skin Sheet Reactor, *Chemical Engineering & Technology*, 22 (1999) 931-934.
- [28] D. Bahnemann, Photocatalytic water treatment: solar energy applications, *Solar Energy*, 77 (2004) 445-459.
- [29] L. Bousselmi, S.-U. Geissen, H. Schroeder, Textile wastewater treatment and reuse by solar catalysis: results from a pilot plant in Tunisia, *Water Science and Technology*, 49 (2004) 331-337.
- [30] A. Zapata, I. Oller, C. Sirtori, A. Rodríguez, J.A. Sánchez-Pérez, A. López, M. Mezcuca, S. Malato, Decontamination of industrial wastewater containing pesticides by combining large-scale homogeneous solar photocatalysis and biological treatment, *Chemical Engineering Journal*, 160 (2010) 447-456.

- [31] I. Oller, S. Malato, J.A. Sánchez-Pérez, M.I. Maldonado, W. Gernjak, L.A. Pérez-Estrada, J.A. Muñoz, C. Ramos, C. Pulgarín, Pre-industrial-scale Combined Solar Photo-Fenton and Immobilized Biomass Activated-Sludge Biotreatment, *Industrial & Engineering Chemistry Research*, 46 (2007) 7467-7475.
- [32] H. Yung-Tse, S.-G. Joanna, B. Michal, Treatment of Landfill Leachate, in: *Hazardous Industrial Waste Treatment*, CRC Press, 2006, pp. 441-494.
- [33] C. Gottschalk, J.A. Libra, A. Saupe, *Ozonation of Water and Waste Water: A Practical Guide to Understanding Ozone*, Strauss GmbH, Mörlenbach, 2010.
- [34] P. Ilies, D.S. Mavinic, The effect of decreased ambient temperature on the biological nitrification and denitrification of a high ammonia landfill leachate, *Water Research*, 35 (2001) 2065-2072.
- [35] G. Ruiz, D. Jeison, R. Chamy, Nitrification with high nitrite accumulation for the treatment of wastewater with high ammonia concentration, *Water Research*, 37 (2003) 1371-1377.
- [36] J.J. Pignatello, E. Oliveros, A. MacKay, Advanced oxidation processes for organic contaminant destruction based on the fenton reaction and related chemistry, *Critical Reviews in Environmental Science and Technology*, 36 (2006) 1-84.
- [37] V.J.P. Vilar, T.F.C.V. Silva, M.A.N. Santos, A. Fonseca, I. Saraiva, R.A.R. Boaventura, Evaluation of solar photo-Fenton parameters on the pre-oxidation of leachates from a sanitary landfill, *Solar Energy*, 86 (2012) 3301-3315.
- [38] J. Bacardit, I. Oller, M.I. Maldonado, E. Chamarro, S. Malato, S. Esplugas, Simple Models for the Control of Photo-Fenton by Monitoring H₂O₂, *Journal of Advanced Oxidation Technologies*, 10 (2007) 219-228.
- [39] L. Prieto-Rodríguez, I. Oller, A. Zapata, A. Agüera, S. Malato, Hydrogen peroxide automatic dosing based on dissolved oxygen concentration during solar photo-Fenton, *Catalysis Today*, 161 (2011) 247-254.
- [40] C.N. Sawyer, P.L. McCarty, G.F. Parkin, *Chemistry for Environmental Engineering and Science*, fifth edition ed., McGraw-Hill, New York, 2003.
- [41] J. De Laat, T.G. Le, Effects of chloride ions on the iron (III)-catalyzed decomposition of hydrogen peroxide and on the efficiency of the Fenton-like oxidation process, *Applied Catalysis B: Environmental*, 66 (2006) 137-146.
- [42] G.L. Truong, J.D. Laat, B. Legube, Effects of chloride and sulfate on the rate of oxidation of ferrous ion by H₂O₂, *Water Research*, 38 (2004) 2384-2394.
- [43] J. Peñuela, J.D. Martínez, M.L. Araujo, F. Brito, G. Lubes, M. Rodríguez, V. Lubes, Speciation of the nickel (II) complexes with oxalic and malonic acids studied in 1.0 mol dm⁻³ NaCl at 25° C, *Journal of Coordination Chemistry*, 64 (2011) 2698-2705.
- [44] C. Sawyer, P. McCarty, G. Parkin, *Chemistry for Environmental Engineering and Science*, McGraw-Hill Education, 2003.
- [45] W. Stumm, J.J. Morgan, *Aquatic Chemistry: Chemical Equilibria and Rates in Natural Waters*, Wiley, 2013.
- [46] S. Malato, P. Fernández-Ibáñez, M.I. Maldonado, J. Blanco, W. Gernjak, Decontamination and disinfection of water by solar photocatalysis: Recent overview and trends, *Catalysis Today*, 147 (2009) 1-59.

- [47] A. Machulek Júnior, F.H. Quina, F. Gozzi, V.O. Silva, J.E.F. Moraes, Fundamental Mechanistic Studies of the Photo-Fenton Reaction for the Degradation of Organic Pollutants, in: T. Puzyn, A. Mostrag-Szlichtyng (Eds.) *Organic Pollutants*, Rijeka: InTech, 2011, pp. 1-22.
- [48] Y. Wu, S. Zhou, F. Qin, H. Peng, Y. Lai, Y. Lin, Removal of humic substances from landfill leachate by Fenton oxidation and coagulation, *Process Safety and Environmental Protection*, 88 (2010) 276-284.
- [49] L. Zhang, A. Li, Y. Lu, L. Yan, S. Zhong, C. Deng, Characterization and removal of dissolved organic matter (DOM) from landfill leachate rejected by nanofiltration, *Waste Management*, 29 (2009) 1035-1040.
- [50] J.B. Christensen, D.L. Jensen, C. GRØN, Z. Filip, T.H. Christensen, Characterization of the dissolved organic carbon in landfill leachate-polluted groundwater, *Water Research*, 32 (1998) 125-135.
- [51] M.E. Balmer, B. Sulzberger, Atrazine degradation in irradiated iron/oxalate systems: effects of pH and oxalate, *Environmental Science & Technology*, 33 (1999) 2418-2424.
- [52] B.C. Faust, R.G. Zepp, Photochemistry of aqueous iron (III)-polycarboxylate complexes: roles in the chemistry of atmospheric and surface waters, *Environmental Science & Technology*, 27 (1993) 2517-2522.
- [53] F.C. Moreira, R.A.R. Boaventura, E. Brillas, V.J.P. Vilar, Degradation of trimethoprim antibiotic by UVA photoelectro-Fenton process mediated by Fe(III)-carboxylate complexes, *Applied Catalysis B: Environmental*, 162 (2015) 34-44.
- [54] H. Zhang, H.J. Choi, C.-P. Huang, Optimization of Fenton process for the treatment of landfill leachate, *Journal of Hazardous Materials*, 125 (2005) 166-174.
- [55] A. Zapata, T. Velegraki, J. Sánchez-Pérez, D. Mantzavinos, M. Maldonado, S. Malato, Solar photo-Fenton treatment of pesticides in water: Effect of iron concentration on degradation and assessment of ecotoxicity and biodegradability, *Applied Catalysis B: Environmental*, 88 (2009) 448-454.
- [56] H. Krýsová, J. Jirkovský, J. Krýsa, G. Mailhot, M. Bolte, Comparative kinetic study of atrazine photodegradation in aqueous $\text{Fe}(\text{ClO}_4)_3$ solutions and TiO_2 suspensions, *Applied Catalysis B: Environmental*, 40 (2003) 1-12.
- [57] M. Pérez-Moya, M. Graells, L.J. del Valle, E. Centelles, H.D. Mansilla, Fenton and photo-Fenton degradation of 2-chlorophenol: Multivariate analysis and toxicity monitoring, *Catalysis Today*, 124 (2007) 163-171.
- [58] Metcalf, Eddy, *Wastewater Engineering Treatment and Reuse*, 4th ed., Metcalf & Eddy, 2005.
- [59] J.E. Alleman, Elevated nitrite occurrence in biological wastewater treatment systems, *Water Science and Technology*, 17 (1984) 409-419.
- [60] K. Isaka, S. Yoshie, T. Sumino, Y. Inamori, S. Tsuneda, Nitrification of landfill leachate using immobilized nitrifying bacteria at low temperatures, *Biochemical Engineering Journal*, 37 (2007) 49-55.

4 Integration of solar photo-Fenton and biological oxidation processes for leachate treatment at pre-industrial scale - Biodegradability enhancement assessment

An integrated leachate treatment strategy, combining a solar photo-Fenton reaction to enhance the biodegradability of the leachate from an aerated lagoon, with an activated sludge process, under aerobic and anoxic conditions, is proposed to achieve COD target values and nitrogen content according to legislation. The efficiency and performance of the photo-Fenton reaction, concerning sludge removal after acidification, defining the optimum phototreatment time to reach a biodegradable wastewater that can be further oxidized in a biological reactor and, activated sludge biological process, defining the nitrification and denitrification reaction rates, alkalinity balance and methanol necessary as external carbon source, were evaluated in an integrated system at pre-industrial scale. The plant is composed by a photocatalytic system with 39.52 m² of compound parabolic collectors (CPCs) and 2 m³ recirculation tank and an activated sludge biological reactor with 3 m³ capacity.

Leachate biodegradability enhancement by means of a solar driven photo-Fenton process was evaluated using direct biodegradability tests, as Zahn-Wellens method, and indirect measurements as the average oxidation state (AOS), low-molecular-weight carboxylic acids content (fast biodegradable character) and humic substances (recalcitrant character) concentration. Due to the high variability of leachate composition, UV absorbance on-line measurement was established as a useful parameter for photo-Fenton reaction control.

This chapter is based on the research article “Silva, T.F.C.V., Fonseca, A., Saraiva, I., Boaventura, R.A.R., Vilar, V.J.P, *Biodegradability enhancement of a leachate after biological lagooning using a solar driven photo-Fenton reaction, and further combination with an activated sludge biological process, at pre-industrial scale*, Water Research, 47 (2013) 3543-3557, DOI: 10.1016/j.watres.2013.04.008”.

4.1 Introduction

Sanitary landfill leachates are characterized as a complex mixture of different recalcitrant organic and inorganic contaminants, such as humic and fulvic acids [1], Polycyclic Aromatic Hydrocarbons (PAHs) [2, 3], PolyBrominated Biphenyl Ethers (PBDEs) [4, 5], pesticides [6] and heavy metals [7, 8]. The inability of conventional biological technologies to effectively remove those hazardous substances claims for new advanced treatment technologies capable to ensure environment resources protection, in agreement with the objectives proposed by the European Commission to be achieved until 2015 [9].

Advanced oxidation processes have been recognized as highly efficient in biodegradability enhancement of different recalcitrant wastewaters, including textile [10, 11], cork [12, 13], winery [14-17], pharmaceutical [18], paper mill [19] and olive mill wastewaters [20], pesticide-containing wastewaters [21, 22], leachates from sanitary landfills [23, 24] and many others as report by Oller et al. [25]. Malato et al. [26] proposes a decision scheme for selecting the appropriate treatment train, coupling AOPs-Biological processes, as a function of wastewaters characteristics, in terms of TOC content, biodegradability and toxicity. According to the characteristics of leachates resulting from a preliminary biological lagooning, showing a very low biodegradability and high organic carbon content (≈ 1000 mg C/L), the best coupling strategy consists in a pre-oxidation step using an AOP, modifying the structure of the recalcitrant pollutants, transforming them into more simple and easily biodegradable ones, allowing a subsequent biological oxidation to comply with the discharge limits. The best phototreatment time, must be enough to achieve a high biological efficiency, decreasing energy and reactants consumption, and consequently associated costs. The use of renewable solar energy, as UV-Vis photons source, reduces electric power demand when UV lamps are necessary. Muñoz et al. [27] reported that solar driven photo-Fenton process, considering all solar driven-AOPs, is the best option in terms of integrated environmental and economic point of view, taken into account their life-cycle greenhouse gas emission and life-cycle cost. Previous results also showed that solar photo-Fenton process can be selected as the best option for the peroxidation of mature leachates, after preliminary biological lagooning [28, 29], promoting biodegradability enhancement [23, 30], which makes possible to combine with a further biological oxidation system. Speciation and solubility of iron species are the main critical points of photo-Fenton reaction. pH values between 2.6 and 3.0 have been chosen as the optimum conditions, since the predominant iron species in solution is FeOH^{2+} (48%, pH = 2.8, T = 25 °C and 0.5 M ionic strength), which is the most photoactive ferric ion-water complex [31], and at the same time, avoids iron (III) precipitation (< 30 mg Fe/L, considering an ionic strength of 0.5 M, pH = 2.8 and T = 25 °C, as disclosed on the previous chapter).

In the Chapter 3, it was shown that after acidification, the DOC abatement was approximately 27%, which corresponded to a reduction of the humic substances of approximately 33%, indicating that humic acids precipitation is responsible for approximately 72% of the DOC abatement. Evaluation of organic carbon content in the soluble and particulate phase is very important, in order to prevent a further dissolution of those humic acids after neutralization of photo-treated leachate.

Leachates are also characterized by high nitrogen content, mainly in the form of ammonium [32]. Nitrogen removal from photo-treated leachates can be achieved using a sequential biological oxidation by activated sludge under aerobic/anoxic conditions, as demonstrated on the previous chapter and by a study carried out by Vilar et al. [23], where the complete removal of ammonium, nitrites and nitrates was achieved.

The main goal of the present chapter is to describe a complete leachate-suited treatment train, combining a peroxidation process using a solar photo-Fenton reaction to enhance the biodegradability of the leachate downstream from an aerated lagoon, with an activated sludge biological process, under aerobic and anoxic conditions. The target COD values of 500 and 150 mg O₂/L (according to the regulation for discharge into water bodies) and a nitrogen content below 15 mg/L must be achieved. A further objective is to evaluate the efficiency and performance of the photo-Fenton process, considering the sludge removal step after acidification, to define the optimum phototreatment time to reach a biodegradable wastewater that can be further oxidized in a biological reactor and, to obtain the nitrification and denitrification reaction rates.

4.2 Experimental methodology

All the chemicals used in this work, the detailed description of the experimental unit and respective procedures, as well as the analytical methods employed can be consulted in the Chapter 2.

4.3 Results and discussion

4.3.1 Leachate characterization

Leachate was collected from a sanitary landfill located in the North Portugal, covering an area of 20.5 ha, serving a population of 446,378 inhabitants and receives 446,378 tons of municipal solid wastes (MSW) per year since 1999. The leachate treatment plant (LTP) receives in average 100 m³ of leachate per day, and includes the following treatment units: a 15,000 m³ aerated lagoon with pure oxygen injection; an anoxic and an aerobic activated sludge reactors (150 m³); a clarifier (27 m³), a coagulation/flocculation system and a non-aerated final retention lagoon (3000 m³). The treated leachate is then transported to a municipal WWTP.

The aerated lagoon promotes a biological oxidation of the leachate, achieving 88%, 57% and 63% elimination of the biochemical oxygen demand (BOD₅), dissolved organic carbon (DOC) and chemical oxygen demand (COD), respectively, indicating that the biodegradable organic carbon fraction is almost completely removed in the aerated lagoon [29]. Since the organic matter removal in the anoxic and aerobic activated sludge biological reactors is almost negligible, the leachate samples used in this study were collected after biological lagooning, presenting an intense dark-brown colour, associated with a high organic carbon content (DOC = 1253-1707 mg C/L; COD = 3428-4235 mg O₂/L), low biodegradable organic fraction (BOD₅ = 170-340 mg O₂/L; BOD₅/COD = 0.04-0.09; % D_t, after 28 days (Zahn-Wellens test) = 10-20%), and high nitrogen load (N_D = 2.7-3.0 g N/L), being more that 93% associated to ammonium nitrogen form (Table 4.1).

Considering the leachate characteristics after biological lagooning, the treatment strategy adopted in this work, which operates at a scale close to industrial, integrates a pre-oxidation stage consisting in a solar photo-Fenton process, which enhances the bio-treated leachate biodegradability, mainly through humic substances degradation and, a final polishing step through an aerobic/anoxic activated sludge biological oxidation process, to achieve the target COD values of 500 and 150 mg O₂/L (according to the regulation for discharge into water bodies) and nitrogen content below 15 mg/L.

Table 4.1. Characterization of the sanitary landfill leachate after aerobic lagooning throughout 1-year.

Parameter	Leachate after lagooning				Photo-treated leachate after neutralization				Photo-bio treated leachate				ELV ^b
	Exp. A	Exp. B	Exp. C	Exp. D	Exp. A	Exp. B	Exp. C	Exp. D	Exp. A	Exp. B	Exp. C	Exp. D	
Date	07-02	18-03	27-04	10-05	11-03	05-04	09-05	03-06	05-04	09-05	03-06	16-16	
pH	7.9	7.4	8.1	7.7	7.5	6.7	7.1	6.7	7.1	8.4	8.3	7.6	6-9
T (°C)	11.7	12.9	26.0	23.8	22.4	23.9	19.9	25.3	18.8	22.1	23.3	24.5	-
TSS (mg/L)	136	52	112	90	-	-	-	-	60	44	1163	360	60
DIC (mg C/L)	2497	2307	2278	2202	8.6	2.4	12.3	10.0	33.9 (23.7)	0	194 (290)	203	-
CaCO _{3,ic} ^a (g/L)	10.4	9.6	9.6	9.2	0.04	0.01	0.05	0.04	0.14 (0.10)	0	0.81 (1.2)	0.85	-
DOC (mg C/L)	1253	1406	1707	1654	156	195	435	428	63 (44)	30 (10)	170 (254)	179	-
COD (mg O ₂ /L)	3428	4235	4211	4045	228	266	949	1096	210 (146)	94 (32)	667 (998)	346	150
BOD ₅ (mg O ₂ /L)	300	340	170	255	-	-	-	-	13	14	103	59	40
BOD ₅ /COD	0.09	0.08	0.04	0.06	-	-	-	-	0.06	0.14	0.15	0.17	-
Polyphenols (mg caffeic acid/L)	165	172	190	193	5.8	4.3	13.9	9.9	12.6 (7.4)	8.3 (4.8)	18.2 (21.4)	41.6	-
TDI (mg (Fe ²⁺ + Fe ³⁺)/L)	10.6	12.0	12.2	11.1	1.24	0.21	3.58	1.67	2.8 (0.8)	0.7 (0.1)	14.6 (20.9)	3.1	-
Sulphate (g SO ₄ ²⁻ /L)	0.1	0.1	0.09	0.09	14.0	12.1	11.7	12.6	12.1 (15.0)	10.8	12.6 (13.0)	6.5	2000
Chloride (g Cl ⁻ /L)	2.9	2.9	3.1	3.1	2.5	2.7	2.9	3.3	2.8	3.3 (3.2)	2.8 (2.7)	2.9	-
TDN (g N/L)	2.8	2.7	2.9	2.9	2.6	2.5	2.8	2.8	1.3 (1.6)	32x10 ⁻³ (40x10 ⁻³)	14x10 ⁻³ (22x10 ⁻³)	1.6	15x10⁻³
Ammonium (g N-NH ₄ ⁺ /L)	2.2	2.0	1.7	1.9	2.1	2.1	2	1.7	0.5 (0.7)	2x10 ⁻³	2x10 ⁻³	0.5	7.8x10⁻³
Nitrate (g N-NO ₃ ⁻ /L)	<1x10 ⁻³	<1x10 ⁻³	<1x10 ⁻³	<1x10 ⁻³	0.1	0.5	0.4	0.4	<1x10 ⁻³	<1x10 ⁻³	<1x10 ⁻³	0.1	11x10⁻³
Nitrite (g N-NO ₂ ⁻ /L)	0.1	0.5	0.4	0.4	<1x10 ⁻³	3.4x10 ⁻³	4.6x10 ⁻³	<1x10 ⁻³	0.3 (3x10 ⁻³)	33x10 ⁻³ (<1x10 ⁻³)	14x10 ⁻³ (4x10 ⁻³)	0.7	-
P _T (mg P/L)	19.9	26.2	30.7	23.8	0.9	0.9	2.3	2.3	1.0	3	4.2 (3.8)	14.6	10
Colour (Pt-Co units)	-	-	-	-	-	-	-	-	23	19	114	116	-
Turbidity (NTU)	-	-	-	-	-	-	-	-	46	29	638	298	-

*Values in parenthesis refer to the concentration without the effect of dilution in the biological reactor; ^aAlkalinity values considering that at pH less than 8.1 the inorganic carbon is almost in the form of bicarbonates [33]; ^bELV – Emission Limit Values.

4.3.2 Biodegradability enhancement during solar photo-Fenton reaction

In order to evaluate the leachate biodegradability during the photo-Fenton reaction, samples were collected after different H_2O_2 consumed amounts, associated to different degrees of mineralization. As showed in the previous chapter, leachate acidification to $\text{pH} \sim 2.8$, leads to an abatement of DOC (23%-31%) and COD (11%-15%), associated to humic acids precipitation. The presence of suspended solids increases the turbidity of the leachate, decreasing the light penetration and consequently decreasing the photo-Fenton reaction rate, leading to high energy and H_2O_2 consumption to achieve a similar mineralization of the soluble organic matter. In order to evaluate the influence of sludge produced during acidification in the photo-Fenton reaction, two experiments were performed, with and without sludge removal (experiments A and B, respectively).

Figure 4.1 present the evolution of DOC, COD and two parameters, AOS (average oxidation state) and COS (carbon oxidation state), which can be used to evaluate the oxidation degree and oxidative process efficiency, respectively [34, 35]. Thus, they provide indirect information on the biodegradability as they indicate variations in the qualitative composition of the wastewater that could lead to changes in solution biodegradability/toxicity [36].

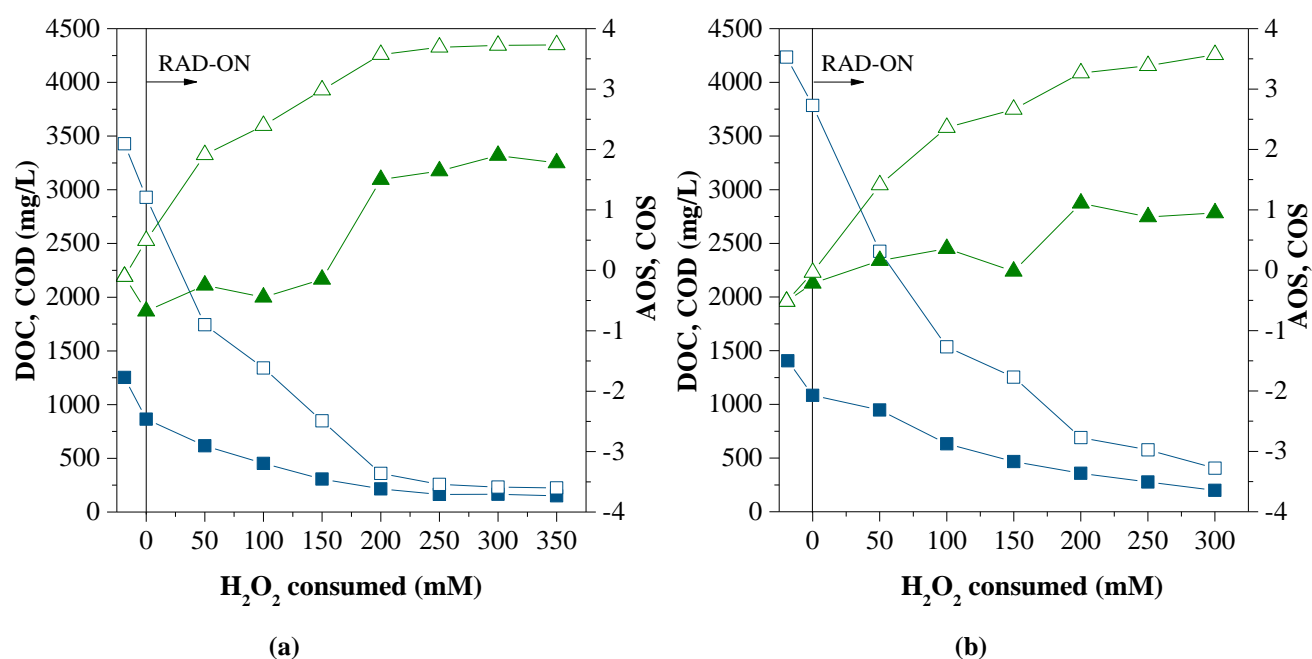


Figure 4.1. DOC (■), COD (□), AOS (▲), and COS (△) evolution as a function of the hydrogen peroxide consumption during the photo-Fenton process: (a) with (Exp. A) and (b) without (Exp. B) sludge removal.

For the experiment with sludge removal (Figure 4.1a), COD has a fast decay (90%) until 200 mM H_2O_2 consumed, showing a strong oxidation of organic matter, which is well correlated with COS increase from -0.1, indicating the presence of rather reduced organic compounds, to +3.7, which means strong mineralization and generation of highly oxidized intermediates. AOS starts at -0.1, and has a high increase between 150 and 200 mM H_2O_2 doses, and remained almost constant for further doses of H_2O_2 . The increase of AOS suggests that more oxidized organic intermediates are formed during the treatment and, after AOS reaches a plateau, the chemistry of the intermediates generated does not vary significantly [37]. For the experiment without sludge removal (Figure 4.1b), COD starts from a higher value than the experiment with sludge removal due to leachate variability, and in order to achieve 90% COD decay it is necessary 250 mM H_2O_2 .

According to Zahn-Wellens test (Figure 4.2 and Figure 4.3), the first two samples (non-treated and after pH adjustment) present a poor biodegradation level, between 4 and 20%. However, as expected, the biodegradability of the leachate was enhanced during the photo-Fenton treatment and a value higher than 70% biodegradation, after only 8 days (or less), was achieved for 200 mM H_2O_2 (sample 6), which is in agreement with the information obtained from AOS and COS profiles.

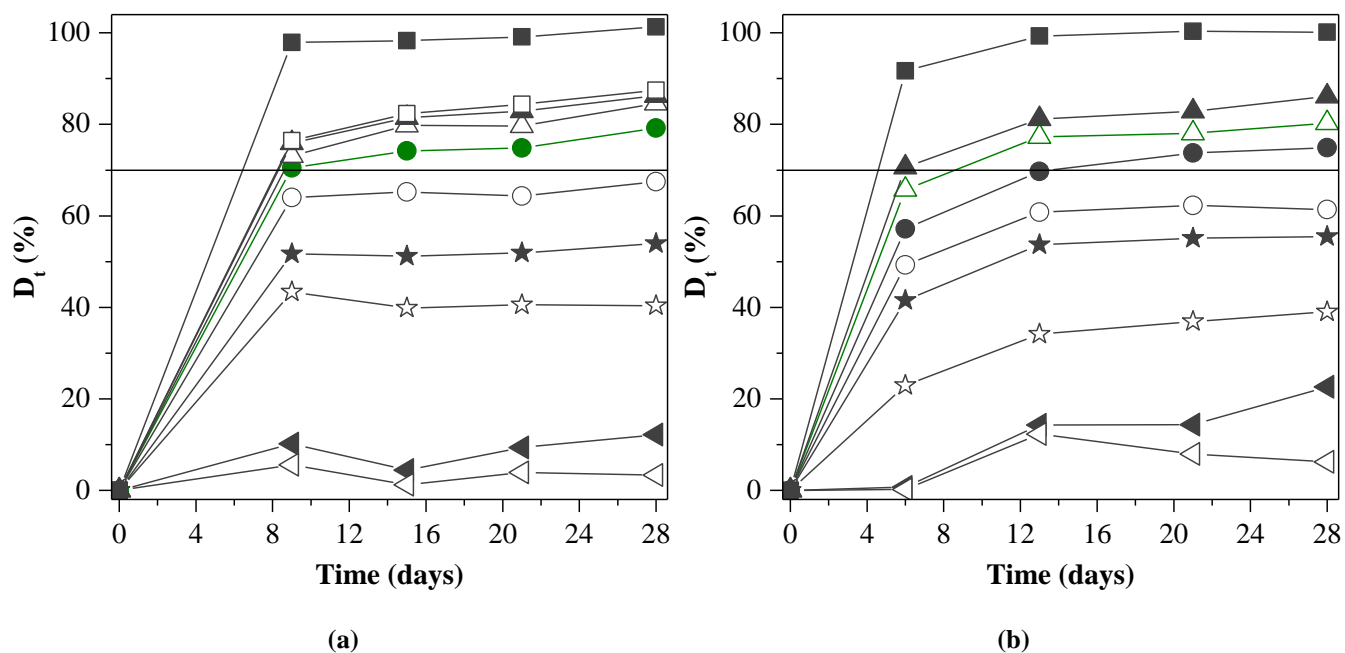
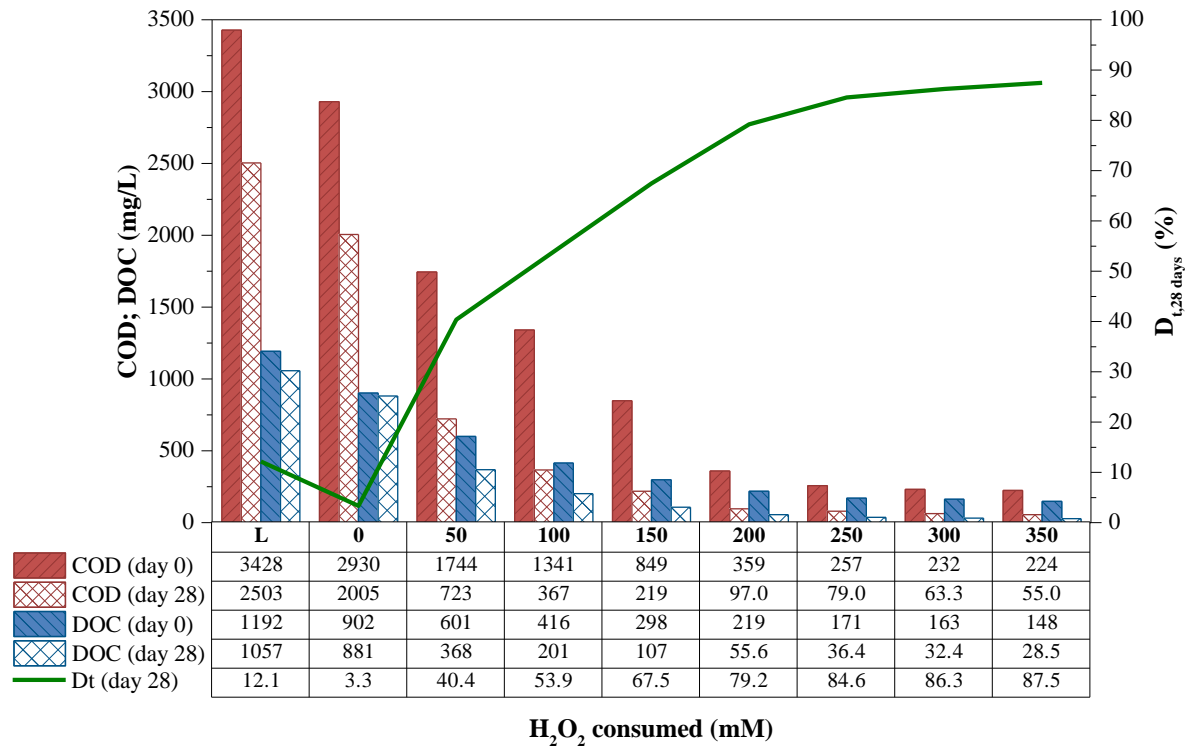
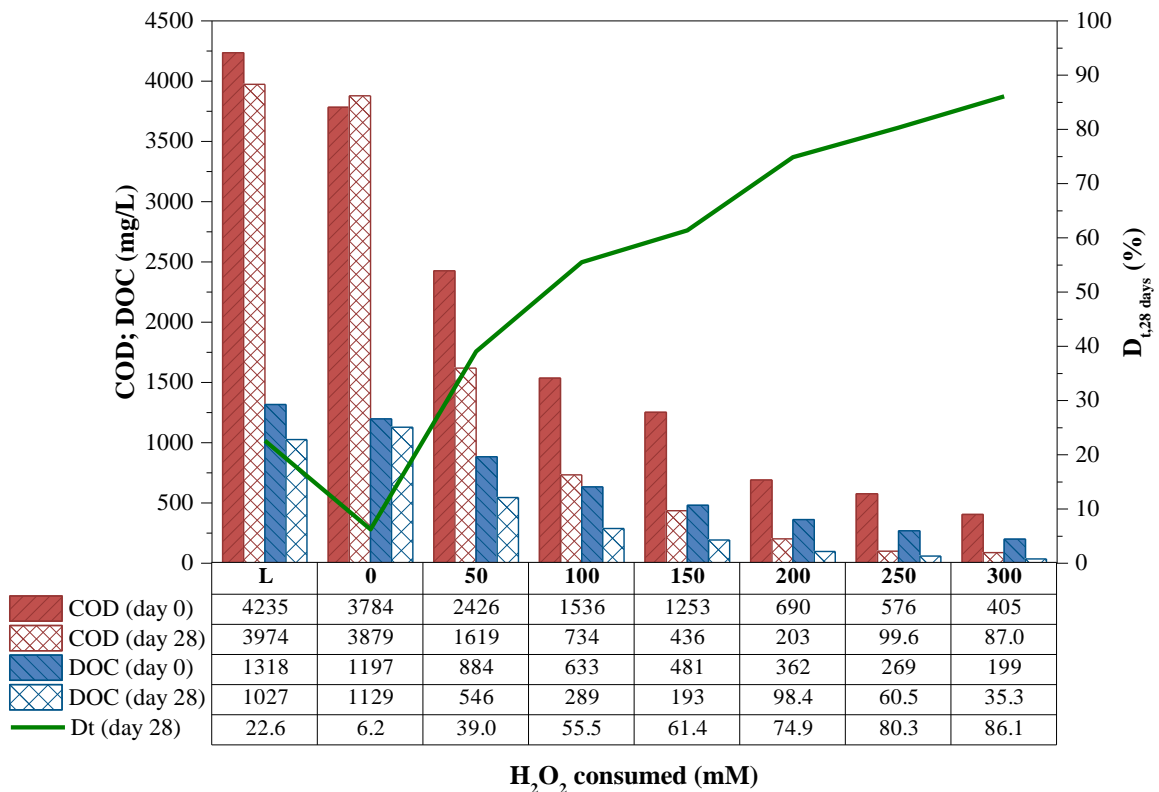


Figure 4.2. Zahn-Wellens test for samples taken during the photo-Fenton process, (a) with (Exp. A) and (b) without (Exp. B) sludge removal: reference (■); initial (◄); after acidification and iron sulphate addition (◁); 50 (☆), 100 (★), 150 (○), 200 (●,●), 250 (△,△), 300 (▲) and 350 (□) mM of H_2O_2 consumed.



(a)



(b)

Figure 4.3. Evaluation of DOC and COD during the Zahn-Wellens test at day 0 and day 28: (a) with (Exp. A) (b) and without (Exp. B) sludge removal after acidification.

Low molecular-weight carboxylate anions concentration also shows the same trend, achieving maximum values between 50 and 75 mg C/L (formate > oxalate > malonate > acetate > propionate > citrate > pyruvate > valerate > maleate), corresponding to 10-17% of DOC, for H_2O_2 doses between 100 and 200 mM H_2O_2 (Figure 4.3).

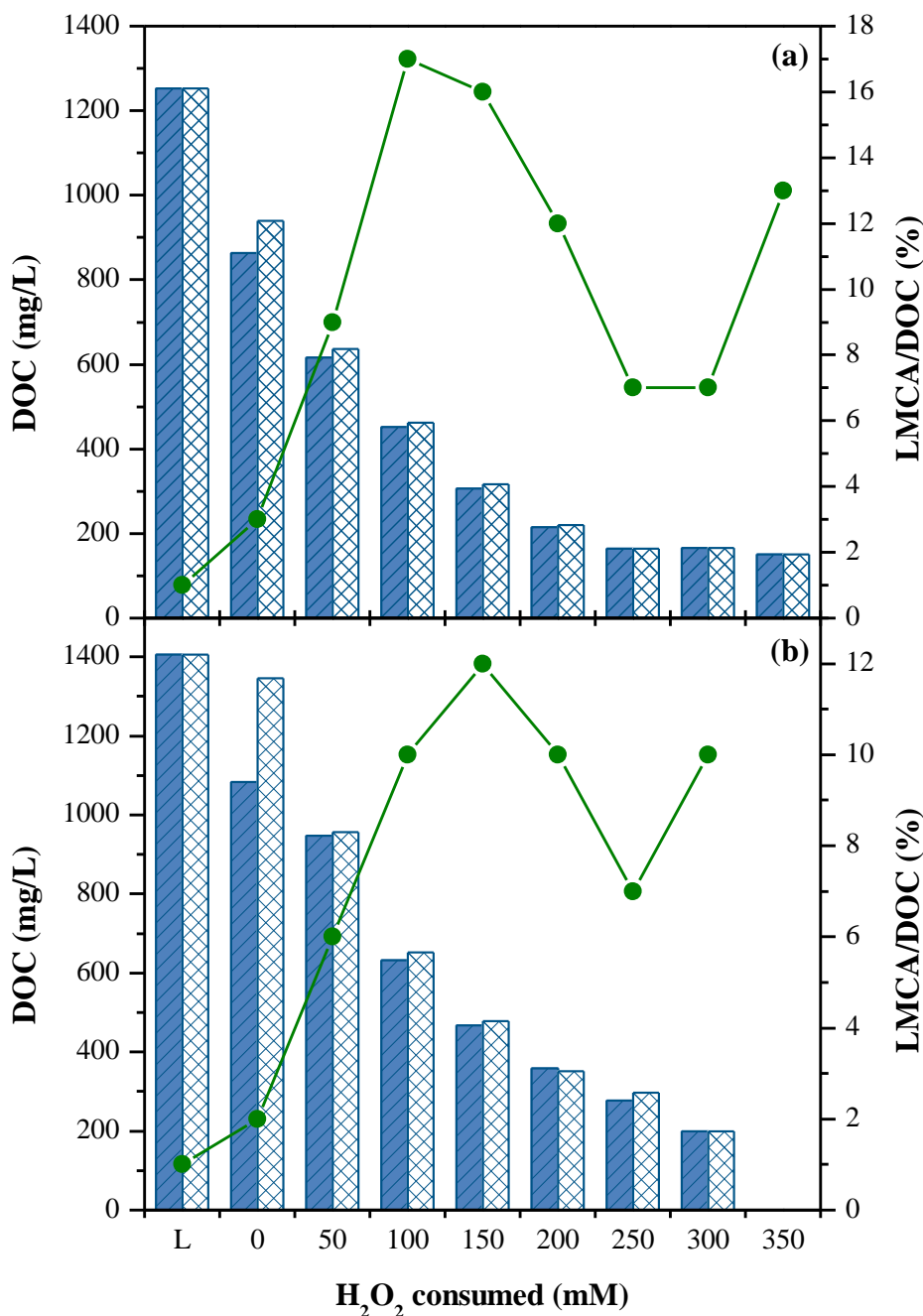


Figure 4.4. Evaluation of DOC at acidic (■) or neutralized (▨) conditions and low-molecular-weight carboxylate anions (LMCA)/DOC ratio (●) as a function of hydrogen peroxide consumption during photo-Fenton process: (a) with (Exp. A) and (b) without (Exp. B) sludge removal after acidification.

Considering the two different target COD values, namely 150 and 500 mg O₂/L, is necessary H₂O₂ doses around 180 mM and 90 mM, respectively, with sludge removal, and around 225 mM and 140 mM, without sludge removal (Figure 4.3), considering a subsequent biological treatment.

For both experiments, the H₂O₂ consumed/DOC oxidized ratio is very similar, with values of 7.9-8.2 (without and with sludge removal) and 10.0 mg H₂O₂/mg DOC, respectively for COD targets values of 500 and 150 mg O₂/L. COD and DOC values at different H₂O₂ consumed amounts (different points of the oxidation process) were determined after neutralization for the experiments with and without sludge removal, which means that humic acids or other organic compounds initially precipitated due to acidification, are dissolved again, if not destroyed. DOC values for the second sample, 0 mM H₂O₂, which corresponds to the sample after acidification step, presents a DOC after neutralization almost equal to the initial leachate (COD after neutralization increased 262 mg C/L), considering the experiment without sludge removal, showing that humic acids or other organic compounds initially precipitated after acidification are dissolved again if pH is neutralized. For the experiment with sludge removal, COD value after neutralization had only a small increase (76 mg C/L), probably due to the fact that a small fraction of sludge was not removed. These results show that a sludge removal step after acidification can be a good option to eliminate 20-30% of the initial leachate organic content, including high recalcitrant humic acids. After 50 mM H₂O₂ consumed, for the experiment without sludge removal, DOC at acidic conditions and after neutralization has the same value, which suggests that humic acids or other organic compounds initially precipitated were removed or transformed into other soluble organic compounds at acidic pH.

The H₂O₂ consumed/DOC oxidized ratio at the optimum phototreatment time defined in Table 4.1 is an important parameter to compare the efficiency of H₂O₂ consumption during the reaction and at the same time can be used to compare the efficiency between different wastewaters with different initial organic carbon content. According to the H₂O₂ consumed/DOC oxidized ratio at the optimum phototreatment time, it can be concluded that the sludge removal after acidification, does not affect the H₂O₂ consumption per unit of DOC oxidized. However, the non-elimination of sludge produced after acidification increases the H₂O₂ consumption to achieve the biodegradability threshold, associated to the H₂O₂ dose necessary to oxidise the particulate organic matter.

Table 4.2. Process variables as performance indicators.

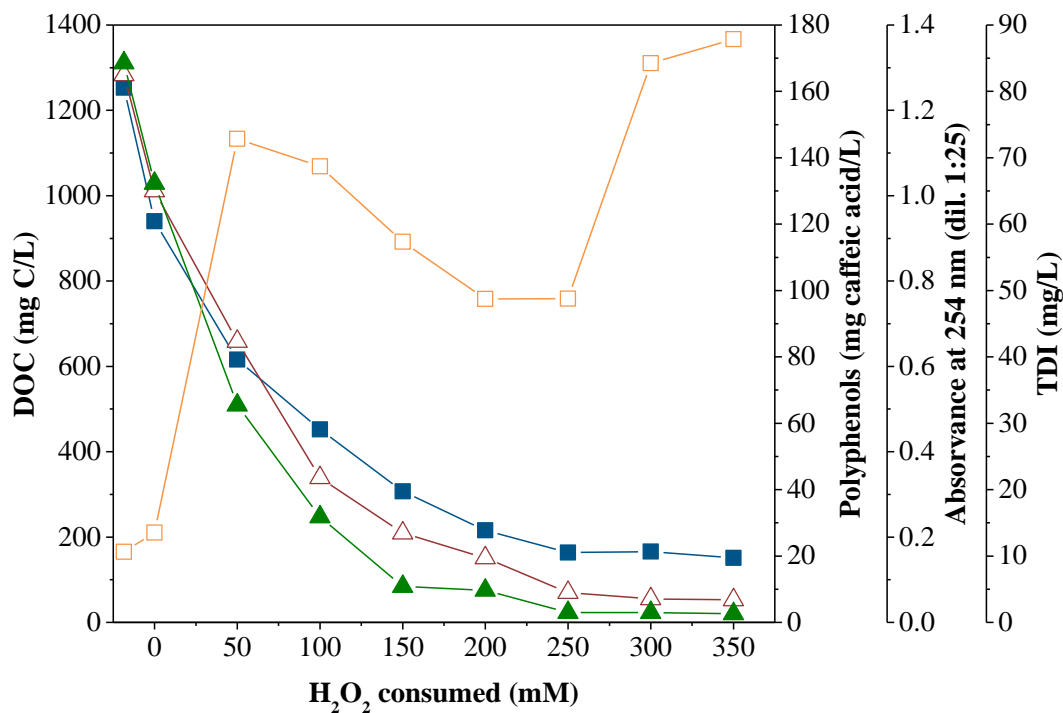
Photo-Fenton (PF)					Biological Treatment			
Parameter	Exp. A	Exp. B	Exp. C	Exp. D	Parameter	Exp. A	Exp. B	Exp. C
pH _m ^a	2.9	2.9	2.7	2.7	VSS (mg/L)	1758	2220	2035
T _m ^a (°C)	21.9	23.8	33.5	40.5	TSS (mg/L)	2915	3977	3418
TDI _m ^a (mg/L)	66.9	34.6	44.9	54.8	VSS/TSS (%)	60	56	60
t _{PF} (h)	-	-	29	43	SSV _{30-min} ¹ (mL/L)	405	735	248
I _{UV} (W/m ²)	16.9	21.7	28.5	23.6	SVI ^m (mg/L)	139	185	73
Q _{UV} (kJ/L)	-	-	84	104				
[H ₂ O ₂] cons. (mM)	350	300	200	275	Nitrification			
[H ₂ SO ₄] (mM)	114	131	99	96	pH _{n,m}	6.9	7.4	7.3
%CaCO ₃ ^b	91	73	97	95	T _{n,m}	18.2	22.6	26.8
[NaOH] (mM)	43	29	29	25	DO _m (mg/L)	1.6	3.7	3.6
DOC _i (mg/L)	1253	1406	1707	1654	t _{BT,n} (h)	356	505	91
DOC _{AA} ^c (mg/L)	864	1084	1239	1327	k _n (mg NH ₄ ⁺ -N/h/g SSV)	0.7±0.1	1.4±0.1	6.9±0.1
DOC _{BN} ^d (mg/L)	151	199	413	427	[NaOH] (mM)/CaCO ₃ (g/L)	113/5.6	172/8.6	400/20.0
DOC _f (mg/L)	156	195	435	428				
Min ^e (%)	88	86	75	74	Denitrification			
Min _{opt} ^f (%)	64/83	67/80	-	-	pH _{d,m}	7.84	8.57	8.8
H ₂ O ₂ /DOC _{ox} ^g (mg H ₂ O ₂ /mg DOC _{ox})	16.9	11.5	8.5	10.4	T _{d,m}	17.2	22.1	26.2
H ₂ O ₂ /DOC _{ox,opt} ^h (mg H ₂ O ₂ /mg DOC _{ox})	7.9/10.0	8.2/10.0	-	-	t _{BT,d} (h)	242	216	167
k _l ⁱ (L/kJ)	-	-	0.02±0.02; 0.009±0.004	0.02±0.01; 0.006±0.001	k _d (mg (NO ₃ ⁻ -N + NO ₂ ⁻ -N)/h/g SSV)	0.9±0.1	2.0±0.4	2.4±0.4
r _d ^j (mg/kJ)	-	-	23±20; 6±2	28±15; 3.5±0.7	C/N (mg CH ₃ OH/mg (NO ₃ ⁻ -N + NO ₂ ⁻ -N))	5.3±0.7	3.0±0.7	3.1±0.8
k _{H₂O₂} ^k (mmol/kJ)	-	-	3±1; 1.9±0.3	4±2; 1.9±0.3	[CH ₃ OH] (mM)	123	239	194
					[H ₂ SO ₄] (mM)/CaCO ₃ (g/L)	0	0	28/2.8

^apH_m, T_m and Fe_m correspond to average values of pH, temperature and total dissolved iron observed during the photo-Fenton experiment; ^bPercentage of consumed acid percentage to neutralize the alkalinity (CaCO_{3,I}/(100.08 × [H₂SO₄]), %); ^cDOC After Acidification; ^dDOC Before Neutralization; ^ePhoto-Fenton mineralization (1-DOC_f/DOC_i, %); ^fPhoto-Fenton mineralization in the optimal point of biodegradability (COD_f < 500/150 mg O₂/L); ^gRatio between H₂O₂ consumed and oxidized DOC (H₂O₂/(DOC_{AA}-DOC_f) × 34.02); ^hRatio between H₂O₂ consumed and oxidized DOC in the optimal point of biodegradability (COD_f < 500/150 mg O₂/L); ⁱPseudo-first-order kinetic constant for DOC degradation (0 < Q_{UV} < 30 kJ_{UV}/L; 30 < Q_{UV} < 100 kJ_{UV}/L); ^jInitial DOC reaction rate (0 < Q_{UV} < 30 kJ_{UV}/L; 30 < Q_{UV} < 100 kJ_{UV}/L); ^kH₂O₂ consumption rate (0 < Q_{UV} < 30 kJ_{UV}/L; 30 < Q_{UV} < 100 kJ_{UV}/L); ^lSS₃₀ - Settled Sludge Volume after 30 minutes of decantation; ^mSVI – Sludge Volume Index.

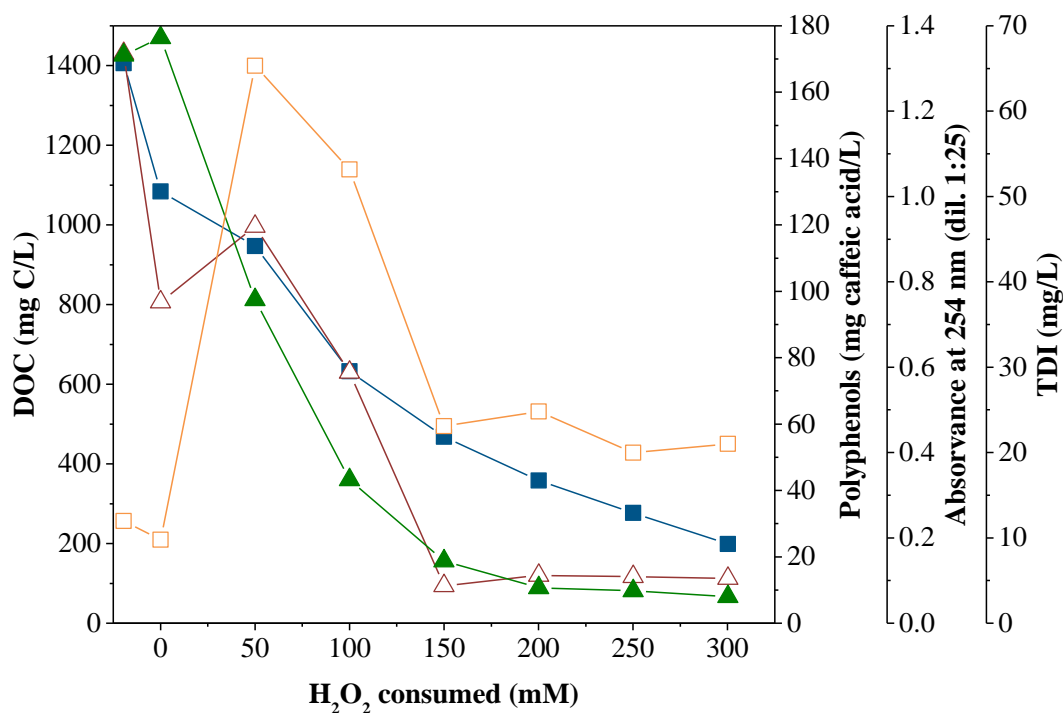
Different authors [38-40] reported high mineralization values regarding the treatment of leachates using Fenton and photo-Fenton processes, although a cautiously analysis of the results must be performed, regarding the evaluation of soluble and particulate organic matter content during the treatment. If precipitation of humic acids or other organic compounds occurs during the acidification process, and if the oxidation treatment time is not enough to degrade those complex molecules present in the particulate phase, after the final effluent neutralization step, those compounds will be redissolved and discharged in water bodies. During the photo-Fenton reaction those organic compounds in the particulate phase will be also attacked by the hydroxyl radicals and will be eventually mineralized. However, the energy and H_2O_2 consumption will be much higher to achieve the same soluble DOC concentration. Beyond that, the high amount of solids decreases the transmissibility of the wastewater, decreasing the efficiency of the photo-Fenton reaction. Sludge elimination can be an interesting option to improve the photo-Fenton process; however the disposal of an acid sludge can be a big problem. The high content of humic acids in the sludge can be a valuable resource, since humic acids can be called “the black gold of agriculture” [41].

Due to high variability of leachate composition, H_2O_2 or UV dose cannot be used as useful parameters for economic online measurement for process control, since depends greatly from initial DOC. Evaluation of UV absorbance at 254 nm, wavelength at which aromatic and unsaturated compounds present a maximum absorption [42], can be used as a fast and economic method for process control. Polyphenols concentration and aromatic content given by absorbance at 254 nm after dilution 1:25 (Figure 4.5), shows a similar profile, leading to 88% and 94% reduction after 200 mM of H_2O_2 consumed for the experiment with sludge removal and 92% and 94% reduction after 250 mM of H_2O_2 consumed for the experiment without sludge removal. For both experiments, absorbance at 254 nm after dilution 1:25 must be lower than 0.3 or 0.08, in order to reach a photo-treated leachate compatible with a biological oxidation process, achieving a final COD below 500 and 150 mg O_2/L , respectively.

Finally, the photo-treated leachate at the optimum phototreatment time is neutralized with NaOH to a pH around 7 under mechanical stirring (a residual concentration of H_2O_2 can be useful to convert all ferrous ions into ferric ions, leading to a higher precipitation extend), before the biological treatment, leading to iron precipitation, followed by a period of 3 h for iron sludge sedimentation. Although the concentration of heavy metals was not measured in the leachates samples used in this work, it was reported in a previous paper [28], for leachate samples collected from the same sanitary landfill in a different time, the presence of the following concentrations: copper (0.1 mg/L); total chromium (2.2 mg/L); manganese (0.9 mg/L); arsenic (95.6 mg/L); lead (36.4 mg/L); zinc (1.2 mg/L); cadmium (0.4 mg/L) and nickel (0.8 mg/L). The neutralization of the photo-treated leachate leading to the precipitation of Fe(II) and Fe(III) can be also an efficient process for the binding and immobilization of the heavy metals by adsorption in the ferrous/ferric sludge, as it was reported by different authors [24, 43, 44].



(a)



(b)

Figure 4.5. DOC (■), absorbance at 254 nm (▲), polyphenols (△) and dissolved iron concentration (□) evolution as a function of hydrogen peroxide consumption during the photo-Fenton process (pH = 2.8; $[Fe^{2+}] = 80$ mg/L): with (Exp. A) (a) and without (Exp. B) (b) sludge removal after acidification.

4.3.3 Integrated systems: solar photo-Fenton pre-oxidation/biological nitrification and denitrification

Two last experiments (C and D) were performed combining the solar photo-Fenton, considering the optimum H_2O_2 dose without sludge removal after acidification, and a further biological oxidation process, with the objective to achieve a final wastewater with a COD content below 500 mg O_2/L . Due to variability of raw leachate composition and preliminary biological lagooning treatment efficiency, leachate samples used in experiments C and D presented values of DOC 20%-30% higher than those observed for experiments A and B. According to $\text{H}_2\text{O}_2/\text{DOC}$ rates, and initial DOC, it was estimated a dose of 235 mM H_2O_2 , to achieve a final wastewater, after biological treatment, with a COD below 500 mg O_2/L . For experiment C it was considered only 200 mM H_2O_2 , in order to know if the biological oxidation process efficiency could be higher than the results obtained in the Zahn-Wellens test. Both kinetics shows similar kinetic profiles (Figure 4.6) with an initial fast degradation rate (23 ± 20 mg $\text{C}/\text{kJ}_{\text{UV}}$; 28 ± 15 mg $\text{C}/\text{kJ}_{\text{UV}}$), and H_2O_2 consumption rate (3 ± 1 mmol $\text{H}_2\text{O}_2/\text{kJ}_{\text{UV}}$; 4 ± 2 mmol $\text{H}_2\text{O}_2/\text{kJ}_{\text{UV}}$), until 30 kJ/L, respectively for the experiments C and D. Until the end of the experiments, reaction and H_2O_2 consumption rates presents values 4-8 times and 2 times lower that those observed in the initial part of reaction, respectively for experiments C and D. The higher consumption rate of H_2O_2 observed in the initial part of experiment D can be attributed to the higher temperature which favours H_2O_2 self-decomposition, being necessary more 25-30% of H_2O_2 to achieve the same mineralization.

For the average pH, chloride and sulphate values observed in experiments C and D (pH = 2.7; 3 g Cl^-/L and 12 g $\text{SO}_4^{2-}/\text{L}$), the predominant iron species in solution are $\text{Fe}(\text{SO}_4)_2^-$ (66.4%) and FeSO_4^+ (33.1%) (considering equilibrium constants at 25 °C and ionic strength of 0.5 M [33, 45-47]), leading to the formation of mainly $\text{SO}_4^{\bullet-}$, which presents a lower oxidant power than HO^{\bullet} radicals. High amounts of sulphuric acid are needed due to the high leachate alkalinity. For example, leachate sample used in experiment C has an alkalinity of 9.6 g CaCO_3/L (considering that at a pH of 8.1, all inorganic carbon corresponds to bicarbonates [33]), consuming 99 mM H_2SO_4 , which corresponds to 97% of the total sulphuric acid needed for the acidification process. If during the preliminary biological lagooning, nitrification is achieved, alkalinity removal can achieve 100% efficiency, decreasing the needs of sulphuric acid in the preliminary acidification process, decreasing sulphates ions concentration, increasing the most photoactive ferric iron-water complex concentration, FeOH^{2+} [31], and consequently increase of the photo-Fenton reaction rate.

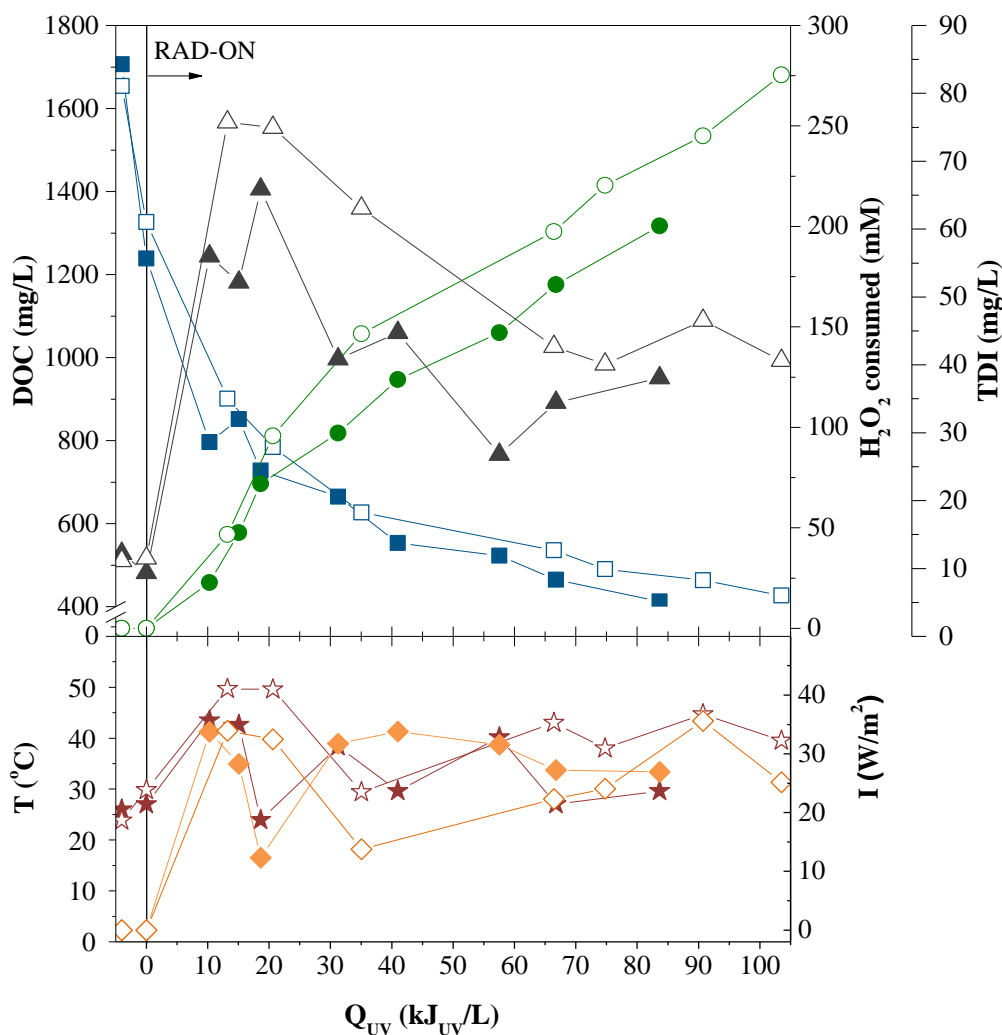


Figure 4.6. Evaluation of the photo-Fenton reaction. (■, □) - DOC; (●, ○) - H₂O₂ consumed; (▲, △) Dissolved Iron; (★, ☆) – Temperature; (◆, ◇) – Average irradiation. Solid symbols: Exp. C (without sludge removal); Open symbols: Exp. D (without sludge removal).

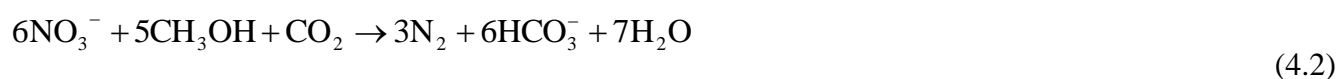
The photo-bio-treated leachate presents COD values lower than 150 mg O₂/L for experiments A and B and lower than 500 mg O₂/L for experiment D (Table 4.1). For experiment C, leachate presented a concentration of humic substances (HS) of 1008 mg C_{HS}/L, representing 59% of the DOC. After acidification, precipitation of humic acids occurred and the remaining humic substance in solution was 671 mg C_{HS}/L, corresponding to 54% of DOC and meaning that 72% of the DOC abatement is attributed to humic acids precipitation. The concentration of humic substances in the photo-treated leachate after neutralization was 126 mg C_{HS}/L, which represents 29% of the remaining DOC, corresponding to a reduction of 87.5%. The bio-photo-treated leachate, experiment D, presents a DOC value of 179 mg C/L, and considering that humic substances are not biodegradable, 74% of the remaining DOC is related to humic substances (Table 4.1).

Figure 4.7 presents the combined system photo-Fenton/biological results for experiments B and C. Under aerobic conditions, it was accumulated more than 84% of the loaded ammonium nitrogen as nitrite, with almost complete ammonium conversion, achieving final values of 1.8 g NO₂⁻-N/L and 0.2 g NO₂⁻-N/L. pH was maintained between 6.8 and 8.0 through NaOH addition. The highest nitrification rate obtained was 6.9 mg NH₄⁺-N/(h.g VSS) consuming 20.0 g CaCO₃ per liter of photo-treated leachate or 9.9 mg CaCO₃ per mg NH₄⁺-N, which is similar to the stoichiometric ratio, 7.14 mg CaCO₃ per mg NH₄⁺-N (Eq. (4.1)) (photo-treated leachate alkalinity was negligible).

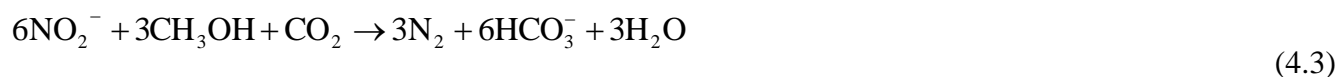


(nitritation, ammonia-oxidising bacteria)

After complete nitrification process, oxygen supply was turned off, methanol was added as external carbon source for the denitrification process and pH was controlled between 7.6 and 9.0, through the addition of H₂SO₄. Maximum denitrification rate of 2.4 mg (NO₂⁻-N + NO₃⁻-N)/(h.g VSS) was observed, with a C/N consumption ratio of 3.1 mg CH₃OH/mg (NO₂⁻-N + NO₃⁻-N) (6.2 g/7.8 mL of commercial methanol per liter of leachate). During denitrification it was produced 2.8 g of alkalinity, as CaCO₃, per liter of leachate, according to the acid addition, which is equivalent to 1.4 g CaCO₃ per g of (NO₂⁻-N + NO₃⁻-N) reduced. According to Equations (4.2) and (4.3), during denitrification is produced 3.57 g (as CaCO₃) of alkalinity per g of NO₂⁻-N or NO₃⁻-N reduced, which is 2 times higher than the value obtained. During denitrification the inorganic carbon concentration increased from 0 to 1.2 g C/L, corresponding to 6.1 g HCO₃⁻/L or 5.0 g CaCO₃/L, equivalent to 2.5 g CaCO₃ per g (NO₂⁻-N + NO₃⁻-N) reduced. So, the overall alkalinity produced was 3.9 g CaCO₃ per g (NO₂⁻-N + NO₃⁻-N) reduced, which is very near to stoichiometric reaction.

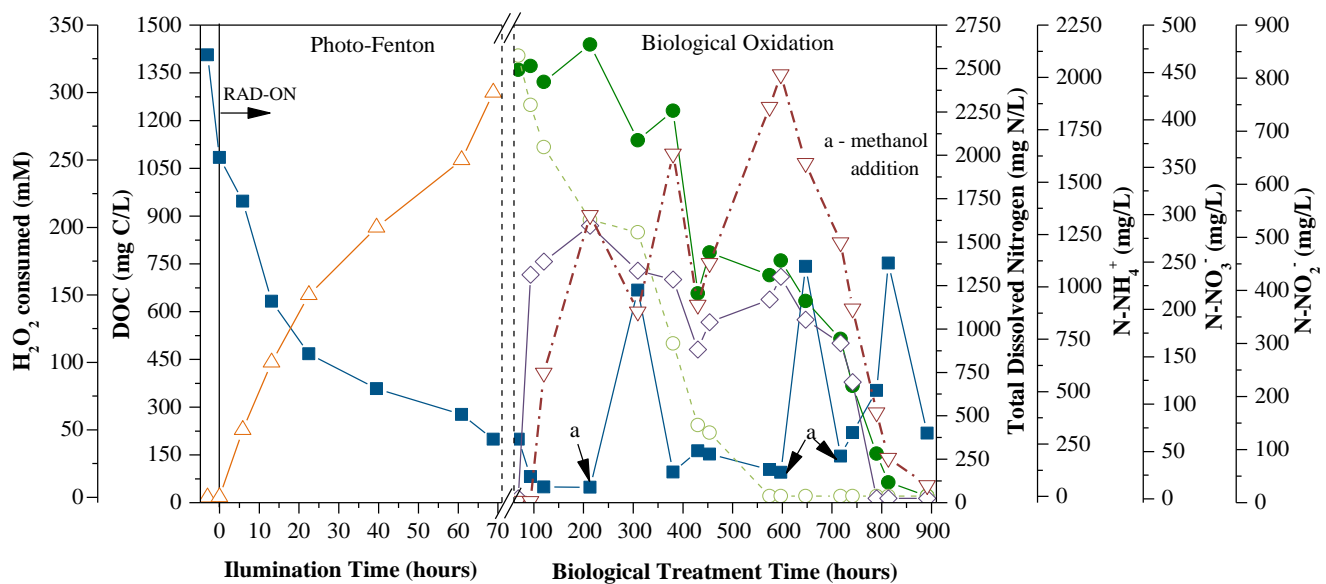


(nitrate removal process)

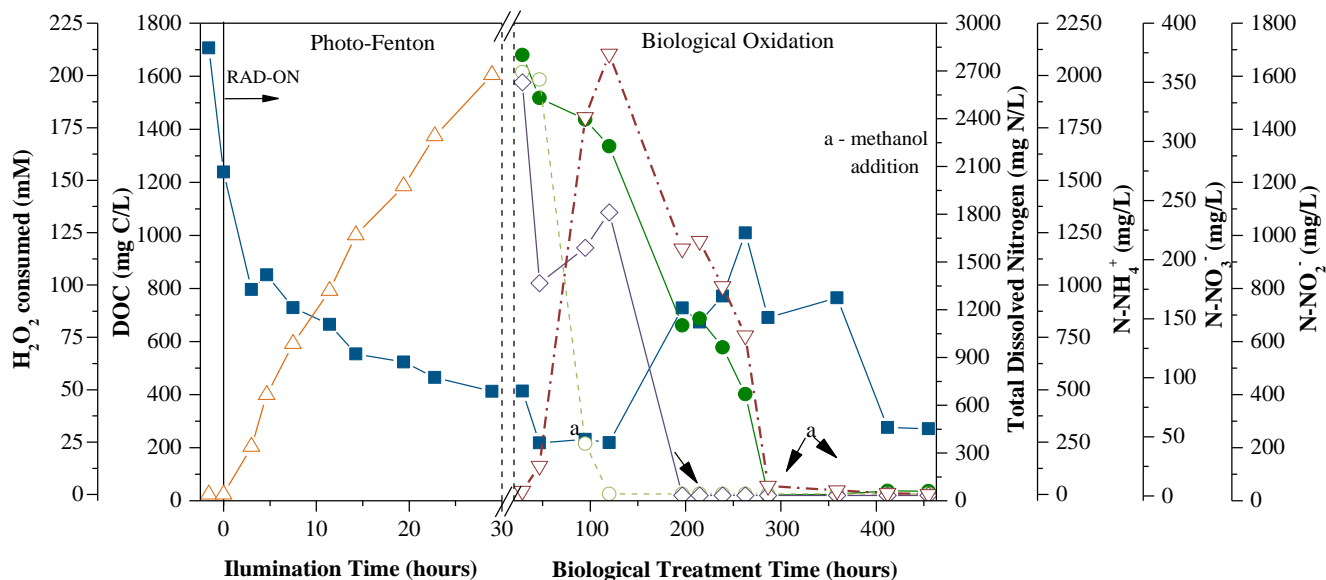


(nitrite removal process)

In the previous chapter, using the same type of photo-treated leachate, it was shown that the maximum nitrification and denitrification rates were 0.49 mg NH₄⁺-N/(h.g VSS) and 0.27 mg (NO₂⁻-N + NO₃⁻-N)/(h.g VSS), which are 14 and 26 times lower than those observed in this section, respectively. This difference is attributed mainly to the low temperatures (<15.5 °C) observed in Chapter 3 (winter season), when compared with an average temperature of 26.8 °C (spring season) observed in experiment C.



(a)



(b)

Figure 4.7. Leachate mineralization by the combined system: photo-Fenton (DOC and H_2O_2 consumed in function of the illumination time); biological nitrification/denitrification (DOC and nitrogen species as function of time). (a) Exp. B (without sludge removal); (b) Exp. C (without sludge removal). ■ - DOC; △ - H_2O_2 consumption; ● - Total Nitrogen; ○ - Ammonium ($\text{NH}_4^+\text{-N}$); ◇ - Nitrate ($\text{NO}_3^-\text{-N}$); ▽ - Nitrite ($\text{NO}_2^-\text{-N}$).

The global efficiency of the combined system for experiment C, in terms of DOC, was approximately 90%, corresponding to 74% (200 mM H_2O_2 consumed) for the chemical oxidation and 16% for the biological oxidation, and approximately 100% for total dissolved nitrogen, achieving a final value below 15 mg N/L.

4.4 Conclusions

An integrated treatment strategy for the treatment of leachates after biological lagooning, combining a pre-oxidation step using a solar photo-Fenton reaction with an activated biological process under anoxic and aerobic conditions was able to yield a final wastewater in agreement with the discharge limits imposed by Portuguese Legislation in terms of COD values ($<150 \text{ mgO}_2/\text{L}$) and nitrogen content ($<15 \text{ mg N/L}$). The preliminary acidification step of the photo-Fenton reaction leads to the precipitation of the majority of humic acids and other organic compounds, and is responsible for an abatement of 20-30% of the soluble DOC. Sludge removal decreases the amount of suspended solids, increasing the transmissibility of the leachate, decreasing the light absorbing species and consequently rising the photo-Fenton reaction rate, and decreasing the consumption of H_2O_2 . The major drawback of sludge elimination step is associated with the disposal of an acid sludge.

The activated sludge biological system operated under aerobic and anoxic conditions, allowed an almost complete nitrogen removal, for levels below 15 mg N/L . A maximum nitrification rate of $6.9 \text{ mg NH}_4^+\text{-N}/(\text{h.g VSS})$ was achieved, consuming 20.0 g CaCO_3 per liter of photo-treated leachate or 9.9 mg CaCO_3 per $\text{mg NH}_4^+\text{-N}$. The maximum denitrification rate observed was $2.4 \text{ mg (NO}_2^-\text{-N} + \text{NO}_3^-\text{-N)}/(\text{h.g VSS})$, with a C/N consumption ratio of $3.1 \text{ mg CH}_3\text{OH}/\text{mg (NO}_2^-\text{-N} + \text{NO}_3^-\text{-N})$.

4.5 References

- [1] H.-j. Fan, H.-Y. Shu, H.-S. Yang, W.-C. Chen, Characteristics of landfill leachates in central Taiwan, *Science of the Total Environment*, 361 (2006) 25-37.
- [2] S. Jonsson, J. Ejlertsson, B.H. Svensson, Behaviour of mono- and diesters of o-phthalic acid in leachates released during digestion of municipal solid waste under landfill conditions, *Advances in Environmental Research*, 7 (2003) 429-440.
- [3] S.K. Marttinen, R.H. Kettunen, J.A. Rintala, Occurrence and removal of organic pollutants in sewages and landfill leachates, *The Science of The Total Environment*, 301 (2003) 1-12.
- [4] M. Osako, Y.-J. Kim, S.-i. Sakai, Leaching of brominated flame retardants in leachate from landfills in Japan, *Chemosphere*, 57 (2004) 1571-1579.
- [5] Y. Wu, S. Zhou, X. Ye, D. Chen, K. Zheng, F. Qin, Transformation of pollutants in landfill leachate treated by a combined sequence batch reactor, coagulation, Fenton oxidation and biological aerated filter technology, *Process Safety and Environmental Protection*, 89 (2011) 112-120.
- [6] C.B. Öman, C. Junstedt, Chemical characterization of landfill leachates – 400 parameters and compounds, *Waste Management*, 28 (2008) 1876-1891.
- [7] D.L. Jensen, A. Ledin, T.H. Christensen, Speciation of heavy metals in landfill-leachate polluted groundwater, *Water Research*, 33 (1999) 2642-2650.
- [8] T.H. Christensen, P. Kjeldsen, P.L. Bjerg, D.L. Jensen, J.B. Christensen, A. Baun, H.-J. Albrechtsen, G. Heron, Biogeochemistry of landfill leachate plumes, *Applied Geochemistry*, 16 (2001) 659-718.
- [9] E. Commission, Decision no 2455/2001/EC of the European parliament and of the council of 20 November 2001, establishing the list of priority substances in the field of water policy and amending directive 2000/60/EC, *Official Journal of the European Communities*, Decision no 2455/2001/EC (2001) L331/331.
- [10] P. Hörsch, A. Speck, F.H. Frimmel, Combined advanced oxidation and biodegradation of industrial effluents from the production of stilbene-based fluorescent whitening agents, *Water Research*, 37 (2003) 2748-2756.
- [11] V.J.P. Vilar, L.X. Pinho, A.M.A. Pintor, R.A.R. Boaventura, Treatment of textile wastewaters by solar-driven advanced oxidation processes, *Solar Energy*, 85 (2011) 1927-1934.
- [12] V.J.P. Vilar, M.I. Maldonado, I. Oller, S. Malato, R.A.R. Boaventura, Solar treatment of cork boiling and bleaching wastewaters in a pilot plant, *Water Research*, 43 (2009) 4050-4062.
- [13] A.M.A. Pintor, V.J.P. Vilar, R.A.R. Boaventura, Decontamination of cork wastewaters by solar-photo-Fenton process using cork bleaching wastewater as H₂O₂ source, *Solar Energy*, 85 (2011) 579-587.
- [14] F.J. Benitez, J.B.d. Heredia, F.J. Real, J.L. Acero, Purification kinetics of winery wastes by ozonation, anaerobic digestion and ozonation plus anaerobic digestion, *Journal of Environmental Science and Health*, A34 (1999) 2023-2041.
- [15] J.B. de Heredia, J. Torregrosa, J. Dominguez, E. Partido, Degradation of wine distillery wastewaters by the combination of aerobic biological treatment with chemical oxidation by Fenton's reagent, *Sustainable Viticulture and Winery Wastes Management*, 51 (2005) 167-174.
- [16] R. Mosteo, J. Sarasa, M.P. Ormad, J. Ovelleiro, Sequential solar photo-Fenton-biological system for the treatment of winery wastewaters, *Journal of Agricultural and Food Chemistry*, 56 (2008) 7333-7338.

- [17] B.S. Souza, F.C. Moreira, M.W. Dezotti, V.J. Vilar, R.A. Boaventura, Application of biological oxidation and solar driven advanced oxidation processes to remediation of winery wastewater, *Catalysis Today*, 209 (2013) 201-208.
- [18] C. Sirtori, A. Zapata, I. Oller, W. Gernjak, A. Agüera, S. Malato, Decontamination industrial pharmaceutical wastewater by combining solar photo-Fenton and biological treatment, *Water Research*, 43 (2009) 661-668.
- [19] A.M. Amat, A. Arques, F. Lopez, M.A. Miranda, Solar photo-catalysis to remove paper mill wastewater pollutants, *Solar Energy*, 79 (2005) 393-401.
- [20] J. Beltrán-Heredia, J. Torregrosa, J. García, J. Domínguez, J. Tierno, Degradation of olive mill wastewater by the combination of Fenton's reagent and ozonation processes with an aerobic biological treatment, *Water Science & Technology*, 44 (2001) 103-108.
- [21] A. Zapata, S. Malato, J.A. Sánchez-Pérez, I. Oller, M.I. Maldonado, Scale-up strategy for a combined solar photo-Fenton/biological system for remediation of pesticide-contaminated water, *Catalysis Today*, 151 (2010) 100-106.
- [22] V.J.P. Vilar, F.C. Moreira, A.C.C. Ferreira, M.A. Sousa, C. Gonçalves, M.F. Alpendurada, R.A.R. Boaventura, Biodegradability enhancement of a pesticide-containing bio-treated wastewater using a solar photo-Fenton treatment step followed by a biological oxidation process, *Water Research*, 46 (2012) 4599-4613.
- [23] V.J.P. Vilar, E.M.R. Rocha, F.S. Mota, A. Fonseca, I. Saraiva, R.A.R. Boaventura, Treatment of a sanitary landfill leachate using combined solar photo-Fenton and biological immobilized biomass reactor at a pilot scale, *Water Research*, 45 (2011) 2647-2658.
- [24] M. Vedrenne, R. Vasquez-Medrano, D. Prato-Garcia, B.A. Frontana-Urbe, J.G. Ibanez, Characterization and detoxification of a mature landfill leachate using a combined coagulation–flocculation/photo Fenton treatment, *Journal of Hazardous Materials*, 205–206 (2012) 208-215.
- [25] I. Oller, S. Malato, J. Sánchez-Pérez, Combination of advanced oxidation processes and biological treatments for wastewater decontamination—a review, *Science of the Total Environment*, 409 (2011) 4141-4166.
- [26] S. Malato, P. Fernández-Ibáñez, M.I. Maldonado, J. Blanco, W. Gernjak, Decontamination and disinfection of water by solar photocatalysis: Recent overview and trends, *Catalysis Today*, 147 (2009) 1-59.
- [27] I. Muñoz, S. Malato, A. Rodríguez, X. Doménech, Integration of Environmental and Economic Performance of Processes. Case Study on Advanced Oxidation Processes for Wastewater Treatment, *Journal of Advanced Oxidation Technologies*, 11 (2008) 270-275.
- [28] E.M.R. Rocha, V.J.P. Vilar, A. Fonseca, I. Saraiva, R.A.R. Boaventura, Landfill leachate treatment by solar-driven AOPs, *Solar Energy*, 85 (2011) 46-56.
- [29] V.J.P. Vilar, J.M.S. Moreira, A. Fonseca, I. Saraiva, R.A.R. Boaventura, Application of Fenton and Solar Photo-Fenton Processes to the Treatment of a Sanitary Landfill Leachate in a Pilot Plant with CPCs, *Journal of Advanced Oxidation Technologies*, 15 (2012) 107-116.
- [30] V.J.P. Vilar, S.M.S. Capelo, T.F.C.V. Silva, R.A.R. Boaventura, Solar photo-Fenton as a pre-oxidation step for biological treatment of landfill leachate in a pilot plant with CPCs, *Catalysis Today*, 161 (2011) 228-234.
- [31] J.J. Pignatello, E. Oliveros, A. MacKay, Advanced oxidation processes for organic contaminant destruction based on the fenton reaction and related chemistry, *Critical Reviews in Environmental Science and Technology*, 36 (2006) 1-84.

- [32] S. Renou, J. Givaudan, S. Poulain, F. Dirassouyan, P. Moulin, Landfill leachate treatment: Review and opportunity, *Journal of Hazardous Materials*, 150 (2008) 468-493.
- [33] C. Sawyer, P. McCarty, G. Parkin, *Chemistry for Environmental Engineering and Science*, McGraw-Hill Education, 2003.
- [34] A.M. Amat, A. Arques, F. Galindo, M.A. Miranda, L. Santos-Juanes, R.F. Vercher, R. Vicente, Acridine yellow as solar photocatalyst for enhancing biodegradability and eliminating ferulic acid as model pollutant, *Applied Catalysis B: Environmental*, 73 (2007) 220-226.
- [35] A. Arques, A.M. Amat, A. García-Ripoll, R. Vicente, Detoxification and/or increase of the biodegradability of aqueous solutions of dimethoate by means of solar photocatalysis, *Journal of Hazardous Materials*, 146 (2007) 447-452.
- [36] J. Scott, D. Ollis, Integration of chemical and biological oxidation processes for water treatment: II. Recent illustrations and experiences, *Journal of Advanced Oxidation Technologies*, 2 (1997) 374-381.
- [37] V. Sarria, S. Parra, N. Adler, P. Peringer, N. Benitez, C. Pulgarin, Recent developments in the coupling of photoassisted and aerobic biological processes for the treatment of biorecalcitrant compounds, *Catalysis Today*, 76 (2002) 301-315.
- [38] H. Zhang, H.J. Choi, C.-P. Huang, Optimization of Fenton process for the treatment of landfill leachate, *Journal of Hazardous Materials*, 125 (2005) 166-174.
- [39] O. Primo, M.J. Rivero, I. Ortiz, Photo-Fenton process as an efficient alternative to the treatment of landfill leachates, *Journal of Hazardous Materials*, 153 (2008) 834-842.
- [40] Y. Wu, S. Zhou, F. Qin, H. Peng, Y. Lai, Y. Lin, Removal of humic substances from landfill leachate by Fenton oxidation and coagulation, *Process Safety and Environmental Protection*, 88 (2010) 276-284.
- [41] Humintech (2010), *Humic & Fulvic Acids: the Black Gold of Agriculture?*, in, New AG International, Available at <http://www.humintech.com/pdf/humicfulvicacids.pdf>, on 4th October 2011.
- [42] M. Mrkva, Evaluation of Correlations between Absorbance at 254 nm and COD of Rivers Waters, *Water Research*, 17 (1983) 231-235.
- [43] M. Gabriela Garcia, J. d'Hiriart, J. Giullitti, H. Lin, G. Custo, M.d.V. Hidalgo, M.I. Litter, M.A. Blesa, Solar light induced removal of arsenic from contaminated groundwater: the interplay of solar energy and chemical variables, *Solar Energy*, 77 (2004) 601-613.
- [44] C.T. Benatti, A.C.S. da Costa, C.R.G. Tavares, Characterization of solids originating from the Fenton's process, *Journal of Hazardous Materials*, 163 (2009) 1246-1253.
- [45] G.L. Truong, J.D. Laat, B. Legube, Effects of chloride and sulfate on the rate of oxidation of ferrous ion by H₂O₂, *Water Research*, 38 (2004) 2384-2394.
- [46] J. De Laat, T.G. Le, Effects of chloride ions on the iron (III)-catalyzed decomposition of hydrogen peroxide and on the efficiency of the Fenton-like oxidation process, *Applied Catalysis B: Environmental*, 66 (2006) 137-146.
- [47] J. De Laat, T.G. Le, Kinetics and modeling of the Fe (III)/H₂O₂ system in the presence of sulfate in acidic aqueous solutions, *Environmental Science & Technology*, 39 (2005) 1811-1818.

5 Integration of biological nitrification-denitrification, solar photo-Fenton and biological oxidation processes for raw leachate treatment, at pre-industrial scale

A multistage treatment system, at pre- industrial scale, was designed for the treatment of a mature raw landfill leachate, including: a) an activated sludge biological oxidation (ASBO), under aerobic and anoxic conditions; b) a solar photo-Fenton process to enhance the bio-treated leachate biodegradability, with and without sludge removal after acidification; and c) a final polishing step, with further ASBO.

The raw leachate was characterized by a high concentration of humic substances (HS) (1211 mg C_{HS}/L), representing 39% of the dissolved organic carbon (DOC) content, and a high nitrogen content, mainly in the form of ammonium nitrogen (>3.8 g NH_4^+-N/L).

In the first biological oxidation step, a 95% removal of total nitrogen and a 39% mineralization in terms of DOC reduction were achieved, remaining only the recalcitrant fraction, mainly attributed to HS (57% of DOC). Under aerobic conditions, the highest nitrification rate obtained was 8.2 mg $NH_4^+-N/h/g$ of volatile suspended solids (VSS), and under anoxic conditions, the maximum denitrification rate obtained was 5.8 mg ($NO_2^- - N + NO_3^- - N$)/(h.g VSS), with a C/N consumption ratio of 2.4 mg CH_3OH/mg ($NO_2^- - N + NO_3^- - N$).

The precipitation of humic acids (37% of HS) after acidification of the bio-treated leachate corresponds to 96% of the DOC abatement. The amount of UV energy and H_2O_2 consumption during the photo-Fenton reaction was 30% higher in the experiment without sludge removal and, consequently, the reaction rate was 30% lower. The phototreatment process led to the depletion of HS $>80\%$, of low-molecular-weight carboxylate anions $>70\%$ and other organic micropollutants, thus resulting in a total biodegradability increase of $>70\%$.

The second biological oxidation allowed to obtain a final treated leachate in compliance with legal discharge limits regarding water bodies (with the exception of sulphate ions), considering the experiment without sludge.

Finally, the high efficiency of the overall treatment process was further reinforced by the total removal percentages attained for the identified organic trace contaminants ($>90\%$).

This chapter is based on the research article “Silva, T.F.C.V., Silva, M.E.F., Cunha-Queda, A.C., Fonseca, A., Saraiva, I., Sousa, M.A., Gonçalves, C., Alpendurada, M.F, Boaventura, R.A.R, Vilar, V.J.P, *Multistage treatment system for raw leachate from sanitary landfill combining biological nitrification-denitrification/solar photo-Fenton/biological processes, at a scale close to industrial - Biodegradability enhancement and evolution profile of trace pollutants*, Water Research, 47 (2013) 6167-6186, DOI: 10.1016/j.watres.2013.07.036”.

5.1 Introduction

Although the disposal of solid wastes in sanitary landfills constitutes nowadays the most common method of waste management [1, 2], the generation of leachates is inevitable, mainly due to rainwater percolation through wastes and their decomposition products [3], leading to a complex mixture of high-strength organic and inorganic contaminants [4-6]. Different recalcitrant contaminants include personal care products (PCPs), pharmaceuticals, hormones, phthalates, humic and fulvic acids [7], PAHs [8, 9], PBDEs [10, 11], pesticides [5] and heavy metals [12, 13].

During the last years, publications regarding sanitary landfill leachates treatment rose continuously. The scientific community research interests have been focused on biological, membrane and advanced oxidation processes (AOPs) technologies for the treatment of leachates. Leachates are normally characterized by a high non-biodegradable organic fraction. In order to reach the necessary quality level of the final effluent fully reducing leachates' negative impact in the environment, in compliance with discharge regulations and at an affordable price, the best treatment system can be obtained using a combination of different technologies, including: i) aerobic and anaerobic biological processes; ii) chemical and physical methods (flotation, coagulation/flocculation, chemical precipitation, adsorption, ammonium stripping, chemical oxidation and ion exchange); iii) membrane filtration (microfiltration, ultrafiltration, nanofiltration and reverse osmosis); iv) AOPs (TiO_2/UV , $\text{H}_2\text{O}_2/\text{UV}$, Fenton ($\text{Fe}^{2+}/\text{H}_2\text{O}_2$), photo-Fenton ($\text{Fe}^{2+}/\text{H}_2\text{O}_2/\text{UV}$), electro-Fenton, electro-photo-Fenton, ozone (O_3 , O_3/UV , and $\text{O}_3/\text{H}_2\text{O}_2$), etc.) [14-16].

Rocha et al. [17] and Vilar et al. [18] applied different photochemical ($\text{H}_2\text{O}_2/\text{UV}$), heterogeneous (TiO_2/UV , $\text{TiO}_2/\text{H}_2\text{O}_2/\text{UV}$) and homogenous ($\text{Fe}^{2+}/\text{H}_2\text{O}_2/\text{UV}$) photocatalytic processes, including also the Fenton reaction ($\text{Fe}^{2+}/\text{H}_2\text{O}_2$), to the treatment of real leachates, after preliminary lagooning, from the same sanitary landfill where the pre-industrial plant used in this work was installed. The photo-Fenton reaction provided degradation rates 20 times higher than the heterogeneous photocatalytic processes. Different other results reported by Vilar et al. [19-21] showed that the solar photo-Fenton oxidation process is an effective technology to improve the biodegradability of mature landfill leachates, allowing to combine AOPs with biological oxidation systems, minimizing chemicals consumption and energy. Furthermore, in the Chapters 3 and 4, it was presented the first pre-industrial plant for leachates treatment from sanitary landfills. The treatment strategy consisted on a pre-oxidation of the leachate after lagooning, enhancing its biodegradability and allowing its further coupling with a biological oxidation system, under aerobic and anoxic conditions, to achieve complete nitrogen removal by nitrification and post-denitrification, using methanol as external carbon source. From June 2010 to May 2011, an

extensive physicochemical characterization of the leachate after lagooning showed its high recalcitrant character, mainly associated with the presence of humic substances (HS), which represented almost 59% of the organic carbon content. The acidification of the leachate after lagooning to a pH near 2.8 was a critical point in the photo-Fenton reaction. It was showed that, after acidification, the DOC abatement was approximately 27%, which corresponded to a reduction of HS of ca. 33%, indicating that the precipitation of the humic acids corresponded to approximately 72% of the DOC abatement. Different authors [22-24] reported high mineralization values regarding leachates treatment using Fenton and photo-Fenton processes, although a cautious result analysis must be performed, considering the evaluation of soluble and particulate organic matter content during the treatment. If humic acids precipitation occurs during the acidification process and if the oxidation treatment time is not long enough to degrade those complex molecules present in the particulate phase, after the final effluent neutralization step, those compounds may be redissolved and discharged into water resources.

This chapter presents a multistage treatment system for raw leachates from a sanitary landfill, at a pre-industrial scale, combining: an activated sludge oxidation process under aerobic and anoxic conditions, promoting nitrification and denitrification reactions in order to achieve a complete removal of nitrogen compounds and the biodegradable organic carbon fraction; followed by a solar photo-Fenton oxidation process (degradation of the most recalcitrant compounds and enhancement of the bio-treated raw leachate biodegradability, without the interference of nitrogen species); and finally an aerobic biological degradation process, for the complete removal of the remaining biodegradable organic compounds. Nitrification and denitrification biological reaction rates were evaluated, as well as alkalinity and methanol consumption, herein used as external carbon source for the denitrification reaction. The solar photo-oxidation efficiency was evaluated considering the sludge removal after acidification and the influence of HS and low-molecular-weight carboxylate anions (LMCA) concentrations in biodegradability enhancement, determined by the Zahn-Wellens test. Finally, some persistent organic micropollutants were identified and their evolution profiles followed-up along the multistage bio-photo-bio-treatment process.

5.2 Experimental methodology

All the chemicals used in this work, the detailed description of the experimental unit and respective procedures, as well as the employed analytical methods can be consulted in the Chapter 2.

5.3 Results and discussion

5.3.1 Leachate characterization

Table 5.1 presents the main characteristics of the raw leachate used in this work. The raw leachate was collected before the aerated lagoon, installed at the sanitary landfill, and it presents an intense dark-brown colour associated to the high concentration of humic substances (>1211 mg C_{HS}/L), which corresponds to 39% and 13% of DOC (2503 mg C/L) and COD (7426 mg O_2/L), respectively. It has also a high nitrogen concentration (4080 mg N/L), mainly in the form of ammonium (95%) and low values of BOD_5/COD (0.18), indicating a low biodegradability fraction. According to leachate classification proposed by Chian and DeWalle [25], as high pH values ($pH > 7.5$), COD values between 4000 and 10,000 mg O_2/L , BOD_5/COD in the range of 0.1-0.3, age higher than 10 years and humic substances concentration higher than 30% in terms of organic compounds, can be classified between intermediate and old leachate. In old mature leachates, the dominant organic fraction is refractory (non-biodegradable), since volatile fat acids are converted to biogas (CH_4 , CO_2) by the methanogenic microorganisms [25]. According to the leachates characteristics, the treatment strategy adopted in this work consists in a multistage treatment system with three sequential steps: preliminary biological treatment by activated sludge under aerobic and anoxic conditions promoting the removal of the biodegradable organic carbon fraction and nitrogen; a solar photo-Fenton process to oxidize the recalcitrant organic compounds into more biodegradable ones; being possible to couple with a second aerated activated sludge process, to achieve complete removal of residual biodegradable organic carbon and nitrogen.

5.3.2 1st Biological oxidation

Figure 5.1 shows the evolution of dissolved organic carbon and nitrogen content during the 1st biological oxidation process. Fast biodegradable organic carbon fraction was totally removed after 24 h, achieving 22% mineralization, with a kinetic constant of 19 mg $DOC/(h.g VSS)$. The slow biodegradable organic fraction was almost totally removed, according to the BOD_5 final value achieved, with a kinetic constant of 1.8 mg $DOC/(h.g VSS)$, leading to a final mineralization of 39%. The remaining organic carbon fraction can be considered recalcitrant, mainly attributed to humic substances, which represented 57% of DOC at the end of the 1st biological treatment. The slight decrease in humic substances concentration, approximately 11%, can be attributed mainly to adsorption in the activated sludge.

Table 5.1. Physico-chemical characterization of the landfill leachate at different treatment phases.

Parameters	RL ^a	LBT1 ^a	LAA ^a		LPF ^a		LPFN ^a		LBT2 ^a		ELV ^b
			With Sludge	Without Sludge	With Sludge	Without Sludge	With Sludge	Without Sludge	With Sludge	Without Sludge	
pH	8.1	8.4	2.9	2.9	3.0	3.1	7.0	7.4	8.0	7.9	6-9
T (°C)	26.4	25.2	26.5	24.1	32.5	30.2	32.5	23.4	22.6	21.3	
TSS (mg/L)	126	900	1500	93	800	358	132	11	126	45	60
VSS (mg/L)	94	690	1320	93	525	160	76	2	82	31	
DOC (mg C/L)	2503	1534	1200	1200	518	261	577	248	196	45	
TIC (mg C/L)	4119	1903	0	0	0	0	5.9	3.2	176	122	-
Alkalinity ^c (g CaCO ₃ /L)	17.1	8.0	0	0	0	0	0.025	0.013	0.73	0.51	-
Mineralization in each process ^d (%)	-	39	11	13	-	-	27	38	15	8	
Accumulated mineralization (%)	-	39	50	52	-	-	77	90	92	98	
COD (mg O ₂ /L)	7426	4864	4041	3720	1243	408	1305	436	467	117	150
BOD ₅ (mg O ₂ /L)	1325	200	-	-	-	-	-	-	14	12	40
BOD ₅ /COD	0.18	0.04	-	-	-	-	-	-	0.03	0.08	
Humic substances (mg C _{HS} /L)	977 (1211) ^e	872	550	550	50	26	92	30	91	30	
HS/DOC (%)	39	57	46	46	10	10	16	12	46	67	
HS/COD (%)	13	18	12	15	4	6	7	7	20	26	
Abs 254 nm (diluted 1:25)	-	1.466	1.160	1.030	0.082	0.086	0.111	0.106	-	-	
TDI (mg (Fe ²⁺ + Fe ³⁺)/L)	4.8	7.9	23.3 ^f	19.7 ^f	30.7	22.9	3.6	0.5	1.1	0.7	
Sulfate (mg SO ₄ ²⁻ /L)	42	6831	-	14522	-	13917	14233	14079	13931	13803	2000
Chloride (mg Cl ⁻ /L)	3549	3370	-	3122	-	3136	3209	3171	3192	3060	
Total Nitrogen (mg N/L)	4080	210	219	182	227	195	221	194	232	8,80	15
Ammoniacal nitrogen (mg NH ₄ ⁺ -N/L)	3864	23	-	34	-	67	64	53	125	<1	8
Nitrate (mg NO ₃ ⁻ -N/L)	<1	<1	-	<1	-	<1	<1	<1	<1	<1	11
Nitrite (mg NO ₂ ⁻ -N/L)	139	<1	-	<1	-	<1	3	<1	2	2	
Total Phosphorous (mg P/L)	35	25	-	-	-	-	8	<1	4	<1	10

^aRL – Raw Leachate; LBT1 – Leachate after 1st biological treatment; LAA – Leachate after acidification; LPF – Leachate after Photo-Fenton reaction; LPFN - Leachate after Photo-Fenton reaction and neutralization; LBT2 – Leachate after 2nd biological treatment; ^bELV – Emission Limit Values; ^cAlkalinity values considering that at pH less than 8.3 the inorganic carbon is almost in the form of bicarbonates [26]; ^dMineralization in each treatment stage relatively to the initial DOC (2503 mg/L); ^eHumic substances concentration in the raw leachate was 1211 mg C_{HS}/L. The mixture of the raw leachate with the activated sludge resulted in 977 mg C_{HS}/L; ^fHigh values due to contamination in reactor.

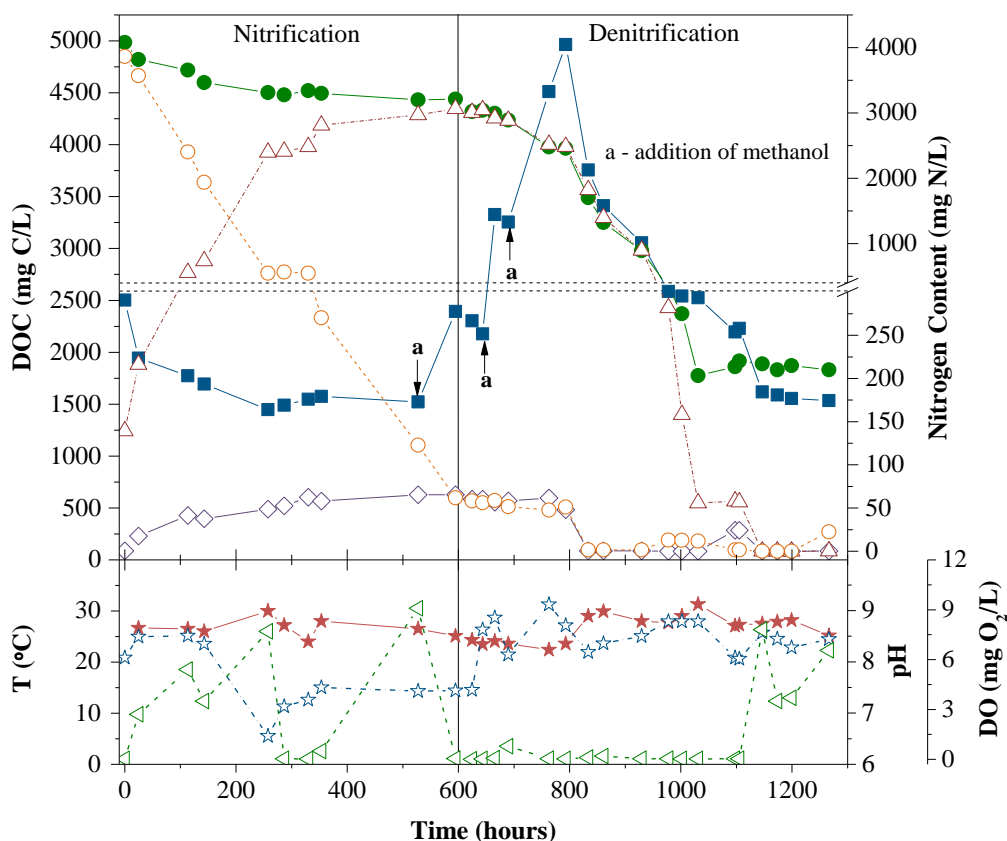


Figure 5.1. Biological nitrification/denitrification of the raw leachate. ■ - DOC; ● - Total Dissolved Nitrogen; ○ - Ammonium (NH₄⁺-N); ◇ - Nitrate (NO₃⁻-N); △ - Nitrite (NO₂⁻-N); ★ - Temperature (T); ☆ - pH; ◁ - Dissolved Oxygen (DO).

The SVI obtained during 1st biological treatment was 96 mL/g, indicating a good sludge settleability, normally below 100 mL/g [27]. Regarding the food to microorganism (biomass) ratio (F/M), it was achieved an acceptable value of 0.08 g substrate/g biomass/day, since typical values for the BOD F/M ratio reported in literature vary from 0.04 g/g/day, for extended aeration processes, to 1.0 g/g/day, for high rate processes [27].

Biological nitrogen removal requires a two-step process: aerobic nitrification of ammonia to nitrite (Eq. (2.1)) and then nitrite is converted to nitrate (Eq. (5.2)); anoxic denitrification of nitrate/nitrite to nitrogen gas (Eq. (5.3)).

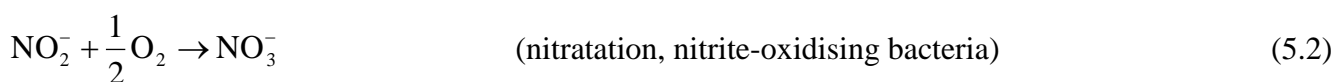
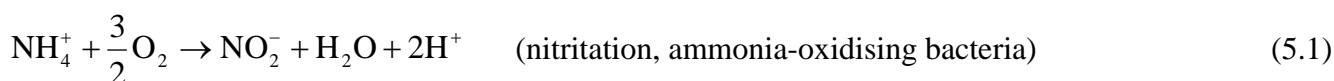
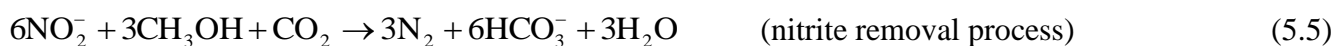
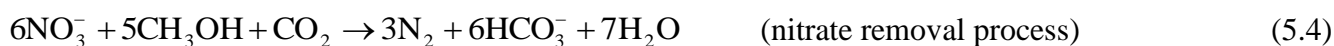


Figure 5.1 shows that under aerobic conditions, it was accumulated more than 96% of the loaded ammonium nitrogen as nitrite, with 98% ammonium conversion, achieving final values of 3 g NO_2^- -N/L and 60 mg NO_2^- -N/L. pH was maintained between 7.5 and 8.5 through the addition of NaOH, as reported by Alleman [28] which showed that the optimal pH values are between 7.9 and 8.2 for nitrification.

Nitrification reaction stopped between 287 and 353 hours due to a problem in the base dosing pump, achieving a pH value of 6.6 and also a problem with the compressor, resulting in very low dissolved oxygen concentration values (<0.1 mg O_2 /L). The highest nitrification rate obtained was 8.2 mg NH_4^+ -N/(h.g VSS) ($T = 26.9$ °C) consuming 4.5 g CaCO_3 per liter (Table 5.2) of raw leachate or 1.2 mg CaCO_3 per mg NH_4^+ -N, which is 6 times lower than the stoichiometric ratio, 7.14 mg CaCO_3 per mg NH_4^+ -N, (Eq. (2.1)). Raw leachate presents initially an inorganic carbon concentration of 4119 mg C/L, which corresponds to 20.9 g HCO_3^- /L or 17.1 g CaCO_3 /L, considering that at pH = 8.0, inorganic carbon is almost in the form of bicarbonates [26]. Until 143 h of nitrification, 2205 mg/L (11.2 g HCO_3^- /L or 9.2 g CaCO_3 /L) of inorganic carbon was consumed, and 1927 mg NH_4^+ -N/L was oxidized, leading to an alkalinity consumption of 4.8 mg CaCO_3 per mg NH_4^+ -N. At 115 h, pH was 6.6, inorganic carbon concentration was negligible, and consequently, nitrification stopped.

Spagni and Marsili-Libelli [29] reported nitrification rates between 4.9 and 12.6 mg N/(h.g VSS) ($T = 20$ °C) for a leachate with 1199 mg NH_4^+ -N/L (COD = 2055 mg O_2 /L), achieving nitrification and COD removal efficiencies in average of 98% and 20%, respectively. Ruiz et al. [30] showed that setting DO concentration at 0.7 mg/L, it was possible to accumulate more than 65% of the loaded ammonia nitrogen as nitrite with 98% ammonia conversion (initial ammonia concentration of 610 NH_4^+ -N/L). Below 0.5 mg/L of DO, ammonia was accumulated and over a DO of 1.7 mg/L complete nitrification to nitrate was achieved. In our case, despite DO concentration was in average 3.2 mg/L, the nitrification process (nitrite oxidation to nitrate) was almost negligible. This can be attributed to the high pH values, possible free ammonia in the reactor, which favoured the ammonia oxidizing bacteria and inhibited the nitrite-oxidizing organisms, as reported by Canziani et al. [31], Villaverde et al. [32] and Suthersan and Ganczarcczyk [33].

Complete nitrification requires 2 mol of oxygen per mol of ammonia to be nitrified (Eqs. (2.1) and (5.2)). If denitrification is to be considered after a nitrification process, partial nitrification to nitrite implies 25% less oxygen demand compared to complete nitrification, and this shortcut of the nitrate would mean a reduction in the total carbon source required for denitrification, because carbon is needed for conversion of nitrate to nitrite, which can yield up to 40% savings in methanol consumption (Eqs. (5.4) and (5.5)).



After 25 days, oxygen supply was turned off, methanol was added as external carbon source for the denitrification process and pH was controlled between 8.0 and 9.0, through the addition of H₂SO₄. After a preliminary denitrification lag phase period of 4 days, characterized by a low denitrification rate of 1.3 mg (NO₂⁻-N + NO₃⁻-N)/(h.g VSS), attributed to the denitrifying bacteria adaptation to the high nitrite concentration, maximum denitrification rate of 5.8 mg (NO₂⁻-N + NO₃⁻-N)/(h.g VSS) was observed, with a C/N consumption ratio of 2.4 mg CH₃OH/mg (NO₂⁻-N + NO₃⁻-N) (7.4 g/9.4 mL of commercial methanol per liter of leachate).

Table 5.2. Process variables as performance indicators.

1 st Biological Treatment			Photo-Fenton (PF)		
	Parameter		Parameter	With Sludge	Without Sludge
	VSS (mg/L)	1581	pH _m	2.8	2.9
	TSS (mg/L)	2257	T _m (°C)	40.5	35.2
	SVI (mg/L)	96	Fe _m	37.6	33.0
	<i>k</i> _{0-25h} ^a (mg DOC/(h.g VSS))	19	t _{PF} (h)	25.1	38.0
	<i>k</i> _{25-258h} ^b (mg DOC/(h.g VSS))	1.8	I _{UV} (W/m ²)	26.1	22.6
Nitrification	pH _{n,m}	7.6	Q _{UV} (kJ/L)	54.5	80.4
	T _{n,m}	26.9	[H ₂ SO ₄] (mM)	104	104
	DO _m (mg/L)	3.2	[H ₂ O ₂]cons. (mM)	250	265
	t _{BT,n} (h)	600	H ₂ O ₂ /DOC _{ox} ^f (mg H ₂ O ₂ /mg DOC _{ox})	13.6	9.5
	<i>k</i> _n (mg NH ₄ ⁺ -N/(h.g SSV))	8.2	<i>k</i> _l ^c (L/kJ)	0.020±0.006	0.016±0.001
	[NaOH] (mM)/CaCO ₃ (g/L)	90/4.5	<i>r</i> ₀ ^d (mg/kJ)	20±6	12±1
	pH _{d,m}	8.4	<i>k</i> _{H₂O₂} ^e (mmol/kJ)	4.6±1.1	3.2±0.2
Denitrification	T _{d,m}	26.4	T _{fm} ^f (g C/h/m ²)	1.72	1.01
	t _{BT,d} (h)	430	T _{fv} ^g (L/h/m ²)	1.18	0.95
	<i>k</i> _d (mg (NO ₃ ⁻ -N + NO ₂ ⁻ -N)/(h.g SSV))	5.8			
	C/N (mg CH ₃ OH/mg (NO ₃ ⁻ -N + NO ₂ ⁻ -N))	2.4			
	[CH ₃ OH] (mM)	231			
	[H ₂ SO ₄] (mM)/CaCO ₃ (g/L)	53/5.3			

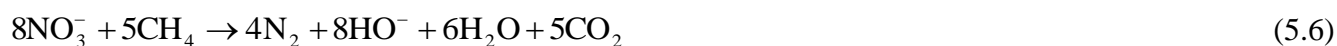
^aDOC removal rate between 0 and 25 hours; ^bDOC removal rate between 25 and 258 hours; ^cPseudo-first-order kinetic constant for DOC degradation (Q_{UV}>10 kJ_{UV}/L); ^dInitial DOC reaction rate (Q_{UV}>10 kJ_{UV}/L); ^eH₂O₂ consumption rate (Q_{UV}>10 kJ_{UV}/L); ^fMass treatment factor ((DOC_i - DOC_f) × V_t/(t_{PF} × A_r)); ^gVolume treatment factor (V_t/(t_{PF} × A_r)).

Between 750 and 850 h, an increase of pH until 9.3 (due to a problem in the dosing pump), resulted in a complete conversion of ammonia from the ionic form, NH₄⁺, to the molecular form, NH₃, and combined with the release of high amounts of nitrogen gas due to denitrification reaction, lead to NH₃ stripping, and flotation of activated sludge.

During denitrification it was produced 5.3 g of alkalinity, as CaCO_3 , per liter of leachate, according to the acid addition, which is equivalent to 1.7 g CaCO_3 per g of $(\text{NO}_2^- \text{-N} + \text{NO}_3^- \text{-N})$ reduced. According to Eqs. (5.4) and (5.5), during denitrification it is produced 3.57 g (as CaCO_3) of alkalinity per g of $\text{NO}_2^- \text{-N}$ or $\text{NO}_3^- \text{-N}$ reduced, which is 2 times higher than the obtained value. Moreover, during denitrification the inorganic carbon concentration increased from 0 to 1.9 g C/L, corresponding to 9.7 g $\text{HCO}_3^- \text{/L}$ or 8.0 g $\text{CaCO}_3 \text{/L}$, equivalent to 2.6 g $\text{CaCO}_3 \text{/g}$ $(\text{NO}_2^- \text{-N} + \text{NO}_3^- \text{-N})$ reduced. So, the overall alkalinity produced was 4.3 g $\text{CaCO}_3 \text{/g}$ $(\text{NO}_2^- \text{-N} + \text{NO}_3^- \text{-N})$ reduced, which is very near to stoichiometric reaction.

Different methanol demands, as external carbon source, for denitrification process of landfill leachates have been reported: 2.43 g $\text{CH}_3\text{OH/g}$ $\text{NO}_3^- \text{-N}$ (3.6 g COD/g $\text{NO}_3^- \text{-N}$) [34], 2.8-3.0 g $\text{CH}_3\text{OH/g}$ $\text{NO}_3^- \text{-N}$ (4.5-4.1 g COD/g $\text{NO}_3^- \text{-N}$) [35], which is more than 1.3 times higher than the stoichiometric mass ratio between consumed methanol and nitrate (1.90 g $\text{CH}_3\text{OH/g}$ $\text{NO}_3^- \text{-N}$). However, when nitrite is the predominant specie in solution, methanol consumption during denitrification is approximately 40% less (1.15 g $\text{CH}_3\text{OH/g}$ $\text{NO}_2^- \text{-N}$). Comparing with the values obtained in our study, methanol consumption was more than two times higher when compared with the stoichiometric mass ratio.

Modin et al. [36] studied the denitrification using methane as external carbon source, showing a C/N ratio of 7.1 g $\text{CH}_4 \text{-C/g}$ $\text{NO}_3^- \text{-N}$, approximately 13 times higher than the stoichiometric mass ratio, according to Eq. (5.6) [37].



Considering a continuous biological treatment system, with a flow rate of 100 m³/day, it would be necessary an anoxic lagoon (560 m³) followed by an aerobic lagoon (500 m³), with a retention time of 5.6 days and 5.0 days, respectively, to achieve complete denitrification of 3.1 kg $\text{NO}_2^- \text{-N/m}^3$ and nitrification of 3.9 kg $\text{NH}_4^+ \text{-N/m}^3$, considering an average VSS of 4 g/L. In order to minimize the consumption of methanol and alkalinity, the treatment sequence can be anoxic followed by an aerobic reactor, with recirculation to the anoxic reactor: (i) to take advantage of the biodegradable organic fraction of the raw leachate, which corresponds to 54% of the organic carbon necessary for denitrification, being necessary only 3.4 kg $\text{CH}_3\text{OH/m}^3$, (ii) to take advantage of the raw leachate alkalinity (17.1 kg $\text{CaCO}_3 \text{/m}^3$), and the alkalinity produced during denitrification (13.3 kg $\text{CaCO}_3 \text{/m}^3$), which is sufficient to achieve complete nitrification of 4 kg $\text{NH}_4^+ \text{-N/m}^3$ (19.2 kg $\text{CaCO}_3 \text{/m}^3$).

5.3.3 Solar photo-Fenton Oxidation

After almost complete removal of nitrogen and biodegradable organic carbon fraction, and further clarification of the wastewater, the bio-treated leachate was pumped to the recirculation tank of the photoreactor system, and it was acidified until pH 3.0, through the addition of sulphuric acid ($3.0 \text{ L H}_2\text{SO}_4/\text{m}^3$). The bio-treated leachate presented 8.0 g alkalinity in terms of CaCO_3 (considering that at pH 8.4, alkalinity is mainly due to bicarbonates), and the amount of sulphuric acid needed to neutralize alkalinity corresponds to 77% of the total acid used during acidification. However, considering that in a full scale plant, the alkalinity of raw leachate and that produced during denitrification, can be used for nitrification, achieving a final bio-treated leachate with a very low alkalinity, which will reduce substantially the amount of sulphuric acid necessary to perform acidification, decreasing sulphate ion concentration, resulting in a substantially increase of photo-Fenton reaction efficiency due to an higher fraction of more photoactive ferric water complexes than ferric sulphate complexes.

After acidification, it was observed an increase of 67% and 91% in the TSS and VSS, respectively, correlated with humic acids precipitation, leading to humic substances and DOC concentration abatement of 37% and 22%, respectively. This indicates that precipitation of the humic acids (37% of the humic substances), corresponds to approximately 96% of DOC abatement. In Chapter 3, it was performed an HS analysis to the acid sludge resulted from the acidification step, and results revealed a concentration of 130 mg C_{HS} per gram of dry sludge, which corresponded to production of 2.7 kg of HS sludge per cubic meter of leachate. Considering the same concentration of HS in the sludge, 2.5 kg of HS sludge per cubic meter of leachate were produced according to results observed in this work.

In order to assess the influence of sludge produced after acidification in the photo-Fenton reaction, it was performed two experiments, with and without sludge removal. The photo-Fenton reactions were conducted at an initial pH of 2.8, achieved after the addition of iron and the first dose of H_2O_2 (500 mg/L), and with an initial iron concentration of 80 mg Fe^{2+}/L , reported in a previous work [21], as the optimum iron concentration for this kind of leachate and photoreactor. This pH value was selected for the photo-Fenton reaction because it avoids iron precipitation [38]. During the reaction, H_2O_2 was supplied in multiple small additions, maintaining the H_2O_2 concentration between 100 and 500 mg $\text{H}_2\text{O}_2/\text{L}$, which has been reported to improve the oxidation rate, avoiding that hydrogen peroxide can be rate-limiting if applied in concentrations that are too low and, minimizing the consumption of H_2O_2 per amount of COD oxidized, considering that high concentration of hydrogen peroxide can compete with contaminants for the hydroxyl radicals generated and also self-decompose into oxygen and water [39, 40].

Observing the overall photo-Fenton process (see Table 5.1, Table 5.2 and Figure 5.2), for the experiment without sludge removal, it was consumed 54.5 kJ/L of accumulated UV energy and 250 mM of H_2O_2 , corresponding to a mineralization of 52% and a specific consumption of 13.6 mg of H_2O_2 per mg of oxidized DOC. While for the experiment with sludge removal it was consumed a little more amount of accumulated UV energy and H_2O_2 , equivalent to 80.4 kJ/L and 265 mM, respectively. However, the mineralization value was higher, 79%, and the consumed H_2O_2 concentration per unit of DOC was lesser, corresponding to 9.5 mg of H_2O_2 per mg of oxidized DOC. The mass and volumetric treatment factors (T_{fm} and T_{fv}), defined as the amount of organics substances or volume of contaminated water, respectively, that the system is able to treat per unit of time and surface of solar collectors [41], were 0.95 g C/h/m² and 1.01 L/h/m² for the experiment without acid sludge removal, and 1.18 g C/h/m² and 1.72 L/h/m² for the experiment with acid sludge removal.

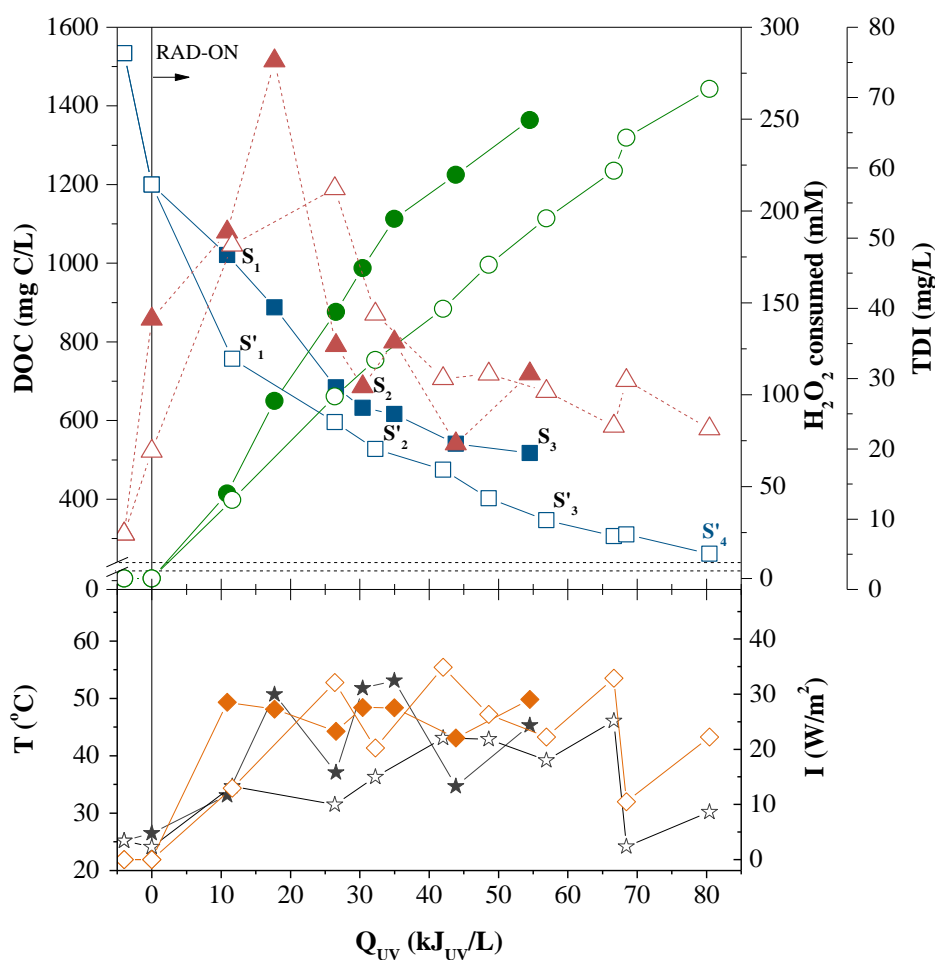


Figure 5.2. DOC (\square , \blacksquare), H_2O_2 consumption (\circ , \bullet), total dissolved iron (TDI) concentration (\triangle , \blacktriangle), temperature (T - \star , \blackstar) and average radiation intensity (I - \diamond , \blacklozenge) evolution as a function of the accumulated UV energy per liter of leachate during the photo-Fenton process (pH = 2.8; $[Fe^{2+}] = 80$ mg/L), with (open symbols) and without (solid symbols) sludge removal.

Figure 5.2 shows that for the same H_2O_2 dose (220 mM), at similar average reaction temperature and average solar UV power, the mineralization efficiency was 80% and 65% for the experiments with and without sludge removal, considering the dissolved organic carbon. The amount of UV energy and H_2O_2 consumed is 30% higher for the experiment without sludge removal, and consequently, reaction velocity is 30% smaller (see Table 5.2). The presence of suspended solids decreases light penetration, competing as photons absorbers with H_2O_2 and iron species, being necessary a higher reaction time and consequently a higher energy consumption, and also will increase energy and H_2O_2 consumption to achieve the same mineralization of dissolved organic matter, related to the degradation of particulate organic matter, as it can be seen by the reduction of more than 50% in TSS and VSS (Table 5.1).

After photo-bio-treated leachate neutralization, consuming 1.0 kg CaCO_3 of alkalinity per cubic meter of leachate, the concentration of humic substances remained approximately constant for experiment without sludge, and increased approximately 184% for experiment without sludge removal. This indicates dissolution of humic acids present in the particulate phase, which were not totally destroyed during the photo-oxidation, and consequently will be discharged to the receiving water bodies, without treatment, as there are recalcitrant to biological oxidation.

Complete nitrogen removal was not achieved during the first biological treatment, mainly due to organic nitrogen. During the photo-Fenton oxidation it can be observed the oxidation of the organic nitrogen to ammonium nitrogen, which increased from 22.5 to 67.3 mg $\text{NH}_4^+\text{-N/L}$ (Figure 5.3). However, total nitrogen remained approximately constant during the phototreatment.

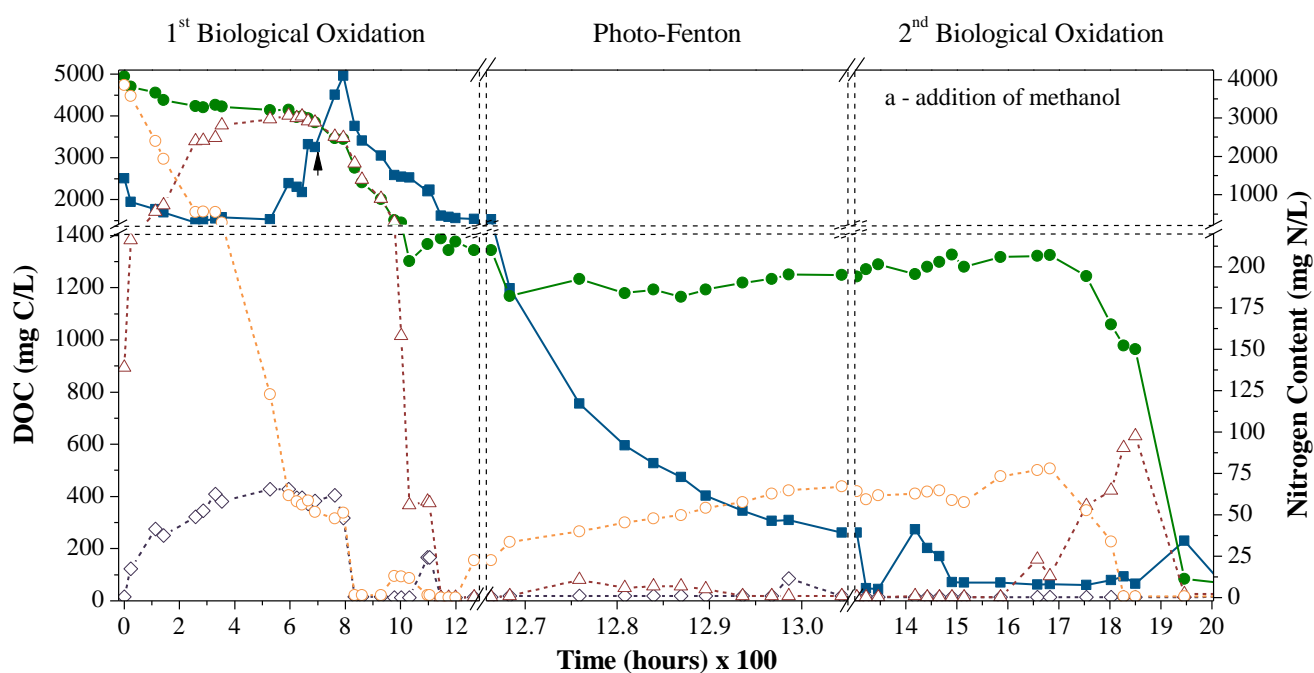


Figure 5.3. Biological/photo-Fenton/Biological treatment sequence of the raw leachate. ■ - DOC; ● - Total Dissolved Nitrogen; ○ - Ammonium ($\text{NH}_4^+\text{-N}$); ◇ - Nitrate ($\text{NO}_3^-\text{-N}$); △ - Nitrite ($\text{NO}_2^-\text{-N}$).

With the purpose to assess the leachate's biodegradability variation in the course of the treatment process, a Zahn-Wellens test was performed on samples collected at different treatment stages, for both the experiments analysed so far - with and without sludge removal (Figure 5.4 and Figure 5.5). First samples were collected before and after the 1st biological oxidation process (raw leachate - RL and LBT1, respectively), as well as after the acidification point (LAA). These samples were coincident for both experiments. The remaining samples were taken during the photo-Fenton reaction, after certain doses of H₂O₂ and UV energy (see Figure 5.5), for the experiments executed without (S₁, S₂ and S₃) and with (S'₁, S'₂, S'₃ and S'₄) removal of the acidic sludge produced during the acidification step.

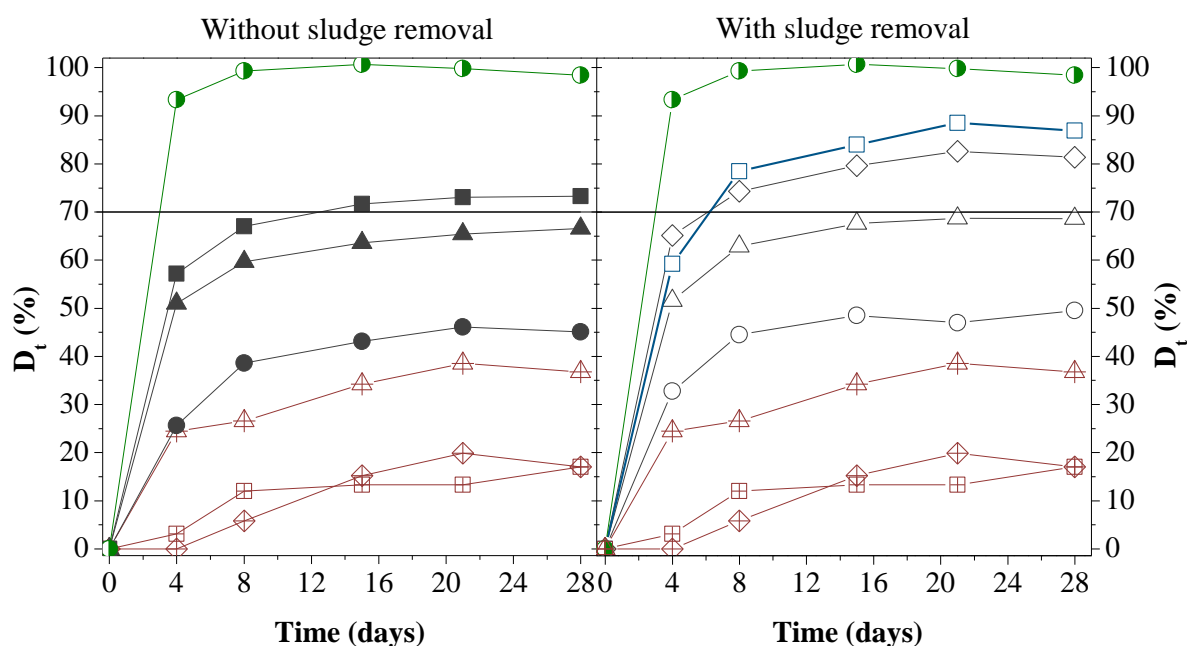


Figure 5.4. Zahn-Wellens test for samples collected before and after the 1st biological treatment and after acidification (cross symbols), and for some samples taken during the photo-Fenton process without (solid symbols) and with (open symbols) sludge removal after acidification: \triangle - Raw Leachate; \boxplus - LBT1; \diamond - LAA; \bullet - S₁; \blacktriangle - S₂; \blacksquare - S₃; \circ - S'₁; \triangle - S'₂; \diamond - S'₃; \square - S'₄; \bullet - Reference.

According to the Zahn-Wellens test, the raw leachate presented a biodegradability percentage of 27% and 37%, after 8 and 28 days, respectively, which is in agreement with the mineralization results obtained in the 1st biological treatment, easily (22%) and slowly (39%) biodegradable organic fraction. Furthermore, COD and DOC values obtained at the end of the 1st biological oxidation were rather close to those achieved by the Zahn-Wellens test. Regarding samples collected before and after acidification, these presented a poor biodegradability percentage (17%), contrary to what happened during the photo-Fenton reaction. Herein, as could be expected [42, 43], it is observed a biodegradability enhancement; concomitantly with a decrease of HS concentration (95% and 83%, for experiments without and with sludge, respectively).

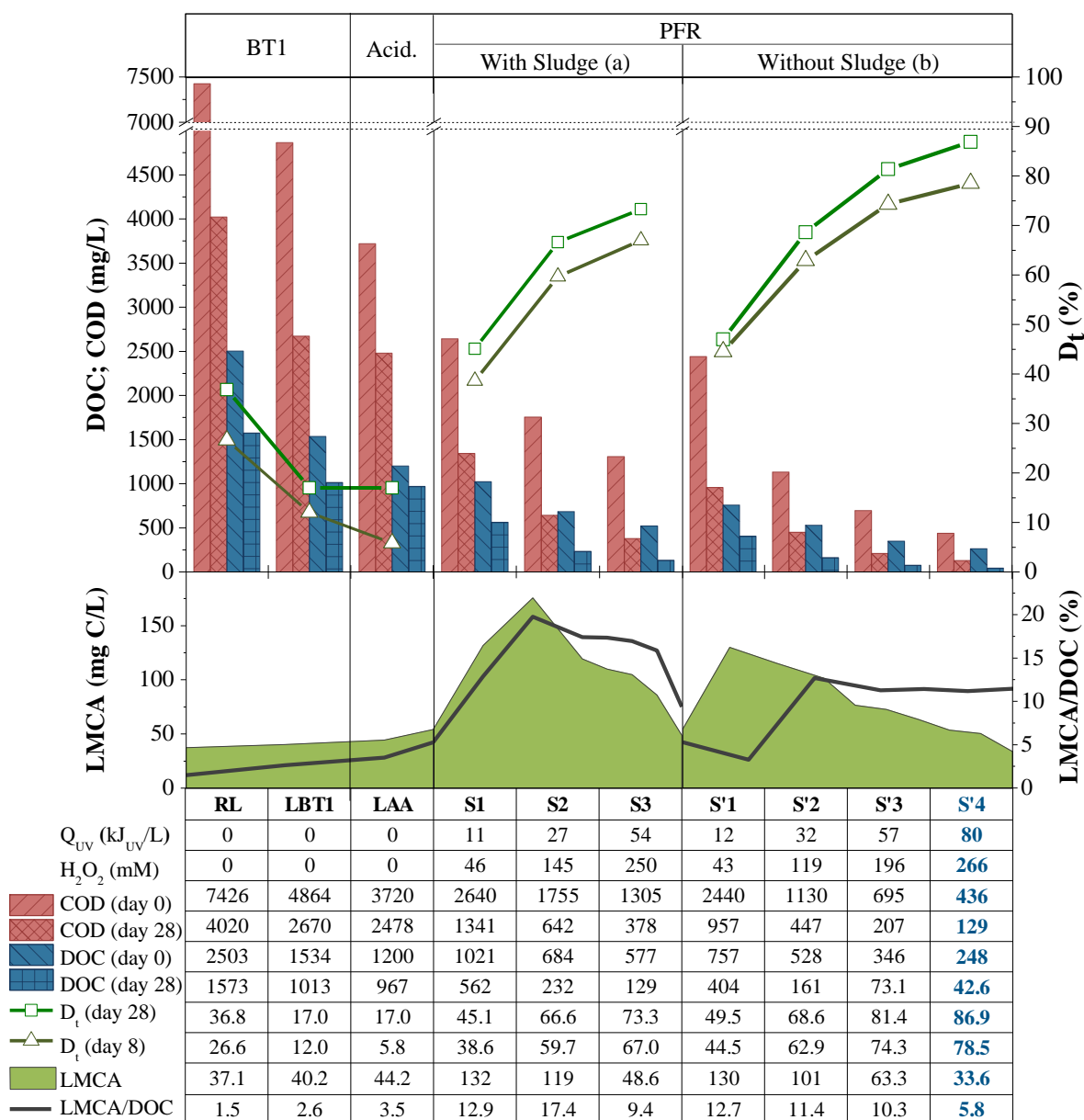


Figure 5.5. Evaluation of DOC and COD during the Zahn-Wellens test at day 0 and day 28; percentage of biodegradation (D_t) during Zahn-Wellens test at day 8 and day 28; low-molecular-weight carboxylate anions (LMCA) and LMCA/DOC ratio, during combined system 1st biological treatment (BT1)/photo-Fenton reaction (PFR), without (a) and with (b) sludge removal after acidification (Acid.).

The achieved D_t values were higher than 70%, after only 8 and 15 days, corresponding to a H₂O₂ consumption of 196-266 and 250 mM, for experiments with and without sludge removal, respectively. After a quick analysis of Figure 5.4, the treatment stage corresponding to sample S₃ could look like a good endpoint for the pre-oxidation process in the experiment without sludge, given that biodegradability was already higher than 70%. However, if the final purpose of the treatment is the discharge of the treated leachate into water bodies, it would certainly be a better choice to stop the photoreaction in a point close to sample S₄, since then the DOC content is low enough to achieve a

COD below 150 mg O₂/L (see Figure 5.5) after biological oxidation. These results are in agreement with others obtained in the Chapter 4, where it was demonstrated that for DOC values lower than 300 mg/L at the end of the phototreatment, it is possible to achieve COD values below 150 mg O₂/L (discharge limit in water bodies) in a subsequent biological treatment.

As aforementioned, Figure 5.5 presents the Zahn-Wellens results, at day 0 and day 28, for some samples collected in specific treatment points. Furthermore, this figure also displays the concentration evolution profile of LMCA during the whole photo-Fenton reaction, as well as LMCA/DOC ratio. As predicted, the concentration of total LMCA showed an initial increase followed by a strong decrease, suggesting there was first the breakdown of recalcitrant macromolecules into short-chain carboxylic acids, followed by their degradation [44]. Figure 5.5 shows maximum LMCA concentration values between 175 and 130 mg C/L (formate > oxalate > phthalate > malonate > acetate > pyruvate > valerate > citrate), corresponding to 13-20% of DOC and a biodegradability percentage higher than 50%, for H₂O₂ doses between 43 and 145 mM.

5.3.4 2nd Biological oxidation

The neutralized photo-bio-treated leachate suffered a final biological oxidation, resulting in a complete elimination of biodegradable organic carbon fraction (82%) and nitrogen content (95%), regarding the experiment without acid sludge (Figure 5.3). In order to perform the last nitrification it was necessary again a long period, mainly attributed to the loss of biomass in the first denitrification step, associated to the foam produced in result of the nitrogen gas release.

Table 5.1 presents the characteristics of the bio-photo-bio-treated leachate resulted from the two experiments with and without sludge removal. Humic substances concentration didn't suffer any modification during the 2nd biological treatment, representing 46% and 67% of the final DOC, respectively for the experiments without and with sludge removal after acidification. In both experiments, the biological reactor operated with values of SVI close to 100 mL/g and BOD F/M ratio equivalent to 0.2 g/g/day, and it was achieved values of COD below 500 mg O₂/L (DOC < 196 mg C/L). However, to obey the more stringent regulations related to effluent discharge into receiving water bodies, COD < 150 mg O₂/L, only the experiment performed with sludge removal after acidification reached those requirements, with the exception of sulphate, whose concentration greatly exceeded the discharge limits.

The COD and DOC values obtained after the 2nd biological treatment, for samples S₃ and S'₄ (experiments without and with acid sludge removal, respectively), are in accordance with the results of the Zahn-Wellens test (Figure 5.5).

5.3.5 Organic trace contaminants identification and evolution profile

Using the analytical GC-MS methods described in Chapter 2 (section 2.6), an initial target screening analysis was conducted on the raw leachate, as well as on other samples collected in key points of the treatment process, in order to identify and assess the evolution profile of potential trace organic contaminants. Standard solutions were used as reference for the identification and quantification of several VOCs, pesticides, phenols, phthalates, PAHs and PCBs, commonly present in sanitary landfill leachates. However, within the 84 target compounds, only 13 were actually identified and quantified, among which 3 VOCs (benzene, 1,2-dichloroethane and 1,2-dichloropropane), 4 phenols (2-nitrophenol, 2,4-dimethylphenol, 4-chloro-3-methylphenol and p-tert-octylphenol) and 6 PAHs (naphthalene, fluorene, phenanthrene, fluoranthene, pyrene and dibenzo[a,h]anthracene) (Table 5.3). Therefore, a non-target screening analysis followed, aiming at the identification of other distinct chromatographic peaks, obtained through the four analytical methods.

Figure 5.6 presents the GC-MS total ion chromatograms obtained for raw leachate samples (RL), leachate after the 1st biological treatment (LBT1), leachate after the photo-Fenton reaction and subsequent neutralization (LPFN) and the final effluent obtained after the 2nd biological treatment (LBT2). In this way, it was possible to evaluate the individual contribution of each biological treatment (1st biotreatment: RL-LBT1; 2nd biotreatment: LPFN-LBT2) and photo-Fenton process (phototreatment: LBT1-LPFN), for the removal and/or formation of each identified contaminant. Table 5.4 displays the correspondence between each peak identified by spectrum comparison against reference spectra from NIST library and the respective compound characteristics. Simply by visual inspection, it is easily inferred the high efficiency of the overall treatment process, comparing the RL and BLBT2 chromatograms (Figure 5.6), as well as by the >90% total removal efficiencies calculated for the identified contaminants, presented in Table 5.4.

Furthermore, the obtained results showed that many of the identified contaminants were originally relatively biodegradable, being significantly removed (>80%) after the first biotreatment process. However, the photo-Fenton reaction also played an important role for the leachate biodegradability increase (>70%), as stated by the >50% removal of several recalcitrant compounds (Table 5.4). One exception was spotted for compound corresponding to peak 1, identified as ethanol, 1-methoxy, acetate, which was produced in large amounts during the phototreatment stage (-975%), probably as a result of the degradation of other more complex aromatic compounds, as previously reported in literature. The 2nd biotreatment process efficiency was already quite low, which is in agreement with its aforementioned contribution to the elimination of the residual biodegradable organic carbon fraction.

Table 5.3. Contaminants' concentrations ($\mu\text{g/L}$) along the leachate treatment process.

	Contaminants	RL*	LBT1*	LAA*	LPF*	LPFN*	LBT2*
Pesticides	Hexachlorobutadiene	<0.01	<0.01	<0.01	<0.01	<0.01	<0.01
	Dichlobenil	<0.01	<0.01	<0.01	<0.01	<0.01	<0.01
	EPTC ^b	<0.01	<0.01	<0.01	<0.01	<0.01	<0.01
	Pentachlorobenzene	<0.01	<0.01	<0.01	<0.01	<0.01	<0.01
	Molinate	<0.01	<0.01	<0.01	<0.01	<0.01	<0.01
	Trifluralin	<0.005	<0.005	<0.005	<0.005	<0.005	<0.005
	α -HCH ^c	<0.01	<0.01	<0.01	<0.01	<0.01	<0.01
	Hexachlorobenzene	<0.01	<0.01	<0.01	<0.01	<0.01	<0.01
	β -HCH ^c	<0.01	<0.01	<0.01	<0.01	<0.01	<0.01
	γ -HCH ^c	<0.01	<0.01	<0.01	<0.01	<0.01	<0.01
	Diazinon	<0.01	<0.01	<0.01	<0.01	<0.01	<0.01
	Fonofos	<0.01	<0.01	<0.01	<0.01	<0.01	<0.01
	Chlorothalonil	<0.01	<0.01	<0.01	<0.01	<0.01	<0.01
	δ -HCH ^c	<0.01	<0.01	<0.01	<0.01	<0.01	<0.01
	Alachlor	<0.01	<0.01	<0.01	<0.01	<0.01	<0.01
	Heptachlor	<0.01	<0.01	<0.01	<0.01	<0.01	<0.01
	S-Metolachlor	<0.01	<0.01	<0.01	<0.01	<0.01	<0.01
	Aldrin	<0.01	<0.01	<0.01	<0.01	<0.01	<0.01
	Dichlofluanid	<0.01	<0.01	<0.01	<0.01	<0.01	<0.01
	Pendimethalin	<0.01	<0.01	<0.01	<0.01	<0.01	<0.01
	Quinalphos	<0.01	<0.01	<0.01	<0.01	<0.01	<0.01
	2,4-DDE ^d	<0.005	<0.005	<0.005	<0.005	<0.005	<0.005
	Endosulfan I	<0.01	<0.01	<0.01	<0.01	<0.01	<0.01
	4,4'-DDE ^d	<0.005	<0.005	<0.005	<0.005	<0.005	<0.005
	2,4-DDD ^e	<0.005	<0.005	<0.005	<0.005	<0.005	<0.005
	Endrin	<0.01	<0.01	<0.01	<0.01	<0.01	<0.01
	Endosulfan II	<0.01	<0.01	<0.01	<0.01	<0.01	<0.01
	4,4'-DDD ^e	<0.005	<0.005	<0.005	<0.005	<0.005	<0.005
	2,4-DDT ^f	<0.01	<0.01	<0.01	<0.01	<0.01	<0.01
	Endosulfan sulfate	<0.01	<0.01	<0.01	<0.01	<0.01	<0.01
	4,4'-DDT ^f	<0.01	<0.01	<0.01	<0.01	<0.01	<0.01
	o,p-methoxychlor	<0.01	<0.01	<0.01	<0.01	<0.01	<0.01
	p,p-methoxychlor	<0.01	<0.01	<0.01	<0.01	<0.01	<0.01
VOCs	Dichloromethane	<0.67 ^a	<0.67	<0.67	<0.67	<0.67	<0.67
	1,2-(E)-Dichloroethylene	<0.71	<0.71	<0.71	<0.71	<0.71	<0.71
	1,1-Dichloroethane	<0.77	<0.77	<0.77	<0.77	<0.77	<0.77
	1,2-(Z)-Dichloroethylene	<0.77	<0.77	<0.77	<0.77	<0.77	<0.77
	Bromochloromethane	<0.63	<0.63	<0.63	<0.63	<0.63	<0.63
	Chloroform	<0.68	<0.68	<0.68	<0.68	<0.68	<0.68
	Benzene	3.13	<0.28	<0.28	<0.28	<0.28	<0.28
	1,2-Dichloroethane	2.09	<0.33	<0.33	<0.33	<0.33	<0.33
	Trichloroethene	<0.71	<0.71	<0.71	<0.71	<0.71	<0.71
	1,2-Dichloropropane	0.87	<0.77	<0.77	<0.77	<0.77	<0.77
	Bromodichloromethane	<0.71	<0.71	<0.71	<0.71	<0.71	<0.71
	Tetrachloroethene	<0.67	<0.67	<0.67	<0.67	<0.67	<0.67
	Dibromochloromethane	<0.59	<0.59	<0.59	<0.59	<0.59	<0.59
	1,2-Dibromomethane	<0.59	<0.59	<0.59	<0.59	<0.59	<0.59
	Tribromomethane	<0.59	<0.59	<0.59	<0.59	<0.59	<0.59

Table 5.3. Contaminants' concentrations ($\mu\text{g/L}$) along the leachate treatment process.

	Contaminants	RL*	LBT1*	LAA*	LPF*	LPFN*	LBT2*
Phenols	2-Chlorophenol	<0.01	<0.01	<0.01	<0.01	<0.01	<0.01
	2-Nitrophenol	3.31	1.15	1.02	0.12	0.11	0.03
	2,4-Dimethylphenol	3.21	0.44	0.21	<0.01	<0.01	<0.01
	2,4-Dichlorophenol	<0.01	<0.01	<0.01	<0.01	<0.01	<0.01
	4-chloro-3-methylphenol	71.41	19.67	24.62	0.35	0.18	0.14
	2,4,6-Trichlorophenol	<0.03	<0.03	<0.03	<0.03	<0.03	<0.03
	p-tert-octylphenol	1.51	0.22	0.13	<0.005	<0.005	<0.005
	Pentachlorophenol	<0.05	<0.05	<0.05	<0.05	<0.05	<0.05
	4-Nonylphenol	<0.005	<0.005	<0.005	<0.005	<0.005	<0.005
Phtalates / PAHs / PCBs	Naphthalene	0.04	<0.001	<0.001	<0.001	<0.001	<0.001
	Dimethyl phtalate	<0.1	<0.1	<0.1	<0.1	<0.1	<0.1
	2-Bromonaphthalene	<0.001	<0.001	<0.001	<0.001	<0.001	<0.001
	Diethyl phtalate	<0.1	<0.1	<0.1	<0.1	<0.1	<0.1
	Fluorene	0.04	<0.001	<0.001	<0.001	<0.001	<0.001
	Phenanthrene	0.06	0.005	<0.001	<0.001	<0.001	<0.001
	Anthracene	<0.001	<0.001	<0.001	<0.001	<0.001	<0.001
	PCB 28	<0.001	<0.001	<0.001	<0.001	<0.001	<0.001
	PCB 52	<0.001	<0.001	<0.001	<0.001	<0.001	<0.001
	Di-n-buthyl phtalate	<0.1	<0.1	<0.1	<0.1	<0.1	<0.1
	Fluoranthene	0.03	<0.001	<0.001	<0.001	<0.001	<0.001
	PCB 101	<0.001	<0.001	<0.001	<0.001	<0.001	<0.001
	Pyrene	0.008	<0.001	<0.001	<0.001	<0.001	<0.001
	PCB 153	<0.001	<0.001	<0.001	<0.001	<0.001	<0.001
	PCB 138	<0.001	<0.001	<0.001	<0.001	<0.001	<0.001
	Benz[a]anthracene	<0.001	<0.001	<0.001	<0.001	<0.001	<0.001
	Chrysene	<0.001	<0.001	<0.001	<0.001	<0.001	<0.001
	PCB 180	<0.001	<0.001	<0.001	<0.001	<0.001	<0.001
	Di-2-ethylhexyl phtalate	<0.1	<0.1	<0.1	<0.1	<0.1	<0.1
	Di-n-octyl phtalate	<0.1	<0.1	<0.1	<0.1	<0.1	<0.1
	Benzo[k]fluoranthene	<0.001	<0.001	<0.001	<0.001	<0.001	<0.001
	Benzo[b]fluoranthene	<0.001	<0.001	<0.001	<0.001	<0.001	<0.001
	Benzo[a]pyrene	<0.001	<0.001	<0.001	<0.001	<0.001	<0.001
	Perylene	<0.001	<0.001	<0.001	<0.001	<0.001	<0.001
	Dibenzo[a,h]anthracene	0.006	<0.001	<0.001	<0.001	<0.001	<0.001
	Indeno[1,2,3-cd]pyrene	<0.001	<0.001	<0.001	<0.001	<0.001	<0.001
	Benzo[ghi]perylene	<0.001	<0.001	<0.001	<0.001	<0.001	<0.001

*RL – Raw leachate; LBT1 – Leachate after 1st biological treatment; LAA – Leachate after acidification; LPF – Leachate after Photo-Fenton reaction; LPFN - Leachate after Photo-Fenton reaction and neutralization; LBT2 – Leachate after 2nd biological treatment; ^aConcentration below the respective quantification limit; ^bEPTC – S-ethyl dipropyl(thiocarbamate); ^cHCH - Hexachlorocyclohexane; ^dDDE – Dichlorodiphenyldichloroethylene; ^eDDD – Dichlorodiphenyldichloroethane; ^fDDT - Dichlorodiphenyltrichloroethane.

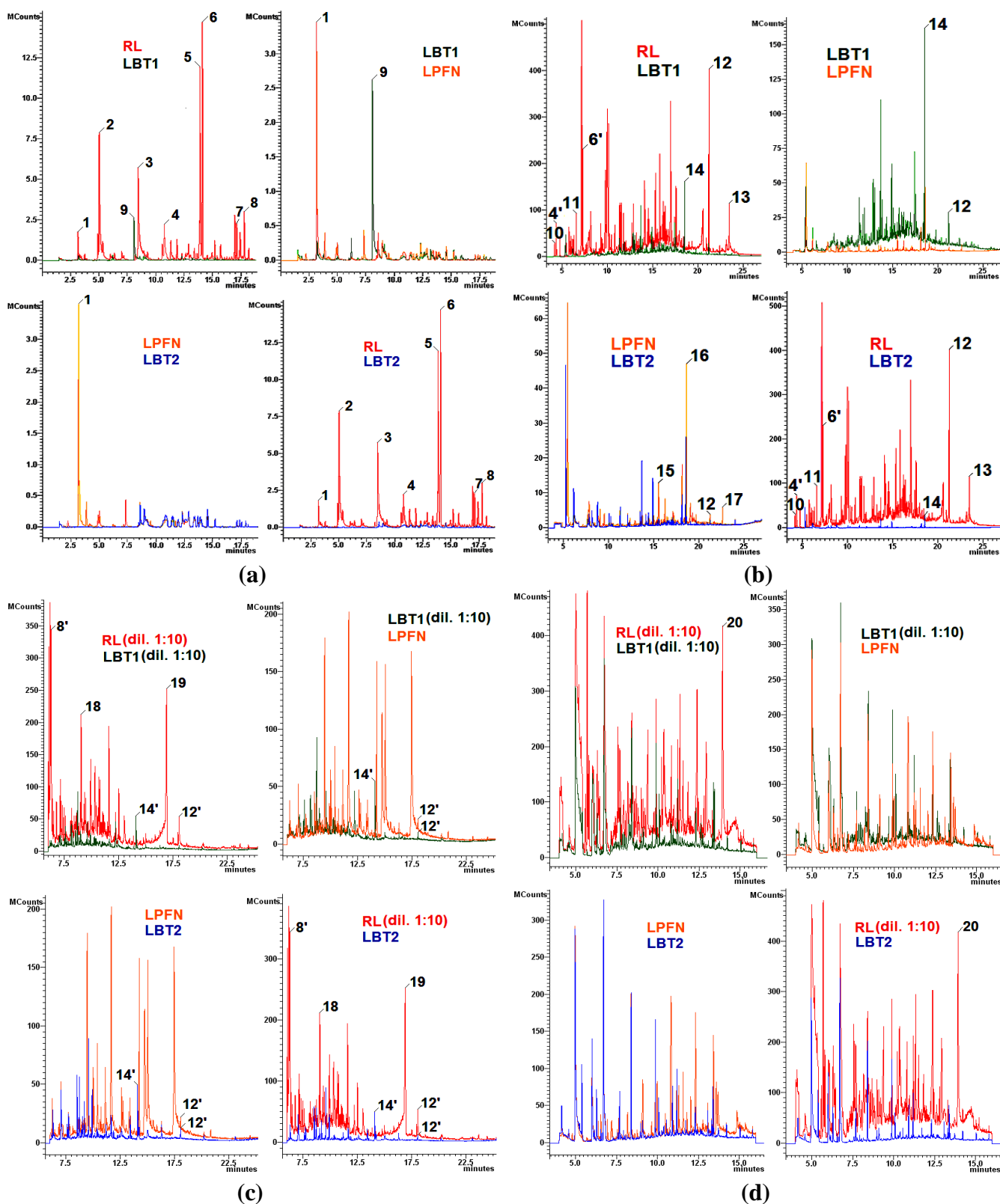


Figure 5.6. Non-target screening analysis of leachate samples, collected at different treatment points, by the four methods described in Chapter 2 (section 2.6): (a) VOCs; (b) PAHs, PCBs and phthalates; (c) pesticides; (d) phenols. Identification of contaminants removed and formed during different treatment stages (correspondence between the compound and the respective peak number is displayed in the Table 5.4) (RL – Raw Leachate; LBT1 – Leachate after 1st biological treatment; LPFN - Leachate after Photo-Fenton reaction and neutralization; LBT2 – Leachate after 2nd biological treatment (final effluent)).

Table 5.4. Contaminants identified in the different leachate samples collected along the treatment process, after target and non-screening analyses by the four methods described in Chapter 2 (section 2.6): structural characterization, fitting probability and removal efficiency during the different treatment stages (RL-Raw Leachate; LBT1-Leachate after 1st biological treatment; LPFN-Leachate after Photo-Fenton reaction and neutralization; LBT2-Leachate after 2nd biological treatment (final effluent)).

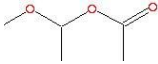
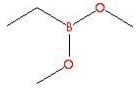
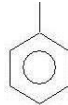
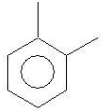
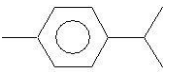
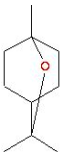
Peak	Contaminant	Molecular Weight (g/mol)	CAS no.	Molecular Formula	Structural Formula	Fitting Probability (%)	Area/Concentration in different samples	Removal(+)/Formation(-) (%)
<i>Non-target screening (Area)</i>								
1	Ethanol, 1-methoxy-, acetate	118	4382-77-8	C ₅ H ₁₀ O ₃		90	RL: 5.864e6 LBT1: 1.320e6 LPFN: 1.353e7 LBT2: n.d.*	RL-LBT1: +77 LBT1-LPFN: -925 LPFN-LBT2: +100 RL-LBT2: +100
2	Boronic acid, ethyl-, dimethyl ester	102	7318-82-3	C ₄ H ₁₁ BO ₂		70	RL: 3.694e7 LBT1: 3.022e5 LPFN: n.d. LBT2: n.d.	RL-LBT1: +99 LBT1-LPFN: +100 LPFN-LBT2: n.a.** RL-LBT2: +100
3	Toluene	92	108-88-3	C ₇ H ₈		53	RL: 4.309e7 LBT1: 3.578e6 LPFN: 2.046e6 LBT2: 1.844e6	RL-LBT1: +92 LBT1-LPFN: +43 LPFN-LBT2: +10 RL-LBT2: +96
4	o-Xylene	106	95-47-6	C ₈ H ₁₀		39	RL: 1.703e7 LBT1: 9.771e5 LPFN: n.d. LBT2: n.d.	RL-LBT1: +94 LBT1-LPFN: +100 LPFN-LBT2: n.a. RL-LBT2: +100
4'							RL: 1.661e8 LBT1: n.d. LPFN: n.d. LBT2: n.d.	RL-LBT1: +100 LBT1-LPFN: n.a. LPFN-LBT2: n.a. RL-LBT2: +100
5	4-Isopropyltoluene	134	99-87-6	C ₁₀ H ₁₄		57	RL: 4.891e7 LBT1: 7.974e5 LPFN: n.d. LBT2: n.d.	RL-LBT1: +98 LBT1-LPFN: +100 LPFN-LBT2: n.a. RL-LBT2: +100
6	Eucalyptol	154	470-82-6	C ₁₀ H ₁₈ O		83	RL: 4.796e7 LBT1: 1.414e5 LPFN: n.d. LBT2: n.d.	RL-LBT1: +99 LBT1-LPFN: +100 LPFN-LBT2: n.a. RL-LBT2: +100
6'							RL: 4.275e8 LBT1: 4.631e6 LPFN: 2.118e6 LBT2: n.d.	RL-LBT1: +99 LBT1-LPFN: +54 LPFN-LBT2: +100 RL-LBT2: +100

Table 5.4. Contaminants identified in the different leachate samples collected along the treatment process, after target and non-screening analyses by the four methods described in Chapter 2 (section 2.6): structural characterization, fitting probability and removal efficiency during the different treatment stages (RL-Raw Leachate; LBT1-Leachate after 1st biological treatment; LPFN-Leachate after Photo-Fenton reaction and neutralization; LBT2-Leachate after 2nd biological treatment (final effluent)).

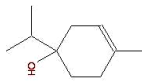
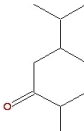

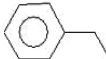
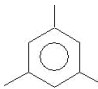
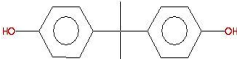
Peak	Contaminant	Molecular Weight (g/mol)	CAS no.	Molecular Formula	Structural Formula	Fitting Probability (%)	Area/Concentration in different samples	Removal(+)/Formation(-) (%)
7	3-Cyclohexen-1-ol, 4-methyl-1-(1-methylethyl)-	154	562-74-3	C ₁₀ H ₁₈ O		53	RL: 7.781e6 LBT1: 3.323e5 LPFN: 2.546e5 LBT2: 1.877e5	RL-LBT1: +96 LBT1-LPFN: +23 LPFN-LBT2: +26 RL-LBT2: +98
8	Cyclohexanone, 2-methyl-5-(1-methylethyl)-, trans	154	499-70-7	C ₁₀ H ₁₈ O		74	RL: 1.014e7 LBT1: 3.194e5 LPFN: 2.371e5 LBT2: 1.781e5	RL-LBT1: +97 LBT1-LPFN: +26 LPFN-LBT2: +25 RL-LBT2: +98
8'							RL: 4.710e9 LBT1: 1.688e8 LPFN: 4.060e7 LBT2: 1.837e7	RL-LBT1: +96 LBT1-LPFN: +76 LPFN-LBT2: +56 RL-LBT2: +99
9	Disulfide, dimethyl	94	624-92-0	C ₂ H ₆ S ₂		95	RL: 1.674e6 LBT1: 1.428e7 LPFN: n.d. LBT2: n.d.	RL-LBT1: -753 LBT1-LPFN: +100 LPFN-LBT2: n.a. RL-LBT2: +100
10	Ethylbenzene	106	100-41-4	C ₈ H ₁₀		69	RL: 4.986e7 LBT1: n.d. LPFN: n.d. LBT2: n.d.	RL-LBT1: +100 LBT1-LPFN: n.a. LPFN-LBT2: n.a. RL-LBT2: +100
11	1,3,5-Trimethylbenzene	120	108-67-8	C ₉ H ₁₂		62	RL: 1.548e8 LBT1: 3.444e7 LPFN: 1.150e6 LBT2: n.d.	RL-LBT1: +78 LBT1-LPFN: +97 LPFN-LBT2: +100 RL-LBT2: +100
12	Bisphenol A <i>or</i> Phenol, 4,4'-(1-methylethylidene)bis-	228	80-05-7	C ₁₅ H ₁₆ O ₂		86	RL: 1.097e9 LBT1: 6.615e7 LPFN: 6.564e6 LBT2: 4.023e6	RL-LBT1: +94 LBT1-LPFN: +90 LPFN-LBT2: +39 RL-LBT2: +99
12'							RL: 1.527e9 LBT1: 1.581e8 LPFN: 2.738e7 LBT2: 2.267e7	RL-LBT1: +90 LBT1-LPFN: +83 LPFN-LBT2: +17 RL-LBT2: +99

Table 5.4. Contaminants identified in the different leachate samples collected along the treatment process, after target and non-screening analyses by the four methods described in Chapter 2 (section 2.6): structural characterization, fitting probability and removal efficiency during the different treatment stages (RL-Raw Leachate; LBT1-Leachate after 1st biological treatment; LPFN-Leachate after Photo-Fenton reaction and neutralization; LBT2-Leachate after 2nd biological treatment (final effluent)).

Peak	Contaminant	Molecular Weight (g/mol)	CAS no.	Molecular Formula	Structural Formula	Fitting Probability (%)	Area/Concentration in different samples	Removal(+)/Formation(-) (%)
13	1-Phenanthrene carboxylic acid, 1,2,3,4,4a,9,10,10a-octahydro-1,4a-dimethyl-7-(1-methylethyl)-, [1R-(1.alpha., 4a.beta., 10a.alpha.)]-	300	1740-19-8	C ₂₀ H ₂₈ O ₂		81	RL: 2.715e8 LBT1: n.d. LPFN: n.d. LBT2: n.d.	RL-LBT1: +100 LBT1-LPFN: n.a. LPFN-LBT2: n.a. RL-LBT2: +100
14	Phenol, 2,6-bis(1,1-dimethylethyl)-4-nitro-	251	728-40-5	C ₁₄ H ₂₁ NO ₃		72	RL: n.d. LBT2: 3.373e8 LPFN: n.d. LBT2: 3.888e7	RL-LBT1: -100 LBT1-LPFN: +100 LPFN-LBT2: -100 RL-LBT2: +100
14'							RL: n.d. LBT1: 1.282e9 LPFN: n.d. LBT2: 1.143e8	RL-LBT1: -100 LBT1-LPFN: +100 LPFN-LBT2: -100 RL-LBT2: +100
15	4-Amino-7-diethylamino-chromen-2-one	232	107995-76-6	C ₁₃ H ₁₆ N ₂ O ₂		73	RL: 6.184e7 LBT1: 2.925e7 LPFN: 1.967e7 LBT2: 4.832e6	RL-LBT1: +53 LBT1-LPFN: +38 LPFN-LBT2: +75 RL-LBT2: +92
16	7,9-Di-tert-butyl-1-oxaspiro(4,5)deca-6,9-diene-2,8-dione	276	82304-66-3	C ₁₇ H ₂₄ O ₃		88	RL: n.d. LBT1: n.d. LPFN: 7.097e7 LBT2: 3.765e6	RL-LBT1: n.a. LBT1-LPFN: n.a. LPFN-LBT2: +95 RL-LBT2: n.a.
17	Benzyl butyl phtalate	312	85-68-7	C ₁₉ H ₂₀ O ₄		79	RL: n.d. LBT1: n.d. LPFN: 9.528e6 LBT2: n.d.	RL-LBT1: n.a. LBT1-LPFN: n.a. LPFN-LBT2: +100 RL-LBT2: n.a.
18	Acenaphthene	154	83-32-9	C ₁₂ H ₁₀		72	RL: 4.191e9 LBT1: 2.466e8 LPFN: 3.890e7 LBT2: 2.870e7	RL-LBT1: +94 LBT1-LPFN: +84 LPFN-LBT2: +26 RL-LBT2: +99
19	Cyclic octaatomic sulfur	256	10544-50-0	S ₈		97	RL: 1.210e10 LBT1: n.d. LPFN: n.d. LBT2: n.d.	RL-LBT1: +100 LBT1-LPFN: n.a. LPFN-LBT2: n.a. RL-LBT2: +100

Table 5.4. Contaminants identified in the different leachate samples collected along the treatment process, after target and non-screening analyses by the four methods described in Chapter 2 (section 2.6): structural characterization, fitting probability and removal efficiency during the different treatment stages (RL-Raw Leachate; LBT1-Leachate after 1st biological treatment; LPFN-Leachate after Photo-Fenton reaction and neutralization; LBT2-Leachate after 2nd biological treatment (final effluent)).

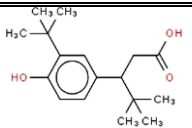
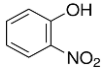
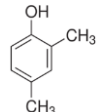
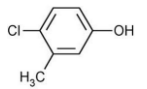
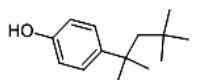
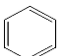

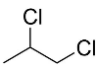
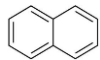
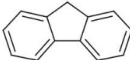

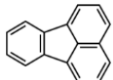
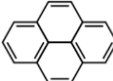
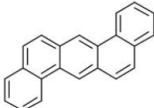
Peak	Contaminant	Molecular Weight (g/mol)	CAS no.	Molecular Formula	Structural Formula	Fitting Probability (%)	Area/Concentration in different samples	Removal(+)/Formation(-) (%)
20	3,5-di-tert-Butyl-4-hydroxyphenylpropionic acid	278	20170-32-5	C ₁₇ H ₂₆ O ₃		84	RL: 1.243e10 LBT1: n.d. LPFN: n.d. LBT2: n.d.	RL-LBT1: +100 LBT1-LPFN: n.a. LPFN-LBT2: n.a. RL-LBT2: +100
Target screening (Concentration in µg/L)								
Phenols	2-Nitrophenol	139	88-75-5	C ₆ H ₅ NO ₃		n.a.	RL: 3.31 LBT1: 1.15 LPFN: 0.11 LBT2: 0.03	RL-LBT1: +65 LBT1-LPFN: +90 LPFN-LBT2: +73 RL-LBT2: +99
	2,4-Dimethylphenol	122	105-67-9	C ₈ H ₁₀ O		n.a.	RL: 3.21 LBT1: 0.44 LPFN: n.d. LBT2: n.d.	RL-LBT1: +86 LBT1-LPFN: +100 LPFN-LBT2: n.a.** RL-LBT2: +100
	4-chloro-3-methylphenol	143	59-50-7	C ₇ H ₇ ClO		n.a.	RL: 71.41 LBT1: 19.67 LPFN: 0.18 LBT2: 0.14	RL-LBT1: +72 LBT1-LPFN: +99 LPFN-LBT2: +22 RL-LBT2: +99
	p-tert-octylphenol	206	140-66-9	C ₁₄ H ₂₂ O		n.a.	RL: 1.51 LBT1: 0.22 LPFN: n.d. LBT2: n.d.	RL-LBT1: +85 LBT1-LPFN: +100 LPFN-LBT2: n.a. RL-LBT2: +100
VOCs	Benzene	78	71-43-2	C ₆ H ₆		n.a.	RL: 3.13 LBT1: n.d. LPFN: n.d. LBT2: n.d.	RL-LBT1: +100 LBT1-LPFN: n.a. LPFN-LBT2: n.a. RL-LBT2: +100
	1,2-Dichloroethane	99	107-06-2	C ₂ H ₄ Cl ₂		n.a.	RL: 2.09 LBT1: n.d. LPFN: n.d. LBT2: n.d.	RL-LBT1: +100 LBT1-LPFN: n.a. LPFN-LBT2: n.a. RL-LBT2: +100
	1,2-Dichloropropane	113	78-87-5	C ₃ H ₆ Cl ₂		n.a.	RL: 0.87 LBT1: n.d. LPFN: n.d. LBT2: n.d.	RL-LBT1: +100 LBT1-LPFN: n.a. LPFN-LBT2: n.a. RL-LBT2: +100

Table 5.4. Contaminants identified in the different leachate samples collected along the treatment process, after target and non-screening analyses by the four methods described in Chapter 2 (section 2.6): structural characterization, fitting probability and removal efficiency during the different treatment stages (RL-Raw Leachate; LBT1-Leachate after 1st biological treatment; LPFN-Leachate after Photo-Fenton reaction and neutralization; LBT2-Leachate after 2nd biological treatment (final effluent)).

Peak	Contaminant	Molecular Weight (g/mol)	CAS no.	Molecular Formula	Structural Formula	Fitting Probability (%)	Area/Concentration in different samples	Removal(+)/Formation(-) (%)
PAHs	Naphthalene	128	91-20-3	C ₁₀ H ₈		n.a.	RL: 0.04 LBT1: n.d. LPFN: n.d. LBT2: n.d.	RL-LBT1: +100 LBT1-LPFN: n.a. LPFN-LBT2: n.a. RL-LBT2: +100
	Fluorene	166	86-73-7	C ₁₃ H ₁₀		n.a.	RL: 0.04 LBT1: n.d. LPFN: n.d. LBT2: n.d.	RL-LBT1: +100 LBT1-LPFN: n.a. LPFN-LBT2: n.a. RL-LBT2: +100
	Phenanthrene	178	85-01-8	C ₁₄ H ₁₀		n.a.	RL: 0.06 LBT1: 0.005 LPFN: n.d. LBT2: n.d.	RL-LBT1: +92 LBT1-LPFN: +100 LPFN-LBT2: n.a. RL-LBT2: +100
	Fluoranthene	202	206-44-0	C ₁₆ H ₁₀		n.a.	RL: 0.03 LBT1: n.d. LPFN: n.d. LBT2: n.d.	RL-LBT1: +100 LBT1-LPFN: n.a. LPFN-LBT2: n.a. RL-LBT2: +100
	Pyrene	202	129-00-0	C ₁₆ H ₁₀		n.a.	RL: 0.008 LBT1: n.d. LPFN: n.d. LBT2: n.d.	RL-LBT1: +100 LBT1-LPFN: n.a. LPFN-LBT2: n.a. RL-LBT2: +100
	Dibenzo[a,h]anthracene	278	53-70-3	C ₂₂ H ₁₄		n.a.	RL: 0.006 LBT1: n.d. LPFN: n.d. LBT2: n.d.	RL-LBT1: +100 LBT1-LPFN: n.a. LPFN-LBT2: n.a. RL-LBT2: +100

*n.d. – not detected; ** n.a. – not applicable.

5.4 Conclusions

A multistage treatment system consisting in three sequential steps, activated sludge biological process/chemical oxidation system based on the photo-Fenton reaction/activated sludge biological process, showed to be a successful approach for the treatment of stabilized raw leachates from sanitary landfills, concerning the elimination of organic matter and nitrogen compounds.

Raw leachate presents a recalcitrant character, associated mainly to HS and a high ammonium nitrogen content. Biological treatment with activated sludge, under aerobic and anoxic conditions, achieved 39% mineralization of the organic carbon and 95% reduction of the nitrogen content. The highest nitrification rate obtained was 8.2 mg $\text{NH}_4^+\text{-N}$ per hour and gram of volatile suspended solids (VSS) ($T = 26.9\text{ }^\circ\text{C}$; $\text{pH} = 7.6$), consuming 4.5 g CaCO_3 per liter of raw leachate or 1.2 mg CaCO_3 per mg $\text{NH}_4^+\text{-N}$. The maximum denitrification rate obtained was 5.8 mg ($\text{NO}_2^-\text{-N} + \text{NO}_3^-\text{-N}$)/(h.g VSS) ($T = 26.4\text{ }^\circ\text{C}$; $\text{pH} = 8.4$), with a C/N consumption ratio of 2.4 mg CH_3OH per mg ($\text{NO}_2^-\text{-N} + \text{NO}_3^-\text{-N}$) (7.4 g/9.4 mL of commercial methanol per liter of leachate), with an overall alkalinity production of 4.3 g CaCO_3 per g ($\text{NO}_2^-\text{-N} + \text{NO}_3^-\text{-N}$) reduced.

The phototreatment process led to the depletion of HS (>80%), of low-molecular-weight carboxylate anions (>70%) and other organic micropollutants, thus resulting in a total biodegradability increase to >70%, being possible to couple it with a further biological treatment, achieving a final wastewater quality in agreement with discharge limits into receiving water bodies, with the exception of sulphate ions. Although humic acids and other organic compounds can be easily removed from the leachate by precipitation at $\text{pH}\sim 3.0$, leading to a high decrease of dissolved organic carbon and consequently decrease of the phototreatment time and reactants consumption, the elimination of the acid sludge can be a big concern.

5.5 References

- [1] H. Robinson, P. Maris, The treatment of leachates from domestic waste in landfill sites, *Journal (Water Pollution Control Federation)*, (1985) 30-38.
- [2] J. Lema, R. Mendez, R. Blazquez, Characteristics of landfill leachates and alternatives for their treatment: a review, *Water, Air, and Soil Pollution*, 40 (1988) 223-250.
- [3] S. Renou, J. Givaudan, S. Poulain, F. Dirassouyan, P. Moulin, Landfill leachate treatment: Review and opportunity, *Journal of Hazardous Materials*, 150 (2008) 468-493.
- [4] A. Baun, A. Ledin, L. Reitzel, P.L. Bjerg, T.H. Christensen, Xenobiotic organic compounds in leachates from ten Danish MSW landfills—chemical analysis and toxicity tests, *Water Research*, 38 (2004) 3845-3858.
- [5] C.B. Öman, C. Junestedt, Chemical characterization of landfill leachates – 400 parameters and compounds, *Waste Management*, 28 (2008) 1876-1891.
- [6] L. Zhang, A. Li, Y. Lu, L. Yan, S. Zhong, C. Deng, Characterization and removal of dissolved organic matter (DOM) from landfill leachate rejected by nanofiltration, *Waste Management*, 29 (2009) 1035-1040.
- [7] H.-j. Fan, H.-Y. Shu, H.-S. Yang, W.-C. Chen, Characteristics of landfill leachates in central Taiwan, *Science of the Total Environment*, 361 (2006) 25-37.
- [8] S. Jonsson, J. Ejlertsson, B.H. Svensson, Behaviour of mono- and diesters of o-phthalic acid in leachates released during digestion of municipal solid waste under landfill conditions, *Advances in Environmental Research*, 7 (2003) 429-440.
- [9] S.K. Marttinen, R.H. Kettunen, J.A. Rintala, Occurrence and removal of organic pollutants in sewages and landfill leachates, *The Science of The Total Environment*, 301 (2003) 1-12.
- [10] M. Osako, Y.-J. Kim, S.-i. Sakai, Leaching of brominated flame retardants in leachate from landfills in Japan, *Chemosphere*, 57 (2004) 1571-1579.
- [11] Y. Wu, S. Zhou, X. Ye, D. Chen, K. Zheng, F. Qin, Transformation of pollutants in landfill leachate treated by a combined sequence batch reactor, coagulation, Fenton oxidation and biological aerated filter technology, *Process Safety and Environmental Protection*, 89 (2011) 112-120.
- [12] D.L. Jensen, A. Ledin, T.H. Christensen, Speciation of heavy metals in landfill-leachate polluted groundwater, *Water Research*, 33 (1999) 2642-2650.
- [13] T.H. Christensen, P. Kjeldsen, P.L. Bjerg, D.L. Jensen, J.B. Christensen, A. Baun, H.-J. Albrechtsen, G. Heron, Biogeochemistry of landfill leachate plumes, *Applied Geochemistry*, 16 (2001) 659-718.
- [14] J. Wiszniowski, D. Robert, J. Surmacz-Gorska, K. Miksch, J. Weber, Landfill leachate treatment methods: A review, *Environmental Chemistry Letters*, 4 (2006) 51-61.
- [15] A.A. Abbas, G. Jingsong, L.Z. Ping, P.Y. Ya, W.S. Al-Rekabi, Review on Landfill Leachate Treatments, *Journal of Applied Sciences Research*, 5 (2009) 534-545.
- [16] A.Ž. Gotvajn, T. Tišler, J. Zagorc-Končan, Comparison of different treatment strategies for industrial landfill leachate, *Journal of Hazardous Materials*, 162 (2009) 1446-1456.

- [17] E.M.R. Rocha, V.J.P. Vilar, A. Fonseca, I. Saraiva, R.A.R. Boaventura, Landfill leachate treatment by solar-driven AOPs, *Solar Energy*, 85 (2011) 46-56.
- [18] V.J.P. Vilar, J.M.S. Moreira, A. Fonseca, I. Saraiva, R.A.R. Boaventura, Application of Fenton and Solar Photo-Fenton Processes to the Treatment of a Sanitary Landfill Leachate in a Pilot Plant with CPCs, *Journal of Advanced Oxidation Technologies*, 15 (2012) 107-116.
- [19] V.J.P. Vilar, S.M.S. Capelo, T.F.C.V. Silva, R.A.R. Boaventura, Solar photo-Fenton as a pre-oxidation step for biological treatment of landfill leachate in a pilot plant with CPCs, *Catalysis Today*, 161 (2011) 228-234.
- [20] V.J.P. Vilar, E.M.R. Rocha, F.S. Mota, A. Fonseca, I. Saraiva, R.A.R. Boaventura, Treatment of a sanitary landfill leachate using combined solar photo-Fenton and biological immobilized biomass reactor at a pilot scale, *Water Research*, 45 (2011) 2647-2658.
- [21] V.J.P. Vilar, T.F.C.V. Silva, M.A.N. Santos, A. Fonseca, I. Saraiva, R.A.R. Boaventura, Evaluation of solar photo-Fenton parameters on the pre-oxidation of leachates from a sanitary landfill, *Solar Energy*, 86 (2012) 3301-3315.
- [22] H. Zhang, H.J. Choi, C.-P. Huang, Optimization of Fenton process for the treatment of landfill leachate, *Journal of Hazardous Materials*, 125 (2005) 166-174.
- [23] O. Primo, M.J. Rivero, I. Ortiz, Photo-Fenton process as an efficient alternative to the treatment of landfill leachates, *Journal of Hazardous Materials*, 153 (2008) 834-842.
- [24] Y. Wu, S. Zhou, F. Qin, H. Peng, Y. Lai, Y. Lin, Removal of humic substances from landfill leachate by Fenton oxidation and coagulation, *Process Safety and Environmental Protection*, 88 (2010) 276-284.
- [25] E.S.K. Chian, F.B. DeWalle, Sanitary landfill leachate and their treatment, *Journal of the Environmental Engineering Division* 2(1976) 411-431.
- [26] C. Sawyer, P. McCarty, G. Parkin, *Chemistry for Environmental Engineering and Science*, McGraw-Hill Education, 2003.
- [27] Metcalf, Eddy, *Wastewater Engineering Treatment and Reuse*, 4th ed., Metcalf & Eddy, 2005.
- [28] J.E. Alleman, Elevated nitrite occurrence in biological wastewater treatment systems, *Water Science and Technology*, 17 (1984) 409-419.
- [29] A. Spagni, S. Marsili-Libelli, Nitrogen removal via nitrite in a sequencing batch reactor treating sanitary landfill leachate, *Bioresource technology*, 100 (2009) 609-614.
- [30] G. Ruiz, D. Jeison, R. Chamy, Nitrification with high nitrite accumulation for the treatment of wastewater with high ammonia concentration, *Water Research*, 37 (2003) 1371-1377.
- [31] R. Canziani, V. Emondi, M. Garavaglia, F. Malpei, E. Pasinetti, G. Buttiglieri, Effect of oxygen concentration on biological nitrification and microbial kinetics in a cross-flow membrane bioreactor (MBR) and moving-bed biofilm reactor (MBBR) treating old landfill leachate, *Journal of Membrane Science*, 286 (2006) 202-212.
- [32] S. Villaverde, M. Fernandez, M. Uruena, F. Fdz-Polanco, Influence of substrate concentration on the growth and activity of a nitrifying biofilm in a submerged biofilter, *Environmental technology*, 18 (1997) 921-928.

- [33] S. Suthersan, J. Ganczarczyk, Inhibition of nitrite oxidation during nitrification. Some observations, *Water pollution research journal of Canada*. Burlington ON, 21 (1986) 257-266.
- [34] D. Kulikowska, E. Klimiuk, Removal of organics and nitrogen from municipal landfill leachate in two-stage SBR reactors, *Polish Journal of Environmental Studies*, 13 (2004) 389-396.
- [35] M. Christensson, E. Lie, T. Welander, A comparison between ethanol and methanol as carbon sources for denitrification, *Water Science and Technology*, 30 (1994) 83-90.
- [36] O. Modin, K. Fukushi, K. Yamamoto, Denitrification with methane as external carbon source, *Water Research*, 41 (2007) 2726-2738.
- [37] C.W. Randall, J.L. Barnard, H.D. Stensel, in: W.W. Eckenfelder, J.F. Malina, J.W. Patterson (Eds.) *Design and retrofit of wastewater treatment plants for biological nutrient removal*, Technomic Pub. Co., Lancaster, Pa., 1992.
- [38] J.J. Pignatello, E. Oliveros, A. MacKay, Advanced oxidation processes for organic contaminant destruction based on the fenton reaction and related chemistry, *Critical Reviews in Environmental Science and Technology*, 36 (2006) 1-84.
- [39] J. Bacardit, I. Oller, M.I. Maldonado, E. Chamarro, S. Malato, S. Esplugas, Simple Models for the Control of Photo-Fenton by Monitoring H₂O₂, *Journal of Advanced Oxidation Technologies*, 10 (2007) 219-228.
- [40] L. Prieto-Rodríguez, I. Oller, A. Zapata, A. Agüera, S. Malato, Hydrogen peroxide automatic dosing based on dissolved oxygen concentration during solar photo-Fenton, *Catalysis Today*, 161 (2011) 247-254.
- [41] J.B. Gálvez, S.M. Rodríguez, *Solar Detoxification*, United Nations Educational, Scientific and Cultural Organization, 2003.
- [42] C. Pulgarin, M. Invernizzi, S. Parra, V. Sarria, R. Polania, P. Péringier, Strategy for the coupling of photochemical and biological flow reactors useful in mineralization of biorecalcitrant industrial pollutants, *Catalysis Today*, 54 (1999) 341-352.
- [43] J. Wiszniowski, D. Robert, J. Surmacz-Gorska, K. Miksch, S. Malato, J.-V. Weber, Solar photocatalytic degradation of humic acids as a model of organic compounds of landfill leachate in pilot-plant experiments: influence of inorganic salts, *Applied Catalysis B: Environmental*, 53 (2004) 127-137.
- [44] M.A. Oturan, M. Pimentel, N. Oturan, I. Sirés, Reaction sequence for the mineralization of the short-chain carboxylic acids usually formed upon cleavage of aromatics during electrochemical Fenton treatment, *Electrochimica Acta*, 54 (2008) 173-182.

6 Scale-up and economic analysis of the photo-Fenton system for landfill leachate treatment

This chapter presents the scale-up and cost analysis of a photo-Fenton process, using solar and/or artificial radiation, for the treatment of 100 m³ per day of a sanitary landfill leachate previously oxidized in a biological system.

The scale-up of the photo-oxidation system, taking into account the CPCs (compound parabolic collectors) area and land requirements for its installation and/or the number of UV lamps (with 4 kW and 20,000-h of lifetime each), was performed considering the following data: i) the average global UV irradiance and insolation in the specific location of the sanitary landfill; ii) the amount of UV energy and H₂O₂ necessary for the photo-Fenton reaction in order to achieve two different target COD values, i.e., 1000 and 150 mg O₂/L (values according to the Portuguese discharge regulations into sewerage systems and water bodies, respectively). Regarding the optimal conditions, the plant includes 3836 and 6056 m² of CPCs, or 25 and 39 UV lamps, to achieve the above mentioned target COD values. A third plant configuration, combining simultaneous natural and artificial radiation, requires 2446 and 3862 m² of CPCs and, 19 and 30 UV lamps, respectively.

Total photo-Fenton costs were based on the project's contingencies, engineering and setup and spare parts, personnel, maintenance, electricity and chemicals supply. Thus, the total unitary costs for the optimal conditions aiming to achieve COD values of 1000 and 150 mg O₂/L, were, respectively: i) 6.8 and 11.0 €/m³ using only CPCs; ii) 7.2 and 11.7 €/m³ resorting just to UV lamps; and iii) 6.7 and 10.9 €/m³ combining CPCs and UV lamps. The cost of the H₂O₂ reactant represents more than 30% of the total yearly cost.

6.1 Introduction

Mature leachates present a high non-biodegradable organic fraction mainly due to the presence of humic and fulvic acids. The best treatment strategy to reach the required level of purification to fully reduce environmental negative impacts and to meet discharge regulations, at comfortable prices, consists in a multistage treatment process. This strategy may include primary, secondary and tertiary processes, as those reported in UK Environment Agency guidance [1].

Advanced oxidation processes (AOPs) have been reported to significantly enhance the biodegradability of mature landfill leachates [2-4] and, therefore, are particularly suitable to be combined with biological oxidation systems [5-7]. Amongst AOPs, the solar photo-Fenton process has been selected as the best option for the pre-oxidation of mature leachates [4, 8].

The photo-Fenton reaction consists of the Fenton reaction ($\text{H}_2\text{O}_2 + \text{Fe}^{2+} \rightarrow \text{Fe}^{3+} + \text{OH}^- + \text{OH}^\bullet$) in the presence of UV-Vis radiation. The radiation has a positive effect on the reaction rate by promoting the photoreduction of ferric ions to ferrous ions, producing additional hydroxyl radicals. The regenerated Fe^{2+} ions react with H_2O_2 , generating more hydroxyl radicals. Thus, low amounts of iron are needed for the treatment of wastewaters using a photo-Fenton process [9].

In the Chapter 5, the first pre-industrial plant for leachates treatment from a sanitary landfill located in the North of Portugal, combining: i) an aerobic/anoxic biological system (3.5 m³ capacity); ii) a solar photo-Fenton oxidation process, using 39.52 m² of compound parabolic collectors (CPCs), and iii) a further aerobic biological treatment. This multistage treatment system lead to a final effluent with COD and total nitrogen concentrations below 150 mg O₂/L and 15 mg N/L, respectively, which is in agreement with the discharge limits into receiving water bodies, imposed by the Portuguese Legislation. Given the promising results and in order to scale-up the process, a cost analysis must be performed to assess the economic viability of the process.

Few studies have reported cost analysis for AOPs applied to water/wastewater treatment (see Table 6.1). Cassano et al. [10] reported the operating costs for the combination of a sequential batch biofilter granular reactor (SBBGR) and a solar photo-Fenton (SphF) process for the treatment of municipal landfill leachate (COD_i = 2.8-3.6 g/L; DOC_i = 0.9-1.2 g/L; N-NH_{4,i} = 1.5-2.0 g/L). The operating costs were 3.26 €/m³ (2.54€/m³ for SBBGR and 0.72€/m³ for SphF) and 4.13€/m³ (2.54€/m³ for SBBGR and 1.59€/m³ for SphF) for a final COD of 500 and 160 mg O₂/L, respectively.

Table 6.1. Total expenditure with different treatment strategies using AOPs.

Effluent	Process ^c	Initial characteristics	Final characteristics	Observations	Cost	Reference
Landfill leachate	O ₃		TOC = 223 mg/L	-	5184 ^f ATS/m ³	Bauer and Fallmann [11]
	O ₃ /UV		TOC = 213 mg/L	UV radiation = 150 W	4704 ^f ATS/m ³	
	UV/H ₂ O ₂	TOC = 545 mg/L	TOC = 474 mg/L	UV radiation = 150 W	1954 ^f ATS/m ³	
	ALphF		TOC = 218 mg/L	UV radiation = 2×400 W	864 ^f ATS/m ³	
	SphF		TOC = 218 mg/L	Flat basin	84 ^f ATS/m ³	
Water containing acetaminophen (0.5 mM)	SphF (100 m ² of CPCs)	DOC ≈ 50 mg/L	DOC ≈ 35 mg/L	One H ₂ O ₂ addition	0.37 €/m ³	Carra et al. [12]
				Continuous H ₂ O ₂ dosage	0.51 €/m ³	
				PI controlled H ₂ O ₂ dosage	0.40 €/m ³	
				One H ₂ O ₂ addition	1.33 €/m ³	
Landfill leachate	SBBGR enhanced by O ₃ SBBGR + SphF SBBGR/O ₃ + SphF SBBGR + SphF SBBGR/O ₃	COD = 2.8-3.6 g/L DOC = 0.9-1.2 g/L NH ₄ ⁺ -N = 1.5-2.0 g/L Cl ⁻ = 3.0-4.0 g/L SO ₄ ²⁻ = 1.0-1.5 g/L	COD < 500 mg/L COD < 160 mg/L	SBBGR final:	3.2 ^f €/m ³	Cassano et al. [10]
				COD = 1200 mg/L	3.2 ^f €/m ³	
				DOC = 425 mg/L	4.8 ^f €/m ³	
				NH ₄ ⁺ -N = 6 mg/L	4.1 ^f €/m ³	
				NO _x -N = 9 mg/L	5.7 ^f €/m ³	
Fuel-contaminated groundwater (2044 m ³ /day) with BTEX ^a	Pt-TiO ₂	BTEX = 2 mg/L	BTEX = 5 µg/L	Solar radiation	US\$ 1.4/m ³	Crittenden et al. [13]
Landfill leachate	SBBGR enhanced by O ₃	DOC = 0.9-1.2 g/L COD = 2.2-3.2 g/L	DOC = 290 mg/L COD = 495 mg/L	Discharge in sewerage system	4 ^f €/m ³	Di Iaconi et al. [14]
Apple juice wastewater	SphF/Ferrioxalate	TOC = 678 mg/L	TOC = 102 mg/L	-	10.9 ^f €/m ³	Durán et al. [15]
Real wastewater resulting from an integrated gasification combined cycle power station	ALphF (40 L)			Initial addition of H ₂ O ₂ .	34 ^f €/m ³	Durán et al. [16]
	ALphF (40 L)	Removal of 4.5 g of TOC		Continuous addition of O ₂ and H ₂ O ₂ .	10 ^f €/m ³	
	SphF/Ferrioxalate (35 L)			-	6 ^f €/m ³	
Wastewater from chip-board production (10 m ³ /day)	SphF	COD _i = 2000-4000 mg/L	COD _f = 60%-100% of COD _i	-	9 €/m ³	Eduardo da Hora Machado et al. [17]
Wastewater contaminated with pesticides (6,000 m ³ /year)	TiO ₂ – persulfate			CPCs (300 m ²)	18 €/m ³	Gálvez and Rodríguez [18]
	SphF	TOC = 100 mg/L	TOC = 20 mg/L	CPCs (200 m ²)	9.5 €/m ³	
Industrial effluent (1000 m ³ /year) contaminated with Orange II (0.2 mM)	SphF - Fe/Nafion/C catalysts			CPC fixed	10.4 €/m ³	Gumy et al. [19]
	SphF	Complete colour removal		CPC homogeneous	7.2 €/m ³	
	SphF - Fe/Nafion/C catalysts			Flat fixed	12.5 €/m ³	

Table 6.1. Total expenditure with different treatment strategies using AOPs.

Effluent	Process ^c	Initial characteristics	Final characteristics	Observations	Cost	Reference
Wastewater contaminated with Paracetamol (~1mM)	SphF	DOC = 100 mg/L	DOC = 20 mg/L	CPCs (100 m ² ; t _{30w} = 2h) Comp. biodegradability	3.45 €/m ³	Jordá et al. [20]
			DOC = 65 mg/L	CPCs (100 m ² ; 34 W/m ² ; 25 min); biodegradability sufficiently high for a downstream BT ^e	0.74 €/m ³	
Wastewater from a sewage system, in Malaysia	Solar detoxification with TiO ₂	-	-	FPC ^d (1000 L/m ² ; 40 W/m ²)	US\$ 9.5/m ³	Jubran et al. (2000)
		-	-	CPC (600 L/m ² ; 30 W/m ²)	US\$ 11.1/m ³	
Domestic effluents with low concentration of antibiotics (150 m ³ /day)	SphF (secondary treatment)	Complete antibiotics removal		-	0.85 €/m ³	Michael et al. [21]
Tannery industrial effluent	SphF + Electrocoagulation	COD = 11,878 mg/L	COD = 107 mg/L	-	US\$ 66.2 ^f /m ³	Módenes et al. [22]
Textile effluent	SphF	COD = 1636 mg/L	COD = 33-196 mg/L		US\$ 6.9 ^f /m ³	Módenes et al. [23]
	ALphF				US\$ 18 ^f /m ³	
Industrial wastewater (2500 m ³ /year) containing alpha-methyl-phenylglycine (500 mg/L)	SphF	-	-	Discontinuous mode	14.1 €/m ³	Muñoz et al. [24]
	ALphF	-	-	Continuous mode	12.1 €/m ³	
	O ₃	-	-	Continuous mode	15.1 €/m ³	
Industrial ecotoxic wastewater (10 m ³ /d) contaminated with a mixture of five commercial pesticides (OPMDI ^b)	SphF/MBR	DOC = 500 mg/L	DOC = 13 mg/L	SphF mineraliz. = 57%	2.51 €/m ³	Pérez et al. [25]
		DOC = 200 mg/L	DOC = 14 mg/L	SphF mineraliz. = 40%	2.15 €/m ³	
		DOC = 50 mg/L	DOC = 13 mg/L	SphF mineraliz. = 33%	1.53 €/m ³	
		DOC = 50 mg/L	DOC = 11 mg/L	SphF mineraliz. = 20%	1.19 €/m ³	
Landfill leachate (40 m ³ /day)	Coagulation + SphF	DOC = 13 g/L	DOC = 8 g/L	DOC removed in coagulation = 17% SphF mineraliz. = 27%	43 €/m ³	De Torres-Socías et al. [3]
Wastewater contaminated with pesticides (200 m ³ /day)	Solar detoxification with TiO ₂	C = 500 µL	C = 0.1 µL	400 m ² of CPCs	US\$ 0.7/ m ³	Vidal et al. [26]

^aBTEX - benzene, toluene, ethylbenzene and xylene; ^bOPMDI - Oxamyl, Pyrimethanil, Methomyl, Dimethoate, Imidacloprid; ^cTreatment processes used: O₃ – Ozonation, ALphF – Artificial Light photo-Fenton, SphF – Solar photo-Fenton, SBBGR - Sequencing batch biofilter granular reactor, Pt-TiO₂ – Platinized titanium dioxide, SphF - Fe/Nafion/C catalysts – SphF with supported Fe/Nafion/C catalysts, MBR – Membrane bioreactor; ^dFPC – Flat plate collector; ^eBT – Biological Treatment; ^fOperating Costs; 1 ATS = 0.07267 €.

Durán et al. [16] presented an operating cost of 6.0 €/m³ for the treatment of a real wastewater by a solar photo-Fenton process. Jordá et al. [20] reported a treatment cost of 0.74 €/m³ for a paracetamol-containing wastewater (~1 mM; 100 mg DOC/L) using a photo-Fenton system. Pérez et al. [25] carried out an economic assessment on a solar photo-Fenton/membrane bioreactor (MBR) combined process, to treat industrial ecotoxic wastewaters (mixture of five commercial pesticides, ranging from 50-500 mg DOC/L). The authors showed that a 30% total cost reduction could be achieved by treating higher daily volumes, resulting in competitive costs that vary from 1.1-1.9 €/m³, depending on the pollution load. Gumy et al. [19] reported a cost of 7.2 €/m³ for the treatment of an industrial effluent (1000 m³/year) containing Orange II (0.2 mM) using a solar photo-Fenton process. Vidal et al. [26] reported a treatment capacity of 42 L/h/m² and a cost of 1 US\$/m³ for wastewater containing 500 µg/L of selected pesticides, with a maximum discharge level of 0.1 µg/L, using a solar TiO₂ photocatalytic system based on CPCs technology.

Amongst solar driven-AOPs, solar driven photo-Fenton processes have been considered the best option considering their life-cycle greenhouse gas emission and life-cycle cost [24]. Bauer and Fallmann [11] estimated the operational costs of several AOPs for the treatment of a landfill leachate with an initial TOC of 545 mg/L, such as O₃, O₃/UV, UV/H₂O₂, Fe²⁺/H₂O₂/UV and solar driven photo-Fenton. The study led to the conclusion that the photo-Fenton system driven by sunlight was by far the cheapest when compared with the other tested AOPs. Reagents costs were 18.7 €/kg of removed TOC.

The photo-Fenton process driven by natural light can be considered an environmentally sound technology as it generates low to zero waste and prevents pollution, according to Chapter 34 of Agenda 21 (resolution from United Nations Conference on Environment and Development (UNCED) held in Rio de Janeiro, Brazil, in 1992).

This work is about the scale-up and cost analysis of a solar/UV photo-Fenton system for the treatment of a sanitary leachate, previously oxidised in an aerated lagoon, taking into account two different target COD values, 1000 and 150 mg O₂/L, as required by the Portuguese discharge regulations into sewerage systems and water bodies, respectively. The area of the CPCs and the number of UV lamps were calculated according to the monthly variation of solar radiation power. The costs of solar UV photons or electric UV photons were also calculated and compared. Three different treatment set-ups were proposed for the photo-Fenton reaction considering the use of i) only natural sunlight through CPCs technology, ii) only UV lamps and iii) the combination of natural and artificial radiation, according to the UV radiation needs throughout the year. Finally, the main operation variables affecting the costs of the proposed treatment line were identified.

6.2 Experimental methodology

The scale-up and the economical assessment were performed only for the photo-Fenton process, based on results obtained in 3 experiments. Experiment 1 (which corresponds to test carried out with acid sludge removal presented in Chapter 5) consisted of three treatment steps: i) anoxic/aerobic biological treatment of the raw leachate; ii) photo-Fenton reaction of the bio-treated leachate; and iii) anoxic/aerobic biological treatment of the neutralized photo-bio-treated leachate. For experiments 2 and 3 (which correspond to tests 5 and 9, respectively, presented in the Chapter 3), only the photo-Fenton reaction step was applied to the bio-treated leachate collected after the aerated lagoon of the leachate treatment plant (LTP), installed at a municipal solid waste (MSW) sanitary landfill nearby Porto. Table 6.2 summarizes the values of the main physico-chemical characteristics of the bio-treated leachate samples (BTLs) used in the three photo-reaction experiments.

Table 6.2. Characteristics of the bio-treated leachate used in the photo-Fenton reactions.

Parameters	Experiment 1 ^a	Experiment 2 ^b	Experiment 3 ^b
pH	8.4	7.0	6.5
T (°C)	25.2	26.4	27.5
TSS (mg/L)	900	407	121
Dissolved Inorganic Carbon (mg/L)	1903	575	200
Alkalinity ^c (g CaCO ₃ /L)	7.94	2.40	0.83
DOC (mg C/L)	1534	1129	1135
COD (mg O ₂ /L)	4864	3775	2945
BOD ₅ (mg O ₂ /L)	200	-	-
BOD ₅ /COD	0.04	-	-
Total Dissolved Iron (mg (Fe ²⁺ + Fe ³⁺)/L)	7.9	7.9	6.6
Sulphate (mg SO ₄ ²⁻ /L)	6831	292	340
Chloride (mg Cl ⁻ /L)	3370	3601	3665
Total Dissolved Nitrogen (mg N/L)	210	859	1377
Ammonium Nitrogen (mg NH ₄ ⁺ -N/L)	23	1	19
Nitrate (mg NO ₃ ⁻ -N/L)	<1	757	1297
Nitrite (mg NO ₂ ⁻ -N/L)	<1	<1	<1
Total Phosphorous (mg P/L)	25	40	7

^aBiological oxidation was performed in the pre-industrial scale plant, located at the sanitary landfill; ^bBiological oxidation was performed in the aerated lagoon of the leachate treatment plant, located at the sanitary landfill; ^cAlkalinity values considering that at pH less than 8.3, the inorganic carbon was almost in the form of bicarbonates.

All the chemicals used in this work, the detailed description of the experimental unit and respective procedures, as well as the employed analytical methods can be consulted in the Chapter 2.

6.3 Results and discussion

6.3.1 Bio-treated leachate characterization

The conditions for scale-up and economical assessment of the photo-Fenton process were selected from 31 experiments performed during 1 year (Chapters 3-5). The different characteristics of the bio-treated samples were taken into account, in terms of nitrogen species, sulphates, DOC and alkalinity. The BTLS presents a high organic matter content (DOC = 1129-1534 mg C/L; COD = 2945-4864 mg O₂/L) and an intense dark-brown colour, mainly due to the presence of humic substances. A high nitrogen load (859-1377 mg N/L), with more than 83% in the form of nitrate, can be observed in the BTLS used in experiments 2 and 3 (see Table 6.2). These results indicate a high efficiency of the nitrification process in the aerated lagoon of the LTP. The BTLS used in experiment 1 presents low nitrogen content, high sulphate concentration and a low biodegradable fraction (BOD₅ = 200 mg O₂/L; BOD₅/COD = 0.04). These characteristics indicate the presence of recalcitrant organic matter, and consequently the need for the application of AOPs as post or intermediate treatment, depending on the COD target value to be achieved. The variability of the bio-treated leachate composition in terms of DOC and alkalinity has a high influence on the photo-Fenton treatment time (i.e. UV energy and H₂O₂ consumption) and on the amount of acid required to achieve a pH around 2.6-2.9, respectively.

6.3.2 Performance of the biological and photo-Fenton oxidation processes

Previous to the photo-Fenton reaction, in experiment 1, raw leachate was biologically treated in the pre-industrial plant, under aerobic/anoxic conditions, achieving almost complete nitrogen removal (95%) through nitrification/denitrification. The maximum nitrification and denitrification rates obtained were 8.2 mg NH₄⁺-N/g VSS/h (T_m = 26.9 °C, pH_m = 7.6 and DO_m = 3.2 mg/L) and 5.8 mg (NO₃⁻-N+NO₂⁻-N)/g VSS/h (T_m = 26.4 °C and pH_m = 8.4), respectively. Throughout nitrification, about 90 mM of sodium hydroxide (~4.5 g CaCO₃/L) was added to compensate for the raw leachate alkalinity (17.1 g CaCO₃/L). During denitrification, methanol was added as external carbon source (2.4 mg CH₃OH/ mg (NO₃⁻-N+NO₂⁻-N)), and sulphuric acid (53 mM) was added to compensate the alkalinity produced during denitrification.

The solar photo-Fenton experiments were performed at optimum operating conditions: i) pH was kept between 2.6-2.9 (to avoid iron precipitation [27]); ii) initial iron dose was 80 mg Fe²⁺/L (optimum value obtained in a previous work [28], for a leachate collected from the same sanitary landfill); and iii) H₂O₂ concentration was maintained in the range 100-500 mg/L during the entire reaction (to improve the

oxidation reaction rate, minimizing the H_2O_2 consumption [29]). The photo-Fenton reaction showed a mineralization efficiency between 57% and 80%, consuming 80-225 mM of H_2O_2 and 20-67 kJ/L of accumulated UV energy, and led to DOC values below 500 mg/L in all experiments (Table 6.3).

6.3.3 Evaluation of the yearly solar irradiation and CPCs area requirements

Table 6.3 presents the main process operation variables necessary for scale-up and economical assessment of a photo-Fenton system for the treatment of bio-treated leachate. The target COD values considered were 1000 and 150 mg O_2/L , according to Portuguese discharge regulations into sewerage systems and water bodies, respectively. It should be noted that: i) for discharge into water bodies, the photo-Fenton reaction must be performed until a biodegradable level is reached, able to be further biologically oxidized, in order to achieve a final COD equal or less than 150 mg O_2/L ; and ii) for discharge into sewerage systems, the photo-Fenton reaction must be carried out until achieving a maximum COD value of 1000 mg O_2/L . In the last case, an additional biological oxidation is not needed, as this step will be implemented in the domestic wastewater treatment plant (WWTP). In addition to experiments 1, 2 and 3, an ideal situation was defined. In the latter, a leachate with intermediate characteristics between the BTLS used in the experiments 2 and 3 was considered.

Figure 6.1 shows the average solar radiation power, insolation and cloud factor, according to the specific location of the sanitary landfill. Maximum values of approximately 20 W/m^2 in spring and summer seasons were recorded. This is in agreement with the lower cloud factor values associated with atmospheric transparency affected by all the atmospheric components that can absorb or scatter solar radiation. The total yearly hours of insolation depend on geographic location and were estimated by Gálvez and Rodríguez [18]. Values between 3500 h near the equator parallel to 2500 h from 40th and 50th parallels were obtained. In the present study, the total yearly hours of insolation and yearly average global UV radiation power, observed in the sanitary landfill, were 2944 hours and 17 W/m^2 , respectively. Accordingly, the total collectors' area (A_{CPC}) needed for the treatment of 100 m^3 of bio-treated leachate per day (annual average value), considering the two different COD targets and leachate characteristics, was between 3836-13525 m^2 .

Table 6.3. Operation data for the treatment of 100 m³/day of sanitary landfill leachate.

Parameter	Experiment 1		Experiment 2		Experiment 3	Optimal	
	1000*	150*	1000*	150*	1000*	1000*	150*
Daily flow – Q _d (m ³ /day)	100	100	100	100	100	100	100
Yearly volume - V _y ^a (m ³)	36500	36500	36500	36500	36500	36500	36500
Yearly average global UV irradiation – I _m ^b (W/m ²)	17	17	17	17	17	17	17
Total yearly hours of insolation – t _{ins} ^b (h)	2944	2944	2944	2944	2944	2944	2944
Yearly accumulated UV energy – E _y ^c (kJ _{UV} /m ²)	180809	180809	180809	180809	180809	180809	180809
DOC _i (mg C/L)	1534	1534	1129	1129	1135	~1200	~1200
DOC _f (mg C/L)	498	306	400	234	493	~518	~252
Min. ^d (%)	68	80	65	79	57	57	79
Alkalinity (g CaCO ₃ /L)	8.0	8.0	2.4	2.4	0.8	0	0
H ₂ SO ₄ /HCl (mM)	61/0	61/0	44/38	44/38	14	14	14
pH _m ^e	2.8	2.9	2.6	2.6	2.7	2.6-2.9	2.6-2.9
T _m ^e (°C)	33.9	35.2	34.3	37.0	41.1	30-40	30-40
Fe _m ^e (mg/L)	39.0	33.0	61.9	51.6	60.0	30-60	30-60
H ₂ O ₂ consumed (mM)	140	225	80	180	80	80	180
t _{PF} (h)	19.1	30.4	7.9	11.9	6.4	6-8	10-12
I _{UV} ^e (W/m ²)	25.0	25.9	25.7	24.8	33.1	25-33	25-33
Q _{UV} (kJ/L)	40	67	19	30	20	19	30
A _{CPC} ^f (m ²)	8075	13525	3836	6056	4037	3836	6056
T _{fm} (g C/h/m ²)	1.59	1.13	2.36	1.83	1.97	2.20	1.94
T _{fv} (L/h/m ²)	1.54	0.92	3.23	2.05	3.07	3.22	2.05
Land area required for the implementation of the CPCs – A _{land} (m ²)	24024	40175	11370	18030	12036	11370	18030
Number of solar photons per unit of time and potency - N _{ps} (photons/(W.h))	5.8x10 ²¹	5.8x10 ²¹	5.8x10 ²¹	5.8x10 ²¹	5.8x10 ²¹	5.8x10 ²¹	5.8x10 ²¹
Number of UV photons required – N _{uv} (photons)	2.4 x10 ³⁰	3.9x10 ³⁰	1.1x10 ³⁰	1.8x10 ³⁰	1.2x10 ³⁰	1.1x10 ³⁰	1.8x10 ³⁰

^aYearly volume of leachate generated from the sanitary landfill ($V_y = 365 \times Q_d$); ^bValues obtained from the integration of the yearly UV radiation data since August of the 2010 until July of the 2011, using 4 W/m² as the integration limit; ^cAccumulated UV energy since August of the 2010 until July of the 2011 ($E_y = 3.6 \times I_m \times t_{ins}$); ^dPhoto-Fenton mineralization ($1 - \text{DOC}_f / \text{DOC}_i$, %); ^epH_m, T_m, Fe_m and I_{UV} corresponds to average pH values, average temperature, average dissolved iron and average UV irradiance power observed during the photo-Fenton experiments; ^fCPCs area required ($A_{CPC} = 1000 \times Q_{UV} \times V_y / E_y$); *Targets COD expressed in mg O₂/L.

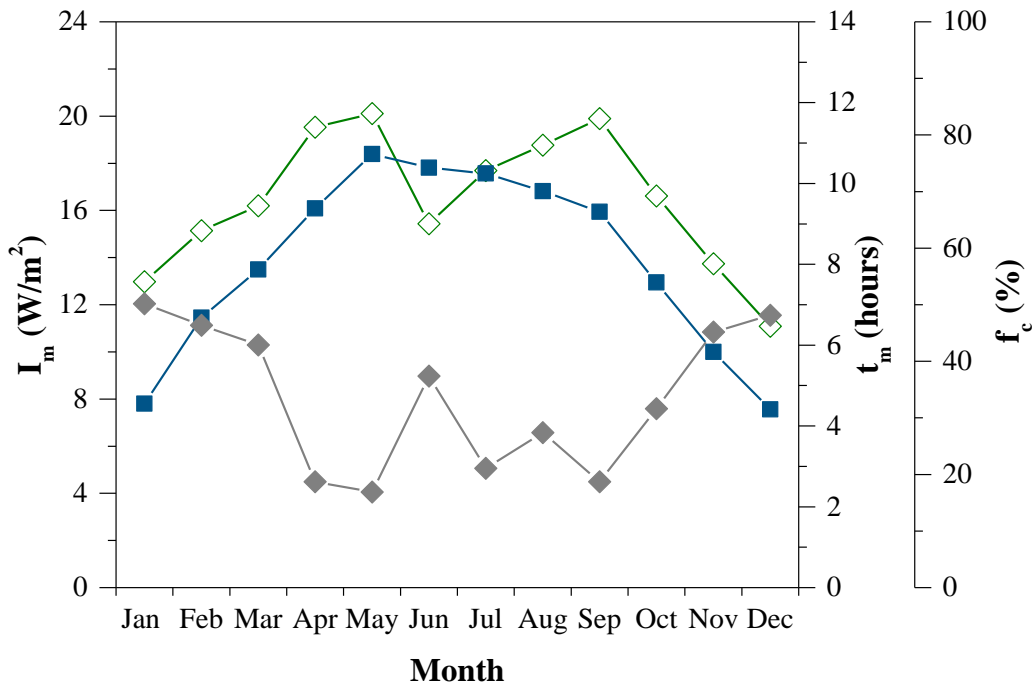


Figure 6.1. Average global UV irradiance (\diamond - I_m), insolation (\blacksquare - t_m) and ‘cloud factor’ (\blacklozenge - f_c) for global UV irradiance during the years 2010 and 2011 nearby Porto, Portugal.

The total collectors’ area (A_{CPC}) was calculated from the Eq. (6.1):

$$A_{CPC} = \frac{Q_{UV} \times V_y}{I_m \times t_{ins}} \quad (6.1)$$

where Q_{UV} is the accumulated UV energy required for the leachate treatment by the photo-Fenton reaction, V_y is the yearly volume of leachate generated from the sanitary landfill, I_m is the yearly average global UV radiation power and t_{ins} is the total yearly hours of insolation.

Based on the CPC area, Table 6.3 also presents the number of UV photons required, which is calculated from the Eq. (6.2):

$$N_{uv} = N_{ps} I_m t_{ins} A_{CPC} \quad (6.2)$$

where N_{uv} is the number of photons emitted up to wavelength of 387 nm, N_{ps} is the number of photons emitted up to wavelength of 387 nm per unit of time and potency according to the standard ASTM solar spectrum (assuming constant spectral distribution) (5.8×10^{21} photons/W/h) [18], I_m is the yearly average global UV irradiation (W/m²), t_{ins} is the total yearly hours of insolation (h) and A_{CPC} is the surface area of solar collector field (m²).

The maximum mass and volumetric treatment factors (T_{fm} and T_{fv}) (Eqs. (6.3) and (6.4)) are defined as the amount of removed organic substances ($\Delta m = (DOC_i - DOC_f) \times V_y$) or volume of contaminated water (V_y), respectively, which the system is able to treat per unit of time (t_{ins}) and area of solar collectors (A_{CPC}). In order to achieve a final COD of 1000 mg O₂/L, T_{fm} and T_{fv} values were 2.36 g C/h/m² and 3.23 L/h/m². If the goal is to achieve a final COD after biological treatment of 150 mg O₂/L, the T_{fm} and T_{fv} values were 1.83 g C/h/m² and 2.05 L/h/m².

$$T_{fm} = \frac{\Delta m(\text{g C})}{t_{ins}(\text{h}) \times A_{CPC}(\text{m}^2)} = \frac{(DOC_i - DOC_f) \times V_y}{t_{ins} \times A_{CPC}} \tag{6.3}$$

$$T_{fv} = \frac{V_y}{t_{ins} \times A_{CPC}} \tag{6.4}$$

Solar fixed collectors are south oriented (northern hemisphere) in order to capture the maximum amount of global UV energy, and tilted horizontally to a degree equal to the latitude (Porto city: 41°). The amount of land required for the implementation of the CPCs was calculated based on the total CPCs area required (2.04 m² modules tilted 41°) and on the distance between the CPCs parallel rows, in order to minimize the shadowing between collectors. For this purpose, the angle of sunlight at noon on 21 December (lowest maximum sun elevation; 26°) was used as a design parameter to define the CPCs row separation value at 3.94 m. Each CPC module of 2.04 m² occupies 5.55 m² of land, as can be seen in Figure 6.2.

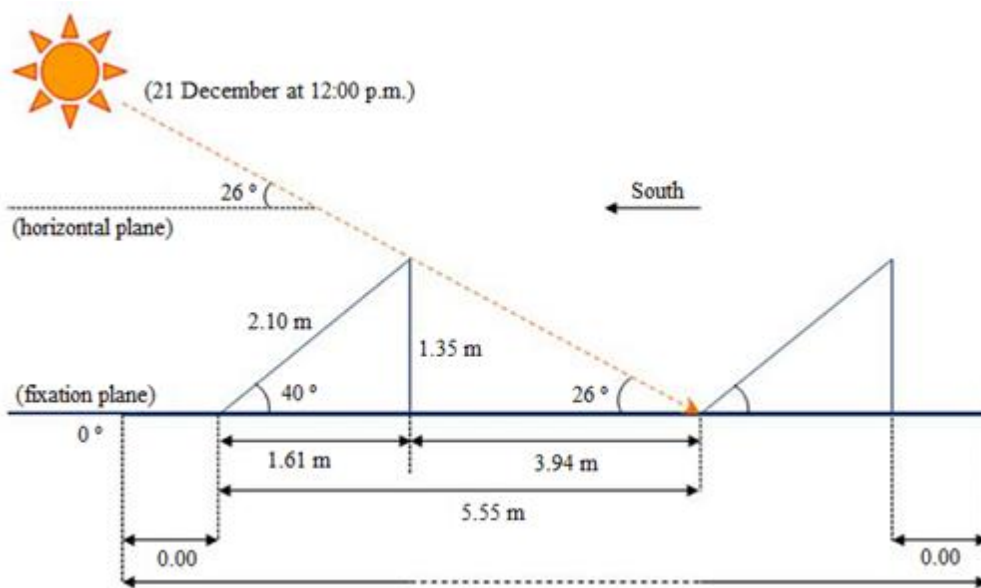


Figure 6.2. Illustrative scheme of the CPCs' configuration to a local with 41° of latitude.

Navntoft et al. [30] analysed 4 years of solar UV radiation measurements performed on tilted and horizontal planes located at Plataforma Solar de Almería, Spain. The authors showed that a photoreactor tilted 37° (local latitude), equator faced, will receive annually about 3-4% more UV energy than the horizontal plane. However, it was also showed that the best choice is to use different inclinations for each month (January (58.3°); February (50.3°), March (39.4°), April (27.8°), May (18.7°), June (14.4°), July (16.2°), August (23.6°), September (34.5°), October (46.1°), November (55.8°) and December (60.4°)) in order to have normal sun incidence onto the plane of interest, achieving 10% to 12% global UV gains. This is due to the large diffuse component in the UV range, a product of large Rayleigh scattering and aerosol absorption.

Considering the high land area required for the CPCs' implementation, i.e., 11370-40175 m² equivalent to 2.3 and 8.0 soccer fields (50 m \times 100 m), the costs with electric UV photons production were analysed together with the costs associated to capturing solar UV photons.

6.3.4 Solar UV photons versus electric UV photons

The comparison between solar and electric UV photons was performed considering only the costs associated with the photoreactor, given the similarity in the costs related to the rest of system [18]. The estimative of the unitary cost of the CPCs, according to their area, was given, five years ago, by the Portuguese Company Ao Sol Energias Renováveis, Lda, which had the CPCs patent (see Table 6.4). The company no longer exists.

Table 6.4. Estimative of the unitary cost of the CPCs according to their area.

A_{CPC} (m ²)	Cost (€)	A_{CPC} (m ²)	Cost (€)	A_{CPC} (m ²)	Cost (€)
12	1112	69	330	3448	158
14	974	230	215	4598	154
16	877	345	198	6897	145
23	658	1149	173	11494	129
29	555	2299	164	22989	89
46	412	2874	161	-	-

Table 6.5 shows the estimated yearly levelized cost (considering a fixed charge rate (FCR) of 12%, which is equivalent to 20-year plant depreciation period) to capture different number of solar UV photons (between the lowest and highest amount of UV photons needed to achieve a final COD of 150 and 1000 mg O₂/L), using: (i) different possible yearly average UV global irradiation; (ii) the Eq. (6.1)

to calculate the amount of CPC area required; and (iii) a power regression to express the CPC costs as a function of CPC area, according to values presented in Table 6.4. The total yearly hours of insolation depends on geographic location, and were estimated by Gálvez and Rodríguez [18] between 3500 h near the equator parallel to 2500 h from 40th and 50th parallels. In this study, it was used 2944 h with a yearly average global UV irradiation of 17 W/m².

Table 6.5. Estimative of costs to capture of 1.1×10^{30} , 1.8×10^{30} , 2.4×10^{30} and 3.9×10^{30} solar UV photons at different conditions of solar irradiation (FCR = 12%, 20 years).

Solar UV photons	E_y (kJ _{UV} /m ²)	I_m (W _{UV} /m ²)	t_{ins} (h)	A_{CPC} (m ²)	Investment Cost (€)	Yearly Cost (€/year)	Photon Cost (€/1x10 ²⁵ photons)
1.1×10³⁰	504000	40	3500	1355	232866	27944	0.25
	441000	35	3500	1548	262673	31521	0.29
	378000	30	3500	1806	301857	36223	0.33
	270000	25	3000	2529	408893	49067	0.45
	191520	20	2660	3565	567061	68047	0.62
	180809	17	2944	3776	594704	71364	0.65
	135000	15	2500	5057	757243	90869	0.83
	90000	10	2500	7586	1058919	127070	1.16
	27000	5	1500	25287	2866047	343926	3.13
1.8×10³⁰	504000	40	3500	2217	363100	43572	0.24
	441000	35	3500	2533	409577	49149	0.27
	378000	30	3500	2956	470675	56481	0.31
	270000	25	3000	4138	641449	76974	0.43
	191520	20	2660	5834	852135	102256	0.57
	180809	17	2944	6179	893674	107241	0.60
	135000	15	2500	8276	1137925	136551	0.76
	90000	10	2500	12414	1591260	190951	1.06
	27000	5	1500	41379	4306871	516825	2.87
2.4×10³⁰	504000	40	3500	2956	470675	56481	0.24
	441000	35	3500	3378	530921	63711	0.27
	378000	30	3500	3941	616082	73930	0.31
	270000	25	3000	5517	813741	97649	0.41
	191520	20	2660	7778	1081018	129722	0.54
	180809	17	2944	8239	1133714	136046	0.57
	135000	15	2500	11034	1443571	173228	0.72
	90000	10	2500	16552	2018671	242240	1.01
	27000	5	1500	55172	5463692	655643	2.73
3.9×10³⁰	504000	40	3500	4803	725587	87070	0.22
	441000	35	3500	5489	810306	97237	0.25
	378000	30	3500	6404	920479	110458	0.28
	270000	25	3000	8966	1215799	145896	0.37
	191520	20	2660	12639	1615135	193816	0.50
	180809	17	2944	13388	1693867	203264	0.52
	135000	15	2500	17931	2156819	258818	0.66
	90000	10	2500	26897	3016069	361928	0.93
	27000	5	1500	89655	8163229	979587	2.51

Table 6.6 presents the estimated costs associated to the generation of electric UV photons, which were predicted considering UV lamps of 4 kW, with dominant emission spectrum at 365 nm, and according to manufacturer data, an average lamp life time (t_{LL}) of 20,000 hours and average efficiency of UV-photon production of about 20%, during its lifetime.

Table 6.6. Estimative of costs associated to the generation of electric UV photons (lamps with 4 kW, 20,000 hours of total operation and 8760 hours of yearly operation (t_{LO})), comparing electricity cost of 0.10 and 0.15 €/kWh (FCR=12%, 20 years).

Number of Electric UV photons	Unitary cost (€)	1.1×10³⁰	1.8×10³⁰	2.4×10³⁰	3.9×10³⁰
Number of lamps		24	39	52	84
Lamp, Ballast and accessories	500	11869	19421	25895	42080
Lamp reactor cost	100	2374	3884	5179	8416
A) Investment cost	600	14242	23306	31074	50496
Yearly electricity cost (0.10€/kWh)	3504	83176	136106	181474	294896
Lamp replacement	219	5198	8507	11342	18431
Labour cost of lamp replacement	3.15	75	122	163	265
B) Operation cost	3726	88449	144735	192980	313592
Yearly cost: A×FCR+B	3798	90158	147532	196709	319652
Cost per 1×10²⁵ UV photons		0.82	0.82	0.82	0.82
Lamp, Ballast and accessories	500	11869	19421	25895	42080
Lamp reactor cost	100	2374	3884	5179	8416
A) Investment cost	600	14242	23306	31074	50496
Yearly electricity cost (0.15€/kWh)	5256	124764	204159	272212	442344
Lamp replacement	219	5198	8507	11342	18431
Labour cost of lamp replacement	3.15	75	122	163	265
B) Operation cost	5478	130037	212788	283717	461040
Yearly cost: A×FCR+B	5550	131746	215585	287446	467100
Cost per 1×10²⁵ UV photons		1.20	1.20	1.20	1.20

The number of lamps (N_L) was calculated using Eq. (6.5), considering 8760 hours of operation per year (t_{LO}), a photonic flux (ϕ) of 5.29×10^{24} photons/s and the required photons number (N_{UV}). The photonic flux was calculated based on the energy of 1-photon ($E_{ph} = h \times c / \lambda$, [31]) and the UV lamp characteristics, using Eq. (6.6):

$$N_L = \frac{N_{UV}}{\phi \times t_{LO}} \quad (6.5)$$

$$\varphi = \frac{P_L \times \lambda}{h \times c} \eta \quad (6.6)$$

where P_L is the lamp power (4,000 W), λ is the maximum emission peak wavelength (365 nm), h is the Planck constant (6.63×10^{-34} J×s), c is the speed of light (3.0×10^8 m/s) and η is the lamp efficiency (20%).

The annual costs associated to the UV lamp replacement (C_R), as well as the cost associated to the labor needed to this operation (C_{LR}) were given by Eq. (6.7) and (6.8), respectively:

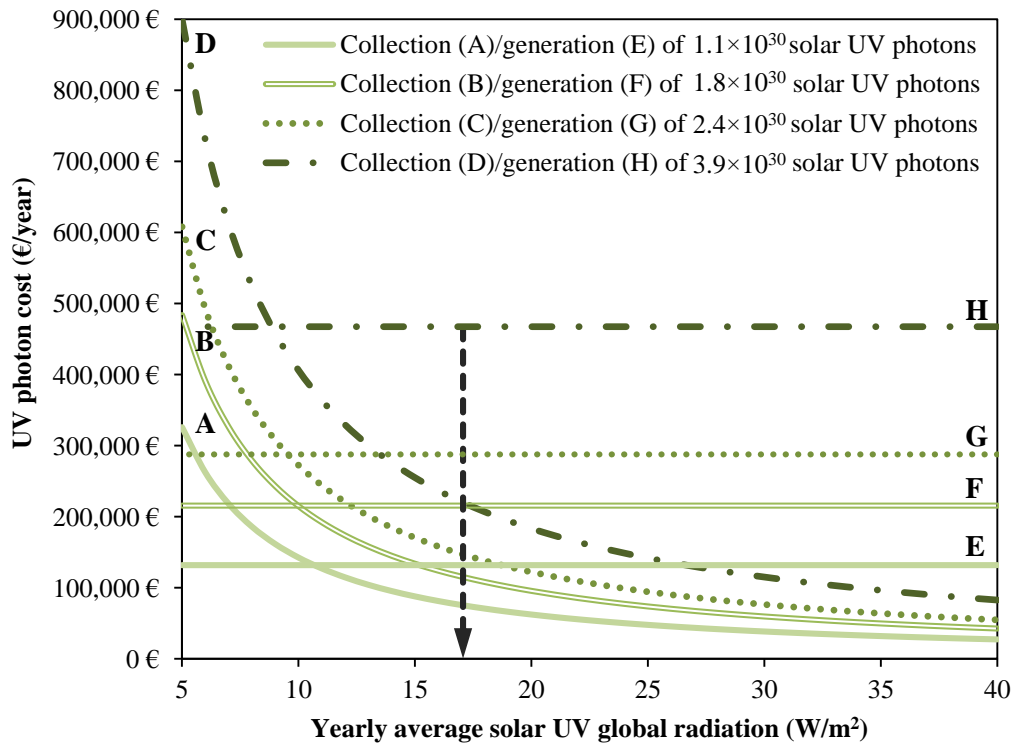
$$C_R = C_L \times \frac{t_{LO}}{t_{LL}} \quad (6.7)$$

$$C_{LR} = C_{LR,IL} \times \frac{t_{LO}}{t_{LL}} \quad (6.8)$$

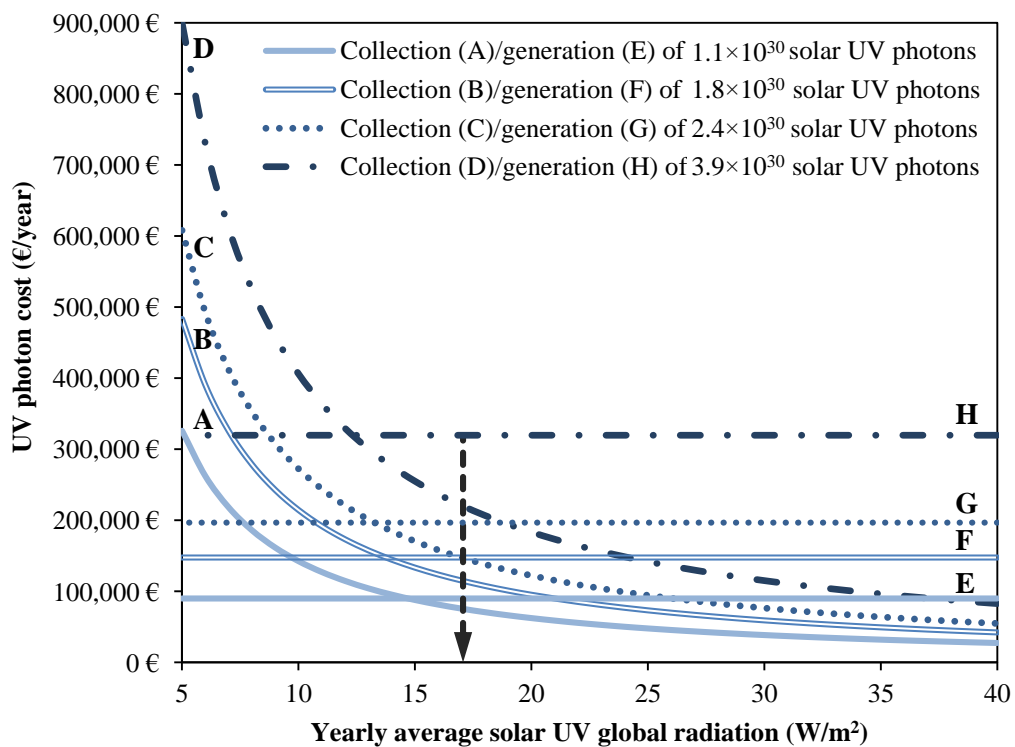
where C_L and $C_{LR,IL}$ are the costs with 1-lamp and the labor to replace 1-lamp, respectively, and the t_{LO} and the t_{LL} are the operation and life times of the lamp, respectively.

Figure 6.3 shows the cost comparison amongst UV photons produced by CPC technology and electric lamps, taking into account four different values of UV photons collected ($N_{UV} = 1.1 \times 10^{30}$, 1.8×10^{30} , 2.4×10^{30} and 3.9×10^{30} UV photons, which correspond to the lowest and highest amount of UV photons (N_{UV}) presented in the Table 6.3), and considering two different costs of electric energy (0.10 and 0.15 €/kWh). The UV photon cost for CPCs was calculated applying a power regression between the total yearly cost and the yearly average solar UV global radiation according to the values presented in Table 6.5. The electric UV photons cost corresponds to the total yearly cost presented in the Table 6.6, which is independent of the yearly average solar UV global radiation. The main difference on the total yearly cost, considering both types of photons sources, is related to the investment and operation components. Using solar energy the investment cost is higher than the operational cost. On the other hand, the opposite happens when using electrical power [18, 24, 32].

Figure 6.3 shows that for a yearly average solar UV global radiation of 17 W/m^2 (correspondent to the yearly average radiation observed at the sanitary landfill), the cost of electric UV photons generation is higher than the cost of solar UV photons collection and is independent of the UV photons number and electricity cost studied. However, the difference between these costs increases proportionally to the electric energy cost.



(a)



(b)

Figure 6.3. Costs of UV photons collected using CPCs and UV photons generated with electric lamps (electricity costs of (a) 0.15 €/kWh and (b) 0.10 €/kWh) (Based on Gálvez and Rodríguez [18] and information obtained in a market study).

Taking as an example the experiments with the highest and the lowest UV photons requirements (3.9×10^{30} and 1.1×10^{30}), the cost of the electric UV photons production is 1.6 and 1.3 times higher than the cost of solar UV photons capture, considering an electricity cost of 0.10 €/kWh. If the electricity cost increases to 0.15 €/kWh, this scenario is aggravated and as a result, the cost of electrical photons becomes 2.3 and 1.8 higher than the cost of solar photons, respectively.

It is evident that electrical photons are more expensive than solar photons. However, the CPCs implementation is unreasonable since a high land area is required for the CPCs' implementation, mainly for the treatment of leachate in the same conditions of Experiment 1 ($A_{land} > 24000 \text{ m}^2$). Considering this limitation, the possible combination of natural and artificial radiation, taking into account the monthly accumulated UV energy, was evaluated.

6.3.5 Assessment of CPCs area and UV lamps requirements according to monthly variations of solar radiation

Another promising setup for the radiation source, in the treatment of sanitary landfill leachates by the photo-Fenton reaction, is the simultaneous application of CPCs and UV lamps. In order to evaluate this scenario, it was calculated the accumulated solar UV energy for each month and the correspondent CPCs area. The latter was performed taking into account the accumulated UV energy (Q_{UV}) required in each experiment, the leachate's volume to be treated, meeting the final goals of COD less than 150 and 1000 mg O₂/L. Figure 6.4 presents the monthly accumulated solar UV energy (E_m) and the leachate's volume to be treated (V_m), as well as the CPCs area (A_{CPC}) and the number of UV lamps required (4 kW, continuous 24-h operation), considering that the smallest CPCs area (relative to the month with higher radiation) would be implemented.

The minimum CPCs area was achieved in May, ranging between 2446 and 8626 m² ($Q_{UV} = 19$ and 67 kJ/L, respectively), since it was the month with higher accumulated solar UV energy. Implementing the CPCs areas obtained for May, the use of UV lamps would not be needed, considering the COD targets and UV doses for each experiment conditions. On the other hand, in December, in order to compensate the lack of solar radiation, 18 to 65 UV lamps would be needed (maximum number of UV lamps), with a nominal power of 4 kW and in continuous 24-h operation, aiming at COD values below 1000 and 150 mg O₂/L. This can be considered a good alternative for minimizing the operational costs related to electrical energy, as well as the investment costs associated to solar technologies.

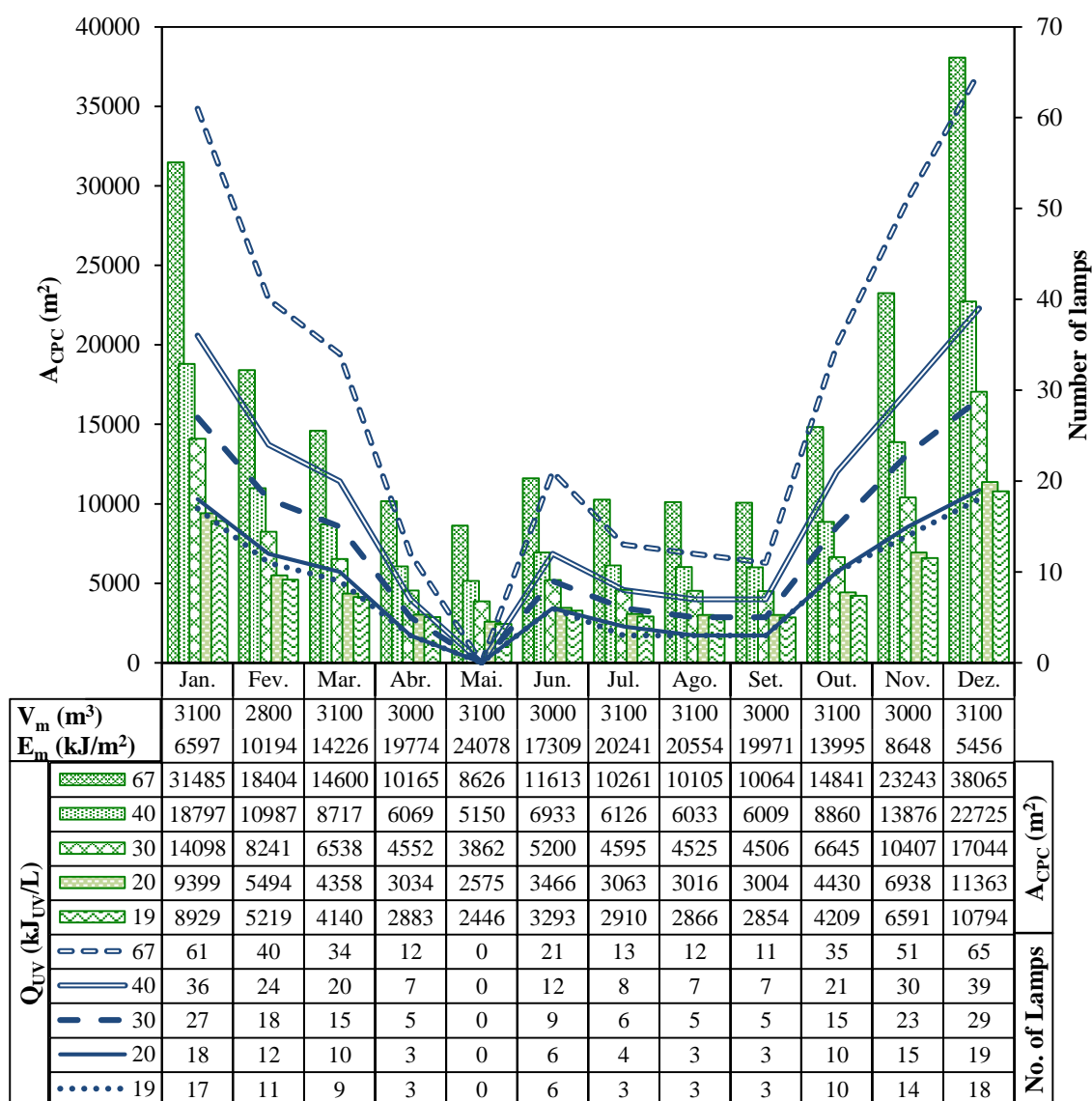


Figure 6.4. Assessment of CPCs area (bars) and number of lamps (lines) required for each month of the year, considering different operating conditions.

6.3.6 Reagents costs

The consumption of reagents and the unitary cost associated with experiments 1-3 and operation in optimal conditions are presented in Table 6.7. As expected, the bio-treated leachate with low alkalinity and ammonium (which works as buffer) contents, results in 76% reduction of sulphuric acid requirements for the preliminary acidification step of the photo-Fenton process. Consequently, the sulphate concentration decreases and the photo-Fenton reaction velocity increases since the predominant iron species will be $FeOH^{2+}$, which is the most photoactive ferric-water complex [9, 27].

Table 6.7. Cost associated to reagents consumption, considering different operability conditions.

		Reagent					Total	Total annual cost (€)		
		H ₂ O ₂	FeSO ₄	H ₂ SO ₄	HCl	NaOH				
% (w/w)		50 ^b	-	98	33	30	-	-		
ρ (kg/L)		1.1	-	1.84	1.16	1.33	-	-		
Reagent cost (€/ton)		390	300	155	115	160	-	-		
Consumption (L/m ³)	Exp. 1	1000 ^a	9	0.4 ^c	3.3	0	1.9	-	-	
		150 ^a	14.4	0.4 ^c	3.3	0	1.9	-	-	
	Exp. 2	1000 ^a	5	0.4 ^c	1	3.6	1.9	-	-	
		150 ^a	11.3	0.4 ^c	1	3.6	1.9	-	-	
	Exp. 3	1000 ^a	4.8	0.4 ^c	0.8	0	1.6	-	-	
	Optimal	1000 ^a	5	0.4 ^c	0.8	0	1.6	-	-	
		150 ^a	11.3	0.4 ^c	0.8	0	1.6	-	-	
	Unitary cost (€/m ³)	Exp. 1	1000 ^a	3.71	0.12	0.94	0	0.4	5.17	188,995
			150 ^a	5.97	0.12	0.94	0	0.4	7.43	271,321
		Exp. 2	1000 ^a	2.12	0.12	0.28	0.48	0.4	3.4	124,519
150 ^a			4.78	0.12	0.28	0.48	0.4	6.06	221,370	
Exp. 3		1000 ^a	2.12	0.12	0.23	0	0.34	2.81	102,582	
Optimal		1000 ^a	2.12	0.12	0.23	0	0.34	2.81	102,582	
	150 ^a	4.78	0.12	0.23	0	0.34	5.47	199,437		

^aCOD targets expressed in mg O₂/L; ^bValue expressed in % (w/v); ^cValues expressed in kg/m³.

For the optimal conditions, the cost with methanol in a biological pre-oxidation step was calculated, considering that the raw leachate presented 4 g/L of nitrogen and taking into account the methanol consumption reported in Chapter 5. Figure 6.5 shows that at optimal conditions the cost with H₂O₂ is the most representative, considering or not the methanol addition. In the absence of methanol addition, the cost of H₂O₂ corresponds to 87 and 76% of the yearly total cost of reagents (199,438 € and 102,583 €), respectively for COD target values of 150 and 1000 mg O₂/L. If the methanol addition is taken into account, the contribution of H₂O₂ decreases, representing 68 and 49% of the total annual amount spent on reagents (255,648 € and 158,793 €), respectively for COD target values of 150 or 1000 mg O₂/L. Methanol costs are also important and equal to 22 and 35%, considering the same COD target values.

Cassano et al. [10] obtained an unit cost for H₂O₂ of 1.24 € per 1 m³ of bio-treated leachate fed to the photo-Fenton process, which is approximately 4 times less than the amount obtained for the Experiment 2, considering a target COD of 150 mg O₂/L. This discrepancy can be associated with the leachate physico-chemical characteristics at the beginning of photo-Fenton reaction. The leachate used by the authors presented TSS, DOC and COD concentrations 5.0, 2.6 and 3.2 times lower, respectively.

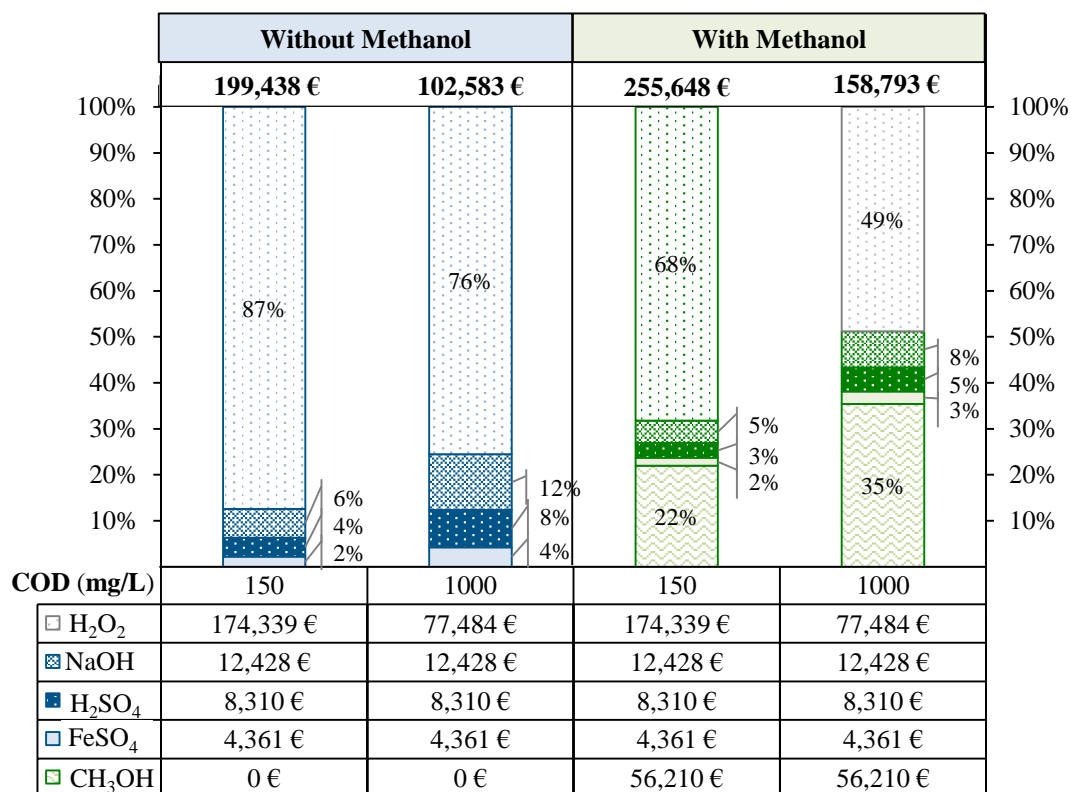


Figure 6.5. Yearly total cost of reagents for the optimal conditions, with and without methanol contribution, considering target COD values of 150 and 1000 mg O₂/L.

Bauer and Fallmann [11] achieved a total reagents cost of 84 ATS/m³ (6.1 €/m³) for the treatment of a landfill leachate, considering DOC abatement from 545 to 218 mg/L, using a photo-Fenton process under artificial and solar radiation. The total reagents cost is only 11.5% higher than the unitary cost achieved in this work for the optimal conditions, regarding the COD target of 150 mg O₂/L ($\Delta\text{DOC} \approx 1200\text{-}252$ mg/L). The main leachate characteristics that influence the photo-Fenton reagents cost are alkalinity and organic matter content. The optimization of the preliminary biological pretreatment, considering the minimization of those two variables, allows a considerable reduction on photo-Fenton reagents cost.

In order to minimize the consumption of methanol and alkalinity, the bio-treatment sequence could be an anoxic reactor followed by an aerobic reactor with recirculation to the anoxic reactor, taking advantage of the: i) biodegradable organic carbon fraction of the raw leachate, which corresponds to 54% of the organic carbon necessary for denitrification; and ii) raw leachate alkalinity in addition to the one produced during denitrification, which would be sufficient to reach complete nitrification. Moreover, this pretreatment promotes the removal of the biodegradable organic carbon fraction and, consequently, also contributes for the reduction of accumulated UV energy and H₂O₂ consumption, during photo-Fenton reaction.

6.3.7 Total cost: comparison of the leachate phototreatment using CPCs and/or UV lamps

The overall costs associated with the sanitary landfill leachate treatment by a photo-Fenton process to achieve a final wastewater with a COD of 150 and 1000 mg O₂/L, were determined: i) taking into account facilities, project's contingencies, system engineering and assembly, spare parts, personnel, maintenance material, electric and chemical supplies; and ii) not considering the costs related to the biological treatments, before or after the photo-Fenton process.

The total yearly cost (*TYC*) with the leachate phototreatment is based on the initial installation cost and the operating costs (*OC*) [18, 33], according to Eq. (6.9):

$$TYC = TCR \times FCR + OC \quad (6.9)$$

where, TCR is the total capital required for the initial investment with the facility, including piping and tanks, auxiliary equipment and control and others (direct cost), more contingencies and spare parts (indirect cost); FCR is the fixed charge rate, estimated in 12% for 20-year plant depreciation. The product of the TCR by the FCR represents the annual capital cost. The operating costs include the expenses with consumables (reagents), operation and maintenance, and electricity and lamps replacement when artificial light is used.

The scale-up and economic assessment of the photocatalytic facility were performed considering: i) operating conditions of the experiments 1, 2 and 3 and the optimal settings; ii) a leachate derived from a biological pre-oxidation process; iii) leachate final COD values below 150 or 1000 mg O₂/L; iv) three different setups to take advantage of the UV radiation. The setups consider i) the use of only natural sunlight, through CPCs technology, for capturing UV photons (Table 6.8); ii) the application of artificial radiation using solely UV lamps (Table 6.9); iii) the combination of natural and artificial radiation, using CPCs and UV Lamps, according to the UV radiation energetic needs along the year (Table 6.10).

The usage of CPCs requires a high initial investment with the total capital required comprised between 800,000 € and 2,000,000 €. This amount can be amortized along 20-year, with a 12% FCR, corresponding to about 39 and 49% of the total yearly cost (see Table 6.8 and Figure 6.6), depending on the characteristics of the leachate. It is possible to observe, in Table 6.2 and Table 6.8, that the cost of the photo-Fenton process increases proportionally to pollution load, as reported by Pérez et al. [25].

Table 6.8. Yearly cost associated to sanitary landfill leachate treatment using CPC technology considering different operating conditions.

Target COD (mg O ₂ /L)	Experiment 1		Experiment 2		Experiment 3	Optimal	
	150	1000	150	1000	1000	150	1000
Direct Cost:							
CPCs area (m ²)	13525	8075	6056	3836	4037	6056	3836
A – Total collector cost	1,656,061 €	1,142,731 €	899,841 €	599,709 €	628,420 €	899,841 €	599,709 €
B – Piping and tanks (8% of A)	132,485 €	91,419 €	71,987 €	47,977 €	50,274 €	71,987 €	47,977 €
C – Auxiliary equipment and controls (10% of A)	165,606 €	114,273 €	89,984 €	59,972 €	62,842 €	89,984 €	59,971 €
D – Others (15% of A)	248,409 €	171,410 €	134,976 €	89,956 €	94,263 €	134,976 €	89,956 €
Total Direct Cost (TDC = A + B + C + D)	2,202,561 €	1,519,837 €	1,196,788 €	797,613 €	835,799 €	1,196,788 €	797,613 €
Indirect Cost:							
E – Contingencies (12% of TDC)	264,307 €	182,380 €	143,615 €	95,714 €	100,296 €	143,615 €	95,714 €
F – Spare parts (1% of TDC)	22,026 €	15,198 €	11,968 €	7,976 €	8,358 €	11,968 €	7,976 €
Total Capital Required (TCR = TDC + E + F)	2,488,894 €	1,717,416 €	1,352,370 €	901,303 €	944,452 €	1,352,370 €	901,303 €
Yearly Cost:							
G – Capital (12% of TCR, 20 years)	298,667 €	206,090 €	162,284 €	108,156 €	113,334 €	162,284 €	108,156 €
H – Consumables	271,322 €	188,995 €	221,374 €	124,519 €	102,583 €	199,438 €	102,583 €
I – Operation and maintenance ^a	37,800 €	37,800 €	37,800 €	37,800 €	37,800 €	37,800 €	37,800 €
Total Yearly Cost (TYC = G + H + I)	607,789 €	432,885 €	421,457 €	270,476 €	253,717 €	399,522 €	248,539 €
Unitary Cost (UC = TYC/V_y)	16.65 €/m³	11.86 €/m³	11.55 €/m³	7.41 €/m³	6.95 €/m³	10.95 €/m³	6.81 €/m³

^aThe costs associated with the operation and maintenance include the expenses with personal and electric power.

Table 6.9. Yearly cost associated to sanitary landfill leachate treatment with resource to UV lamps (4 kW, 20000 hours of total operation and 8760 hours of yearly operation) considering different operating conditions.

Target COD (mg O ₂ /L)	Experiment 1		Experiment 2		Experiment 3	Optimal	
	150	1000	150	1000	1000	150	1000
Direct Cost:							
Cost with lamps:							
Number of lamps (NL ^a)	86	51	39	25	26	39	25
A – Lamp, Ballast and accessories (500NL)	43,000 €	25,500 €	19,500 €	12,500 €	13,000 €	19,500 €	12,500 €
B – Lamp reactor cost (100NL)	8,600 €	5,100 €	3,900 €	2,500 €	2,600 €	3,900 €	2,500 €
Lamp Total Cost (LTC = A + B)	51,600 €	30,600 €	23,400 €	15,000 €	15,600 €	23,400 €	15,000 €
C – Pimping and tanks ^b	132,485 €	91,419 €	71,987 €	47,977 €	50,274 €	71,987 €	47,977 €
D – Auxiliary equipment and control ^b	165,607 €	114,273 €	89,984 €	59,971 €	62,842 €	89,984 €	59,971 €
E – Others ^b	248,410 €	171,410 €	134,976 €	89,956 €	94,263 €	134,976 €	89,956 €
Total Direct Cost (TDC = LTC + C + D + E)	598,100 €	407,703 €	320,347 €	212,904 €	222,979 €	320,347 €	212,904 €
Indirect Cost:							
F – Contingencies (12% of TDC)	71,772 €	48,924 €	38,442 €	25,548 €	26,757 €	38,442 €	25,548 €
G – Spare parts (1% de TDC)	5,981 €	4,077 €	3,203 €	2,129 €	2,230 €	3,203 €	2,129 €
Total Capital Required (TCR = TDC + F + G)	675,853 €	460,704 €	361,993 €	240,581 €	251,966 €	361,993 €	240,581 €
Yearly cost:							
H – Capital (12% of TCR, 20 years)	81,102 €	55,284 €	43,439 €	28,870 €	30,236 €	43,439 €	28,870 €
I – Consumables	271,322 €	188,995 €	221,374 €	124,519 €	102,583 €	199,438 €	102,583 €
J – Operation and maintenance	37,800 €	37,800 €	37,800 €	37,800 €	37,800 €	37,800 €	37,800 €
K – Electricity cost (0.10€/kWh)	301,344 €	178,704 €	136,656 €	87,600 €	91,104 €	136,656 €	87,600 €
L – Lamp replacement ^a	18,834 €	11,169 €	8,541 €	5,475 €	5,694 €	8,541 €	5,475 €
M – Labour cost with lamp replacement ^a	271 €	161 €	123 €	79 €	82 €	123 €	79 €
Total Yearly Cost (TYC = H + I + J + K + L + M)	710,673 €	472,114 €	447,933 €	284,343 €	267,499 €	425,997 €	262,406 €
Unitary Cost (UC = TYC/V_y)	19.47 €/m³	12.93 €/m³	12.27 €/m³	7.79 €/m³	7.33 €/m³	11.67 €/m³	7.19 €/m³

^aThe number of lamps, as well as the cost with the UV lamps replacement and the cost associated to the labour can be calculated from the Eq.s (6.5)-(6.8). ^bThe costs associated with the secondary equipment (rubrics C, D and E) were considered equal to those achieved in the case of using only CPCs (rubrics B, C and D of the Table SM-6, respectively), since the difference between solar and electric UV photons is only affected by the photocatalytic reactor, being the remaining components fairly similar [18].

Table 6.10. Yearly cost associated to sanitary landfill leachate treatment combining CPCs technology with UV lamps (4 kW, 20,000 hours of total operation and 8,760 hours of yearly operation) considering different operating conditions.

Target COD (mg O ₂ /L)	Experiment 1		Experiment 2		Experiment 3	Optimal	
	150	1000	150	1000	1000	150	1000
Direct Cost							
Principal Equipment:							
Collectors area	8626	5150	3862	2446	2575	3862	2446
A – Total collector cost	1,204,096 €	781,519 €	603,544 €	396,832 €	415,624 €	603,544 €	396,832 €
Number of lamps (NL)	66	40	30	19	20	30	19
B – Lamp, Ballast and accessories (500NL)	33,000 €	20,000 €	15,000 €	9,500 €	10,000 €	15,000 €	9,500 €
C – Lamp reactor cost (100NL)	6,600 €	4,000 €	3,000 €	1,900 €	2,000 €	3,000 €	1,900 €
Principal Equipment Total Cost (PETC = A + B + C)	1,243,696 €	805,519 €	621,544 €	408,232 €	427,624 €	621,544 €	408,232 €
D – Piping and tanks (8% of PETC)	99,496 €	64,442 €	49,723 €	32,659 €	34,210 €	49,723 €	32,659 €
E – Auxiliary equipment and controls (10% of PETC)	124,370 €	80,552 €	62,154 €	40,823 €	42,762 €	62,154 €	40,823 €
F – Others (15% of PETC)	186,554 €	120,828 €	93,232 €	61,235 €	64,144 €	93,232 €	61,235 €
Total Direct Cost (TDC = PETC + D + E + F)	1,654,115 €	1,071,340 €	826,653 €	542,949 €	568,740 €	826,653 €	542,949 €
Indirect Cost							
G – Contingencies (12% of TDC)	198,494 €	128,561 €	99,198 €	65,154 €	68,249 €	99,198 €	65,154 €
H – Spare parts (1% of TDC)	16,541 €	10,713 €	8,267 €	5,429 €	5,687 €	8,267 €	5,429 €
Total Capital Required (TCR = TDC + G + H)	1,869,150 €	1,210,614 €	934,118 €	613,532 €	642,676 €	934,118 €	613,532 €
Yearly Cost							
I – Capital (12% of TCR, 20 years)	224,298 €	145,274 €	112,094 €	73,624 €	77,121 €	112,094 €	73,624 €
J – Consumables	271,322 €	188,995 €	221,374 €	124,519 €	102,583 €	199,438 €	102,583 €
K – Operation and maintenance	37,800 €	37,800 €	37,800 €	37,800 €	37,800 €	37,800 €	37,800 €
L – Electricity cost^a	105,792 €	62,678 €	46,339 €	28,858 €	30,317 €	46,339 €	28,858 €
M – Lamp replacement^a	2,156 €	1,277 €	944 €	588 €	618 €	944 €	588 €
N – Labour cost with lamp replacement^a	95 €	56 €	42 €	26 €	27 €	42 €	26 €
Total Yearly Cost (TYC = I + J + K + L + M + N)	641,463 €	436,081 €	418,593 €	265,415 €	248,466 €	396,657 €	243,479 €
Unitary Cost (UC = TYC/V_y)	17.57 €/m³	11.95 €/m³	11.47 €/m³	7.27 €/m³	6.81 €/m³	10.87 €/m³	6.67 €/m³

^aMinimum CPCs area and maximum number of UV lamps required throughout the year which correspond to the values obtained in May and December, respectively (months in which it wouldn't be necessary to use UV lamps and it would be necessary to use the highest amount of UV lamps, respectively); ^bThese amounts change monthly according to needs of UV lamps number expressed on Figure 6.4.

Comparing the total unitary cost (Table 6.8) with the volumetric treatment factor (Table 6.3), one can verify that, in general, the unitary cost decreases with the increase of the treatment factor. This means that, as expected, the increment of the amount of contaminated wastewater to be treated leads to the reduction of the total unitary cost [25]. The leachate phototreatment has an average cost of 0.021 € per hour and square meter. Regarding the optimal conditions, it can be seen that in order to achieve a target COD of 150 mg O₂/L instead 1000 mg O₂/L, the unitary cost increases from 6.8 until 11.0 €/m³. Depending on the legislation applied in each municipality, it can be advantageous the discharge into the aquatic environment or to pay to discharge into the sewerage system.

De Torres-Socías et al. [3] performed a cost analysis for the treatment of 40 m³/day of a landfill leachate, previously treated by a physico-chemical process, using a solar photo-Fenton process (27% mineralization, final DOC = 8 g/L). The estimated operating cost was 43€/m³. This value is considerably higher (about 4 times) than the one obtained in this study (for optimal conditions and COD < 150 mg O₂/L), most likely due to the high organic load, which required a substantially higher amount of H₂O₂ (22 g/L) and energy (137 kJ/L) to achieve an effluent with a biodegradability higher than 70%. However, the cost per unit of DOC removal was only 1.2 times greater (14.3 € per 1 kg of DOC eliminated when compared to 11.6 € per 1 kg of DOC removed).

Gumy et al. [19] estimated a unitary treatment cost of 7.2 €/m³, considering the treatment of 1000 m³ per year of a wastewater contaminated with 0.2 mM of Orange II (TOC~38 mg/L), using a solar-photo-Fenton reaction. This treatment cost is very similar (+5%) to the value obtained in the present study, considering a COD target of 1000 mg O₂/L, in the optimal conditions. Gálvez and Rodríguez [18] presented a study of a solar detoxification plant with 200 m² of CPCs, for the treatment of 6000 m³/year of a wastewater containing pesticides, using Fenton's reagent. The authors obtained an annual treatment cost of 9.5 €/m³, which is quite close (-13%) to the value calculated in our study, considering a COD target of 150 mg O₂/L, in the optimal conditions. The unitary treatment cost for a wastewater from a sewage system, in Malaysia, using a solar detoxification process with TiO₂ and CPCs technology was reported by Jubran et al. [34]. They achieved a value of US\$ 42 per 1000 gallons (≈8.3 €/m³). Even though a different photocatalytic process was used, the cost obtained is in the range of the values presented in this work, for the same UV photons capture system.

The use of UV lamps was considered with approximately 20,000 hours of lifetime, in a continuous operation during 24 hours per day and 365 days per year (8760 hours), and with a nominal power of 4 kW, corresponding to a photonic flux of 5.29×10²⁴ photons/s. As expected, the expense with the leachate treatment is greater when using UV lamps rather than the situation in which CPCs are exclusively used. When only UV lamps are used an increment on the costs is verified and is associated

to electric power and the costs with reagents remain the same, when compared with CPCs technology, as reported by García-Montaño et al. [35]. The drastic increase of electric power cost represents between 27%, for optimal settings, and 42%, for experiment 1, of the total yearly cost. In return, the contribution of amortization capital is very low, corresponding to less than 12% of the annual cost (see Table 6.9 and Figure 6.6). The unitary cost with electric power (2.4-8.3 €/m³) is by far lower than the cost obtained by Bauer and Fallmann [11] (56.7 €/m³), considering the treatment of 8 L of leachate with a UV lamp of 400 W.

Table 6.9 shows that for the different treatment conditions, the total unitary cost decreases from 19.5 to 7.3 €/m³, being in optimal conditions equal to 11.7 and 7.2 €/m³, regarding targets COD of 150 and 1000 mg O₂/L, respectively. The total cost in order to achieve a COD of 150 mg O₂/L was very close to the amount estimated by Muñoz et al. [24] (12.1 €/m³), considering the treatment of 2500 m³ per year of an industrial wastewater containing 500 mg/L of alpha-methyl-phenylglycine.

The use of CPCs and UV lamps reduce the yearly capital cost in more than 20% and the annual expenses related to electric power and lamps replacement in 60%, when compared to the application of only CPCs or UV lamps, respectively. The costs with consumables, operation and maintenance remain the same (see Table 6.10 and Figure 6.6).

Di Iaconi et al. [14] presented an operating cost of 4 €/m³ for a medium-age landfill leachate treatment, using a sequencing batch biofilter granular reactor enhanced by ozonation, with the purpose of disposal into sewerage system. The cost obtained is only 15% lower than the value obtained in this work using the optimal conditions, to reach a COD below 1000 mg O₂/L (4.7 €/m³). The total unitary cost obtained for this configuration varies between 17.6 and 6.8 €/m³, regarding experiments 1, 2 and 3, being in the best conditions equal to 10.9 and 6.7 €/m³, for COD values of 150 and 1000 mg O₂/L, respectively.

In Portugal, the Regulatory Institute for Water and Wastes (IRAR, in Portuguese: Instituto Regulador de Águas e Resíduos) [36] identified 341 waste dumps, 8 closed sanitary landfills and 34 open sanitary landfills. In 2006, the leachate of 19% of the 42 reported landfills was discharged directly in a WWTP for full treatment. For the other cases (4 closed landfills and 30 open landfills), the leachate was discharged into one of the 32 existing LTPs (Leachate Treatment Plants), either for: i) pre-treatment and subsequent final treatment in a WWTP (47% of the situations); or ii) for full treatment and disposal into water bodies (64%). IRAR showed that for about 80% of existing landfills, the leachate treatment efficiency doesn't fulfil the requisites originally defined in the projects. Furthermore, it was verified that, in general, in order to achieve a higher treatment efficiency for stabilized leachates, it is necessary the usage of membrane separation units, where the total cost can range between 3.9 and 10.8 €/m³. One of

the sanitary landfills uses an evaporation/condensation system over membrane units for the leachate treatment, resulting in a final wastewater with high quality but at much superior costs (25 €/m³). Given the current Portuguese situation, it can be said that the treatment strategies proposed in this work are promising and economically viable.

Figure 6.6 also compares the total unitary cost for each treatment configuration (CPCs; UV lamps and CPCs + UV lamps) aiming to achieve COD values below 150 and 1000 mg O₂/L. For all situations, the total costs based on experiment 1 greatly exceed the costs based on experiments 2 and 3, mostly due to the initial concentration of sulphate and alkalinity (which implies the addition of higher amounts of sulphuric acid). This negatively affects the photo-Fenton reaction rates and increases the energetic needs, requiring a higher CPCs area and more UV lamps.

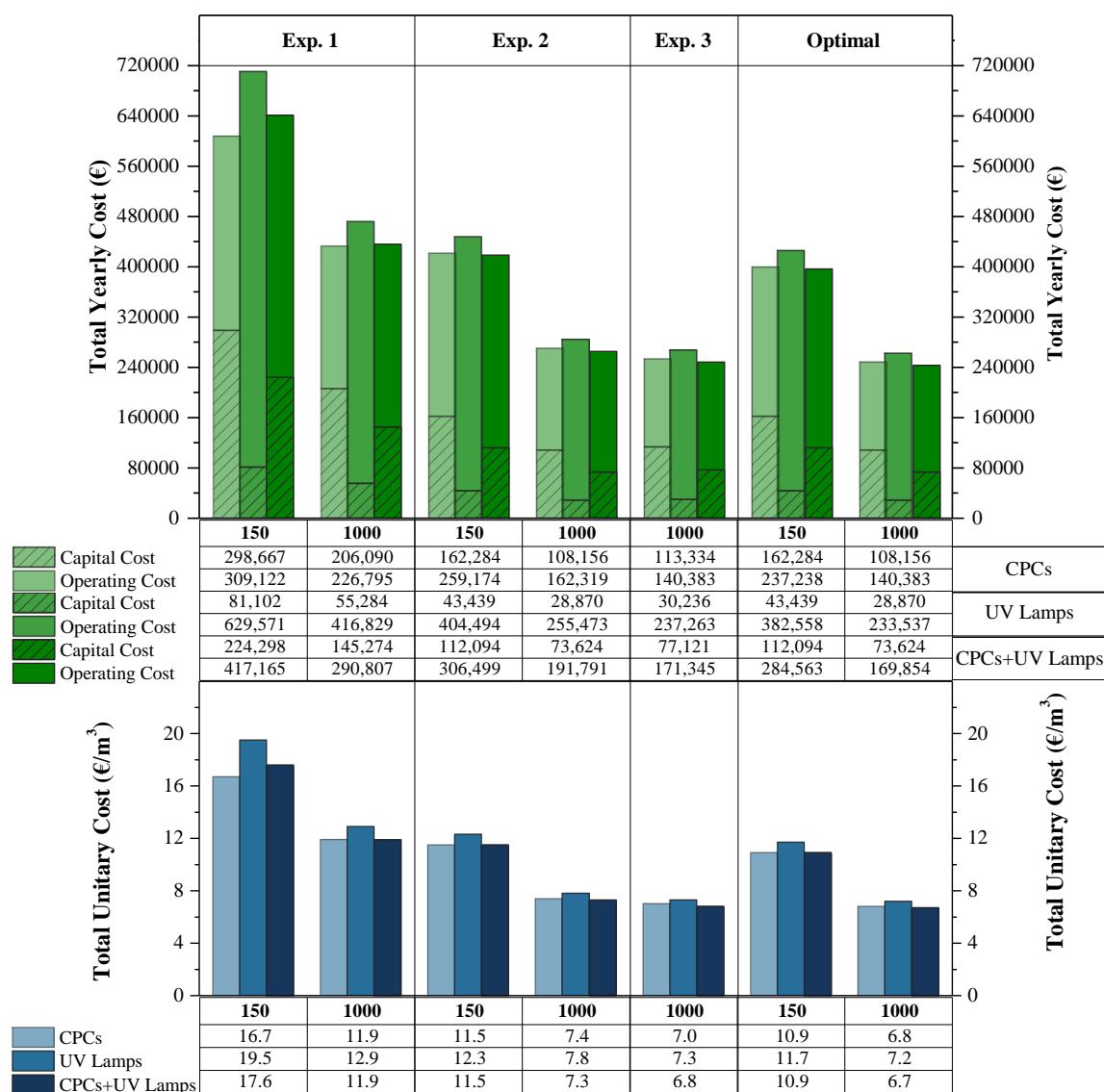


Figure 6.6. Total cost for the sanitary landfill leachate's treatment using different set-ups.

For all scenarios, the expense associated with H₂O₂ consumption represents, in average, 30 and 39% of the total yearly cost, respectively for final COD values of 1000 or 150 mg O₂/L. The *in-situ* electro-generation of H₂O₂ [37, 38] can be a good approach to decrease H₂O₂ costs.

The use of only CPCs or the combination of CPCs and UV lamps can be considered the best configurations. However, according to UV radiation distribution along the year nearby Porto, in December, even for the best conditions, 10794 m² of CPCs would be needed, which corresponds to a land area of 43173 m², the equivalent to 8.6 soccer fields. Thus, the usage of CPCs should be disregarded, since the best choice is the integration of CPCs and UV lamps, taking into account the monthly energetic needs. It should also be noted that: i) the costs with UV lamps were calculated estimating 4 kW power and 20000 h lifetime; and ii) the efficiency of UV lamps for the treatment of effluents with low transmissibility, such as leachates, using a photo-Fenton is not well known.

According to the Guidance for the Treatment of Landfill Leachate [1], the treatment of 400 m³ leachate per day with an initial COD of 6000 mg O₂/L, using a sequencing batch reactor (SBR) with further disposal into a sewer, has a total cost of 4.12 £/m³ (4.8 €/m³): i) a capital expenditure of 1,000,000 £, corresponding to a yearly unitary cost of 0.83 £/m³ (0.97 €/m³) considering a FCR of 12%; ii) an operational expenditure (plant operation, maintenance, and reagents or transport) of 0.80 £/m³ (0.94 €/m³); and iii) a discharge cost, including sewer connections of 2.50 £/m³ (2.92 €/m³).

In the present study, associating the costs related to SBR and disposal into sewer with the costs obtained in the optimal conditions, to achieve COD values lower than 1000 and 150 mg O₂/L, the complete treatment of the leachate would have a total unitary cost of about 11.5 and 14.7 €/m³, respectively. To reach a COD value of 1000 mgO₂/L, the treatment sequence would be: i) biological oxidation in a SBR (1.9 €/m³); ii) photo-Fenton reaction, using as UV photons source the combination of CPCs and UV lamps (6.7 €/m³); and iii) disposal into sewerage system (2.9 €/m³). If the goal is to achieve a COD value of 150 mg O₂/L, the treatment sequence would be: i) biological oxidation (1.9 €/m³); ii) photo-Fenton reaction using the combination of CPCs and UV lamps as UV photons source (10.9 €/m³); iii) biological oxidation (1.9 €/m³); and iv) disposal into water bodies (no costs associated). It should be noted that the costs regarding the discharge into sewerage systems can vary according to the legislation applied in each municipality.

According to an example given in the “Guidance for the Treatment of Landfill Leachate” [1], when leachate is transported to a WWTP, without any previous treatment, the estimated cost was 17.50 £/m³ (20.45 €/m³) [1]. This greatly exceeds the values presented in this work considering the treatment strategy adopted.

As a final remark, proper operation of the biological pre-treatment is a key point to minimize the leachate phototreatment costs.

6.4 Conclusions

The scale-up of a photo-Fenton plant for the treatment of biologically oxidised landfill leachate was successfully designed considering the combined use of solar light, through CPCs technology, and artificial radiation (UV lamps), according to UV radiation energetic needs for the photo-oxidation step along the year.

Appropriate operation of the preliminary biological oxidation, leading to a leachate with low alkalinity and organic matter content, substantially reduces the costs associated with the photo-oxidation system.

Although the collection of solar photons through CPCs technology presents a higher investment cost, the generation of electrical photons showed to be more costly mainly due to higher operation costs.

The cost analysis for leachate treatment using a photo-Fenton system led to a total unitary cost, aiming to achieve COD values of 1000 and 150 mg O₂/L, respectively of: 6.8 and 11.0 €/m³, using only CPCs; 7.2 and 11.7 €/m³, resorting just to UV lamps; and 6.7 and 10.9 €/m³, combining CPCs and UV lamps.

For all scenarios, the H₂O₂ costs represent between 30 to 39% of the total yearly cost.

The maximum mass and volumetric treatment factors (T_{fm} and T_{fv}) obtained were 1.83 g C/h/m² and 2.04 L/h/m² to achieve a final COD after biological treatment of 150 mg O₂/L, considering a total of 2944 hours of insolation and a yearly average solar UV radiation of 17 W/m² (data collected at the location of the sanitary landfill).

6.5 References

- [1] U.E. Agency, Guidance for the Treatment of Landfill Leachate, Sector Guidance Note IPPC S5.03, in: I.P.P.a.C. (IPPC) (Ed.), 2007.
- [2] R. Chemlal, N. Abdi, N. Drouiche, H. Lounici, A. Pauss, N. Mameri, Rehabilitation of Oued Smar landfill into a recreation park: Treatment of the contaminated waters, *Ecological Engineering*, 51 (2013) 244-248.
- [3] E. De Torres-Socías, L. Prieto-Rodríguez, A. Zapata, I. Fernández-Calderero, I. Oller, S. Malato, Detailed treatment line for a specific landfill leachate remediation. Brief economic assessment, *Chemical Engineering Journal*, 261 (2015) 60-66.
- [4] E.M.R. Rocha, V.J.P. Vilar, A. Fonseca, I. Saraiva, R.A.R. Boaventura, Landfill leachate treatment by solar-driven AOPs, *Solar Energy*, 85 (2011) 46-56.
- [5] R. Chemlal, L. Azzouz, R. Kernani, N. Abdi, H. Lounici, H. Grib, N. Mameri, N. Drouiche, Combination of advanced oxidation and biological processes for the landfill leachate treatment, *Ecological Engineering*, 73 (2014) 281-289.
- [6] V.J.P. Vilar, E.M.R. Rocha, F.S. Mota, A. Fonseca, I. Saraiva, R.A.R. Boaventura, Treatment of a sanitary landfill leachate using combined solar photo-Fenton and biological immobilized biomass reactor at a pilot scale, *Water Research*, 45 (2011) 2647-2658.
- [7] Y. Wu, S. Zhou, X. Ye, D. Chen, K. Zheng, F. Qin, Transformation of pollutants in landfill leachate treated by a combined sequence batch reactor, coagulation, Fenton oxidation and biological aerated filter technology, *Process Safety and Environmental Protection*, 89 (2011) 112-120.
- [8] V.J.P. Vilar, J.M.S. Moreira, A. Fonseca, I. Saraiva, R.A.R. Boaventura, Application of Fenton and Solar Photo-Fenton Processes to the Treatment of a Sanitary Landfill Leachate in a Pilot Plant with CPCs, *Journal of Advanced Oxidation Technologies*, 15 (2012) 107-116.
- [9] S. Malato, P. Fernández-Ibáñez, M.I. Maldonado, J. Blanco, W. Gernjak, Decontamination and disinfection of water by solar photocatalysis: Recent overview and trends, *Catalysis Today*, 147 (2009) 1-59.
- [10] D. Cassano, A. Zapata, G. Brunetti, G. Del Moro, C. Di Iaconi, I. Oller, S. Malato, G. Mascolo, Comparison of several combined/integrated biological-AOPs setups for the treatment of municipal landfill leachate: Minimization of operating costs and effluent toxicity, *Chemical Engineering Journal*, 172 (2011) 250-257.
- [11] R. Bauer, H. Fallmann, The photo-Fenton oxidation—a cheap and efficient wastewater treatment method, *Research on Chemical Intermediates*, 23 (1997) 341-354.
- [12] I. Carra, E. Ortega-Gómez, L. Santos-Juanes, J.L. Casas López, J.A. Sánchez Pérez, Cost analysis of different hydrogen peroxide supply strategies in the solar photo-Fenton process, *Chemical Engineering Journal*, 224 (2013) 75-81.
- [13] J.C. Crittenden, R.P.S. Suri, D.L. Perram, D.W. Hand, Decontamination of water using adsorption and photocatalysis, *Water Research*, 31 (1997) 411-418.
- [14] C. Di Iaconi, M. De Sanctis, S. Rossetti, A. Mancini, Bio-chemical treatment of medium-age sanitary landfill leachates in a high synergy system, *Process Biochemistry*, 46 (2011) 2322-2329.

- [15] A. Durán, J.M. Monteagudo, A. Carnicer, I. San Martín, P. Serna, Solar photodegradation of synthetic apple juice wastewater: Process optimization and operational cost study, *Solar Energy Materials and Solar Cells*, 107 (2012) 307-315.
- [16] A. Durán, J.M. Monteagudo, I. San Martín, Photocatalytic treatment of an industrial effluent using artificial and solar UV radiation: An operational cost study on a pilot plant scale, *Journal of Environmental Management*, 98 (2012) 1-4.
- [17] A. Eduardo da Hora Machado, T. Padovani Xavier, D. Rodrigues de Souza, J. Antonio de Miranda, E. Thomas Fleury Mendonça Duarte, R. Ruggiero, L. de Oliveira, C. Sattler, Solar photo-Fenton treatment of chip board production waste water, *Solar Energy* 77 (2004) 583-589.
- [18] J.B. Gálvez, S.M. Rodríguez, *Solar Detoxification*, United Nations Educational, Scientific and Cultural Organization, 2003.
- [19] D. Gumy, P. Fernández-Ibáñez, S. Malato, C. Pulgarin, O. Enea, J. Kiwi, Supported Fe/C and Fe/Nafion/C catalysts for the photo-Fenton degradation of Orange II under solar irradiation, *Catalysis Today*, 101 (2005) 375-382.
- [20] L.S.-J. Jordá, M.M.B. Martín, E.O. Gómez, A.C. Reina, I.M.R. Sánchez, J.L.C. López, J.A.S. Pérez, Economic evaluation of the photo-Fenton process. Mineralization level and reaction time: The keys for increasing plant efficiency, *Journal of Hazardous materials*, 186 (2011) 1924-1929.
- [21] I. Michael, E. Hapeshi, C. Michael, A.R. Varela, S. Kyriakou, C.M. Manaia, D. Fatta-Kassinos, Solar photo-Fenton process on the abatement of antibiotics at a pilot scale: Degradation kinetics, ecotoxicity and phytotoxicity assessment and removal of antibiotic resistant enterococci, *Water Research*, 46 (2012) 5621-5634.
- [22] A.N. Módenes, F.R. Espinoza-Quiñones, F.H. Borba, D.R. Manenti, Performance evaluation of an integrated photo-Fenton – Electrocoagulation process applied to pollutant removal from tannery effluent in batch system, *Chemical Engineering Journal*, 197 (2012) 1-9.
- [23] A.N. Módenes, F.R. Espinoza-Quiñones, D.R. Manenti, F.H. Borba, S.M. Palácio, A. Colombo, Performance evaluation of a photo-Fenton process applied to pollutant removal from textile effluents in a batch system, *Journal of Environmental Management*, 104 (2012) 1-8.
- [24] I. Muñoz, S. Malato, A. Rodríguez, X. Doménech, Integration of environmental and economic performance of processes. Case study on advanced oxidation processes for wastewater treatment. , *Journal of Advanced Oxidation Technologies*, 11 (2008) 270-275.
- [25] J.A.S. Pérez, I.M.R. Sánchez, I. Carra, A.C. Reina, J.L.C. López, S. Malato, Economic evaluation of a combined photo-Fenton/MBR process using pesticides as model pollutant. Factors affecting costs, *Journal of Hazardous materials*, (2012).
- [26] A. Vidal, A.I. Díaz, A. El Hraiki, M. Romero, I. Muguruza, F. Senhaji, J. González, Solar photocatalysis for detoxification and disinfection of contaminated water: pilot plant studies, *Catalysis Today*, 54 (1999) 283-290.

- [27] J.J. Pignatello, E. Oliveros, A. MacKay, Advanced oxidation processes for organic contaminant destruction based on the fenton reaction and related chemistry, *Critical Reviews in Environmental Science and Technology*, 36 (2006) 1-84.
- [28] V.J.P. Vilar, T.F.C.V. Silva, M.A.N. Santos, A. Fonseca, I. Saraiva, R.A.R. Boaventura, Evaluation of solar photo-Fenton parameters on the pre-oxidation of leachates from a sanitary landfill, *Solar Energy*, 86 (2012) 3301-3315.
- [29] J. Bacardit, I. Oller, M.I. Maldonado, E. Chamarro, S. Malato, S. Esplugas, Simple Models for the Control of Photo-Fenton by Monitoring H₂O₂, *Journal of Advanced Oxidation Technologies*, 10 (2007) 219-228.
- [30] L.C. Navntoft, P. Fernandez-Ibañez, F. Garreta, UV solar radiation on a tilted and horizontal plane: Analysis and comparison of 4 years of measurements, *Solar Energy*, 86 (2012) 307-318.
- [31] J.G. Webster, *The Measurement, Instrumentation, and Sensors: Handbook*, Springer Verlag, 1999.
- [32] J.R. Bolton, K.G. Bircher, W. Tumas, C.A. Tolman, Figures-of-merit for the technical development and application of advanced oxidation technologies for both electric-and solar-driven systems (IUPAC Technical Report), *Pure and Applied Chemistry*, 73 (2001) 627-637.
- [33] G. Matthur, D. Goswami, C. Jotshi, A simulation program for predicting solar detoxification costs, in: *Energy Conversion Engineering Conference, 1996. IECEC 96., Proceedings of the 31st Intersociety, IEEE, 1996*, pp. 1703-1708.
- [34] B.A. Jubran, A.F. Ismail, T. Pervez, Prediction of the performance of a solar water detoxification system under Malaysian climatic conditions, *Energy Conversion and Management*, 41 (2000) 1-12.
- [35] J. García-Montañó, N. Ruiz, I. Muñoz, X. Domènech, J.A. García-Hortal, F. Torrades, J. Peral, Environmental assessment of different photo-Fenton approaches for commercial reactive dye removal, *Journal of Hazardous Materials*, 138 (2006) 218-225.
- [36] IRAR, *Gestão e tratamento de lixiviados produzidos em aterros sanitários de resíduos urbanos, Relatório IRAR nº 03/2008*, Lisboa, 2008.
- [37] K.V. Plakas, A.J. Karabelas, S.D. Sklari, V.T. Zaspalis, Toward the development of a novel electro-Fenton system for eliminating toxic organic substances from Water. Part 1. In situ generation of hydrogen peroxide, *Industrial & Engineering Chemistry Research*, 52 (2013) 13948-13956.
- [38] E. Brillas, I. Sirés, M.A. Oturan, Electro-Fenton process and related electrochemical technologies based on Fenton's reaction chemistry, *Chemical Reviews*, 109 (2009) 6570-6631.

7 Evaluation of solar photo-Fenton reaction parameters on the treatment of landfill leachate after biological and physico-chemical oxidation, at lab-scale

In the present chapter it is evaluated the effect of the main photo-Fenton (PF) reaction variables on the treatment of a sanitary landfill leachate collected at the outlet of a leachate treatment plant, which includes aerated lagooning followed by aerated activated sludge and a final coagulation-flocculation step.

The PF experiments were performed in a lab-scale compound parabolic collector (CPC) photoreactor using artificial solar radiation. The photocatalytic reaction rate was determined while varying the total dissolved iron concentration (20 – 100 mg Fe^{2+} /L), solution pH (2.0 - 3.6), operating temperature (10 - 50°C), type of acid used for acidification (H_2SO_4 , HCl and H_2SO_4+HCl) and UV irradiance (22 – 68 W/m^2).

This work also tries to elucidate the role of ferric hydroxides, ferric sulphate and ferric chloride species, by taking advantage of ferric speciation diagrams, in the efficiency of the PF reaction when applied to leachate oxidation. The molar fraction of the most photoactive ferric species, $FeOH^{2+}$, was linearly correlated with the PF pseudo-first order kinetic constants obtained at different solution pH and temperature values. Ferric ion speciation diagrams also showed that the presence of high amounts of chloride ions negatively affected the PF reaction, due to the decrease of ferric ions solubility and scavenging of hydroxyl radicals for chlorine radical formation. The increment of the PF reaction rates with temperature was mainly associated with the increase of the molar fraction of $FeOH^{2+}$.

The optimal parameters for the photo-Fenton reaction were: pH = 2.8 (acidification agent: H_2SO_4); $T = 30^\circ C$; $[Fe^{2+}] = 60$ mg/L and UV irradiance = 44 W_{UV}/m^2 , achieving 72% mineralization after 25 kJ_{UV}/L of accumulated UV energy and 149 mM of H_2O_2 consumed.

This chapter is based on the research article “Silva, T.F.C.V., Ferreira, R., Soares, P.A., Manenti, D.R., Fonseca, A., Saraiva, I., Boaventura, R.A.R, Vilar, V.J.P, *Insights into solar photo-Fenton reaction parameters in the oxidation of a sanitary landfill leachate at lab-scale*, Journal of Environmental Management, 164 (2015) 32-40, DOI: 10.1016/j.jenvman.2015.08.030 ”.

7.1 Introduction

Leachate treatment plant (LTP) design constitutes nowadays a challenge for environmental engineers, mainly due to the recalcitrant character of leachates with high organic (e.g. humic and fulvic acids) and inorganic contaminants concentration (e.g. ammonium nitrogen, heavy metals) [1, 2]. Normally, resulting in a complex LTP to achieve a final wastewater with quality enough to be discharged into receiving water bodies, at comfortable costs, without the generation of further wastes. LTP normally combines different processes, as: (i) conventional combined treatment with domestic sewage or recycling back the treated effluent to the landfill; (ii) aerobic and anaerobic biological processes; (iii) chemical and physical methods (flotation, coagulation/flocculation, adsorption, chemical precipitation, chemical oxidation, ammonium stripping and ion exchange); (iv) membrane filtration (microfiltration, ultrafiltration, nanofiltration and reverse osmosis); (v) advanced oxidation processes - AOPs (TiO_2/UV , $\text{H}_2\text{O}_2/\text{UV}$, Fenton ($\text{Fe}^{2+}/\text{H}_2\text{O}_2$)/photo-Fenton ($\text{Fe}^{2+}/\text{H}_2\text{O}_2/\text{UV}$)/electro-Fenton/electro-photo-Fenton, ozone (O_3 , O_3/UV , and $\text{O}_3/\text{H}_2\text{O}_2$), etc.) [3-10].

The photo-Fenton reaction has been proposed as a good option for biodegradability enhancement of old recalcitrant leachates from sanitary landfills [7, 11-15], being possible to couple it with a further biological process to achieve the discharge limits. In the Chapters 3-5, the first results at pre-industrial plant scale for the treatment of leachates after lagooning, by combining a solar photo-Fenton oxidation process using 39.52 m² of compound parabolic collectors (CPCs) and an aerobic/anoxic biological system (3.5 m³ capacity), were presented. According to the results obtained, two of the main observed drawbacks were related to: (i) the inner filter effect consisting in the absorption of photons by other absorbing species, mainly humic acids, associated with the dark-brown colour intrinsic to leachates; and (ii) the high amount of suspended solids generated during the acidification step required by the photo-Fenton reaction, due to the precipitation of some organic compounds with ferric ions. The high amount of suspended solids decreases the light penetration, competes with H_2O_2 and iron species as photons absorbers, and leads to a high consumption of H_2O_2 during the phototreatment due to the oxidation of particulate organic matter. Considering these aspects, a preliminary physico-chemical process can be a good option to significantly reduce the organic load (through the sludge production) and the light absorption species, boosting the phototreatment efficiency.

This study mainly focuses on the optimization of sanitary landfill leachate treatment, collected at the outlet of a LTP, which includes biological oxidation and physico-chemical processes, by a photo-Fenton reaction mediated by artificial solar radiation, taking into account the (i) total dissolved iron (TDI) concentration, (ii) solution pH, (iii) operating temperature (T), (iv) type of acid used in the acidification,

and (v) UV irradiance (I). Simultaneously, the role of ferric hydroxides, ferric sulphate and ferric chloride complexes, in the PF reaction efficiency, was assessed through the use of ferric ion speciation diagrams, taking into account the solution pH, temperatures and acid type used in the acidification step.

7.2 Experimental methodology

Leachate samples were collected at the outlet of a LTP, from a Municipal Solid Waste Sanitary Landfill located in northern Portugal, receiving on average 150 m³ of leachate per day, which comprises the following treatment units: (i) an aerated lagoon with pure oxygen injection (15,000 m³); (ii) an anoxic and an aerobic activated sludge reactors (150 m³ each); (iii) a coagulation/flocculation tank (27 m³) and (iv) a final retention lagoon (3000 m³). The treated leachate is transported to a municipal WWTP since it does not meet the discharge regulations into sewerage systems and water bodies (Decree-Law no. 236/98 – Table 7.1). Table 7.1 presents the main physico-chemical characteristics of the leachate used in the photo-Fenton oxidation tests.

Table 7.1. Characterization of sanitary landfill leachate samples, at the outlet of the LTP (after coagulation/flocculation), used for the experiments with sulphuric and hydrochloric acids.

Parameters	Unities	Experiments only with sulphuric acid	Experiments with hydrochloric acid	ELV ^b
pH	Sorënsen scale	6.91	6.94	6.0-9.0
Temperature	°C	20.6	21.2	-
TSS	mg/L	68	52	60
VSS	mg/L	48	36	-
COD	mg O ₂ /L	2770	2527	150
BOD ₅	mg O ₂ /L	330	370	40
BOD ₅ /COD	-	0.12	0.15	-
Total Dissolved Carbon	mg C/L	2065	2081	-
Total Inorganic Carbon	mg C/L	1205	1233	-
Alkalinity ^a	g CaCO ₃ /L	5.02	5.14	-
DOC	mg C/L	860	848	-
Total Dissolved iron	mg Fe/L	8.35	10.37	2.0 ^c
Conductivity	mS/cm	22.3	23.7	-
Chloride	mg Cl ⁻ /L	3156	4658	-
Sulphate	mg SO ₄ ²⁻ /L	2866	293	2000
Total Dissolved Nitrogen	mg N/L	2686	2625	15 ^d
Nitrate	mg N-NO ₃ ⁻ /L	<1	9.3	11
Nitrite	mg N-NO ₂ ⁻ /L	625	567	-
Ammonium	mg N-NH ₄ ⁺ /L	1933	1948	8
Phosphate	mg PO ₄ ³⁻ /L	9.1	9.2	-
Sodium	mg Na ⁺ /L	2704	2677	-
Potassium	mg K ⁺ /L	2132	2186	-
Magnesium	mg Mg ²⁺ /L	419	403	-
Calcium	mg Ca ²⁺ /L	292	308	-

^aAlkalinity values considering that for pH < 8.3, the inorganic carbon was almost in the form of bicarbonates [16]; ^bEmission limit values for wastewater disposal into aquatic environment, imposed by the Portuguese legislation and established in the Decree-Law no. 236/98; ^cTotal iron; ^dTotal nitrogen.

All the chemicals used in this work, the detailed description of the experimental unit and respective procedures, as well as the employed analytical methods can be consulted in the Chapter 2. The operational conditions used in the experiments are displayed in Table 7.2.

Table 7.2. Operational conditions used in the photo-Fenton experiments.

Group of experiments	I ^a (W _{UV} /m ²)	Acid Type	T (°C)	pH	TDI ^b (mg/L)
I	44	H ₂ SO ₄	20	2.8	20
					40
					60
					80
					100
II	44	H ₂ SO ₄	20	2.0	60
				2.4	
				2.8	
				3.2	
				3.6	
III	44	H ₂ SO ₄	10	2.8	60
			20		
			30		
			40		
			50		
IV	44	H ₂ SO ₄	30	2.8	60
		HCl+ H ₂ SO ₄			
		HCl			
V	22	H ₂ SO ₄	30	2.8	60
	44				
	68				

^aUV Irradiance; ^bTotal dissolved iron concentration.

7.3 Results and discussion

7.3.1 Leachate characterization

The leachate showed an intense yellow-brown colour associated to the high concentration of humic substances (HS), as reported in the Chapter 5, achieving values near 1.2 g C_{HS}/L for a raw leachate. It was also characterized by a high organic content (DOC = 848-860 mg C/L, COD = 2.5-2.8 g O₂/L), with low biodegradability (BOD₅ = 330-370 mg O₂/L; BOD₅/COD = 0.12-0.15). Additionally, leachate presented high alkalinity (5.0-5.1 g CaCO₃/L, most in the form of bicarbonate, as pH < 8.3) and nitrogen content, mainly in the forms of NH₄⁺ (1.9-2.0 g N-NH₄⁺/L) and NO₂⁻ (567-625 mg N-NO₂⁻/L), even after the preliminary treatments. It also presented high conductivity (22.3-23.7 mS/cm) associated with the high concentration of sulphate, chloride, potassium, sodium, magnesium and calcium ions (see Table 7.1).

7.3.2 Solar photo-Fenton reaction: Influence of iron concentration

The photo-Fenton reaction under simulated solar radiation was tested at five different initial iron concentrations (20, 40, 60, 80 and 100 mg Fe²⁺/L), as can be seen in Figure 7.1, considering a pH = 2.8, T = 20°C and I = 44 W_{UV}/m² (Table 7.2).

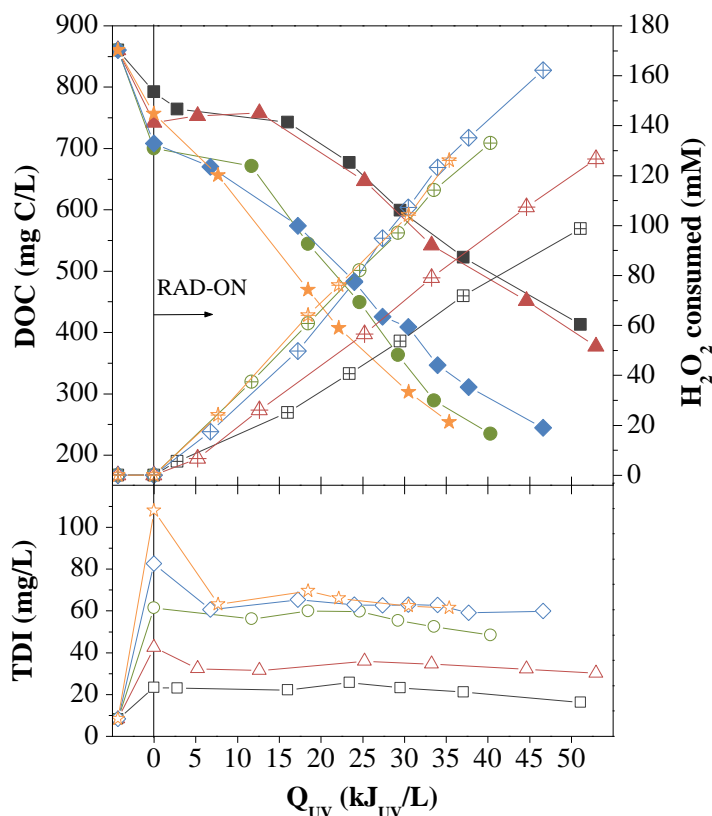


Figure 7.1. Evaluation of the DOC (closed symbols), H₂O₂ consumed (crossed symbols) and TDI concentration (open symbols) during the photo-Fenton reaction for different iron concentrations. Operational conditions: pH = 2.8 (H₂SO₄), T = 20°C, I = 40 W_{UV}/m²; (■, □, ▤) – [Fe] = 20 mg/L; (▲, △, ▴) – [Fe] = 40 mg/L; (●, ○, ⊕) – [Fe] = 60 mg/L; (◆, ◇, ⊕) – [Fe] = 80 mg/L; (★, ☆, ✨) – [Fe] = 100 mg/L.

As shown in Figure 7.1, the preliminary acidification step ($Q_{UV} < 0$ kJ/L) resulted in a DOC abatement between 8-19%, most likely due to the precipitation of some humic acids, which were not removed in the LTP. Henceforward, it was possible to see the occurrence of an induction period ($0 < Q_{UV} < 15$ kJ/L) for the two lowest iron concentrations associated with a low H₂O₂ consumption rate. This behaviour suggests that after the first H₂O₂ addition and subsequent ferrous ions oxidation, the rate-limiting step of the reaction is the ferrous ions regeneration (reduction of Fe³⁺ to Fe²⁺) [17]. This is attributed to the light absorbing species (inner filter effect) present in the leachate, as for instance fulvic acids (aromatic structure) [18] and nitrates, thereby decreasing the amount of photons available to be absorbed by the iron complexes. Usually, the direct photolysis of organic contaminants, such as humic substances, has a

low quantum yield, leading to a loss of the absorbed photons. From Figure 7.1, it was also possible to observe that the higher the iron concentration, the lower the induction period, being almost null for the three highest iron contents tested. This means that a high catalyst concentration is required to compete efficiently for the photons with the other light absorbing species.

According to the induction time, reaction rate and H_2O_2 consumption rate (Table 7.3), there is no significant difference among the experiments carried out with the three highest iron concentrations. This is in agreement with the average TDI in solution (55-65 mg/L) for those trials. During the experiments, principally for the two highest iron concentrations, a decrease in the pH was observed. This is related to the formation of low-molecular-weight carboxylic acids resulting from the humic substances degradation, which have a high content of carboxylic groups (9 meq of carboxylic acids per gram of carbon) [19]. Consequently, the presence of ferric-carboxylates complexes in the solution can enhance the reaction rate, due to its ability of make use of photons at higher wavelengths, overcoming the inner filter effects. Considering that a lower iron concentration reduces the operating costs, the catalyst concentration of 60 mg Fe^{2+} /L was selected as the optimum TDI concentration for further studies.

7.3.3 Solar photo-Fenton reaction: Influence of solution pH

The solution pH plays an important role in the efficiency of the photo-Fenton reaction, since it greatly influences the molar fraction of the iron-water complexes (e.g. FeOH^{2+} , $\text{Fe}(\text{OH})_2^+$, etc.), iron-organic complexes (e.g. oxalic, formic, etc.) and iron-inorganic complexes (e.g. chlorides, sulphates, etc.). Therefore, the influence of solution pH on the leachate photo-treatment was also assessed in the range 2.0 - 3.6 (Table 7.2). Figure 7.2 and Table 7.3 show that the best results are obtained at pH 2.8. This is in agreement with Pignatello et al. [20], who indicated that this pH avoids Fe^{3+} precipitation, and the predominant iron-water species in solution is FeOH^{2+} , which is the most photoactive ferric ion-water complex and can absorb light until 410 nm. In our case, although the optimum pH value is the same, the explanation does not fully apply due to the presence of large amounts of sulphate and chloride ions in the leachate. Preliminary acidification constitutes the major drawback of the photo-Fenton process, since it increases the costs associated with reactants consumption (acid for acidification and base for neutralization) and increases the salts content (e.g. SO_4^{2-} , Cl^- , Na^+ , Ca^{2+}). Furthermore, the presence of Cl^- and SO_4^{2-} can result in a strong negative effect in the photo-Fenton reaction through the formation of complexes with iron, leading to the formation of less reactive radicals, Cl^\bullet , Cl_2^\bullet and SO_4^\bullet , and possible formation of carcinogenic chlorinated organic intermediates [21].

Table 7.3. Variables and kinetic parameters of the photo-Fenton process for all experiments.

Changed parameter	t (h)	Q _{UV} (kJ/L)	T _m ^a (°C)	pH _m ^a	TDI _m ^a (mg/L)	H ₂ O ₂ (mM)	DOC _F ^b (mg/L)	Red. _{DOC} ^c (%)	Kinetic parameters					
									COD degradation			H ₂ O ₂ consumption		Q _{UV} ^h (kJ/L)
									k ^d (L/kJ)	r ₀ ^e (mg/kJ)	R ^{2,f}	k _H ^g (mmol/kJ)	R ^{2,f}	
TDI=20 mg/L	13.8	51.1	21.4	2.74	21.9	99	413	52.0	0.017 ± 0.001	13 ± 1	0.997	2.1 ± 0.1	0.999	> 16.0
TDI=40 mg/L	14.3	53.0	20.6	2.76	32.8	127	377	56.2	0.017 ± 0.002	13 ± 2	0.991	2.5 ± 0.1	0.999	> 12.6
TDI=60 mg/L	10.9	40.3	20.3	2.86	55.3	133	235	72.7	0.038 ± 0.004	25 ± 3	0.991	3.3 ± 0.1	0.996	> 11.7
TDI=80 mg/L	12.6	46.6	20.2	2.78	62.0	162	244	71.6	0.030 ± 0.002	20 ± 1	0.994	3.9 ± 0.4	0.990	> 17.2
TDI=100 mg/L	9.6	35.4	20.1	2.74	64.5	126	254	70.5	0.034 ± 0.002	23 ± 1	0.998	3.6 ± 0.2	0.998	> 7.7
pH=2.0	8.0	29.6	20.2	2.00	53.7	27	725	15.7	-	-	-	0.94 ± 0.05	0.998	> 0
pH=2.4	9.3	34.2	20.0	2.42	60.4	78	448	47.9	0.019 ± 0.002	13 ± 1	0.995	2.4 ± 0.3	0.993	> 11.1
pH=2.8	10.9	40.3	20.3	2.86	55.3	133	235	72.7	0.038 ± 0.004	25 ± 3	0.991	3.3 ± 0.1	0.996	> 11.7
pH=3.2	11.0	40.6	20.4	3.19	35.6	111	434	49.5	0.031 ± 0.005	20 ± 3	0.993	3.6 ± 0.6	0.994	> 15.5
pH=3.6	7.8	28.9	20.5	3.60	34.9	44	609	29.2	0.005 ± 0.001	3.5 ± 0.8	0.990	1.5 ± 0.1	0.998	> 10.8
T=10°C	12.8	47.5	10.1	2.81	30.2	81	378	56.0	0.023 ± 0.003	13 ± 2	0.991	2.6 ± 0.2	0.998	> 29.0
T=20°C	10.9	40.3	20.3	2.86	55.3	133	235	72.7	0.038 ± 0.004	25 ± 3	0.991	3.3 ± 0.1	0.996	> 11.7
T=30°C	6.8	25.1	30.1	2.80	55.0	149	237	72.4	0.058 ± 0.006	35 ± 4	0.995	7.2 ± 0.2	0.998	> 8.5
T=40°C	4.6	17.0	39.5	2.81	58.3	196	193	77.6	0.09 ± 0.02	48 ± 5	0.998	13 ± 3	0.991	> 5.9
T=50°C	5.3	19.4	50.1	2.81	40.3	216	195	77.3	0.071 ± 0.005	44 ± 3	0.996	12 ± 1	0.990	> 3.0
H ₂ SO ₄	6.8	25.1	30.1	2.80	55.0	149	237	72.4	0.058 ± 0.006	35 ± 4	0.995	7.2 ± 0.2	0.998	> 8.5
HCl	8.0	29.6	30.8	2.83	28.3	99	417	50.5	0.025 ± 0.003	15 ± 2	0.991	3.4 ± 0.2	0.998	> 15.5
H ₂ SO ₄ +HCl	8.5	31.2	30.6	2.83	30.3	95	398	52.7	0.025 ± 0.002	16 ± 1	0.995	4.0 ± 0.2	0.997	> 11.7
I=22W/m ²	11.3	20.8	30.2	2.81	37.6	146	332	61.4	0.049 ± 0.005	31 ± 3	0.990	9.7 ± 0.5	0.997	5.5 - 18.9
I=44W/m ²	6.8	25.1	30.1	2.80	55.0	149	237	72.4	0.058 ± 0.006	35 ± 4	0.995	7.2 ± 0.2	0.998	> 8.5
I=68W/m ²	7.0	40.0	31.8	2.81	31.2	121	275	68.0	0.027 ± 0.002	16 ± 1	0.995	3.5 ± 0.2	0.993	> 5.7

^aAverage values of temperature, pH and total dissolved iron observed during the photo-Fenton experiments; ^bFinal DOC; ^cDOC Total reduction (1-DOC_F/DOC_i, %); ^dPseudo-first-order kinetic constant for DOC degradation; ^eInitial DOC reaction rate; ^fCoefficient of determination; ^gH₂O₂ consumption rate; ^hValue or interval of energy from which the kinetic parameters were calculated.

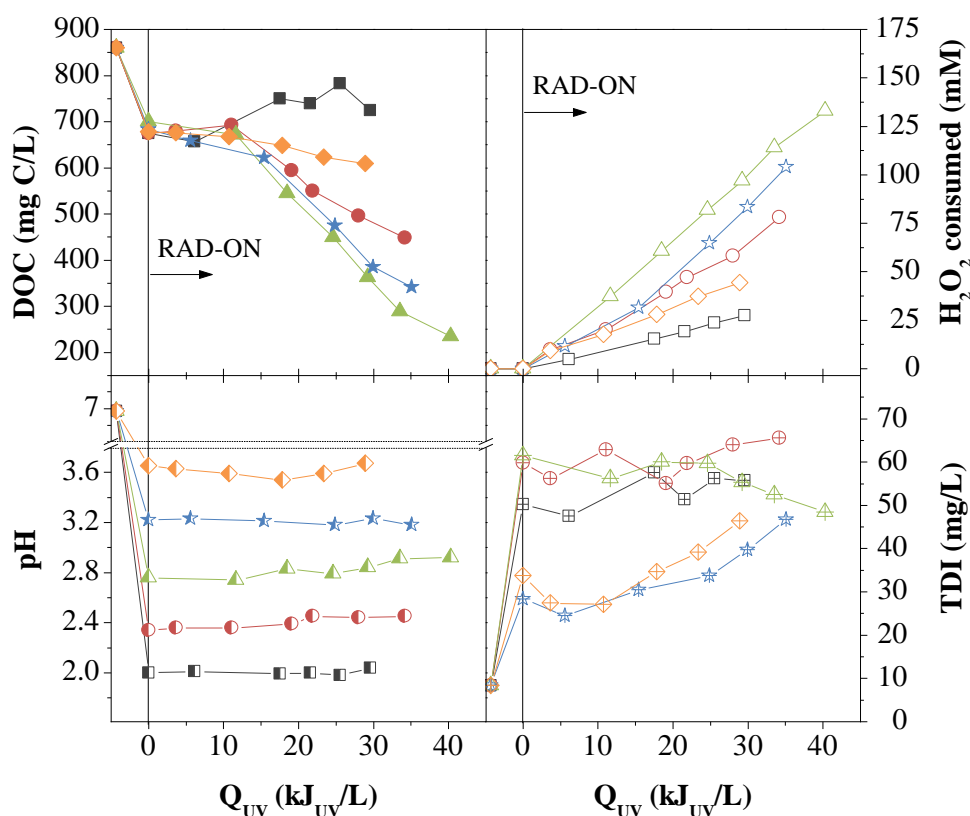


Figure 7.2. Evaluation of the DOC (closed symbols), H_2O_2 consumed (open symbols), pH (H_2SO_4) (semi-filled symbols) and TDI concentration (crossed symbols) during photo-Fenton reaction for different pH values. Operational conditions: $[\text{Fe}] = 60 \text{ mg/L}$, $T = 20^\circ\text{C}$, $I = 40 \text{ W}_{\text{UV}}/\text{m}^2$; (■, □, ▣, ⊞) – pH = 2.0; (●, ○, ⊙, ⊕) – pH = 2.4; (▲, △, ▴, ⊲) – pH = 2.8; (★, ☆, ⚡, ✦) – pH = 3.2; (◆, ◇, ⚡, ⊕) – pH = 3.6.

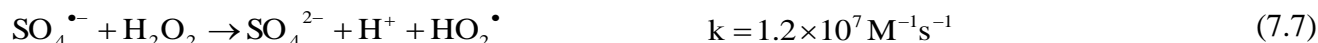
Taking into account the importance of the type of iron complexes formed during the photo-Fenton reaction, theoretical speciation diagrams of iron (III) including $\text{Fe}(\text{OH})_{3(s)}$ formation were performed (see Figure 7.3 and Table 7.4), considering the experimental conditions of each assay. It should be noted that only iron-water, iron-sulphate and iron-chloride complexes were considered since sulphate and chloride were the main anions found and/or added to the leachate. So, it is necessary to bear in mind that the information provided by the speciation diagrams must be used carefully and cannot be taken for granted, since this type of effluent presents a myriad of compounds and its degradation can originate much more, which can also affect the type of iron complex formed. As regards sulphates and chlorides content after acidification and iron addition, the ferric ion speciation diagram (Figure 7.3 and Table 7.4) shows that at pH 2.8, where the best results were achieved, the predominant iron species in solution are FeSO_4^+ (59.4%), $\text{Fe}(\text{SO}_4)_2^-$ (29.5%), Fe^{3+} (4.4%), $\text{Fe}(\text{OH})_2^+$ (2.9%), FeOH^{2+} (2.4%) and FeCl^{2+} (1.3%), leading to the simultaneous formation of $\text{SO}_4^{\cdot-}$, HO^{\cdot} and Cl^{\cdot} radicals, according to Eqs. (7.1) to (7.3) [22]:



Nevertheless, the sulphate radical is mostly produced under acidic conditions by the scavenging of the hydroxyl radical by the hydrogensulphate ions (Eq. (7.4)), since the FeSO_4^+ species has a very low photolysis quantum yield [23].



Depending on the operating conditions, the sulphate radical can oxidise some reactive oxygen species, including the H_2O_2 (Eq. (7.5)-(7.9)) and can consume ferrous ions (Eq. (7.10)) [23]. Beyond that, even being a strong oxidant, compared to HO^\bullet [24, 25], this species is slightly less reactive and more selective, affecting the organic compounds oxidation rates [26, 27].



Furthermore, in acidic medium, the concentration of H^+ rises, which also can have negative effects on the leachate mineralization (see Figure 7.2), since it can (i) react with H_2O_2 (Eq. (7.11)), yielding the peroxonium ion (H_3O_2^+), therefore decreasing substantially its reactivity with Fe^{2+} ions, and (ii) work as a scavenger of the HO^\bullet (Eq. (7.12)) [28-31].



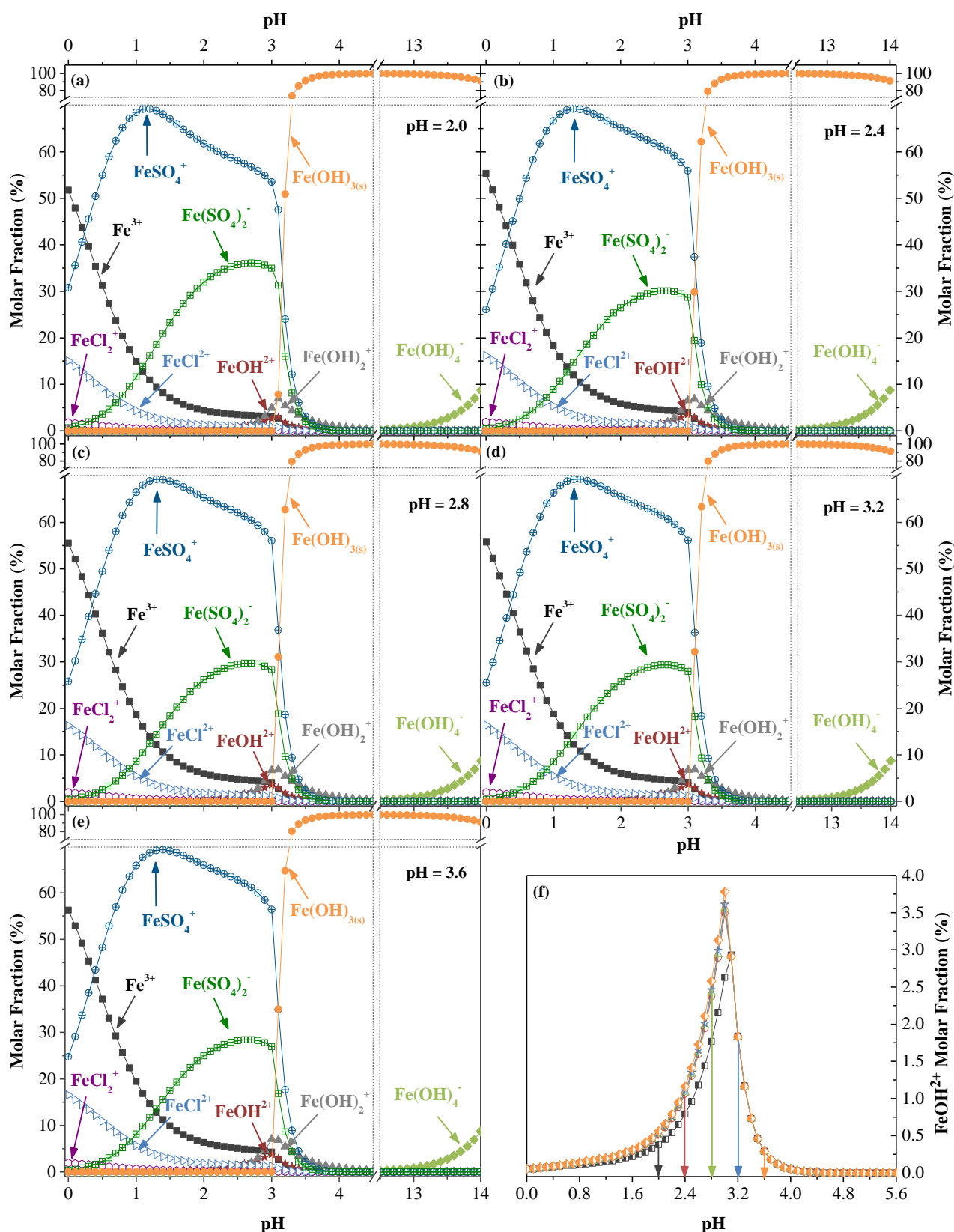


Figure 7.3. Theoretical Fe^{3+} speciation diagrams as a function of solution pH in the conditions of the experiments performed at different pH values: (a) 2.0; (b) 2.4; (c) 2.8; (d) 3.2; and (e) 3.6. Comparison of the theoretical molar fraction of FeOH^{2+} as a function of pH in the conditions of the experiments performed at different pH values (f): 2.0 (■); 2.4 (●); 2.8 (▲); 3.2 (★); and 3.6 (◆).

Table 7.4. Concentration of iron, chloride and sulphate added in the photo-Fenton reaction, and theoretical molar fraction of Fe^{3+} species, associated to pH value in different experiments.

Experiment	pH	Concentration (mM)			Molar fraction (%)							
		Fe	Cl ⁻	SO ₄ ²⁻	Fe ³⁺	FeOH ²⁺	Fe(OH) ₂ ⁺	FeCl ₂ ⁺	FeCl ²⁺	FeSO ₄ ⁺	Fe(SO ₄) ₂ ⁻	Fe(OH) ₃ (s)
pH=2.0	2.0	1.07	89	121	4.38	0.38	0.07	0.15	1.28	61.77	31.96	0.00
pH=2.4	2.4	1.07	89	95	4.82	1.06	0.50	0.17	1.42	62.50	29.52	0.00
pH=2.8	2.8	1.07	89	93	4.36	2.42	2.85	0.15	1.28	59.36	29.54	0.00
pH=3.2	3.2	1.07	89	92	1.31	1.83	5.44	0.05	0.39	18.33	9.32	63.31
pH=3.6	3.6	1.07	89	88	0.08	0.29	2.18	0.00	0.02	1.14	0.56	95.72
T=10°C	2.8	1.07	89	93	5.56	1.74	3.82	0.21	1.22	56.38	31.04	0.00
T=20°C	2.8	1.07	89	93	4.36	2.42	2.85	0.15	1.28	59.36	29.54	0.00
T=30°C	2.8	1.07	89	93	3.56	3.38	2.22	0.12	1.37	61.99	27.30	0.00
T=40°C	2.8	1.07	89	93	2.95	4.60	1.75	0.09	1.47	64.02	25.05	0.00
T=50°C	2.8	1.07	89	93	1.53	3.78	0.85	0.04	0.95	40.32	14.03	38.45
H ₂ SO ₄	2.8	1.07	89	93	3.56	3.38	2.22	0.12	1.37	61.99	27.30	0.00
HCl	2.8	1.07	229	4.12	7.56	7.49	5.06	1.79	7.92	6.46	0.13	63.31
H ₂ SO ₄ +HCl	2.8	1.07	201	20.8	7.72	7.56	5.07	1.38	7.01	32.33	3.24	35.42

So, high amounts of sulphate and hydrogen ions, as well as low amounts of FeOH^{2+} species greatly affect the photo-Fenton reaction efficiency.

If the PF reaction is conducted at pH values higher than 3.0, iron begins to precipitate as $\text{Fe}(\text{OH})_{3(s)}$ (Figure 7.3), decreasing the mineralization rates. This is in agreement with the iron profile for each experiment presented in Figure 7.2, leading to an average dissolved iron concentration of ca. 35 mg/L, for the experiments at pH 3.2 and 3.6. Nevertheless, taking into account the ferric ions speciation diagram, at pH 3.6 all iron is the form of $\text{Fe}(\text{OH})_{3(s)}$, which is not in agreement with the experimental results. This can be explained by the presence of synthetic and natural complexing agents in the leachate samples (e.g. ethylenediaminetetraacetic acid (EDTA) and humic substances) [32-34], as also other organic species generated during the oxidation process (e.g. citric, oxalic and others carboxylic acids), that could form soluble ferric iron complexes (Fe^{3+}L), being possible to work at higher pH values [17, 35-37]. Some iron organic complexes can be photolysed (Eq. (7.13)) using higher light wavelengths, leading eventually to higher reaction rates through absorption of more solar photons (e.g. Fe(III)-oxalate complexes is efficient up to 500 nm with a quantum yield between 1.0 and 1.2) [20].



Additionally, the precipitation of iron (III) hydroxides occurs slowly [38, 39], a fact that may explain the inconsistency between the speciation diagram and the TDI concentration at the beginning of experiment at pH 3.6.

Linking the information obtained by the speciation diagrams (Table 7.4 and Figure 7.3) with the reaction kinetic data (Table 7.3 and Figure 7.2), an interesting relationship was observed. For a pH interval among 2.4 and 3.6, the photo-Fenton apparent reaction constant is directly proportional to the theoretical amount of FeOH^{2+} species (the most photoactive complex), obtained from the speciation diagrams, considering the working pH, as can be seen in the Figure 7.4a. This suggests that the photo-Fenton reaction efficiency is mostly affected by the concentration of FeOH^{2+} in solution, since this species is an additional source of hydroxyl radicals.

According to the speciation diagrams (Figure 7.3), maintaining chloride concentration constant (89 mM) and increasing sulphate concentration from 88 to 95 mM (Table 7.4), FeOH^{2+} species present a maximum molar fraction at about pH 3.0, corresponding to an average molar concentration of 3.9×10^{-2} mM. Thus, an increment in the reaction rate could have been achieved by increasing the pH up to 3.0, yielding a pseudo-first-order kinetic constant of 0.058 L/kJ, according to the linear regression presented in the Figure 7.4a.

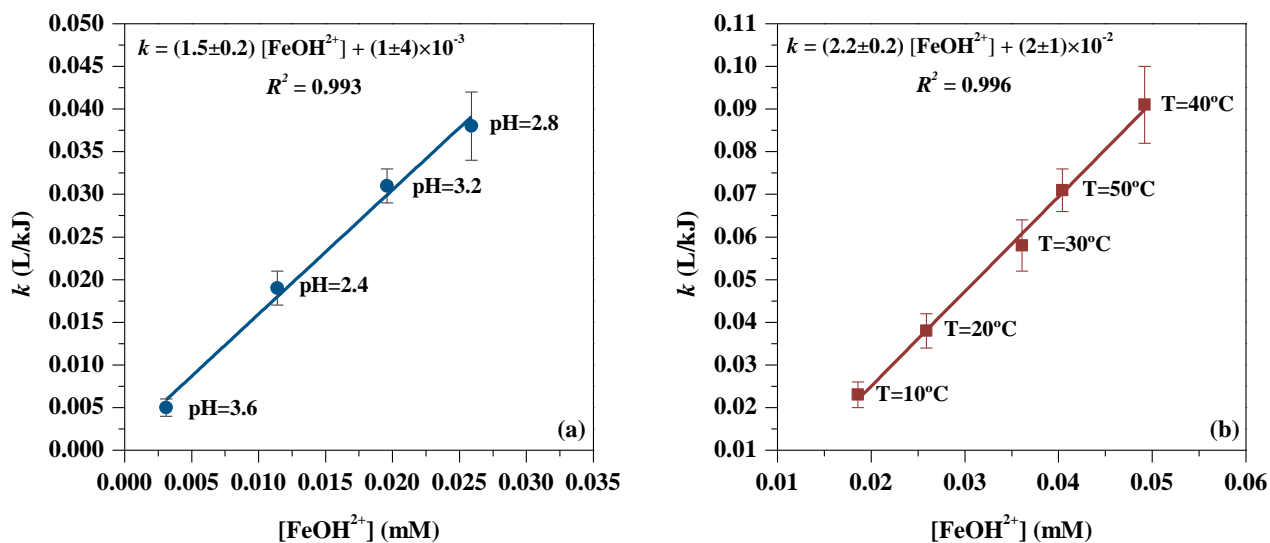


Figure 7.4. Representation of the pseudo-first-order kinetic constant for DOC degradation as a function of the theoretical FeOH^{2+} concentration, for the tests performed at different values of pH (a) and temperature (b).

7.3.4 Solar photo-Fenton reaction: Influence of temperature

Solar driven photo-Fenton reaction has some unique advantages since it can use the entire solar spectrum to: (i) photochemical reactions, which are activated by solar UV/visible photons between 300-500 nm; and (ii) thermal reactions involved in the ferric ion reduction using wavelengths higher than 500 nm, mostly according to Eqs. (7.14)-(7.16).



Previous studies reported an increase of the leachate temperature during solar AOPs, achieving values near 50°C [11, 15, 40, 41], associated to the presence of light absorbing species for wavelengths higher than 500 nm, responsible by the intense dark colour of the leachates. In contrast, another prior investigation performed at pre-industrial plant scale for *in situ* leachate treatment, showed that during winter, the average temperature for the solar-driven photo-Fenton reaction did not rise above 13°C. Given these possible temperature variations in a full-scale treatment, the influence of this parameter on the leachate treatment performance was evaluated from 10 to 50°C, keeping constant all the other variables (see Table 7.2).

Figure 7.5 shows that low temperatures lead to higher induction periods, indicating that the thermal reactions involved in the reduction of the ferric ion are more important than the photoreduction of ferric ions during this preliminary reaction period. Figure 7.5 and Table 7.3 also disclose that the increase of leachate temperature had a positive effect on the reaction rate, increasing 4 times by raising the temperature from 10°C to 40°C. The increase of the reaction rate can be attributed to two different factors: (i) production of more hydroxyl radicals resulting from a higher ferric ion reduction rates through thermal reactions (Eqs. (7.14)-(7.16)) [39]; and (ii) increment of the molar fraction of FeOH^{2+} , which is the most photoactive iron-water complex [42].

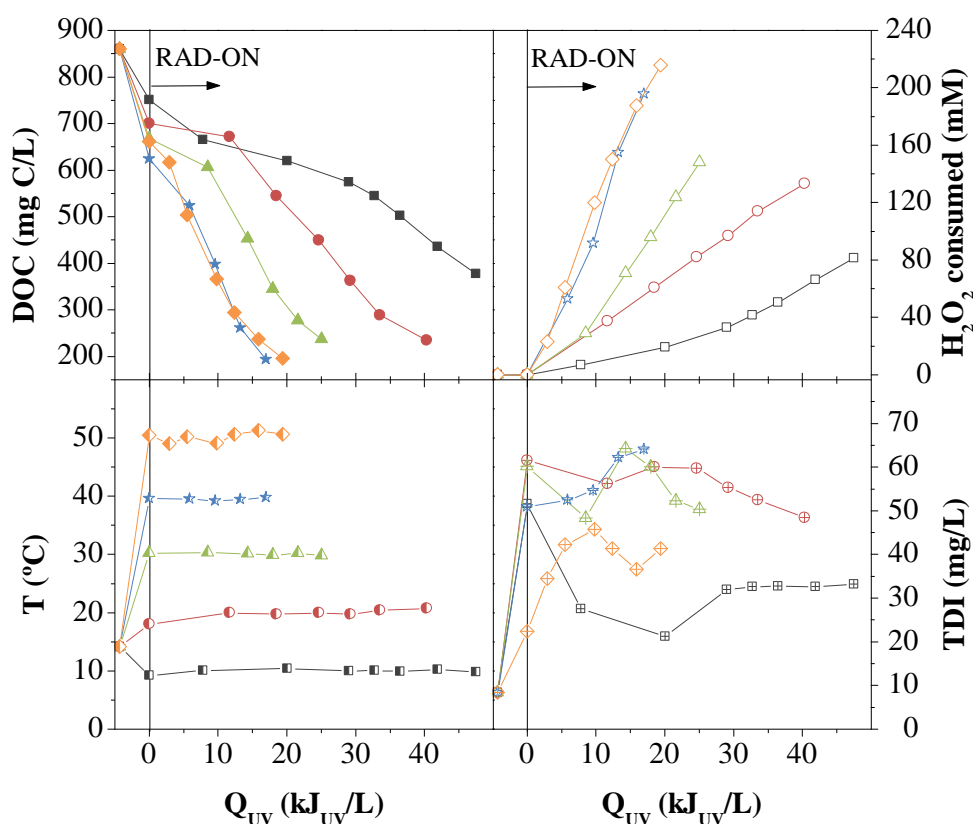


Figure 7.5. Evaluation of the DOC (closed symbols), H_2O_2 consumed (open symbols), temperature (semi-filled symbols) and TDI concentration (crossed symbols) during the photo-Fenton reaction for different temperature values. Operational conditions: $\text{pH} = 2.8$ (H_2SO_4); $[\text{Fe}] = 60 \text{ mg/L}$, $I = 40 \text{ W}_{\text{UV}}/\text{m}^2$; (■, □, ▣, ⊞) – $T = 10^\circ\text{C}$; (●, ○, ⊙, ⊕) – $T = 20^\circ\text{C}$; (▲, △, ⊲, ⊳) – $T = 30^\circ\text{C}$; (★, ☆, ⚡, ⚡) – $T = 40^\circ\text{C}$; (◆, ◇, ⬠, ⬠) – $T = 50^\circ\text{C}$.

Regarding the temperature interval studied (10 - 50°C), it can be assessed from Figure 7.4b that the reaction rate (Table 7.3) is also linearly dependent on the theoretical FeOH^{2+} concentration, calculated from the iron (III) speciation diagrams (Table 7.4 and Figure 7.6), considering the experimental conditions used for each test.

From the speciation diagrams, it was possible to note that increasing the leachate temperature, the maximum molar fraction of FeOH^{2+} is achieved at lower pH values. For instance, considering 10 and 50°C, the amount of this species is higher at pH 3.1 and 2.7 (3.0 and 5.1%, respectively). Given that, in a leachate treatment plant, the oxidation rate can be slightly increased if the photo-Fenton reaction is performed at higher pH (3.1) during winter, and lower pH (2.7) during summer.

Figure 7.5 shows that higher temperatures lead to an increase of H_2O_2 consumption to achieve the same mineralization, principally for temperatures above 30°C, which can be associated with two main factors: (i) the thermal ferric ion reduction reactions and (ii) H_2O_2 decomposition at high temperatures (the rate of H_2O_2 decomposition doubles when the temperature rises 10°C, in addition, because of the exothermic nature of the reaction, the rate of decomposition of H_2O_2 self-accelerates).

Considering temperature interval between 20°C and 40°C, the TDI concentration remained approximately constant during the experiments with an average concentration in the range 55-58 mg/L. For the temperature of 10°C, TDI concentration decreased substantially at the beginning of the reaction and remained approximately constant (30 mg/L) during the reaction, which can be attributed to the complexation with degradation by-products. Figure 7.5 also indicates that for the temperature of 50°C, ferric and ferrous ion solubility decreases substantially, which is in agreement with the speciation diagrams (see Table 7.4 and Figure 7.6). However, in this case, the reaction kinetics was similar to that observed at 40°C since dissolved iron concentration was sufficient to catalyse the reaction.

This means that, although temperature control in an industrial plant is economically non-viable, this parameter must be taken into account in the calculation of CPCs area, according to the annual average temperature (winter and summer).

Since the reaction performance at 30°C led to good efficiency and lesser decomposition of H_2O_2 than at 40 and 50°C, it was selected for the additional tests.

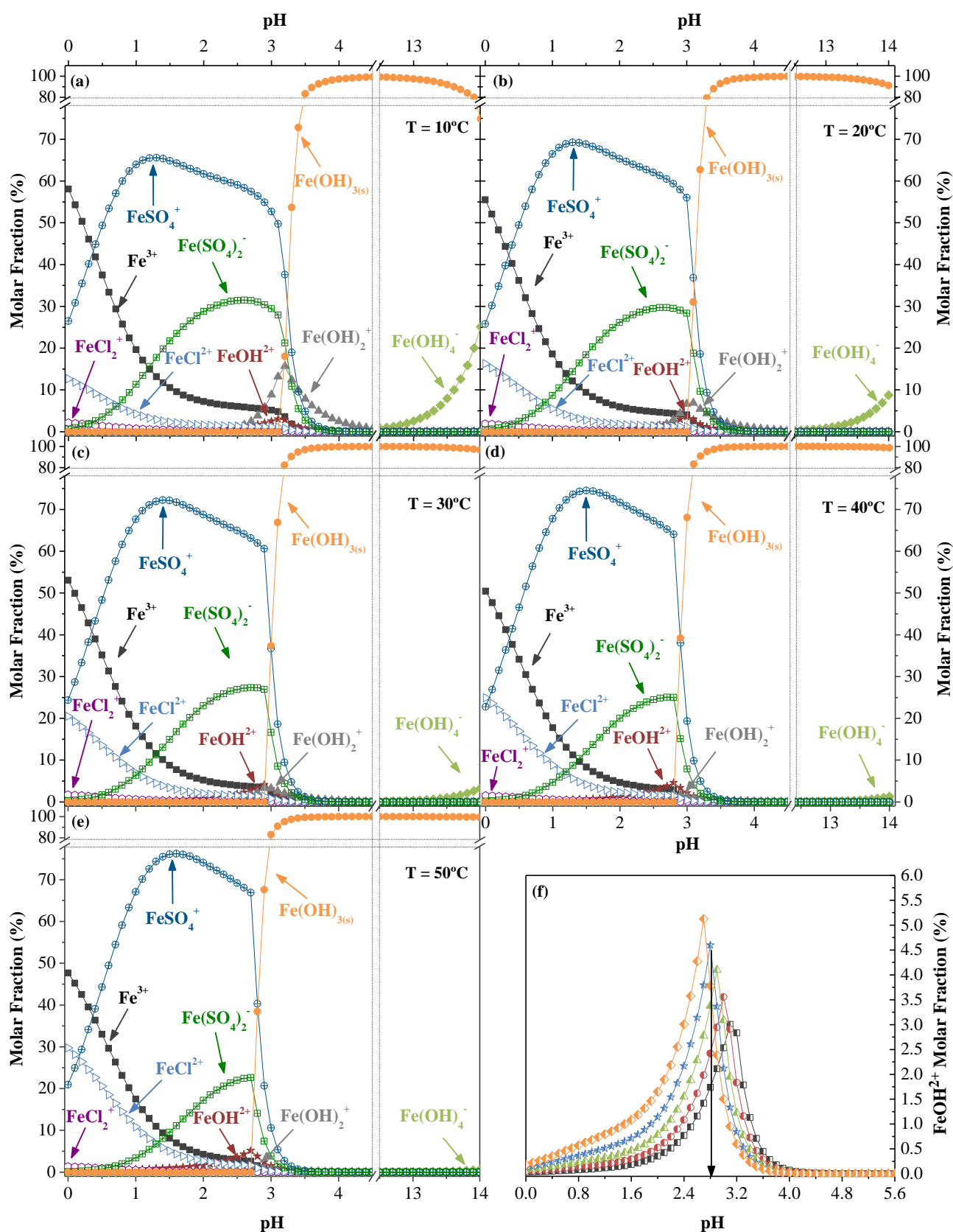
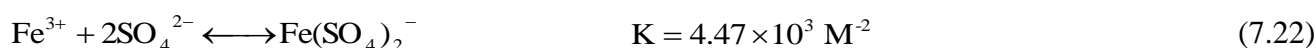
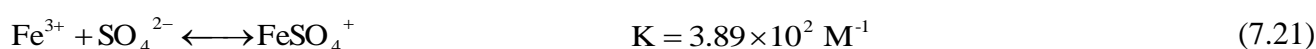
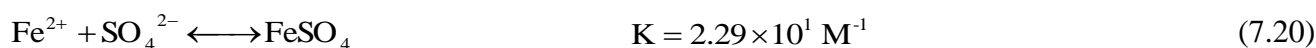
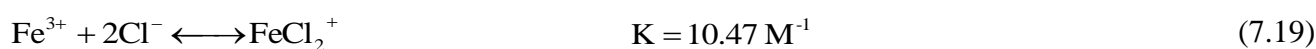
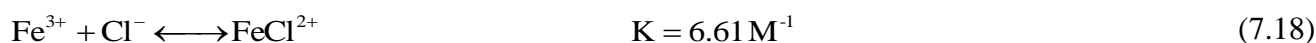
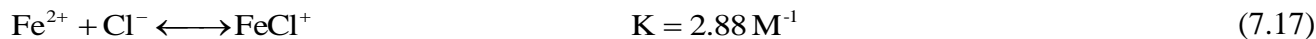


Figure 7.6. Theoretical Fe^{3+} speciation diagrams as a function of solution pH in the conditions of the experiments performed at different temperature values: (a) 10°C; (b) 20°C; (c) 30°C; (d) 40°C; and (e) 50°C. Comparison of the theoretical molar fraction of FeOH^{2+} as a function of pH in the conditions of the experiments performed at different temperature values (f): 10°C (■); 20°C (◻); 30°C (▲); 40°C (★); and 50°C (◆).

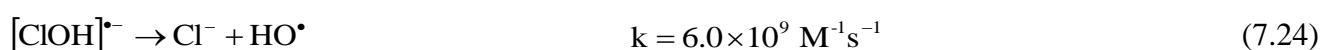
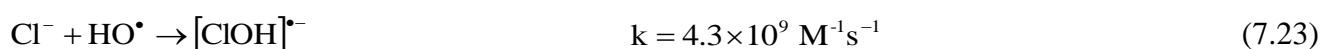
7.3.5 Solar photo-Fenton reaction: Influence of acid type

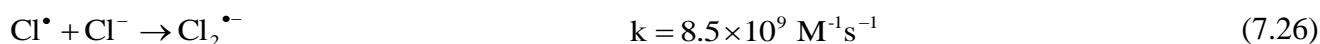
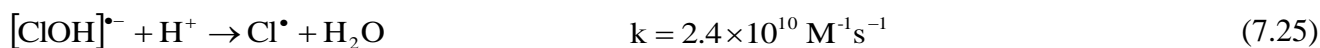
It is well known that higher photo-Fenton reaction rates are achieved at acidic pH and therefore acidification of neutral wastewaters is necessary. Commonly, sulphuric acid is used in the acidification step of the photo-Fenton reaction since it is a strong acid and commercially available in high concentration (>96% < > $[H^+] \approx 37 \text{ M}$) at low price. However, the discharge limit imposed by the Portuguese legislation for the sulphate ions is merely 2 g/L. On the other hand, HCl is commercially available at similar price but only at 37% ($[H^+] \approx 12 \text{ M}$). However, discharge regulations into water bodies do not include chloride ions concentration. Most often, the sanitary landfill leachate presents a high alkalinity and buffer capacity, due to the high bicarbonate content, which requires the addition of high amounts of acid to achieve the desired acidic pH values for the photo-Fenton reaction (as reported in the Chapters 3-5). Thus, the influence of chloride and sulphate ions on leachate phototreatment was assessed.

The presence of high concentration of chloride and sulphate ions can affect the photo-Fenton reaction rate due to four possible reasons [26, 43, 44]: (i) complexation reactions with Fe^{2+} and Fe^{3+} , which can affect the distribution and the reactivity of the iron species (Eqs. (7.17)-(7.22) for IS = 0.1 M):

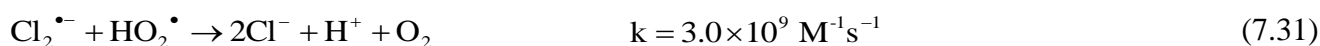
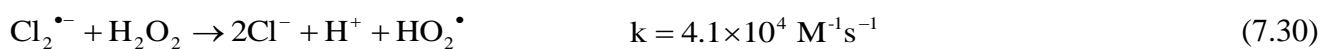
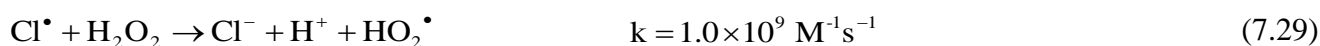
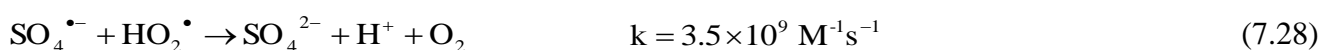
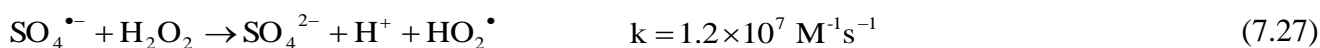


(ii) scavenging of hydroxyl radicals and formation of less reactive inorganic radicals (Cl^\bullet , $Cl_2^{\bullet-}$ and $SO_4^{\bullet-}$) (Eqs. (7.4) and (7.23)-(7.26)):





(iii) H_2O_2 decomposition due to less reactive chloride and sulphate radicals, increasing the reagent consumption (Eqs. (7.27)-(7.31)):



(iv) oxidation reactions involving these inorganic radicals.

Figure 7.7 illustrates the photo-Fenton reaction efficiency for the sanitary landfill leachate treatment using H_2SO_4 or HCl individually, or combined (the amount of H_2SO_4 added was conditioned to the limit of 2 g $\text{SO}_4^{2-}/\text{L}$, taking into account the addition of iron sulphate, as iron source) in the acidification stage. It can be seen that the best option is to use only H_2SO_4 in the acidification step. Furthermore, in the presence of such high concentration of chloride ions, the presence of 2 g/L of sulphate doesn't affect the reaction rate.

Unlike what was inferred from the tests at different values of pH and temperature, where the kinetic constants were directly related to the theoretical FeOH^{2+} concentration, herein the opposite just happens. The FeOH^{2+} concentration is higher, but the reaction rate is lower. It should be noted that the amount of HCl required to achieve a pH of 2.8, leads to a final concentrations of chloride ions (≥ 200 mM) higher than sulphate ions (93 mM), when just H_2SO_4 was employed (see Table 7.4). This causes a significant change in the ionic composition of the reactional medium while in the other tests only occurred a slight change in the sulphate concentration (trials with pH variation) and temperature. The presence of such high chloride concentration results in a competitive formation of more FeCl^{2+} and FeCl_2^+ species (see Table 7.4). Even taking into account the considerable amount of FeOH^{2+} species, the iron-chloride complexes present higher molar absorptivity under UV radiation and photo-decompose with higher quantum yields [23]. Moreover, De Laat et al. [45] have simulated the distribution of inorganic radicals

as a function of solution pH, considering the presence of NaCl 0.1 M, and it was observed that, at pH 2.8, all hydroxyl radicals (HO^\bullet) are converted in dichlorine anion radicals ($\text{Cl}_2^{\bullet-}$), which is a much less reactive species. On the other hand, in the presence of high sulphate concentrations, the amount of HSO_4^- is higher (about 5.4, 0.2 and 1.2 mM, for experiments with H_2SO_4 , HCl and $\text{H}_2\text{SO}_4 + \text{HCl}$, respectively – data not showed), and even if HSO_4^- converts all HO^\bullet in $\text{SO}_4^{\bullet-}$, this radical can be more reactive than $\text{Cl}_2^{\bullet-}$, hence the photo-oxidation rate is higher.

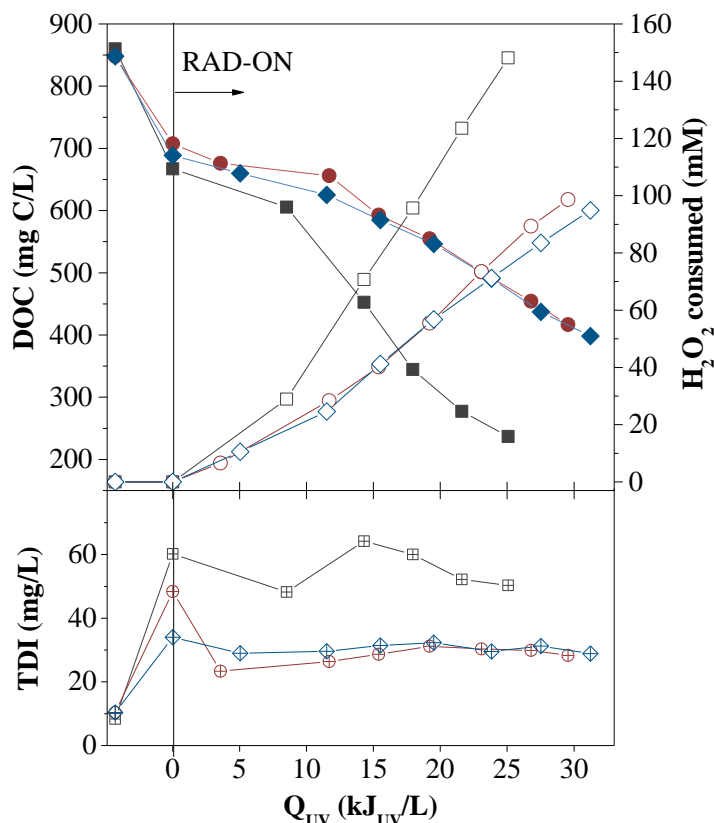


Figure 7.7. Evaluation of the DOC (closed symbols), H_2O_2 consumed (open symbols) and TDI concentration (crossed symbols) during the photo-Fenton reaction for different acid types. Operational conditions: pH = 2.8; $T = 30^\circ\text{C}$; $[\text{Fe}] = 60 \text{ mg/L}$, $I = 40 \text{ W}_{\text{UV}}/\text{m}^2$; (■, □, ▣) – H_2SO_4 ; (●, ○, ⊕) – HCl ; (◆, ◇, ⊞) – $\text{H}_2\text{SO}_4 + \text{HCl}$.

Looking at the iron profile (Figure 7.7), it can be observed that when HCl is used in the acidification procedure, the TDI concentration decreases at the beginning of photo-Fenton reaction and remains approximately constant during the experiments, achieving average TDI concentrations near 30 mg/L. This behaviour is in accordance with the theoretical Fe^{3+} speciation diagrams (Figure 7.8), where it was predicted that when HCl or H_2SO_4 were only used, $\text{Fe}(\text{OH})_{3(s)}$ was formed at $\text{pH} \geq 2.7$ or $\text{pH} \geq 3.0$, respectively.

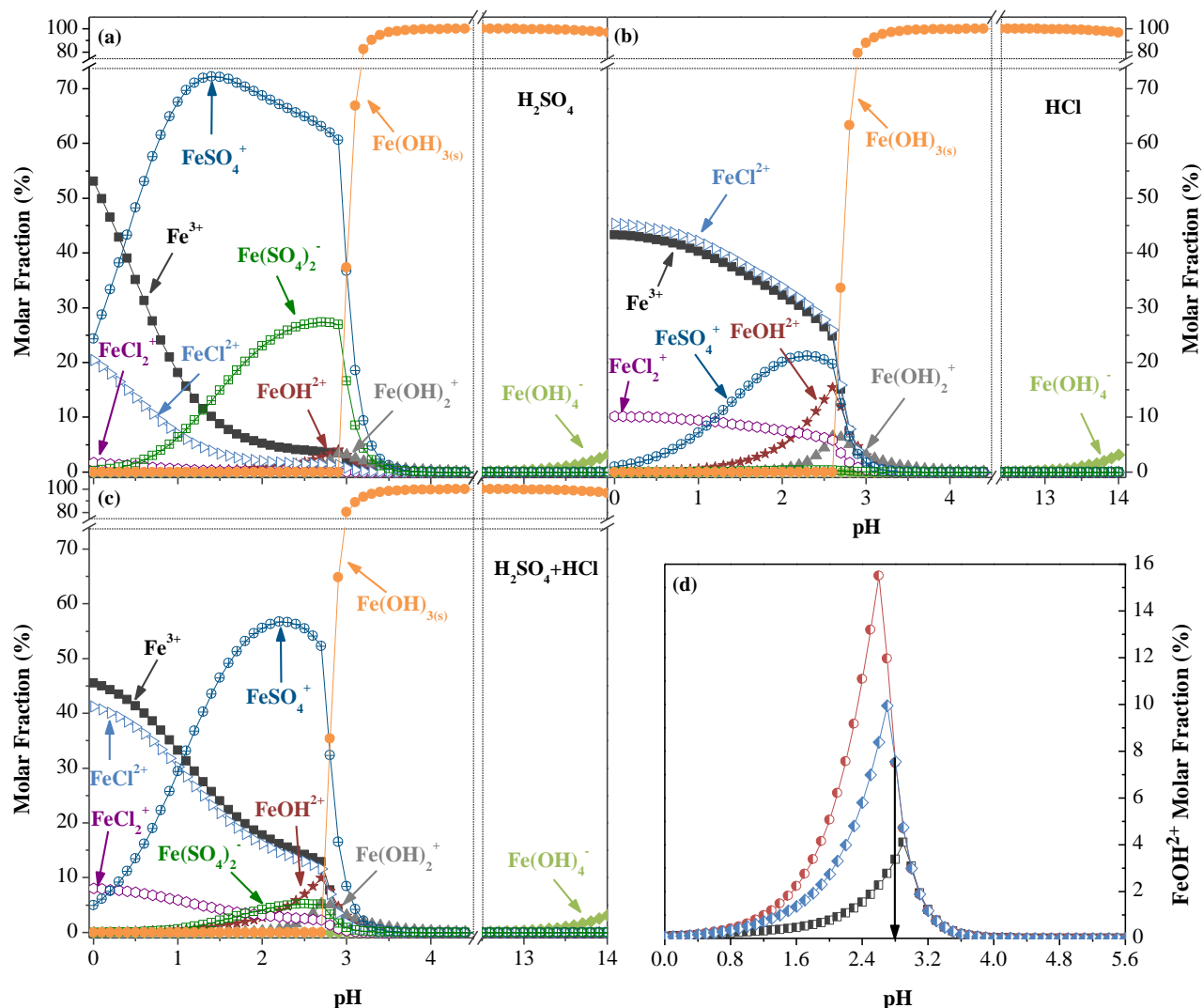


Figure 7.8. Theoretical Fe^{3+} speciation diagrams as a function of solution pH in the conditions of the experiments performed with different acid types: (a) H_2SO_4 ; (b) HCl ; (c) $\text{H}_2\text{SO}_4 + \text{HCl}$. Comparison of the theoretical molar fraction of FeOH^{2+} as a function of pH in the conditions of the experiments performed with different acid types (d): H_2SO_4 (■); HCl (●) and $\text{H}_2\text{SO}_4 + \text{HCl}$ (◆).

Crossing the kinetic data with the average TDI concentration, the reaction rate increased 2.3 times and the average dissolved iron concentration rose from 30 to 55 mg/L (tests with HCl and H_2SO_4 , respectively). An analogous situation was observed for the group of experiments where the iron concentration was changed, at 20 °C (using only H_2SO_4). In this case it was observed that the increment of the average dissolved iron concentration from 30 to 55 mg/L (tests with a desired TDI concentration of 40 and 60 mg/L, respectively), led to an enhancement of the reaction rate of 2.2 times. This behaviour suggests that the lack of iron, when the HCl was used, can also clarify the loss of the photo-Fenton reaction efficiency.

Considering the results presented above, the best option is to only use sulphuric acid in the preliminary acidification step of the photo-Fenton reaction, leading to higher mineralization rates. Regarding the high amount of ammonium in the leachate, a preliminary biological nitrification to nitrates/nitrites can be an interesting approach for the consumption of the leachate alkalinity, reducing considerably the amount of acid necessary for the acidification in the photo-Fenton reaction.

7.3.6 Solar photo-Fenton reaction: Influence of irradiance

Solar irradiance in a clear day usually rises from early morning to achieve a maximum intensity between 12:00 and 16:00, according to the location and season, and decreases again during the afternoon. In Chapter 6, it was reported a monthly average solar UV radiation power in the specific location of the sanitary landfill (north of Portugal), where the leachate was collected, of ca. $20 \text{ W}_{\text{UV}}/\text{m}^2$, in spring and summer seasons, and $11 \text{ W}_{\text{UV}}/\text{m}^2$ in winter and autumn seasons. The insolation at the sanitary landfill was of 2944 hours per year and the yearly average global UV radiation power was $17 \text{ W}_{\text{UV}}/\text{m}^2$. Considering that the irradiance varies greatly along the day due to atmospheric conditions (clouds, rain and fog), location and season and, high irradiances are associated to higher temperatures, the influence of the irradiance on the photo-Fenton reaction efficacy must be evaluated.

Figure 7.9 shows that increasing the UV irradiance from 22 to $44 \text{ W}_{\text{UV}}/\text{m}^2$, the photo-Fenton reaction rate: (i) is almost similar in terms of accumulated UV energy, although the H_2O_2 consumption decreases; and (ii) increases ca. 56% (from $0.09 \pm 0.01 \text{ h}^{-1}$ to $0.21 \pm 0.03 \text{ h}^{-1}$), considering the reaction time. Increasing the irradiance up to $68 \text{ W}_{\text{UV}}/\text{m}^2$, the photo-Fenton reaction rate: (i) decreases about 50% when compared with the other UV irradiance values, which can be attributed to a loss of photons; and (ii) stays approximately the same in terms of reaction time. This means that considering the optical length of the reactor (borosilicate glass tube with 46.4 mm internal diameter), higher doses of iron are necessary to absorb all the photons for irradiances higher than $44 \text{ W}_{\text{UV}}/\text{m}^2$. The decrease of H_2O_2 consumption with the increase of the irradiance may be attributed to the predominance of the photochemical pathway concerning the ferric ions regeneration in detriment of the thermal process.

As the maximum UV irradiance recorded in Portugal is around $44 \text{ W}_{\text{UV}}/\text{m}^2$ (spring and summer), it is possible to conclude that all photons reaching the reaction medium will be absorbed, considering the path length of the photoreactors. For lower irradiances (autumn and winter), the kinetic rate remains constant in terms of accumulated UV energy, but the reaction takes longer time.

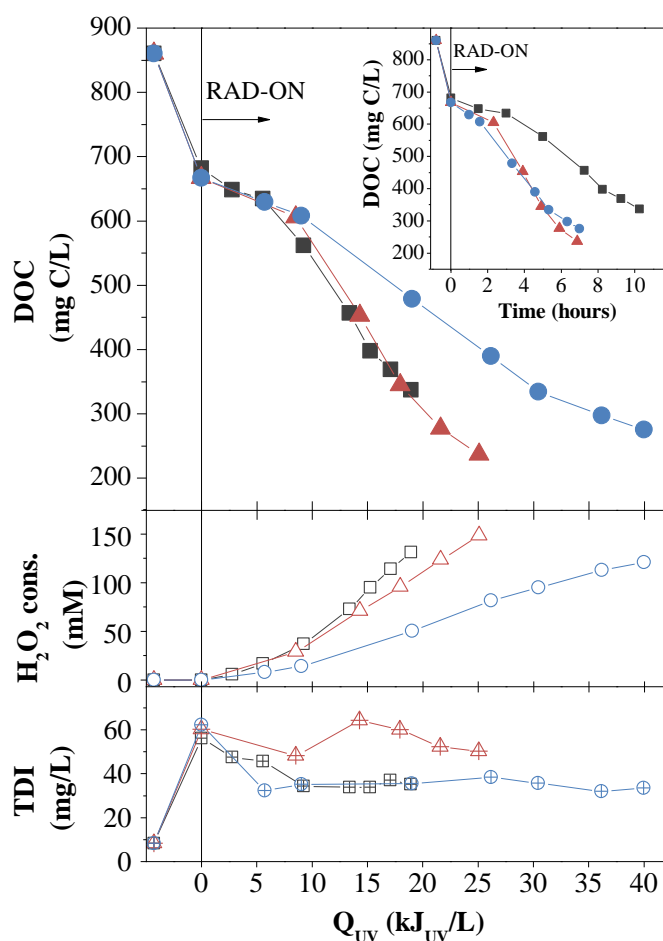


Figure 7.9. Evaluation of the DOC (closed symbols), H_2O_2 consumed (open symbols) and TDI concentration (crossed symbols) during the photo-Fenton reaction for different values of solar irradiance. Operational conditions: $\text{pH} = 2.8$ (H_2SO_4); $T = 30^\circ\text{C}$; $[\text{Fe}] = 60 \text{ mg/L}$; ($\blacksquare, \square, \boxplus$) – $I = 22 \text{ W}_{\text{UV}}/\text{m}^2$; (\bullet, \circ, \oplus) – $I = 44 \text{ W}_{\text{UV}}/\text{m}^2$; ($\blacklozenge, \diamond, \lozenge$) – $I = 68 \text{ W}_{\text{UV}}/\text{m}^2$.

As mentioned in the introduction section, two of the main drawbacks reported in Chapters 3-5 regarding the use of the PF reaction in the treatment of leachates, are associated with: (i) the dark-brown colour intrinsic to leachates and (ii) the high amount of suspended solids generated at the beginning of PF reaction. Therefore, it was decided to collect the leachate after a physico-chemical process. From this study, using the leachate after the coagulation/flocculation treatment step, the optimum PF reaction variables were: $[\text{Fe}^{2+}] = 60 \text{ mg/L}$, $\text{pH} = 2.8$ and $T = 30^\circ\text{C}$, using as acidification agent only H_2SO_4 and an irradiance of $44 \text{ W}_{\text{UV}}/\text{m}^2$. In these conditions, 72% DOC reduction is achieved after $25 \text{ kJ}_{\text{UV}}/\text{L}$ of accumulated UV energy and an H_2O_2 consumption of 149 mM , leading to a final DOC concentration of 237 mg/L . The phototreatment time corresponding to a final DOC of 250 mg/L was established according to the results presented in Chapter 4. In these conditions, the leachate presents a high biodegradability, being able to be further oxidised in a biological reactor, resulting in final COD in agreement with the discharge limit ($150 \text{ mg O}_2/\text{L}$) for disposal into water bodies.

Comparing with the results reported in Chapter 5, where the photo-oxidation reaction ($\text{pH} = 2.8$ (H_2SO_4); $\text{TDI}_m = 33$ mg/L ($\text{TDI}_{\text{added}} = 80$ mg/L); $T_m = 35^\circ\text{C}$; $I_m = 23$ W/m²) was directly applied to a leachate just after an aerobic lagooning stage, the coagulation/flocculation treatment step decreased in about 69% and 44% the required UV energy and H_2O_2 necessary for the photo-Fenton reaction, respectively, in order to achieve a similar final DOC (261 mg/L).

7.4 Conclusions

A solar photo-Fenton (PF) oxidation process showed to be an interesting approach for the mineralization of recalcitrant leachates, and can be integrated in a treatment strategy consisting of the following steps: aerated lagooning, aerated activated sludge, coagulation/flocculation, photo-Fenton oxidation and aerated/anoxic activated sludge.

The coagulation/flocculation step improves substantially the efficiency of the PF reaction, both in terms of energy (69% less) and H_2O_2 consumption (44% less), mainly associated with the decrease on TSS (ca. 75% less) and precipitation of humic acids during the physico-chemical step.

Regarding the PF reaction variables it was possible to conclude that: (i) the best iron concentration was 60 mg/L and above this content the mineralization degree is not affected; (ii) the best pH value was 2.8, since iron precipitation is avoided and the highest FeOH^{2+} concentration is achieved, nevertheless, according to ferric speciation diagrams, the reaction rate constant could be improved if the pH was increased to 3.0; (iii) the rise of leachate temperature benefits the reaction rate until 40°C, mostly attributed to the production of more hydroxyl radicals resulting from a higher ferric ion reduction through thermal reactions and an increment of the FeOH^{2+} molar fraction; however, mainly above 30°C, more H_2O_2 was spent to achieve the same mineralization; (iv) higher reaction rates were achieved when using only H_2SO_4 instead of HCl and $\text{H}_2\text{SO}_4 + \text{HCl}$, since (1) H_2SO_4 is commercially available at higher concentration than HCl but at the similar price, being necessary a much lesser amount to acidify the leachate, (2) the Cl^\bullet and Cl_2^\bullet radicals are less reactive than $\text{SO}_4^{\bullet-}$, and (3) the ferric ions solubility decreases in the presence of high chlorides content; (v) during spring and summer, when the irradiance is around 44 $\text{W}_{\text{UV}}/\text{m}^2$ at maximum, considering the path length of the photoreactors, energy losses will be negligible, and, over autumn and winter, the kinetic reaction rate remains constant in terms of accumulated UV energy, but the reaction takes a longer time.

Ferric ion speciation diagrams showed to be a good tool to predict the dissimilarities on the photo-Fenton reaction performance, according to the solution pH, temperature, concentration of chloride and sulphate ions. When the pH and temperature values were individually changed, it was possible to achieve a linear relation between the pseudo-first order kinetic constant and the theoretical FeOH^{2+} content. Furthermore, in a full-scale plant, speciation diagrams can be used to predict the optimum pH value, taking into account the leachate temperature variability and the amount of sulphate and chloride ions, and also the required phototreatment time for a further biological treatment with high efficiency.

7.5 References

- [1] A. Baun, A. Ledin, L.A. Reitzel, P.L. Bjerg, T.H. Christensen, Xenobiotic organic compounds in leachates from ten Danish MSW landfills--chemical analysis and toxicity tests, *Water Research*, 38 (2004) 3845-3858.
- [2] C.B. Öman, C. Junestedt, Chemical characterization of landfill leachates - 400 parameters and compounds, *Waste Management*, 28 (2008) 1876-1891.
- [3] S. Renou, J.G. Givaudan, S. Poulain, F. Dirassouyan, P. Moulin, Landfill leachate treatment: Review and opportunity, *Journal of Hazardous materials*, 150 (2008) 468-493.
- [4] Y. Deng, J.D. Englehardt, Hydrogen peroxide-enhanced iron-mediated aeration for the treatment of mature landfill leachate, *Journal of Hazardous materials*, 153 (2008) 293-299.
- [5] D. Hermosilla, M. Cortijo, C.P. Huang, Optimizing the treatment of landfill leachate by conventional Fenton and photo-Fenton processes, *Science of the Total Environment*, 407 (2009) 3473-3481.
- [6] E.M.R. Rocha, V.J.P. Vilar, A. Fonseca, I. Saraiva, R.A.R. Boaventura, Landfill leachate treatment by solar-driven AOPs, *Solar Energy*, 85 (2011) 46-56.
- [7] M. Umar, H.A. Aziz, M.S. Yusoff, Trends in the use of Fenton, electro-Fenton and photo-Fenton for the treatment of landfill leachate, *Waste Management*, 30 (2010) 2113-2121.
- [8] J.J. Wu, C.-C. Wu, H.-W. Ma, C.-C. Chang, Treatment of landfill leachate by ozone-based advanced oxidation processes, *Chemosphere*, 54 (2004) 997-1003.
- [9] M. Panizza, C.A. Martinez-Huitle, Role of electrode materials for the anodic oxidation of a real landfill leachate – Comparison between Ti–Ru–Sn ternary oxide, PbO₂ and boron-doped diamond anode, *Chemosphere*, 90 (2013) 1455-1460.
- [10] S.S. Abu Amr, H.A. Aziz, New treatment of stabilized leachate by ozone/Fenton in the advanced oxidation process, *Waste Management*, 32 (2012) 1693-1698.
- [11] V.J.P. Vilar, T.F.C.V. Silva, M.A.N. Santos, A. Fonseca, I. Saraiva, R.A.R. Boaventura, Evaluation of solar photo-Fenton parameters on the pre-oxidation of leachates from a sanitary landfill, *Solar Energy*, 86 (2012) 3301-3315.
- [12] S. Cortez, P. Teixeira, R. Oliveira, M. Mota, Evaluation of Fenton and ozone-based advanced oxidation processes as mature landfill leachate pre-treatments, *Journal of Environmental Management*, 92 (2011) 749-755.
- [13] J.L. de Morais, P.P. Zamora, Use of advanced oxidation processes to improve the biodegradability of mature landfill leachates, *Journal of Hazardous materials*, 123 (2005) 181-186.
- [14] H.-s. Li, S.-q. Zhou, Y.-b. Sun, P. Feng, J.-d. Li, Advanced treatment of landfill leachate by a new combination process in a full-scale plant, *Journal of Hazardous materials*, 172 (2009) 408-415.
- [15] V.J.P. Vilar, E.M.R. Rocha, F.S. Mota, A. Fonseca, I. Saraiva, R.A.R. Boaventura, Treatment of a sanitary landfill leachate using combined solar photo-Fenton and biological immobilized biomass reactor at a pilot scale, *Water Research*, 45 (2011) 2647-2658.

- [16] C. Sawyer, P. McCarty, G. Parkin, *Chemistry for Environmental Engineering and Science*, McGraw-Hill Education, 2003.
- [17] M. Silva, A. Trovó, R. Nogueira, Degradation of the herbicide tebuthiuron using solar photo-Fenton process and ferric citrate complex at circumneutral pH, *Journal of Photochemistry and Photobiology A: Chemistry*, 191 (2007) 187-192.
- [18] C.-H. Liao, M.-C. Lu, S.-H. Su, Role of cupric ions in the H_2O_2/UV oxidation of humic acids, *Chemosphere*, 44 (2001) 913-919.
- [19] S.E. Cabaniss, Carboxylic acid content of a fulvic acid determined by potentiometry and aqueous Fourier transform infrared spectrometry, *Analytica Chimica Acta*, 255 (1991) 23-30.
- [20] J.J. Pignatello, E. Oliveros, A. MacKay, *Advanced Oxidation Processes for Organic Contaminant Destruction Based on the Fenton Reaction and Related Chemistry*, *Critical Reviews in Environmental Science and Technology*, 36 (2006) 1-84.
- [21] J. Kiwi, A. Lopez, V. Nadtochenko, Mechanism and kinetics of the OH-radical intervention during Fenton oxidation in the presence of a significant amount of radical scavenger (Cl⁻), *Environmental Science & Technology*, 34 (2000) 2162-2168.
- [22] A. Machulek Júnior, F.H. Quina, F. Gozzi, V.O. Silva, J.E.F. Moraes, Fundamental Mechanistic Studies of the Photo-Fenton Reaction for the Degradation of Organic Pollutants, in: T. Puzyn, A. Mostrag-Szlichtyng (Eds.) *Organic Pollutants*, Rijeka: InTech, 2011, pp. 1-22.
- [23] A. Machulek Jr, J.E.F. Moraes, L.T. Okano, C.A. Silvério, F.H. Quina, Photolysis of ferric ions in the presence of sulfate or chloride ions: implications for the photo-Fenton process, *Photochemical & Photobiological Sciences*, 8 (2009) 985-991.
- [24] J.T. Jasper, D.L. Sedlak, Phototransformation of wastewater-derived trace organic contaminants in open-water unit process treatment wetlands, *Environmental Science & Technology*, 47 (2013) 10781-10790.
- [25] T. Zeng, W.A. Arnold, Pesticide photolysis in prairie potholes: probing photosensitized processes, *Environmental Science & Technology*, 47 (2012) 6735-6745.
- [26] P. Neta, R.E. Huie, A.B. Ross, Rate constants for reactions for inorganic radicals in aqueous solution, *Journal of Physical and Chemical Reference Data*, 17 (1988) 1027-1247.
- [27] J. De Laat, T.G. Le, Kinetics and modeling of the Fe (III)/ H_2O_2 system in the presence of sulfate in acidic aqueous solutions, *Environmental Science & Technology*, 39 (2005) 1811-1818.
- [28] A. El-Ghenymy, S. Garcia-Segura, R.M. Rodríguez, E. Brillas, M.S. El Begrani, B.A. Abdelouahid, Optimization of the electro-Fenton and solar photoelectro-Fenton treatments of sulfanilic acid solutions using a pre-pilot flow plant by response surface methodology, *Journal of Hazardous materials*, 221 (2012) 288-297.
- [29] M.M. Ghoneim, H.S. El-Desoky, N.M. Zidan, Electro-Fenton oxidation of Sunset Yellow FCF azo-dye in aqueous solutions, *Desalination*, 274 (2011) 22-30.
- [30] J. Feng, X. Hu, P.L. Yue, H.Y. Zhu, G.Q. Lu, Degradation of azo-dye orange II by a photoassisted Fenton reaction using a novel composite of iron oxide and silicate nanoparticles as a catalyst, *Industrial & Engineering Chemistry Research*, 42 (2003) 2058-2066.

- [31] J.W.T. Spinks, R.J. Woods, *An introduction to radiation chemistry*, (1990).
- [32] D.L. Jones, K.L. Williamson, A.G. Owen, Phytoremediation of landfill leachate, *Waste Management*, 26 (2006) 825-837.
- [33] N. Klamerth, S. Malato, A. Agüera, A. Fernández-Alba, Photo-Fenton and modified photo-Fenton at neutral pH for the treatment of emerging contaminants in wastewater treatment plant effluents: A comparison, *Water Research*, 47 (2013) 833-840.
- [34] X. Liu, F.J. Millero, The solubility of iron hydroxide in sodium chloride solutions, *Geochimica et Cosmochimica Acta*, 63 (1999) 3487-3497.
- [35] Y. Sun, J.J. Pignatello, Activation of hydrogen peroxide by iron (III) chelates for abiotic degradation of herbicides and insecticides in water, *Journal of Agricultural and Food Chemistry*, 41 (1993) 308-312.
- [36] Y. Sun, J.J. Pignatello, Organic intermediates in the degradation of 2, 4-dichlorophenoxyacetic acid by iron (3+)/hydrogen peroxide and iron (3+)/hydrogen peroxide/UV, *Journal of Agricultural and Food Chemistry*, 41 (1993) 1139-1142.
- [37] N. Klamerth, S. Malato, M.I. Maldonado, A. Agüera, A. Fernández-Alba, Modified photo-Fenton for degradation of emerging contaminants in municipal wastewater effluents, *Catalysis Today*, 161 (2011) 241-246.
- [38] Y. Deng, Formation of iron(III) hydroxides from homogeneous solutions, *Water Research*, 31 (1997) 1347-1354.
- [39] S. Malato, P. Fernández-Ibáñez, M.I. Maldonado, J. Blanco, W. Gernjak, Decontamination and disinfection of water by solar photocatalysis: Recent overview and trends, *Catalysis Today*, 147 (2009) 1-59.
- [40] V.J.P. Vilar, S.M.S. Capelo, T.F.C.V. Silva, R.A.R. Boaventura, Solar photo-Fenton as a pre-oxidation step for biological treatment of landfill leachate in a pilot plant with CPCs, *Catalysis Today*, 161 (2011) 228-234.
- [41] V.J.P. Vilar, J.M.S. Moreira, A. Fonseca, I. Saraiva, R.A.R. Boaventura, Application of Fenton and Solar Photo-Fenton Processes to the Treatment of a Sanitary Landfill Leachate in a Pilot Plant with CPCs, *Journal of Advanced Oxidation Technologies*, 15 (2012) 107-116.
- [42] F.C. Moreira, R.A.R. Boaventura, E. Brillas, V.J.P. Vilar, Degradation of trimethoprim antibiotic by UVA photoelectro-Fenton process mediated by Fe(III)-carboxylate complexes, *Applied Catalysis B: Environmental*, 162 (2015) 34-44.
- [43] A.E. Martell, R.M. Smith, *Critical stability constants*, Plenum Press, New York, 1977.
- [44] J. De Laat, T.G. Le, Effects of chloride ions on the iron (III)-catalyzed decomposition of hydrogen peroxide and on the efficiency of the Fenton-like oxidation process, *Applied Catalysis B: Environmental*, 66 (2006) 137-146.
- [45] J. De Laat, G. Truong Le, B. Legube, A comparative study of the effects of chloride, sulfate and nitrate ions on the rates of decomposition of H₂O₂ and organic compounds by Fe(II)/H₂O₂ and Fe(III)/H₂O₂, *Chemosphere*, 55 (2004) 715-723.

8 Nitrification and denitrification kinetic parameters of a mature sanitary landfill leachate

The purpose of this work is to assess the effect of the main nitrification and denitrification variables on the nitrogen's biological removal via nitrite, from mature leachates. The leachate samples were collected after an aerated lagoon, at a LTP nearby Porto, presenting a high amount of dissolved organic carbon (1.1-1.2 g DOC/L), ammonium nitrogen (1.0-1.5 g NH₄⁺-N/L) and alkalinity (4.6-6.7 g CaCO₃/L). The experiments were carried out in a 1-L lab-scale batch reactor, equipped with a pH, temperature and dissolved oxygen (DO) control system, in order to determine the reaction kinetic constants at unchanging conditions.

The nitrification reaction rate was evaluated while varying the (i) operating temperature (15, 20, 25 and 30 °C), (ii) DO concentration interval (0.5-1.0, 1.0-2.0 and 2.0-4.0 mg/L) and (iii) solution pH (not controlled, 7.5-8.5 and 6.5-7.5). At the beginning of most assays, it was verified that the ammonia stripping occurred simultaneously to the nitrification, reaching up to 31 % removal of total dissolved nitrogen. The denitrification kinetic constants and the methanol consumptions were calculated testing (i) diverse values of pH interval (6.5-7.0, 7.0-7.5, 7.5-8.0, 8.0-8.5 and 8.5-9.0), (ii) different temperatures (20, 25 and 30 °C) and (iii) the addition of phosphate ions (30 mg PO₄³⁻/L), using the previously nitrified effluent.

The maximum nitrification rate obtained was 37±2 mg NH₄⁺-N/(h.g VSS) (25 °C, 1.0-2.0 mg O₂/L, pH not controlled), consuming 5.3±0.4 mg CaCO₃/mg NH₄⁺-N. The highest denitrification rate achieved was 27±1 mg NO₂⁻-N/(h.g VSS) (pH between 7.5 and 8.0, 30°C, adding 30 mg PO₄³⁻/L), with a C/N consumption ratio of 1.6±0.1 mg CH₃OH/mg NO₂⁻-N and an overall alkalinity production of 3.2±0.1 mg CaCO₃/mg NO₂⁻-N. The denitrification process showed to be sensitive to all studied parameters, while the nitrification reaction did not suffer significant change when DO content was changed.

The two most abundant groups in the nitrification and denitrification processes, as indicated by the 454-pyrosequencing analysis of the 16S rRNA gene, were affiliated to Saprospiraceae/Nitrosomonadaceae and Hyphomicrobiaceae/Saprospiraceae, respectively. The abundance of Nitrosomonadaceae and Hyphomicrobiaceae (in particular, Hyphomicrobium) in the nitrification and denitrification process, respectively, is in agreement with the nitrifying and denitrifying activity of these bacterial members.

This chapter is based on the research article “Silva, T.F.C.V., Vieira, E.S.S., Lopes, A.R., Bondoso, J., Nunes, O.C., Fonseca, A., Saraiva, I., Boaventura, R.A.R, Vilar, V.J.P, *Determination of Nitrification and Denitrification Kinetic Parameters of a Sanitary Landfill Leachate and Characterization of the Bacterial Communities*, submitted to *Bioresource Technology*, 2015”.

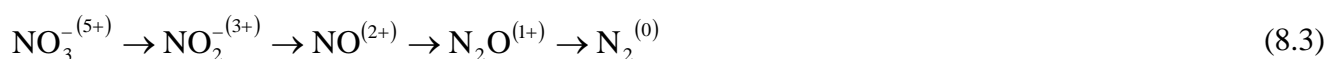
8.1 Introduction

Sanitary landfill leachates are characterized as a complex mixture of diverse organic and inorganic contaminants [1, 2], which are usually removed by combining different treatment processes [3, 4]. Due to its simplicity, reliability, high cost-effectiveness and to the high nitrogen content (mostly in the NH_4^+ -N form) inherent in this type of effluent, the activated sludge biological process is almost always applied in leachate treatment plants (LTPs) [5, 6]. Up to date, the nitrification reaction followed by a denitrification step is the biological process most used for nitrogen removal from wastewaters [7].

The nitrification reaction is a litho-autotrophic microbiological mechanism, occurring under aerobic conditions, where the carbon dioxide is the carbon source and the molecular oxygen is the final electron acceptor. Usually, nitrification reaction takes place in two steps: (i) first, ammonium nitrogen is oxidised into nitrite (nitritation) by the ammonia-oxidising bacteria (AOB), frequently *Nitrosomonas*, according to the Eq. (8.1); and (ii) then, in more restrictive operating conditions, the nitrite is converted into nitrate (nitrataion) by the nitrite-oxidising bacteria (NOB), such as *Nitrobacter* or *Nitrospira*, in agreement with the Eq. (8.2) [8-10]. In wastewater treatment processes with high organic load, the AOB and NOB coexist with organo-heterotrophic bacteria, since these are the most responsible for the conversion of organic nitrogen compounds, such as proteins and amino acids, into simplest products, including the ammonium ions [11-13].

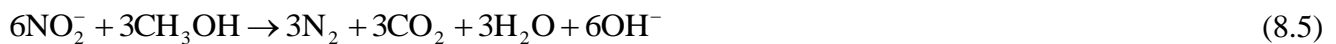


In contrast, the denitrification reaction is widely distributed among prokaryotic microorganisms, being coupled with chemo-organo-heterotrophy or chemo-litho-autotrophy. It occurs under anoxic conditions, because an ionic nitrogen oxide compound acts as the final electron acceptor. The denitrification process involves the dissimilatory reduction of nitrate and/or nitrite into atmospheric nitrogen, through a sequential production of gaseous nitrogen oxide intermediates. The linear pathway of the reductive steps is shown in the Eq. (8.3) (where the values between parenthesis represent the oxidation states of each nitrogen specie) [8, 9, 14]:



Each oxidised nitrogen substrate is catalysed by a specific enzyme (NO_3^- , NO_2^- , NO or N_2O reductase) and attends as electron acceptor on the denitrifying bacteria respiration, commonly, attached to the oxidation of a biodegradable organic compound as electron donor for energy generation [8, 9].

Although, in general, leachates contain a high organic matter content, their biodegradable fraction decreases with aging, due to the releasing of recalcitrant molecules (mainly humic and fulvic acids) from the solid wastes deposited in the landfills. [5]. This fact combined with that of denitrification step being preceded by nitrification (where the biodegradable carbon is already oxidized) often leads to the need of adding an external carbon source to accomplish the denitrification reaction. Several carbon sources have been used on this process, e.g., methanol, ethanol, glucose, methane, acetic and benzoic acid [15-19]. Among the various carbon sources commercially available, methanol is widely used, mainly because it is the cheaper, it reduces the sludge production and its residual content can be easily removed by aeration [15, 17, 20]. The Eqs. (8.4) - (8.6) represent the energy-yielding reactions involved in denitrification, where the methanol provides energy to bacteria, such as *Hyphomicrobium*, and the gaseous dinitrogen is released to the atmosphere [12]:



The biological nitrogen removal via nitrite, instead of nitrate, could be a good option since nitrite is an intermediate of both nitrification and denitrification reactions. Thus, the nitrification could be stopped at nitrite and the denitrification could start from there, by reducing the nitrite into nitrogen gas, thereby saving about 25 % in the oxygen demand for the nitrification, 40 % in the needs of external carbon source for the denitrification and 50 % in the size of the anoxic reactor [21, 22]. This shortcut was effectively implemented by Spagni and Marsili-Libelli [23], on the treatment of sanitary landfill leachate with an average initial concentration of ammonium nitrogen of 1199 mg $\text{NH}_4^+\text{-N/L}$, using a sequencing batch reactor (SBR), at bench-scale. The authors achieved efficiencies of 98 and 95 % on the nitrification and denitrification reactions, respectively, saving about 35 % on the external carbon source.

The extension of the nitrification reaction can be influenced by diverse abiotic factors, being the most important the temperature, pH, dissolved oxygen (DO) deficiency, the presence of toxic or inhibitory substances and the substrate concentration. The nitrite build-up occurs when, individually or in combination, certain deviations in the abiotic factors repress the action of the nitrite-oxidizing bacteria in detriment of the ammonia-oxidising bacteria. The denitrification process can be affected by the energy source, the temperature, the pH and the presence of oxygen, since the bacteria begin to respire with oxygen and stop to denitrify [8].

The main goal of the present work is to assess how the variation of certain operating conditions may affect the reaction rates of nitrification and denitrification via nitrite, in a full-scale biological treatment of a mature leachate, since this process is almost always incorporated in LTPs. To achieve our goal, at lab-scale, the influence of: i) temperature, dissolved oxygen (DO) concentration and pH, on the nitrification of a leachate collected at the outlet of an aerobic lagoon; and (ii) pH interval, operating temperature and phosphate addition, on the denitrification of a nitrified leachate, was assessed. The biological sludge used in both nitrification and denitrification reactions was previously adapted to aerobic and anoxic conditions, respectively. Furthermore, the composition and structure of the corresponding bacterial communities were assessed, using 454-pyrosequencing of the 16S rRNA gene.

8.2 Experimental methodology

A set of 16 experiments was conducted in a respirometer, working as an activated sludge biological reactor, at lab-scale, in order to calculate the kinetic constants of nitrification and denitrification reactions under controlled conditions. Table 8.1 shows a short description of the operating conditions applied on each test.

For nitrification assays, the activated sludge was collected from an aerobic biological reactor of a leachate treatment plant (LTP), and it was acclimated for 3 months to the landfill leachate in aerobic conditions, prior to the first test. During the acclimation process, the leachate collected after aerobic lagooning was successively fed to a 10-L batch bioreactor ($24 < t \text{ (h)} < 48$, $22 < T \text{ (}^\circ\text{C)} < 28$; $6.5 < \text{pH} < 9.0$ (through the NaOH addition, after the leachate alkalinity exhaustion); $0.5 < \text{DO (mg/L)} < 4$), up to almost complete oxidation of ammonium into nitrite ($> 95\%$). This reactor was kept running throughout entire nitrification test period, since it was the source of biomass for the experiments in the respirometer. The obtained bio-treated leachate was saved for later use on the denitrification tests and on the acclimation of the denitrifying bacteria.

Table 8.1. Operating conditions adopted in the nitrification and denitrification tests.

	Group of experiments	V _{leachate} (mL)	V _{biomass} ^c (mL)	T (°C)	DO interval (mg/L)	pH interval
Nitrification	I Effect of pH	880 ^a	20 ^d	25	1.0 – 2.0	6.5 – 7.5
						7.5 – 8.5
						Not controlled
	II Effect of DO	880 ^a	20 ^d	25	1.0 – 2.0	Not controlled
		880 ^a	20 ^d			
		870 ^a	30 ^d			
III Effect of Temperature	870 ^a	30 ^d	15	0.5 – 1.0	Not controlled	
			20			
			25			
			30			
Denitrification	I Effect of pH	950 ^b	50 ^e	30	< 0.1	6.5 – 7.0
						7.0 – 7.5
						7.5 – 8.0
						8.0 – 8.5
	II Effect of Temperature	950 ^b	50 ^e	20	< 0.1	7.5 – 8.0
				25		
30						
III <u>Phosphate addition</u>	950 ^b	50 ^e	30	< 0.1	7.5 – 8.0	
	<u>950^b</u>	<u>50^e</u>	<u>30</u>		<u>< 0.1</u>	<u>7.5 – 8.0</u>

^aLeachate after aerobic lagooning; ^bLeachate after nitrification; ^cAmount of biomass after centrifugation (2000 rpm, 3 min);

^dBiological sludge previously adapted to aerobic regime and leachate after aerobic lagooning; ^eBiological sludge previously adapted to anoxic regime and nitrified leachate.

For denitrification tests startup, a 10-L batch bioreactor ($48 < t \text{ (h)} < 72$; $25 < T \text{ (°C)} < 30$; $7.0 < \text{pH} < 9.5$ (through the H₂SO₄ (50 %) addition; DO < 0.1 mg/L) was inoculated with a fraction of activated sludge from the nitrification reactor, and successively fed with nitrified leachate, up to almost complete reduction of nitrite into gaseous dinitrogen (> 90 %). After 4 months of acclimation, this reactor was also kept in operation in parallel with the respirometer, as biomass source.

To assess the bacterial community composition and structure, 6 mixed liquor samples were collected from both reactors (3 from the nitrification (N) reactor and 3 from the denitrification (D) reactor), in different batches and at the initial (I), middle (M) and final (F) treatment stages. The total bacterial genomic DNA was extracted from each sample and the 16S rRNA gene diversity was assessed by 454-pyrosequencing, according to the experimental procedure described in Chapter 2 (section 2.7).

All the chemicals used in this work, the detailed description of the experimental unit and respective procedures, as well as the employed analytical methods can be consulted in the Chapter 2. Table 8.2 only presents the main characteristics of the leachate used in the nitrification and denitrification assays.

Table 8.2. Physico-chemical characterization of the leachate used in the nitrification and denitrification tests.

Parameter	Unities	Nitrification tests	Denitrification tests
pH	Sorensen scale	8.3 ± 0.5	7.8 ± 0.2
Total dissolved carbon (TDC)	g C/L	2.5 ± 0.3	1.2 ± 0.1
Dissolved inorganic carbon (DIC)	g C/L	1.4 ± 0.2	0.05 ± 0.01
Alkalinity ^a	g CaCO ₃ /L	5.7 ± 0.9	0.19 ± 0.04
Dissolved organic carbon (DOC)	g C/L	1.14 ± 0.07	1.2 ± 0.1
Total dissolved nitrogen (N _D)	g N/L	1.3 ± 0.2	1.1 ± 0.2
Total ammonia nitrogen	g N-NH ₄ ⁺ /L	1.3 ± 0.2	0.03 ± 0.02
Nitrate	g N-NO ₃ ⁻ /L	0.02 ± 0.01	0.03 ± 0.02
Nitrite	g N-NO ₂ ⁻ /L	0.08 ± 0.01	1.1 ± 0.2
Phosphate	g PO ₄ ³⁻ /L	0.04 ± 0.01	0.015 ± 0.04
Sulphate	g SO ₄ ²⁻ /L	0.12 ± 0.01	0.13 ± 0.03
Chloride	g Cl ⁻ /L	2.47 ± 0.06	2.5 ± 0.2
Sodium	g Na ⁺ /L	2.07 ± 0.06	2.7 ± 0.1
Potassium	g K ⁺ /L	1.95 ± 0.05	2.06 ± 0.03
Magnesium	g Mg ²⁺ /L	0.29 ± 0.02	0.24 ± 0.01
Calcium	g C a ²⁺ /L	0.46 ± 0.08	0.58 ± 0.05

^aAlkalinity values considering that, for pH < 11, the inorganic carbon was in the form of carbonates and bicarbonates [24].

8.3 Results and discussion

8.3.1 Nitrification

8.3.1.1 General Remarks

During all nitrification tests, the nitrate concentration was negligible, indicating that only the nitrification reaction occurred, leading to the accumulation of nitrite inside the biological reactor. Whereby, the nitrification kinetic constants were calculated in terms of ammonia removal and nitrite formation. The cause of nitrite build-up was almost certainly due to the presence of free ammonia (NH₃), which has been described as being more inhibitory for the NOB (0.08-0.82 mg NH₃-N/L) than for the AOB (8.2-123 mg NH₃-N/L) [10, 25]. Throughout the experiments, the maximum concentration of free ammonia ranged between 29 and 469 mg NH₃-N/L (see Table 8.3), which came to be inhibitory for both nitrifying bacteria species. The amount of un-ionised ammonia ([NH₃-N]) was correlated with the concentration of total ammonia nitrogen ([TAN] = [NH₃-N + NH₄⁺-N], determined directly by ionic chromatography), the solution pH and the temperature (in °C), according to the Eq. (8.7) [25]:

$$[\text{NH}_3 - \text{N}] = \frac{\text{TAN} \times 10^{\text{pH}}}{e^{6344/(273+T)} + 10^{\text{pH}}} \quad (8.7)$$

Table 8.3. Operating conditions and kinetic parameters of the nitrification process for all experiments.

pH range	pH _m	DO range (mg/L)	DO _m (mg/L)	T (°C)	VSS (g/L)	TAN _i (mg/L)	t _r ^a (h)	TAN _{AS} ^b (%)	NH ₃ -N _{max} (mg/L)	k_n^c	k_a^d	Alkalinity ^e	Δt^f (h)	
										$\left(\frac{\text{mg NO}_2^- - \text{N}}{\text{g VSS} \cdot \text{h}} \right)$	$\left(\frac{\text{mg NH}_4^+ - \text{N}}{\text{g VSS} \cdot \text{h}} \right)$	$\left(\frac{\text{mg CaCO}_3}{\text{mg NH}_4^+ - \text{N}} \right)$		
Group I Not controlled	8.91	0.5-1.0	1.26	15	2.92	1155	16	0.1	217	2.3 ± 0.1	2.6 ± 0.1	6.3 ± 0.3	3-16	
	8.92		0.99	20	3.25	1488	24	13.9	378	21 ± 2	21 ± 1	5.5 ± 0.6	19-24	
	8.75		0.53	25	2.76	1750	14	23.1	469	32 ± 1	34 ± 2	5.2 ± 0.5	10-14	
	8.59		0.41	30	3.48	1471	13	30.9	469	31 ± 1	30 ± 2	5.2 ± 0.3	7-11	
Group II Not controlled	8.75	0.5-1.0	0.53		2.76	1750	14	23.1	469	32 ± 1	34 ± 2	5.2 ± 0.5	10-14	
	8.73	1.0-2.0	1.35	25	2.19	1074	16	14.3	340	34 ± 2	37 ± 2	5.3 ± 0.4	9-14	
	8.91	2.0-4.0	3.07		2.30	1089	16	31.1	383	29 ± 2	29 ± 3	5.1 ± 0.5	8-13	
Group III Not controlled	6.5-7.5	7.02	1.83		1.94	973	14	2.8	29	9.4 ± 0.4	9.7 ± 0.5	5.9 ± 0.6	6-14	
	7.5-8.5	8.18	1.0-2.0	1.26	25	1.92	1012	16	8.3	126	24 ± 1	26 ± 2	5.7 ± 0.4	10-16
	8.73		1.35		2.19	1074	16	14.3	340	34 ± 2	37 ± 2	5.3 ± 0.4	9-14	

^aTotal reaction time; ^bTotal ammonia nitrogen fraction removed by ammonia stripping $((A_1 - A_2) \times \text{VSS}) / (t_r \times \text{TAN}_i) \times 100$, where A_1 and A_2 are the areas below the curves of the Figure 8.2 related to TAN and NO₂⁻-N, respectively); ^cNitrification's reaction rate, expressed in the terms of nitrite formation, whose values correspond to the slopes on the respective Δt (Figure 8.2); ^dNitrification's reaction rate, expressed in the terms of ammonium removal, whose values correspond to the slopes on the respective Δt (Figure 8.2); ^eAlkalinity consumption during nitrification reaction, considering the amount of NaOH added, when necessary, and that, for pH < 11, the inorganic carbon was in the form of carbonates and bicarbonates [24], whose values correspond to the slopes on the respective Δt (Figure 8.2); ^fTime interval considered for the calculus of the nitrification's reaction rate and alkalinity's consumption.

Furthermore, in practically all tests, it was verified that it was possible to divide the reaction into two distinct periods: (i) a first phase, where the nitrification process occurred together with the ammonia stripping (phenomenon which can take place at high pH values), before the nitrification stabilization [26]; and (ii) a second phase, where almost only the nitrification reaction was observed. Hence, in order to clarify the general behaviour of the experiments performed along the nitrification studies, initially, in this subsection, will just be displayed, as example, the test performed without pH control, at 25 °C, dissolved oxygen (DO) between 0.5-1.0 mg/L and an average concentration of volatile suspended solids (VSS) of 2.76 g/L (Figure 8.1). As can be inferred from total dissolved nitrogen, total ammonia nitrogen (TAN) and total nitrite-nitrogen (TNN) profiles, up to the 8-hours, a considerable fraction of the ammonia was lost by air-stripping, reducing the total nitrogen content by about 25%. After that, the concentration of total nitrogen remained sensibly constant. However, only after 10-hours working (moment from which pH began to decrease quickly), the TAN depletion rate became closest to the TNN formation rate, as indicated by the kinetic constants of 34 ± 2 mg $\text{NH}_4^+\text{-N}/(\text{h.g VSS})$ and 32 ± 1 mg $\text{NO}_2^-\text{-N}/(\text{h.g VSS})$, respectively. Until then, the TAN removal rate (42 ± 1 mg $\text{NH}_4^+\text{-N}/(\text{h.g VSS})$) was ca. 2 times higher than the TNN production rate (21 ± 2 mg $\text{NO}_2^-\text{-N}/(\text{h.g VSS})$).

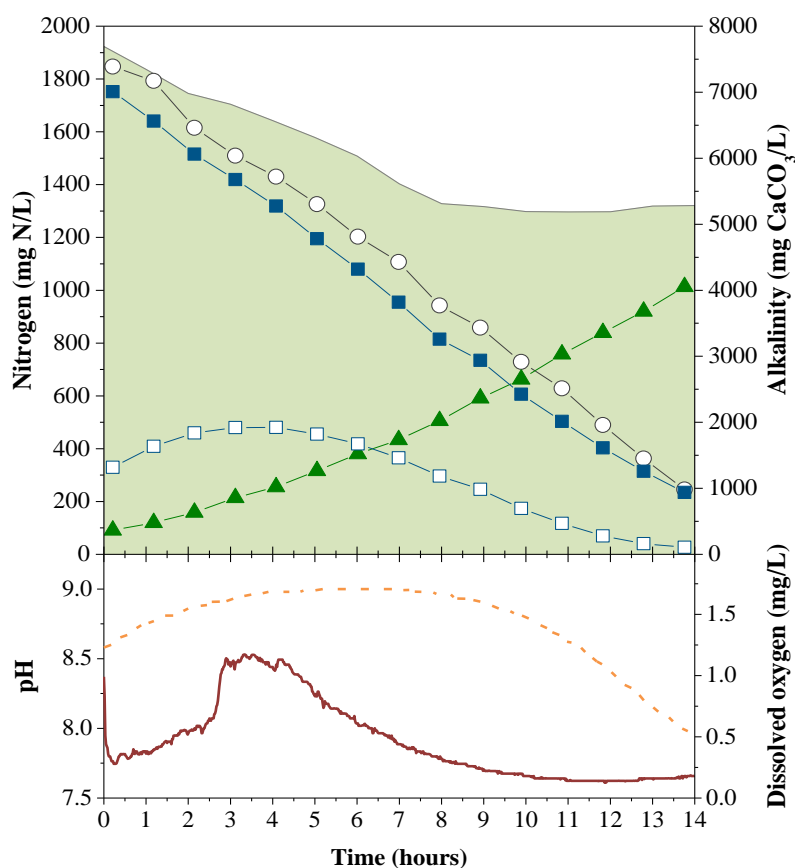


Figure 8.1. Evolution of total dissolved nitrogen (■), total ammonia nitrogen (■ - $\text{NH}_4^+\text{-N} + \text{NH}_3\text{-N}$), free ammonia (□ - $\text{NH}_3\text{-N}$), total nitrite-nitrogen (▲ - $\text{NO}_2^-\text{-N}$), alkalinity (○), pH (---) and dissolved oxygen (—) during a nitrification test (pH not controlled, OD = 0.5-1.0, T = 25 °C, VSS = 2.76 g/L).

The air stripping process consists in the mass transfer of a volatile compound from a liquid phase to a gas stream [14, 27]. In the present work, ammonia stripping also occurred together with the nitrification reaction. This phenomenon was favoured by the high pH values observed during the tests, as can be depicted in Figure 8.1. The pH rise, observed at the beginning of the experiments, was due to the CO₂ stripping that was significantly faster than the NH₃ stripping, before the equilibrium conditions were achieved, since the Henry's constant for CO₂ (150 atm/mole fraction, at 20 °C) is greater than for NH₃ (0.76 atm/mole fraction, at 20°C) [28-30]. Along the nitrification tests, the total ammonia nitrogen removal by air stripping varied between 0.1 and 31.1%, depending on the operating conditions (see Table 8.3). Similarly, Jokela et al. [31] attested the occurrence of air stripping, during the nitrification of a landfill leachate by a suspended carrier biofilm process, losing about 10 – 30% of nitrogen.

Given the above, the calculation of the nitrification kinetic constants (Table 8.3) was performed taking into account only the period where the ammonia stripping no longer occurred. This period coincided with the moment where the pH drop was faster and the free ammonia content was below 200 mg NH₃-N/L.

8.3.1.2 Influence of the operating parameters

In order to evaluate and predict the behaviour of nitrification reaction, face to potential variations in the operating conditions, 8 experiments were carried out, over approximately 16-hours each, where the influence of the temperature (Group I – 15, 20, 25 and 30 °C), dissolved oxygen (DO) content interval (Group II – 0.5-1.0, 1.0-2.0 and 2.0-4.0 mg/L) and pH interval (Group III – not controlled, 7.5-8.5 and 6.5-7.5) was assessed (Table 8.3). The Figure 8.2 illustrates the profiles of total ammonia nitrogen (TAN) removal and nitrite-nitrogen production per amount of volatile suspended solids used on each experiment, along time, and the alkalinity removal, as a function of TAN removal. The respective maximum reaction rates were obtained from the slopes of these plots, in the respective time interval (see Table 8.3).

The Group I of experiments revealed that: i) for operating temperatures of 15 °C, the activated sludge was almost completely inhibited and, therefore, the extent of the nitrification reaction was very low (2.6 ± 0.1 mg NH₄⁺-N/(h.g VSS)); ii) increasing the temperature from 15 to 25 °C, the nitrification rate increased about 3.1 mg NH₄⁺-N/(h.g VSS) per each Celsius degree, achieving a maximum value of 34 ± 4 mg NH₄⁺-N/(h.g VSS); and iii) for temperatures above the 25°C, the reaction rate was not improved. These results are in agreement with the literature, where the optimum temperature was set in the range of 25-35°C, for the general biological activity [14], and 28-32°C for the nitrification process [12].

Moreover, Shammas [32] studied the interaction of temperature, pH and biomass on the nitrification reaction and found that, using high VSS concentrations (3200 mg/L), the maximum nitrification rate was not affected by increasing the operating temperature from 25 to 33°C. Likewise, Gabarró et al. [33] investigated the influence of the temperature on the AOB activity on the partial nitrification (PN) of a mature leachate, with 6 g NH₄⁺-N/L, in an SBR. During the PN stabilization period, they achieved average specific nitrogen loading rates of 34 ± 4 and 35 ± 10 mg N/(h.g VSS) for 25 and 35 °C, respectively, which perfectly agrees with the nitrification performance disclosed in the present work.

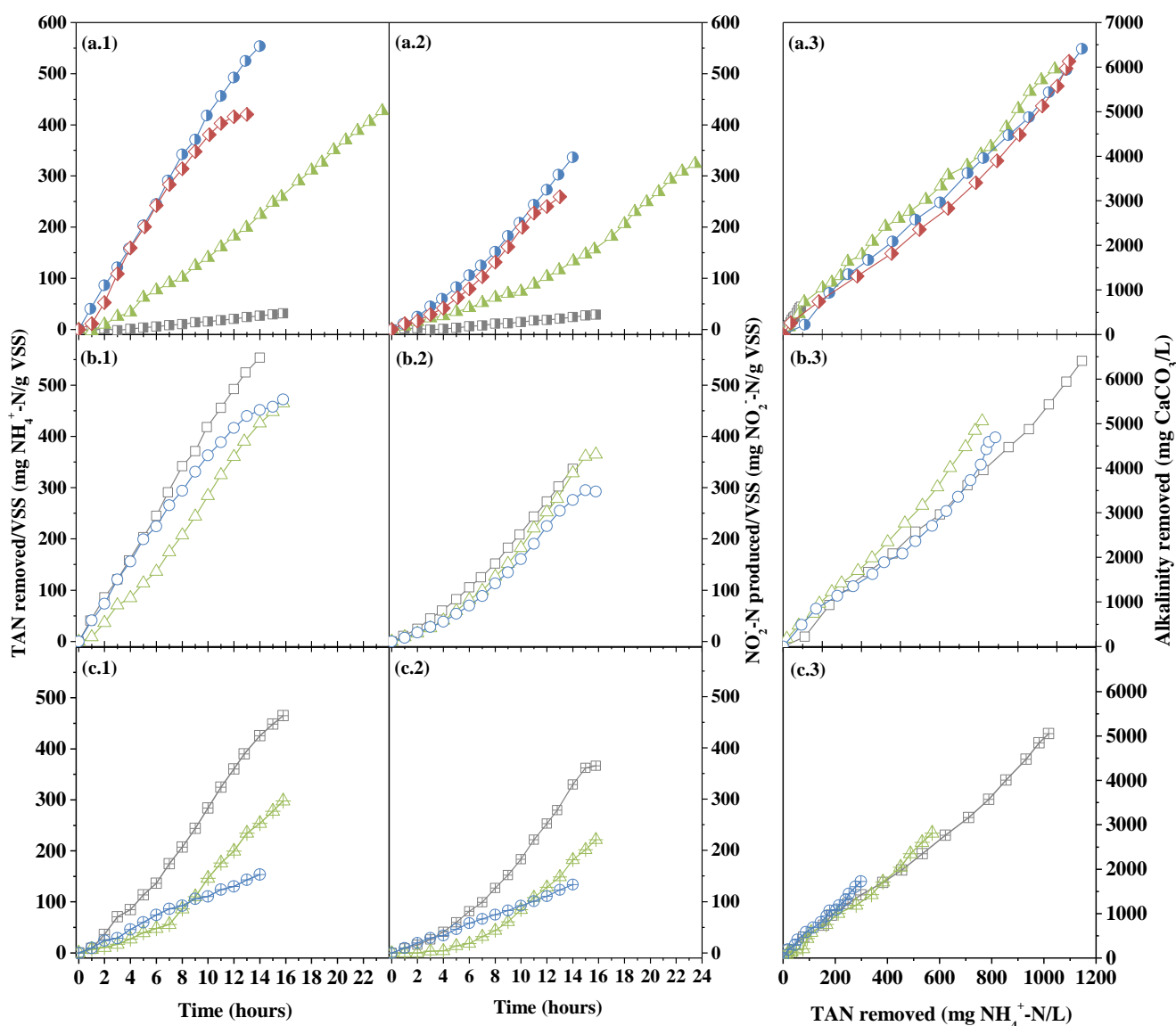


Figure 8.2. Representation of the (.1) TAN removed/VSS ratio, and the (.2) NO₂⁻-N produced/VSS ratio, as a function of time, and the (.3) alkalinity removed, as a function of TAN removed, along all nitrification tests, for different (a) temperature values (15 °C, ■; 20 °C, ▲; 25 °C, ● and 30 °C, ◆), (b) DO intervals (0.5-1.0 mg/L, □; 1.0-2.0 mg/L, △ and 2.0-4.0 mg/L, ○) and (c) pH intervals (6.5-7.5, ⊕; 7.5-8.5, ▲ and not controlled, ⊞).

The Group II results show that the variation of DO content practically had no impact on the reaction rate, which is justified by the fact that nitrification should be mediated by AOB, and these bacteria are more robust than the NOB at low oxygen concentrations [9]. Hanaki et al. [34] explained the nitrite build-up, at low DO, by the difference on the saturation constant (as DO) between the AOB and NOB. For activated sludge processes, the half-saturation constant for O_2 varies between 0.16-0.5 and 0.34-2.5 mg O_2/L , respectively [9]. Increasing the DO interval from 0.5-1.0 to 1.0-2.0 mg/L (average concentrations of 0.53 and 1.35 mg/L, respectively), the maximum nitrification rate did not increase more than 10%. And, for the DO interval of 2.0-4.0 mg/L ($DO_m = 3.1$ mg/L), the reaction rate even decreased marginally between 15 and 22% (as NH_4^+-N), most probably due to the inhibition of the AOB by the aerobic heterotrophic bacteria [11].

Regarding the third group of experiments, it was verified that the decrease of the pH value (from 8.7 until 7.0, considering the average values) led to the linear decrease of the nitrification reaction rate, from 37 ± 2 to 9.7 ± 0.5 mg $NH_4^+-N/(h.g VSS)$. This phenomenon was even more evident at pH values below 7, since during the test conducted in the pH range of 6.5-7.5, it was observed that pH decreased more and more slowly as it was approaching the lowest operation limit (see Figure 8.3). So, in the absence of alkalinity ($DIC < 30$ mg/L) and knowing that during nitrification the release of H^+ ions occurs, it was possible to presume that the reaction was near the end. These results are in accordance with the literature, where it is reported that for pH values higher than 6.7, the nitrification process begins to accelerate [12]. Furthermore, Shammas [32] studied the pH influence on the nitrification reaction and also concluded that the increment of the solution pH improves the maximum nitrification rate. This enhancement can be explained by the high alkalinity which favours the operation of the enzymatic systems within the nitrifying bacteria [12].

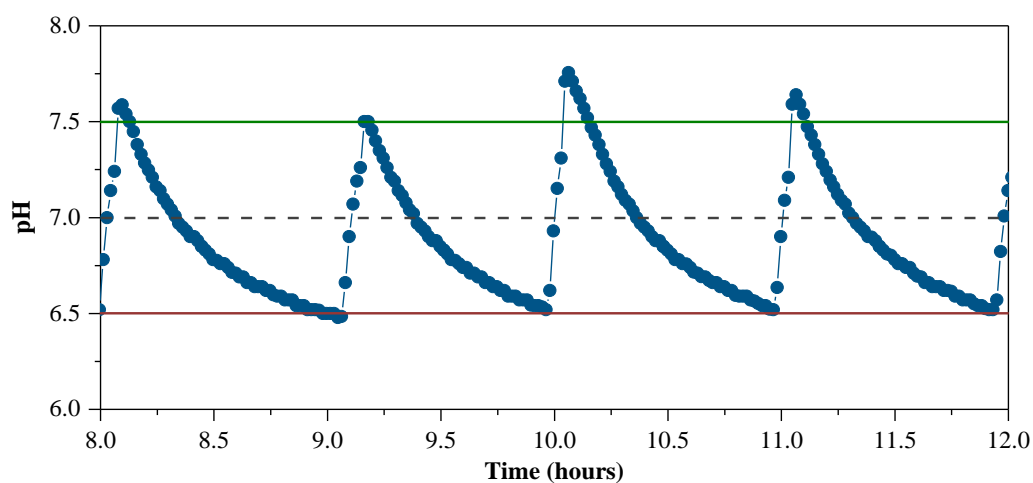


Figure 8.3. Evolution of the pH profile along the test carried out in the pH interval of 6.5-7.5, between the 8 and 12 hours.

Throughout the experiments, 5.5 ± 0.5 mg CaCO_3 were consumed on average per 1 mg of $\text{NH}_4^+\text{-N}$ oxidised to accomplish the nitrification reaction, which is about 23% lesser than the stoichiometric ratio (7.1 mg $\text{CaCO}_3/\text{mg NH}_4^+\text{-N}$ [12]). Except for the tests conducted in the pH ranges of 6.5-7.5 and 7.5-8.5, where it was needed to add NaOH to keep the pH value within the intended interval, all the alkalinity nullified by the releasing of the H^+ ions was provided by the leachate.

It should also be noted that along these assays, commonly, the total amount of ammonia lost by air stripping was raised by the increasing of the temperature, dissolved oxygen concentration, pH value and initial amount of TAN (see Table 8.3), as expected [28, 29]. Looking at the Group II of experiments, it could be noticed that for the lowest DO range, the percentage of ammonia stripping was not the lowest because the initial TAN content was about 34% higher, and consequently, being the pH and temperature values similar in all tests, the amount of available free ammonia was also higher.

8.3.2 Denitrification

Aiming the projection and assessment of the denitrification process performance when an alteration on the operating conditions occurs, 8 tests were conducted, during approximately 12-36 hours. Throughout each denitrification test, the nitrate concentration was negligible, therefore, the maximum denitrification reaction rate was determined in terms of nitrite removal, regarding the influence of pH (Group I, pH ranges: 6.5-7.0, 7.0-7.5, 7.5-8.0, 8.0-8.5 and 8.5-9.0), temperature (Group II – 20, 25 and 30 °C) and phosphate addition (Group III – without and with addition of 30 mg $\text{PO}_4^{3-}/\text{L}$, respectively). All variables and kinetic parameters achieved can be consulted in Table 8.4 while the respective reaction profiles can be observed in Figure 8.4. Figure 8.4 represents the ratio between the amount of nitrite-nitrogen removed and the VSS concentration, as a function of time, and the amount of methanol consumed and alkalinity produced, as a function of $\text{NO}_2^-\text{-N}$ reduced, in all experiments. The maximum reaction rates, as well as the methanol consumption and the alkalinity production, were obtained from the respective slopes (see Table 8.4).

The 1st Group of experiments disclosed that the pH interval between 7.5 and 8.5 was the most favourable to the good performance of the denitrification reaction at 30°C, leading to a maximum reaction rate of 19.4 ± 0.7 mg $\text{NO}_2^-\text{-N}/(\text{h.g VSS})$. Besides that, this test also presented the lowest values of methanol consumption and alkalinity production. The pH range between 8.0 and 8.5 also showed itself quite proficient, being the specific reaction rate only 11% lower. However, the application of this interval would result in an increasing of methanol and acid to be used. The higher inhibition rate was observed for the lowest pH range (6.5-7.0), being the reaction rate only 5.5 ± 0.1 mg $\text{NO}_2^-\text{-N}/(\text{h.g VSS})$, about 72% lower than the maximum kinetic constant.

Table 8.4. Operating conditions and kinetic parameters of the denitrification process for all experiments.

	pH range	pH _m	T (°C)	VSS (g/L)	NO ₂ ⁻ -N _i (mg/L)	$k_{\text{desn.}}^{\text{a}}$ $\left(\frac{\text{mg NO}_2^- - \text{N}}{\text{g VSS.h}}\right)$	Methanol ^b $\left(\frac{\text{mg CH}_3\text{OH}}{\text{mg NO}_2^- - \text{N}}\right)$	Alkalinity ^c $\left(\frac{\text{mg CaCO}_3}{\text{mg NO}_2^- - \text{N}}\right)$
Group I	6.5-7.0	6.77		3.72	1389	5.5 ± 0.1	1.72 ± 0.08	3.5 ± 0.1
	7.0-7.5	7.15		2.86	982	15.8 ± 0.2	1.62 ± 0.06	3.4 ± 0.1
	7.5-8.0	7.86	30	3.24	1475	19.4 ± 0.7	1.61 ± 0.06	3.2 ± 0.1
	8.0-8.5	8.14		2.92	1046	17.5 ± 0.4	1.67 ± 0.07	3.8 ± 0.1
	8.5-9.0	8.90		3.34	1221	13.5 ± 0.2	1.69 ± 0.06	3.4 ± 0.1
Group II		7.42	20	2.00	1421	1.4 ± 0.1	4.3 ± 0.2	---
	7.5-8.0	7.78	25	2.70	1070	11.1 ± 0.3	2.19 ± 0.06	3.6 ± 0.1
		7.86	30	3.24	1475	19.4 ± 0.7	1.61 ± 0.06	3.2 ± 0.1
Group III		7.86		3.24	1475	19.4 ± 0.7	1.61 ± 0.06	3.2 ± 0.1
	7.5-8.0	7.85^d	30	2.10^d	909^d	27 ± 1^d	1.6 ± 0.1^d	3.2 ± 0.1^d

^aDenitrification's reaction rate, expressed in the terms of nitrite reduction, whose values correspond to the slopes in Figure 8.4; ^bMethanol consumption during denitrification reaction, whose values correspond to the slopes in Figure 8.4; ^cAlkalinity production during denitrification reaction, considering the amount of H₂SO₄ added, and that, for pH < 11, the inorganic carbon was in the form of carbonates and bicarbonates [24], whose values correspond to the slopes in Figure 8.4; ^dValues for the experiment with the addition of 30 mg/L of phosphate ions.

The results concerning the pH variation are in agreement with literature, where it was reported that the optimum pH for denitrification was around 7.5-8.5 and for low pH values (< 7) the reaction rate may become slower [8, 12, 14]. At acidic pH (~6.8), the denitrification process can be inhibited by the presence of free nitrous acid (HNO₂), which is related to the nitrite ([NO₂⁻-N]) concentration, pH and temperature (in °C), according to Eq. (8.8) [9, 25]:

$$[\text{HNO}_2 - \text{N}] = \frac{\text{NO}_2^- - \text{N}}{e^{-2300/(273+T)} \times 10^{\text{pH}}} \quad (8.8)$$

It should be noted that, during the test performed at the lowest pH interval, the HNO₂ content ranged between 0.26-0.47 mg HNO₂-N/L (data not shown), while in the remaining tests the HNO₂ concentration did not exceed 0.1 mg HNO₂-N/L. Philips et al. [9] reported that the denitrification is inhibited by the HNO₂ in concentrations above 0.04 mg HNO₂-N/L.

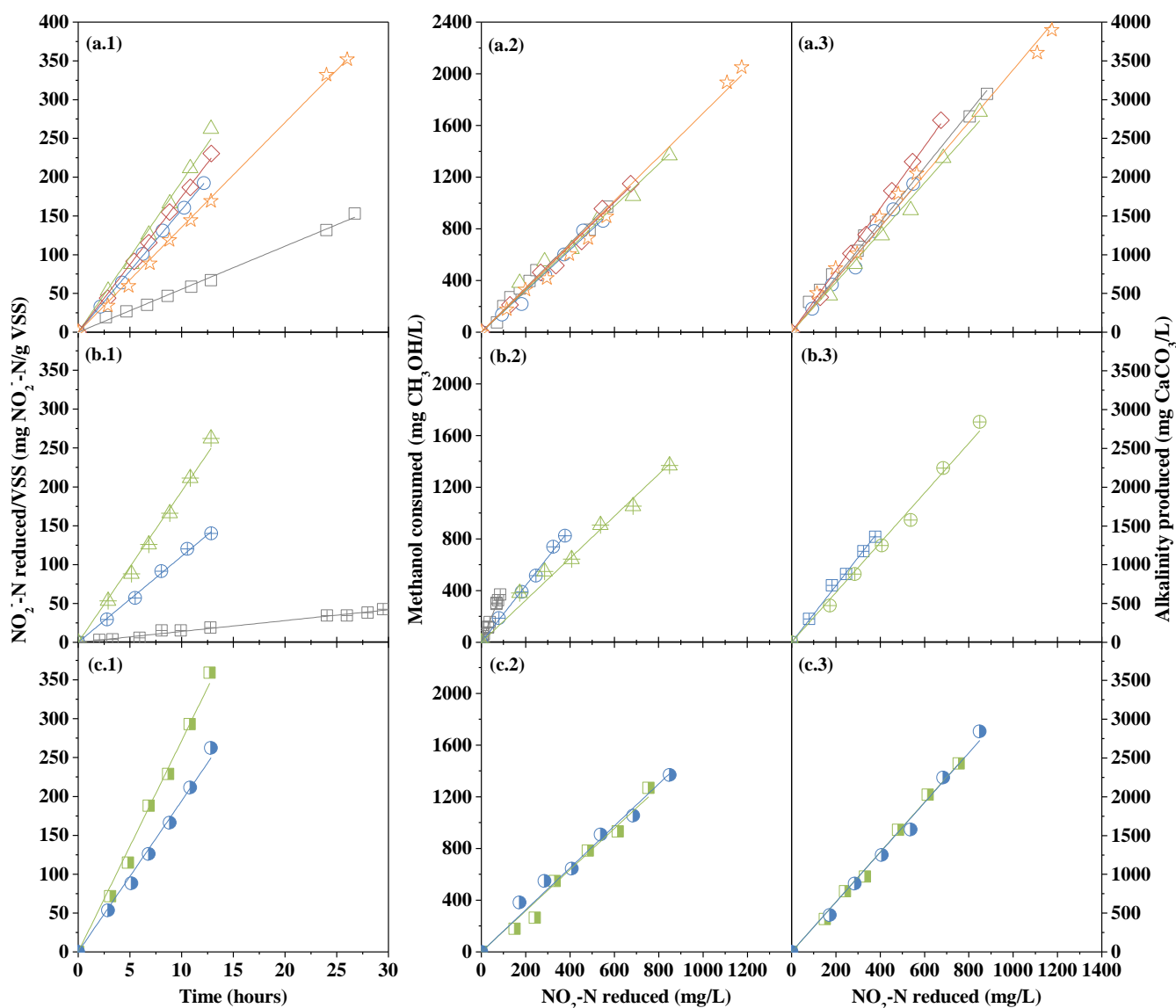


Figure 8.4. Representation of the (.1) $\text{NO}_2\text{-N reduced/VSS}$ ratio, as a function of time, and the (.2) methanol consumed and (.3) alkalinity removed, as a function of $\text{NO}_2\text{-N reduced}$, along all denitrification tests, regarding (a) different pH intervals (6.5-7.0, □; 7.0-7.5, ○; 7.5-8.0, △; 8.0-8.5, ◇ and 8.5-9.5, ☆), (b) different temperatures (20 °C, ▣; 25 °C, ⊕ and 30 °C, △) and (c) the addition (■) or not (●) of phosphate ions.

From the Group II of experiments, it was possible to infer that: i) between 20 and 30°C, per each Celsius degree of temperature increase, the denitrification rate rose about 1.8 mg $\text{NO}_2\text{-N/(h.g VSS)}$; and ii) for temperatures below 20 °C, the extension of the denitrification reaction was very low. In addition to the fact that the highest reaction rate was achieved at 30 °C, the lowest methanol consumption and alkalinity production was achieved at the same conditions. However, in a full-scale plant, only on the summer, the biological reactor would present temperatures near 30 °C. Since heating/cooling systems are very expensive, in the rest of the year, the denitrification reaction rate would be strongly conditioned by the ambient temperature, which should be taken into account on the LTP design.

In the 3rd Group of experiments, it was evaluated the addition of phosphate, which is a source of phosphorous, one of the most important nutrients for the microorganisms [14]. In fact, the denitrification reaction presupposes a previous nitrification process, and then part of the initial phosphate from the leachate had already been removed. The phosphate addition enhanced the biomass activity during the denitrification, resulting in 39% increase on the kinetic constant, consuming only 16 mg of PO_4^{3-} per 1-L of leachate (data not shown), keeping the consumption of methanol and acid. In a biological treatment system at full-scale, the lack of phosphorous can be compensated by the utilization of phosphoric acid instead of the sulphuric acid used to nullify the alkalinity produced.

Considering all the denitrification experiments carried out, with exception of test 20 (where it was not possible to determine the alkalinity production and the methanol consumption was clearly an outlier), on average, it was consumed 1.73 ± 0.07 mg of CH_3OH per each mg of NO_2^- -N removed, which was only 13% higher than the mass stoichiometric ratio (1.53 mg CH_3OH /mg NO_2^- -N, considering the methanol used for denitrification reaction and for cellular synthesis or sludge production [12, 35]). At the same time it was produced 3.4 ± 0.1 mg of CaCO_3 per each mg of NO_2^- -N reduced, which was only 4.8% lower than the mass stoichiometric ratio (3.57 mg CaCO_3 /mg NO_2^- -N [12, 14]).

In order to take advantage of the alkalinity consumption, during nitrification, and the alkalinity production, during denitrification, and thereby, suppress the need of chemicals to correct the pH value, the best approaches to obtain a leachate in a full-scale LTP with a nitrogen content below 15 mg/L (emission limit value for discharge into water bodies) would be: i) the use of a SBR, alternating between the aerobic and anoxic cycles so as to maintain the leachate's pH among 7.5-8.5; or ii) the use of an anoxic continuous flow reactor followed by an aerobic one, with recirculation to the anoxic reactor (also taking advantage of some biodegradable organic matter of the leachate that could be used for the denitrification reaction).

8.3.3 Characterization of the bacterial communities

The phylogenetic composition and diversity of the bacterial community inhabiting the biological treatment of the mature landfill leachate under aerobic and anoxic conditions, respectively, was assessed by a 454-pyrosequencing analysis of the 16S rRNA gene. A total of 20 209 16S rRNA sequences were obtained. Per sample, the number of high-quality sequences ranged between 2 490 and 4 358. Given these variability and according to the recommendation of QIIME pipeline instructions [36], the samples were normalized by rarefaction to 2 400 sequences per sample.

Alpha diversity was evaluated determining the richness estimator Chao 1 [37], and the diversity indices Simpson, Shannon and PD [38-40] (Table 8.5). Beta diversity was evaluated using the unweighted UniFrac metric (Figure 8.5) [41].

Table 8.5. Diversity indices of the bacterial communities of the nitrification (N) and denitrification (D) reactors, at the initial (I), middle (M) and final (F) treatment stages.

Sample	Nitrification Reactor			Denitrification Reactor		
	NI	NM	NF	DI	DM	DF
No. OTUs ^a	401	451	359	225	173	194
Chao 1	523	614	502	352	276	281
Shannon index	6.95	7.39	6.82	4.09	3.12	4.05
Simpson index	0.98	0.99	0.98	0.76	0.61	0.80
PD ^b	38.7	43.2	31.9	25.9	20.4	20.4

^aOperational taxonomic units; ^b Phylogenetic diversity.

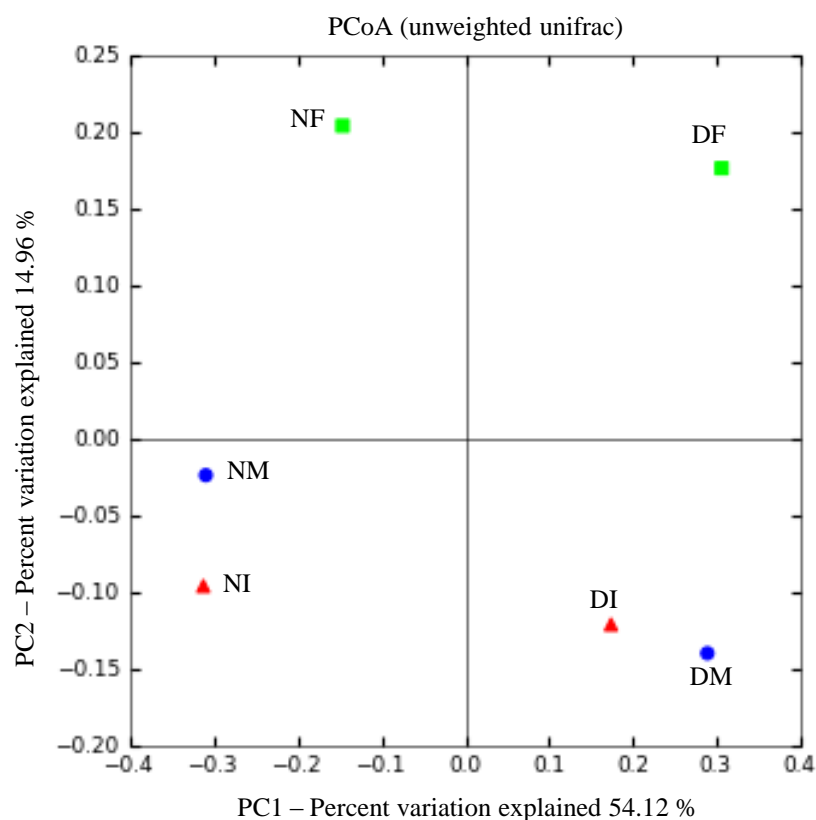


Figure 8.5. PCoA biplot depicting the dissimilarities between the bacterial communities from each biological sludge sample, based on the unweighted UniFrac distances.

The bacterial diversity, as revealed by the values of diversity coverage (Chao 1), number of OTUs, Shannon index and phylogenetic diversity (PD), was higher in the nitrification treatment than in the denitrification (Table 8.5) In addition, the relative abundance of each bacterial member in the nitrification reactor was more homogeneous (co-abundance of microorganisms) than in denitrification reactor, as revealed by Simpson index values, which measures the evenness of the communities. These differences were also observed when analysing the beta diversity as depicted in the unweighted unifracs based PCoA (Figure 8.5), as the nitrification and denitrification bacterial communities are separated over a gradient of 54.1 % dissimilarity.

Although the dissimilarity between the bacterial communities from the nitrification and denitrification processes, in both reactors only 0.7 % and 0.1 % of the sequences obtained, respectively, were not classified as Bacteria. The abundance of each phylogenetic group is expressed as the percentage of the total number of rarefied bacterial sequences (2400) affiliated at each taxonomic level, classified using RDP Classifier at a confidence threshold of 80%. The bacterial sequences obtained in the present study were affiliated to 23 phyla out of which only 6 presented abundance above 1 %, whose distribution is displayed in Figure 8.6.

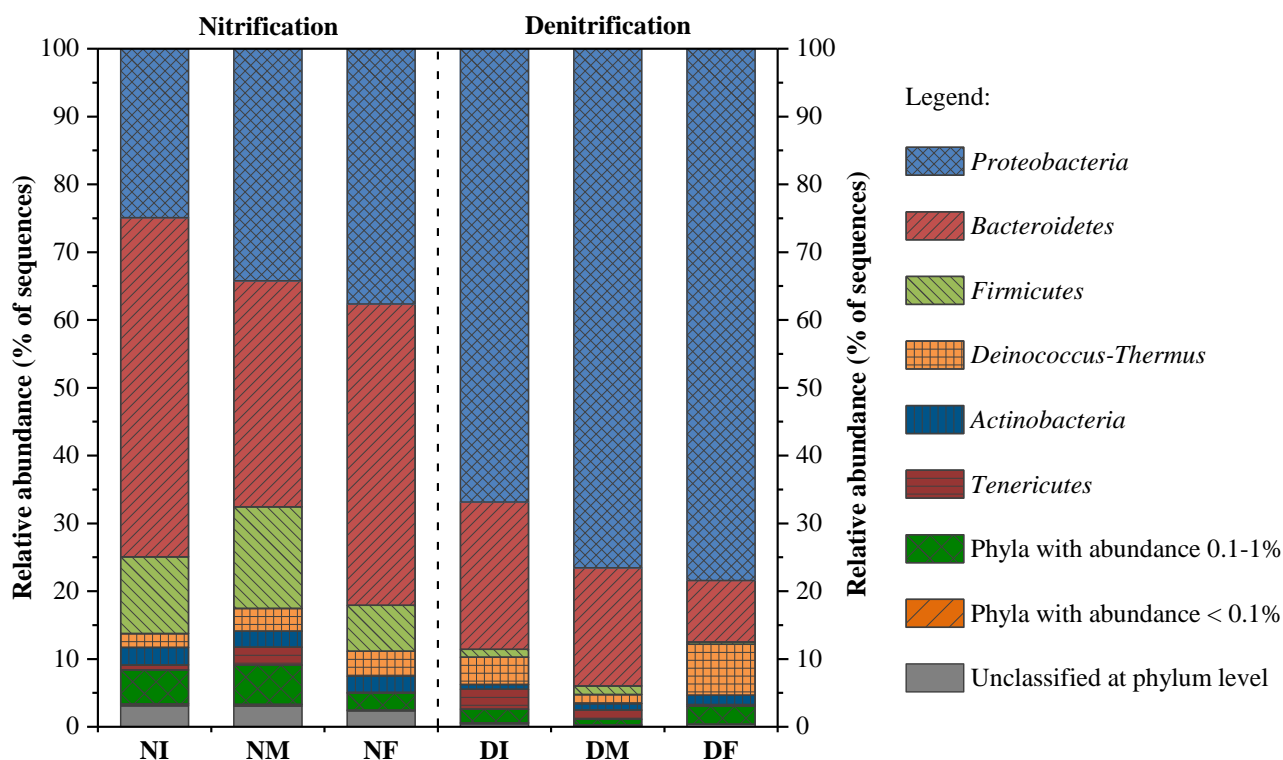


Figure 8.6. Relative abundance of the members affiliated to the different phyla present in each biological sludge sample. Phyla with abundance ranging from 0.1-1% include *Acidobacteria*, *Chloroflexi*, *Gemmatimonadetes*, GNO2, SAR406, *Spirochaetes*, *Synergistetes*, *Thermotogae*, TM7, *Verrucomicrobia* and WPS-2. Phyla with abundance < 0.1% include OD1, OP9, OP11, SR1, WS6, WYO.

Considering the bacterial community of the nitrification reactor, the 6 most abundant phyla were *Bacteroidetes* (42.6 %), *Proteobacteria* (32.2 %), *Firmicutes* (11.0 %), *Deinococcus-Thermus* (3.0 %), *Actinobacteria* (2.4 %) and *Tenericutes* (1.2%). Whereas for denitrification reactor the 6 most abundant phyla were *Proteobacteria* (73.9 %), *Bacteroidetes* (16.1 %), *Deinococcus-Thermus* (4.3 %), *Tenericutes* (1.5 %), *Actinobacteria* (1.0%) and *Firmicutes* (0.9 %).

Within the nitrification reactor, the most abundant members belonged to *Bacteroidetes* phylum and were mainly affiliated to the classes *Sphingobacteriia* (60.8 %), *Bacteroidia* (18.4 %) and *Flavobacteriia* (7.2 %). Members affiliated to *Sphingobacteriia* and *Flavobacteriia* are known to be involved in the degradation of slowly biodegradable organic matter, such as complex organic molecules, including humic acids [42, 43]. The class *Sphingobacteriia* included the most abundant family, from all of the sequences obtained from nitrification process, which was *Saprospiraceae* (16.1%) (Table 8.6).

Regarding the proteobacterial members, most were affiliated to the classes *Betaproteobacteria* (67.6 %), *Alphaproteobacteria* (20.7 %) and *Gammaproteobacteria* (9.1 %). In addition, members affiliated to *Betaproteobacteria*, in particular to *Nitrosomonadaceae* (6.9%) and *Comamonadaceae* (5.7%) were also among the three most abundant families (Table 8.6). Bacteria belonging to *Nitrosomonadaceae* are associated with the oxidation of ammonia into nitrite [44, 45] and, in the present study, during the nitrification reaction, there was nitrite accumulation. Thus, the presence/abundance of these members in the nitrification reactor is in agreement with the results obtained from the nitrification tests. Moreover, as expected, none of the OTUs was affiliated to *Nitrobacteriaceae*, which embraces nitrite-oxidising bacteria that are strongly inhibited by the presence of free ammonia, as previously mentioned.

Additionally, the high abundance of members affiliated to the families *Saprospiraceae* and *Comamonadaceae* was not surprising as these members are usually present in activated sludge plants from municipal and industrial wastewater treatment plants [46-48]. Moreover, the family *Comamonadaceae* is a group of prokaryotes which is phylogenetically coherent but physiologically heterogeneous, encompassing different genera: aerobic organotrophs, anaerobic denitrifiers, hydrogen oxidizers, iron (III)-reducing bacteria, photoautotrophic and photoheterotrophic bacteria, and fermentative bacteria [49, 50]. Among these genera, there is also a group of bacteria which plays an important role in the biodegradation of aromatic compounds and toxic wastes [49]. So, the presence and high abundance of *Comamonadaceae* members in the treatment of an effluent like the landfill leachates, where a myriad of different compounds are present, is perfectly conceivable. Even more, bacteria from this family were already identified elsewhere [43], where the landfill leachate was treated by aerated partial nitrification using a SBR.

Table 8.6. Relative abundance (> 1%) of the families belonging to the bacterial phyla with an abundance higher than 1% in nitrification or/and denitrification reactors.

Phylum	Class	Order	Family	Nitrification				Denitrification			
				NI	NM	NF	Mean	DI	DM	DF	Mean
<i>Bacteroidetes</i>	<i>Bacteroidia</i>	<i>Bacteroidales</i>	<i>Porphyromonadaceae</i>	3.50	3.58	2.33	3.14	0.63	0.38	0.25	0.42
			<i>Cryomorphaceae</i>	0.38	0.17	1.50	0.68	0.08	0.00	0.00	0.03
	<i>Flavobacteriia</i>	<i>Flavobacteriales</i>	<i>Flavobacteriaceae</i>	1.67	0.67	1.88	1.40	1.71	2.71	0.58	1.67
			<i>Balneolaceae</i>	1.71	2.58	2.13	2.14	1.83	1.00	0.29	1.04
	<i>Sphingobacteriia</i>	<i>Sphingobacteriales</i>	<i>Chitinophagaceae</i>	2.42	2.08	1.67	2.06	0.38	0.50	0.25	0.38
			<i>Saprospiraceae</i>	24.04	8.92	15.33	16.10	5.96	4.38	4.88	5.07
<i>Deinococcus-Thermus</i>	<i>Deinococci</i>	<i>Deinococcales</i>	<i>Deinococcaceae</i>	2.04	3.33	3.63	3.00	4.00	1.33	7.50	4.28
<i>Firmicutes</i>	<i>Clostridia</i>	<i>Clostridiales</i>	<i>Clostridiaceae</i>	4.33	5.96	4.83	5.04	0.54	0.88	0.29	0.57
<i>Proteobacteria</i>	<i>Alphaproteobacteria</i>	<i>Caulobacterales</i>	<i>Caulobacteraceae</i>	0.00	0.00	0.13	0.04	0.96	0.33	2.04	1.11
		<i>Rhizobiales</i>	<i>Hyphomicrobiaceae</i>	0.58	1.29	1.96	1.28	50.67	64.04	44.67	53.13
			<i>Phyllobacteriaceae</i>	0.33	1.38	0.75	0.82	0.67	0.29	1.04	0.67
		<i>Rhodobacterales</i>	<i>Rhodobacteraceae</i>	1.50	2.63	3.46	2.53	1.50	1.50	3.38	2.13
		<i>Sphingomonadales</i>	<i>Sphingomonadaceae</i>	0.88	1.08	1.08	1.01	0.13	0.00	0.00	0.04
	<i>Betaproteobacteria</i>	<i>Burkholderiales</i>	<i>Burkholderiaceae</i>	0.46	0.63	0.71	0.60	0.92	0.88	1.46	1.08
			<i>Comamonadaceae</i>	4.04	6.83	6.08	5.65	1.25	0.54	1.00	0.93
		<i>Nitrosomonadales</i>	<i>Nitrosomonadaceae</i>	6.25	5.96	8.58	6.93	0.21	0.04	0.13	0.12
	<i>Gammaproteobacteria</i>	<i>Rhodocyclales</i>	<i>Rhodocyclaceae</i>	0.79	1.17	1.67	1.21	0.00	0.04	0.08	0.04
		<i>Xanthomonadales</i>	<i>Xanthomonadaceae</i>	0.71	0.96	1.08	0.92	6.75	6.54	11.00	8.10
<i>Thiotrichales</i>		<i>Piscirickettsiaceae</i>	0.00	0.00	0.08	0.03	0.92	0.63	10.54	4.03	
<i>Tenericutes</i>	<i>Mollicutes</i>	<i>Acholeplasmatales</i>	<i>Acholeplasmataceae</i>	0.58	2.04	0.08	0.90	2.83	1.25	0.25	1.44
		<i>Anaeroplasmatales</i>	<i>Anaeroplasmataceae</i>	0.17	0.58	0.04	0.26	0.08	0.08	0.00	0.06

Considering the bacterial communities from denitrification reactor proteobacterial members were the most abundant and were mainly affiliated to the classes *Alphaproteobacteria* (78.3%), *Gammaproteobacteria* (16.7 %) and *Betaproteobacteria* (4.8 %). The most abundant families were *Hyphomicrobiaceae* (53.1 %), *Xanthomonadaceae* (8.1 %), which belong, respectively, to *Alphaproteobacteria* and *Gammaproteobacteria* (see Table 8.6). In the denitrification reactor, about 74.7 % of the total sequences were classified to genus level. In contrast, only about 15.1 % of the overall nitrification sequences were classified at genus level (data not shown). Curiously, 51.9% out of 74.7% corresponded to the genus *Hyphomicrobium* from the family *Hyphomicrobiaceae*. These results indicate the potential role of these members in the denitrification reactor. In fact, members from this genus are known as denitrifiers. Moreover, this bacterium is known to use methanol as external carbon source, which agrees with the present study use of methanol, both at the start-up period as throughout the denitrification experiments [15, 51, 52]. In addition, members belonging to *Bacteroidetes* were mainly affiliated to the classes *Sphingobacteriia* (58.6 %), *Flavobacteriia* (14.6 %) and *Bacteroidia* (7.3 %), as observed for bacterial communities from the nitrification reactor. The existence of common members on both reactors would already be expected since the activated sludge of the denitrification reactor was inoculated from the nitrification reactor. In particular, the *Sphingobacteriia* members affiliated to *Saprospiraceae* (5.1%) were among the three most abundant members (see Table 8.6).

8.4 Conclusions

The biological nitrification revealed to be efficient on the removal of TAN from a high-strength leachate, from an old sanitary landfill. About 31% of the TAN was removed by ammonia stripping, which is favoured by the high initial values of pH and TAN content of the leachates, at the beginning of the nitrification reaction. The abundance of *Nitrosomonadaceae* members in nitrification reactor samples suggests that the remaining TAN was oxidised into nitrite by these bacteria, whose activity was strongly inhibited by low values of temperature (< 20 °C) and pH (< 7.5) and just slightly affected by variations in the DO concentration.

The reduction of the nitrite ions into gaseous nitrogen, through the denitrification reaction, may have been mediated by bacteria from the genus *Hyphomicrobium*, whose performance was strongly affected by alterations in the operating temperature, very inhibited by low pH values (< 7.0) and quite benefited by the presence of phosphorous.

Besides the presence of bacteria from the families *Nitrosomonadaceae* and *Hyphomicrobiaceae*, responsible by the nitrification and denitrification reactions, respectively, the 454-pyrosequencing analysis of the 16S rRNA gene also revealed the presence of bacteria associated to the classes *Sphingobacteriia* and *Flavobacteriia* on both reactors, which have been reported as responsible for the degradation of complex organic matter, one of the main constituents of the mature landfill leachates. Summarizing, these results suggest that reactions involving (i) oxidation/reduction of nitrogen species and (ii) degradation of organic matter were mostly mediated by bacteria from the phyla *Proteobacteria* and *Bacteroidetes*, respectively.

8.5 References

- [1] C.B. Öman, C. Junestedt, Chemical characterization of landfill leachates – 400 parameters and compounds, *Waste Management*, 28 (2008) 1876-1891.
- [2] P. Kjeldsen, M.A. Barlaz, A.P. Rooker, A. Baun, A. Ledin, T.H. Christensen, Present and Long-Term Composition of MSW Landfill Leachate: A Review, *Critical Reviews in Environmental Science and Technology*, 32 (2002) 297-336.
- [3] J. Wiszniewski, D. Robert, J. Surmacz-Gorska, K. Miksch, J. Weber, Landfill leachate treatment methods: A review, *Environmental Chemistry Letters*, 4 (2006) 51-61.
- [4] A.A. Abbas, G. Jingsong, L.Z. Ping, P.Y. Ya, W.S. Al-Rekabi, Review on Landfill Leachate Treatments, *Journal of Applied Sciences Research*, 5 (2009) 534-545.
- [5] S. Renou, J. Givaudan, S. Poulain, F. Dirassouyan, P. Moulin, Landfill leachate treatment: Review and opportunity, *Journal of Hazardous materials*, 150 (2008) 468-493.
- [6] U.E. Agency, Guidance for the Treatment of Landfill Leachate, Integrated Pollution Prevention and Control (IPPC), in, Sector Guidance Note IPPC S5.03, 2007.
- [7] G. Ruiz, D. Jeison, O. Rubilar, G. Ciudad, R. Chamy, Nitrification–denitrification via nitrite accumulation for nitrogen removal from wastewaters, *Bioresource Technology*, 97 (2006) 330-335.
- [8] M. Henze, P. Harremoës, J.I.C. Jansen, E. Arvin, Basic Biological Processes, in: *Wastewater Treatment: Biological and Chemical Processes*, Second Edition, Springer-Verlag, Berlin, 1997.
- [9] S. Philips, H.J. Laanbroek, W. Verstraete, Origin, causes and effects of increased nitrite concentrations in aquatic environments, *Reviews in environmental science and biotechnology*, 1 (2002) 115-141.
- [10] R. Canziani, V. Emondi, M. Garavaglia, F. Malpei, E. Pasinetti, G. Buttiglieri, Effect of oxygen concentration on biological nitrification and microbial kinetics in a cross-flow membrane bioreactor (MBR) and moving-bed biofilm reactor (MBBR) treating old landfill leachate, *Journal of Membrane Science*, 286 (2006) 202-212.
- [11] L.-k. Wang, G.-m. Zeng, Z.-h. Yang, L.-l. Luo, H.-y. Xu, J. Huang, Operation of partial nitrification to nitrite of landfill leachate and its performance with respect to different oxygen conditions, *Biochemical Engineering Journal*, 87 (2014) 62-68.
- [12] M.H. Gerardi, *Nitrification and Denitrification in the Activated Sludge Process*, Wiley, 2003.
- [13] H.K. Trivedi, Simultaneous Nitrification and Denitrification (Symbio® Process), in: L.K. Wang, N.K. Shamas, Y.-T. Hung (Eds.) *Advanced Biological Treatment Processes*, Humana Press, 2009.
- [14] Metcalf, Eddy, *Wastewater Engineering Treatment and Reuse*, 4th ed., Metcalf & Eddy, 2005.
- [15] M. Ginige, J. Bowyer, L. Foley, J. Keller, Z. Yuan, A comparative study of methanol as a supplementary carbon source for enhancing denitrification in primary and secondary anoxic zones, *Biodegradation*, 20 (2009) 221-234.
- [16] M. Martiensen, R. Schöps, Biological treatment of leachate from solid waste landfill sites—Alterations in the bacterial community during the denitrification process, *Water Research*, 31 (1997) 1164-1170.

- [17] J.-J. Her, J.-S. Huang, Influences of carbon source and C/N ratio on nitrate/nitrite denitrification and carbon breakthrough, *Bioresource Technology*, 54 (1995) 45-51.
- [18] J.A. Torà, J.A. Baeza, J. Carrera, J.A. Oleszkiewicz, Denitrification of a high-strength nitrite wastewater in a sequencing batch reactor using different organic carbon sources, *Chemical Engineering Journal*, 172 (2011) 994-998.
- [19] F. Thalasso, A. Vallecillo, P. García-Encina, F. Fdz-Polanco, The use of methane as a sole carbon source for wastewater denitrification, *Water Research*, 31 (1997) 55-60.
- [20] J. Park, Y. Yoo, Biological nitrate removal in industrial wastewater treatment: which electron donor we can choose, *Applied Microbiology and Biotechnology*, 82 (2009) 415-429.
- [21] S. Villaverde, F. Fdz-Polanco, P.A. García, Nitrifying biofilm acclimation to free ammonia in submerged biofilters. Start-up influence, *Water Research*, 34 (2000) 602-610.
- [22] O. Turk, D.S. Mavnic, Preliminary assessment of a shortcut in nitrogen removal from wastewater, *Canadian Journal of Civil Engineering*, 13 (1986) 600-605.
- [23] A. Spagni, S. Marsili-Libelli, Nitrogen removal via nitrite in a sequencing batch reactor treating sanitary landfill leachate, *Bioresource Technology*, 100 (2009) 609-614.
- [24] C. Sawyer, P. McCarty, G. Parkin, *Chemistry for Environmental Engineering and Science*, McGraw-Hill Education, 2003.
- [25] A. Anthonisen, R. Loehr, T. Prakasam, E. Srinath, Inhibition of nitrification by ammonia and nitrous acid, *Journal (Water Pollution Control Federation)*, (1976) 835-852.
- [26] N.K. Shamas, L. K.Wang, ZuchengWu, *Waste Stabilization Ponds and Lagoons*, in: L.K. Wang, N.C. Pereira, Y.-T. Hung (Eds.) *Biological Treatment Processes*, Humana Press, 2009.
- [27] D. Green, R. Perry, *Perry's Chemical Engineers' Handbook*, Eighth Edition, McGraw-Hill Education, 2007.
- [28] S. Marttinen, R. Kettunen, K. Sormunen, R. Soimasuo, J. Rintala, Screening of physical–chemical methods for removal of organic material, nitrogen and toxicity from low strength landfill leachates, *Chemosphere*, 46 (2002) 851-858.
- [29] J.C. Campos, D. Moura, A.P. Costa, L. Yokoyama, F.V.d.F. Araujo, M.C. Cammarota, L. Cardillo, Evaluation of pH, alkalinity and temperature during air stripping process for ammonia removal from landfill leachate, *Journal of Environmental Science and Health, Part A*, 48 (2013) 1105-1113.
- [30] N.J. Horan, *Nutrient Removal from Wastewaters*, Taylor & Francis, 1994.
- [31] J. Jokela, R. Kettunen, K. Sormunen, J. Rintala, Biological nitrogen removal from municipal landfill leachate: low-cost nitrification in biofilters and laboratory scale in-situ denitrification, *Water Research*, 36 (2002) 4079-4087.
- [32] N.K. Shamas, Interactions of Temperature, pH, and Biomass on the Nitrification Process, *Journal (Water Pollution Control Federation)*, 58 (1986) 52-59.
- [33] J. Gabarró, R. Ganigué, F. Gich, M. Ruscalleda, M.D. Balaguer, J. Colprim, Effect of temperature on AOB activity of a partial nitrification SBR treating landfill leachate with extremely high nitrogen concentration, *Bioresource Technology*, 126 (2012) 283-289.

- [34] K. Hanaki, C. Wantawin, S. Ohgaki, Nitrification at low levels of dissolved oxygen with and without organic loading in a suspended-growth reactor, *Water Research*, 24 (1990) 297-302.
- [35] N.K. Shammass, L. K.Wang, Emerging Attached-Growth Biological Processes, in: L.K. Wang, N.K. Shammass, Y.-T. Hung (Eds.) *Advanced Biological Treatment Processes*, Humana Press, 2009.
- [36] J.G. Caporaso, J. Kuczynski, J. Stombaugh, K. Bittinger, F.D. Bushman, E.K. Costello, N. Fierer, A.G. Pena, J.K. Goodrich, J.I. Gordon, QIIME allows analysis of high-throughput community sequencing data, *Nature methods*, 7 (2010) 335-336.
- [37] A. Chao, Nonparametric estimation of the number of classes in a population, *Scandinavian Journal of statistics*, (1984) 265-270.
- [38] E.H. Simpson, Measurement of diversity, *Nature*, (1949).
- [39] C.E. Shannon, W. Weaver, *The mathematical theory of communication*, University of Illinois Press, Urbana, IL, 1963.
- [40] D.P. Faith, Conservation evaluation and phylogenetic diversity, *Biological conservation*, 61 (1992) 1-10.
- [41] C. Lozupone, R. Knight, UniFrac: a new phylogenetic method for comparing microbial communities, *Applied and environmental microbiology*, 71 (2005) 8228-8235.
- [42] J. Gabarró, P. González-Cárcamo, M. Rusalleda, R. Ganigué, F. Gich, M.D. Balaguer, J. Colprim, Anoxic phases are the main N₂O contributor in partial nitrification reactors treating high nitrogen loads with alternate aeration, *Bioresource Technology*, 163 (2014) 92-99.
- [43] J. Gabarró, E. Hernández-del Amo, F. Gich, M. Rusalleda, M.D. Balaguer, J. Colprim, Nitrous oxide reduction genetic potential from the microbial community of an intermittently aerated partial nitrification SBR treating mature landfill leachate, *Water Research*, 47 (2013) 7066-7077.
- [44] B.-C. Kim, S. Kim, T. Shin, H. Kim, B.-I. Sang, Comparison of the bacterial communities in anaerobic, anoxic, and oxic chambers of a pilot A2O process using pyrosequencing analysis, *Current microbiology*, 66 (2013) 555-565.
- [45] L. Pal, B. Kraigher, B. Brajer-Humar, M. Levstek, I. Mandic-Mulec, Total bacterial and ammonia-oxidizer community structure in moving bed biofilm reactors treating municipal wastewater and inorganic synthetic wastewater, *Bioresource Technology*, 110 (2012) 135-143.
- [46] Y. Xia, Y. Kong, T.R. Thomsen, P. Halkjær Nielsen, Identification and Ecophysiological Characterization of Epiphytic Protein-Hydrolyzing Saprospiraceae ("Candidatus Epiflobacter" spp.) in Activated Sludge, *Applied and Environmental Microbiology*, 74 (2008) 2229-2238.
- [47] C. Kragelund, C. Levantesi, A. Borger, K. Thelen, D. Eikelboom, V. Tandoi, Y. Kong, J. Krooneman, P. Larsen, T.R. Thomsen, Identity, abundance and ecophysiology of filamentous bacteria belonging to the Bacteroidetes present in activated sludge plants, *Microbiology*, 154 (2008) 886-894.
- [48] A.A. Khardenavis, A. Kapley, H.J. Purohit, Simultaneous nitrification and denitrification by diverse *Diaphorobacter* sp, *Applied Microbiology and Biotechnology*, 77 (2007) 403-409.

- [49] K. Kersters, P.d. Vos, M. Gillis, J. Swings, P. Vandamme, E. Stackebrandt, Introduction to the Proteobacteria, in: M. Dworkin, S. Falkow, E. Rosenberg, K.-H. Schleifer, E. Stackebrandt (Eds.) *The Prokaryotes: A Handbook on the Biology of Bacteria*, Springer, 2006.
- [50] A. Willems, The Family Comamonadaceae, in: E. Rosenberg, E.F. DeLong, S. Lory, E. Stackebrandt, F. Thompson (Eds.) *The Prokaryotes: Alphaproteobacteria and Betaproteobacteria*, Springer-Verlag Berlin Heidelberg, 2014.
- [51] C. Martineau, C. Villeneuve, F. Mauffrey, R. Villemur, Complete genome sequence of *Hyphomicrobium nitratorans* strain NL23, a denitrifying bacterium isolated from biofilm of a methanol-fed denitrification system treating seawater at the Montreal Biodome, *Genome announcements*, 2 (2014) e01165-01113.
- [52] T. Urakami, J. Sasaki, K.-I. Suzuki, K. Komagata, Characterization and Description of *Hyphomicrobium denitrificans* sp. nov., *International journal of systematic bacteriology*, 45 (1995) 528-532.

9 Depuration of mature sanitary landfill leachate using biological nitrification followed by coagulation and photo-Fenton reaction, combining solar and artificial radiation, at pre-industrial scale

In this chapter a new methodology for the treatment of landfill leachates, after aerobic lagooning, was developed and adjusted, at a scale close to industrial. This methodology involves an aerobic biological pre-oxidation by activated sludge, a coagulation/sedimentation step (240 mg Fe³⁺/L, at pH 4.2, 14-hours settling) and a photo-oxidation through photo-Fenton reaction (60 mg Fe²⁺, at pH 2.8) combining solar and artificial radiation, promoting the recalcitrant molecules degradation and consequent biodegradability enhancement.

The results demonstrate that the aerobic biological process applied to a leachate after aerobic lagooning, with high organic and nitrogen content (DOC = 1.1-1.5 g C/L; COD = 3.0-4.3 g O₂/L and N_D = 0.8-3.0 g N/L) and low biodegradability (BOD₅/COD = 0.07-0.13), is capable to oxidise between 62 and 99% of the ammonium nitrogen (NH₄⁺-N_f = 8-250 mg/L), consuming only the affluent alkalinity (CaCO_{3,f} = 0-1.6 g/L), achieving alkalinity reductions between 70 and 100%.

The coagulation/sedimentation stage led to the humic acids precipitation, promoting a marked change in leachate colour, from dark-brown to yellowish-brown, which is related to the presence of fulvic acids, accompanied by a reduction of 60% on DOC (DOC_f ≈ 400 mg/L), 58% on COD (COD_f ≈ 1200 mg/L) and 88% on TSS (supernatant TSS = 135 mg/L), obtaining an amount of acid sludge of about 300 mL/L.

From the photo-Fenton trials, it was concluded that the best option would be combining natural sunlight with artificial radiation (~1.3 kW/m³), thus optimizing the indirect costs. According to Zahn-Wellens test, a leachate, with 419 mg DOC/L after coagulation, would have to be photo-oxidized until a DOC and an 254 nm absorbance (1:25 dilution) lesser than 300 mg/L and 0.13, respectively, consuming approximately 100 mM of H₂O₂ and 7.4 kJ/L of accumulated UV energy, in order to achieve an effluent than can be biologically treated in compliance with the COD discharge limit (< 150 mg O₂/L) into water bodies. The biological process subsequent to the photocatalytic system would promote a 59% mineralization, being the final COD of approximately 115 mg O₂/L. If the ultimate goal is the discharge into sewerage system (COD < 1000 mgO₂/L), the full treatment would be finalized in the photo-treatment step, with a COD of about 950 mg O₂/L after a mineralization of 21% and a consumption of 1.5 kJ/L of UV energy and 76 mM of H₂O₂.

The scale-up of a photocatalytic facility with a capacity to treat 100 m³ of leachate per day showed the need to implement 1500 and 295 m² of CPCs, or 38 and 8 UV-Vis lamps (with 4kW and 20,000-h of lifetime each), targeting a COD value lesser than 150 and 1000 mg O₂/L, respectively. Combining solar and artificial radiation, it would be need 957 and 188 m² of CPCs (considering the month of higher irradiance), and 30 and 6 lamps (considering the month of lesser irradiance), respectively. The cost of the photo-Fenton step, aiming a COD lower than 150 and 1000 mg O₂/L, respectively, prowled: 5.7 and 4.2 €/m³, resorting just to CPCs; 5.79 and 4.22 €/m³, using only UV-Vis-Lamps; and 5.69 and 4.17 €/m³, combining CPCs and lamps. The cost with H₂O₂ corresponds to about 44% of the total yearly cost.

9.1 Introduction

Under the protocol established between FEUP/LSRE and EFACEC Engineering and Systems, a project named LFOTOBIO was developed. The generic objective of the project was the development and optimization of a solar photocatalytic technology for leachates treatment and, eventually, other recalcitrant industrial wastewaters, with the purpose of upgrading wastewater treatment plants using this new technology. The present thesis started under that project and the first results were presented in the Chapters 3, 4, 5 and 6. The set of experiments carried out in that context allowed to define a leachate treatment strategy composed by the following stages:

- (i) Anoxic/aerobic lagooning of the raw leachate, promoting the elimination of the biodegradable organic matter fraction and nitrogen, through nitrification/denitrification reactions.

The lagooning process would consist in a non-aerated lagoon in series with an aerated lagoon, with recirculation, in order to (a) use the biodegradable organic matter as carbon source for denitrification, and (b) eliminate alkalinity during nitrification, taking advantage of the alkalinity produced along the denitrification, besides the raw leachate alkalinity. The resulting effluent would be characterized by a low alkalinity, low nitrogen and low biodegradability mainly associated with high humic substances content. It can be used also a sequential batch reactor, combining cycles of nitrification and denitrification, to promote this first biological step.

- (ii) Coagulation/sedimentation of the leachate after lagooning, using ferric chloride at acid pH, in order to reduce the amount of recalcitrant organic matter mainly due to the humic acids precipitation and suspended solids, changing the effluent colour from dark/brown to yellow/brown after sedimentation, synonymous of the major presence of fulvic acids, which increases significantly the light transmissibility in the subsequent photo-oxidation process.

The need to use high amounts of acid to correct the pH value, in addition to the increment of the operating costs, also leads to an abrupt increase of sulphate ions concentrations, assuming the use of sulphuric acid. This results in the formation of sulphate-ferric complexes with much lower photoactivity than ferric hydroxo complexes, decreasing the photo-Fenton reaction rate, being necessary a larger amount of UV energy for the photo-treatment step. Therefore, for the proper operation of this step, it is important to minimize the leachate buffer capacity, through the alkalinity consumption during the biological nitrification that takes place in the lagoon.

- (iii) Photo-Fenton reaction combining natural solar light with artificial radiation. This process includes the addition of a ferrous solution (about 60 mg Fe^{2+} /L) and hydrogen peroxide at pH 2.8, since the most photoactive iron species prevail, thus maximizing the production of hydroxyl radicals and avoiding the iron hydroxide precipitation.

The photo-Fenton reaction rate is drastically reduced by suspended solids, since they negatively affect the light penetration in the reactional medium and absorb the UV-Vis photons.

The photo-oxidized leachate must have a DOC concentration between 220-280 mg/L and an absorbance at 254 nm less than 0.08 (after dilution 1:25), in order to meet the discharge limit for chemical oxygen demand ($\text{COD} < 150 \text{ mg O}_2/\text{L}$), at the end of a subsequent biological treatment.

- (iv) Activated sludge biological treatment (sequential batch reactor) of the photo-oxidised leachate, after neutralization, under aerobic and anoxic conditions, with the purpose of eliminating the remaining fraction of nitrogen and biodegradable organic matter, obtaining a final effluent in agreement with the discharge limits imposed by legislation.

Based on the first results and conclusions from the study at the solar pre-industrial plant, the initial configuration was adjusted in order to implement a treatment strategy similar to the one described above. The new plant comprises also a coagulation/sedimentation cylindrical tank and a set of UV-Vis lamps was inserted in the recirculation tank of the photocatalytic system, which allows to use solar and/or artificial radiation.

It was initially planned the use of the leachate after treatment in the LTP, which comprises a lagoon with oxygen injection, an activated sludge biological reactor and a settling tank. However, at the beginning of the experimental period, the effluent from the LTP presented high alkalinity ($> 10 \text{ g CaCO}_3/\text{L}$), which required the use of the aerobic biological reactor of the pre-industrial plant to promote the nitrification reaction. Since it was not possible to implement the complete strategy previously described, it was decided to use a methodology based on the first three steps of the process initially defined:

- (i) Initial biological oxidation by activated sludge under aerobic conditions, to promote nitrification and the elimination of the alkalinity still existing in the leachate collected at the LTP, thus decreasing the sulphuric acid consumption in the subsequent coagulation step;
- (ii) Coagulation with ferric chloride at acid pH, followed by sedimentation, to reduce the amount of suspended solids and organic compounds, such as humic acids, through precipitation, thus increasing the light penetration in the reactional medium and consequently the phototreatment efficiency.
- (iii) Photo-Fenton oxidation combining ferrous ion with hydrogen peroxide and UV-Vis radiation, using natural solar radiation, collected from 20.8 m^2 of compound parabolic collectors (CPCs), and/or artificial radiation, emitted by UV-Vis lamps (2 or 4) with a rated power between 850 and 1200 W. This treatment step promotes the degradation of recalcitrant organic compounds, such as fulvic acids, into simplest molecules, leading to biodegradability enhancement, until the point

(DOC \approx 250 mg/L) wherein a downstream biological treatment would allow to meet the discharge limit into water bodies (COD < 150 mg O₂/L).

Bear in mind the methodology adopted, the following objectives were established:

- Leachate characterization along all stages (biological oxidation, coagulation and photo-oxidation);
- Individual efficiency assessment of the:
 - biological reactor, under aerobic regime;
 - coagulation/sedimentation stage, for different values of pH and different settling times;
 - photo-Fenton reaction, in the optimal conditions obtained at the lab-scale, using solar and/or artificial radiation and changing the number and rated power of the lamps;
- Evaluation of the leachate treatment train, integrating the biological oxidation process with the coagulation/sedimentation and the photo-oxidation;
- Economic analysis of the phototreatment step, based on the test conducted under the optimal operating conditions.

9.2 Experimental methodology

During the trial period concerning this chapter, 15 experiments were carried out at the pre-industrial scale plant, combining biological oxidation with physico-chemical processes (coagulation/sedimentation with ferric chloride) and photo-oxidation (photo-Fenton reaction) using UV solar/artificial radiation.

All the chemicals used in this work, the detailed description of the experimental unit and respective procedures, as well as the employed analytical methods can be consulted in the Chapter 2. Table 9.1 just shows a brief description of the experiments presented in this chapter.

It should be noted that the initial biological treatment was always performed under aerobic conditions (trying to keep the dissolved oxygen concentration between 0.5-1.0 mg O₂/L), without NaOH addition during nitrification reaction, being only consumed the leachate alkalinity.

With the exception of experiments 5 and 6, at the end of photo-Fenton reaction, DOC was between 220 and 280 mg/L. These values are very close to the DOC values obtained in the Chapter 4, for a photo-treated leachate corresponding to an easily biodegradable effluent, allowing to obtain a final COD in agreement with the discharge limit (150 mg O₂/L) for disposal into water bodies, after a subsequent biological treatment.

Table 9.1. Description of the tests performed.

Test	Coagulation			Photo-Oxidation			Observations
	Fe ³⁺ (mg/L)	pH	Sed. ^a (h)	Rad.	Fe ²⁺ _{ad.} (mg/L)	pH	
1	240	2.8	14	Solar	60	2.8	At the beginning of the photo-Fenton reaction, a fast consumption of H ₂ O ₂ occurred, resulting in the decrease of the solution pH, requiring the addition of NaOH for pH correction. This situation was observed in all tests.
2	240	3.0	14	Solar	60	2.8	It was observed the existence of gas trapped in the acidic sludge settled at the bottom of coagulation tank, which decreased the sedimentation efficiency, leading to a supernatant with higher amount of TSS.
3	240	3.0	3	Artificial (4×1 kW)	60	2.8	It was observed that a settling time of 3 hours in the coagulation tank was not enough to achieve a low content of TSS in the supernatant.
4	240	3.0	3	Artificial (4×1 kW)	60	2.8	
5	-	-	-	Artificial (4×1 kW)	60	2.8	High H ₂ O ₂ and energy consumption during photo-Fenton, due to absence of coagulation.
6	-	-	-	Artificial (4×1 kW)	60	2.8	Acidification until pH 4, in order to reduce the NaOH consumption at the beginning of photo-reaction.
7	240	-	3	Artificial (4×1 kW)	60	2.8	Only FeCl ₃ was added in the coagulation step, in order to verify if H ₂ O ₂ addition (at the beginning of phototreatment) was enough to decrease the pH value till the optimum for photo-Fenton reaction and, thus, avoiding the need for NaOH addition. It was disclosed that for pH > 5, the H ₂ O ₂ addition was not sufficient for leachate acidification.
8	240	4.5	3	Artificial (4×1 kW)	60	2.8	It was verified that, only for pH ≤ 4, the H ₂ O ₂ was quickly consumed, lowering the pH value.
9	240	4.2	14	Artificial (4×1 kW)	60	2.8	Coagulation carried out at pH 4.2, since the iron sulphate addition leads to acidification to pH 4, and then the H ₂ O ₂ addition, at the beginning of photo-Fenton oxidation, is capable to reduce the pH until the optimum value, with lower NaOH consumption.
10	240	4.2	14	Solar Artificial (4×1 kW)	60	2.8	The use of solar radiation together with artificial radiation led to a decrease of the total amount of energy needed and 50% of electricity.

Table 9.1. Description of the tests performed.

Test	Coagulation			Photo-Oxidation			Observations
	Fe ³⁺ (mg/L)	pH	Sed. ^a (h)	Rad.	Fe ²⁺ _{ad.} (mg/L)	pH	
11	120	4.2	14	Solar Artificial (4×1 kW)	60	2.8	The reduction of the iron content in the coagulation step led to higher energy and H ₂ O ₂ consumption during photo-oxidation.
12	240	4.2	14	Artificial (2×1.2 kW)	60	2.8	The use of two lamps at maximum power (1.2 kW) slightly increased the reaction time, but decreased the total energy required.
13	240	4.2	14	Artificial (2×0.85 kW)	60	2.8	The use of two lamps at the minimum power (0.85 kW) made the process less efficient.
14	240	4.2	14	Artificial (2×1.2 kW)	60	2.8	Validation test for the conditions used in test 12.
15	240	4.2	14	Solar Artificial (2×1.2 kW)	60	2.8	Experiment performed at the best conditions, for further biodegradability evaluation of the leachate during photo-Fenton oxidation, through the Zahn-Wellens test.

^aSedimentation time.

9.3 Results and discussion

9.3.1 Evaluation of the biological oxidation efficiency

The biological reactor (BR) effectiveness assessment was based on the characterization of the landfill leachate along the treatment, for the experiments 1-15, mostly in terms of alkalinity and ammonium nitrogen removal. The effluent fed to BR was transferred from the LTP settling tank, after aerobic lagooning and aerobic biological oxidation with activated sludge. The inoculation of BR was performed using the mixed liquor of the activated sludge reactor of the LTP, already adapted to the inhibitory compounds present in this kind of wastewater.

Table 9.2 shows the values of all parameters analysed at the beginning (RB_0) and end (RB_F) of each batch BR test, as well as the removal efficiency of total dissolved carbon (TDC); dissolved inorganic carbon (DIC); dissolved organic carbon (DOC); alkalinity; chemical oxygen demand (COD); 5-day biochemical oxygen demand (BOD₅); total dissolved nitrogen (N_D) and ammonium nitrogen (NH₄⁺-N).

Table 9.2. Physico-chemical characterization of the landfill leachate before and after biological treatment.

Test	Sample	pH	T (°C)	TDC (mg/L)	DIC (mg/L)	DOC (mg/L)	Alkalinity ^a (g CaCO ₃ /L)	COD (mg/L)	BOD ₅ (mg/L)	$\frac{BOD_5}{COD}$	SO ₄ ²⁻ (mg/L)	Cl ⁻ (mg/L)	N _{TD} (mg/L)	N-NH ₄ ⁺ (mg/L)	N-NO ₃ ⁻ (mg/L)	N-NO ₂ ⁻ (mg/L)	P _T (mg/L)
1	RB1.0	7.5	27.6	4039	2544	1495	10.6	4084	480	0.12	344	3269	2958	2170	0.56	151	14.3
	RB1F	7.1	24.4	1151	7.5	1144	0.03	3724	40	0.01	337	2908	1919	224	4.87	1392	8.6
	% Rem.^b	-	-	71.5	99.7	23.5	99.7	8.8	91.7	-	-	-	35.1	89.7	-	-	-
2	RB2.0	7.3	29.2	1820	462	1357	1.93	4162	315	0.08	268	3266	2126	559	4.60	1276	11.4
	RB2F	6.7	29.0	1191	< 5	1191	< 0.02	3902	45	0.01	257	3239	1887	212	8.98	1543	8.5
	% Rem.^b	-	-	34.6	100	12.2	100	6.2	85.7	-	-	-	11.2	62.1	-	-	-
3	RB3.0	7.4	29.6	1867	496	1370	2.07	4166	300	0.07	408	3464	2116	611	6.67	1295	12.6
	RB3F	6.5	21.8	1240	13.8	1226	0.06	3809	50	0.01	464	3676	1492	137	8.93	1422	10.3
	% Rem.^b	-	-	33.6	97.2	10.5	97.1	8.5	-	-	-	-	29.4	77.6	-	-	-
4	RB4.0	7.3	22.0	1803	575	1228	2.40	3969	410	0.10	467	3676	1371	244	7.28	1075	15
	RB4F	6.9	19.0	1230	70	1160	0.29	3820	67.5	0.02	309	3502	1268	49	15.2	1204	9.6
	% Rem.^b	-	-	31.8	87.8	5.5	87.9	3.8	83.5	-	-	-	7.5	79.9	-	-	-
5	RB5.0	7.5	26.2	2197	873	1325	3.64	4261	380	0.09	303	3710	1304	339	11.9	766	7.3
	RB5F	7.3	21.8	1461	211	1250	0.88	4091	70	0.02	201	3300	1237	9.6	4.75	1123	6.9
	% Rem.^b	-	-	26.2	75.8	5.7	75.8	4.0	81.6	-	-	-	5.1	97.2	-	-	-
6	RB6.0	7.6	25.2	2167	810	1358	3.37	3590	450	0.13	246	3527	1267	294	2.22	673	10.5
	RB6F	7.1	16.2	1264	82.8	1181	0.34	3267	145	0.04	201	3313	1236	10	4.72	1162	7.4
	% Rem.^b	-	-	41.7	89.8	13.0	89.9	9.0	67.8	-	-	-	2.4	96.6	-	-	-
7	RB7.0	7.4	19.6	1772	547	1226	2.28	4169	390	0.09	204	3312	1285	204	4.17	901	12.2
	RB7F	7.1	20.2	1299	82.9	1216	0.35	4019	200	0.05	197	3086	1213	19.4	15.1	1053	8.9
	% Rem.^b	-	-	26.7	84.8	0.8	84.6	3.4	48.7	-	-	-	5.6	90.5	-	-	-
8	RB8.0	7.7	21.8	2480	1151	1329	4.80	3904	490	0.13	254	3321	1159	488	3.47	409	9.5
	RB8F	7.4	18.8	1403	171	1233	0.71	3679	90	0.02	164	2963	1067	7.54	14.6	937	6.5
	% Rem.^b	-	-	43.4	85.1	7.2	85.2	5.8	81.6	-	-	-	7.9	98.5	-	-	-

Table 9.2. Physico-chemical characterization of the landfill leachate before and after biological treatment.

Test	Sample	pH	T (°C)	TDC (mg/L)	DIC (mg/L)	DOC (mg/L)	Alkalinity ^a (g CaCO ₃ /L)	COD (mg/L)	BOD ₅ (mg/L)	$\frac{BOD_5}{COD}$	SO ₄ ²⁻ (mg/L)	Cl ⁻ (mg/L)	N _{TD} (mg/L)	N-NH ₄ ⁺ (mg/L)	N-NO ₃ ⁻ (mg/L)	N-NO ₂ ⁻ (mg/L)	P _T (mg/L)
9	RB9.0	7.8	25.2	2680	1436	1244	5.98	4047	440	0.11	159	3167	1125	638	1.27	192	7.7
	RB9F	7.5	15.8	1275	218	1058	0.91	3746	130	0.04	182	2822	961	9.28	3.35	854	7.2
	% Rem.^b	-	-	52.4	84.8	15.0	84.8	7.4	70.5	-	-	-	14.6	98.5	-	-	-
10	RB10.0	7.8	23.2	2528	1299	1228	5.41	3632	360	0.10	193	3050	832	523	0.82	182	6.8
	RB10F	7.6	15.6	1416	310	1106	1.29	3443	175	0.05	142	2866	767	16.9	3.04	723	6.4
	% Rem.^b	-	-	44.0	76.1	9.9	76.2	5.2	51.4	-	-	-	7.8	96.8	-	-	-
11	RB11.0	7.8	23.8	2372	1224	1148	5.10	4052	310	0.08	421	2927	853	521	1.94	167	9.4
	RB11F	7.7	14.4	1465	369	1096	1.54	3127	75	0.02	412	2830	714	8.94	9.05	662	8.5
	% Rem.^b	-	-	38.2	69.9	4.5	69.8	22.8	75.8	-	-	-	16.3	98.3	-	-	-
12	RB12.0	7.7	23.8	2683	1440	1243	6.00	3065	290	0.10	342	3034	1244	672	4.41	136	9.7
	RB12F	7.7	14.8	1333	319	1015	1.33	2952	90	0.03	261	2709	781	91.6	24.2	773	8.2
	% Rem.^b	-	-	50.3	77.8	18.3	77.8	3.7	69.0	-	-	-	37.2	86.4	-	-	-
13	RB13.0	7.7	20.2	2487	1233	1254	5.14	3645	360	0.10	173	2692	981	334	8.43	277	7.5
	RB13F	7.6	13.1	1358	233	1125	0.97	3308	95	0.03	258	2578	856	15.3	31.0	864	6.9
	% Rem.^b	-	-	41.4	81.1	10.3	81.1	9.2	73.6	-	-	-	12.7	95.4	-	-	-
14	RB14.0	7.6	17.4	2115	895	1220	3.73	3674	300	0.08	310	2686	1045	273	21.5	553	9.4
	RB14F	7.3	12.4	1175	134	1041	0.56	3410	90	0.03	526	2727	888	29.3	23.0	978	8.3
	% Rem.^b	-	-	44.4	85.0	14.7	85.0	7.2	70.0	-	-	-	15.0	89.3	-	-	-
15	RB15.0	7.5	19.0	2102	922	1181	3.84	3786	320	0.09	675	2792	1202	416	14.0	603	10
	RB15F	6.8	14.8	1055	52.5	1002	0.22	3566	110	0.03	538	2454	1105	68	20.7	1069	9.8
	% Rem.^b	-	-	49.8	94.3	15.2	94.3	5.8	65.6	-	-	-	8.1	83.7	-	-	-

^aAlkalinity values considering that at pH lower than 8.3 the inorganic carbon is almost in the form of bicarbonates [9]; ^bRemoval percentage (100 – 100 × RB₀/RB_F).

The reduction of the organic matter content during the biological tests was relatively low (1-24%, for DOC and 2-23%, for COD), which together with the low values of the BOD₅/COD ratio, confirm the low leachate biodegradability. Similar finding was got by Spagni and Marsili-Libelli [1], that obtained an average COD removal of 20% using a sequencing batch reactor (SBR) for the treatment of an old leachate.

The recalcitrant character of the leachate suggests that a simple biological oxidation is not enough to achieve a final effluent in agreement with the discharge limits, requiring the use of a non-conventional treatment technology, such as advanced oxidation processes (AOPs), which have been reported to enhance significantly the biodegradability of different recalcitrant wastewaters [2-6].

As previously mentioned, the biological treatment was performed under aerobic conditions, in order to promote only the nitrification reaction, just consuming the inorganic carbon of the leachate. The biological oxidation was interrupted when the final values of alkalinity and/or ammonium nitrogen tended to zero, ranging between 7.5 – 250 mg NH₄⁺-N/L and 0 – 1.6 mg CaCO₃/L, respectively (see Figure 9.1). During this step, on average, 9.1 mg of CaCO₃ was consumed per 1 mg of NH₄⁺-N converted, which is 27% higher than the stoichiometric ratio (7.14 mg CaCO₃/mg NH₄⁺-N) [7, 8].

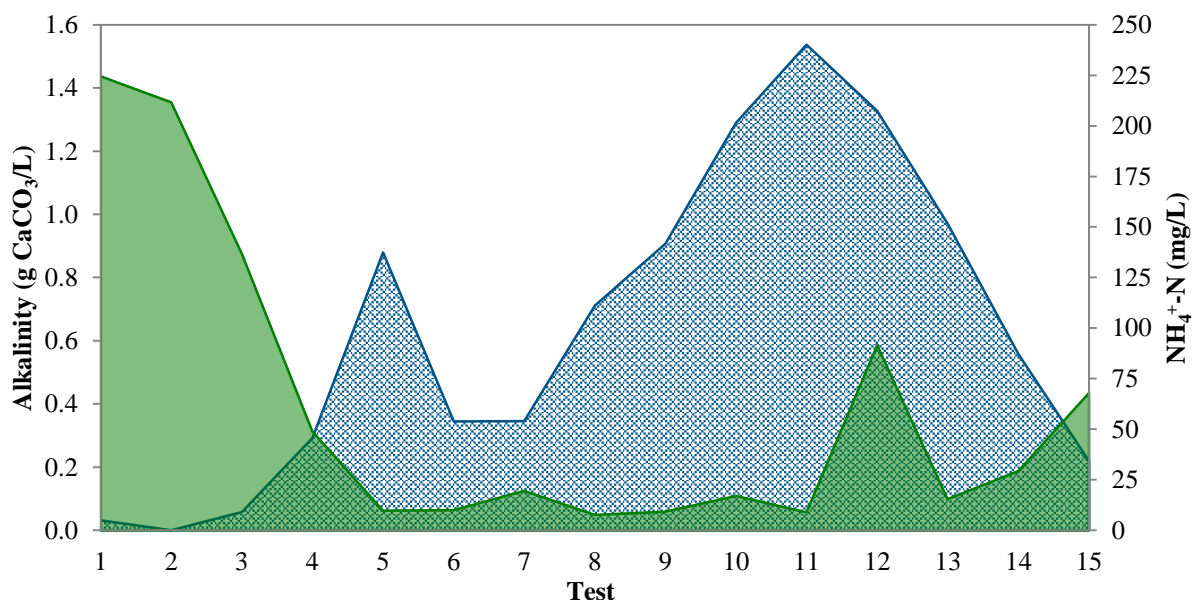


Figure 9.1. Variation of the alkalinity (■) and ammonium nitrogen content (■) at the end of the biological treatment.

Although the biological reactor was continuously aerated, the air supplied was not enough for microbial oxygen consumption needs, and the average dissolved oxygen (DO) content was below 0.5 mg/L (see Figure 9.2). DO was even null at the beginning of the nitrification process, and therefore the limiting step of this reaction. The DO concentration was only above zero ($DO_m = 0.36$ mg/L) throughout all reaction for test 1, due to the low amount of activated sludge. Considering this limitations, the nitrification kinetic constant was only calculated for test 1, achieving a value of 6.3 mg NH_4^+-N/g VSS/h ($T_m = 26$ °C; $pH_m = 7.7$). This specific ammonia oxidation rate was 23% lesser than the one presented in Chapter 5, using a raw leachate with almost the double of the ammonia content, under similar pH ($pH_m = 7.6$) and temperature ($T_m = 27$ °C) conditions, but with higher concentration of dissolved oxygen ($DO_m = 3.2$ mg/L). Spagni and Marsili-Libelli [1] obtained nitrification rates between 12.6 and 4.9 mg N/g VSS/h ($T = 20$ °C; $NH_4^+-N_i = 1199$ mg/L), which is in agreement with the results obtained in this work. For the remaining tests, it was possible to observe that the time required for the nitrification reaction was higher for leachates with higher ammonium content, lower operating temperatures and lower VSS content (Figure 9.2 and Figure 9.3).

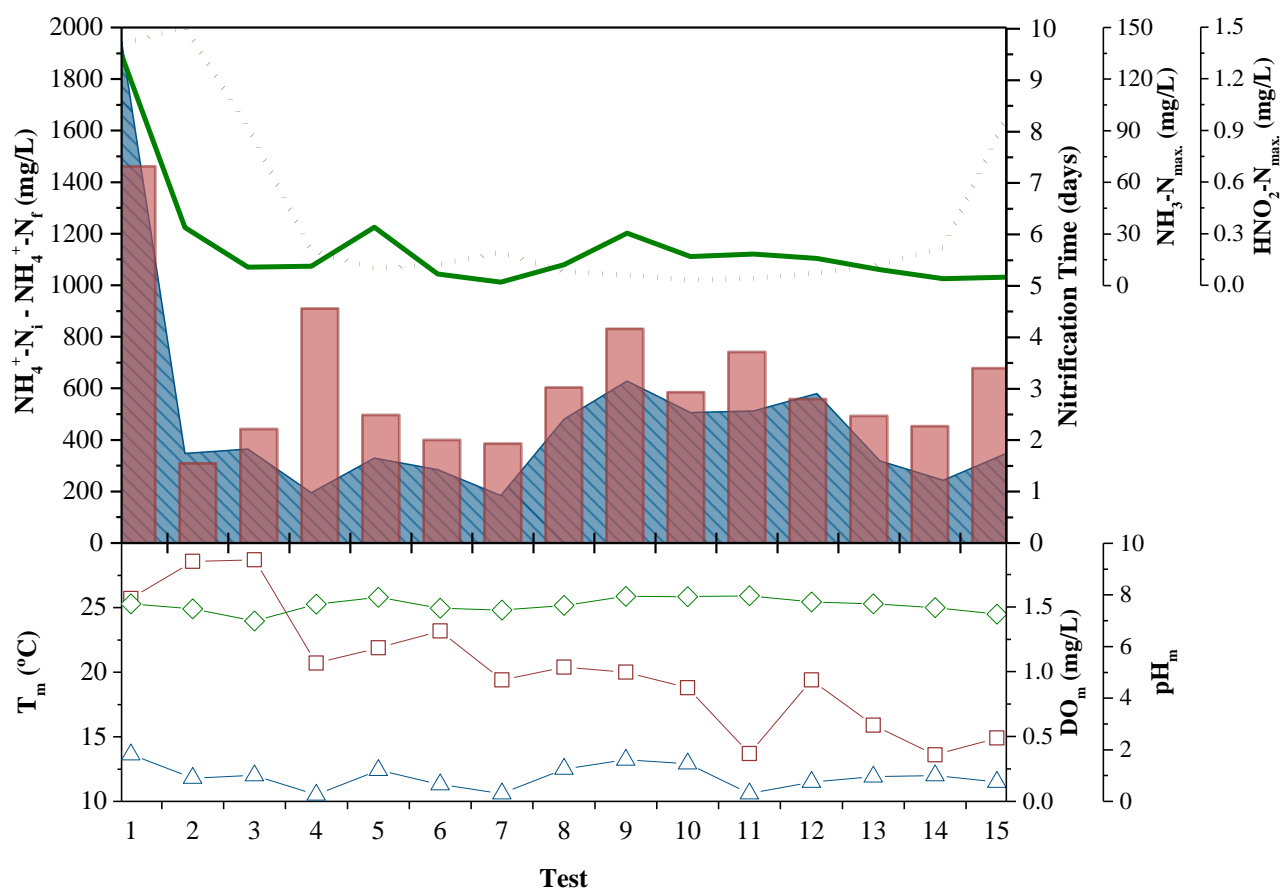


Figure 9.2. Amount of ammonium nitrogen eliminated (■), time required for the nitrification reaction (■), maximum contents of free ammonia (—) and free nitrous acid (····), and average values of temperature (□), dissolved oxygen (△) and pH (◇), for each biological test.

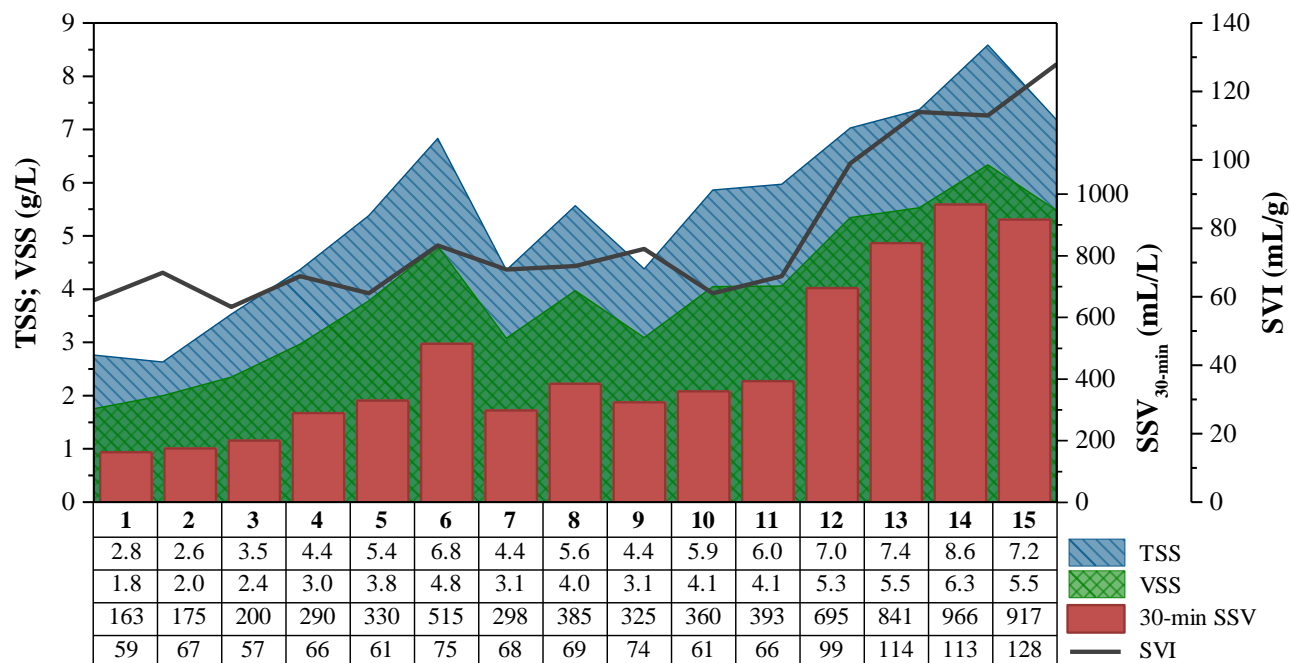


Figure 9.3. Evolution of total suspended solids (TSS), volatile suspended solids (VSS), 30-min settled sludge volume (SSV_{30-min}) and sludge volumetric index (SVI), in the biological reactor, along the experimental period.

Table 9.2 shows that during the nitrification process, ammonium was mainly converted in nitrites whose concentration increased from 17 to 821%, indicating that only the nitrification reaction occurred, leading to the accumulation of nitrite inside the biological reactor [10, 11]. It can also be observed that, contrary to what would be supposed, the amount of total dissolved nitrogen decreased (2 – 37%), being the formation of nitrous nitrogen lesser than the loss of ammonium nitrogen, suggesting that part of ammonium was lost by ammonia stripping.

The nitrification reaction takes place in two steps: (i) first, ammonium nitrogen is oxidised into nitrite (nitritation) by the ammonia-oxidising bacteria (AOB), according to the Eq. (9.1); and (ii) then, in more restrictive operating conditions, the nitrite is converted into nitrate (nitrataion) by the nitrite-oxidising bacteria (NOB), in agreement with Eq. (9.2) [10, 12, 13].



The extension of the nitrification can be influenced by diverse abiotic factors, being the most important the temperature, pH, dissolved oxygen (DO) deficiency, the presence of toxic or inhibitory substances and the substrate concentration [12]. The nitrite build-up occurs when, individually or in combination, certain deviations in the abiotic factors repress the action of the NOB in detriment of the ABO.

The nitration reaction can especially be inhibited by: (i) cold temperatures ($< 14^{\circ}\text{C}$), since the nitrite oxidation by NOB is slower than the ammonium oxidation by AOB [8, 10]; (ii) high pH values, since the optimal pH values are between 7.2 and 7.6 for NOB and between 7.9 and 8.2 for AOB [13, 14]; (iii) low DO content ($< 0.5 \text{ mg/L}$), since the oxygen deficit affects more significantly the activity of NOB than that of AOB, thus being the nitrite oxidation strongly inhibited [8, 10, 15]; (iv) high concentrations of un-ionised ammonia (NH_3), which has been described as being more inhibitory for NOB ($0.08\text{-}0.82 \text{ mg NH}_3\text{-N/L}$) than for AOB ($8.2\text{-}123 \text{ mg NH}_3\text{-N/L}$) [13, 16]; and (v) a content of free nitrous acid or un-ionised nitrous acid (HNO_2) higher than $0.06\text{-}0.83 \text{ mg HNO}_2\text{-N/L}$ [10, 16].

The amounts of un-ionised ammonia ($[\text{NH}_3\text{-N}]$) and un-ionised nitrous acid ($[\text{HNO}_2\text{-N}]$) are directly related to the concentrations of total ammonia nitrogen ($[\text{TAN}] = [\text{NH}_3\text{-N} + \text{NH}_4^+\text{-N}]$) and nitrite ($[\text{NO}_2^-\text{-N}]$), respectively, the pH and the temperature (in $^{\circ}\text{C}$), and can be estimated from the following equations:

$$[\text{NH}_3 - \text{N}] = \frac{\text{TAN} \times 10^{\text{pH}}}{e^{6344/(273+T)} + 10^{\text{pH}}} \quad (9.3)$$

$$[\text{HNO}_2 - \text{N}] = \frac{\text{NO}_2^- - \text{N}}{e^{-2300/(273+T)} \times 10^{\text{pH}}} \quad (9.4)$$

Given the exposed above and looking at the Figure 9.2, it can be inferred that the cause of the nitrite accumulation is the combination of low dissolved oxygen content along with the presence of free ammonia and free nitrous acid (maximum concentrations between $2.0\text{-}134 \text{ mg NH}_3\text{-N/L}$ and $0.03\text{-}1.5 \text{ mg HNO}_2\text{-N/L}$, respectively). The free ammonia seems to be the abiotic factor that more represses the nitrite oxidation into nitrate, rising up to values that, according to Anthonisen et al. [16], can inhibit both the species of nitrifying bacteria.

The ammonium nitrogen conversion to nitrite could be a good option, since the nitrite is an intermediate, both of nitrification and denitrification reactions. Thus, the nitrification could be stopped at nitrite and the denitrification could start from there, by reducing the nitrite into nitrogen gas, thereby saving 25% in the oxygen demand for the nitrification and 40% in the needs of external carbon source for the denitrification [17].

Throughout this chapter it will be explained that a leachate downstream from the biological oxidation, with high amounts of nitrite, affects directly the hydrogen peroxide consumption in the subsequent photo-Fenton reaction. So, in the future, two measures could be implemented in the first biological oxidation process, regarding a proficient integration of the treatment strategy under consideration, namely: (i) to perform nitrification-denitrification via nitrite, taking into account the alkalinity balance (consumed during nitrification plus the produced along denitrification), in order to assure that the sulphate concentration (added as sulphuric acid and ferrous sulphate, in the coagulation and photo-oxidation steps, respectively) does not exceed 2000 mg/L; or (ii) to carry out complete nitrification to nitrate, optimizing the operating conditions (pH, OD and temperature) and the ammonium nitrogen load fed to the biological reactor (for instance, using a sequential batch reactor (SBR) with 100 m³ capacity, being the treated volume of 25 m³, which means a dilution of four times of the inlet leachate), minimizing the inhibition of nitrite-oxidising bacteria.

Figure 9.3 shows an oscillation on solids profile, with a progressive growing trend (TSS = 2.6 – 8.6 g/L and VSS = 1.7 – 6.3 g/L), keeping the VSS/TSS ratio between 64 and 76%, along all biological oxidation trials. The increment in solids content was associated with the microbial growth and the existence of solids in the leachate fed to the biological reactor, while the decreasing was due to the purge of sludge. In the course of the experimental period, the values of the settled sludge volume at 30 min, and the sludge volumetric index increased up to a maximum of 966 mL/L and 128 mL/g, respectively, indicating a poor sludge settling (SVI > 100 mL/g) [18]. The weak settleability perceived, mainly in the last four experiments, was most likely caused by the increment of the sludge age and by the very low food to microorganism ratio (F/M) [19], which ranged among 0.01 and 0.05 g BOD₅ per 1 g of VSS per day.

9.3.2 Evaluation of the coagulation/sedimentation efficiency

Previous results showed that the preliminary acidification process of the photo-Fenton reaction led to the formation of high amounts of sludge, increasing the turbidity and decreasing the light penetration and consequently decreasing the photo-Fenton reaction rate, thus demanding high energy and H₂O₂ consumption to achieve a biodegradable effluent able to be coupled with a biological process (Chapters 3-5). Considering these aspects it was decided to perform an intermediate step of coagulation/sedimentation, whose main purposes are: (i) removal of the recalcitrant organic matter fraction, corresponding to the humic acids present in the effluent downstream the biological treatment; and (ii) leachate clarification, in order to improve the efficiency of the upstream photo-oxidation step.

In this process, ferric chloride was selected as coagulant, since the photo-Fenton reaction is carried out with iron. Initially, the coagulation tests were performed at pH 2.8, since the photo-Fenton reaction is more efficient at pH between 2.8 and 3.0 [20]. However, for the photo-oxidation experiments, the addition of an alkaline solution was required due to the pronounced decrease of pH, at the beginning of the photo-Fenton reaction (this will be explained in the next sub-section). Bearing in mind the minimization of this unavoidable consumption of sodium hydroxide in the subsequent phototreatment process, the coagulation step was also performed at higher pH values, and a pH of 4.2 was selected as probable the optimum (discussion still going on). Moreover, Ntampou et al. [21] claimed that the optimum pH value for the leachate treatment by coagulation, using ferric chloride (7 mmol Fe³⁺/L), was around 4.5.

Since the coagulation pH had to be chosen taking into account the following photo-Fenton reaction and there was no significant difference between the coagulation efficiencies at pH 3.0 and 4.2, only the coagulant dose was tested, varying the ferric ion concentration between 120 and 600 mg Fe³⁺/L to evaluate its influence on the coagulation/sedimentation process. The jar-test stirring speed was set at 100 rpm (equivalent to stirring speed in the coagulation tank). Figure 9.4 and Figure 9.5 show the evolution of the colour, DOC concentration, and total suspended solids in the supernatant, and volume of settled sludge after 30 minutes, for different additions of ferric chloride.

Increasing the coagulant dose from 120 to 600 mg/L, it was observed an increment (i) in the DOC removal from 37% to 82%, (ii) in the TSS removal from 26% to 77% and (ii) in the amount of acid sludge generated, approximately, from 120 to 600 mL/L (after half an hour). Figure 9.5 also shows that the increment in the coagulant dose led to a change in the effluent colour, from dark-brown (associated to humic acids) to yellow-brown and light yellow (associated to fulvic acids), which is related to the precipitation of the negatively charged humic acids [22, 23]. The insoluble Fe(III)-HA complexes are created when two or more iron coordination positions are occupied by HA ligand donor groups, forming an internal ring structure, mostly due to the reactions with the HA functional groups that contain oxygen, such as COOH, C=O and phenolic OH groups [24].

Figure 9.6 presents the images of an experiment where humic substances were extracted from a biologically oxidised leachate by the acid-base treatment method [25, 26], with a DAX-8 resin column. Figure 9.6b shows the dark colour of the humic substances extracted from the column. The sludge volume was measured every 30 minutes, along 4.5 hours of sedimentation. After 2 hours, for the experiments performed with the three higher iron doses, it was observed the flotation of a fraction of the solid phase, probably due to the large amount of gas entrapped in the sludge.

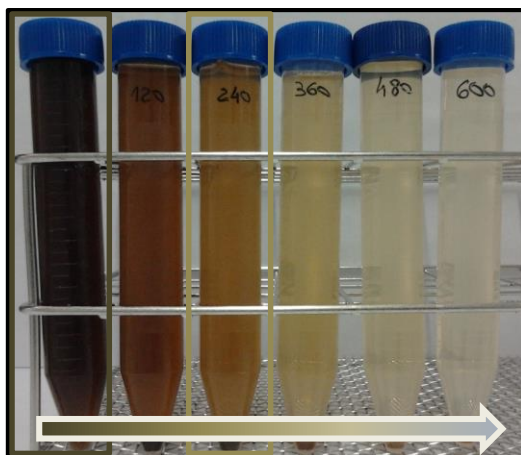


Figure 9.4. Evolution of the supernatant colour for coagulant doses from 0 to 600 mg Fe³⁺/L.

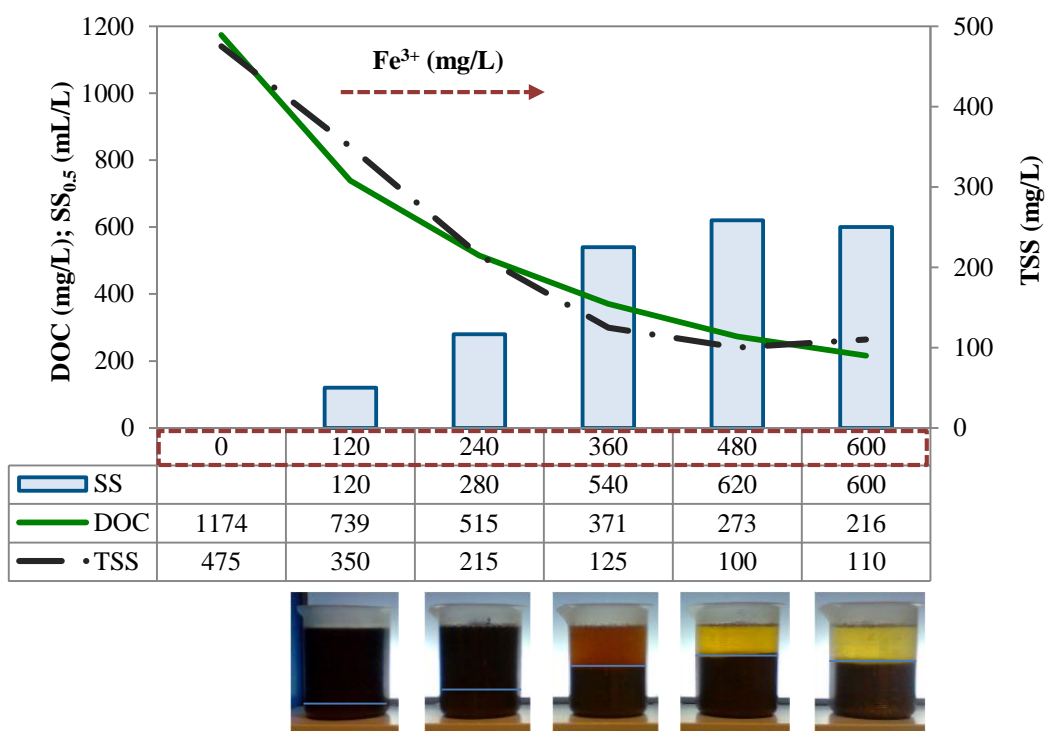


Figure 9.5. Dissolved organic carbon (DOC), 30-min settled sludge volume (SS) and total suspended solids (TSS) in the supernatant, as a function of coagulant concentration (pH 4.2).

Aziz et al. [27] also showed that the removal of colour, turbidity, suspended solids and COD increased with the increasing of FeCl₃ dose. For instance, the COD decreased 27% and 51%, when using 200 and 1200 mg/L of FeCl₃ (COD_i = 1533-3600 mg/L), respectively. They likewise concluded that the organic matter is the main responsible for the leachate colour. On the other hand, Amokrane et al. [28] indicated that to achieve a COD reduction of 55% (COD_i = 4100 mg/L; DOC_i = 1430 mg/L), the optimal iron dose, for landfill leachate pretreatment by coagulation, was 0.035 mol/L (FeCl₃), which is 4.8 times higher than the dose obtained by Aziz et al [27].

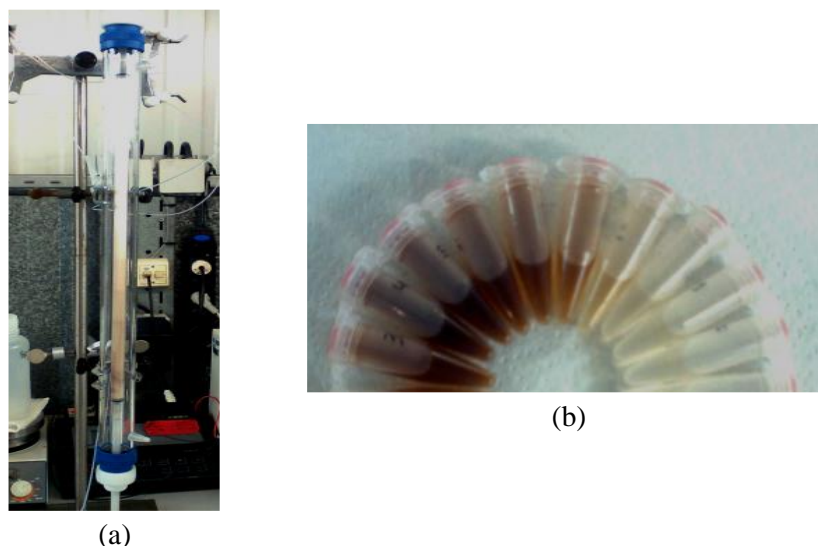


Figure 9.6. Extraction of humic substances from landfill leachate. (a) XAD-8 resin column after passing the leachate previously nitrified and acidified. (b) Eluate samples collected at different times.

The coagulation step only promotes the transfer of the organic matter from the dissolved phase to the particulate phase, leading to the formation of high amounts of acidic sludge, which currently constitutes a serious problem and needs to be forwarded to the landfill. The coagulant dose selected was $240 \text{ mg Fe}^{3+}/\text{L}$ due to three main factors: i) minimum dose of coagulant able to precipitate the humic acids and yield a light yellow leachate; ii) minimum dose of coagulant allowing to obtain a leachate with low suspended solids and avoid the sludge flotation; iii) minimum production of acidic sludge and maximum amount of organic matter to be oxidised in the phototreatment.

The coagulation tests performed at pre-industrial scale, using the same coagulant dose, showed a much higher efficiency than that obtained in the jar-test, leading to an effluent with characteristics close to the leachate obtained with the addition of $360 \text{ mg Fe}^{3+}/\text{L}$ in the jar-test (see Figure 9.7).

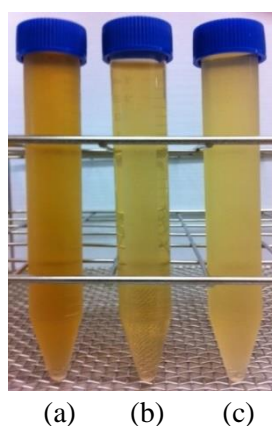


Figure 9.7. Comparison between the test performed in the pre-industrial scale plant using $240 \text{ mg Fe}^{3+}/\text{L}$ (b), with the tests performed in the jar-test using 240 (a) and 360 (c) $\text{mg Fe}^{3+}/\text{L}$.

Table 9.3 shows the values of the main analysed parameters, at the beginning (CT₀ = BR_F) and the end (CT_F) of each test, as well as the removal efficiency of TSS, DOC and COD. The concentration of the TSS at the end of the experiment (TSS_{CT_F}) refers to the value after the sedimentation period (Sed.) and acid sludge removal. In the tests 5 and 6, the coagulation step was not carried out, aiming at comparing the tests conducted in this set with those reported in Chapters 3, 4 and 5. Whenever the values presented in the table refer to the moment after acidification, very low DOC and COD removals (< 35%) were obtained. In the trial 7, only ferric chloride was added, in order to verify if the H₂O₂ addition, in the subsequent photo-oxidation, would be enough to lower the pH value until the desired one, and it was verified that, during coagulation, the organic matter removal was about 30% lesser than the average. Finally, the experiment 11 was performed with less coagulant, with the intention of checking whether the yield of photo-Fenton reaction was significantly affected. As will be seen, the use of a lower iron dose led to a decrease in efficiency both of coagulation and photo-oxidation.

With exception of tests 5, 6 and 11, during the coagulation process, the chloride ions concentration increased in average 540 mg/L, which is very close to the stoichiometric amount of this ion (490 mg/L) added as ferric chloride commercial solution (considering the information of manufacturer: 40% FeCl₃ and 1% HCl). The sulphate ions concentration simultaneously increased, during the coagulation step, but in this case, due to sulphuric acid addition. By the analysis of the Table 9.3 and Figure 9.8, it appears that, in general, the acid needs increase proportionally to the alkalinity concentration of the leachate fed to the coagulation tank. Therefore, it is extremely important to achieve the complete removal of alkalinity in the nitrification biological step in order to reduce the acid requirements. High doses of sulphuric acid will lead to high amounts of sulphate ions in the treated leachate, exceeding the discharge limit imposed by the Portuguese legislation (2 g/L). Beyond that, high sulphate content reduces significantly the photo-Fenton reaction rate, as previously discussed in Chapter 7.

According to Table 9.3 and Figure 9.9, with exception of tests 5, 6 and 11, the coagulation step led to DOC and COD removal efficiencies above 40% (average removal efficiency of 60 and 58%, respectively). Ntampou et al [21] achieved similar results (COD removal of approximately 54%) using 4 mM of ferric ion (223 mg Fe³⁺/L) in the coagulation of a stabilized leachate. These values are in agreement with those presented by Amokrane et al. [28]. The authors reported DOC and COD removal efficiencies of approximately 10 – 25% for young leachates, and about 50 – 65% for stabilized leachates or biologically oxidised leachates.

Table 9.3. Physico-chemical characterization of the landfill leachate before and after coagulation/sedimentation process.

Test	V (m ³)	Fe ³⁺ (mg/L)	Sed. ^a (h)	H ₂ SO ₄ (mM)	Sample	pH	T (°C)	TSS (mg/L)	DOC (mg/L)	COD (mg/L)	DIC (mg/L)	Alkalinity ^b (g CaCO ₃ /L)	NH ₄ ⁺ -N (mg/L)	SO ₄ ²⁻ (mg/L)	Cl ⁻ (mg/L)
1	2.1	240	14	29.8	CT1.0	7.10	24.4	288	1144	3724	7.50	0.03	224	337	2908
					CT1F	2.69	24.0	44	456	1554	< 0.1	< 4×10 ⁻⁴	146	3188	3518
					% Rem.^c	-	-	84.7	60.1	58.3	-	> 98.6	35.2	-	-
2	2.0	240	14	35.9	CT2.0	6.73	29.0	1252	1191	3902	< 0.1	< 4×10 ⁻⁴	212	257	3239
					CT2F	2.85	25.8	252	556	1877	< 0.1	< 4×10 ⁻⁴	144	3670	3727
					% Rem.^c	-	-	79.9	53.3	51.9	-	-	32.0	-	-
3	2.6	240	3	31.8	CT3.0	6.46	21.8	480	1226	3809	13.8	0.06	137	464	3676
					CT3F	2.99	22.4	480	435	1463	< 0.1	< 4×10 ⁻⁴	53.9	3311	3950
					% Rem.^c	-	-	0	64.5	61.6	-	> 99.3	60.6	-	-
4	2.5	240	3	33.8	CT4.0	6.93	19.0	322	1160	3820	70.0	0.29	49.0	309	3502
					CT4F	2.95	22.2	375	436	1609	4.00	0.02	44.3	3438	4007
					% Rem.^c	-	-	-	62.4	57.9	-	94.3	9.47	-	-
5	1.4	-	-	44.9	CT5.0	7.30	21.8	132	1250	4091	211	0.88	9.63	201	3300
					CT5F	2.99	22.4	705	856	2690	1.73	0.01	15.0	4377	3416
					% Rem.^c	-	-	-	31.5	34.2	-	99.2	-	-	-
6	1.5	-	-	18.8	CT6.0	7.06	16.2	780	1181	3267	82.8	0.34	10.0	201	3313
					CT6F	3.99	17.8	760	971	3021	< 0.1	< 4×10 ⁻⁴	8.35	2017	3423
					% Rem.^c	-	-	2.6	17.8	7.5	-	> 99.9	16.6	-	-
7	2.5	240	3	-	CT7.0	7.07	20.2	655	1216	4019	82.9	0.35	19.4	197	3086
					CT7F	5.50	16.8	413	702	2403	6.60	0.03	15.8	199	3565
					% Rem.^c	-	-	36.9	42.3	40.2	-	92.0	18.8	-	-
8	2.4	240	14	6.4	CT8.0	7.43	18.8	285	1233	3679	171	0.71	7.54	164	2963
					CT8F	4.85	15.8	524	505	1936	5.30	0.02	4.36	698	3619
					% Rem.^c	-	-	-	59.0	47.4	-	96.9	42.2	-	-

Table 9.3. Physico-chemical characterization of the landfill leachate before and after coagulation/sedimentation process.

Test	V (m ³)	Fe ³⁺ (mg/L)	Sed. ^a (h)	H ₂ SO ₄ (mM)	Sample	pH	T (°C)	TSS (mg/L)	DOC (mg/L)	COD (mg/L)	DIC (mg/L)	Alkalinity ^b (g CaCO ₃ /L)	NH ₄ ⁺ -N (mg/L)	SO ₄ ²⁻ (mg/L)	Cl ⁻ (mg/L)
9	2.5	240	14	13.4	CT9.0	7.54	15.8	175	1058	3746	217	0.91	9.28	182	2822
					CT9F	4.18	13.8	72	388	1141	4.49	0.02	4.57	1333	3528
					% Rem.^c	-	-	58.9	63.3	69.5	-	97.9	50.7	-	-
10	2.4	240	14	18.4	CT10.0	7.59	15.6	496	1106	3443	309	1.29	16.9	142	2866
					CT10F	4.27	12.4	116	374	1162	1.93	0.01	2.04	1690	3365
					% Rem.^c	-	-	76.6	66.2	66.3	-	99.4	88.0	-	-
11	2.5	120	14	18.8	CT11.0	7.76	14.4	540	1096	3127	368	1.54	8.94	412	2830
					CT11F	4.31	14.8	416	613	2060	9.37	0.04	3.37	2202	3040
					% Rem.^c	-	-	23.0	44.1	34.1	-	97.5	62.3	-	-
12	2.3	240	14	19.5	CT12.0	7.67	14.8	492	1015	2952	318	1.33	91.6	261	2709
					CT12F	4.18	13.2	220	382	1297	10.7	0.04	12.3	1679	3256
					% Rem.^c	-	-	55.3	62.4	56.1	-	96.6	86.6	-	-
13	2.3	240	14	13.6	CT13.0	7.60	13.1	164	1125	3308	233	0.97	15.3	258	2578
					CT13F	4.29	10.4	168	410	1363	5.46	0.02	22.6	1397	3267
					% Rem.^c	-	-	-	63.6	58.8	-	97.7	-	-	-
14	2.5	240	14	9.4	CT14.0	7.26	12.4	360	1041	3410	134	0.56	29.3	526	2727
					CT14F	4.24	10.2	200	422	1498	7.82	0.03	26.5	1254	3308
					% Rem.^c	-	-	44.4	59.5	56.1	-	94.2	9.41	-	-
15	2.9	240	14	4.4	CT15.0	6.82	14.8	528	1002	3566	52.5	0.22	68.0	538	2454
					CT15F	4.20	9.4	40	419	936	6.08	0.03	32.9	901	2861
					% Rem.^c	-	-	92.4	58.2	73.8	-	88.4	51.6	-	-

^aSedimentation time; ^bAlkalinity values considering that at pH below 8.0 the inorganic carbon is almost in the form of bicarbonates ; ^cRemoval percentage (100 – 100 × RB₀/RB_F).

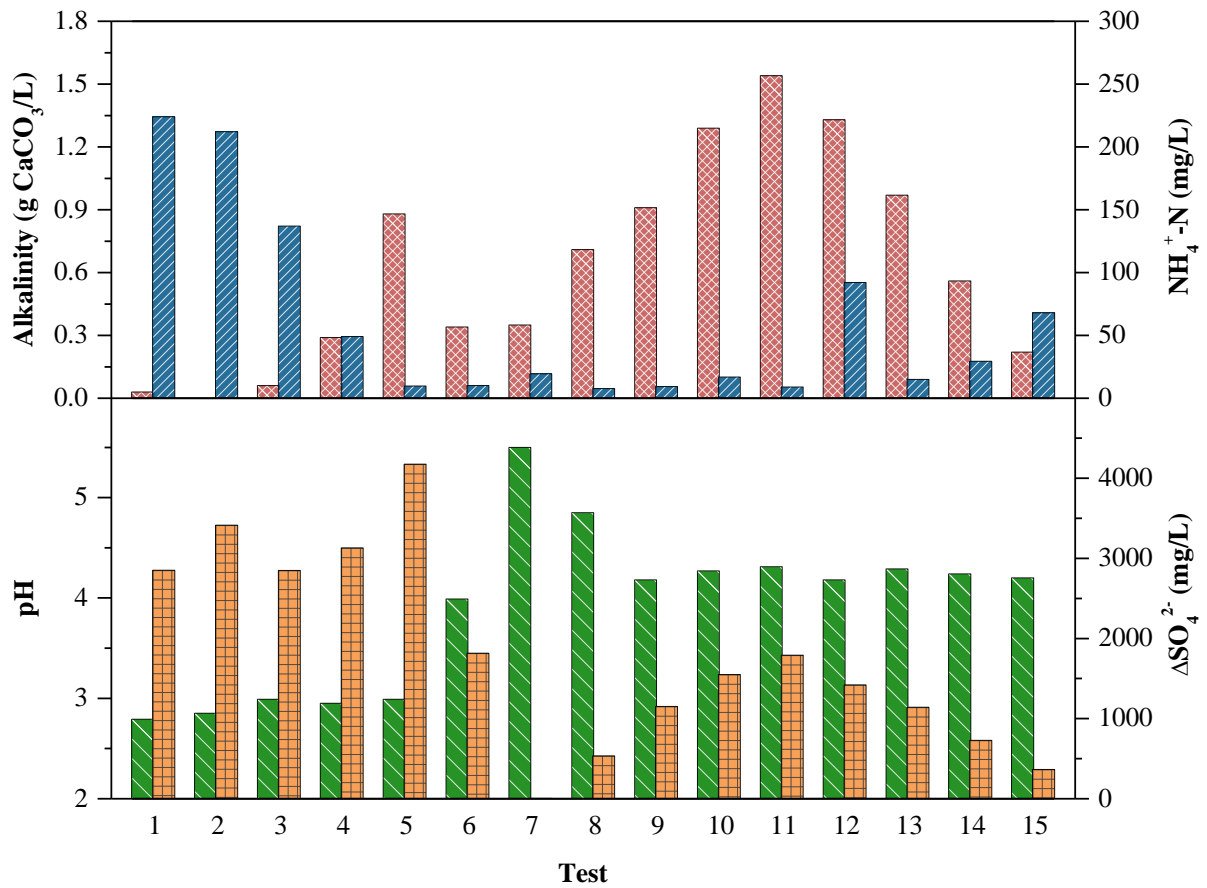


Figure 9.8. Variation of the initial values of alkalinity (■) and $\text{NH}_4^+\text{-N}$ (■), final pH (■) and sulphate increment (■), during the coagulation step.

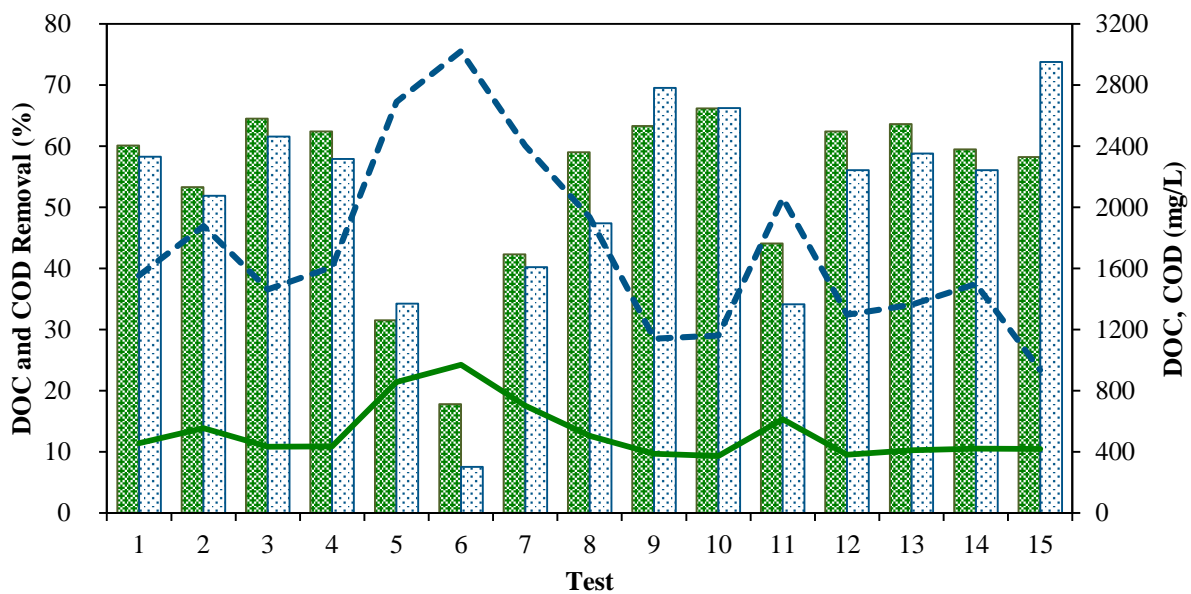


Figure 9.9. Evolution of DOC (■) and COD (■) removal along the experimental period, and values of DOC (—) and COD (---) at the end of the coagulation step.

The marked decay of the organic matter is most likely related to the removal of humic substances, mainly humic acids, leading to a change in the leachate colour, from dark-brown, characteristic of humic acids solutions, to brownish yellow, typical of fulvic acids solutions (see Figure 9.4), resulting in approximately 300 mL (measured after 30 minutes; in the next day the sludge content was about 240 mL/L) of acidic iron sludge per 1-L of coagulated leachate.

Wu et al. [29] investigated the dissolved organic matter (DOM) composition during a multistage leachate treatment strategy, including biological oxidation through SBR, coagulation, Fenton reaction and biological aerated filtering (BAF). The DOM of the landfill leachate was fractionated in each stage into humic acid (HA), fulvic acid (FA) and hydrophilic (Hyl) fractions. The coagulation step achieved a removal efficiency of 71%, 53% and 37% for HA, Hyl and FA, respectively. This indicates that the high molecular weight (MW) humic acids are preferentially eliminated in this stage.

Yoon et al. [30] reported similar results for the treatment of a leachate from an aerated lagoon with a ferric iron driven coagulation process, using an ultrafiltration system for the organic compounds fractionation. The authors showed that along the coagulation process, the organics with MW > 500 Da were removed more easily (59 – 73%) than the organics with a MW < 500 Da (18%). The humic substances can be removed from the aqueous phase by coagulation-sedimentation according to two mechanisms [21, 31]: (i) charge neutralization by binding the cationic metal on the negatively charged functional groups of the humic acids, reducing their solubility; and (ii) adsorption, by adhesion of amorphous metal hydroxides onto the produced precipitates. As previously reported, the photo-Fenton rate is drastically reduced by the presence of suspended solids due to three main factors: i) decrease of the light penetration in the reactional medium; ii) absorption of UV-Vis photons, decreasing its availability for the photo-oxidation process; iii) degradation of the particulate organic matter.

Aiming at correctly operate the subsequent phototreatment step, the coagulation/sedimentation stage should be performed: (i) using ferric chloride, with a concentration of 240 mg of Fe³⁺ per 1-L of landfill leachate, after suitable aerobic biological oxidation; (ii) at pH 4.2, once it was the ideal to initiate the subsequent photo-Fenton reaction, ensuring that the sulphate ion concentration remains below the discharge limit (2 g/L); and (iii) with a sedimentation period of approximately 14 hours, achieving a supernatant's TSS content lower than 250 mg/L.

9.3.3 Evaluation of the photo-Fenton reaction efficiency

Concerning the assessment of leachate treatment using a photo-treatment, 15 tests were executed, under different operating conditions: i) type and intensity of the radiation source (solar and/or artificial, 2/4 UV lamps); ii) leachate with or without coagulation/sedimentation pretreatment; and iii) initial pH of the leachate. Table 9.4 shows the main characteristics of the leachate after the photo-oxidation process. The pre-treatment of the leachate using a biological oxidation/coagulation/sedimentation process enhances significantly the efficiency of the photo-Fenton oxidation (tests 1 and 2), achieving a reaction rate more than four times higher, consuming 24% less solar energy and 77% less H_2O_2 when compared to the test performed with the leachate without any pre-treatment (experiment 5 presented in Chapter 3 and represented in Figure 9.10 as 5') to obtain a final effluent with a DOC value of 250 mg/L (Figure 9.10). The oxidation time required to achieve a DOC value of 250 mg/L was established in Chapter 4 as the optimum phototreatment time to obtain an easily biodegradable effluent, wherein the final COD of a downstream biological treatment would be in agreement with the discharge limit (150 mg O_2/L) for disposal into water bodies.

The induction period of almost 10 $\text{kJ}_{\text{UV}}/\text{L}$ observed in DOC profile of the photo-Fenton reaction applied to the raw leachate (experiment 5') was almost completely eliminated when using the pre-treated leachate (Figure 9.10), mainly due to the absence of high molecular weight humic acids. This represents a major decrease in the photo-Fenton reaction costs related to H_2O_2 consumption, number of UV lamps, area of CPCs required and area of land for CPCs implementation.

Figure 9.10 shows that to obtain a leachate with a DOC value of 250 mg/L it was necessary 88 m H_2O_2 and 4.9 $\text{kJ}_{\text{UV}}/\text{L}$ for test 1 and 122 mM H_2O_2 and 8.1 $\text{kJ}_{\text{UV}}/\text{L}$ for test 2. Although higher amounts of energy and reactants had been required for test 2, higher values of average UV irradiance and temperature were observed for test 2 ($I_{\text{m},2} = 25.8 \text{ W}/\text{m}^2$ and $T_{\text{m},2} = 38.9^\circ\text{C}$, $I_{\text{m},1} = 14.3 \text{ W}/\text{m}^2$ and $T_{\text{m},1} = 27.1^\circ\text{C}$). This difference can be mainly associated with the fact that in the second test the leachate sample had (i) a higher DOC concentration (556 vs. 456 mg/L), which led to a higher total amount of H_2O_2 consumed, since the specific H_2O_2 consumption is practically the same (15.1 and 14.3 mg of H_2O_2 per mg of oxidised DOC, in the tests 1 and 2, respectively), and (ii) a higher total suspended solids concentration (253 vs. 44 mg/L).

Table 9.4. Main characteristics of the leachate after the photo-oxidation process.

Test	Radiation		Pretreatment ^b	V (m ³)	TSS _i ^c (mg/L)	pH _i ^c	pH _m ^d	T _m ^d (°C)	Fe _m ^d (mg/L)	t (h)	Q _{UV} (kJ/L)	EE ^e (kWh/m ³)	NaOH ^f (mM)	H ₂ O ₂ ^g (mM)	DOC _i ^c (mg/L)	DOC _f ^h (mg/L)	Min ⁱ (%)	H ₂ O ₂ /C ^j ($\frac{\text{mg H}_2\text{O}_2}{\text{mg DOC}}$)
	Source ^a	Intensity																
1	Sol.	14.3 W/m ²	BT + Coag.	1.0	44	2.69	2.52	27.1	72.4	7.0	7.3	-	34.9	123	456	178	61.0	15.1
2	Sol.	25.8 W/m ²	BT + Coag.	1.0	253	2.85	2.59	38.9	74.0	4.2	9.2	-	34.9	140	556	222	60.1	14.3
3	Art.	4×1000 W	BT + Coag.	1.4	480	2.99	2.64	42.1	75.9	6.2	19.7	16.3	27.9	125	435	176	59.5	16.4
4	Art.	4×1000 W	BT + Coag.	1.4	575	2.95	2.58	32.4	81.5	9.8	30.3	23.3	34.9	174	436	193	55.7	24.4
5	Art.	4×1000 W	BT	1.4	705	2.99	2.68	38.6	31.1	23.6	72.8	67.4	56.9	250	856	437	48.9	20.3
6	Art.	4×1000 W	BT	1.5	760	3.99	2.62	33.0	59.2	18.6	53.5	49.6	23.0	203	971	520	46.4	15.3
7	Art.	4×1000 W	BT + Coag.	1.5	413	5.50	3.11	35.1	60.2	11.9	34.3	31.8	16.0	187	702	292	58.4	15.5
8	Art.	4×1000 W	BT + Coag.	1.4	524	4.85	2.64	29.9	53.8	11.8	36.5	25.0	17.0	202	505	198	60.8	22.4
9	Art.	4×1000 W	BT + Coag.	1.6	72	4.18	2.69	28.3	52.1	7.0	19.0	15.0	14.0	119	388	222	42.8	24.4
10	Sol./Art.	23.7 W/m ² + 4×1000 W	BT + Coag.	1.7	116	4.27	2.59	29.0	56.3	5.3	17.7	7.5	12.0	133	374	172	54.0	22.4
11	Sol./Art.	14.1 W/m ² + 4×1000 W	BT + Coag.	1.7	416	4.31	2.72	31.9	49.8	13.3	46.0	25.9	12.0	170	613	229	62.6	15.1
12	Art.	2×1200 W	BT + Coag.	1.4	220	4.18	2.59	25.2	56.7	8.1	15.0	10.9	11.0	115	382	240	37.2	27.6
13	Art.	2×850 W	BT + Coag.	1.3	168	4.29	2.67	15.6	58.7	13.2	18.6	13.3	12.0	125	410	232	43.4	23.9
14	Art.	2×1200 W	BT + Coag.	1.4	200	4.24	2.60	23.5	54.5	7.2	13.3	12.3	16.0	115	422	286	32.2	28.8
15	Sol./Art.	17.1 W/m ² + 2×1200 W	BT + Coag.	1.8	40	4.20	2.77	22.6	49.5	5.7	12.2	7.6	14.0	127	419	205	51.1	20.2

^aSol. – Solar, Art. – Artificial; ^bBT – Biological treatment, Coag. – Coagulation; ^cInitial values of TSS, pH and DOC (equal to the final value of coagulation); ^dAverage values of pH, temperature and dissolved iron concentration, during the photo-Fenton reaction; ^eElectricity consumed by the lamps; ^fSodium hydroxide consumed during the photo-Fenton reaction plus the amount to be spent in the neutralization of the photo-treated leachate (~9.5 mM); ^gHydrogen peroxide concentration consumed; ^hFinal value of DOC; ⁱMineralization (1- COD_f/COD_i, %); ^jRatio between the H₂O₂ consumed and DOC oxidised along photo-Fenton (H₂O₂/(COD_i-COD_f) × 34,02).

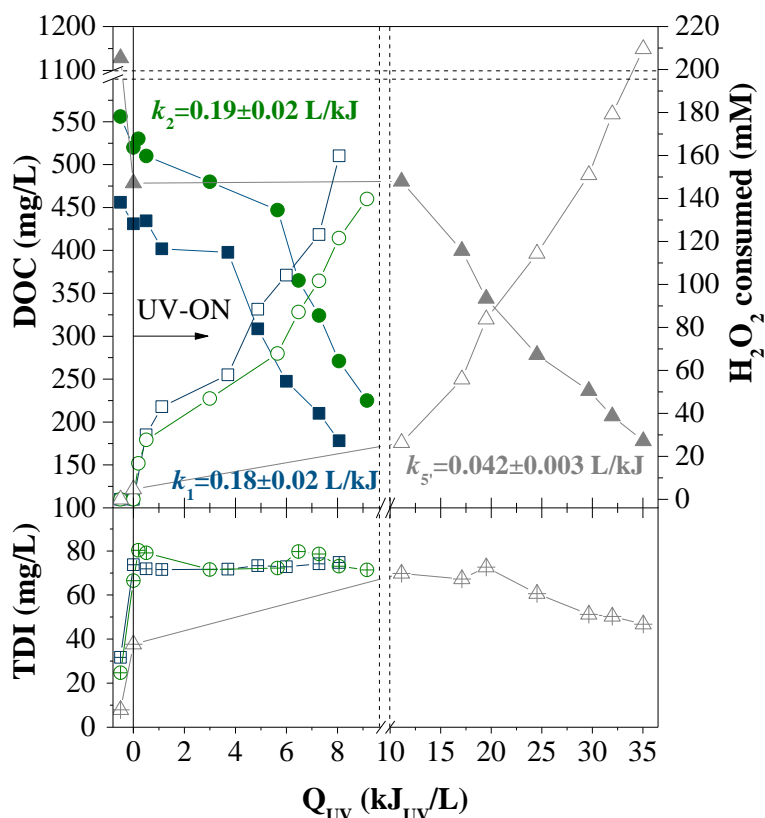


Figure 9.10. Evaluation of DOC (closed symbols), H_2O_2 consumed (open symbols) and TDI concentration (cross symbols), during photo-Fenton reaction ($\text{pH} = 2.8$, $[\text{Fe}] = 60 \text{ mg/L}$), for the experiments performed with solar radiation, with (1 – ■, □, ▤; 2 – ●, ○, ⊕) and without (5' – ▲, △, ⊖) pre-treatment (aerobic biological oxidation and coagulation).

Another difference observed between the current tests and the other ones previously carried out, was the initial phase of the photo-Fenton reaction, when the first H_2O_2 dose (usually 500 mg/L) was added. For experiments 1 to 15 it was observed a high consumption of H_2O_2 and an abrupt decrease of pH to values lower than 2.8, in the initial phase of the photo-Fenton reaction, requiring the addition of NaOH to correct the pH to 2.8. The high H_2O_2 consumption is related to the oxidation of nitrites to nitrates, as can be observed in Figure 9.11.

The conversion of nitrite to nitrate took place by intermediate formation of peroxyntrous acid (ONOOH), through the reaction of nitrous acid (HNO_2) with H_2O_2 [32, 33]:



The peroxyntrous acid in aqueous solution is a particularly unstable yellow species, with $pK_a = 6.8$. However, at alkaline pH its conjugated base, the very stable peroxyntrite anion is the predominant species. In acidic medium, the peroxyntrous acid quickly decomposes itself into nitrate ion (see Eq. (9.6)), releasing hydrogen ions, which promotes the acidification of the leachate [32-34].



The formation of peroxyntrous acid depends on the HNO_2 concentration in solution, which is favoured by acidic conditions. In aqueous solution, the nitrite ion is the conjugated base of the weak acid HNO_2 , whose dissociation is represented by the following equilibrium equation [35, 36]:

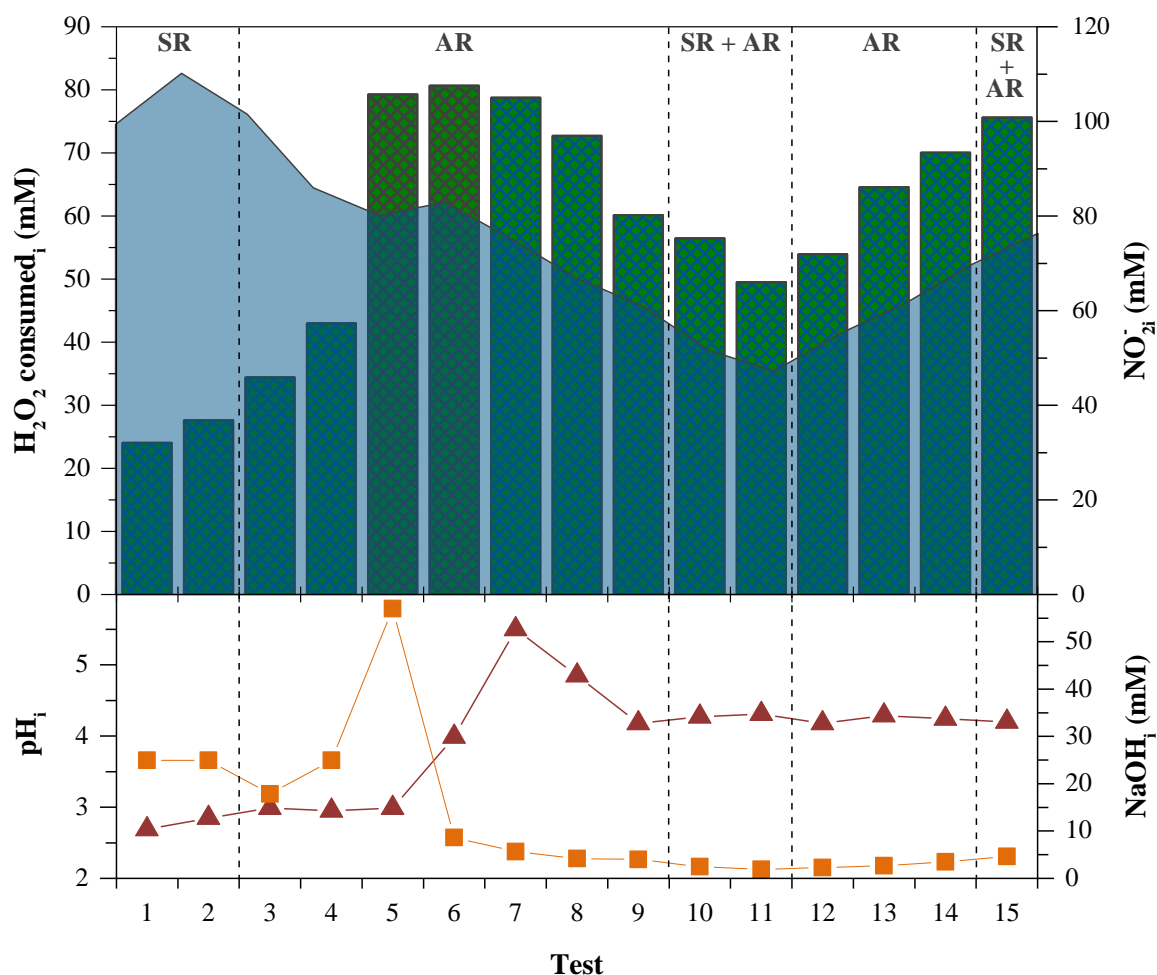
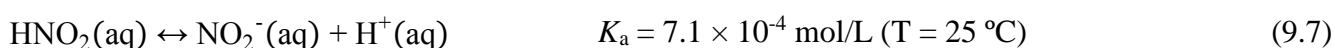


Figure 9.11. Progression of H_2O_2 (■) and NaOH (—□—) consumption, and initial values of NO_2^- -N (■) and pH_i (—▲—), at the beginning of photo-Fenton reactions, using solar (S) and/or artificial (A) radiation (R), along the experiments.

Taking into account the pK_a value (3.15 at 25 °C) of HNO_2 , and the respective distribution diagram (Figure 9.12), it can be disclosed that only for pH below 5, the HNO_2 starts to appear, and barely for pH values below 3.15, $[\text{HNO}_2] > [\text{NO}_2^-]$. This explains the fact that the reaction between H_2O_2 and HNO_2 , and further decomposition of peroxyxynitrite acid, is faster at acidic pH values, which was experimentally observable by the quicker pH decay.

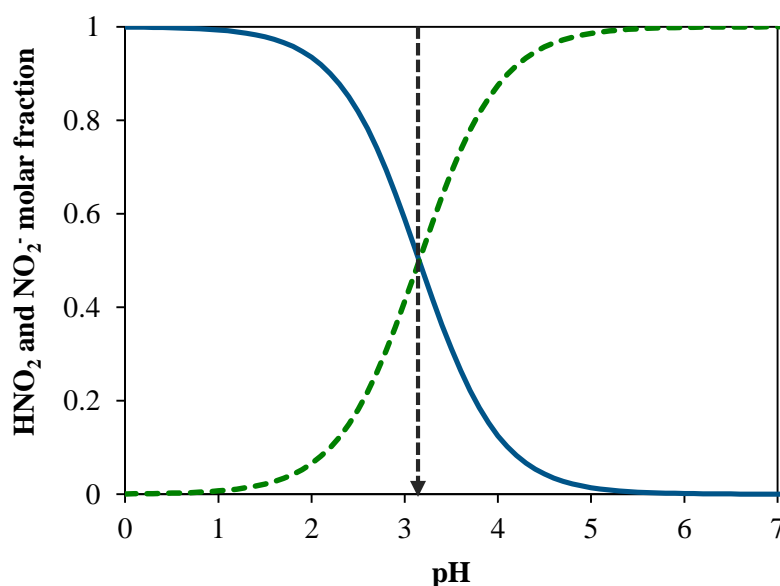


Figure 9.12. Distribution diagram of the molar fractions of nitrous acid (—) and nitrite ion (---), as a function of pH ($T = 25\text{ °C}$).

From Figure 9.11 it can be concluded that the initial H_2O_2 consumption is not directly proportional to the initial nitrite ion concentration, in the following conditions:

- (i) For leachate samples with the same initial pH value, but using a different radiation source, like in experiments 2 and 4 (solar and artificial radiation, respectively, at pH 3). For test 2, the NO_2^- content is higher but a lower H_2O_2 consumption is observed when compared to test 4. In this case, part of the H_2O_2 was photolysed by the UV-C radiation emitted by UV-Vis lamps (which corresponds to about 24% of the UV fraction of the lamp spectrum), increasing the total amount of H_2O_2 consumed in the initial phase of the photo-Fenton reaction.
- (ii) For the same radiation source, but using a leachate with a different initial pH value, such as in experiments 4 and 9 (pH equal to 3.0 and 4.2, respectively; artificial radiation). During the initial phase of test 9, it was consumed more 40% of H_2O_2 than in test 4, even being the NO_2^- concentration 29% lower. This dissimilarity can be attributed to the fact that for higher pH values, the molar fraction of HNO_2 is lower than NO_2^- , and consequently the amount of acid available to react with H_2O_2 is lower, leaving more H_2O_2 free to be photolysed.

It should be also noted that, when the pre-treatment (biological oxidation plus coagulation) was not performed (tests 5 and 6), the concentration of H_2O_2 consumed was not affected by the initial pH value. Moreover, as expected, the NaOH consumed to correct the solution pH considerably decreased for the experiments performed at a higher initial pH. So, if the photo-Fenton reaction was started at pH 4.2 under artificial radiation, on average it will be consumed about 1 mol of H_2O_2 and 0.05 mol of NaOH per 1 mol of NO_2^- fed to the photoreactor.

Figure 9.13 compares three photo-Fenton experiments after the initial biological oxidation: two of them carried out after coagulation at pH 3.0, one using solar radiation (exp. 2) and the other using 4 UV-Vis lamps, each one of 1000 W (exp. 4); and the last one was carried out without a previous coagulation step, but with acidification up to pH 3.0 (exp. 5).

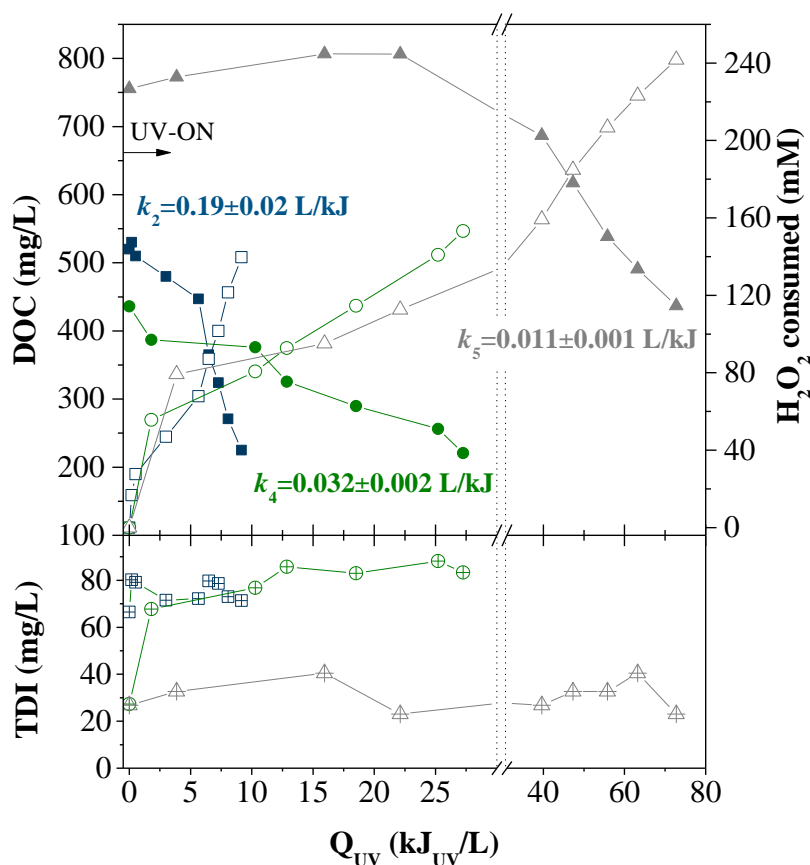


Figure 9.13. Evaluation of DOC (closed symbols), H_2O_2 consumed (open symbols) and TDI concentration (cross symbols), during the photo-Fenton treatment (pH = 2.8, $[\text{Fe}] = 60 \text{ mg/L}$) of the bio-coagulated treated leachate using solar radiation (2 – ■, □, ⊞), 4 UV-Vis lamps (4 – ●, ○, ⊕) and 4 UV-Vis lamps (without coagulation; pH = 3.0) (5 – ▲, △, ⊲).

The bio-treated leachate (without coagulation) exhibited an initial organic load 50% higher than the bio-coagulated leachate, being necessary much more energy to reach the intended DOC value. On the other hand, it is important to bear in mind that the coagulation process only promotes the pollutants transfer from the liquid phase to the solid phase, leading to the formation of chemical sludge, which needs to be treated in order to (i) be deposited in the landfill or (ii), as it contains a high amount of humic acids, be reutilized as fertilizer for agriculture.

From Figure 9.13, it was also possible to infer that in the test performed with solar radiation, even starting with a superior DOC (556 vs. 436 mg/L), the photo-Fenton reaction was more efficient, being the specific H_2O_2 consumption and the amount of accumulated UV energy 1.8 and 2.6 times lower, respectively, to reach a mineralization level 10% greater. Beyond that, the photo-Fenton reaction using solar radiation (exp. 2) was performed at a higher average operating temperature (39 °C compared to 32 °C) and using a higher sedimentation period (14 instead of 3 hours), leading to a more clarified leachate (TSS from exp. 2 was 56% lower than from exp. 4). This means that polychromatic sunlight is more efficient than other light sources with shorter wavelength, since higher wavelengths are able to better overcome the inner filter effects, and can promote the photolysis of ferric ion complexes [2].

Until the assay 5, the coagulation/acidification stage was performed at pH near 3, requiring high amounts of NaOH to neutralize the high concentration of hydrogen ion generated from the decomposition of peroxyxynitrite acid. In order to try to take advantage of this phenomenon, and additionally minimize the NaOH consumption, it was decided to carry out an experiment (exp.6), with acidification up to pH 4.0, and so it would be possible to verify if the H^+ released from the decomposition of peroxyxynitrite acid was enough to achieve the pH of 2.8. From test 6, it was found that, initiating the photo-Fenton reaction at pH 4.0, the leachate pH value decreased to values below 2.8, and it was still necessary to add NaOH to adjust this parameter. Test 6 also showed the ineffectiveness of the photo-treatment applied to the bio-treated leachate without the coagulation step: approximately 200 mM of H_2O_2 and 54 kJ/L of accumulated UV energy were required merely to reach a DOC of 520 mg/L.

Another photo-Fenton reaction (exp. 7) was performed using a bio-coagulated leachate with a pH of 5.5. In this condition, the leachate pH during the initial part of the photo-Fenton reaction remained 5.5 and the oxidation efficiency was negligible due to iron precipitation. The amount of HNO_2 at pH 5.5 (Figure 9.12) is low and consequently the decomposition of H_2O_2 in the presence of nitrites and formation of H^+ is not enough to drop the leachate pH. The same results were obtained for the bio-coagulated leachate at pH 4.5 (exp. 8). So, further experiments were performed using a bio-coagulated leachate with a pH of 4.2, since the addition of ferrous sulphate, in the photo-treatment step, results in a pH abatement of approximately 0.2. Taking into account the results obtained before, along with the values of TSS at the beginning of the photo-oxidation, it was decided that the settling phase would pass to take 14 hours.

Three more photo-Fenton reactions were performed using a bio-coagulated leachate with a pH of 4.2 and a sedimentation time in the coagulation step of 14 hours (Figure 9.14): (i) using 4 UV-Vis lamps (1000 W each) (exp. 9); (ii) combining solar radiation and artificial light (4 UV-Vis lamps) (exp. 10); and (iii) combining solar radiation and artificial light (4 UV-Vis lamps), but applying half of the coagulant dose (exp. 11).

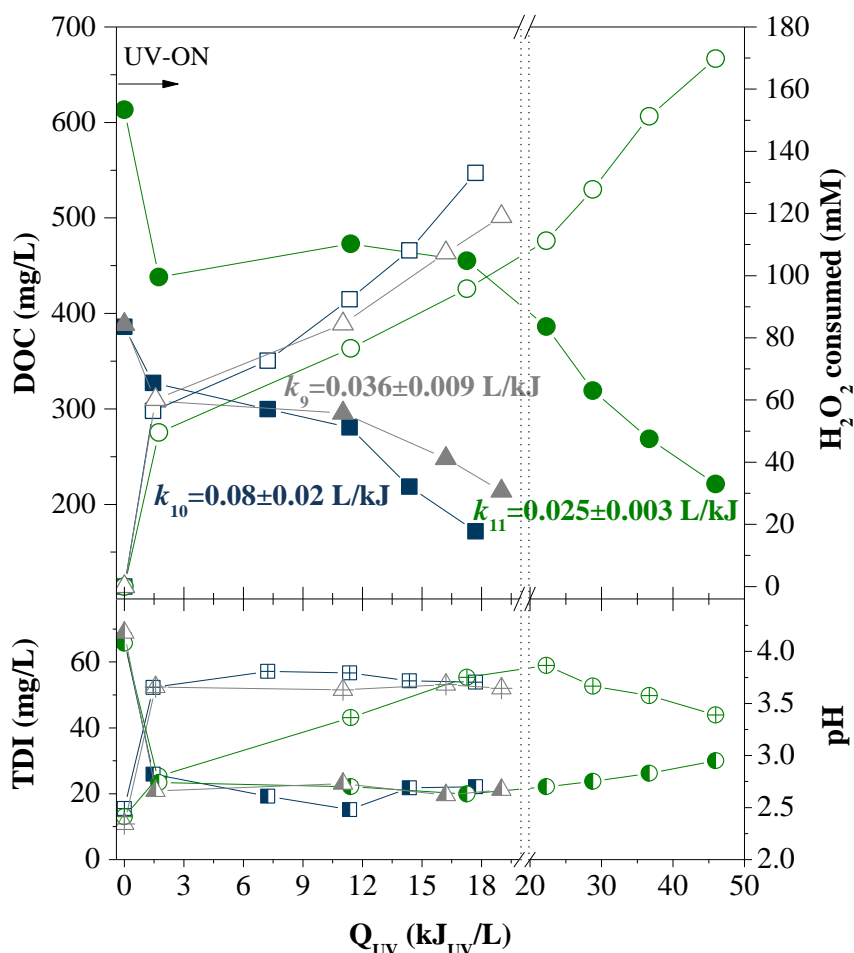


Figure 9.14. Evaluation of DOC (closed symbols), H_2O_2 consumed (open symbols), TDI concentration (cross symbols) and pH (semi-filled symbols) during the photo-Fenton treatment (pH = 2.8, $[\text{Fe}] = 60 \text{ mg/L}$) of the bio-coagulated treated leachate using 4 UV-Vis lamps (9 – $\blacktriangle, \triangle, \triangle, \blacktriangle$) and combining solar radiation with 4 UV-Vis lamps after coagulation with $240 \text{ mg Fe}^{3+}/\text{L}$ (10 – $\blacksquare, \square, \boxplus, \blacksquare$) and $120 \text{ mg Fe}^{3+}/\text{L}$ (11 – $\bullet, \circ, \oplus, \bullet$).

Figure 9.14 shows a steep initial DOC decay of 80, 60 and 190 mg/L for the tests 9, 10 and 11, respectively, due to organic matter precipitation with the Fe^{3+} (obtained through the reaction of H_2O_2 with Fe^{2+}). After that, the DOC profile presents an induction period until approximately 10 kJ/L, for the assays 9 and 10, and 15 kJ/L for assay 11, in which less oxidized compounds are converted into more oxidized ones but without significant mineralization. The second part of the DOC profile follows a pseudo-first kinetic behavior.

The initial DOC abatement was higher in experiment 11, since in this case it was used half of the coagulant dose in the coagulation step, remaining higher amounts of humic acids in solution, than eventually were precipitated with ferric ions at the beginning of the photo-oxidation. Therefore, the dissolved iron concentration that remained in the solution was 50% lower than in experiments 11 and 10.

The amount of accumulated UV energy and H₂O₂ consumption during the photo-oxidation was 3.1 and 1.5 times higher, to achieve a leachate with a DOC value of 250 mg/L, in the experiment 11 (half of the coagulant dose) when compared to experiment 10. The leachate after the coagulation/sedimentation step using 120 mg Fe³⁺/L presented: (i) higher organic load (about 64%), (ii) increased turbidity, (iii) higher coloration (see second tube of the Figure 9.4), and (iii) increased TSS content in the supernatant (416 vs. 116 mg/L), which greatly affects the light penetration into the reactional medium.

The DOC, H₂O₂ consumption, T, pH and dissolved iron concentration profiles are very similar for the experiments performed using only artificial light (exp. 9) or combining solar and artificial light (exp. 10). However, after 10 kJ/L, the reaction rate almost doubled for the experiment combining both radiation sources. The addition of 499 W of natural UV light (24 W/m² of natural solar radiation, CPC area of 20.8 m²) to 1200 W of UV artificial radiation (4 lamps with a rated power of 1000 W, emitting 30% of useful UV radiation), decreased the reaction time and the electric energy consumption was reduced to half.

Figure 9.15 compares the efficiency of the photo-Fenton reaction in the treatment of a bio-coagulated leachate using different number of UV lamps and power (exps. 9, 12 and 13). In all assays, the leachate was submitted to the same pre-treatment: aerobic biological oxidation, where close values of alkalinity were achieved (see Table 9.2); followed by coagulation/sedimentation with 240 mg Fe³⁺/L, at pH 4.2, yielding equivalent values of sulphate ion concentration (see Table 9.3); and a settling period of 14 hours, reaching TSS contents in the supernatant ≤ 220 mg/L (see Table 9.3). The experiment 9 was performed using 4 UV-Vis lamps regulated to a power of 1000 W, while the experiments 12 and 13 were carried out with 2 UV-Vis lamps of 1200 and 850 W, respectively.

Figure 9.15 shows that all trials yielded a similar profile of H₂O₂ consumption and total dissolved iron concentration. To reach a photo-treated leachate with a DOC value of 250 mg/L, in the experiments 9, 12 and 13, it was consumed, respectively: (i) 15.7, 13.2 and 15.9 kJ/L of accumulated UV energy; (ii) 105, 106 and 115 mM of H₂O₂; and (iii) 25.9, 27.3 and 24.5 mg of H₂O₂ per 1 mg of oxidized DOC.

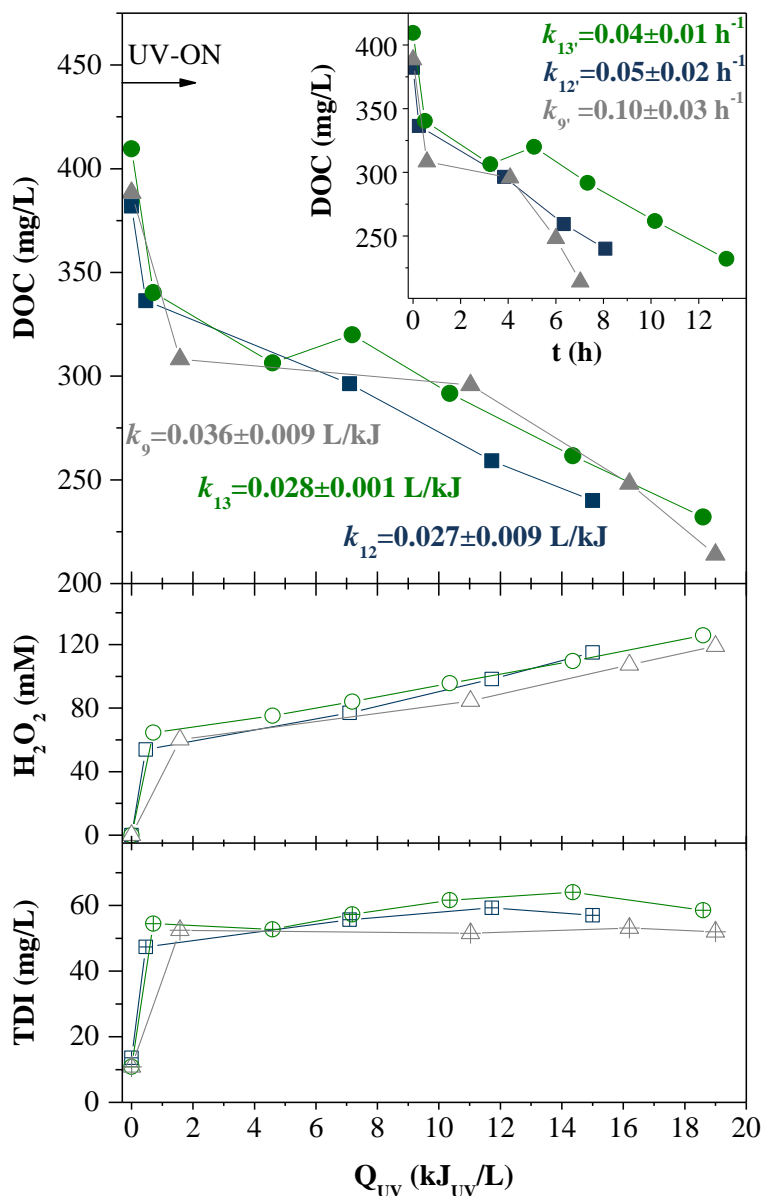
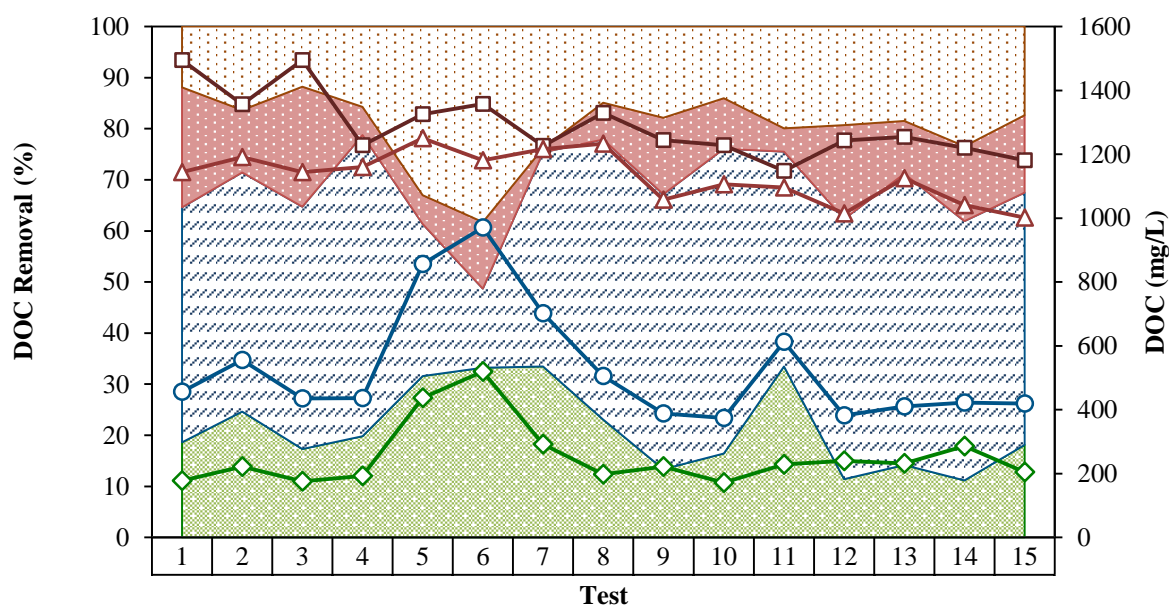


Figure 9.15. Evaluation of DOC (closed symbols), H_2O_2 consumed (open symbols) and TDI concentration (cross symbols), during the photo-Fenton treatment ($\text{pH} = 2.8$, $[\text{Fe}] = 60 \text{ mg/L}$) of the bio-coagulated treated leachate, using 4 lamps of 1000 W (9 – $\blacktriangle, \triangle, \triangle$), 2 lamps of 1200 W (12 – $\blacksquare, \square, \boxplus$) and 2 lamps of 850 W (13 – \bullet, \circ, \oplus).

Considering the configuration of the UV lamps inside the recirculation tank, the best option is to use 2 lamps of 1200 W each, as radiation source, since in this conditions the amount of required UV energy is slightly lesser. Moreover, working with this configuration, it was possible to save on electric energy, spending about 14.6, 12.3 and 14.8 kWh/m^3 , when $4 \times 1000 \text{ W}$, $2 \times 1200 \text{ W}$ and $2 \times 850 \text{ W}$ were applied to the leachate treatment. Besides that, using the rated power of 2400 W, the operating time only increased 1.4 h/m^3 comparing with the power of 4000 W.

Figure 9.16 illustrates the mineralization values obtained in all the multi-stage treatment steps: (i) aerobic biological oxidation (RB); physico-chemical process (CT); and (iii) photo-Fenton reaction (RT). The DOC values of the initial leachate and at the end of each step are also presented. The removal percentages obtained in each treatment stage were determined relatively to the initial DOC.



	Test														
%Rem.RB	23.5	12.2	23.5	5.5	5.7	13.0	0.8	7.2	15.0	9.9	4.5	18.3	10.3	14.7	15.2
%Rem.CT	46.0	46.8	47.4	59.0	29.7	15.5	41.9	54.8	53.9	59.6	42.1	50.9	57.0	50.7	49.4
%Rem.RT	18.6	24.6	17.3	19.8	31.6	33.2	33.4	23.1	13.3	16.4	33.4	11.4	14.2	11.1	18.1
DOCi	1495	1357	1495	1228	1325	1358	1226	1329	1244	1228	1148	1243	1254	1220	1181
DOC_BR	1144	1191	1144	1160	1250	1181	1216	1233	1058	1106	1096	1015	1125	1041	1002
DOC_CT	456	556	435	436	856	971	702	505	388	374	613	382	410	422	419
DOC_RT	178	222	176	193	437	520	292	198	222	172	229	240	232	286	205

Figure 9.16. Evolution of DOC removal in the biological, coagulation/sedimentation and photo-oxidation processes, as well as the initial and final DOC of each stage.

Comparing the organic matter removal efficiency in each treatment process, disregarding for this purpose the tests 5 and 6, since the coagulation step was not performed, it appears that the highest percentage was reached in the coagulation step, being the average value equivalent to 51%, followed by the photo-treatment stage, with an average mineralization of about 20%, consuming 143 mM of H_2O_2 and 21.5 kJ/L of accumulated UV energy to achieve a DOC of 219 mg/L, and finally the biological oxidation with 12%. As final remark one can say that this treatment strategy is able to remove more than 80% of the organic matter present in the sanitary landfill leachate, obtaining at the end a biodegradable effluent, able to be oxidised in a final biological process, in order to fulfil the discharge limits imposed by the Portuguese legislation.

9.3.4 Biodegradability assessment

Taking into account the tests presented until now, in order to obtain a leachate with a DOC value of approximately 250 mg/L, the best treatment strategy combines (Figure 9.17): (i) a biological aerobic oxidation process, in order to remove the biodegradable organic fraction and alkalinity, and promote the conversion of NH_4^+ into NO_2^- ; (ii) followed by a coagulation step, with 240 mg Fe^{3+} /L at pH 4.2 and sedimentation period of 14 hours; and (iii) a photo-Fenton reaction, using solar light together with artificial radiation, emitted by 2 UV-Vis lamps of 1200 W. In order to define the optimal photo-treatment time to reach a biodegradable effluent that can be further biologically oxidized, a Zahn-Wellens test was performed for different photo-oxidised samples of experiment 15, which was carried out using the treatment strategy reported above.

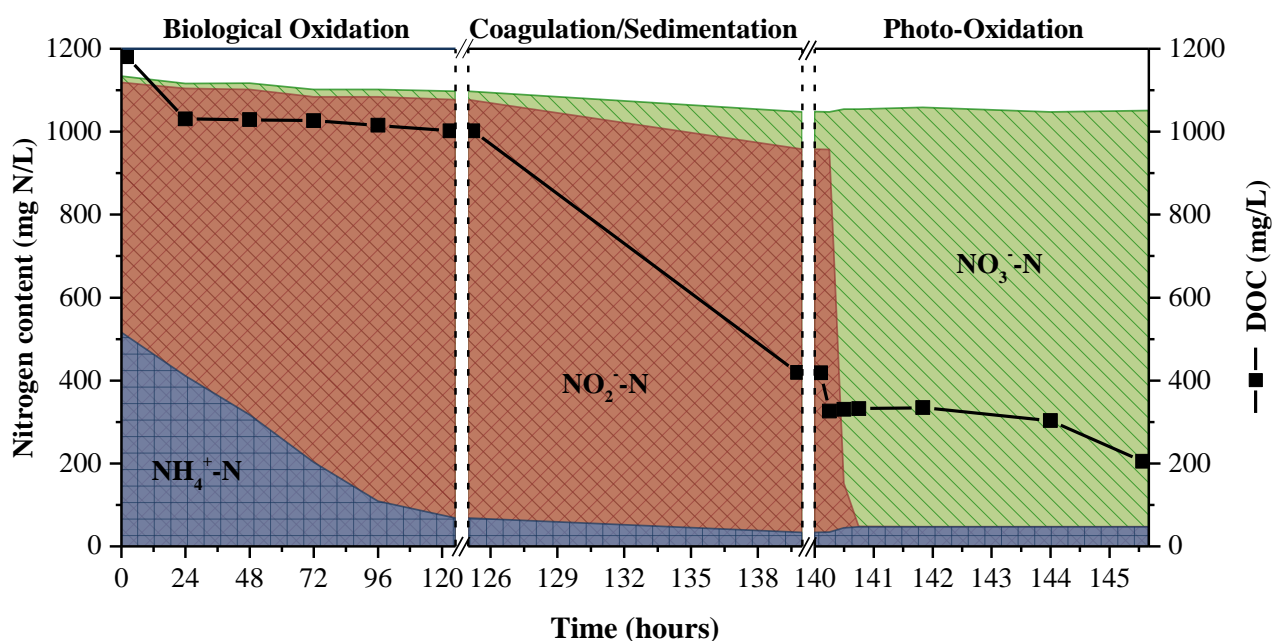


Figure 9.17. Evolution of DOC and nitrogen content (NH_4^+ -N - blue, NO_2^- -N - red and NO_3^- -N - green) along all stages of the multi-treatment process, as a function of time, for the experiment in the best conditions.

Throughout this trial, the biological oxidation was the step with higher treatment time (about 43 h/m³), while the photo-treatment was the one with lesser (c.a. 3.2 h/m³). In the biological process (VSS = 5.47 g/L, $T_m = 15.3$ °C), it was achieved a final pH value of 6.8, a DOC of 1002 mg/L and an alkalinity and ammonium nitrogen of 0.2 g CaCO_3 /L and 68 mg NH_4^+ -N/L, respectively, with a very low nitrification reaction rate of 0.78 mg NH_4^+ -N/(h.g VSS), consuming about 11 mg CaCO_3 /mg NH_4^+ -N. Along this stage, the SVI value was 128 mL/g, suggesting a poor sludge settling, since according to Metcalf and Eddy [18], for a good biomass sedimentation, SVI values below 100 mL/g are desired. The weak settleability could have been caused by the high sludge age, which tends to be raised in sequencing batch

systems, as well as by the very low food to microorganism ratio (F/M) [19], which was only 0.01 g BOD₅ per 1 g of VSS per day. In the coagulation/sedimentation step, 58% of the organic matter fed to the coagulation tank was removed. The final clarified leachate presented a DOC of 419 mg/L, a sulphate ion concentration equal to 900 mg/L, a TSS content of 40 mg/L and pH value equal to 4.2. The photo-oxidation stage was carried out with an average temperature, pH and iron concentration of 22.6 °C, 2.8 and 49.5 mg/L, respectively (see Table 9.4 and Figure 9.18).

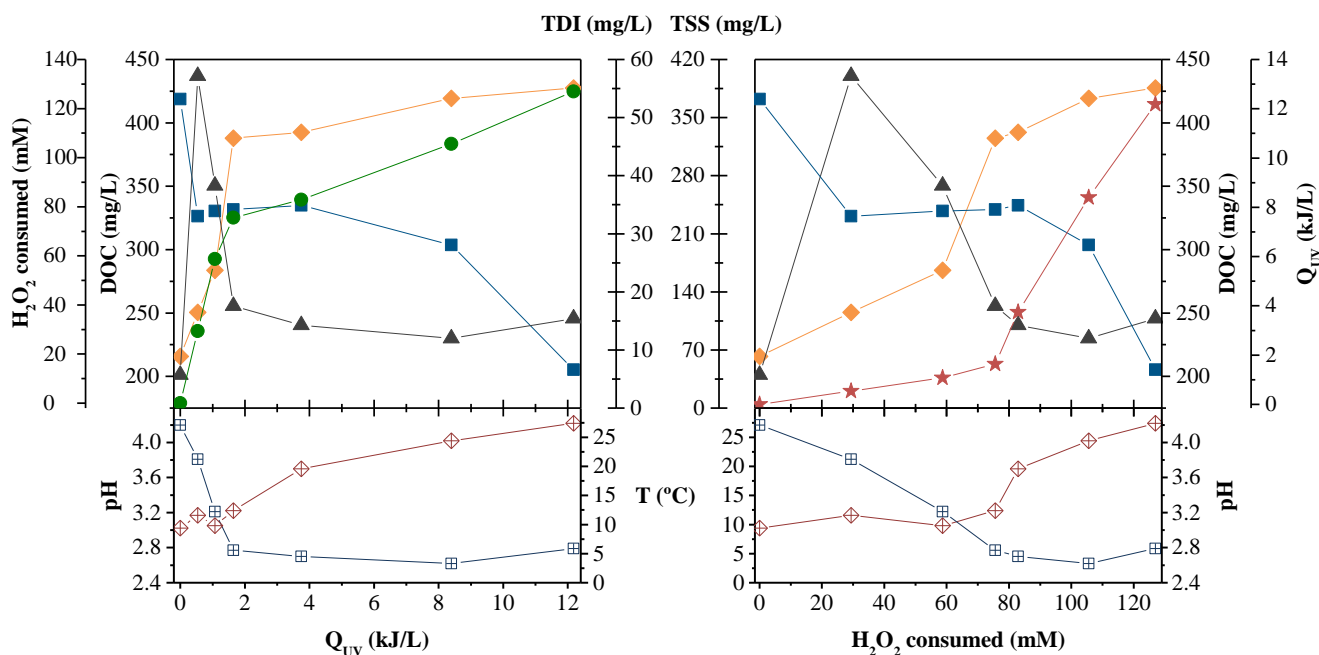


Figure 9.18. Evaluation of DOC (■), H₂O₂ consumed (●), TDI concentration (◆), TSS content (▲), Q_{UV} (★), pH (⊞) and temperature (⊕), as a function of accumulated UV energy and H₂O₂ consumed during the photo-oxidation of the bio-coag-treated leachate.

During the initial period of the photo-Fenton reaction it was observed: (i) a decrease in the DOC value of 93 mg/L and consequent increase of the total suspended solids of 360 mg/L ($0 < Q_{UV} < 0.48$ kJ/L), as a result of ferrous sulphate and H₂O₂ addition, leading to the precipitation of ferric ions with the organic matter which was not removed during the coagulation step; (ii) afterwards an increase of the total dissolved iron concentration and decrease of the TSS content, most likely due to dissolution of the iron precipitate as a result of the release of hydrogen ions from the reaction of H₂O₂ with nitrous acid, but also due to the attack of the hydroxyl radicals generated through the decomposition of the H₂O₂ by the UV-C radiation, until 1.46 kJ/L of accumulated UV energy; (iii) depletion of 60% of the total amount of H₂O₂ required for the reaction up to 1.46 kJ/L, associated with the total conversion of nitrites into nitrates, followed by a slow H₂O₂ consumption rate and stabilization of solution pH (see Figure 9.17); (iv) DOC slight increase until 3.3 kJ/L of accumulated UV energy, suggesting that the initially

precipitated organic material was redissolved and during that period the complex organic molecules were only broken down into simpler ones, still not occurring their complete mineralization into H₂O and CO₂.

Given the results obtained along this trial period, and not being possible to perform a final biological treatment, it became necessary to determine the optimum photo-treatment time, where a biodegradable and non-toxic effluent would be obtained, and a downstream biological oxidation would allow to reach a COD value lesser than 150 mg O₂/L. To do this, a Zahn-Wellens test was applied to the samples collected along the experiment 15. Besides the Zahn-Wellens test, it was also evaluated the absorbance at 254 nm (Abs₂₅₄), the average oxidation state (AOS) and the carbon oxidation state (COS). The two last parameters are calculated from DOC and COD, according to equations (9.8) and (9.9), and indicate the oxidation degree and the efficiency of the oxidative process. While AOS only considers the organic matter in solution, the COS also considers the CO₂ generated by mineralization.

$$\text{AOS} = 4 - 1.5 \frac{\text{COD}}{\text{DOC}} \quad (9.8)$$

$$\text{COS} = 4 - 1.5 \frac{\text{COD}}{\text{DOC}_0} \quad (9.9)$$

where *DOC* is the dissolved organic carbon at the sampling time *t* (mg C/L), *DOC*₀ is the dissolved organic carbon (mg C/L) at the beginning of the photo-Fenton reaction (*Q*_{UV} = 0 kJ/L) and the *COD* is the chemical oxygen demand at the sampling time *t* (mg O₂/L).

Figure 9.19 shows that as the H₂O₂ consumption increases, the values of DOC, COD and Abs₂₅₄ decrease, following a similar tendency, indicating that during the treatment the most complex compounds were degraded into simpler ones until CO₂, H₂O and mineral acids. The AOS values increased initially until 60 mM of H₂O₂ consumed, indicating the formation of more oxidised intermediary compounds. Regarding the COS behaviour, it can be seen an increase from +0.65, indicating the presence of rather oxidised compounds, to +3.4, which means strong mineralization and generation of highly oxidised intermediates.

Figure 9.20 shows the low-molecular-weight carboxylate anions (LMCA) detected along the oxidation reaction period, as well as the fraction of dissolved organic carbon related to the identified carboxylic acids.

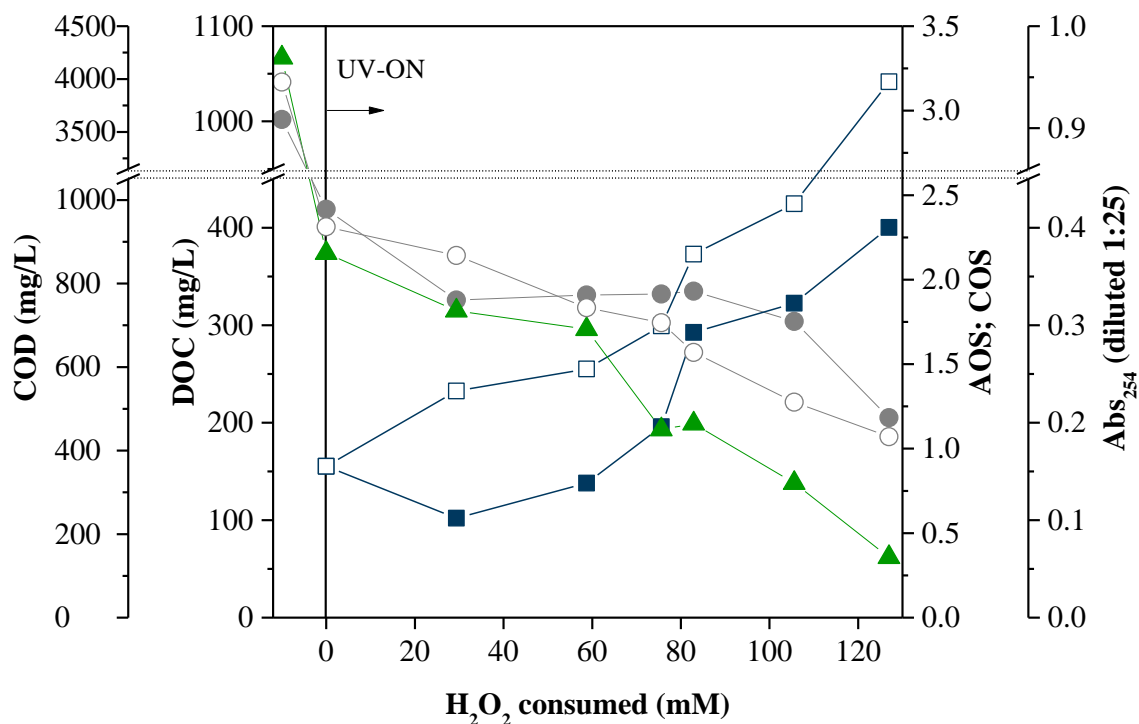


Figure 9.19. Progress of the DOC (●), COD (○), AOS (■), COS (□) and Abs₂₅₄ (▲), as a function of the H₂O₂ consumed, along experiment 15.

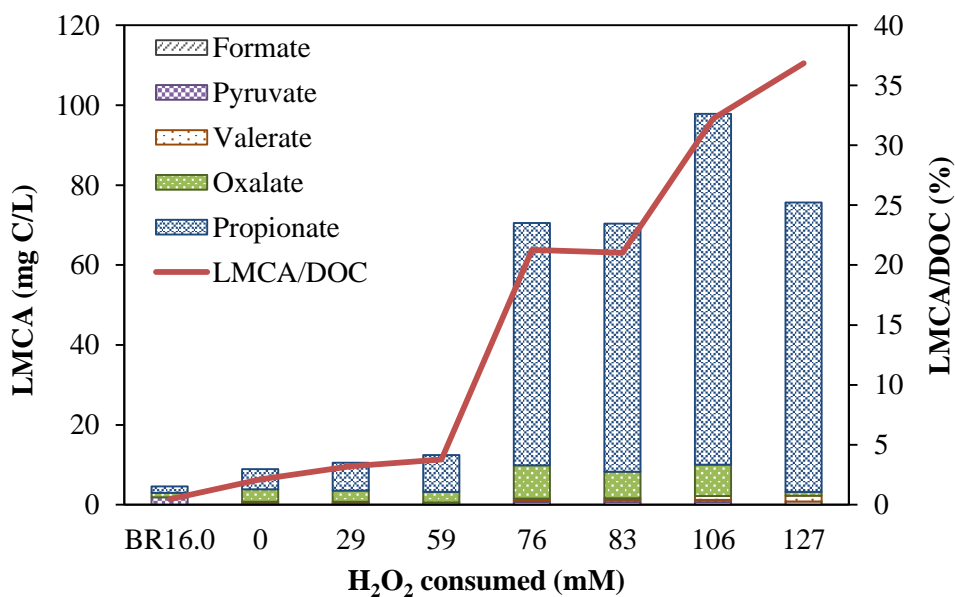


Figure 9.20. Evolution of low-molecular-weight carboxylate anions (LMCA) concentration and LMCA/DOC ratio, along experiment 15.

Initially few LMCA were detected, and throughout the oxidation process higher amounts of LMCA were generated, particularly after 59 mM of H_2O_2 consumed, the point where the H_2O_2 started to be consumed for the reaction itself and not for the indirect conversion of the nitrite into nitrate. The LMCA concentration increased until 106 mM of H_2O_2 consumed, which is in accordance with the pH profile (see Figure 9.18), where a slight decrease of the pH value can be observed. After 106 mM of H_2O_2 consumed, the amount of LMCA started to decrease, as a consequence of LMCA oxidation into CO_2 , H_2O and mineral acids. The tendency of the LMCA concentration together with the increment of LMCA/DOC ratio along the oxidation period, suggests the breakdown of recalcitrant macromolecules into short-chain carboxylic acids, and the consequent enhancement of the leachate biodegradability.

Regarding the proper assessment of the leachate biodegradability, the Zahn-Wellens test was performed for each oxidized sample taken throughout the experiment 15. Figure 9.21 shows that the bio (BR15.0) or bio-coag-treated (CT15F) leachate presents low biodegradability ($\approx 15\%$). During the photo-oxidation process a high enhancement of the leachate biodegradability was observed, achieving values higher than 70%. For the sample corresponding to 106 mM of H_2O_2 consumed, it was obtained a biodegradability percentage of 59% and a final COD value lower than 150 mg O_2/L (see Figure 9.22), at the end of the Zahn-Wellens test (28 days), which is the discharge limit value imposed by the Portuguese legislation (Decree-Law no. 236/98).

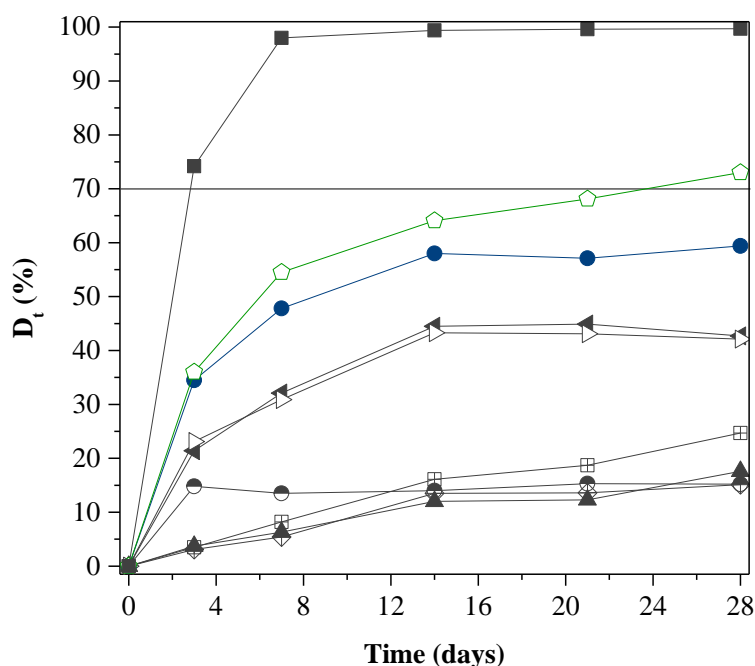


Figure 9.21. Zahn-Wellens test results for samples collected along experiment 15: Reference (■); BR15.0 (●); CT15F (⊕); 29 (▲), 59 (⊞), 76 (◀), 83 (▷), 106 (●) and 127 (◊) mM of H_2O_2 consumed.

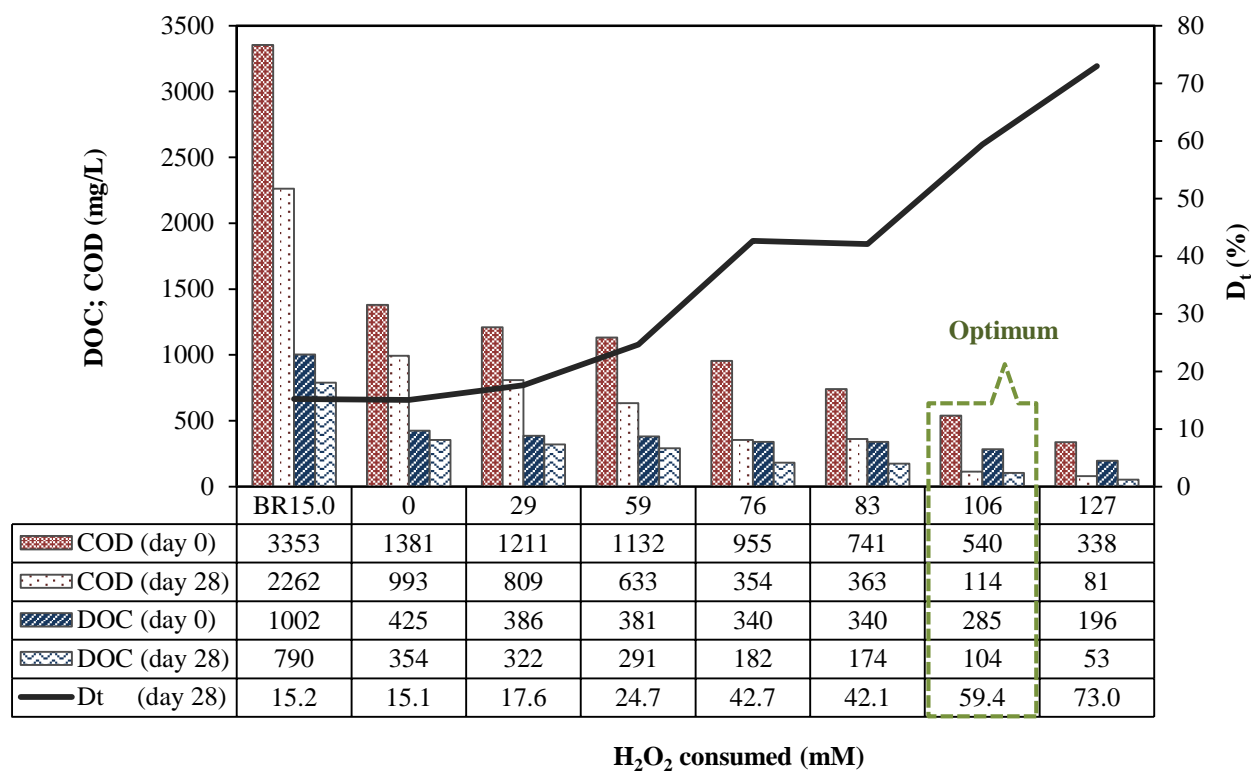


Figure 9.22. Evaluation of DOC and COD at day 0 and 28 of the Zahn-Wellens test and percentage of biodegradability at day 28.

According to results presented previously, the chemical oxidation process of a leachate with a DOC of 419 mg/L, after biological and coagulation/sedimentation pre-treatments, can be stopped after the consumption of 106 mM of H_2O_2 and 7.4 kJ/L of accumulated UV energy, achieving an effluent with DOC = 304 mg/L (27.5% of mineralization), and COD = 114 mg O_2 /L after a downstream biological treatment.

In the hypothesis of the discharge of the treated leachate into sewerage systems, the final COD would have to be lesser than 1000 mg O_2 /L, being the final biological treatment performed in the municipal wastewater treatment plant. In this case, considering the results aforesaid, for an effluent with a DOC approximately equal to 420 mg/L after a physical-chemical treatment process, it can be inferred that the optimum photo-treatment time is achieved for 76 mM of H_2O_2 consumed and 1.5 kJ/L of accumulated UV energy, obtaining a mineralization of 21% and a COD of 955 mg O_2 /L (see COD at day 0 in Figure 9.22).

9.3.5 Economic analysis

In this sub-section, the scale-up and cost estimation for the photo-Fenton process will be presented, based on the results obtained in the preceding sub-chapter, targeting a final wastewater with a COD of 150 or 1000 mg O₂/L, according to Portuguese discharge regulations into water bodies and sewerage systems, respectively. The overall costs were computed: (i) considering the solar/UV facilities, project's contingencies, system engineering and assembly, spare parts, personnel, maintenance material, electric and chemicals supplies; and (ii) not bearing in mind the costs related to biological or physical-chemical treatments, excepting the chemicals. This study was especially based on the book of Gálvez and Rodríguez [37], as previously presented in the Chapter 6 (following the same formulas and steps).

First of all, it was necessary to set some project variables which underpinned the design of a facility capable of treating 100 m³ of leachate per day, since it was the average daily flow of effluent generated in the sanitary landfill. Table 9.5 shows the main process operation variables required for the scale-up and economical assessment of a photo-oxidation plant prepared to treat an effluent from a biological and a coagulation/sedimentation process, with a DOC of about 420 mg/L (experiment 15), followed by: (i) a biological treatment able to oxidize the effluent up to the established limits for discharge into water bodies (COD < 150 mg O₂/L); or (ii) direct discharge into a municipal sewerage system (COD < 1000 mg O₂/L).

Taking into account the two COD targets and the leachate characteristics, the total collectors area required for the treatment of 100 m³/day is 1500 and 295 m², respectively. Comparing the CPCs areas obtained in this Chapter with those ones reported in Chapter 6, even for the optimal conditions, it can be inferred that the implementation of the biological and coagulation/sedimentation pre-treatments, substantially decreased (67% and 89%, for a target COD of 150 and 1000 mg O₂/L, respectively) the land area required, turning more feasible the use of the natural sunlight.

The capacity that the CPCs system has to treat a certain charge of organic matter ($\Delta m = (DOC_i - DOC_f) \times V_y$) or a determined volume of contaminated water (V_y) per unit of time and surface of solar collectors (A_{CPC}) can be estimated through the mass and volumetric treatment factors (T_{fm} and T_{fv}), respectively. Considering the conditions of experiment 15, it was obtained a T_{fm} and a T_{fv} of 0.63 g C/h/m² and 5.5 L/h/m², respectively, to reach a final COD below 150 mg O₂/L, after a subsequent biological oxidation, and 2.4 g C/h/m² and 28 L/h/m², respectively, to achieve a final COD of 1000 mg O₂/L.

Table 9.5. Operation data for the treatment of 100 m³ per day of sanitary landfill leachate.

Parameter	Target COD (mg O ₂ /L)	
	150	1000
Initial-final DOC ^a (mg C/L)	419 - 304	419 - 332
H ₂ O ₂ consumed ^a (mM)	106	76
Average operating temperature – T _m ^a (°C)	20.6	11.3
Accumulated UV energy – Q _{UV} ^a (kJ _{UV} /L)	7.4	1.5
Daily flow – Q _d (m ³ /day)	100	100
Yearly volume - V _y ^b (m ³)	36500	36500
Yearly average global UV irradiation - I _m ^c (W/m ²)	17	17
Total yearly hours of insolation – t _{ins} ^c (h)	2944	2944
Yearly accumulated UV energy – E _y ^d (kJ _{UV} /m ²)	180809	180809
Area of required CPCs – A _{CPC} ^e (m ²)	1500	295
Mass treatment factor – T _{fm} ^f (g C/h/m ²)	0.63	2.4
Volumetric treatment factor – T _{fv} ^g (L/h/m ²)	5.5	28
Land area required for CPCs implementation – A _{Land} (m ²)	5876	1214
Number of solar photons per unit of time and potency [37] - N _{PS} (photons/W/h)	5.8x10 ²¹	5.8x10 ²¹
Number of UV photons required – N _{UV} ^h (photons)	4.4x10 ²⁹	8.6x10 ²⁸

^aData obtained from experiment 15; ^bV_y=365.Q_d; ^cRadiation annual data presented in the Chapter 6; ^dE_y=3.6×I_m×t_{ins};

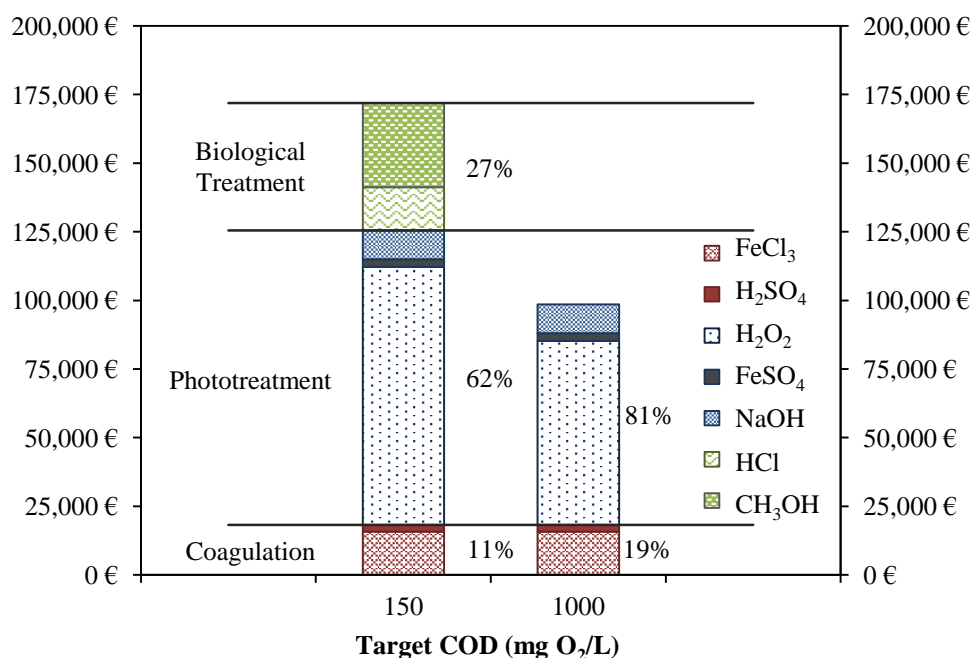
^eA_{CPC}=Q_{UV} × V_y × 1000/E_y; ^fT_{fm}=(DOC_i-DOC_f)×V_y/(t_{ins}×A_{CPC}); ^gT_{fv}=V_y/(t_{ins}×A_{CPC}); ^hN_{UV}=N_{PS}×I_m×t_{ins}×A.

Table 9.6 and Figure 9.23 present the annual costs associated with the chemicals needs, based on the reagents consumption obtained in experiment 15. For both scenarios, the cost associated with the first biological oxidation was not considered, once it was assumed that the leachate alkalinity was enough to achieve the complete conversion of ammonium into nitrites. The hydrochloric acid and methanol costs were determined taking into account the nitrogen content at the end of the photo-Fenton reaction (exp. 15), to be removed in the final biological oxidation step (1.2 mg HCl/mg N and 2.4 mg CH₃OH/mg N, respectively).

The cost with the reagents for the phototreatment stage are the most representative, corresponding to 62% or 81% of the total yearly costs, targeting a COD value lower than 150 or 1000 mg O₂/L, respectively. Beyond that, the contribution of H₂O₂ is about 55% or 68% of the total yearly costs, respectively. It should be underlined that the cost related to H₂O₂ can still be diminished in about 50%, if the complete nitrification (NH₄⁺ → NO₂⁻ → NO₃⁻) occurs in the first biological treatment.

Table 9.6. Cost associated to reagents consumption on each treatment step.

	Coagulation		Photo-Fenton			Biological oxidation		
	FeCl ₃	H ₂ SO ₄	FeSO ₄	H ₂ O ₂	NaOH	HCl	CH ₃ OH	
Reagent								
ρ (kg/L)	1.44	1.84	-	1.10	1.33	1.16	0.79	
Reagent cost (€/ton)	240	155	300	390	160	115	350	
COD < 150 mg O₂/L	Consumption (L/m³) (FeSO ₄ -kg/m ³)	1.25	0.24	0.25	6.00	1.35	3.23	3.04
	Unitary cost (€/m³)	0.43	0.07	0.08	2.57	0.29	0.43	0.84
	Annual cost (€)	15,768	2,498	2,738	93,951	10,486	15,727	30,068
	Step total cost (€)	18,266		107,174			46,408	
	Annual total cost (€)	171,848						
CQO < 1000 mg O₂/L	Consumption (L/m³) (FeSO ₄ -kg/m ³)	1.25	0.24	0.25	4.28	1.35	-	-
	Unitary cost (€/m³)	0.43	0.07	0.08	1.84	0.29	-	-
	Annual cost (€)	15,768	2,498	2,738	67,018	10,486	-	-
	Step total cost (€)	18,266		80,242			-	
	Annual total cost (€)	98,508						

**Figure 9.23.** Annual cost of the reagents employed in each treatment step.

Two of the primordial aims of the leachate treatment strategy presented in this chapter was (i) to remove the alkalinity from the landfill leachate and, (ii) to diminish the amount of suspended solids, as well as other light absorbing species, using the biological and coagulation/sedimentation pre-treatment steps. This way the amount of acid required to acidify the effluent until 2.8, as well the concentration of H_2O_2 required for the photo-Fenton reaction, would be lesser, and consequently the associated costs. Comparing these results with the ones obtained in the Chapter 6 for the optimal conditions, it can be said that the objectives of the present multistage treatment were fully achieved, decreasing 3.4 times the total annual expenses with H_2SO_4 , while the yearly cost associated to the H_2O_2 was reduced by about 1.9 and 1.2 times, for a target COD of 150 and 1000 mg O_2/L , respectively. Considering the costs associated with coagulation/sedimentation and photo-Fenton oxidation steps, since no reactants are required in the first biological process, 37% savings in the chemicals costs was still reached, compared with the photo-Fenton reaction (in optimal conditions) without pre-treatments, in order to attain a COD value of 150 mg O_2/L .

Table 9.7 presents the financial-economic assessment of the phototreatment of 100 m^3/day of the bio-coag-treated leachate, according to the operating conditions of test 15, aiming a final effluent with COD values lower than 150 and 1000 mg O_2/L , based on three different setups to take advantage of the UV radiation: (i) natural UV photons capture through CPCs technology; (ii) artificial UV photons emitted by UV lamps; and (iii) combination of natural and artificial radiation, employing CPCs and UV lamps, in accordance with the UV radiation energetic needs along the year.

Looking at all photocatalytic setups studied, it is notorious that the highest annual expense is related to the reactants consumption, representing in average 60% and 64% of the total yearly cost, aiming a COD lower than 150 and 1000 mg O_2/L , respectively, even neglecting the costs of the reactants used in the final biological oxidation. If the hydrochloric acid and methanol addition is taken into consideration, in the case where a COD lower than 150 mg O_2/L is the target requisite, the contribution of the chemicals increases to 68%, being the total unitary cost approximately equal to 7 €/m³. It should also be noted that the amount spent just with H_2O_2 consumption corresponds to about 44% of the total yearly cost. However, as previously mentioned, this expenditure can be reduced by about 50%, if in the first biological oxidation all ammonium nitrogen was converted into nitrate. Thus, the unitary cost to treat a leachate, in the same conditions than the ones used in experiment 15, would become about 4 €/m³.

Table 9.7. Yearly cost associated to the leachate phototreatment using CPCs technology and/or UV-Vis lamps (4 kW, 20,000 hours of useful lifetime), considering the operability conditions of the test 15, in order to obtain a COD below 150 and 1000 mg O₂/L.

Target COD (mg O ₂ /L)	CPCs		Lamps		CPCs and Lamps	
	150	1000	150	1000	150	1000
Direct Cost						
Principal Equipment:						
Collectors area	1500	295	0	0	957	188
A – Total collector cost	255,269 €	60,109 €	0 €	0 €	170,139 €	44,389 €
Number of lamps (NL)	0	0	38	8	30	6
B – Lamp, Ballast and accessories (500NL)	0 €	0 €	19,000 €	4,000 €	15,000 €	3,000 €
C – Lamp reactor cost (100NL)	0 €	0 €	3,800 €	800 €	3,000 €	600 €
Principal Equipment Total Cost (PETC = A + B + C)	255,269 €	60,109 €	22,800 €	4,800 €	188,139 €	47,989 €
D – Piping and tanks (8% of PETC) ^a	20,422 € ^a	20,422 € ^d	20,422 € ^e	20,422 € ^e	15,051 € ^a	15,051 € ^d
E – Auxiliary equipment and controls (10% of PETC) ^a	25,527 € ^b	25,527 € ^d	25,527 € ^e	25,527 € ^e	18,814 € ^b	18,814 € ^d
F – Others (15% of PETC) ^a	38,290 € ^c	38,290 € ^d	38,290 € ^e	38,290 € ^e	28,221 € ^c	28,221 € ^d
Total Direct Cost (TDC = PETC + D + E + F)	339,508 €	144,348 €	107,039 €	89,039 €	250,225 €	110,075 €
Indirect Cost						
G – Contingencies (12% of TDC)	40,741 €	17,322 €	12,845 €	10,685 €	30,027 €	13,209 €
H – Spare parts (1% of TDC)	3,395 €	1,443 €	1,070 €	890 €	2,502 €	1,101 €
Total Capital Required (TCR = TDC + G + H)	383,644 €	163,113 €	120,954 €	100,614 €	282,754 €	124,385 €
Yearly Cost						
I – Capital (12% ^f of TCR, 20 years)	46,037 €	19,574 €	14,514 €	12,074 €	33,930 €	14,926 €
J – Consumables	125,461 €	98,508 €	125,461 €	98,508 €	125,461 €	98,508 €
K – Operation and maintenance ^g	36,000 €	36,000 €	36,000 €	36,000 €	36,000 €	36,000 €
L – Electricity cost (0.10 €/kWh) ^h	0 €	0 €	33,288 €	7,008 €	11,952 €	2,479 €
M – Lamp replacement ($C_R = (500+7.2)^i \times NL \times t_{LO}^j / t_{LL}^k$) ^h	0 €	0 €	2,110 €	444 €	747 €	155 €
Total Yearly Cost (TYC = I + J + K + L + M + N)	207,498 €	154,082 €	211,374 €	154,034 €	208,101 €	152,071 €
Unitary Cost (UC = TYC/V_y)	5.68 €/m³	4.22 €/m³	5.79 €/m³	4.22 €/m³	5.70 €/m³	4.17 €/m³

^a8% of PETC; ^b10% of PETC; ^c15% of PETC; ^dThe cost associated to the rubrics D, E and F was considered equal to that determined for the target COD of 150 mg O₂/L.; ^eThe expense concerning D, E and F was regarded as identical to that computed when CPCs are exclusively used; ^fFixed charge rate (FCR), for 20-year plant depreciation; ^gThis rubric includes the expenses with personal and electric power, except the one consumed by the lamps; ^hThese amounts change monthly according with needs of UV-Vis lamps number expressed on Table 9.8, when the CPCs technology is combined with UV-Vis lamps; ⁱCost of 1-lamp plus labour cost with the replacement of 1-lamp; ^jLamp operation time; ^kLamp lifetime.

The cost of CPCs was calculated as a function of their area, according to the power regressions presented in the Figure 9.24. This values were provided three years ago by the Portuguese Company Ao Sol Energias Renováveis, Lda (CPCs patent holders), which no longer exists.

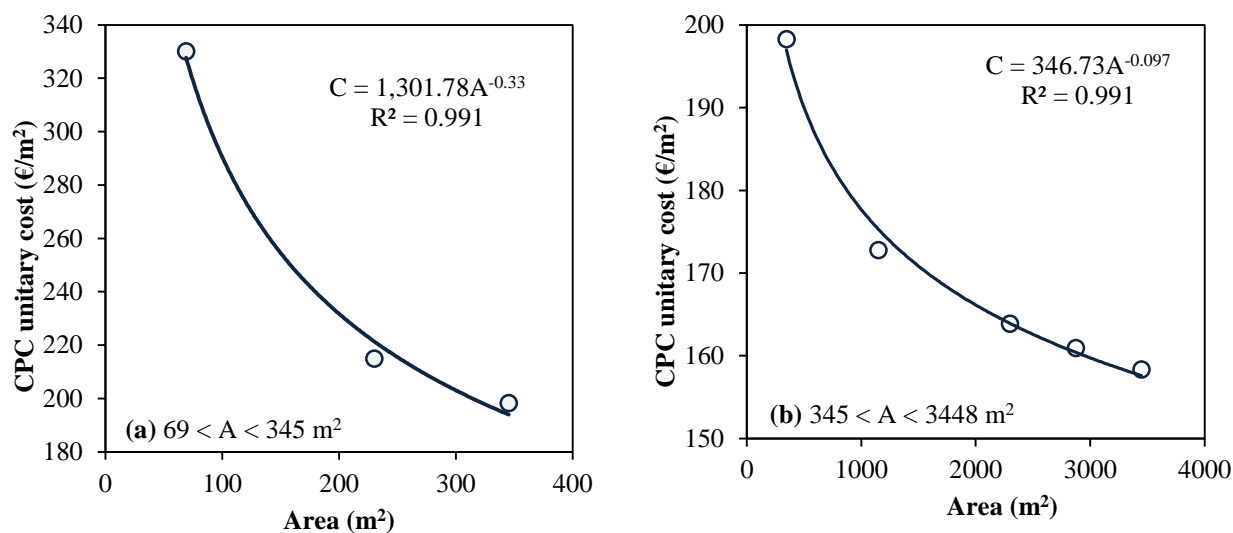


Figure 9.24. Estimative of the CPCs unitary cost as a function of their area, through a power regression used for the calculation of the total expense with CPCs, targeting a COD of 1000 (a) and 150 (b) mg O₂/L.

As regards the cost associated to secondary equipment (rubrics D, E and F of the Table 9.7), it was estimated that: (i) for COD < 1000 mg O₂/L, its value would be equal to the one obtained for the COD < 150 mg O₂/L, since the effluent volume to treat is the same in both cases. The main change is the required CPCs area, which in the first case is much lesser (about 80 %), because less accumulated UV energy is needed (1.5 face to 7.4 kJ/L) to reach the goal; and (ii) when UV lamps are only applied during the phototreatment, the value would be equal to the one found in the case where CPCs are uniquely used, since the comparison amongst the solar photons collection and the electric photons generation is only affected by the photocatalytic reaction system, being the remaining components very analogous as concerns cost and design [37]. For a solar energy system is necessary to include the expenses derived from the solar photons collection. On the other hand, for a system based on UV lamps, additionally to the electrical installation, it is necessary to include the expenses with electricity and replacement of the lamps (rubrics L, M and N).

The total cost with the leachate treatment through the use of artificial radiation can change according with the number of daily working hours of the lamps, because the number of required lamps is calculated as a function of the operating time (see Eqs. (6.5) and (6.6) from Chapter 6). The costs presented in Table 9.7 for the case where only UV lamps are applied were computed estimating that the UV lamps would work during 6-hours per day, since less hours increase the total unitary cost and more hours don't affect this cost, as can be seen in Figure 9.25. In the case wherever UV lamps were combined with CPCs technology, it was considered that the lamps would also work 6-hours per day.

Figure 9.25 shows that the total unitary treatment cost considerably decreases with the increase of lamps daily operation time, but then tends to approximately constant values, becoming independent of the total lamp operating time. According to this profile, if the number of irradiation hours is not a mandatory project requirement, it can be chosen in view of procedural matters, such as the total time allocated to the phototreatment or the surface area available for lamps implementation.

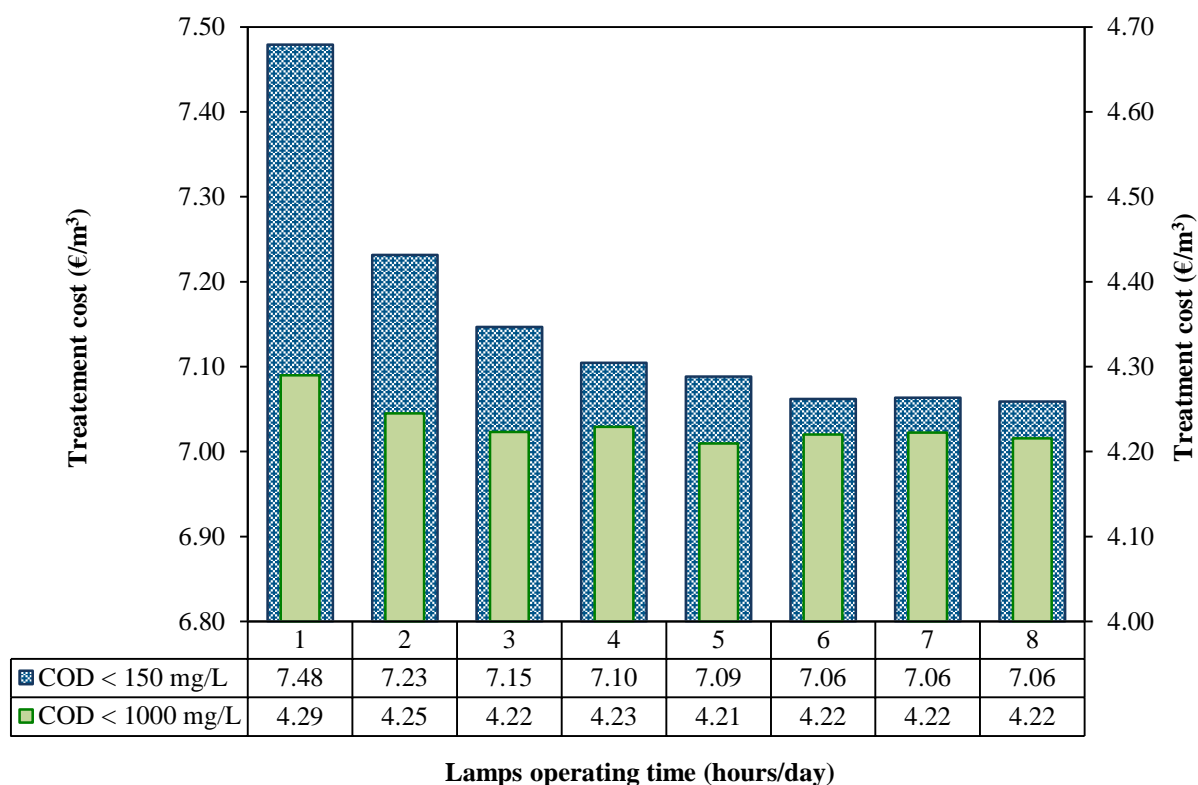


Figure 9.25. Representation of the total unitary cost of the treatment using artificial light, as a function of the lamps operating time in order to obtain a COD lesser than 150 and 1000 mg O₂/L.

The last scenario presented in Table 9.7 contemplates the combination of natural sunlight with artificial radiation. In order to assess this setup, an evaluation of the monthly accumulated solar UV energy was carried out, and the correspondent CPCs area was calculated, taking also into account the accumulated UV energy required to achieve the target COD of 150 and 1000 mg O₂/L. Table 9.8 presents for each month (i) the accumulated solar UV energy (E_m), (ii) the leachate volume to be treated (V_m), (iii) the required CPCs area (A_{CPC}), (iv) the energy captured by the CPCs (E_{CPC}), (v) the lamps electricity consumption (E_L), (vi) the number of the lamp's photons and (vii) the number of UV lamps (with 4kW, in continuous operation during 6-hours) that would be needed, considering that the smallest CPCs area (relative to the month with higher average irradiation) would be implemented.

Table 9.8. CPCs area and number of UV lamps required for all months of the year, targeting a final COD value of 150 or 1000 mg O₂/L.

Month	E _m (kJ/m ²)	V _m (m ³)	A _{CPC} (m ²)		E _{CPC} (kJ)		E _L (kJ)		Lamp photons		No. of Lamps	
			150*	1000*	150*	1000*	150*	1000*	150*	1000*	150*	1000*
Jan.	6597	3100	3492	686	6.3×10 ⁶	1.2×10 ⁶	1.7×10 ⁷	3.3×10 ⁶	2.7×10 ²⁸	5.3×10 ²⁷	28	6
Feb.	10194	2800	2041	401	9.8×10 ⁶	1.9×10 ⁶	1.1×10 ⁷	2.2×10 ⁶	1.8×10 ²⁸	3.5×10 ²⁷	20	4
Mar.	14226	3100	1619	318	1.4×10 ⁷	2.7×10 ⁶	9.4×10 ⁶	1.9×10 ⁶	1.5×10 ²⁸	3.0×10 ²⁷	16	3
Apr.	19774	3000	1127	222	1.9×10 ⁷	3.7×10 ⁶	3.4×10 ⁶	6.6×10 ⁵	5.4×10 ²⁷	1.1×10 ²⁷	6	1
May.	24078	3100	957	188	2.3×10⁷	4.5×10⁶	0	0	0	0	0	0
Jun.	17309	3000	1288	253	1.7×10 ⁷	3.3×10 ⁶	5.7×10 ⁶	1.1×10 ⁵	9.2×10 ²⁷	1.8×10 ²⁷	10	2
Jul.	20241	3100	1138	224	1.9×10 ⁷	3.8×10 ⁶	3.7×10 ⁶	7.2×10 ⁵	5.9×10 ²⁷	1.2×10 ²⁷	6	2
Aug.	20554	3100	1121	220	2.0×10 ⁷	3.9×10 ⁶	3.4×10 ⁶	6.6×10 ⁵	5.4×10 ²⁷	1.1×10 ²⁷	4	1
Set.	19971	3000	1116	219	1.9×10 ⁷	3.8×10 ⁶	3.2×10 ⁶	6.3×10 ⁵	5.1×10 ²⁷	1.0×10 ²⁷	4	1
Oct.	13995	3100	1646	323	1.3×10 ⁷	2.6×10 ⁶	9.6×10 ⁶	1.9×10 ⁶	1.6×10 ²⁸	3.1×10 ²⁷	16	3
Nov.	8648	3000	2578	506	8.3×10 ⁶	1.6×10 ⁶	1.4×10 ⁷	2.8×10 ⁶	2.3×10 ²⁸	4.4×10 ²⁷	24	5
Dec.	5456	3100	4221	829	5.2×10 ⁶	1.0×10 ⁶	1.8×10 ⁷	3.5×10 ⁶	2.9×10 ²⁸	5.6×10 ²⁷	30	6

*COD targets expressed in mg O₂/L.

According to the irradiation profile and reaction energetic needs, the minimum CPCs area was obtained in May, being equivalent to 957 and 188 m², aiming COD values lesser than 150 and 1000 mg O₂/L, respectively. Assuming that the CPCs with this surface area would be installed, UV lamps would not be necessary in May. However, in December about 30 or 6 lamps (maximum value) would be required, in order to compensate the lack of solar irradiation. This is a good option to reduce the electrical energy costs with the lamps and the investment costs with the CPCs. Regarding this scenario (see Table 9.7), the capital cost was computed considering the minimum CPCs area and the maximum number of UV lamps, in order to fulfil all the energetic needs along the year. The annual operating costs with electricity and lamps replacement were calculated by the sum of their parts in each month.

When the CPCs were the selected technology to benefit from UV radiation, the cost with initial investment in tangible fixed capital is the highest, being the total capital required comprised between 163 and 384 thousand euros, amortizable during 20-years at 12% FCR. On the other hand, the use of UV lamps to produce the UV photons resulted in higher operating costs, mostly due to the need of additional electrical power, being the respective annual expenses comprised between 7 and 33 thousand euros. Concerning a target COD of 1000 mg O₂/L, the total yearly cost was practically the same, using any of these two photocatalytic setups, and the total unitary cost was even equal, as can be seen in Table 9.7 and Figure 9.26. Aiming a target COD of 150 mg O₂/L, the total cost was slightly lesser (1.8%) when CPCs were envisioned.

Nevertheless, it is important to remind that the CPCs-based facility was projected considering a yearly average irradiation of 17 W/m^2 , which is not observed along all the year. For instance, in December, the specific accumulated solar UV energy is around 5500 kJ/m^2 (the lowest value found), so if it is decided to treat each month all the leachate produced (3100 m^3), up to a COD lesser than $150 \text{ mg O}_2/\text{L}$, it would be required 4221 m^2 of CPCs, which corresponds to a land area around 16700 m^2 , the equivalent to 4 soccer fields. Alternatively, if it is decided to use the 1500 m^2 of CPCs (c.a. 1.4 soccer fields) initially designed, only 66% of the leachate would be treated from October to March, being necessary an extra storage capacity of approximately 6300 m^3 . So, in order to minimize the utilization of artificial energy resources and taking the maximum advantage of a renewable and sustainable source, the best configuration is the combination of natural sunlight with UV-Vis lamps, thus ensuring the proper performance of the phototreatment step along all the year.

The economic and financial study of the last scenario, where solar and artificial radiation were combined, indeed showed that the investment and operating costs declined, namely: i) the total capital required decreased by about 24-26%, compared with the situation where CPCs were exclusively considered; and ii) the total cost associated to the UV-Vis lamps diminished 64-65%, assuming that only artificial radiation would be applied. This assumption resulted in a total unitary cost of 5.70 €/m^3 (almost the same as the CPCs, which was the lowest), targeting a COD lesser than $150 \text{ mg O}_2/\text{L}$, and 4.17 €/m^3 when the target COD was $1000 \text{ mg O}_2/\text{L}$, which was the lowest cost from all.

Finally, it is performed a comparison (see Figure 9.26) between the costs obtained from the experiments reported in this Chapter with the optimum results achieved in Chapter 6, aiming the same goals and considering the simulated scenarios under identical conditions. In both cases the best option seems to be the combination of CPCs and UV-Vis lamps, leading to a lower unitary cost, considering the most beneficial situation regarding the annual radiation trend in Portugal.

The pre-treatment of the leachate reduces on average the costs associated with the phototreatment step by 49% and 39%, targeting a COD of 150 and $1000 \text{ mg O}_2/\text{L}$, respectively. Thereby, the leachate pre-treatment steps are of extremely importance, improving the efficiency of the photo-Fenton reaction and decreasing the global treatment costs, making this treatment sequence very competitive for implementation at industrial scale. According to the Portuguese Regulatory Institute for Water and Wastes (IRAR, in Portuguese: Instituto Regulador de Águas e Resíduos), 80% of existing leachate treatment plants doesn't fulfill the requisites originally planned in the project [38].

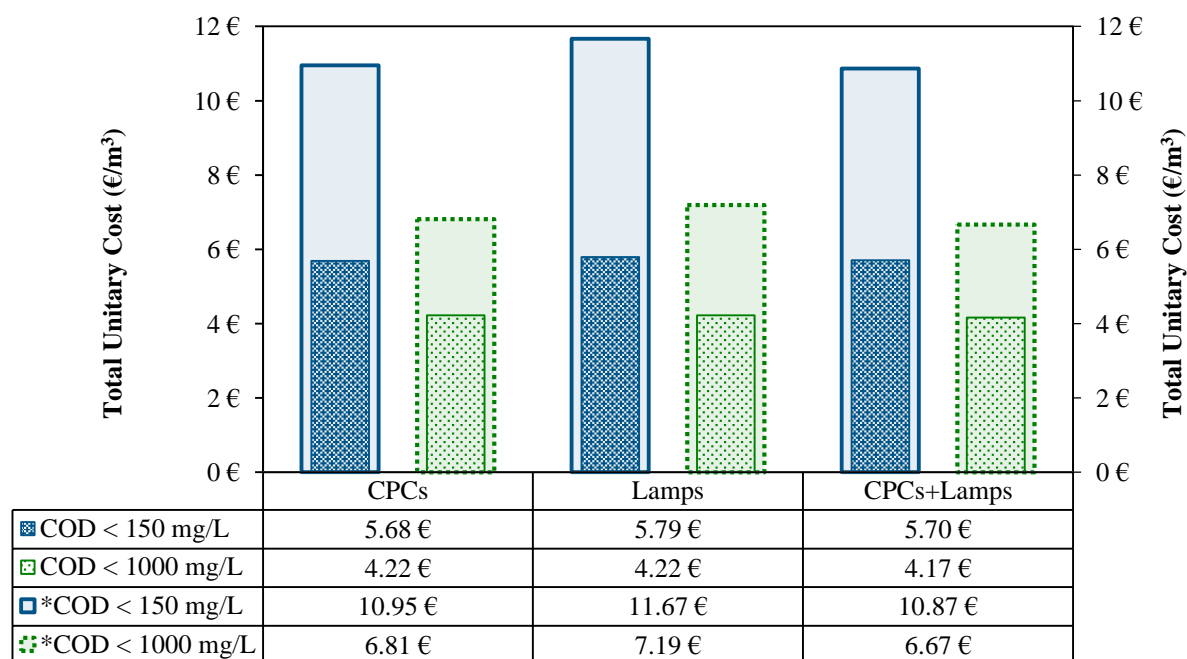


Figure 9.26. Comparison between the total cost of the leachate phototreatment obtained in this chapter and in Chapter 6 (*), considering different process setups, aiming a COD of 150 and 1000 mg O₂/L.

9.3.6 European patent and semi-industrial scale plant

Following the work done in the course of this thesis and under the partnership established between the EFACEC Engineering and Systems, S.A. company and FEUP/LSRE, an European Patent (EP 2784031 A1) was published [39], disclosing a methodology for the treatment of landfill leachates, which comprises the following sequential steps: i) preliminary biological oxidation; ii) coagulation/sedimentation process; iii) photo-Fenton reaction (combining solar and artificial radiation); and iv) final biological oxidation.

In the meantime, under the same protocol established between the FEUP/LSRE and the Company EFACEC Engineering and Systems, S.A. a project named Advanced LFT (FCOMP-01-0202-FEDER-033 960) was developed and financed by FEDER - Fundo Europeu de Desenvolvimento Regional, through COMPETE/POFC - Programa Operacional Factores de Competitividade, of the QREN - Quadro de Referência Estratégico Nacional, under the Incentives System for Research and Technological Development. The main objective of this project was to achieve a multistage treatment system for the treatment of mature leachates at comfortable costs, as described in the Patent. For that, a semi-industrial scale plant (Figure 9.27), with a capacity of treating 20 m³/day of leachate, was constructed and installed in a sanitary landfill nearby Porto.

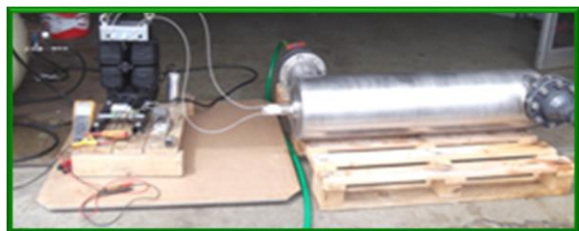


Figure 9.27. Semi-industrial plant for the treatment of 20 m³/day of leachate, developed under the project Advanced LFT.

9.4 Conclusions

The leachate collected after the biological oxidation system of the LTP installed at the sanitary landfill, object of this study, has an average biodegradable organic fraction of 11% (0.14 g C/L), being 71% non-biodegradable organics (1.13 g C/L) attributed to humic substances. Beyond that, the leachate also presents a high nitrogen content (1.3 g N/L), being 43 and 44% in the form of ammonium and nitrite, respectively. Leachates are a high strength complex mixture and consequently an efficient and cost effective universal solution capable of ensuring the environment resources protection has not been found.

The present work presents a multistage treatment process adjustable to the characteristics of leachates from urban sanitary landfills with its own 'mix' of toxic and recalcitrant chemical pollutants, as an eco-efficient and cost effective technology, combining:

- (i) Aerobic biological oxidation to achieve complete conversion of ammonia to nitrates, with simultaneous removal of alkalinity and biodegradable organic carbon fraction;

During this phase, the biological reactor must operate in conditions that ensure complete nitrification to nitrate, minimizing the H_2O_2 consumption in the subsequent photo-Fenton reaction and in the alkalinity consumption, reaching a final pH value around 6.5. This minimizes the sulphuric acid requirements for the acidification step of the photo-Fenton reaction, being able to achieve a final treated leachate in agreement with the discharge limit for sulphate.

- (ii) Physical-chemical process of coagulation/sedimentation with ferric chloride (240 mg Fe^{3+}/L), at pH 4.2 (partial nitrification to nitrite) or 3.0 (complete nitrification to nitrate), followed by a 14-hours settling phase, in order to promote precipitation of the humic acids and the sedimentation of the suspended solids generated, maximizing the light penetration in the photoreactor;

The presence of suspended solids revealed itself, in the first studies, to be a negative factor on the photo-Fenton efficiency, decreasing the capacity of the light to access the reaction medium, increasing the H_2O_2 consumption and preventing the iron catalyst regeneration in different phototreatment cycles. In this regard, the addition of a coagulant followed by a sedimentation period will enhance the precipitation and elimination of recalcitrant organic matter, mostly humic acids, resulting in a yellow colour leachate, mainly attributed to the presence of dissolved fulvic acids, with a low suspended solids content and high UV-visible transmissibility.

- (iii) Photo-Fenton oxidation step ($\text{Fe}^{2+}/\text{H}_2\text{O}_2/\text{UV-Vis}$; 60 mg of Fe^{2+} per 1-L of leachate at pH 2.8) using artificial and solar radiation (CPCs were used to capture UV-visible solar photons), to degrade the most recalcitrant organic compounds, through the generation of powerful reactive chemical species, such as hydroxyl radicals ($\cdot\text{OH}$), turning them into simpler and easily biodegradable organic compounds;

If nitrification reaction predominates in the biological oxidation, the photo-Fenton reaction contemplates an initial phase where the nitrites are indirectly converted into nitrates and hydrogen ions, consuming an extra amount of hydrogen peroxide. Nevertheless, this situation also leads to the need of sodium hydroxide addition to avoid pH values lower than 2.8. Whereby when the leachate presents nitrite ions instead of nitrates, the coagulation must be done at pH 4.2, in order to minimize the sodium hydroxide consumption. However, the complete nitrification in the biological reactor is ideal, thus avoiding the initial hydrogen peroxide consumption.

From the biodegradability trials, in order to achieve a leachate able to be further biologically oxidized to fulfil the COD discharge limit into water bodies (150 mg O_2/L) is mandatory that at the end of the photo-reaction: i) the DOC concentration is around 300 mg/L (initializing with 420 mg/L); and ii) the absorbance at 254 nm (1:25 dilution) is approximately equal to 0.13; resulting in the consumption of about 105 mM of H_2O_2 (or c.a. 60% less, if the leachate present nitrates instead of nitrites) and 7.5 kJ of accumulated UV energy. It was also possible to infer that for the discharge into a sewerage system, the whole treatment would finalize at the phototreatment stage, since the final biological treatment will take place in a municipal WWTP, and in this case the optimum phototreatment time will be obtained after 1.5 kJ of accumulated UV energy, consuming 76 mM of H_2O_2 (or c.a. 85% less, if the leachate present nitrates instead of nitrites), reaching up to a COD value of 955 mg O_2/L .

The H_2O_2 was the reactant that most contributed to the final treatment cost (~44%), while the sulphuric acid and the ferrous iron were the chemicals that contributed less (~1%). The design of a photocatalytic plant capable of treating 100 m^3/day of leachate, after aerobic lagooning, demonstrated the need of implementing 1500 and 295 m^2 of CPCs, which in terms of land occupation corresponds to 5876 and 1214 m^2 , targeting a final COD value below 150 or 1000 mg O_2/L , respectively. Regarding the scenario wherein only artificial radiation is used, it would be required about 38 and 8 UV-Vis lamps, with a rated power of 4 kW, working 6 daily hours, respectively. The combination of solar and artificial radiation, taking into account the energetic needs throughout the year, showed to be the best alternative, being required 957 and 188 m^2 of CPCs (the equivalent to 3711 and 714 m^2 of land area) and, 30 and 6 UV-Vis lamps (working 6 daily hours), respectively. From the economic assessment, it was found that the total unitary costs of the photo-Fenton reaction

applied to the bio-coag-treated leachate, were very close for the three configurations analysed, being on average equal to 5.7 and 4.2 €/m³, targeting a COD value lesser than 150 and 1000 mg O₂/L, respectively.

- (iv) Biological oxidation step under anoxic conditions to promote the denitrification and elimination of the remaining biodegradable organic fraction;

The treatment of a photo-treated leachate with DOC < 300 mg C/L by an aerobic biological process with activated sludge revealed, as reported in the first chapters, to be highly efficient, allowing to obtain a final effluent with COD < 150 mg O₂/L, at a retention time lower than 24-hours. Regarding the denitrification reaction, it was achieved a maximum reaction rate of 5.8 mg (NO₃⁻-N+NO₂⁻-N)/g VSS/h, a minimum methanol consumption of 2.4 g CH₃OH per each gram of NO₃⁻-N+NO₂⁻-N reduced and an alkalinity production of 4.3 g CaCO₃/g (NO₃⁻-N+NO₂⁻-N).

9.5 References

- [1] A. Spagni, S. Marsili-Libelli, Nitrogen removal via nitrite in a sequencing batch reactor treating sanitary landfill leachate, *Bioresource Technology*, 100 (2009) 609-614.
- [2] S. Malato, P. Fernández-Ibáñez, M.I. Maldonado, J. Blanco, W. Gernjak, Decontamination and disinfection of water by solar photocatalysis: Recent overview and trends, *Catalysis Today*, 147 (2009) 1-59.
- [3] V.J.P. Vilar, M.I. Maldonado, I. Oller, S. Malato, R.A.R. Boaventura, Solar treatment of cork boiling and bleaching wastewaters in a pilot plant, *Water Research*, 43 (2009) 4050-4062.
- [4] V.J.P. Vilar, L.X. Pinho, A.M.A. Pintor, R.A.R. Boaventura, Treatment of textile wastewaters by solar-driven advanced oxidation processes, *Solar Energy*, 85 (2011) 1927-1934.
- [5] A. Zapata, S. Malato, J.A. Sánchez-Pérez, I. Oller, M.I. Maldonado, Scale-up strategy for a combined solar photo-Fenton/biological system for remediation of pesticide-contaminated water, *Catalysis Today*, 151 (2010) 100-106.
- [6] I. Oller, S. Malato, J. Sánchez-Pérez, Combination of advanced oxidation processes and biological treatments for wastewater decontamination—a review, *Science of the Total Environment*, 409 (2011) 4141-4166.
- [7] *Wastewater Treatment: Biological and Chemical Processes*, Springer, 2002.
- [8] M.H. Gerardi, *Nitrification and Denitrification in the Activated Sludge Process*, Wiley, 2003.
- [9] C. Sawyer, P. McCarty, G. Parkin, *Chemistry for Environmental Engineering and Science*, McGraw-Hill Education, 2003.
- [10] S. Philips, H.J. Laanbroek, W. Verstraete, Origin, causes and effects of increased nitrite concentrations in aquatic environments, *Reviews in environmental science and biotechnology*, 1 (2002) 115-141.
- [11] A. Spagni, M.C. Lavagnolo, C. Scarpa, P. Vendrame, A. Rizzo, L. Luccarini, Nitrogen removal optimization in a sequencing batch reactor treating sanitary landfill leachate, *Journal of Environmental Science and Health Part A*, 42 (2007) 757-765.
- [12] M. Henze, P. Harremoës, J.I.C. Jansen, E. Arvin, *Basic Biological Processes*, in: *Wastewater Treatment: Biological and Chemical Processes*, Second Edition, Springer-Verlag, Berlin, 1997.
- [13] R. Canziani, V. Emondi, M. Garavaglia, F. Malpei, E. Pasinetti, G. Buttiglieri, Effect of oxygen concentration on biological nitrification and microbial kinetics in a cross-flow membrane bioreactor (MBR) and moving-bed biofilm reactor (MBBR) treating old landfill leachate, *Journal of Membrane Science*, 286 (2006) 202-212.
- [14] J.E. Alleman, Elevated nitrite occurrence in biological wastewater treatment systems, *Water Science and Technology*, 17 (1984) 409-419.
- [15] K. Hanaki, C. Wantawin, S. Ohgaki, Nitrification at low levels of dissolved oxygen with and without organic loading in a suspended-growth reactor, *Water Research*, 24 (1990) 297-302.
- [16] A. Anthonisen, R. Loehr, T. Prakasam, E. Srinath, Inhibition of nitrification by ammonia and nitrous acid, *Journal (Water Pollution Control Federation)*, (1976) 835-852.

- [17] S. Villaverde, F. Fdz-Polanco, P.A. García, Nitrifying biofilm acclimation to free ammonia in submerged biofilters. Start-up influence, *Water Research*, 34 (2000) 602-610.
- [18] Metcalf, Eddy, *Wastewater Engineering Treatment and Reuse*, 4th ed., Metcalf & Eddy, 2005.
- [19] H.K. Trivedi, Simultaneous Nitrification and Denitrification (Symbio® Process), in: L.K. Wang, N.K. Shamas, Y.-T. Hung (Eds.) *Advanced Biological Treatment Processes*, Humana Press, 2009.
- [20] J.J. Pignatello, E. Oliveros, A. MacKay, Advanced oxidation processes for organic contaminant destruction based on the fenton reaction and related chemistry, *Critical Reviews in Environmental Science and Technology*, 36 (2006) 1-84.
- [21] X. Ntampou, A.I. Zouboulis, P. Samaras, Appropriate combination of physico-chemical methods (coagulation/flocculation and ozonation) for the efficient treatment of landfill leachates, *Chemosphere*, 62 (2006) 722-730.
- [22] G. Edge, T. Weller, *The Best of The Growing Edge International, 2000-2005: Select Cream-of-the-crop Articles for Soilless Growers*, New Moon Publishing, 2005.
- [23] R. Nieder, D.K. Benbi, *Carbon and Nitrogen in the Terrestrial Environment*, Springer, 2008.
- [24] S. Park, T.-i. Yoon, The effects of iron species and mineral particles on advanced oxidation processes for the removal of humic acids, *Desalination*, 208 (2007) 181-191.
- [25] L.S. Clesceri, A.E. Greenberg, A.D. Eaton, *Standard Methods for Examination of Water & Wastewater*, 21st ed. ed., American Public Health Association (APHA), American Water Works Association (AWWA) & Water Environment Federation (WEF), 2005.
- [26] E.M. Thurman, R.L. Malcolm, Preparative isolation of aquatic humic substances, *Environmental Science & Technology*, 15 (1981) 463-466.
- [27] H.A. Aziz, S. Alias, M.N. Adlan, Faridah, A.H. Asaari, M.S. Zahari, Colour removal from landfill leachate by coagulation and flocculation processes, *Bioresource Technology*, 98 (2007) 218-220.
- [28] A. Amokrane, C. Comel, J. Veron, Landfill leachates pretreatment by coagulation-flocculation, *Water Research*, 31 (1997) 2775-2782.
- [29] Y. Wu, S. Zhou, X. Ye, D. Chen, K. Zheng, F. Qin, Transformation of pollutants in landfill leachate treated by a combined sequence batch reactor, coagulation, Fenton oxidation and biological aerated filter technology, *Process Safety and Environmental Protection*, 89 (2011) 112-120.
- [30] J. Yoon, S. Cho, Y. Cho, S. Kim, The characteristics of coagulation of fenton reaction in the removal of landfill leachate organics, *Water Science and Technology*, 38 (1998) 209-214.
- [31] J. Duan, J. Gregory, Coagulation by hydrolysing metal salts, *Advances in Colloid and Interface Science*, 100-102 (2003) 475-502.
- [32] A. Saha, S. Goldstein, D. Cabelli, G. Czapski, Determination of optimal conditions for synthesis of peroxyxynitrite by mixing acidified hydrogen peroxide with nitrite, *Free Radical Biology and Medicine*, 24 (1998) 653-659.
- [33] S. Goldstein, G.L. Squadrito, W.A. Pryor, G. Czapski, Direct and indirect oxidations by peroxyxynitrite, neither involving the hydroxyl radical, *Free Radical Biology and Medicine*, 21 (1996) 965-974.

- [34] M. Hughes, H. Nicklin, The chemistry of pernitrites. Part I. Kinetics of decomposition of pernitrous acid, *Journal of the Chemical Society A: Inorganic, Physical, Theoretical*, (1968) 450-452.
- [35] P.B. Kelter, M.D. Mosher, A. Scott, *Chemistry: The Practical Science*, Houghton Mifflin, 2008.
- [36] D. Skoog, D. West, F. Holler, S. Crouch, *Fundamentals of Analytical Chemistry*, Cengage Learning, 2013.
- [37] J.B. Gálvez, S.M. Rodríguez, *Solar Detoxification*, United Nations Educational, Scientific and Cultural Organization, 2003.
- [38] IRAR, (2008) *Gestão e tratamento de lixiviados produzidos em aterros sanitários de resíduos urbanos*. Relatório IRAR n.º 03/2008.
- [39] I.M.A. Saraiva, F.M.A.F. da, V.J.P. Vilar, T.F.C.V. Silva, R.A. da Rocha Boaventura, Method of treating leachate, phototreatment reactors and respective use, in, *Google Patents*, 2014.

10 Final Remarks

This last chapter presents the most relevant results and conclusions reported in the previous chapters, as well as some suggestions for future work.

10.1 Conclusions

The main goal of the present thesis was the development and optimization of a multistage methodology for the treatment of mature landfill leachates, aiming mostly the discharge into water bodies at appellative costs. Regardless the multistage treatment system used, the treatment strategy involved always an activated sludge biological oxidation (ASBO) and a photo-Fenton (PF) reaction. Later, it was also incorporated a coagulation/sedimentation stage. All processes were tested at the lab and pre-industrial scale units equipped with (i) biological reactor, which was prepared to work under aerobic and anoxic conditions, and (ii) photoreactor containing compound parabolic collectors (CPCs) and/or UV-Vis lamps. The results showed that the integration of these three oxidative processes applied to the mature leachate treatment is an interesting and commercially viable option.

10.1.1 Integration of solar photo-Fenton reaction with biological oxidation

The leachate after lagooning pre-treatment showed low biodegradability, mainly due to the presence of a high concentration of humic acids (~59% of DOC) and a high nitrogen load, mainly in the form of ammonium. Firstly, based on the leachate characteristics, an integrated leachate treatment strategy was proposed in Chapters 3 and 4, combining (i) solar PF reaction, as pre-oxidation process, to enhance the leachate's biodegradability, with (ii) ASBO, under aerobic and anoxic conditions, to oxidize the remaining biodegradable organic fraction and completely eliminate nitrogen compounds, through nitrification and denitrification, with the addition of an external carbon source. The tests were conducted in a pre-industrial plant, incorporating a solar photocatalytic system with 39.52 m² of CPCs and an activated sludge reactor with 3.5 m³ capacity. The experimental unit was constructed and installed at a sanitary landfill in order to evaluate the treatment efficiency, under real circumstances of leachate variability and weather conditions.

The preliminary acidification step required by the PF reaction led to the precipitation of humic acids and other organic compounds, and is responsible for an abatement of 20-58% of the soluble DOC. The acid sludge produced after acidification decreased the PF reaction efficiency due to the lower light transmission caused by the higher amount of suspended solids that competed with H₂O₂ and iron species as photons absorbers. Therefore, higher amounts of H₂O₂ and energy were necessary to degrade also the particulate organic matter. The major drawback of sludge elimination is associated with the remediation/disposal of an acid sludge.

The reutilization of iron sludge in consecutive oxidation treatments was not viable precisely due to the increase of suspended solids, leading to lower reaction rates. The leachate photo-oxidation was also strongly affected by weather conditions, mainly due to low values of irradiance and temperature in the winter season, leading to low reaction rates, associated to the effects of the Fenton thermal reaction and molar fraction of ferric species.

The PF reaction was able to enhance the leachate's biodegradability above 70%, according to Zahn-Wellens test. In order to achieve COD target values below 150 mg O₂/L (in agreement with the discharge limit into water bodies) after the final biological oxidation, it was necessary, for the photo-oxidation, a hydrogen peroxide concentration between 180-225 mM. The good results obtained in the PF reaction, even in the presence of high concentrations of sulphate and chloride ions, were attributed to the formation of ferric-carboxylate complexes.

Biological nitrification and denitrification reactions were strongly affected by the low temperatures observed during the winter season. A maximum nitrification rate of 6.9 mg NH₄⁺-N/(h.g VSS) (T = 26.8 °C, pH = 7.3) was achieved, consuming 20.0 g CaCO₃/L or 9.9 mg CaCO₃ per mg NH₄⁺-N. The maximum denitrification rate was 2.4 mg (NO₂⁻-N + NO₃⁻-N)/(h.g VSS) (T = 26.2 °C, pH = 8.8), with a C/N consumption ratio of 3.1 mg CH₃OH/mg (NO₂⁻-N + NO₃⁻-N).

The post-treatment system by ASBO, operating under aerobic and anoxic conditions, allowed an almost complete nitrogen removal, for levels below 15 mg N/L (emission limit value). The global DOC removal efficiency in the combined system was approximately 86%, corresponding 55% to chemical oxidation and 31% to biological oxidation.

Later, in Chapter 5, a multistage treatment system consisting in three sequential steps, ASBO/PF reaction/ASBO, showed to be an interesting approach for the treatment of stabilized raw leachates from sanitary landfills, concerning the elimination of organic matter and nitrogen compounds.

In the 1st ASBO system, under aerobic and anoxic conditions, 39% mineralization and 95% and 53% reduction of the nitrogen and alkalinity content, respectively, were achieved. The highest nitrification rate was 8.2 mg NH₄⁺-N/(h.g VSS) (T = 26.9 °C; pH = 7.6), consuming 21.6 g CaCO₃ per liter of raw leachate or 6.0 mg CaCO₃ per mg NH₄⁺-N. The maximum denitrification rate was 5.8 mg (NO₂⁻-N + NO₃⁻-N)/(h.g VSS) (T = 26.4 °C; pH = 8.4), with a C/N consumption ratio of 2.4 mg CH₃OH per mg (NO₂⁻-N + NO₃⁻-N), with an overall alkalinity production of 4.3 g CaCO₃ per g (NO₂⁻-N + NO₃⁻-N) reduced.

The precipitation of humic acids (37% of HS) after acidification of the bio-treated leachate corresponded to 96% of the DOC abatement. The amount of UV energy and H₂O₂ consumption during the PF reaction was 30% higher in the experiment without sludge removal and, consequently, the reaction rate was 30% lower. The PF process led to the depletion of HS >80%, of low-molecular-weight carboxylate anions >70% and other organic micropollutants >90%, thus resulting in a total biodegradability increase of >70%, being possible to couple it with a further ASBO, achieving a final wastewater quality in agreement with Portuguese discharge limits into receiving water bodies, with the exception of sulphate ions.

Finally, in order to evaluate the feasibility of this approach to leachate treatment at full scale, a scale-up and economic assessment of a PF plant was performed, in Chapter 6. The scale-up and economic assessment of the PF plant, using solar and/or artificial radiation, were based on the operation variables obtained at pre-industrial scale, considering the treatment of 100 m³ per day of a landfill leachate after a biological pre-oxidation process, in order to achieve two targets COD values of 1000 and 150 mg O₂/L, regarding Portuguese discharge regulations into sewerage systems and water bodies, respectively.

The maximum mass and volumetric treatment factors (T_{fm} and T_{fv}) achieved were 2.35 g C/h/m² and 3.22 L/h/m² to achieve a final COD of 1000 mg O₂/L and, 1.83 g C/h/m² and 2.04 L/h/m² to achieve a final COD after biological treatment of 150 mg O₂/L, considering a total of 2944 hours of insolation and a yearly average solar UV radiation of 17 W/m² (data collected at the location of the sanitary landfill). The production of electrical photons was more expensive than solar photons capture, being the main difference, between both UV photons sources, related to investment and operation costs, since, using solar energy, the investment cost is higher than the operational cost and using electric energy, the opposite happens.

The scale-up for the optimal conditions showed the need to implement 3836 and 6056 m² of CPCs, or 25 and 39 UV lamps, to achieve targets COD of 1000 and 150 mg O₂/L, respectively. Considering the combined use of natural and artificial radiation, it is necessary to implement 2446 m² of CPCs and 19 UV lamps, for COD of 1000 mg O₂/L, and 3862 m² of CPCs and 30 UV lamps, for COD of 150 mg O₂/L. For all scenarios, the expense associated just with H₂O₂ consumption represents, on average, about 30 and 39% of the total yearly cost, respectively to target COD of 1000 and 150 mg O₂/L. The economic assessment for optimal conditions led to a total unitary cost, aiming to achieve COD values of 1000 and 150 mg O₂/L, respectively of: 6.8 and 11.0 €/m³, using only CPCs; 7.2 and 11.7 €/m³, resorting just to UV lamps; and 6.7 and 10.9 €/m³, combining CPCs and UV lamps.

It was notorious that the cost of the PF process increased proportionally to the leachate pollution load and alkalinity; consequently its minimization would decrease the total expenditure. Moreover, the results reported in Chapters 3-5 showed that the PF reaction efficiency was considerably affected by the (i) weather conditions, mainly due to low irradiances and temperatures in the winter season, (ii) presence of humic acids (associated with the dark-brown colour intrinsic to leachates), (iii) high amount of suspended solids (resulting from the precipitation of some organic compounds with ferric ions) and (iv) high amounts of sulphate ions due to addition of sulphuric acid required for the acidification step of the PF. Considering all these aspects, it was concluded that the implementation of a preliminary biological nitrification followed by a physico-chemical process would be the best strategy to reduce the content of sulphates and photons absorbing species, during the photo-oxidation, thus also reducing the overall treatment cost. So, it was decided to adapt the pre-industrial plant to this new methodology.

10.1.2 Integration of biological oxidation with coagulation and solar/UV photo-Fenton process

Complementarily to tests conducted at pre-industrial scale, some experiments at lab-scale were performed, under controlled conditions, in order to evaluate and predict the behaviour of the PF process and the nitrification and denitrification reactions, via nitrite, face to potential variations in the operating conditions.

In Chapter 7, the main PF reaction variables (Fe^{2+} concentration, pH, temperature, acid type and UV irradiance) were assessed using (i) a sanitary landfill leachate collected at the outlet of a leachate treatment plant (LTP), which includes aerated lagooning followed by aerated activated sludge and a final coagulation-flocculation step, and (ii) a lab-scale CPC photoreactor with artificial solar radiation. The coagulation/flocculation step improved substantially the efficiency of the PF reaction, both in terms of energy consumption (69% less) and H_2O_2 consumption (44% less), mainly associated with the decrease on TSS (ca. 75% less) and precipitation of humic acids.

Regarding the PF reaction variables it was possible to conclude that: (i) the best iron concentration was 60 mg/L and above this content the mineralization degree is not affected; (ii) the best pH value was 2.8, since the iron precipitation is avoided and the highest FeOH^{2+} concentration is achieved, nevertheless, according to ferric speciation diagrams, the reaction rate constant could be improved if the pH was increased to 3.0; (iii) the rise of leachate temperature benefits the reaction rate until 40°C, mostly attributed to the production of more hydroxyl radicals resulting from a higher ferric ion reduction through thermal reactions and an increment of the FeOH^{2+} molar fraction; however, mainly above 30°C, more H_2O_2 was spent to achieve the same mineralization; (iv) higher reaction rates were achieved when using only H_2SO_4 instead of HCl and $\text{H}_2\text{SO}_4 + \text{HCl}$, since (1) a much lesser amount of H_2SO_4 is required

to acidify the leachate, (2) the Cl^\bullet and $\text{Cl}_2^{\bullet-}$ radicals are less reactive than $\text{SO}_4^{\bullet-}$, and (3) the ferric ions solubility decreases in the presence of high chlorides content; (v) during spring and summer, when the irradiance is around $44 \text{ W}_{\text{UV}}/\text{m}^2$ at maximum, considering the path length of the photoreactors, the energy losses will be negligible, and, over autumn and winter, the kinetic reaction rate remains constant in terms of accumulated UV energy, but the reaction takes a longer time.

Ferric ion speciation diagrams help to predict the dissimilarities on the photo-Fenton reaction performance, according to the solution pH, temperature, concentration of chloride and sulphate ions. When the pH and temperature values were individually changed, it was possible to achieve a linear relation between the pseudo-first order kinetic constant and the theoretical FeOH^{2+} content. Furthermore, in a full-scale plant, speciation diagrams can be used to predict the optimum pH value, taking into account the leachate temperature variability and the amount of sulphate and chloride, and also the required phototreatment time for a further biological treatment with high efficiency.

Chapter 8 refers to the assessment of the effect of the main nitrification (temperature, dissolved oxygen (DO) and pH) and denitrification (pH, temperature and PO_4^{3-} concentration) variables on the nitrogen's biological removal via nitrite, from mature leachates collected after aerobic lagooning or previously nitrified. At the beginning of most nitrification assays, it was verified the occurrence of ammonia stripping simultaneously to nitrification, leading up to 31 % removal of total dissolved nitrogen.

The maximum nitrification rate obtained was $37 \pm 2 \text{ mg NH}_4^+-\text{N}/(\text{h.g VSS})$ (25°C , $1.0\text{-}2.0 \text{ mg O}_2/\text{L}$, pH not controlled), consuming $5.3 \pm 0.4 \text{ mg CaCO}_3/\text{mg NH}_4^+-\text{N}$. The highest denitrification rate achieved was $27 \pm 1 \text{ mg NO}_2^--\text{N}/(\text{h.g VSS})$ (pH between 7.5 and 8.0, 30°C , adding $30 \text{ mg PO}_4^{3-}/\text{L}$), with a C/N consumption ratio of $1.6 \pm 0.1 \text{ mg CH}_3\text{OH}/\text{mg NO}_2^--\text{N}$ and an overall alkalinity production of $3.2 \pm 0.1 \text{ mg CaCO}_3/\text{mg NO}_2^--\text{N}$. The denitrification process showed to be sensitive to all studied parameters, while the nitrification reaction was not significantly affected by the DO content.

The 454-pyrosequencing analysis of the 16S rRNA gene disclosed the presence of bacteria from the families *Nitrosomonadaceae* and *Hyphomicrobiaceae* (in particular, genus *Hyphomicrobium*), in the aerobic and anoxic bio-reactors, which are closely related to the reactions of nitrification and denitrification, respectively. Furthermore, it was also disclosed the attendance of bacteria associated to classes *Sphingobacteriia* and *Flavobacteriia* in both reactors, which have been reported as responsible for the degradation of complex organic matter, one of the main constituents of the mature landfill leachates. As a final point, it was also possible to conclude that, reactions involving (i) oxidation/reduction of nitrogen species and (ii) degradation of organic matter were mostly mediated by bacteria from the phyla *Proteobacteria* and *Bacteroidetes*, respectively.

Finally, in Chapter 9, it was presented a multistage treatment approach adjustable to the characteristics of leachates from urban sanitary landfills with their own 'mix' of toxic and recalcitrant pollutants, as an eco-efficient and cost effective technology, combining: (i) an ASBO, under aerobic conditions, to remove leachate's alkalinity and the biodegradable organic carbon fraction (ii) a coagulation/sedimentation step (240 mg Fe³⁺/L, at pH 4.2, 14-hours settling), to promote humic acids precipitation and reduce the amount of TSS, and (iii) a photo-oxidation process through PF reaction (60 mg Fe²⁺/L, at pH 2.8), combining solar and artificial radiation (since during winter the irradiance is low), to promote the recalcitrant molecules degradation and consequent biodegradability enhancement, until the point (DOC \approx 250 mg/L) wherein a downstream biological treatment would allow to meet the discharge limit into water bodies (COD < 150 mg O₂/L).

The results revealed that the aerobic biological process applied to a leachate after aerobic lagooning, with high organic and nitrogen content (DOC = 1.1-1.5 g C/L; COD = 3.0-4.3 g O₂/L and N_D = 0.8-3.0 g N/L) and low biodegradability (BOD₅/COD = 0.07-0.13), was capable to oxidise between 62 and 99% of the ammonium nitrogen (NH₄⁺-N_f = 8-250 mg/L), consuming only the leachate alkalinity (final concentration between 0-1.6 g CaCO₃/L), achieving alkalinity reductions between 70 and 100%. The coagulation/sedimentation process led to the humic acids precipitation, promoting a marked change in leachate colour, from dark-brown to yellowish-brown, which was related to the presence of fulvic acids, accompanied by a reduction of 60% on DOC (DOC_f \approx 400 mg/L), 58% on COD (COD_f \approx 1200 mg/L) and 88% on TSS (supernatant TSS = 135 mg/L), obtaining an amount of acid sludge of about 300 mL/L. The implementation of the combined system of biological nitrification/coagulation was able to keep the sulphate ions concentration below the legal discharge limit into water bodies (2 g/L), which was not possible in the previous experiments.

The PF reaction showed an initial phase where the nitrites are indirectly converted to nitrates and hydrogen ions, consuming an extra amount of hydrogen peroxide. Nevertheless, this situation also led to the need of sodium hydroxide addition to avoid pH values lower than 2.8. Whereby, when the leachate presents nitrite ions instead of nitrates, the coagulation must be done at pH 4.2, in order to minimize the sodium hydroxide consumption. However, the complete nitrification in the biological reactor is ideal, thus avoiding the initial hydrogen peroxide consumption.

From the photo-Fenton trials, it was concluded that the best option would be combining natural sunlight with artificial radiation (\sim 1.3 kW/m³), thus optimizing the indirect costs. According to Zahn-Wellens test, a leachate, with 419 mg DOC/L after coagulation, would have to be photo-oxidized until a DOC and an 254 nm absorbance (1:25 dilution) lesser than 300 mg/L and 0.13, respectively, consuming approximately 105 mM of H₂O₂ (or c.a. 60% less, if the leachate present nitrates instead of nitrites) and

7.5 kJ/L of accumulated UV energy, in order to achieve an effluent that can be biologically treated in compliance with the COD discharge limit ($< 150 \text{ mg O}_2/\text{L}$) into water bodies. The biological process subsequent to the photocatalytic system would promote a 59% mineralization, being the final COD $\approx 115 \text{ mg O}_2/\text{L}$. If the ultimate goal is the discharge into sewerage system (COD $< 1000 \text{ mgO}_2/\text{L}$), the full treatment would be finalized in the photo-treatment step, since the final biological treatment will take place in a municipal WWTP, with a COD of about $950 \text{ mg O}_2/\text{L}$ after a mineralization of 21% and a consumption of 1.5 kJ/L of UV energy and 76 mM of H_2O_2 (or c.a. 85% less, if the leachate present nitrates instead of nitrites).

The scale-up of a photocatalytic facility with a capacity to treat 100 m^3 of leachate per day showed the need to implement 1500 and 295 m^2 of CPCs, which in terms of land occupation corresponds to 5876 and 1214 m^2 , or 38 and 8 UV-Vis lamps (with 4kW and $20,000\text{-h}$ of lifetime each, working 6 daily hours), targeting a COD value lesser than 150 and $1000 \text{ mg O}_2/\text{L}$, respectively. Combining solar and artificial radiation, only 957 and 188 m^2 of CPCs (considering the month of higher irradiance), and 30 and 6 lamps (considering the month of lesser irradiance), respectively, would be required. From the economic assessment, it was found that the total unitary costs of the PF reaction applied to the bio-coag-treated leachate, were very close for the three configurations analysed, being on average equal to 5.7 and 4.2 €/m^3 , targeting a COD value lesser than 150 and $1000 \text{ mg O}_2/\text{L}$, respectively. The cost with H_2O_2 corresponds to about 44% of the total yearly cost.

The application of this strategy to leachate treatment leads to a final effluent in agreement with the discharge limits into water bodies, imposed by Portuguese legislation, including for sulphate ions. Moreover, the cost of the PF step decreases about 50% when compared to the initial methodology.

10.2 Suggestions for future work

The results presented in Chapter 9 showed that a leachate downstream from biological oxidation, with high amounts of nitrite, affects directly the hydrogen peroxide consumption in the subsequent photo-Fenton reaction. So, in the future, two measures could be implemented in the first biological oxidation process, regarding a proficient integration with the coagulation and photo-Fenton processes, namely: i) to perform nitrification-denitrification via nitrite, taking into account the alkalinity balance (consumed during nitrification and produced along denitrification), in order to assure that the sulphate concentration (added as sulphuric acid and ferrous sulphate, in the coagulation and photo-oxidation steps, respectively) does not exceed 2 g/L; or (ii) to carry out complete nitrification to nitrate, optimizing the operating conditions (pH, OD and temperature) and the ammonium nitrogen load fed to the biological reactor (for instance, using a sequential batch reactor (SBR) with 100 m³ capacity, being the treated volume of 25 m³, which means a dilution factor of four), minimizing the inhibition of nitrite-oxidising bacteria.

It could also be interesting the study of a continuous biological treatment system composed by an anoxic reactor followed by an aerobic one, with recirculation to the anoxic reactor, using raw leachate. Thus, it would be possible to take advantage of the biodegradable organic fraction and alkalinity of the raw leachate.

If nitrification-denitrification is performed in the first biological treatment, additional tests, applying coagulation and photo-Fenton reaction to the leachate previously denitrified, should be conducted, in order to determine the optimal conditions for the treatment of a leachate without nitrogen.

For future work, it is also suggested (i) to conduct photo-Fenton experiments with humic and fulvic acids extracted from the leachate, (ii) the characterization of the leachate along all treatment sequence, by size exclusion chromatography, in order to understand the molecular weight distribution changes, and (iii) the study of the final biological treatment, after a multistage system composed by biological oxidation, coagulation/sedimentation and photo-Fenton reaction.

Finally, efforts must be spent on the (i) development of new designs for photocatalytic reactors using artificial radiation through computational fluid dynamics (CFD) tool, considering the fluid hydrodynamics, lamp emission spectra and power and, respective distribution inside the reactor, and (ii) optimization of the optical system for sunlight capture, based in CPCs systems, in terms of photon and thermal flux and, volumetric capacity per unit of collector area using non imaging optics (NIO) techniques.

